Chapter 6

BEHAVIOR OF BOX-SHAPED CROSS SECTION OF STRUCTURE SUBJECTED TO SOIL LIQUEFACTION

6.1 GENERAL REMARKS

As illustrated in chapter 1, one of the limitations of past studies on buried box-shaped cross sections is that the effects of liquefied soil have not been focused on. Accordingly the dynamic behavior of flexible cross section during soil liquefaction has not been shown experimentally. On the other hand, it is important to understand the effect of earth pressures on bending strains or deflections of structure in order to specify design loads of cross section. In this chapter, dynamic behavior of cross section in the process of pore water pressure build-up and during complete liquefaction is presented based on the series of shaking table tests. The measured curvatures as well as deflections of flexible wall will be illustrated in detail. Calculation will be made to show internal consistency among such measured quantities of structure as earth pressures, deflections of flexible wall and accelerations. The action of the earth pressure on the structure will be discussed based on the results of the calculation.

6.2 CURVATURE AND DEFLECTION OF FLEXIBLE WALL

6.2.1 Definition of monotonic and fluctuating components of curvature

It is convenient for the analysis to divide the time history of curvature into two components, a monotonic component and a fluctuating component. The former consists of the initial curvature before shaking, the accumulated curvature during shaking and the post-shaking

residual value. The latter is the fluctuation due to horizontal motion. The following discussion will be made distinctly on monotonic component and fluctuating component of curvature.

Definition of measured curvature

Dimension of structure model and location of strain gauges used in the shaking table tests are illustrated in Fig.6.1. Bending strain was measured at seven depths of both side of flexible wall of structure (left side SG1～SG7, right side SG8～SG14). Measured bending strain e_b

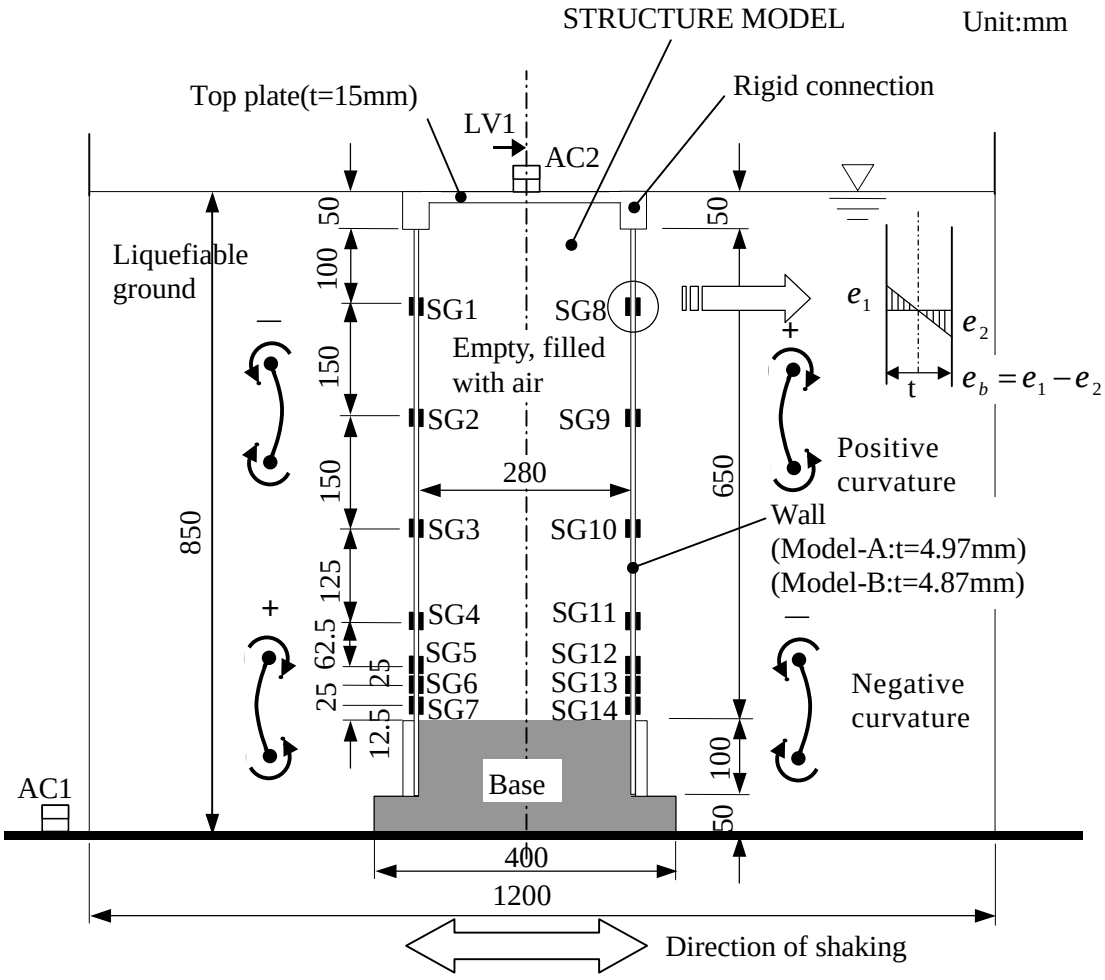

Fig.6.1: Location of strain gauges (SG1～SG14)

($=e_1-e_2$) was converted to curvature ϕ by dividing bending strain by thickness of wall *t* as,

$$f=\frac{e_1-e_2}{t}=\frac{e_b}{t} \tag{6.1}$$

Thickness *t* is either 4.97mm (Structure-A) or 4.87mm (Structure-B). Curvature thus derived is called as the measured curvature hereafter. The definition of either positive or negative curvature is illustrated in Fig.6.1.

Definition of monotonic component

The monotonic component of curvature is extracted from the time history of measured curvature. The moving average computation technique is used for the extraction. The procedure of a moving average computation in this study is shown as what follows:

1. Five sets of sequent data of time history, in which latest 2 data, present data (*i*-th data of time history), and following 2 data, are averaged through all the data of duration time as,

$$\overline{f}_{i,1}=\frac{f_{i-2,0}+f_{i-1,0}+f_{i,0}+f_{i+1,0}+f_{i+2,0}}{5} \qquad (i=3,4,\cdots,N-2) \tag{6.2}$$

where $f_{i-2,0},\cdots,f_{i+2,0}$ are set of raw sequent data of time history, $\overline{f}_{i,1}$ is averaged *i*-th data, and *N* is a number of data.

2. Repeat the previous computation until fluctuation of time history disappears. The *n*-th computation of moving average is expressed as,

$$\overline{f}_{i,n}=\frac{\overline{f}_{i-2,n-1}+\overline{f}_{i-1,n-1}+\overline{f}_{i,n-1}+\overline{f}_{i+1,n-1}+\overline{f}_{i+2,n-1}}{5} \qquad (i=3,4,\cdots,N-2) \tag{6.3}$$

where *n* is number of times of computation (*n*=1 means the first time computation). Schematic diagram of this procedure is depicted in Fig.6.2.

Fig.6.3 shows the time histories of curvature (SG7) with various numbers of times of

computation. It is seen that the fluctuation gradually disappears as the computation is repeated. It takes 800 times of computation to erase fluctuation of time history. For the analysis of curvature for other tests, the same procedure is taken. Table 6.1 summarized the number of times of moving average which erase fluctuations.

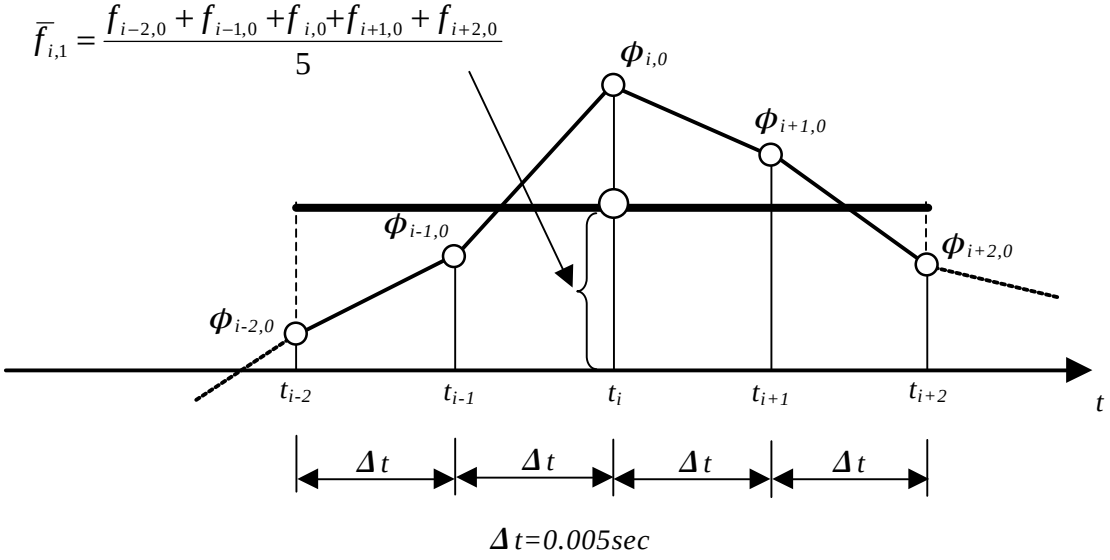

(a) 1st step of computation (i=3,4,…,N-2)

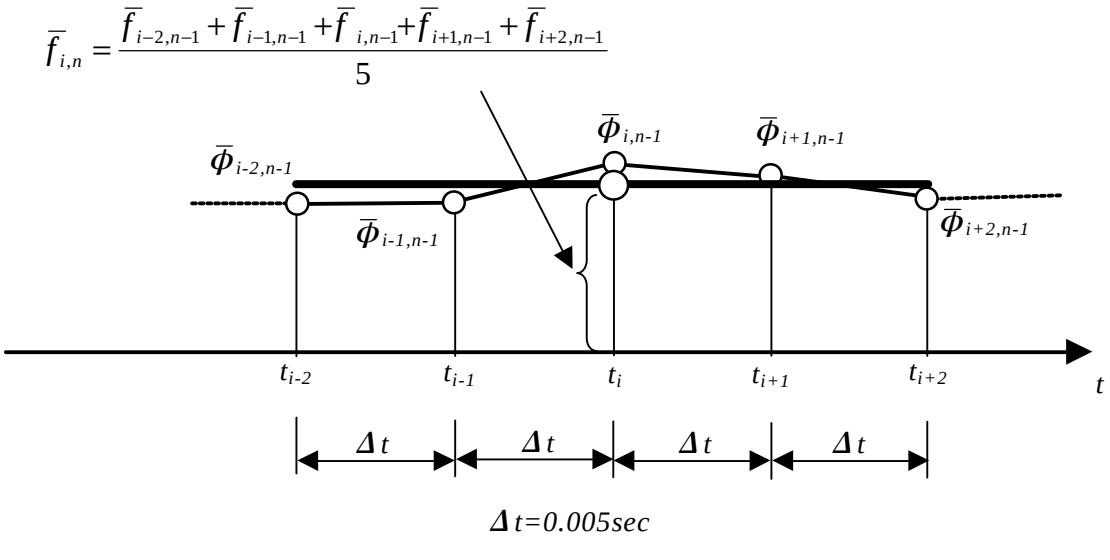

(b) n-th step of computation (i=3,4,…,N-2)

Fig.6.2: Moving average computation at time t_i of sequent data

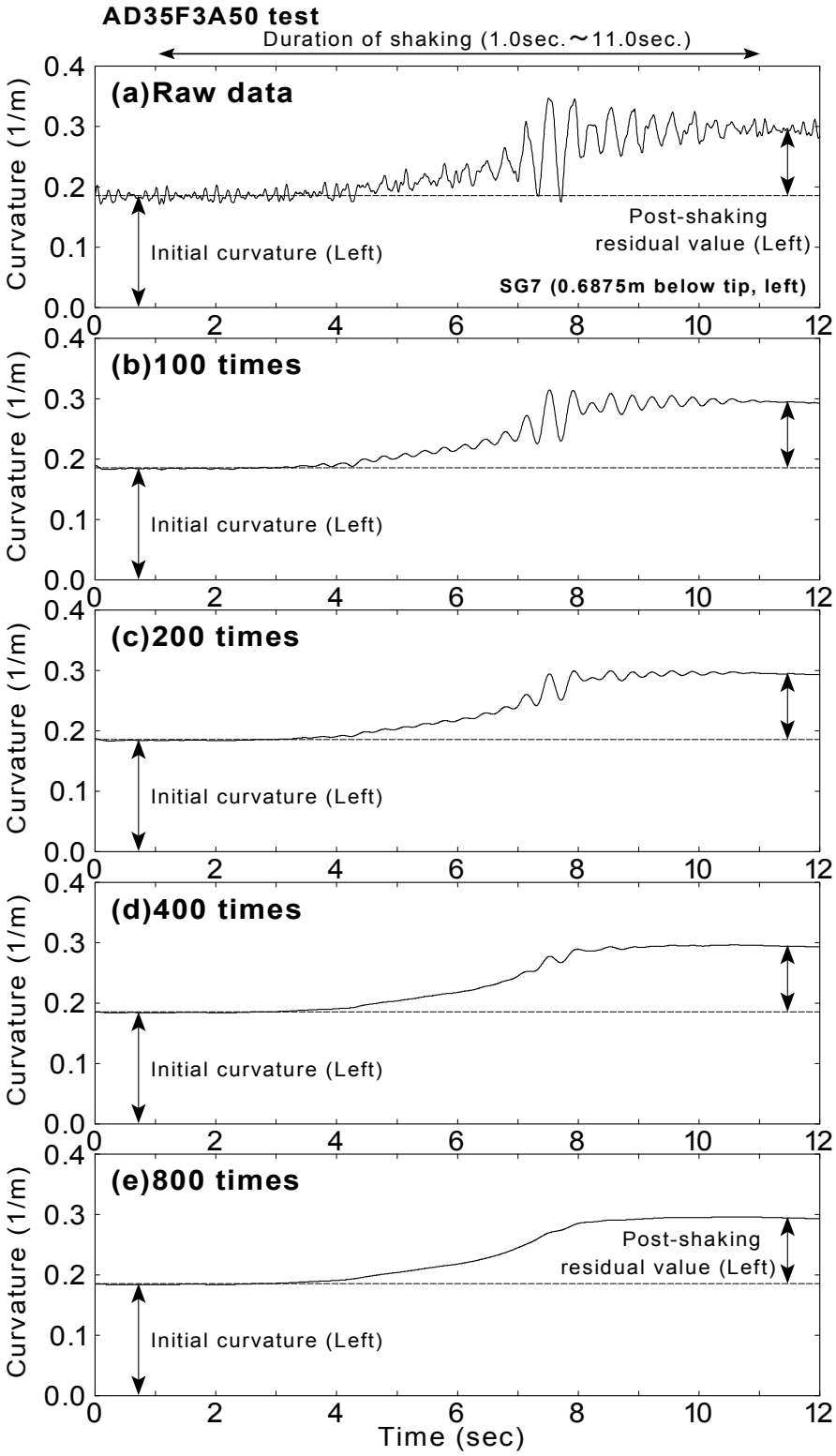

Fig.6.3: Time history of curvature with different times of moving average (SG7, AD35F3A50 test)

Table 6.1: Number of times of moving average calculation for each test

No.	Model of structure	Test	Input frequency (Hz)	Nominal input acc. (m/sec^2)	Number of times of moving average
Model-1	Structure-A	AD35F3A50	3	0.5	800
		AD39F5A50	5	0.5	200
		AD41F3A200	3	2.0	800
		AD61F3A200	3	2.0	800
		AD67F3A500	3	2.0	800
Model-2	Structure-A	AD32F3A500	3	5.0	800
Model-3	Structure-B	BD36F3A500	3	5.0	800
Model-4	Structure-B	BD78F3A500	3	5.0	800

To compare the absolute value between the left and right wall time by time, the sign of time history at the right wall is changed in reverse. Namely,

$$\phi'_{s,\,right\ wall}(t) = -\phi_{s,\,right\ wall}(t) \tag{6.4}$$

where $\phi_{s,\,right\ wall}(t)$ is the monotonic component of curvature at right wall, of which the definition of the sign is defined as illustrated in Fig.6.1. It should be noted that the monotonic component with reversed sign is only for the description of results in figures.

Definition of fluctuating component

Fluctuating component of curvature is calculated by subtracting the time history of monotonic component from the measured time histories of curvature as,

$$\phi_d(t) = \phi(t) - \phi_s(t) \tag{6.5}$$

where $\phi_d(t)$ is the time history of fluctuating component, $\phi(t)$ is the measured time history, and $\phi_s(t)$ is the monotonic component which is derived by the prescribed procedure of moving average computation.

Fig.6.4 illustrates typical time history of monotonic and fluctuating component of curvature at the stem of wall from AD35F3A50 test thus derived (0.6875m below tip, the left wall, SG7, and the right wall ,SG14).

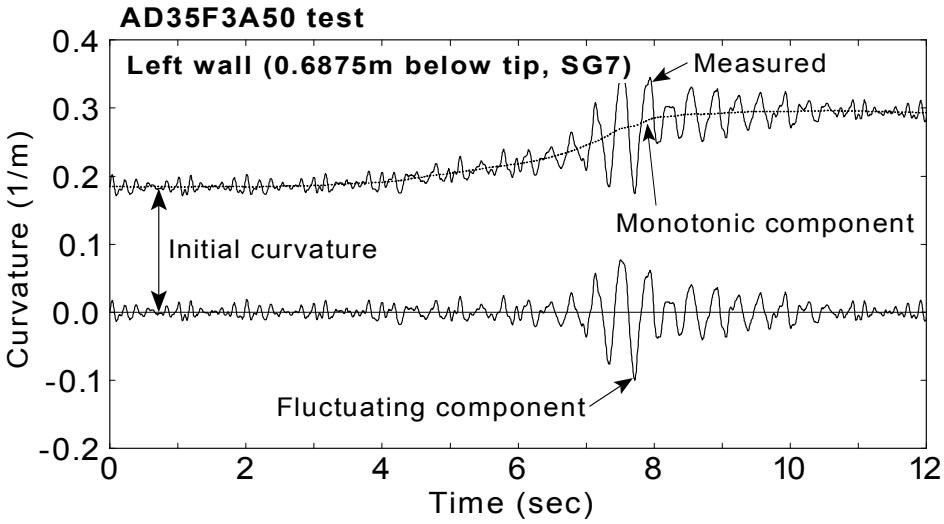

(a) Left wall (stem of wall, 0.6875m below tip, SG7)

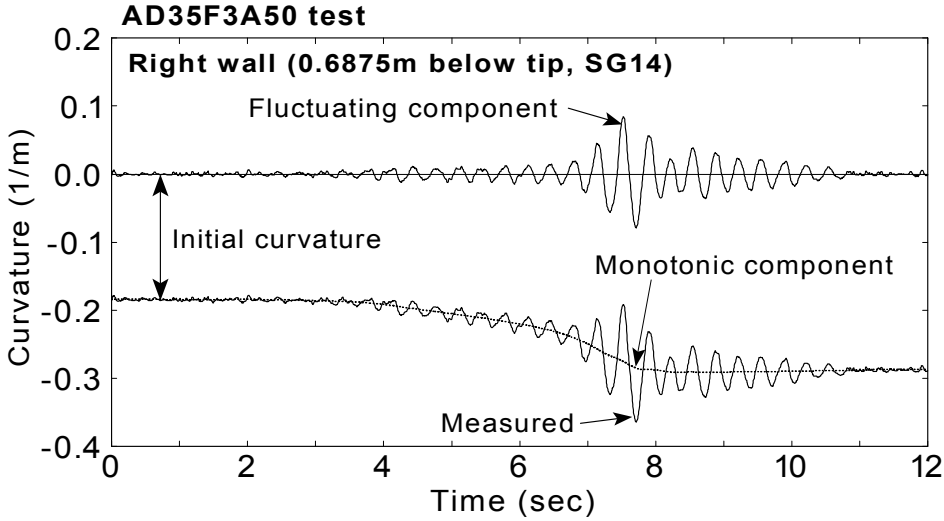

(b) Right wall (stem of wall, 0.6875m below tip, SG14)

Fig.6.4: Monotonic and fluctuating components of curvature (AD35F3A50 test)

6.2.2 Measured curvatures

Typical measurements

The time histories of measured curvatures in AD35F3A50 test at 0.3 m below tip (SG2 and SG9) and the stem of wall (SG7 and SG14), and the horizontal base acceleration are illustrated in Fig.6.5 as typical measurements.

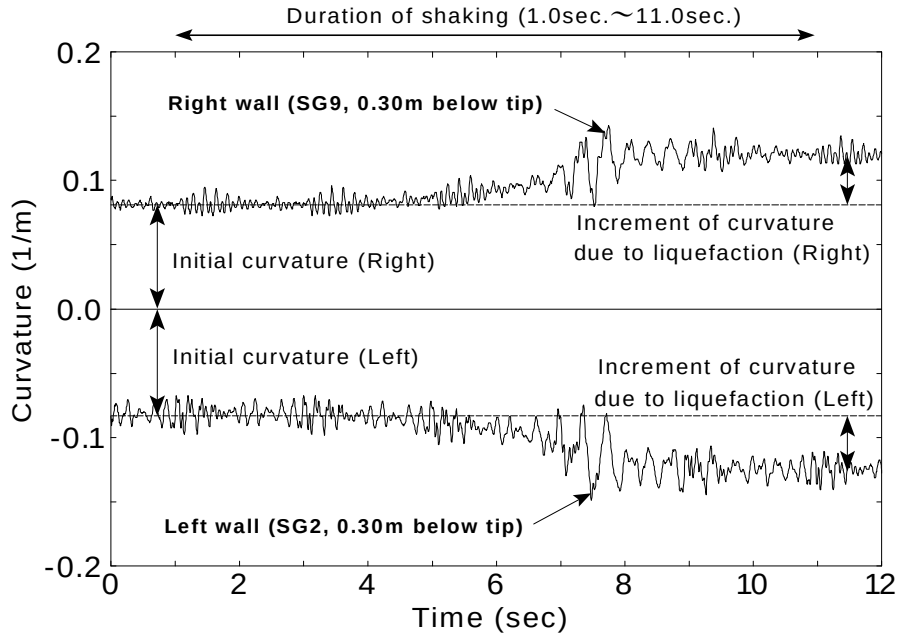

(a) Middle part of the wall (0.30m below tip)

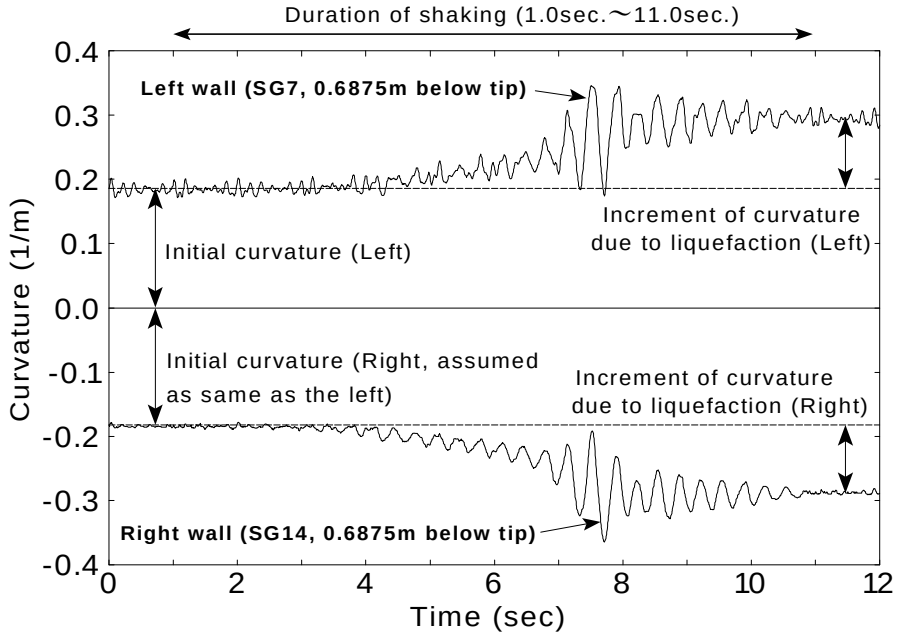

(b) Stem of the wall (0.6875m below tip)

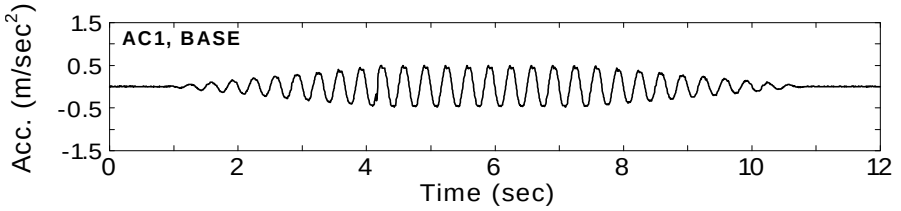

(c) Horizontal base acceleration (Frequency: 3Hz, Acc.: 0.5m/sec^2)

Fig.6.5: Time histories of curvature and acceleration (AD35F3A50 test)

The initial horizontal portion of the curvature time histories (0～1 seconds) indicates the static quantities before shaking. It is clarified that the initial static quantities are exerted by initial lateral earth pressure. The initial curvature and the initial earth pressure are shown to be internally consistent in the chapter 3.

As is seen in Fig.6.5(c), horizontal base acceleration consists of 30 sinusoidal cycles at 3 Hz. However, the response of curvature contains high frequency content, which is about 3 times that of horizontal motion. Moreover, the oscillations with high frequency content are seen before and after excitation (0～1.0 second and 11.0～12.0 seconds), in which no oscillation should occur. This indicates that the oscillations with high frequency content is not exerted by horizontal motion, probably noise, only the oscillation of about 3 Hz could be the response due to horizontal motion.

It is observed that the curvature is gradually increasing in either positive or negative direction with 3Hz of fluctuation as shaking goes on. The flat portion is seen at the end of time history. This is the post-shaking residual value. At 0.3m below tip of left wall (SG2), the post-shaking residual value is negative. In contrast, it is positive at the right wall (SG9). Considering the definition of direction of curvature (see Fig.6.1), both the left and the right wall are bent toward inside of the structure, which is empty, filled with air, after shaking.

At 0.3m below tip of left wall (SG2), the post-shaking residual value is observed to be negative. But it is positive at the stem of the same wall (SG7). This is due to the boundary condition (or fixed condition) of flexible wall. Namely, the stem of the left wall is bent to be convex toward left when the middle of the left wall is bent toward right, inside of structure.

Maximum curvatures

Absolute maximum curvatures measured during shaking and yield curvatures from various tests are summarized in Table 6.2. The time when the yield occurs is also described in the table. The maximum curvature occurs at the stem (SG7 or SG14) of either left or right wall, where curvature and earth pressure are initially large (see e.g. Fig.3.1, Fig.3.3 and Fig.3.4). The maximum curvatures are within the yield curvature, behaving in an elastic manner, except for AD67F3A500 test, BD36F3A500 test, and BD78F3A500 test.

Measurements with yielding of material

Table 6.2: Maximum measured curvatures

Test No.	Nominal input acc. (m/sec^2)	Absolute maximum curvature (1/m)	The time when max. curvature occurred (sec.)	Yield curvature (1/m)	Max. curvature／Yield curvature
AD35F3A50	0.5	0.365	7.710 (SG14)	0.793	0.460
AD39F5A50	0.5	0.312	6.480 (SG7)	0.793	0.393
AD41F3A200	2.0	0.454	4.545 (SG7)	0.793	0.573
AD61F3A200	2.0	0.535	7.885 (SG7)	0.793	0.675
AD67F3A500	2.0	1.181	5.340 (SG14)	0.793	1.489
AD32F3A500	5.0	0.709	7.530 (SG14)	0.793	0.894
BD36F3A500	5.0	1.512	7.875 (SG14)	0.657	2.301
BD78F3A500	5.0	1.002	10.970 (SG7)	0.657	1.525

As illustrated in Table 6.2, the material of structure yielded during shaking in AD67F3A500, BD36F3A500 and BD78F3A500 test. The experimental relationship between bending moment and curvature of wall for both kind of material is illustrated in Fig.6.6. It is seen that the relationship between bending moment and curvature for aluminum alloy (A5083P), which is used in Structure-A of AD67F3A500 test, is linear when curvature is less than the yield curvature. In contrast, slight non-linearity is seen more than curvature of 0.2 (1/m) in Fig.6.6(b) for aluminum (A1070P), which is used in Structure-B of BD36F3A500 and BD78F3A500 test. It causes unclear yield point of aluminum (see Fig.2.11). In this section, the yield curvatures are defined as 0.793 (1/m) for aluminum alloy (A5083P) and 0.657 (1/m) for aluminum (A1070P).

Fig.6.7 illustrates measured time histories from AD67F3A500 test. Time when measured curvature initially exceeds the yield curvature is shown at each depth of wall. It is seen that measured curvature of the right wall at 0.6875m below tip exceeded the yield curvature of 0.753 (1/m) initially at 3.690 seconds. Then the curvature of the left wall at 0.6625m below tip exceeded the yield curvature at 4.67 seconds and 4.82 seconds. The curvature exceeds cyclically the yield curvature at the stem of the wall during strong excitation of 4.0 seconds ～8.0 seconds. After the shaking, the curvature becomes about 0.5(1/m), being within the yield curvature. The portion of wall which is shallower than 0.6625m did not yield.

Fig.6.8 shows the result from BD36F3A500 test. The initial yielding occurs at 2.70 seconds at the stem. The curvature is monotonically increasing with fluctuation after yielding. The curvature fluctuates in the level more than the yielding curvature during 6.0 seconds to

10.0 seconds. The residual curvature after shaking became about 1.0 (1/m), exceeding the yield curvature.

The time histories from BD78F3A500 test are depicted in Fig.6.9. It is seen that the curvature initially exceeds the yield curvature at 3.62 seconds at 0.6875m below tip of right wall. The curvature during shaking is gradually increasing, resulting in post shaking residual value of 0.66(1/m), which is nearly equal to the yielding curvature.

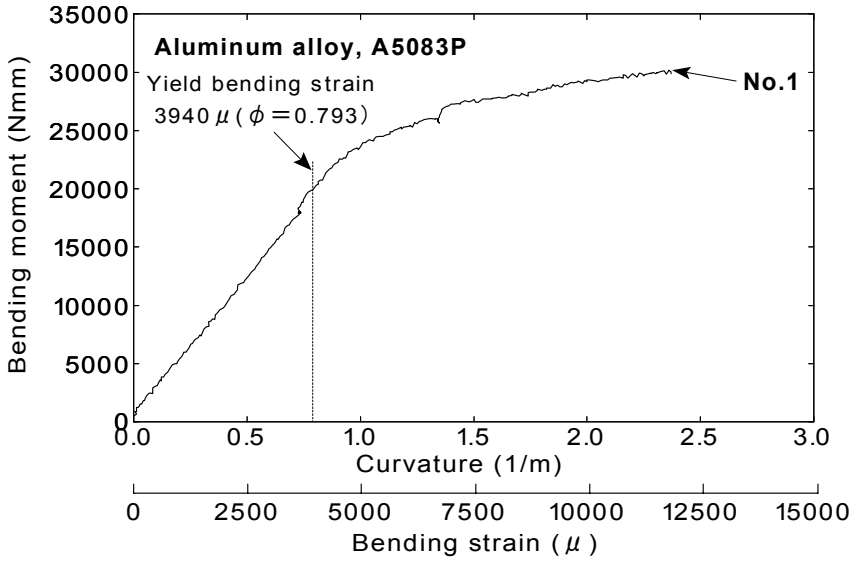

(a) Wall for Structure-A (Aluminum alloy, A5083P)

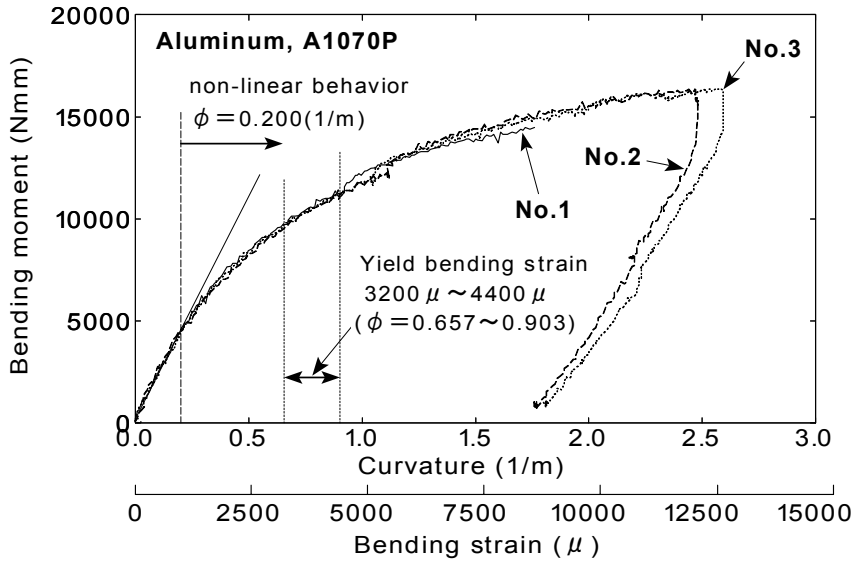

(b) Wall for Structure-B (Aluminum, A1070P)

Fig.6.6: Experimental relationship between bending moment and curvature of wall

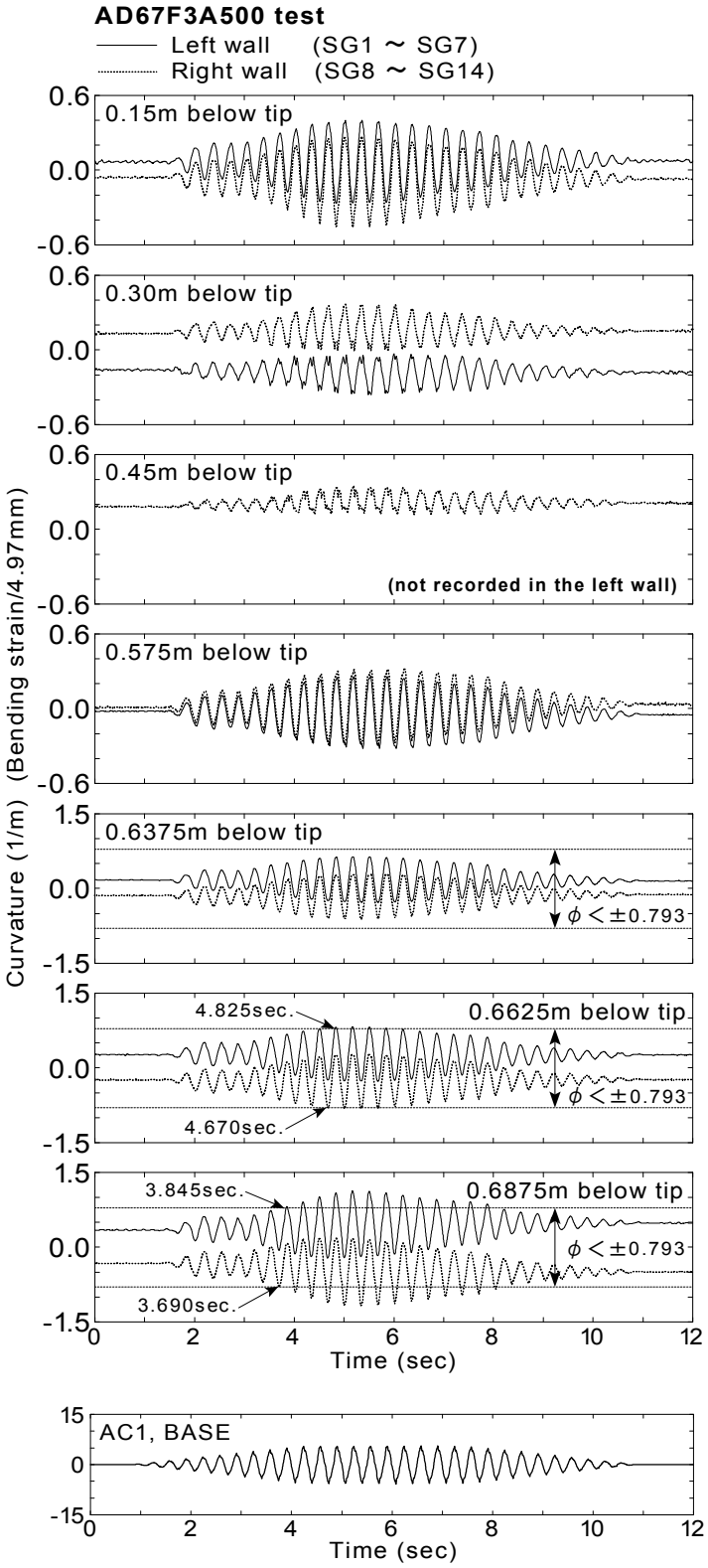

Fig.6.7: Time history of curvature and the time when material yielded (AD67F3A500 test, including monotonic component)

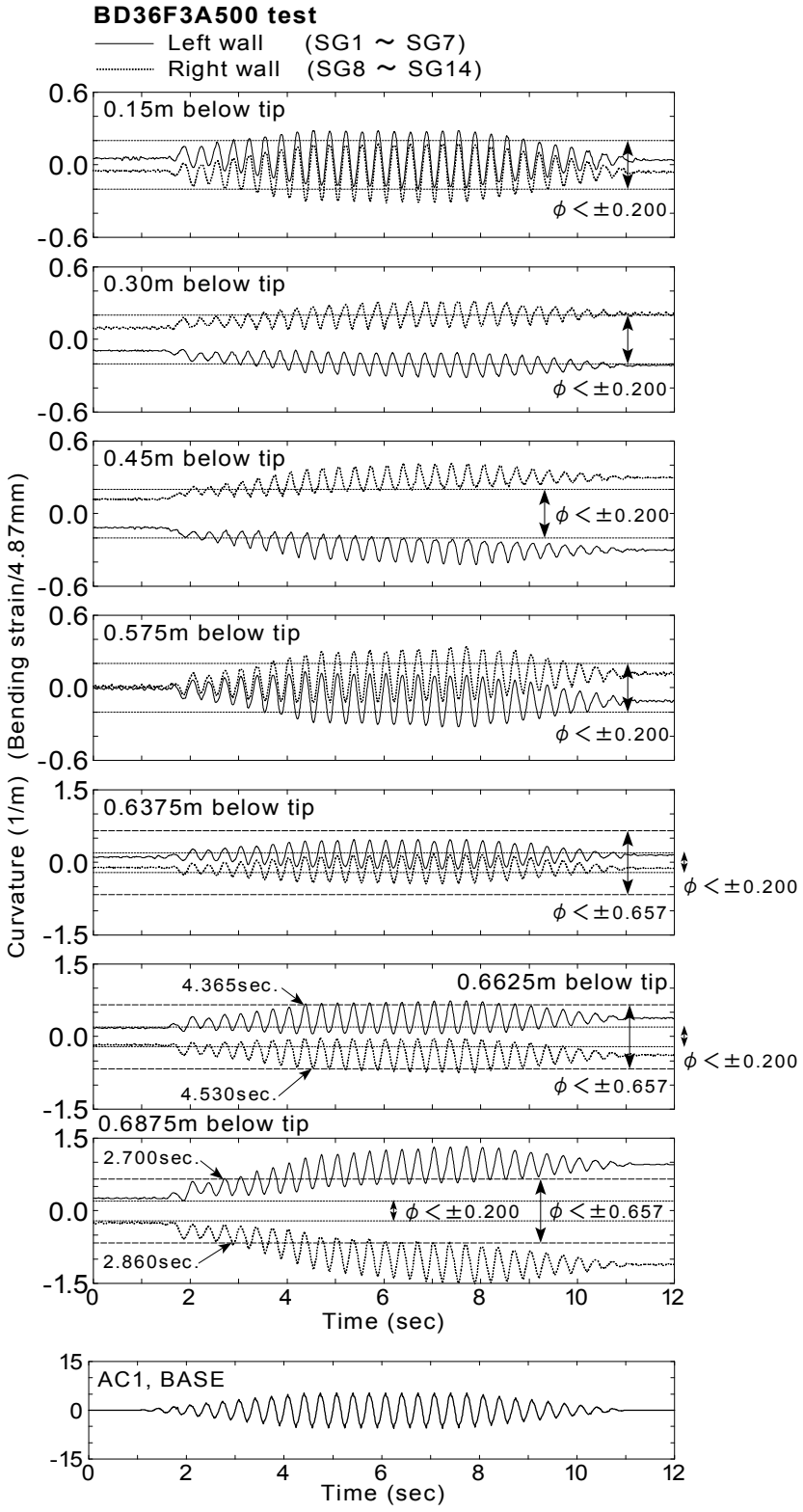

Fig.6.8: Time history of curvature and the time when material yielded (BD36F3A500 test, including monotonic component)

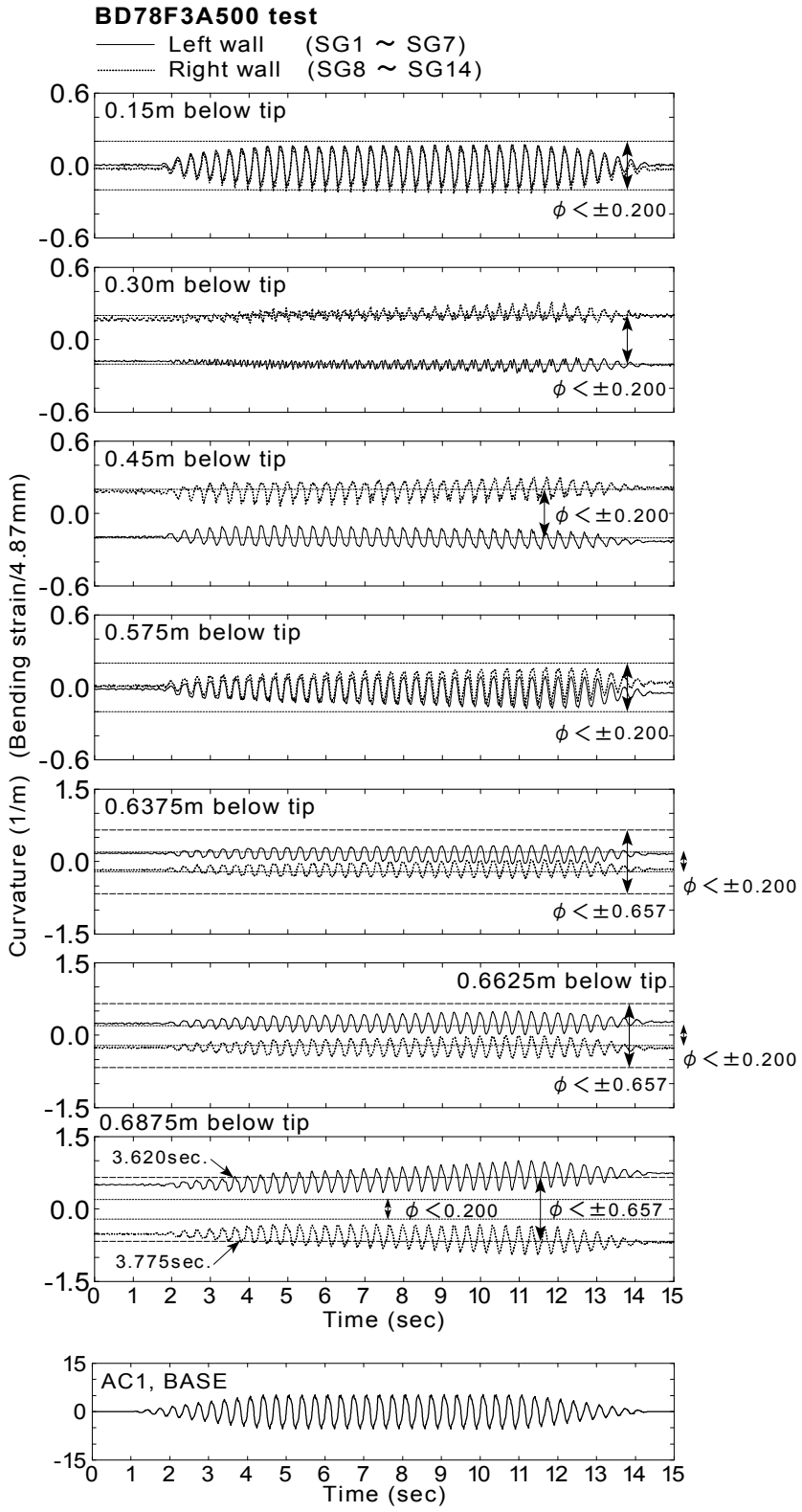

Fig.6.9: Time history of curvature and the time when material yielded (BD78F3A500 test, including monotonic component)

6.2.3 Monotonic component of curvature

Typical results (AD35F3A50 test)

The time histories of monotonic component (800 times of moving average) at 0.6875m below tip (SG7 and SG14) are shown in Fig.6.10. The initial curvature of left wall is derived by measurement before shaking. The initial curvature of right wall is assumed to be the same as left wall since the initial static measurement at right wall (see Table 3.1) is not conducted due to the limitation of data acquisition system. It seems that the absolute value of curvature is consistent between left and right.

The time histories of curvature at the left wall $\phi_{s,left\ wall}(t)$ and the right wall $\phi'_{s,right\ wall}(t)$ are compared in Fig.6.11. Note that the sign of curvature at right wall is reversed by Eq.(6.4) to make the comparison easier in this figure. It is recognized that the amount of the monotonic component in left wall is consistent with that in right wall through duration time.

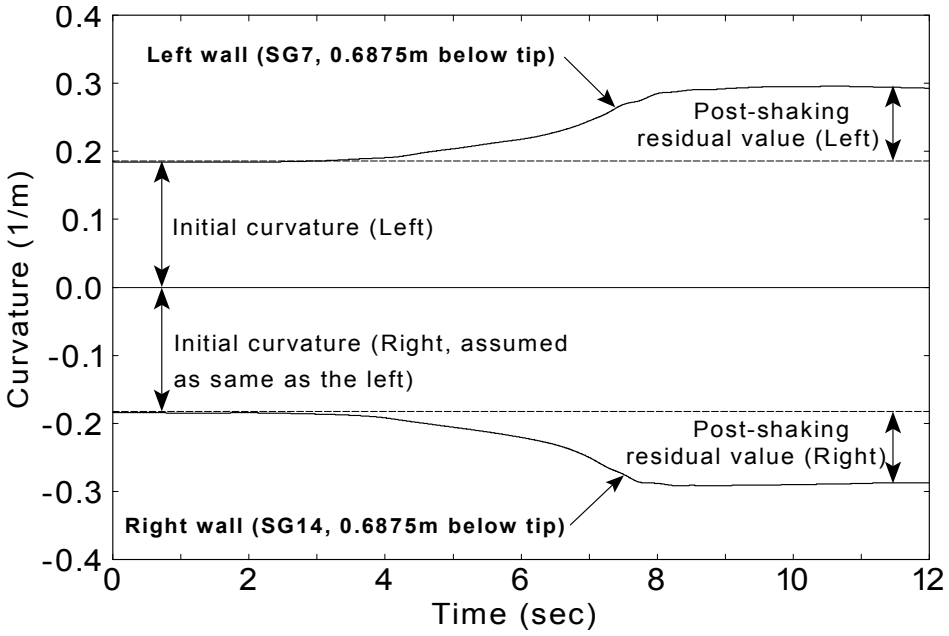

Fig.6.10: Time history of monotonic component of curvature (SG7 and SG14, AD35F3A50 test)

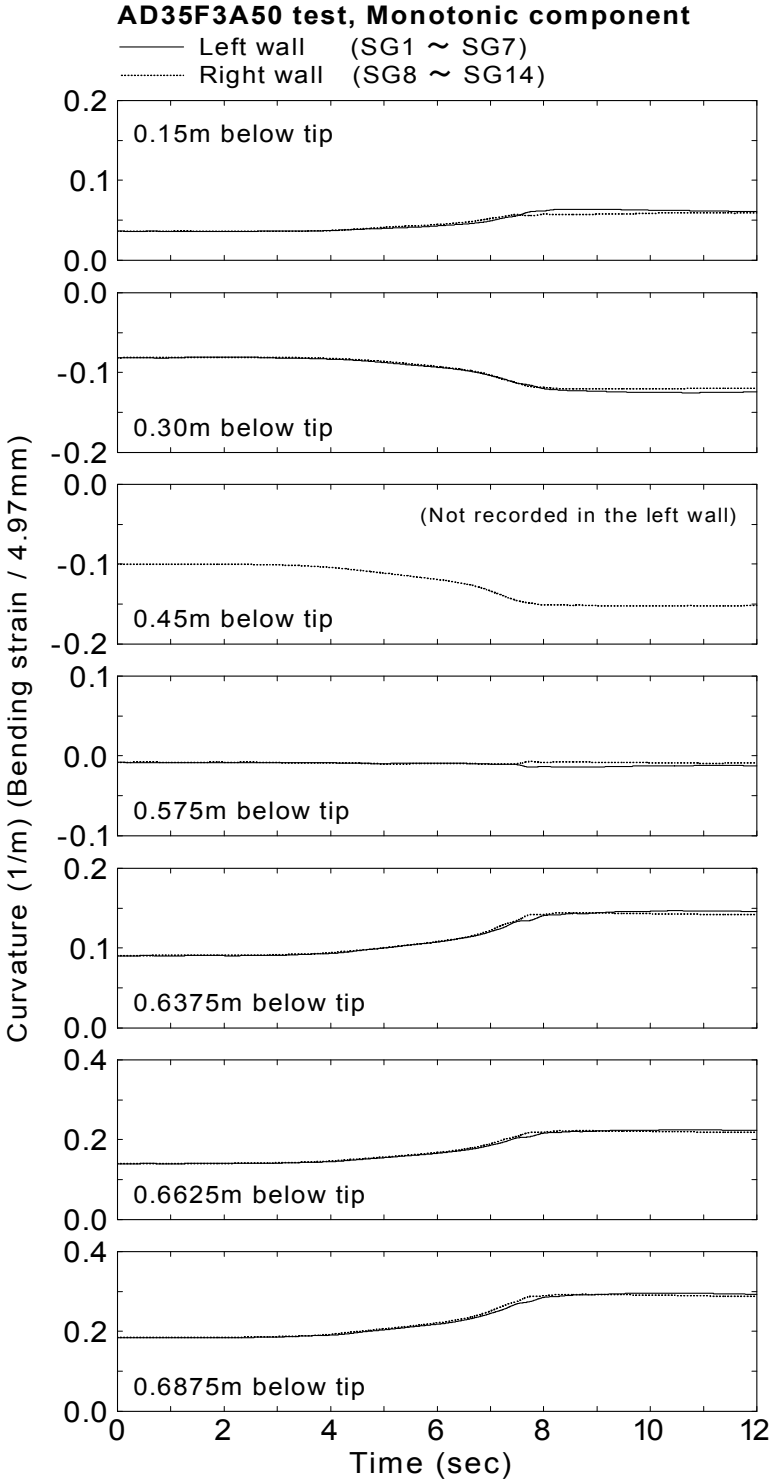

Note: Sign of curvature at right wall is inverted by Eq.(6.4) for the comparison with curvature at the left wall.

Fig.6.11: Comparison of time history of monotonic component (all strain transducers, AD35F3A50 test)

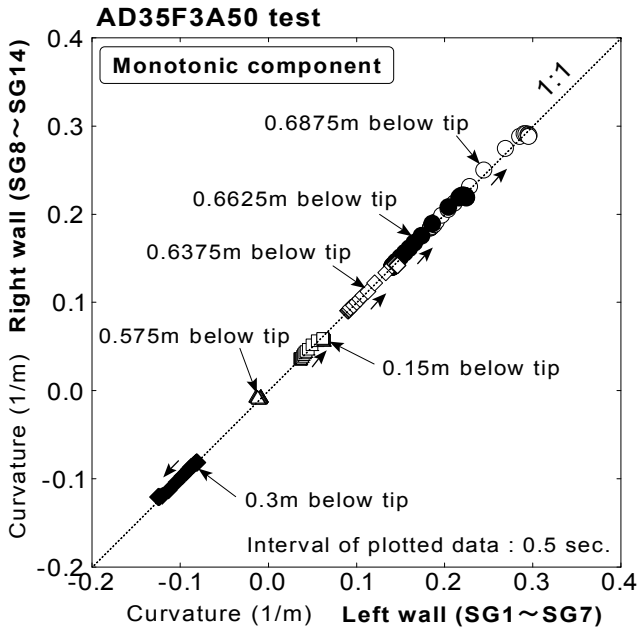

Note: The sign of curvature at right wall is inverted by Eq.(6.4) for comparison.

Fig.6.12: Comparison of monotonic component of curvature between left and right wall (typical result, AD35F3A50 test)

Fig.6.12 compares the monotonic component of curvatures at the same time instance between the left and right walls. Time interval of plotted data is 0.5 seconds. It is seen that plots of data are almost on the line of 1:1, showing a symmetrical deformation of box section of structure during and after shaking.

Results of the test with intense input motion (AD32F3A500 test)

Comparison of monotonic component of curvature between the left and the right wall of structure with the intense input motion is illustrated in Fig.6.13. In the results from AD32F3A500 test which is shaken by intense motion (5.0m/sec^2), however, the amount of monotonic component of right wall at 0.6375m～0.6875m below tip is slightly larger than the left. This kind of behavior is seen in another test with intense input motion. The reason for this is not clear, but only possibility is slight difference of weight of the walls due to earth pressure and pore water pressure transducers and its mechanical connections.

The monotonic component of curvature becomes the same amount when the symmetric structure behaves in an elastic manner. This indicates that lateral earth pressures which act on the structure monotonically from both sides are of equal magnitude.

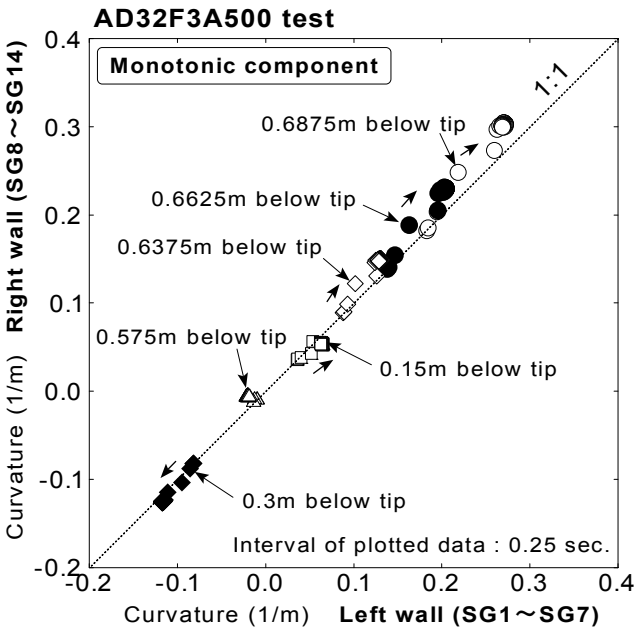

Note: The sign of curvature at right wall is inverted by Eq.(6.4) for comparison.

Fig.6.13: Comparison of monotonic component of curvature between left and right wall (tests with the intense input motion, AD32F3A500 test)

Results of the test with dense backfill (AD67F3A500 and BD78F3A500 test)

The comparisons of amount of monotonic component of curvature from AD67F3A500 and BD78F3A500 test are presented in Fig.6.14. As described previously, the material was yielded by the intense shaking in those tests. The comparisons in Fig.6.14 are limited before yielding of material. As seen, the agreement between left and right wall is fairly good in the model with dense backfill.

Results of tests with yielding of material

Model with loose backfill (BD36F3A500 test)

The monotonic component of curvature from BD36F3A500 test is compared in Fig.6.15. The data before the time of yielding (2.70 seconds) are presented in figure (a) and after the yielding in figure (b).

Note: The sign of curvature at right wall is inverted by Eq.(6.4) for comparison.

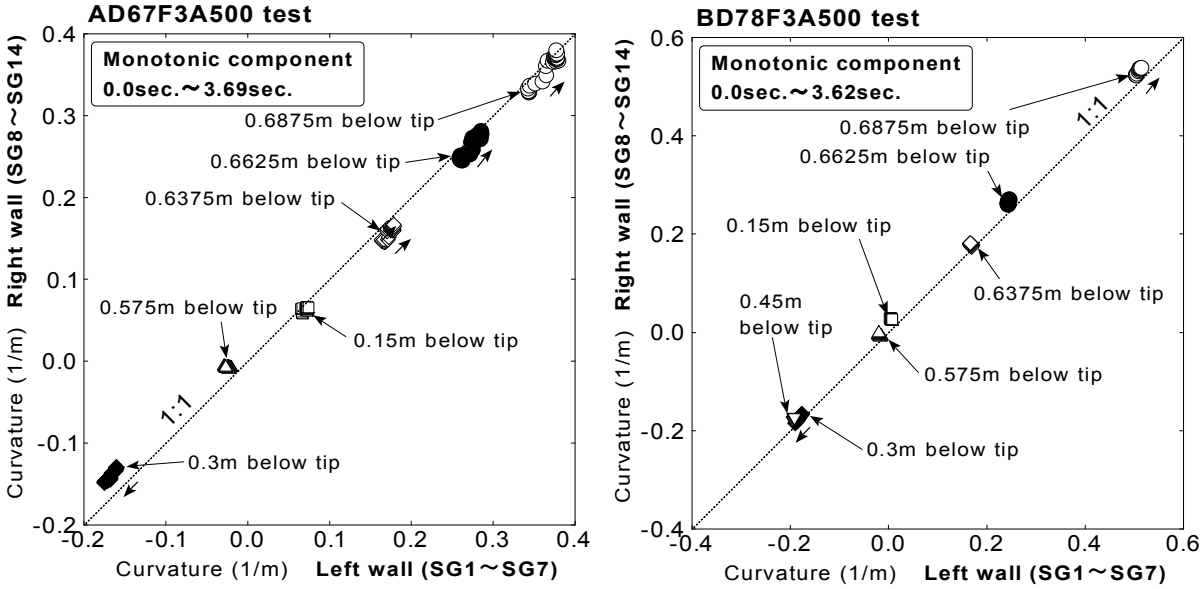

(a) AD67F3A500 test (b) BD78F3A500 test

Fig.6.14: Comparison of monotonic component of curvature between left and right wall (test with dense backfill, before the material yielded)

Note: The sign of curvature at right wall is inverted by Eq.(6.4) for comparison.

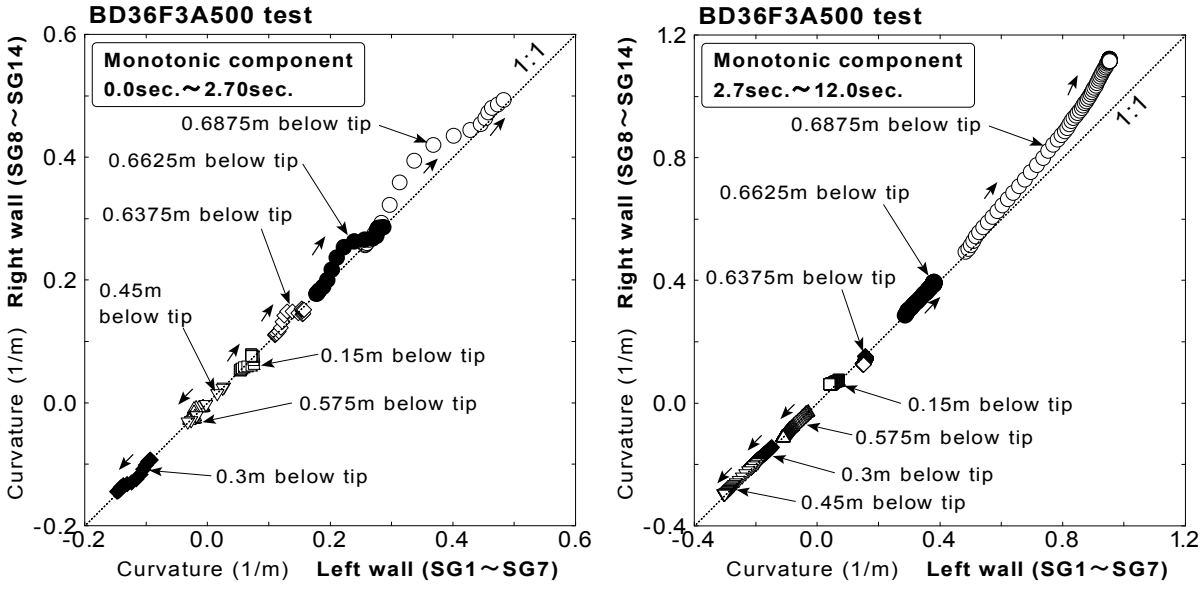

(a) Before yielding (1.0 sec to 2.70 sec) (b) After yielding (2.70 sec to 12.0 sec)

Fig.6.15: Comparison of monotonic component of curvature between left and right wall (yielding of material)

It is observed before yielding that the amount of monotonic component of curvature at right wall of 0.6375m～0.6875m below tip shows slightly larger than that of the left. This feature was observed in AD32F3A500 test as well, in which the test condition is same as BD36F3A500 test except for the material of structure. It is seen after yielding that curvature at 0.6875m below tip of all tests increase in a different way. Curvature at the right wall in DB36F3A500 test is getting larger than the left as shaking goes on. This suggests that the monotonic component of curvature is not always of the same amount if the material yields in a loose backfill.

Model with dense backfill (AD67F3A500 test and BD78F3A500 test, after yielding of material)

The comparison of amount of monotonic component after yielding of material is shown in Fig.6.16. It is also observed that curvature at 0.6875m below tip of all tests increase in a different way in both results. The result from BD78F3A500 test is depicted in figure (c). The monotonic component does not change significantly. It is because the initial lateral earth

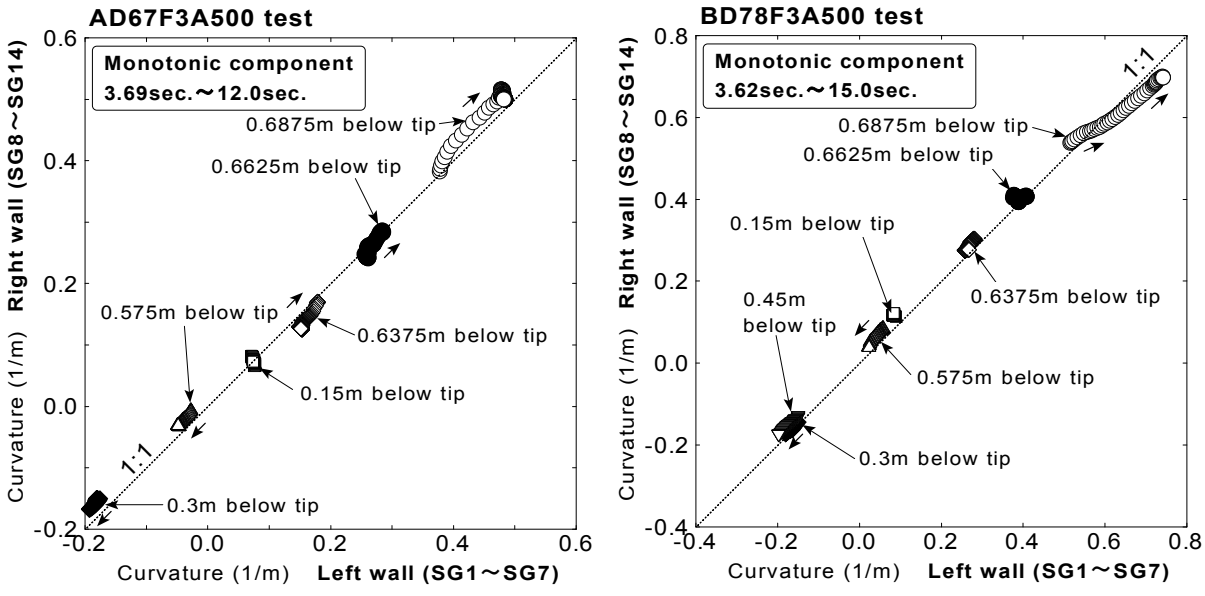

(a) AD67F3A500 test (b) BD78F3A500 test

Fig.6.16: Comparison of monotonic component of curvature between left and right wall (after the material yielded)

pressure at each depth is already as same as the initial overburden pressure due to compacted dense backfill. The earth pressure did not increase by the shaking (see earth pressure in Fig.3.74).

Results from other tests

Comparisons of monotonic component of curvature between the left and the right wall of structure from the other tests are illustrated in Fig.6.17. The structure behaved in an elastic manner in both tests. It is observed that the plots of data move almost on the line of 1:1. It is observed in Fig.6.13(a) of result from AD41F3A200 test that the plots of data move almost on the line of 1:1.

These observations of behavior indicate that the monotonic component of curvature is of the same amount between the left and the right sides as long as the structure behaves in an elastic manner in either loose or dense backfill. This suggests that the monotonic component of lateral earth pressures which act on the structure from both sides are of equal magnitude. It is considered that the same magnitude of lateral earth pressures act on the box section of underground structure in the opposite direction when the shape of structure as well as surrounding liquefied backfill is symmetric. Further discussion based on the beam analysis using monotonic component of earth pressures will be made in Section 6.4.

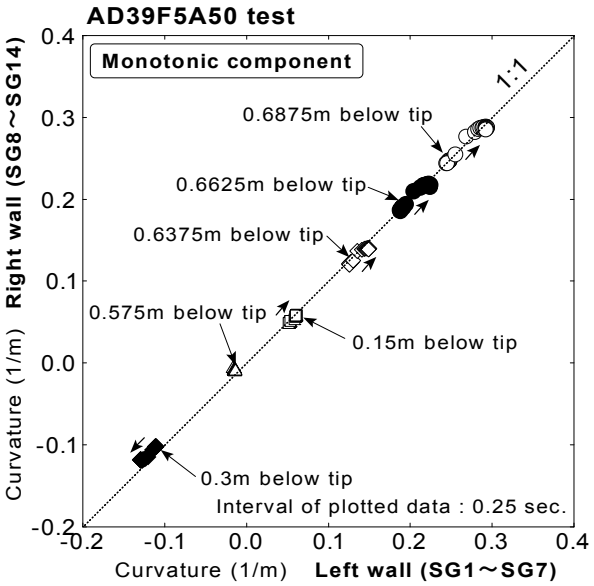

(a) AD39F5A50 test

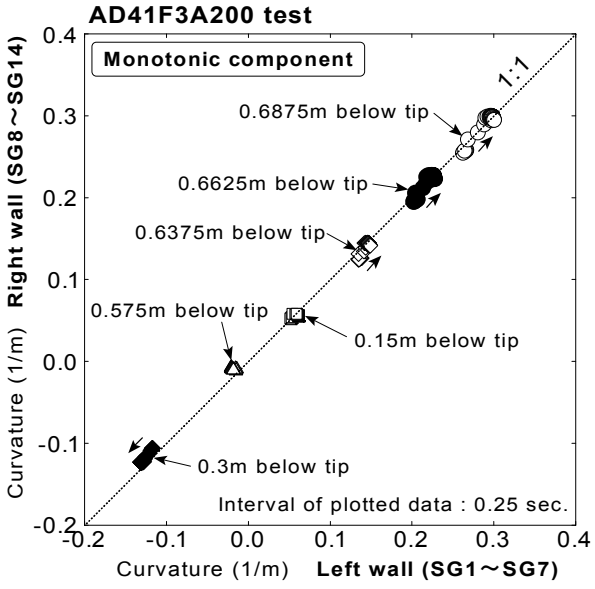

(b) AD41F3A200 test

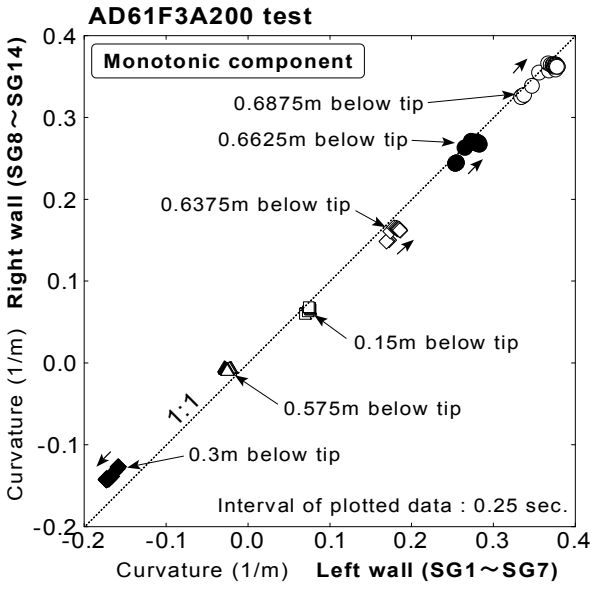

(c) AD61F3A200 test

Fig.6.17: Comparison of monotonic component of curvature between left and right wall

6.2.4 Fluctuating component of curvature

The fluctuating component of curvatures is calculated by Eq.(6.5) for the measured curvatures at both sides of wall in each test.

Typical results (AD35F3A50 test)

Fig.6.18 compares the time histories of fluctuating component of curvature on the left wall with that of right wall at each depth. The time history of fluctuating component at the left wall at 0.45m below tip was not presented since it was recorded incorrectly. It is seen that both time histories agree with reasonably through the depth after about 6 seconds. Agreement is not clear due to noisy response of bending strains before 6 seconds.

Results of the test with intense input motion (AD32F3A500 test)

The time histories from AD32F3A500 test are depicted in Fig.6.19. Although slight difference is seen at the beginning of shaking of 1.5 seconds, both time histories of fluctuating component are identical. This suggests that the equal amount of dynamic earth pressure due to liquefaction of loose backfill acts on the left and right side of structure in the same direction.

Results of the test with dense backfill (AD67F3A500 and BD78F3A500 test)

Fig.6.20(a) illustrates the result from AD67F3A500 test. The time when the initial yield of material is pointed in each time history. It is interesting that the time histories of left wall are identical to those of right wall through duration time irrespective to the yielding of material.

The fluctuating components of curvatures from BD78F3A500 are compared in Fig.6.20(b). It is observed that the amplitude of curvature increases cycle by cycle in spite of constant amplitude of base motion (4.0 seconds to 11.0 seconds). This is considered to be the effect of shear strain of dense backfill, whose amplitude grows gradually with cyclic loading. The curvature in left wall is almost identical to that in right wall.

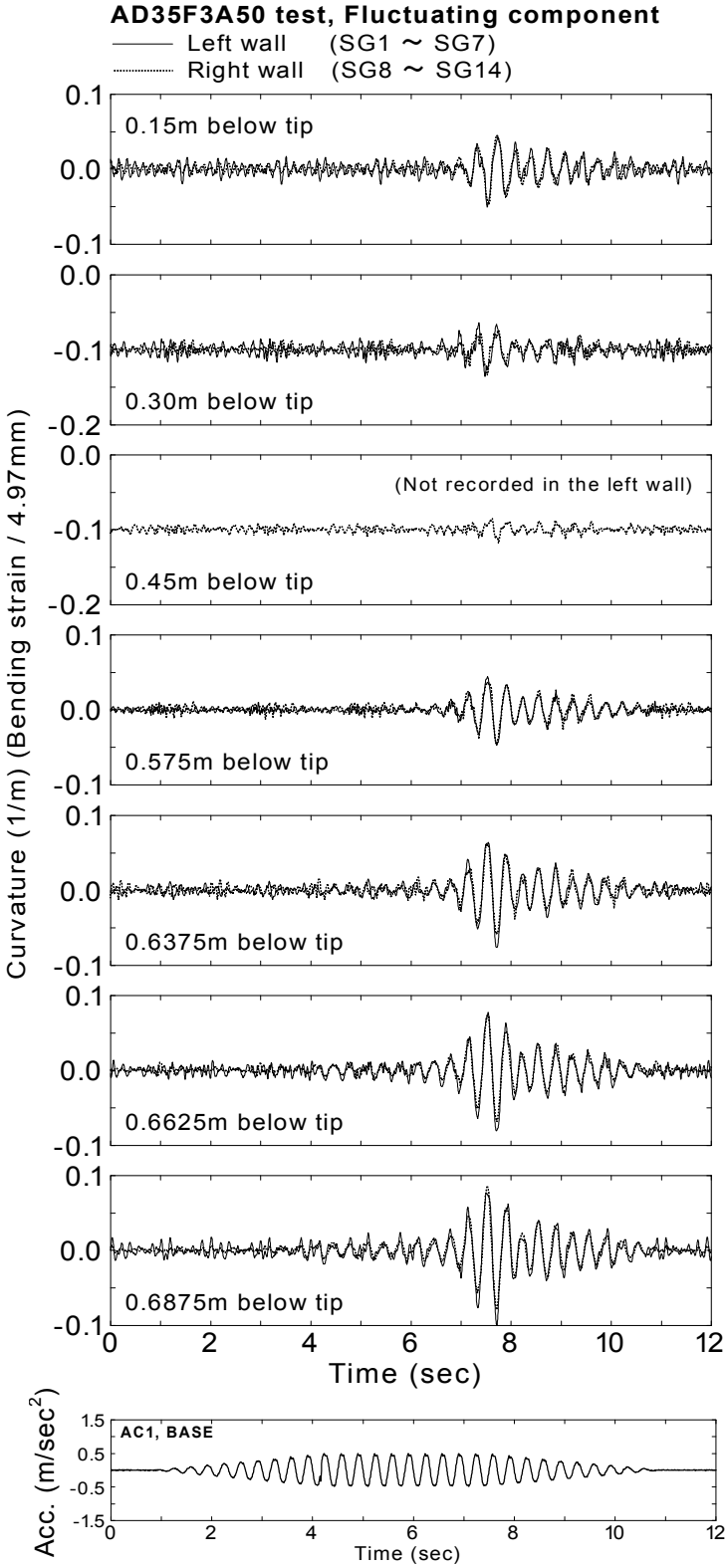

Fig.6.18: Time history of fluctuating component of curvature (typical result, AD35F3A50 test)

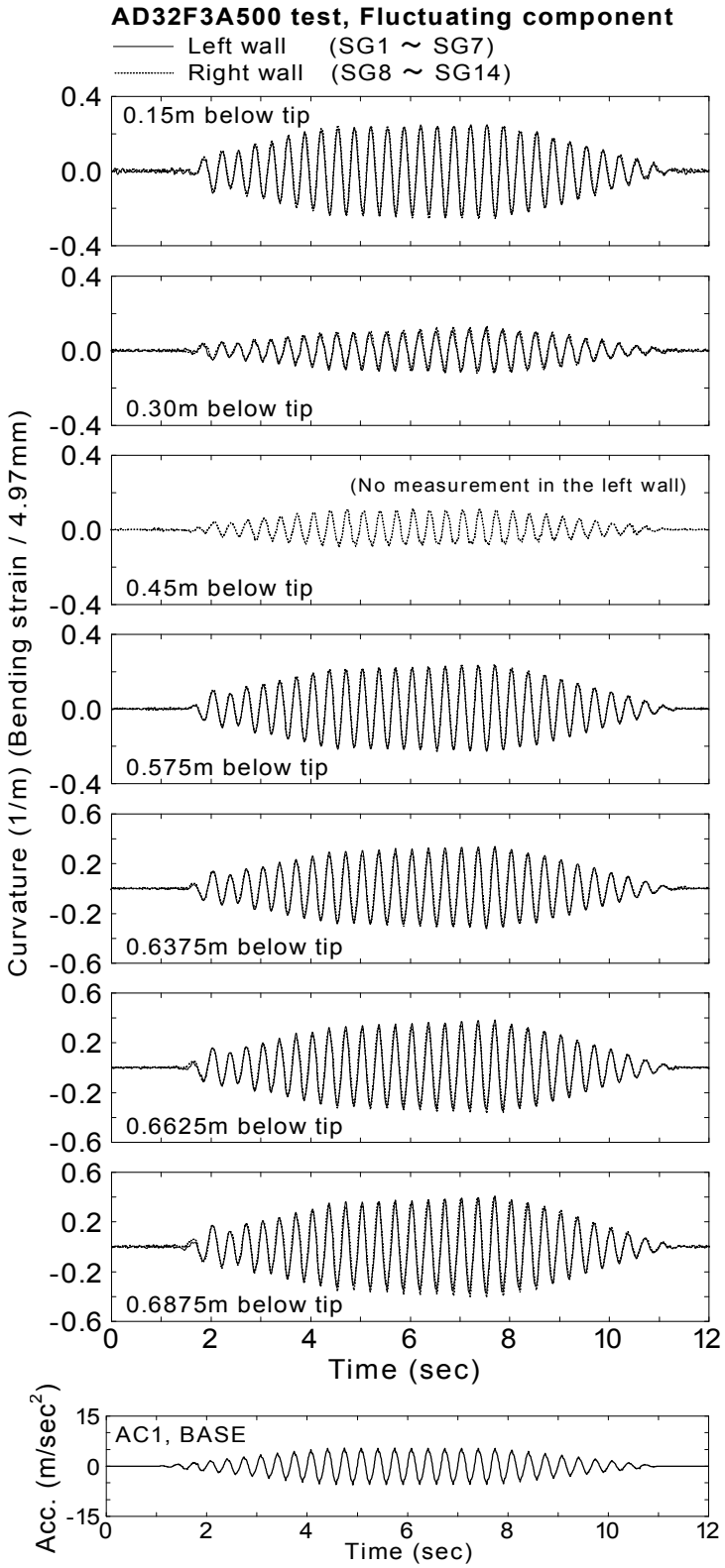

Fig.6.19: Time history of fluctuating component of curvature (intense input motion, AD32F3A500 test)

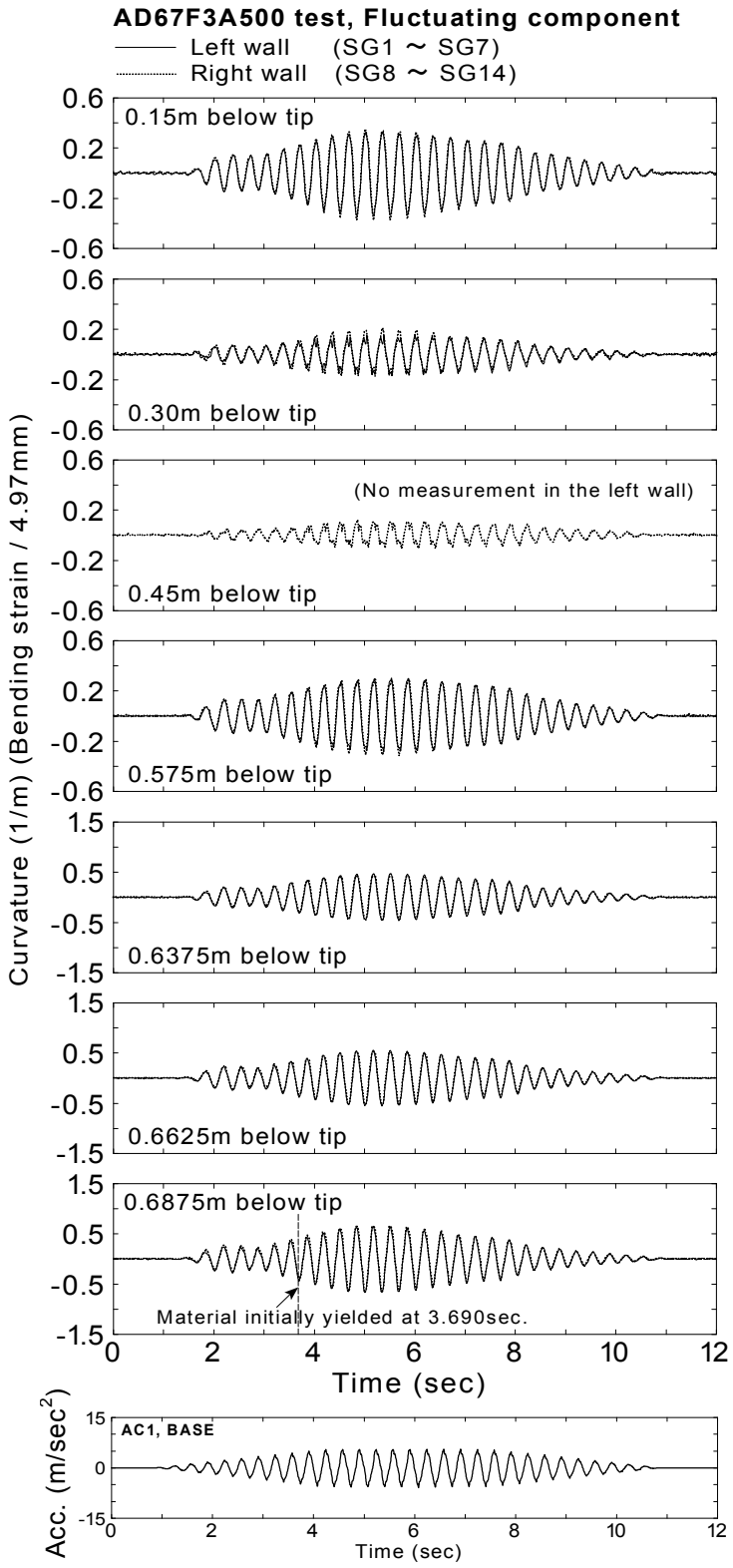

(a) AD67F3A500 test

Fig.6.20: Time history of fluctuating component of curvature (dense backfill)

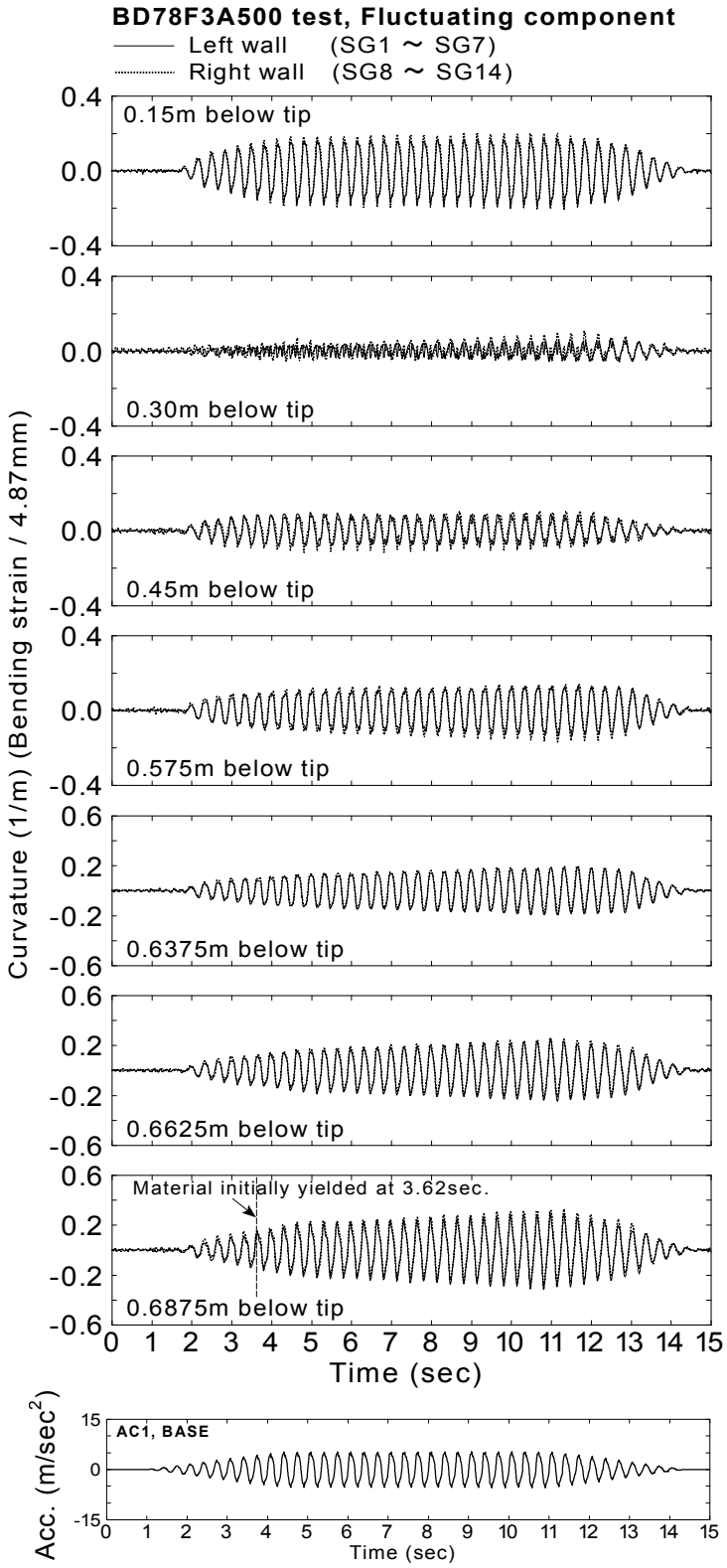

(b) BD78F3A500 test

Fig.6.20: Continued (dense backfill)

Results from tests with yielding of material (BD36F3A500 test)

The time histories of the measured curvatures at both sides of wall from BD36F3A500 test are compared in Fig.6.21. In this test, the maximum curvature became twice greater than the yield curvature. In spite of this, curvatures are almost identical to each other after the yielding of material. It suggests that the symmetric horizontal base motion (sinusoidal motion) brings about the similar response of fluctuating component of curvature even though the material of wall yields.

Results from other tests

Fig.6.22(a) shows time histories from AD39F5A50 test which is shaken by the intensity of $0.5m/sec^2$ at 5Hz. The high frequency content with amplitude about level of 0.02(1/m) already occur before shaking (0sec～1.0sec) at 0.6875m below tip in the left wall. The same level of amplitude is also seen at stationary period after shaking (7.0sec～8.0sec). This indicates that the fluctuating component of curvature less than the level of 0.02(1/m) is not real curvature due to excitation.

The time histories from AD41F3A200 test are depicted in Fig.6.22(b). Although slight difference is seen at the beginning of shaking between 2.0 to 3.0 seconds, both time histories of fluctuating component are identical. The same trend is seen in the AD32F3A500 test in Fig.6.19(b).

The results from AD61F3A200 test are illustrated in Fig.6.22(c). As observed so far, the fluctuating component of curvatures in both sides of wall are of same magnitude in amplitude with no phase difference.

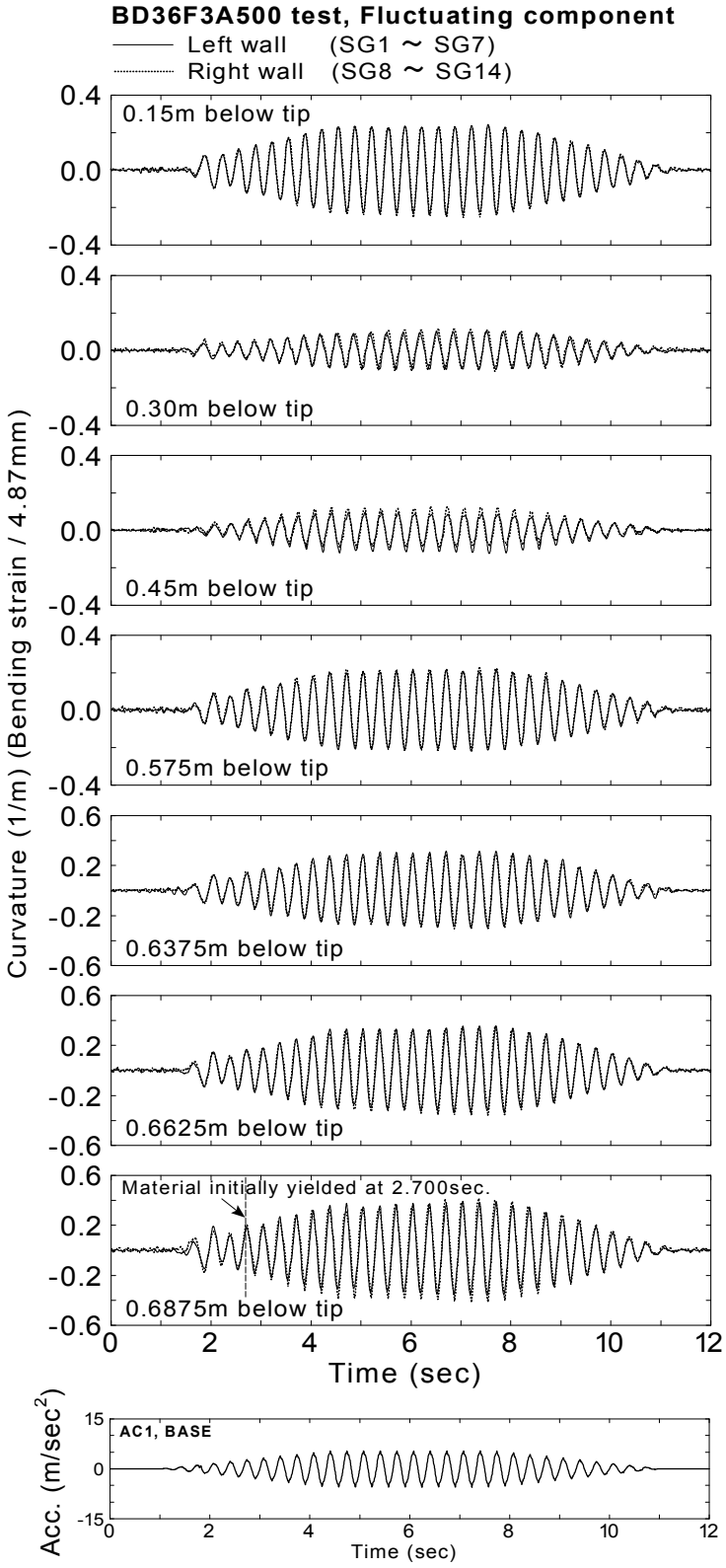

Fig.6.21: Time history of fluctuating component of curvature (yielding of the material, BD36F3A500 test)

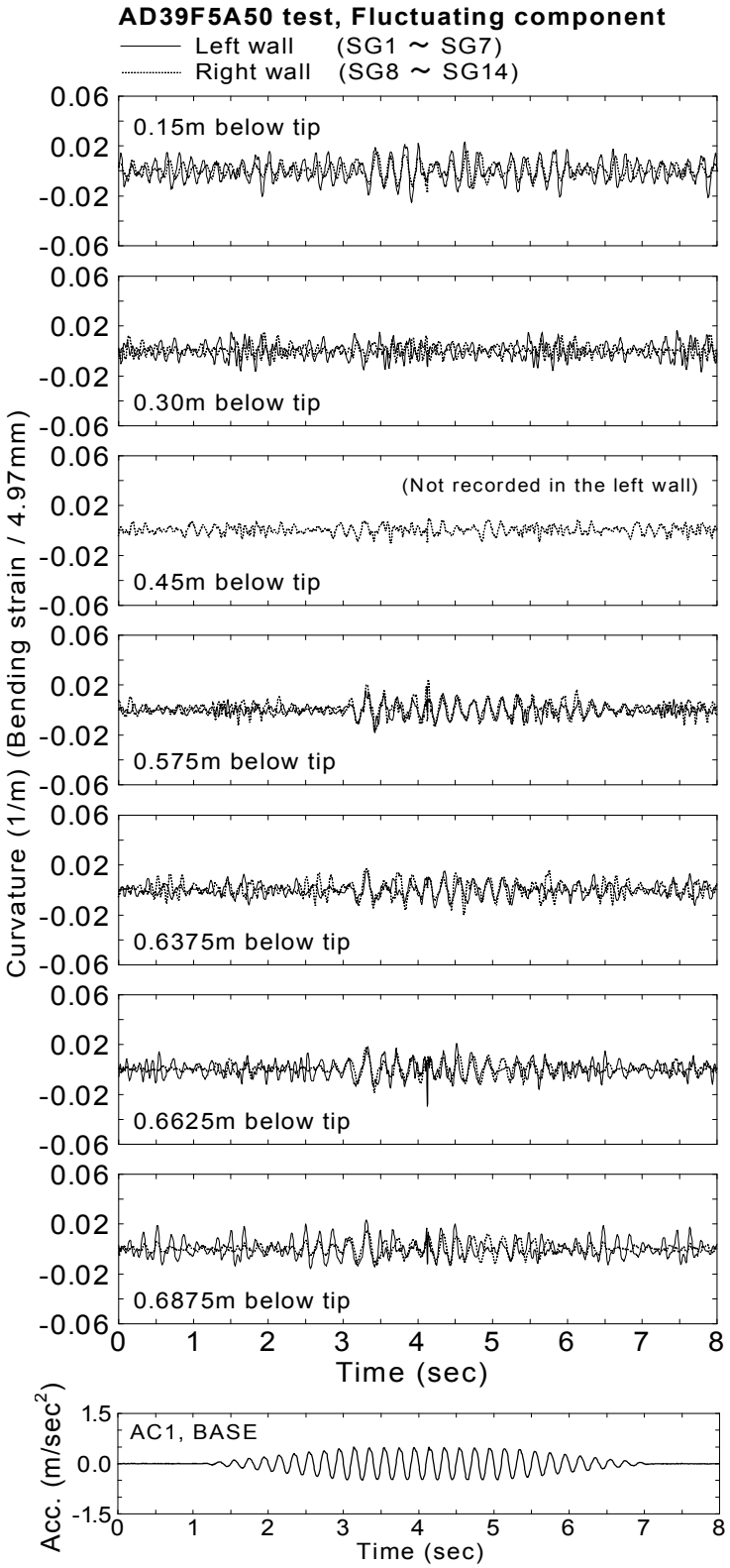

(a) AD39F5A50 test

Fig.6.22: Time history of fluctuating component of curvature (other test results)

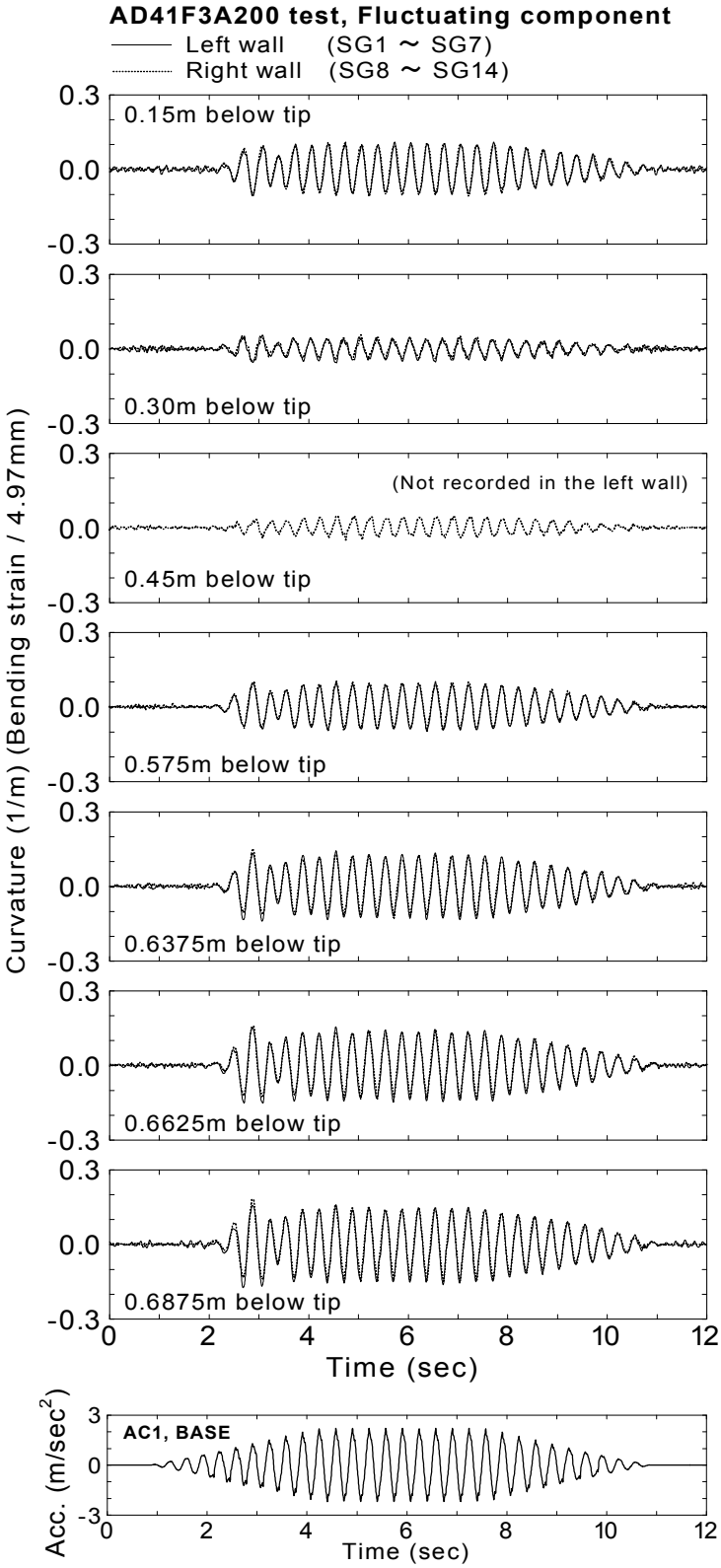

(b) AD41F3A200 test

Fig.6.22: Continued (other test results)

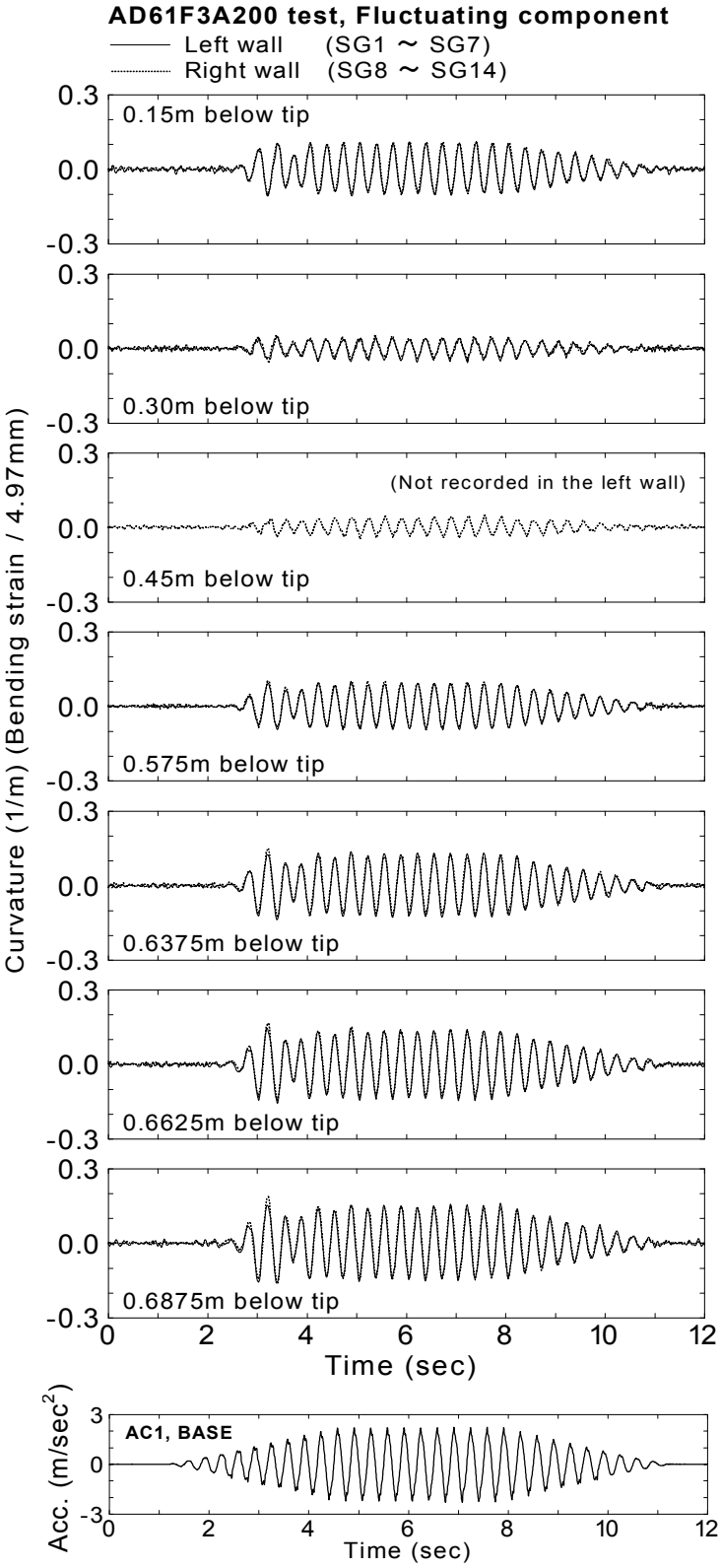

(c) AD61F3A200 test

Fig.6.22: Continued (other test results)

These observations indicate that the fluctuating component of curvature is of same magnitude between both walls of the box section except for the beginning of shaking. This suggests that the equal amount of dynamic earth pressure due to liquefaction of backfill acts on the left and right side of structure in the same direction. It is considered that the amount of fluctuating component of curvature associates with the magnitude of fluctuating component of earth pressures. The study based on the beam analysis will be conducted in Section 6.4 to make further discussion.

6.3 DEFLECTION OF FLEXIBLE WALL

Deflection of walls was calculated by integrating measured curvature twice with respect to depth. The detailed procedure of calculation was presented in the section 4.3.2.

6.3.1 Deflections before and after shaking

Typical results

The calculated deflections of both left and right wall before shaking (t=0.0sec) and after shaking (t=12.0sec) from AD35F3A50 test are illustrated in Fig.6.23(a). The walls are deformed by 2～3mm at its middle toward inside of the structure. It was shown in the chapter 3 that the initial deflection was caused by initial lateral earth pressure, and, measured initial earth pressure and measured curvature are internally consistent (see Fig.3.1).

The amount of deflection at the middle of wall becomes about 4mm after shaking, being greater than the initial deflection. It is considered that liquefied backfill made the earth pressure increase and the deflection accumulate. It is observed that the wall displacements at the top after shaking (t=12.0sec.) were fairly same as before shaking (t=0.0sec.) in both wall, indicating little residual displacement at the top. It is considered to be due to a structural condition of wall and a symmetric property of residual earth pressure. Both walls are connected rigidly by a thick top plate (thickness:15mm) as illustrated in Fig.6.1.

In this case, residual displacements at the top of structure become zero if earth pressure acts on both side of structure in a symmetrical manner. In contrast, some deflections should

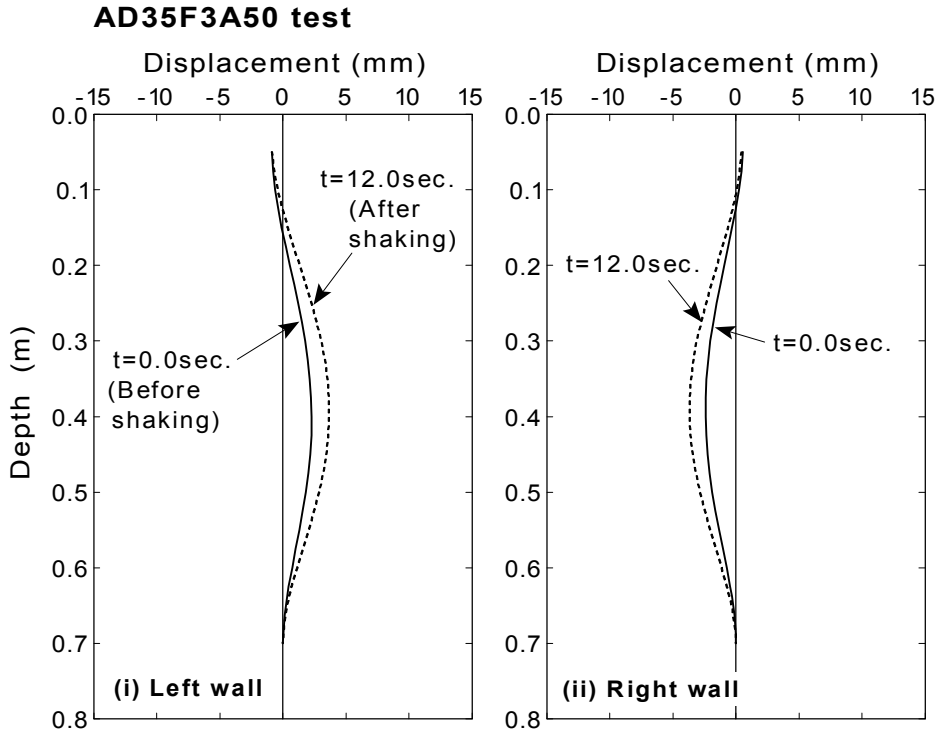

Fig.6.23: Deflections before and after shaking (typical result, AD35F3A50 test)

occur at the middle of both walls. Thus, little residual deflection at the top of wall indicates symmetric action of earth pressure after shaking. The internal consistency between the earth pressure and the deflection when soil liquefies will be examined in the following section.

The relative horizontal displacement between the top of left wall and right wall should be zero since the walls are connected by using the plate with thickness of 15mm at their top. In spite of this, result of calculation shows the horizontal displacement of about -1mm (the left direction) at the top of left wall, and about 1mm (the right direction) in the right wall, amounting 2mm of relative horizontal displacement. The similar trend of relative horizontal displacement is observed in the following results of calculation, suggesting that the horizontal displacements at the top of the wall contain numerical error in the integration of curvature.

Results of tests with intense input motion (AD32F3A500 test)

The deflection in AD32F3A500 test is illustrated in Fig.6.24. This test is the initial shaking of Model No.2 (see Table 3.3). The amount of deflection at the middle of wall after shaking is about 4mm, being equal to the level of the typical test (AD35F3A50 test). This suggests that

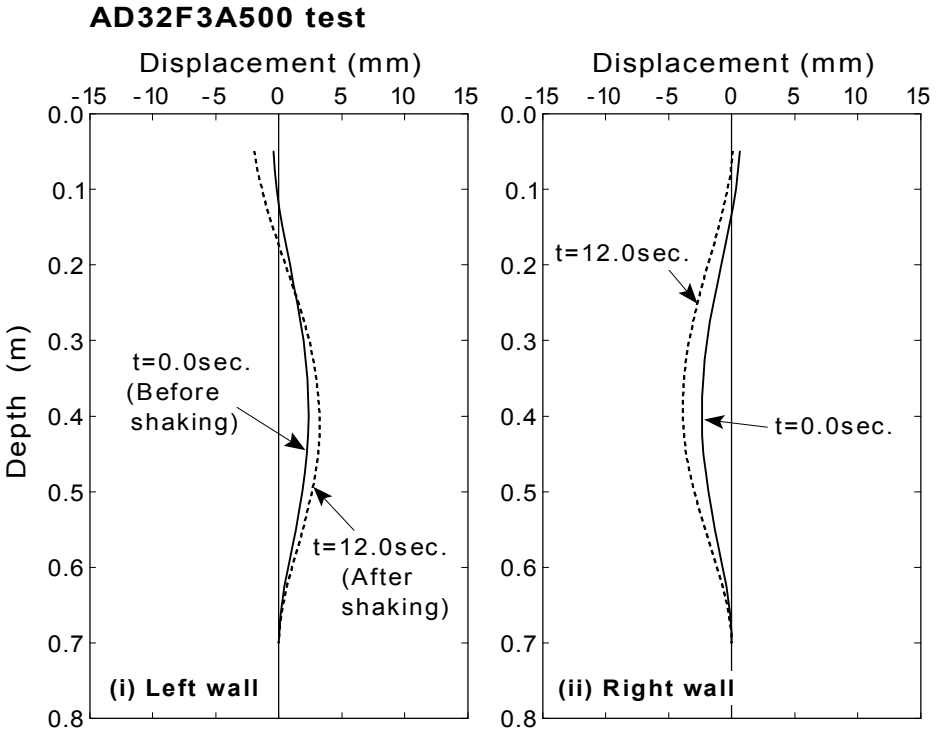

Fig.6.24: Deflections before and after shaking (intense input motion, AD32F3A500 test)

the amount of deflection due to liquefied soil after shaking does not depend on the intensity of shaking.

Results of the test with dense backfill (AD67F3A500 and BD78F3A500 test)

The calculated deflections from AD67F3A500 and BD78F3A500 tests are shown in Fig.6.25. The material yielded initially at 3.69seconds in AD67F3A500 test, at 3.620 seconds in BD78F3A500 test, respectively. After shaking, the level of deflection at the middle of wall becomes about 5mm in AD67F3A500 test. It amounted to 7mm in BD78F3A500 test, being slightly larger than that observed in typical test (about 4mm). It is considered that the large residual deflection in tests with dense backfill causes the yielding of material of wall. It is not due to the density of backfill.

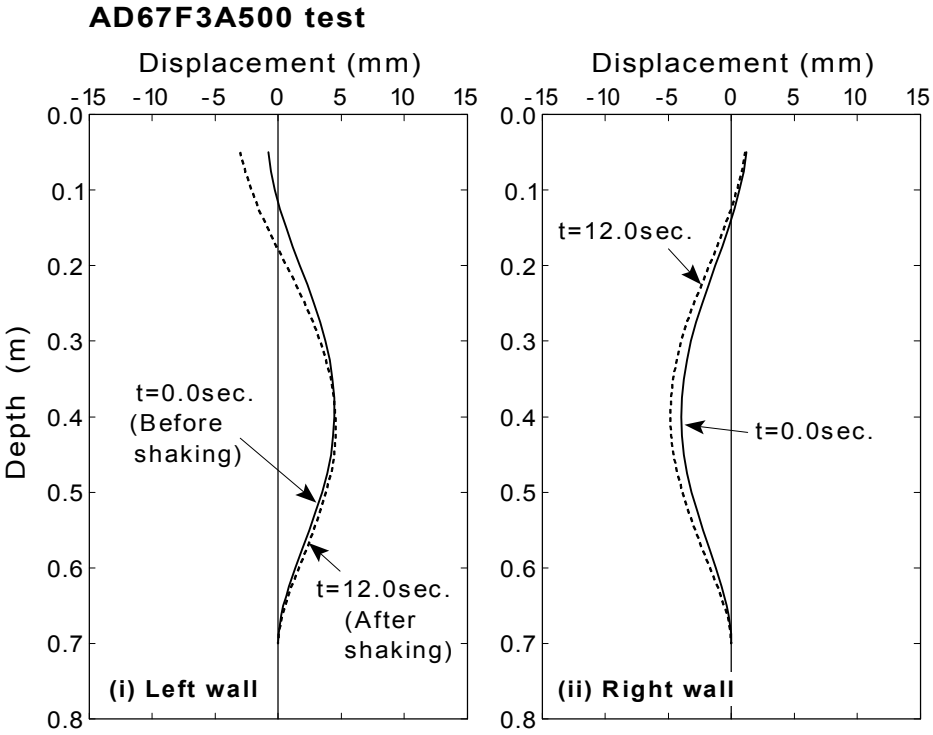

(a) AD67F3A500 test (repeated shaking)

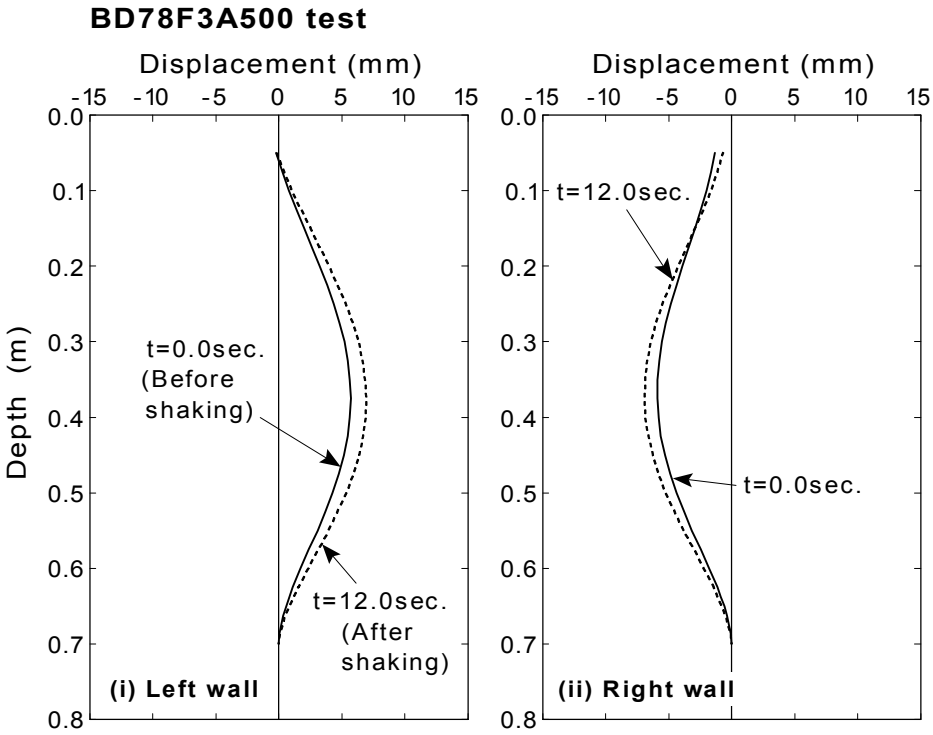

(b) BD78F3A500 test (repeated shaking)

Fig.6.25: Deflections before and after shaking (dense backfill, yielding of material)

Results from tests with yielding of material (BD36F3A500 test)

The results from BD36F3A500 test are illustrated in Fig.6.26. It is remarkable that the deflection at the middle of wall after shaking becomes about 10mm, which is more than twice as much as that before shaking of about 4mm. As illustrated in Fig.6.8, the measured curvature at the bottom of wall after shaking remains about 1.0(1/m), which is about 1.5 times greater than the yield curvature of 0.653(1/m). This suggests that the yielding of material causes the large deflection of wall after shaking.

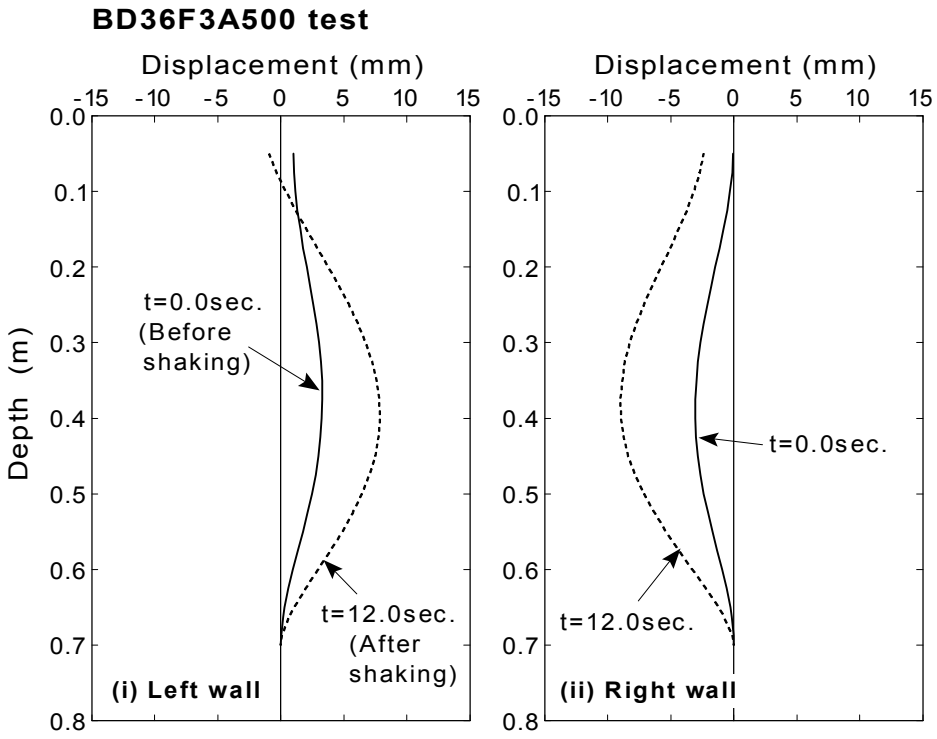

Fig.6.26: Deflections before and after shaking (initial shaking, yielding of material)

Results of other tests

The deflections from AD39F5A50, AD41F3A200 and AD61F3A200 tests are depicted in Fig.6.27. AD39F5A50 test is the second shaking, AD41F3A200 test is the third shaking, and AD61F3A200 test is the tenth shaking of Model No.1. It is seen that the deflection at the middle of the wall after shaking is about 4 to 5mm in these tests, being equal to those of

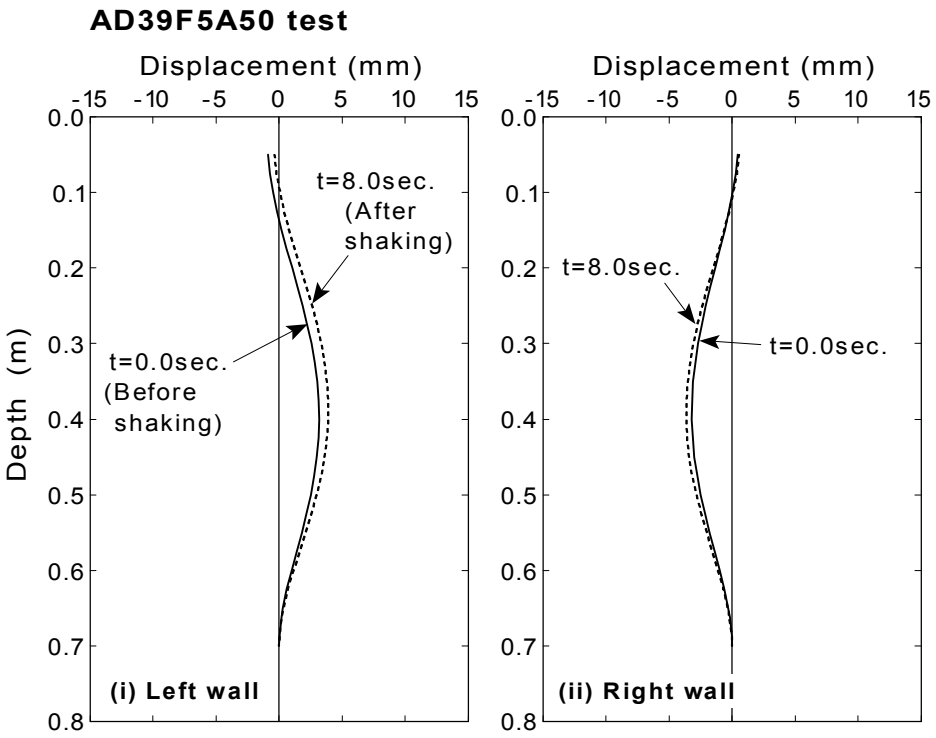

(a) AD39F5A50 test (repeated shaking, shaking of 5Hz in frequency)

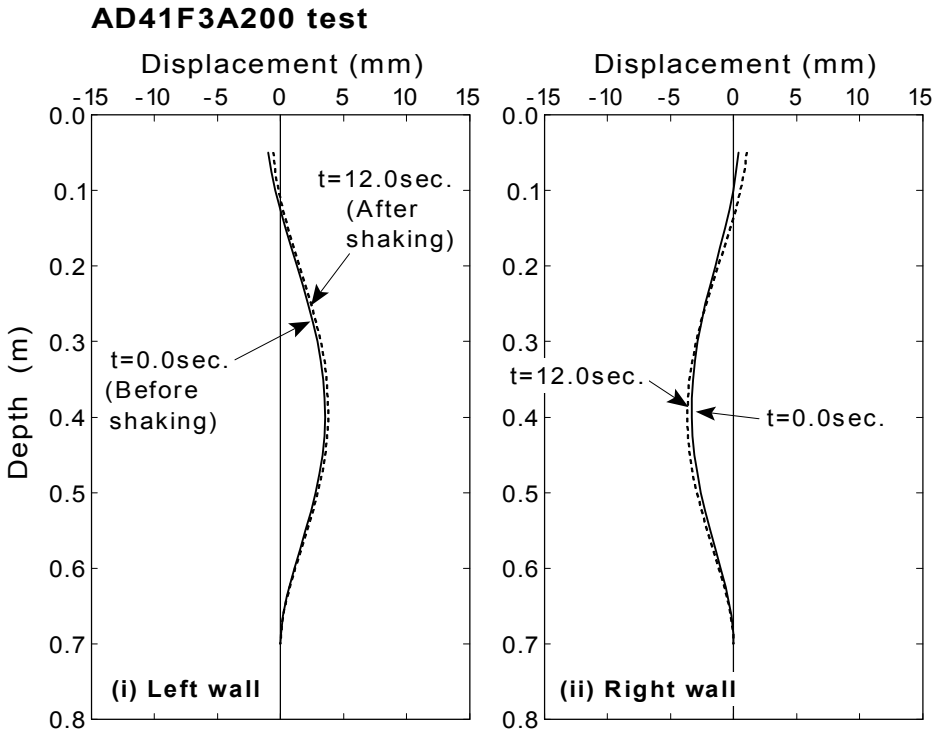

(b) AD41F3A200 test (repeated shaking)

Fig.6.27: Deflections before and after shaking (other test results)

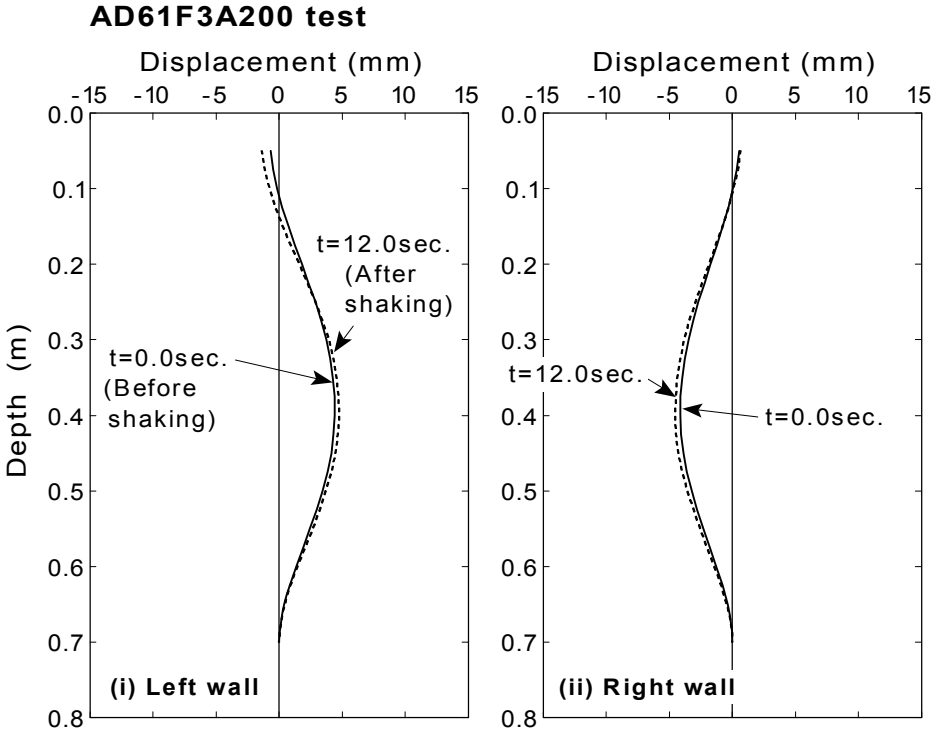

(c) AD61F3A200 test (repeated shaking)

Fig.6.27: Continued

typical or intense input motion tests previously presented.

These observations from all tests suggest that the amount of deflection due to liquefied soil after shaking depends on the yielding of material of wall. The intensity of shaking contributes the occurrence of liquefaction of backfill, but it does not have much effect on the deflection after shaking directly.

6.3.2 Deflections at the maximum displacement during excitation

The profiles of deflection are drawn at each test in order to observe the qualitative feature of deformation of box section of structure. The time i) when the maximum displacement occurs, ii) before or after half a period of input motion (0.165 seconds for 3Hz input motion, 0.1 seconds for 5Hz input motion) from the time of the maximum deflection, and iii) between time i) and ii), are selected for drawing profiles. It is noted that the calculated deflection contains not only fluctuating component but also monotonic component. The qualitative discussion based on the beam analysis will be made in Section 6.4.

Typical results (AD35F3A50 test)

The calculated deflections of both left and right wall during shaking from AD35F3A50 test are illustrated in Fig.6.28. It is seen that the wall moves in either left or right direction due to excitation with the deformation towards inside of the box section. The maximum displacement at the top of the wall reaches about 7mm at 7.725 seconds.

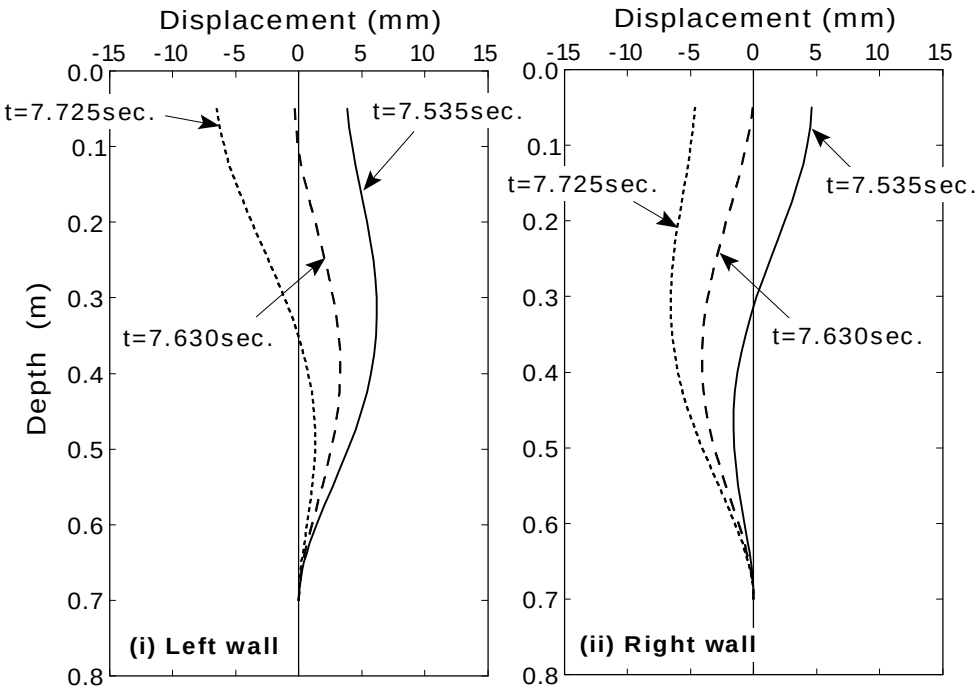

(maximum displacement occurred at 7.725sec)

Fig.6.28: Deflections during shaking (typical test, AD35F3A50 test)

Results of tests with intense input motion (AD32F3A500 test)

The deflection in AD32F3A500 test is illustrated in Fig.6.29. The maximum displacement at the top of the wall during shaking reaches about 25mm. The intense input acceleration of 5.0m/sec^2 brought the large amount of deflection. The qualitative feature of deformation of the box section seems same as that of typical test.

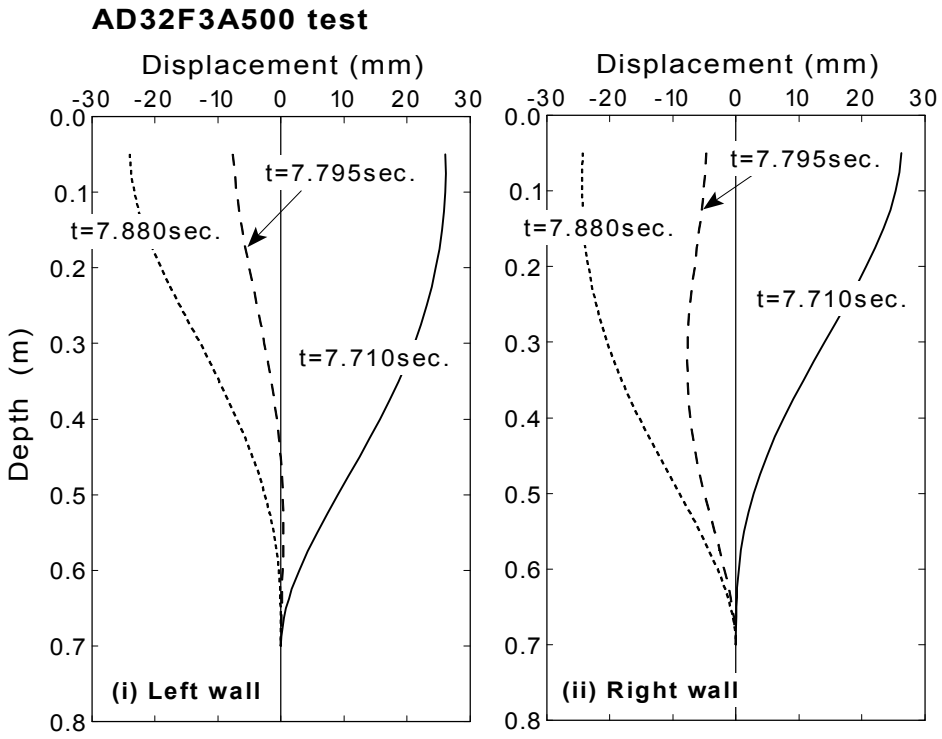

(b) AD32F3A500 test (maximum displacement occurred at 7.710 sec)

Fig.6.29: Deflections during shaking (intense input motion)

Results from tests with dense backfill (AD67F3A500 and BD78F3A500 test)

The deflections from AD67F3A500 test are shown in Fig.6.30(a) and BD78F3A500 test in Fig.6.30(b). No significant difference of feature can be observed comparing to the results from tests using loose backfill except for the amount of maximum deflection.

It was detected by studies conducted in Chapter 5, the resonance occurred and the material yielded initially at 3.69seconds at the bottom of right wall, and at 3.845 seconds at the bottom of left wall. In this test, the displacement at the top of the wall amounted about 40mm, which was much larger than that in BD78F3A500 test. The occurrence of the resonance caused the large amount of dynamic deflection of structure.

Results from tests with yielding of material (BD36F3A500 test)

The deflections from BD36F3A500 test are illustrated in Fig.6.31. The material yielded initially at 2.70 seconds at the bottom of left wall, and at 2.860 seconds at the bottom of right wall. Therefore, the deflection towards inside of structure seems significant as comparing with the results from AD32F3A500 test (see Fig.6.29(b)). On the other hand, the amount of the maximum displacement is about 25mm, being of same level as that in AD32F3A500 test. It seems that the yielding of material of wall affects the monotonic component of deflection more than the amplitude of deflection due to shaking.

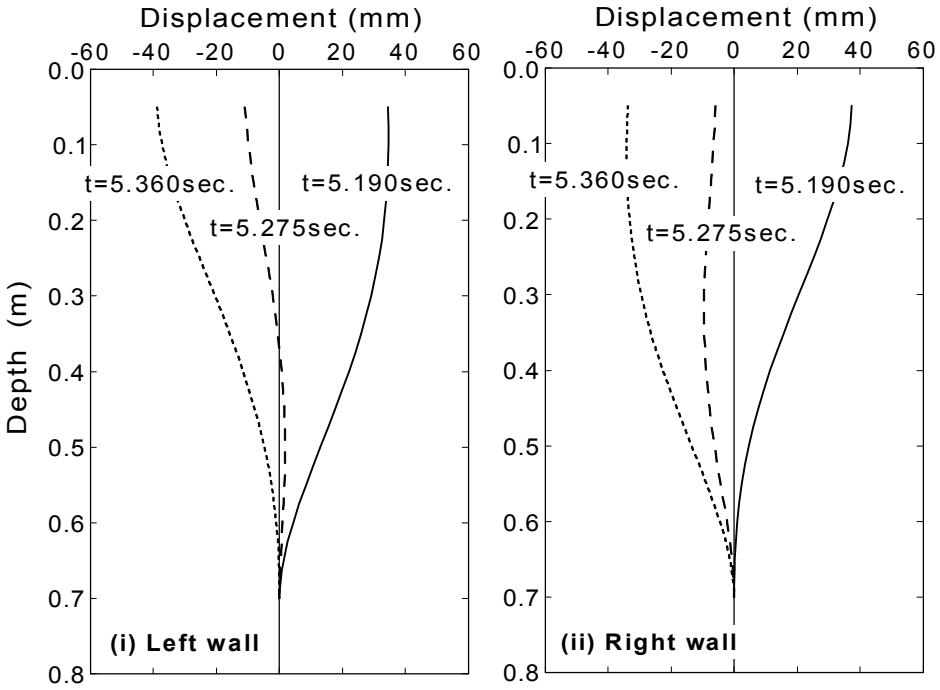

(a) AD67F3A500 test (maximum displacement occurred at 5.190 sec)

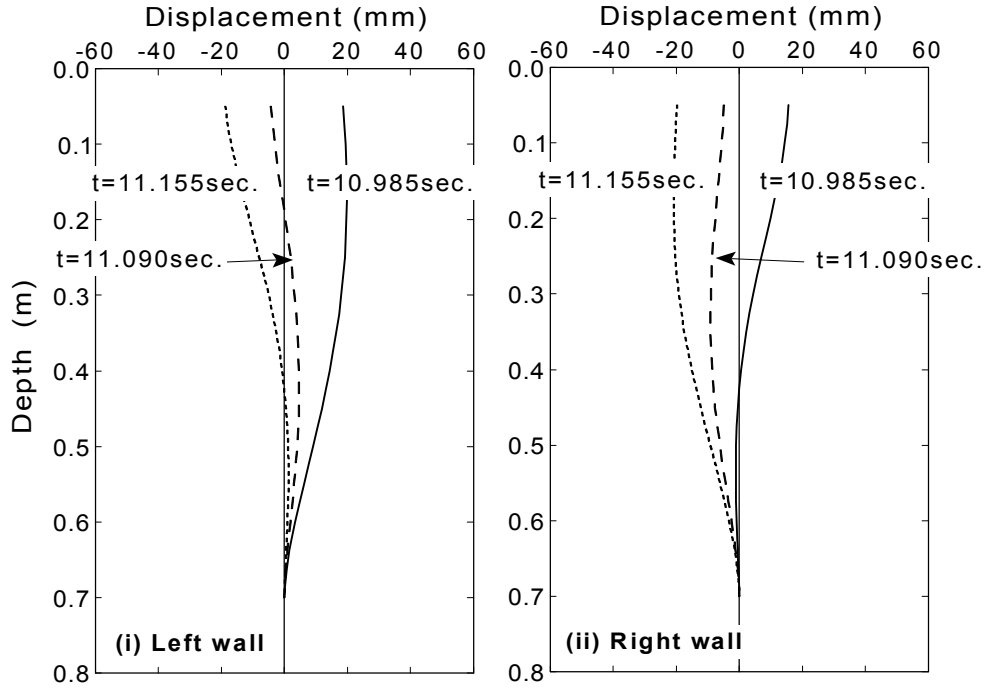

(b) BD78F3A500 test (maximum displacement occurred at 10.985 sec)

Fig.6.30: Deflections during shaking (dense backfill)

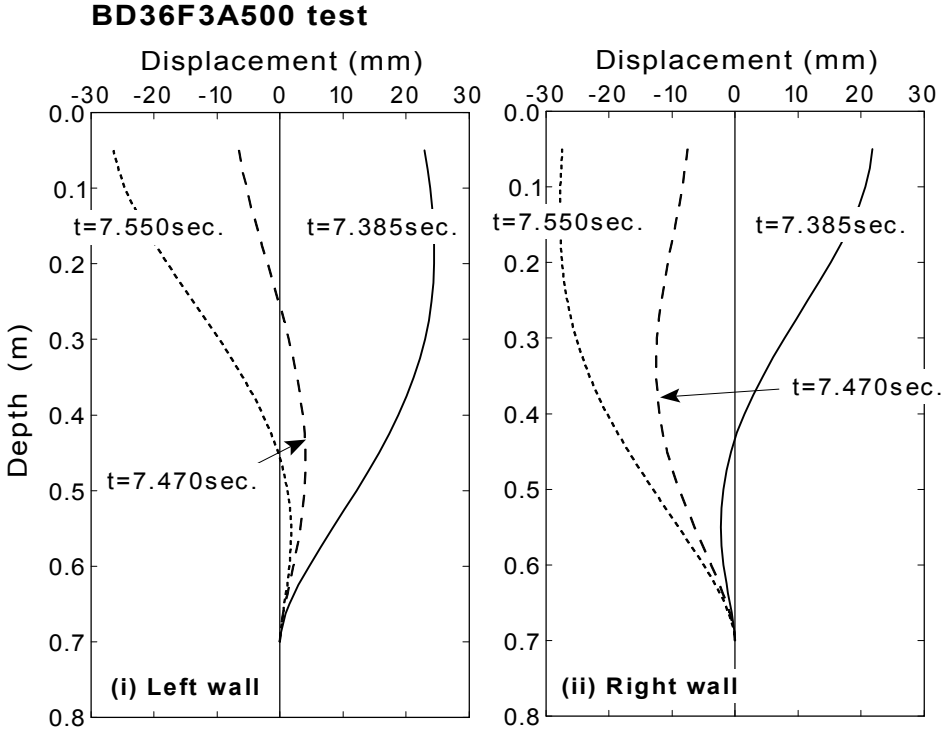

(b) During shaking (Maximum displacement occurred at 7.550 sec)

Fig.6.31: Deflections during shaking (yielding of material, BD36F3A500 test)

Results of other tests

The profiles of deflection from AD39F5A50 test are depicted in Fig.6.32(a). The maximum displacement at the top of the wall seems about 2～3mm, being smaller than that of initial defection of about 4mm at the middle (see Fig.6.27(a)). Taking the time histories of measured curvature shown in Fig.6.22, the effect of noises due to data acquisition system seems to be contained in the calculated deflection.

Fig.6.32(b) present the results from AD41F3A200 test. It is seen that the wall moves in either left or right direction with the deformation towards inside of the box section. It is observed that the deflection at the top of the wall during shaking becomes about the level of 13mm, being as twice as that in AD35F3A50 test.

Fig.6.32(c) presents the results from AD61F3A200 test. The deflection at the top of the wall during shaking becomes about the level of 13mm, being as same as that in AD41F3A200 test.

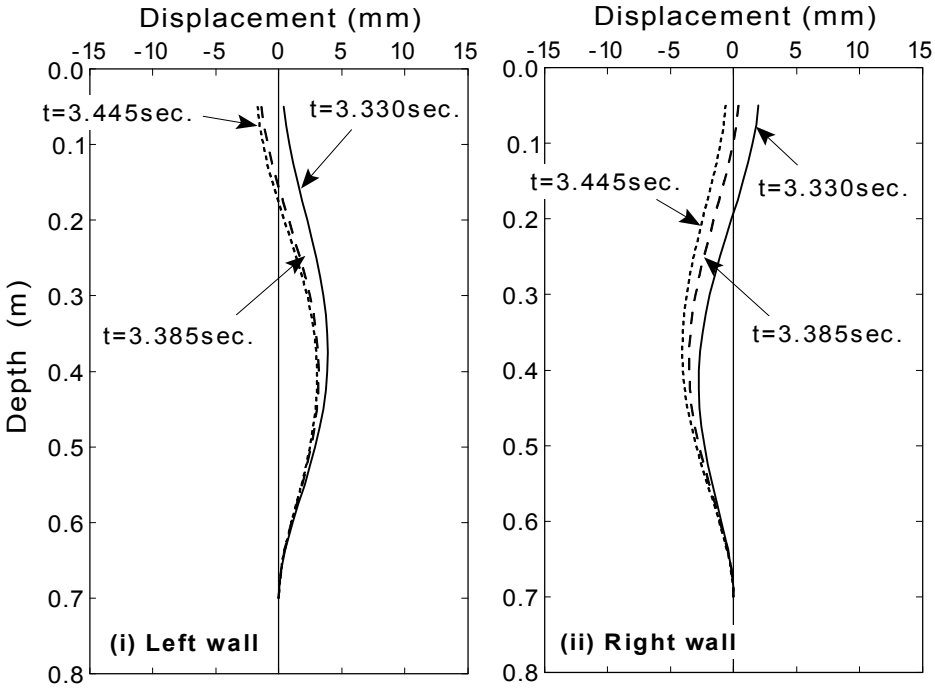

(a) AD39F5A50 test (maximum displacement occurred at 3.445sec)

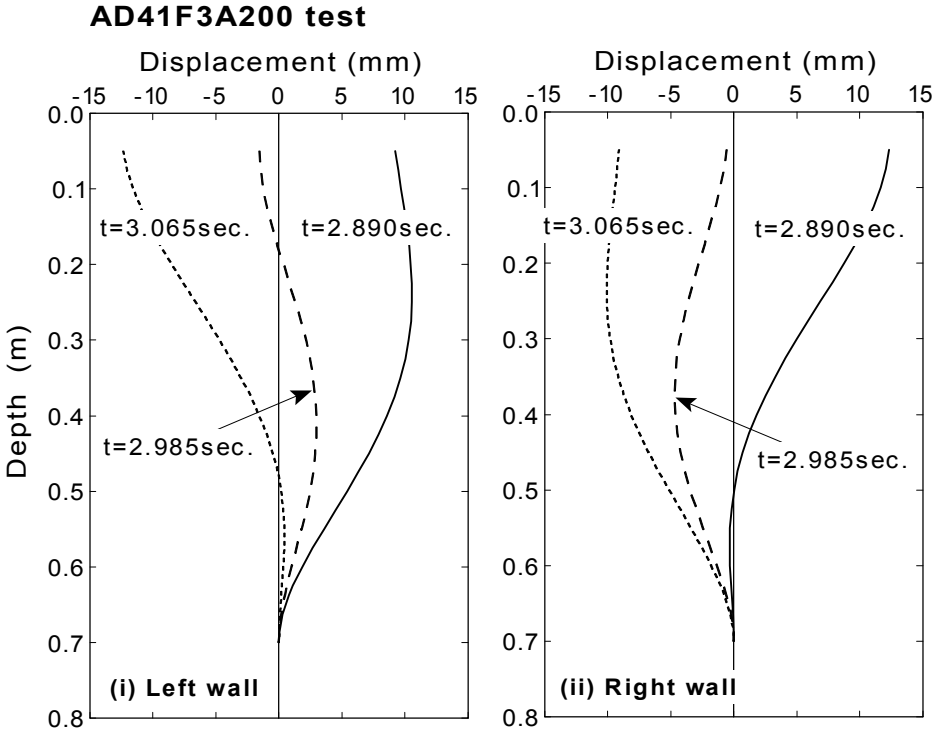

(b) AD41F3A200 test (maximum displacement occurred at 2.890 sec)

Fig.6.32: Deflections during shaking (other test results)

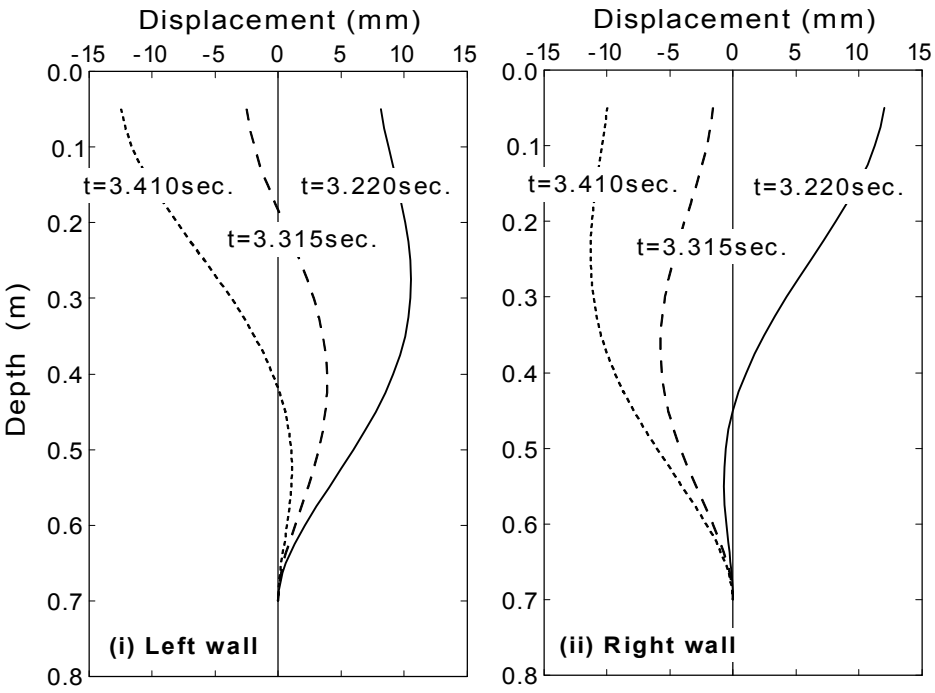

(c) AD61F3A200 test (maximum displacement occurred at 3.220sec)

Fig.6.32: Continued

6.4 ANALYSIS OF DEFORMATION OF CROSS SECTION

In order to build greater confidence in the overall measurements, the measured quantities of structure model will be checked for their internal consistencies. For this purpose, an approach to integrate measured earth pressures to calculate either curvature or deflections will be taken. The calculated quantities of either curvature or deflection will be compared with measured ones to show a reasonable agreement. The tests in which the material behaved in an elastic manner will be selected for the calculation based on the superposition. The action of monotonic and fluctuating component of earth pressure on the structure will be discussed.

6.4.1 Mathematical formulation

As was presented in the previous section, it was convenient for the analysis to distinguish between monotonic component and fluctuating component of responses. The time history of earth pressure will be separated into those components in the following formulation. The monotonic component of curvature will be computed from the monotonic component of earth pressure, and compared with the measured monotonic component of curvature. The fluctuating component of deflection (displacement) will be calculated from the fluctuating component of earth pressure as well as acceleration for comparison with the measured displacement at the top of structure.

Monotonic component

As illustrated in Fig.6.33(a), an actual configuration of a structure is a rectangular box-shape. Considering the following feature of a structure model and earth pressure, the model of structure was reduced to a beam with built-in ends as depicted in Fig.6.33(b).

1. Since the monotonic component of earth pressure is inferred to act on the structure in a symmetric manner (see Fig.6.12 and Fig.6.13), the displacement due to the earth pressure at the top of the structure becomes zero.
2. Since bending stiffness of the top plate is about 27 times larger than that of the wall

(Thickness of the top plate is 3 times as that of walls, see Fig.6.1), rotation does not occur at the rigid connection when the wall deflects.

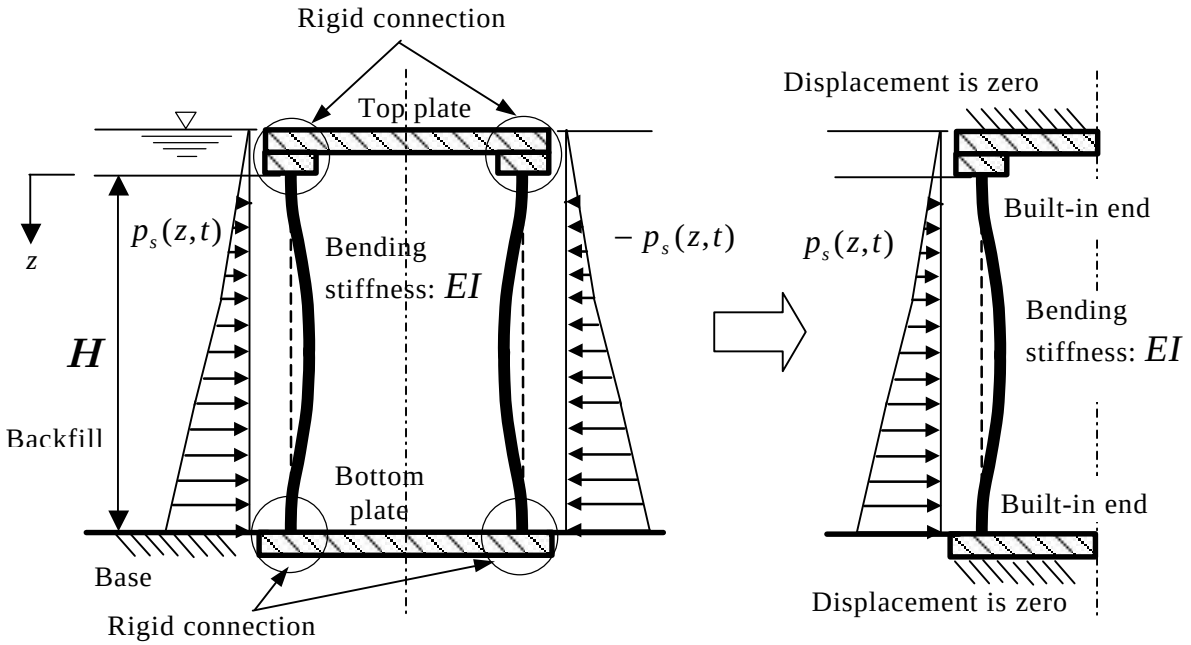

(a) Structure and earth pressure (b) Model of structure

Fig.6.33: Model of structure for calculation with respect to monotonic component

The model illustrated in Fig.6.33(b) can be solved by superposition of loaded earth pressures on an elastic beam. Fig.6.34(a) shows a schematic diagram of superposition of bending moments exerted by distributed loads. Each bending moment produced by piecewise uniformly distributed load p_i(t) as depicted in Fig.6.34(b) can be calculated based on the formula of indeterminate structures (e.g. JSCE, 1986).

Reactions at the top and the bottom of the wall is expressed as

$$R_{ai}(t) = \frac{p_i(t)\cdot b_i}{2}\left\{(2g_i + b_i) - (a_i - g_i)\cdot(2a_i g_i + b_i g_i + a_i b_i)\right\} \tag{6.6}$$

$$R_{bi}(t) = p_i(t)\cdot b_i - R_{ai}(t) \tag{6.7}$$

where,

$$a_i = \frac{a_i}{H} \tag{6.8}$$

$$b_i = \frac{b_i}{H} \tag{6.9}$$

$$g_i = \frac{c_i}{H} \tag{6.10}$$

H : Height of wall (=0.65m)

a_i, b_i, c_i : Heights which define the location of uniformly distributed load (see Fig.6.34(b))

In this series of calculations with respect to monotonic component, the heights a_i, b_i, and c_i are determined as summarized in Table 6.3 considering the location of five earth pressure transducers (see Fig.2.6).

Bending moments at the top and the bottom of the wall are calculated as,

$$M_{ai}(t) = \frac{p_i(t)H^2}{8} b_i \cdot \left\{ (b_i + 2g_i)^2 (2a_i + b_i) + \frac{b_i^2}{3}(2 - 6g_i - 3b_i) \right\} \tag{6.11}$$

$$M_{bi}(t) = \frac{p_i(t)H^2}{8} b_i \cdot \left\{ (2a_i + b_i)^2 (b_i + 2g_i) + \frac{b_i^2}{3}(2 - 6a_i - 3b_i) \right\} \tag{6.12}$$

Considering the reactions and bending moments at both ends, bending moments in section a_i, b_i and c_i are calculated as what follows.

$$M_{1i}(z,t) = R_{ai}(t) \cdot z - M_{ai}(t) \qquad (0 \le z < a_i) \tag{6.13}$$

$$M_{2i}(z,t) = R_{ai}(t) \cdot z - M_{ai}(t) - \frac{p_i(t)}{2}(z - a_i)^2 \qquad (a_i \le z < a_i + b_i) \tag{6.14}$$

$$M_{3i}(z,t) = R_{bi}(t) \cdot (H - z) - M_{bi}(t) \qquad (a_i + b_i \le z \le H) \tag{6.15}$$

Furthermore, deflections in section a_i, b_i and c_i are calculated as

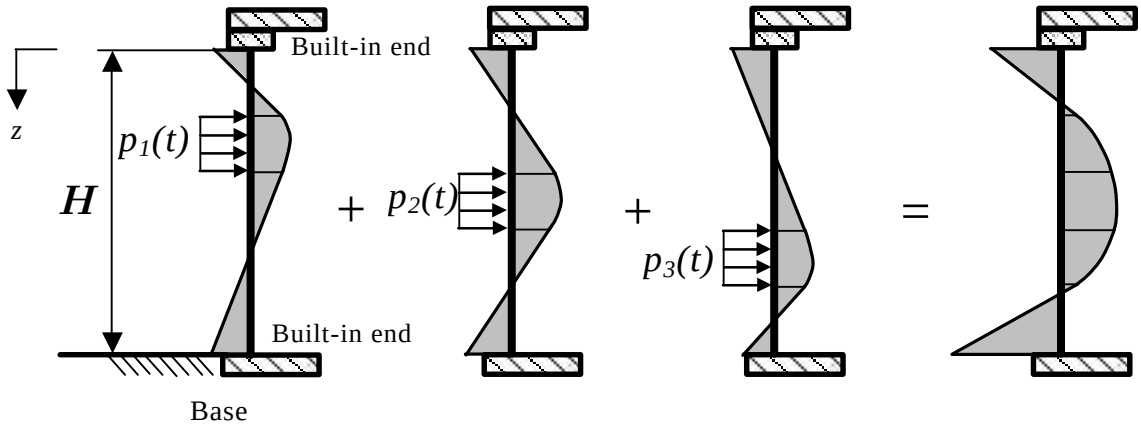

(a) Superposition of bending moments in an elastic beam

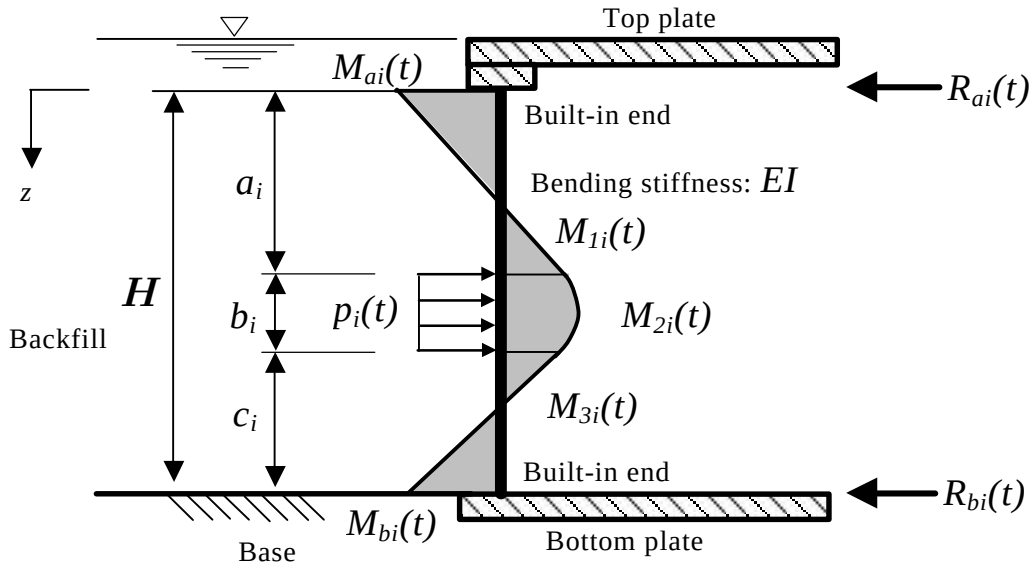

(b) Moment diagram by a uniformly distributed load p_i

Fig.6.34: Schematic diagram of superposition of bending moment

Table 6.3: Height and length used for the calculation

i	Transducer	a_i (m)	b_i (m)	c_i (m)
1	EP6	0.000	0.100	0.550
2	EP7	0.100	0.150	0.400
3	EP8	0.250	0.150	0.250
4	EP9	0.400	0.125	0.125
5	EP10	0.525	0.125	0.000

$H=a_i+b_i+c_i=0.65$m

$$u_{1i}(z,t) = \frac{1}{6EI}\left(3M_{ai}(t)\cdot z^2 - R_{ai}(t)\cdot z^3\right) \qquad (0 \le z < a_i) \tag{6.16}$$

$$u_{2i}(z,t) = \frac{1}{6EI}\left\{3M_{ai(t)}\cdot z^2 - R_{ai}(t)\cdot z^3 + \frac{p_i(t)}{4}(z-a_i)^4\right\} \qquad (a_i \le z < a_i + b_i) \tag{6.17}$$

$$u_{3i}(z,t) = \frac{1}{6EI}\left\{3M_{bi}(t)\cdot (H-z)^2 - R_{bi}(t)\cdot (H-z)^3\right\} \qquad (a_i + b_i \le z \le H) \tag{6.18}$$

Monotonic component of bending moment and deflection at any depth z is derived by superposition of each value due to an uniformly distributed load p_i as

$$M_{mono.}(z,t) = \sum_{i=1}^{5} M_i(z,t) \tag{6.19}$$

$$u_{mono.}(z,t) = \sum_{i=1}^{5} u_i(z,t) \tag{6.20}$$

Consequently, the monotonic component of curvature, $f_{mono.}(z,t)$, is calculated by the following equation.

$$f_{mono.}(z,t) = \frac{M_{mono.}(z,t)}{EI} \tag{6.21}$$

It is herein assumed that the behavior of the beam is in an elastic region.

Fluctuating component

Fig.6.35(a) illustrates a schematic diagram of deformed box-section due to fluctuating component of earth pressure. Considering the following feature of a structure model and earth pressure, the model of structure was reduced to a beam with a roller end at its top and a built-in end at its bottom as depicted in Fig.6.35(b).

1. Since the fluctuating component of earth pressure is inferred to act on the structure by the same amount and in the direction from the consistency of fluctuating component of curvatures (see, Fig.6.18～Fig.6.22), the axial load in the top plate due to the earth

pressure is small enough to neglect.

2. Bending stiffness of the top plate is about 27 times as larger than that of the wall (Thickness of the top plate is 3 times as that of walls, see Fig.6.1), rotation does not occur at the rigid connection when the wall deflects.

Detailed description of model of the structure is depicted in Fig.6.36. Bending moment $M(z,t)$, shear force $V(z,t)$, earth pressure $p(z,t)$ per unit width, acceleration $\ddot{x}(z,t)$ and deflection $u(z,t)$ are functions of space z and time t. The boundary conditions are:

$$\frac{\partial u}{\partial z} = 0 \quad (at\ the\ top) \tag{6.22}$$

$$\frac{\partial u}{\partial z} = 0 \quad (at\ the\ bottom) \tag{6.23}$$

$$u = 0 \quad (at\ the\ bottom) \tag{6.24}$$

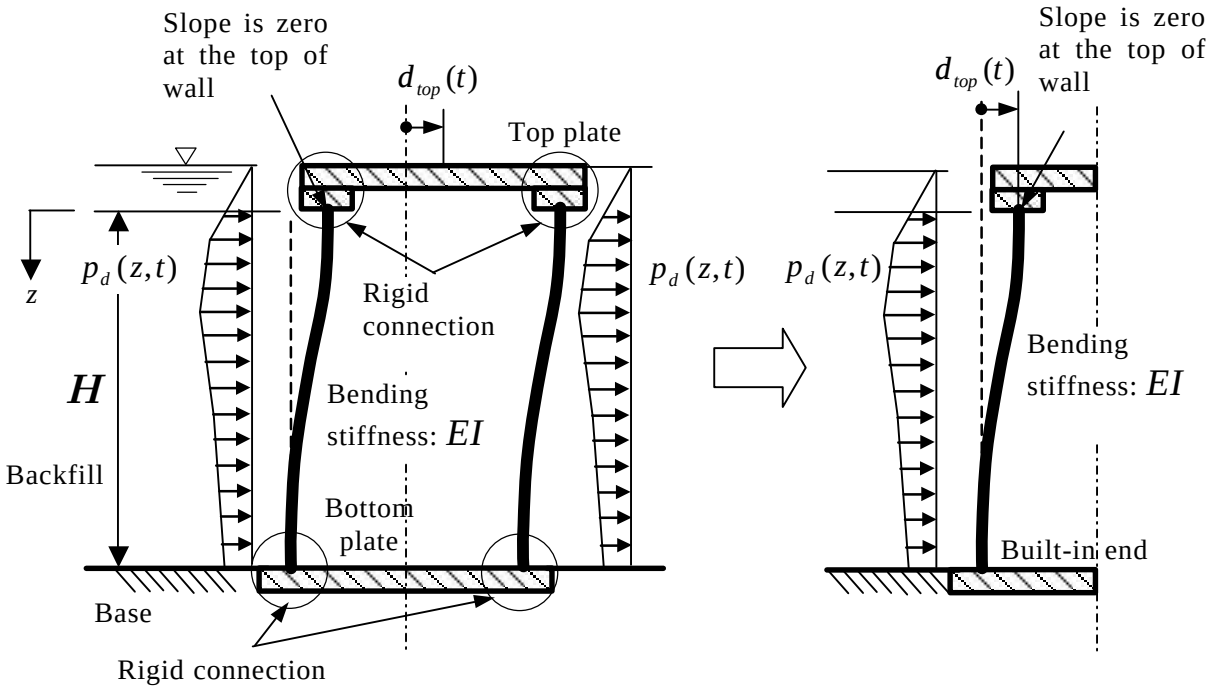

(a) Structure and earth pressure (b) Model of structure

Fig.6.35: Schematic diagram of modeled box section of structure for calculation with respect to fluctuating component

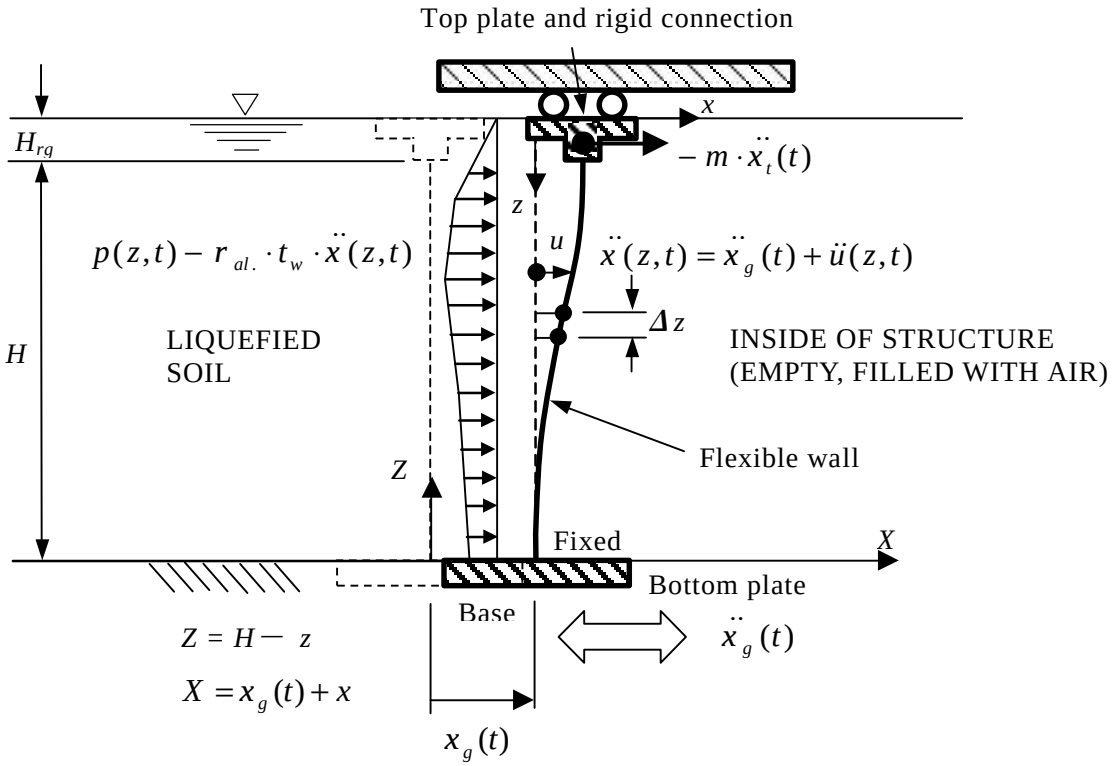

Fig.6.36: Model of wall of the structure

The model shown in Fig.6.36 is indeterminate to the first degree. This type of structure can be solved by superposition. This method requires finding the deflections or deflection angles with one of the supports removed, and then satisfying the given boundary conditions. Procedures to solve the problem are summarized as what follows:

Step1: Remove the redundant supports to reduce the structure to a statically determinate condition. In this problem, the redundant support against rotation at the top of the wall will be removed (see Fig.6.37(a)(i)).

Step2: Calculate the deflection angle at the previous location of redundant support (at the top of wall, see Fig.6.37(b)(i))

Step3: Apply the redundant support a load (M_2, see Fig.6.37(a)(ii)), and find the deflection angle at the redundant support points (at the top of wall, $-q_1$) as functions of the redundant support forces ($-q_1 = M_2 \cdot H/(EI)$, see Fig.6.37 (b)(ii)).

Step4: Use superposition to combine (or to add) the deflections due to the actual loads

(see Fig.6.37(a)(i)) and the redundant support load. The total deflection must agree with the known deflection angles (zero, see Eq.(6.22)) at the redundant support point.

Detailed procedure is presented thereinafter.

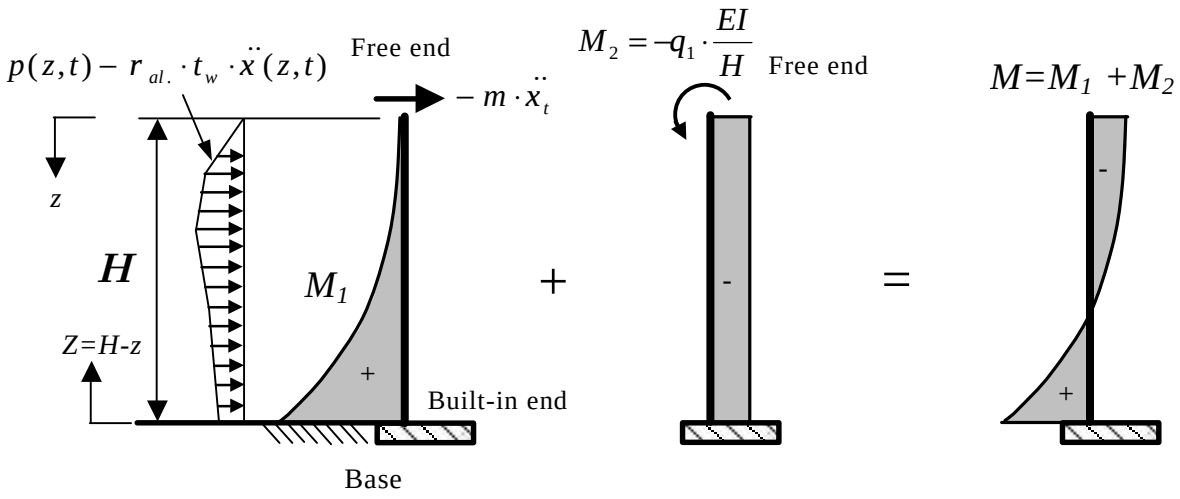

(i) actual loads (ii) redundant support load (iii) Superposed

(a) Bending moment

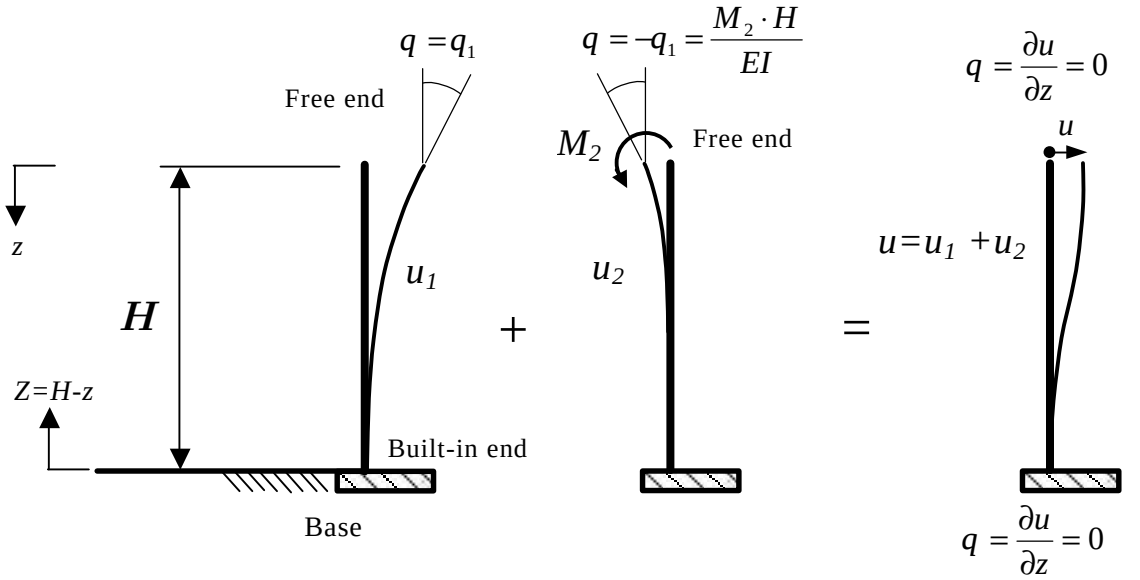

(i) actual loads (ii) redundant support load (iii) Superposed

(b) deflection

Fig.6.37: Bending moment and deflection of structure removing a redundant support

Force equilibrium in the wall

Free-body diagram of the simplified problem of a wall is shown in Fig.6.38. Considering force equilibrium in a small element with height of Δz, shear force increment at the bottom of an element is expressed as,

$$\frac{\partial V(z,t)}{\partial z} dz = p(z,t) \cdot \Delta z - r_{al.} \cdot \Delta z \cdot t_w \cdot \ddot{x}(z,t) \tag{6.25}$$

where $r_{al.}$ is mass density of aluminum $(=2.7)$、t_w is a thickness of wall, $\ddot{x}(z,t)$ is an absolute acceleration. The loading $p(z,t)$ is uniformly distributed in an element. The equation is reduced to be

$$\frac{\partial V(z,t)}{\partial z} = p(z,t) - r_{al.} \cdot t_w \cdot \ddot{x}(z,t) \tag{6.26}$$

On the other hand, moment increment at the bottom of an element is expressed as,

$$\frac{\partial M(z,t)}{\partial z} dz = V(z,t) \cdot \Delta z + \frac{1}{2} p(z,t) \cdot (\Delta z)^2 \tag{6.27}$$

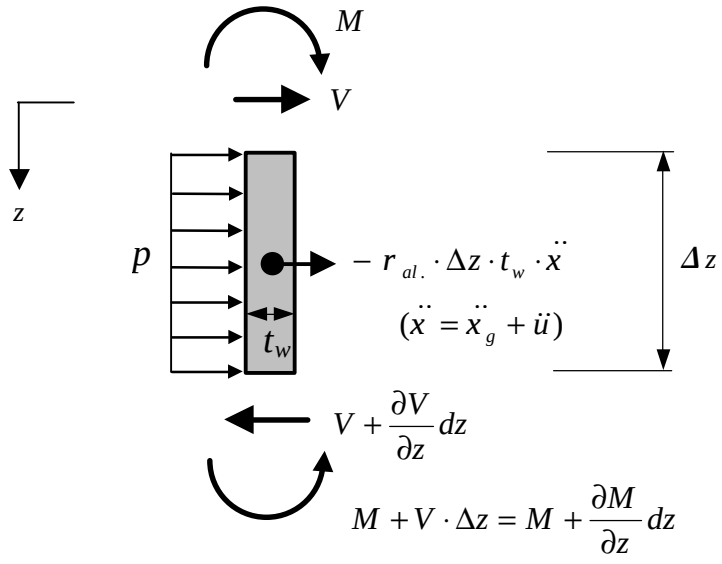

Fig.6.38: Free-body diagram of the wall

Since the height Δz is very small quantity, second term in the right hand is negligible,

$$\frac{1}{2} p(z,t) \cdot (\Delta z)^2 \cong 0 \tag{6.28}$$

Considering Eq.(6.28), Eq.(6.27) is reduced to,

$$V(z,t) = \frac{\partial M(z,t)}{\partial z} \tag{6.29}$$

Substituting Eq.(6.29) into Eq.(6.26), it can be shown that

$$\frac{\partial^2 M(z,t)}{\partial z^2} = p(z,t) - r_{al.} \cdot t_w \cdot \ddot{x}(z,t) \tag{6.30}$$

The above equation can be solved for the structure in which redundant support is removed at each time instance of the base motion time history.

Removing a redundant support (Step1)

The fluctuating component of earth pressure and acceleration can be determined from the measurements. Boundary conditions at the top of wall without redundant support are:

$$M = 0 \quad (at\ the\ top) \tag{6.31}$$

$$\frac{\partial M}{\partial z} = 0 \quad (at\ the\ top) \tag{6.32}$$

Note that above boundary conditions is different from the boundary conditions for actual structure, Eq.(6.22).

Calculation of deflection angle at a redundant support (Step2)

Integrating Eq.(6.30) twice with respect to *z*, the bending moment due to earth pressure and inertia force of wall at any depth and a particular time instance t_1 is calculated as,

$$M_p(z,t_1)=\int_0^z\int_0^x\left[p(z,t_1)-r_{al.}\cdot t_w\cdot\ddot{x}(z,t_1)\right]dzdx+\left[\frac{\partial M(0,t)}{\partial z}\right]\cdot z+M(0,t) \qquad (6.33)$$

where x and z are dummy integration variables. On the other hand, the bending moment at any depth due to inertia force of the top plate, $-m\cdot\ddot{x}_t$, is calculated as,

$$M_{inertia}(z,t_1)=-m\cdot\ddot{x}(z,t_1)\cdot z \qquad (6.34)$$

where *m* is the mass per unit width of the top plate (a half of actual mass). The dimensions of the top plate are illustrated in Fig.6.39, and the values of the mass are summarized in Table 6.4. It should be noted that the half of the mass of the actual top plate is taken into account for the calculation since only the half of the symmetric structure is modeled (see Fig.6.35).

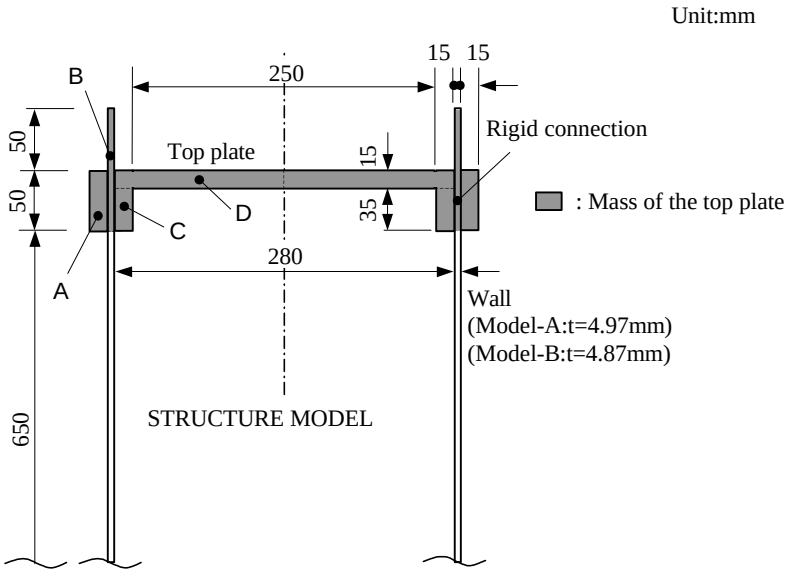

Fig.6.39: Dimensions of the top plate of the structure

Table 6.4: Mass of the top plate considered in the calculation

Portion	Structure-A		Structure-B	
	Dimension (m)	Area (m^2)	Dimension (m)	Area (m^2)
A	0.05×0.015	0.00075	0.05×0.015	0.00075
B	0.10×0.00497	0.000497	0.10×0.00487	0.000487
C	0.035×0.015	0.000525	0.035×0.015	0.000525
D	0.14×0.015	0.0021	0.14×0.015	0.0021
Σ area	—	0.003872	—	0.003862
Mass density ($kNsec^2/m^4$)	2.7		2.7	
Mass m ($Nsec^2/m^2$)	10.454		10.427	

Superposing those bending moments, the bending moment due to actual loads (see Fig.6.37(a)(i))) are calculated as,

$$M_1(z,t_1) = M_p(z,t_1) + M_{inertia}(z,t_1) \tag{6.35}$$

The curvature at any depth and a particular time instance t_1 is related to bending moment as,

$$EI\frac{\partial^2 u}{\partial z^2}(z,t_1) = M_1(z,t_1) \tag{6.36}$$

where EI is bending stiffness of the wall. Integrating Eq.(6.36) once with respect to Z $(=H-z)$ from the bottom toward the top, the deflection angle at any height is calculated as,

$$\theta(Z,t) = \frac{1}{EI}\left[\int_0^Z M_1(\xi,t_1)d\xi\right] + \left.\frac{\partial u}{\partial Z}\right|_{at\ the\ bottom} \tag{6.37}$$

where ξ is a dummy integration variable. The deflection angle at the top of wall, θ_1, is calculated considering the boundary condition at the bottom of wall, $\partial u/\partial Z = 0$, as,

$$\theta_1 = \frac{1}{EI}\left[\int_0^H M_1(\xi,t_1)d\xi\right] \tag{6.38}$$

Application of a load at the redundant support (Step3)

A load which generates deflection angle $-\theta_1$ at the top of wall is expressed as,

$$M_2(z,t_1) = -\theta_1 \cdot \frac{EI}{H} \tag{6.39}$$

Superposition of bending moments and calculation of deflection (Step4)

Consequently, the fluctuating component of actual bending moment of the model structure (Fig.6.37(a)(iii)) is derived superposing as,

$$M_{fluc.}(z,t_1) = M_1(z,t_1) + M_2(z,t_1) \tag{6.40}$$

Curvature at any depth and a particular time instance t_1 is related to bending moment assuming elastic behavior of wall as,

$$\phi(z,t_1) = \frac{\partial^2 u(z,t_1)}{\partial z^2} = \frac{M(z,t_1)}{EI} \tag{6.41}$$

Fluctuating component of deflection at the wall is obtained by integrating Eq.(6.41) twice with respect to *Z (=H-z)* from the bottom toward the top as,

$$u_{fluc.}(Z,t_1) = \frac{1}{EI}\left[\int_0^Z \int_0^\xi M_{fluc.}(\zeta,t_1)\, d\zeta\, d\xi\right] + \left(\left.\frac{\partial u}{\partial Z}\right|_{at\ the\ bottom}\right) \cdot Z + u\,|_{at\ the\ bottom} \tag{6.42}$$

where ξ and ζ are dummy integration variables. The deflection angle at the top of wall is calculated considering the boundary condition at the bottom of wall, $\partial u / \partial Z = 0$, and u=0 as,

$$u\,|_{at\ the\ top} = \frac{1}{EI}\left[\int_0^H \int_0^\xi M_{fluc.}(\zeta,t_1)\, d\zeta\, d\xi\right] \tag{6.43}$$

Thus, at each time step, by using a suitable integration scheme, profiles of earth pressures and accelerations on the wall can be obtained and integrated to compute deflections. Combining calculated deflections at all time steps, complete time histories of those quantities can be obtained.

6.4.2 Approximation of earth pressure and acceleration profiles

Earth pressure profile

Prior to the calculation, the measured earth pressures are separated into the monotonic and fluctuating components by the moving average computation as presented in the previous section. Typical time histories of monotonic component and fluctuating component, as well as measured earth pressures from AD35F3A50 test are illustrated in Fig.6.40. Although compressive earth pressure is defined as positive in this study, note that the negative value of fluctuating component of earth pressure does not mean tensile earth pressure. It is because all the measured earth pressure is actually positive as illustrated in Fig.6.40.

Profiles of earth pressure at the selected time instance are depicted in Fig.6.41(a) for monotonic component and (b) for fluctuating component. It is observed that the shape of distribution of monotonic component shows triangular from the beginning (t=0sec) to the end of shaking (t=10sec). In contrast, the shape of distribution of fluctuating component is complicated in which the sign of earth pressure is opposite between the top and the bottom of the wall. Considering the observed earth pressure profiles and convenience of calculation, each component of earth pressure is approximated differently as shown in Fig.6.42. The monotonic component is approximated by a step function, and the fluctuating component by a linearly interpolated function. As described later, those approximations give good agreement between the calculated and measured curvatures.

All the time history of monotonic component and fluctuating component as well as measured earth pressure are presented in Fig.6.85～Fig.6.91 at the end of this chapter.

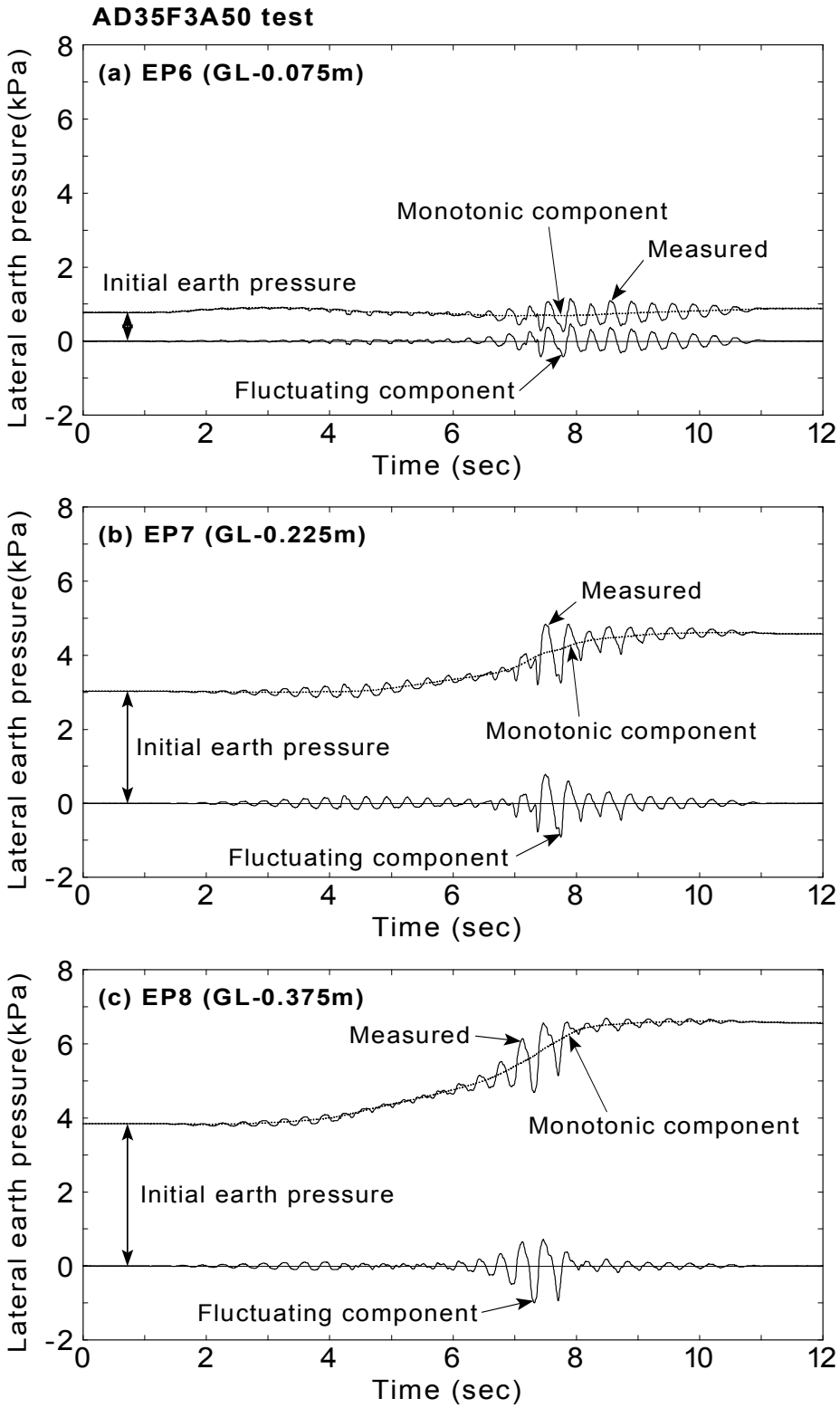

Fig.6.40: Monotonic and fluctuating component of earth pressures considered in the analysis (AD35F3A50 test)

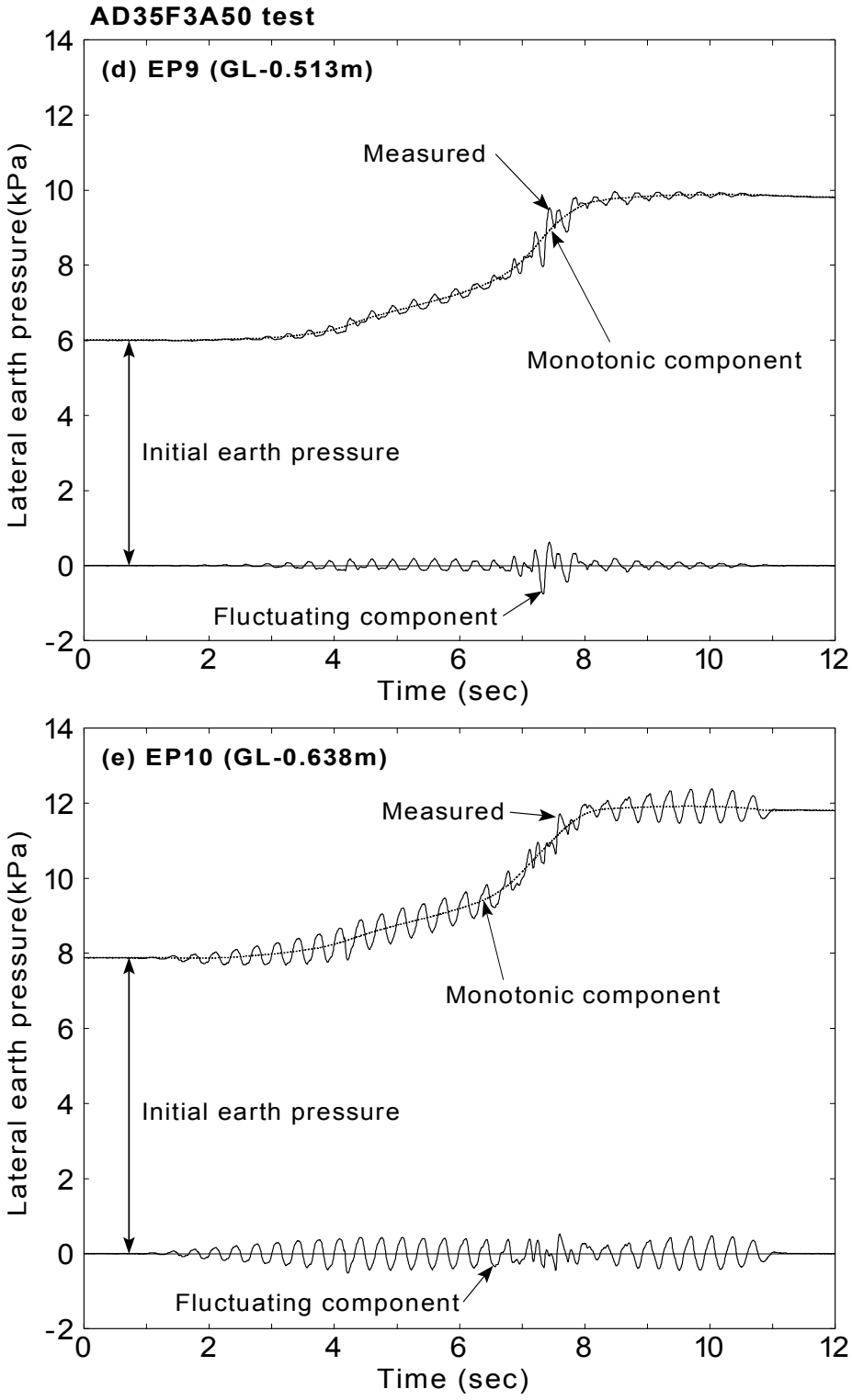

Fig.6.40: Continued

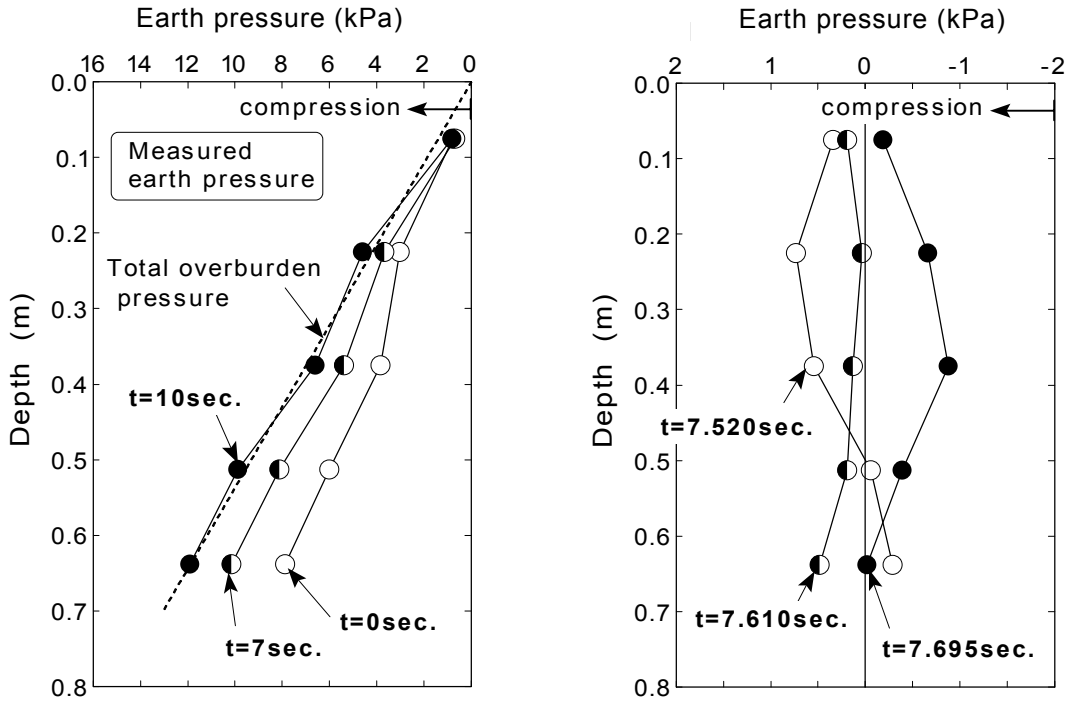

(a) Monotonic component (b) Fluctuating component

Fig.6.41: Typical profile of earth pressures (AD35F3A50 test)

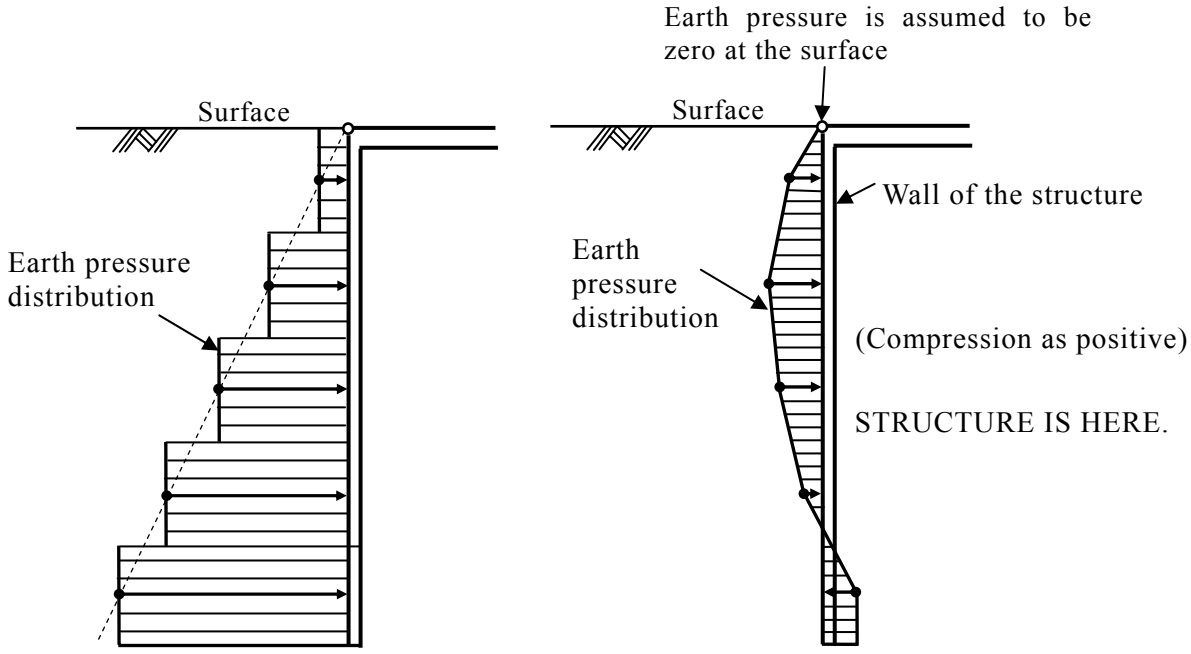

(a) Monotonic component (b) Fluctuating component

Fig.6.42: Approximation of earth pressures for calculation

Acceleration profile at the wall

It is needed to obtain horizontal acceleration profile along the wall for the calculation. Since horizontal accelerations on the structure are measured only at its top and bottom, acceleration profile of wall will be assumed appropriately. Accelerations along the wall $\ddot{x}(z,t)$ are approximated by a deflection of beam with settled end.

Schematic figure of a beam with settled end is illustrated in Fig.6.43. Suppose that bending stiffness of the beam *EI* is constant through the depth, and the displacement u_t occurs at the top built-in end. In this respect, a deflection at any depth of the beam, $u(z)$, is expressed as

$$u(z) = u_t \left(1 - \frac{z}{H}\right)^2 \left\{3 - 2\left(1 - \frac{z}{H}\right)\right\} \tag{6.44}$$

where *H* is the height of the beam.

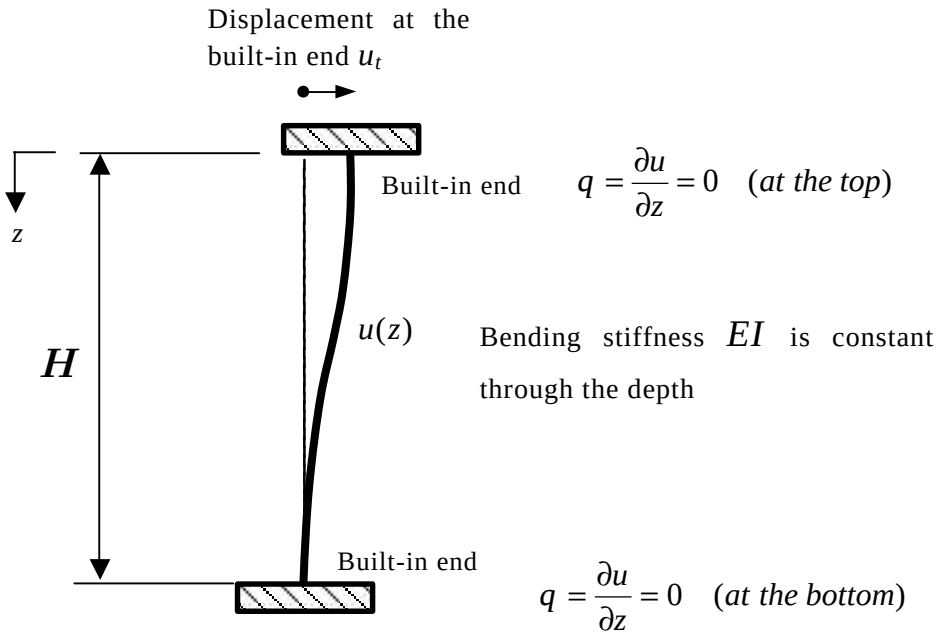

Fig.6.43: Schematic figure of a beam with settled end

Consider absolute acceleration at the top, $\ddot{x}_t(t)$, and the bottom, $\ddot{x}_g(t)$. Applying the distribution expressed by Eq.(6.44) to an acceleration profile, a quantity at the top which corresponds to displacement, u_t, becomes a relative acceleration between the top and the bottom, $(\ddot{x}_t(t) - \ddot{x}_g(t))$. The acceleration profile of beam with settled end is expressed as

$$\ddot{x}(z,t) = \left(\ddot{x}_t(t) - \ddot{x}_g(t)\right)\left(1-\frac{z}{H}\right)^2\left(3-2\left(1-\frac{z}{H}\right)\right)+\ddot{x}_g(t) \quad \textit{at the wall } x=0 \tag{6.45}$$

Approximated acceleration profiles thus obtained from AD35F3A50 test and AD32F3A500 test are illustrated in Fig.6.44 (solid and dashed line). In this figure, absolute accelerations at the top (AC2) and bottom (AC1) of wall are used for accelerations $\ddot{x}_t(t)$ and $\ddot{x}_g(t)$. The calculated horizontal accelerations on the wall obtained from the measured bending curvature are also plotted in the figure. The detailed procedure of calculation of wall acceleration, which was based on the integration of measured curvature and numerical differentiation of deflection of wall, was presented in the section 4.3.3.

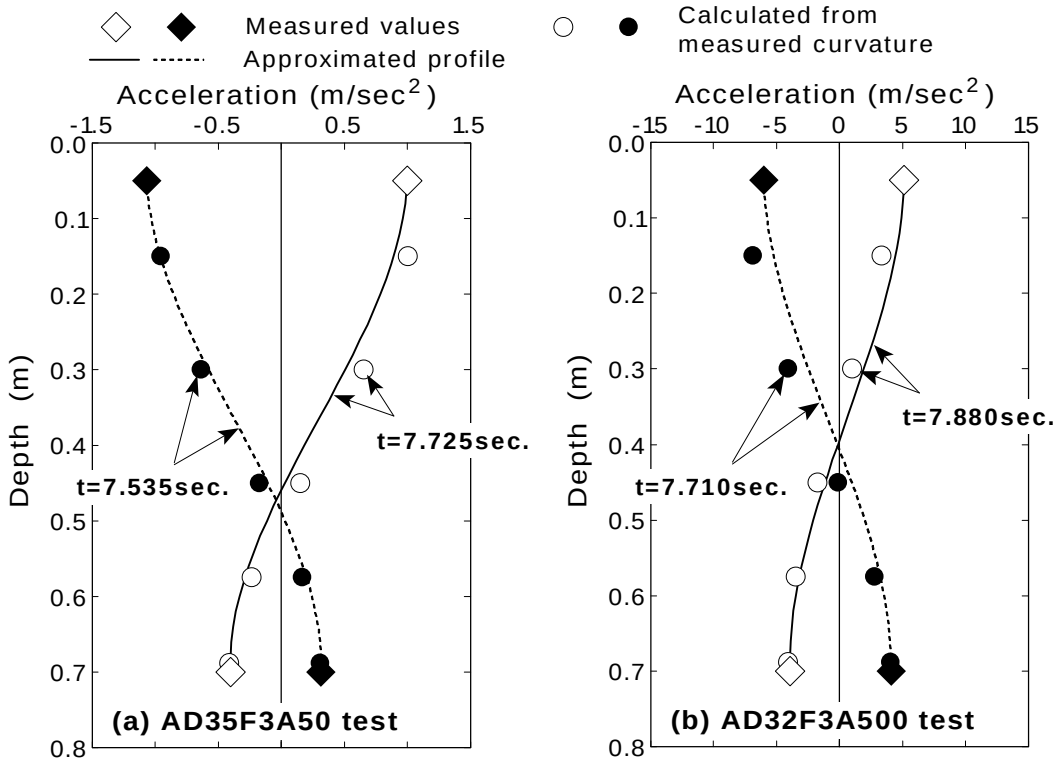

Fig.6.44: Approximated profile of acceleration along the wall

It is seen that the agreement is very good for the test shaken by 0.5m/sec^2 and 5.0m/sec^2 of sinusoidal base motion in spite of simplicity of acceleration profile. It suggests that the approximation by Eq.(6.45) is reasonable. Therefore, this approximation is employed in the calculation of inertia force of wall.

6.4.3 Analysis program

Analysis is going to be conducted using calculation procedure presented in the previous section. Curvatures and displacements at the top of structure will be calculated and compared with the measured quantities. It is assumed that measured earth pressures act as a load on the structure in all the calculation and the structure behaves in an elastic manner. Analysis program is described in Table 6.5. Since the wall yielded in AD67F3A500 test, BD36F3A500 test and BD78F3A500 test, time period before yielding are considered for the analysis. Since the yielding of the material is not taken into account in calculations, BD36F3A500 test is classified in a test of intense input motion in this analysis program.

Table 6.5: Analysis program for curvature and deflection

	Model of structure	Test	Behavior of structure	Time when initial yield occurs (seconds)	Time period considered in the analysis
Typical test	Structure-A	AD35F3A50	Elastic	—	0.0～12.0
Test of intense input motion	Structure-A Structure-B	AD32F3A500 BD36F3A500	Elastic Non-elastic	— 2.700	0.0～12.0 0.0～2.70
Test with dense backfill	Structure-A Structure-B	AD67F3A500 BD78F3A500	Non-elastic Non-elastic	3.690 3.620	0.0～3.69 0.0～3.62
Other tests (Test of repeated shaking)	Structure-A	AD39F5A50 AD41F3A200 AD61F3A200	Elastic Elastic Elastic	— — —	0.0～8.0 0.0～12.0 0.0～12.0

6.4.4 Analysis of monotonic component of curvature

Monotonic component of curvatures are calculated using Eqs.(6.11), (6.12), (6.19) and (6.21), which were induced for the simplified half structure model.

Typical results (AD35F3A50 test)

AD35F3A50 test (maximum acc.=0.5m/sec^2) is the test of initial shaking in Model No.1 (see Table 6.5). Initial relative density was 35%. The profiles of monotonic component of earth pressure used in the calculation of AD35F3A50 test are shown in Fig.6.45(a). The profile of calculated quantities are compared with measured curvatures in Fig.6.45(b).

It is observed that the initial earth pressure increases with time and reaches initial total overburden pressure through the depth at 10 seconds, indicating the complete liquefaction of backfill. The calculated curvature agrees reasonably with the measured curvature. The good agreement between measured and computed curvature suggests that the monotonic component of earth pressure on the wall and curvature are internally consistent.

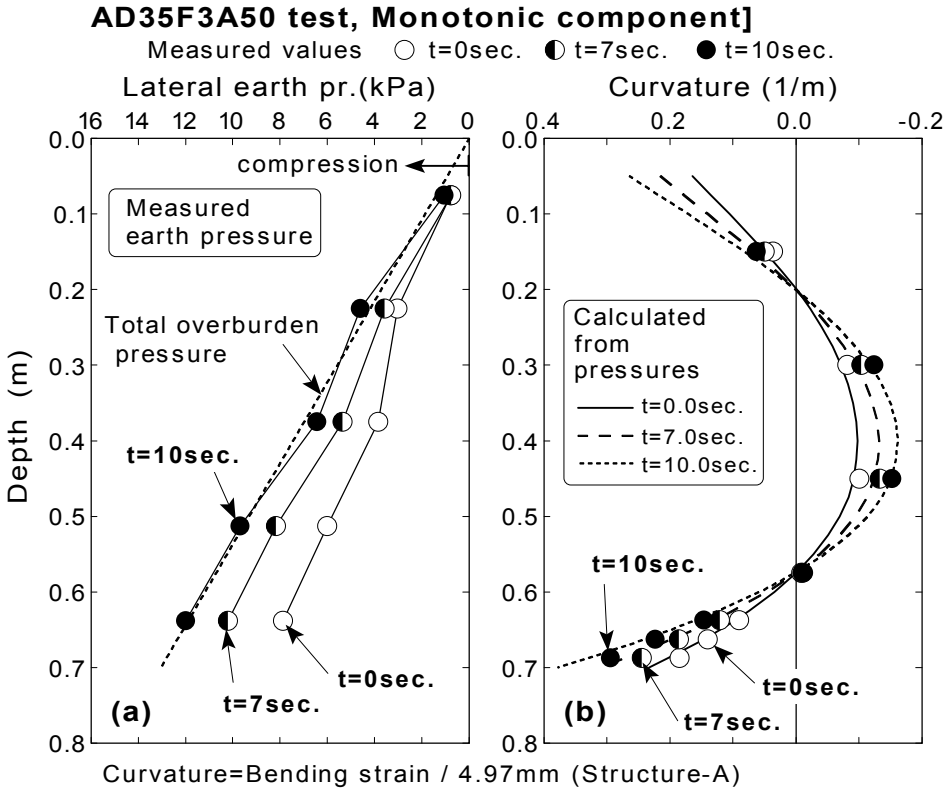

Fig.6.45: Comparison between the monotonic components of measured and calculated curvatures (typical result, AD35F3A50 test)

Results of tests with intense input motion

AD32F3A500 test (Structure-A)

The profile of calculated quantities from AD32F3A500 test are compared with measured curvatures in Fig.6.46. It is seen from Fig.6.46(a)(i) that earth pressure reaches initial total overburden pressure and soil liquefies at 3 seconds (2 seconds after the trigger of shaking). Good agreements are seen between measured and computed curvature as illustrated in Fig.6.46(a)(ii).

The profiles of earth pressure during liquefaction are illustrated in Fig.6.46(b)(i), and comparison between measured and calculated curvature is shown in Fig.6.46(b)(ii). It is observed that the profile of earth pressure does not change with time. It suggests that the state of liquefaction continues with shaking and no dissipation occurs in the backfill. No change with time is seen in the measured curvature. The good agreement is seen between measured and computed curvature.

BD36F3A500 test (Structure-B, before yielding of material)

The profile of calculated quantities from BD36F3A500 test are compared with measured curvatures in Fig.6.47. It is seen that earth pressure has reached the initial total overburden pressure through the depth at about 3 seconds (2 seconds after the trigger of shaking). In this test, the wall yielded initially at 2.7 seconds at the stem of the wall. Good agreements are seen between measured and computed curvature before shaking (t=0 sec.) and t=1.7 seconds as illustrated in Fig.6.47(b). It is seen that the measured curvature at 3 seconds becomes greater than that of calculated curvature. Since the behavior of structure is assumed to be in an elastic manner in the calculation, the curvature which has already yielded is evaluated smaller than that of actual one.

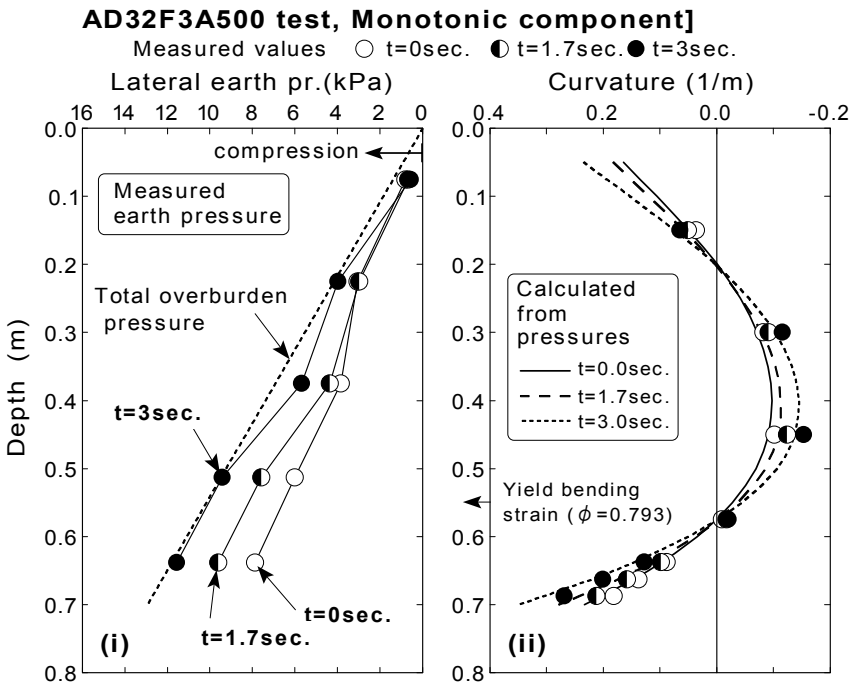

(a) Initial, 1.7 seconds and 3.0 seconds

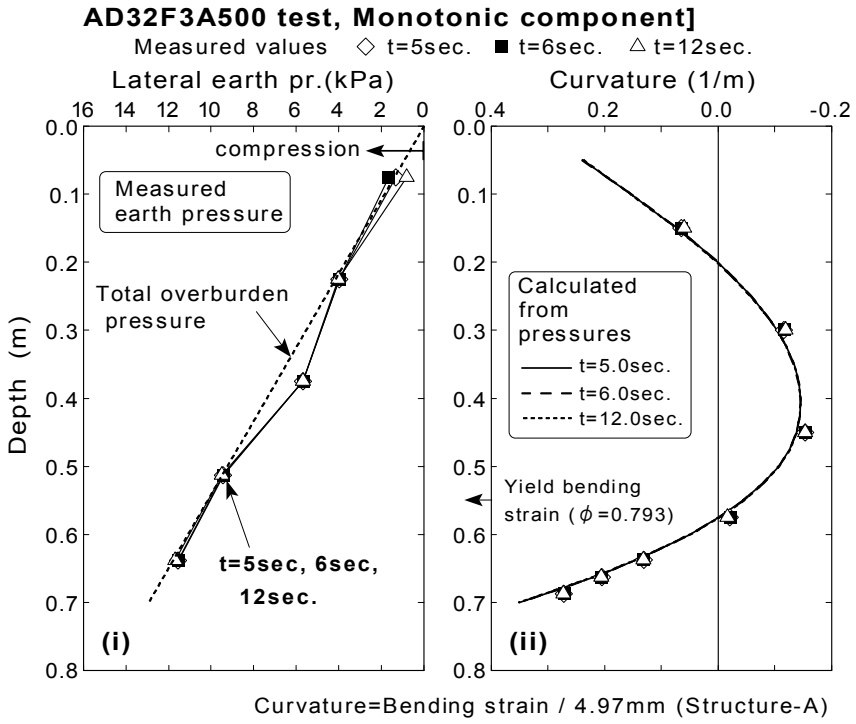

(b) 5.0 seconds, 6.0 seconds and 12.0 seconds (during liquefaction)

Fig.6.46: Comparison between the monotonic components of measured and calculated curvatures (intense input motion, AD32F3A500 test)

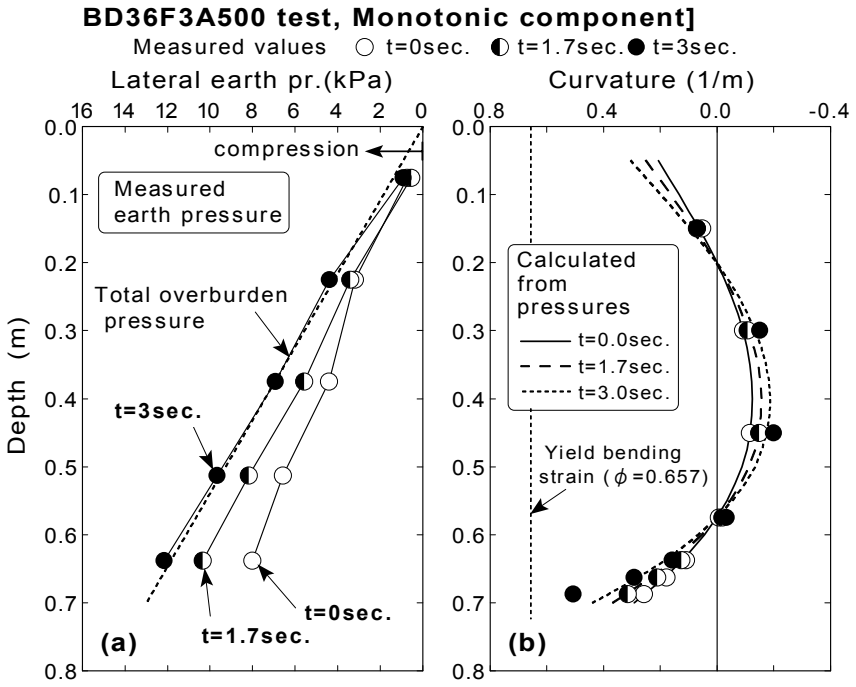

Fig.6.47: Comparison between the monotonic components of measured and calculated curvatures (intense input motion, BD36F3A500 test)

Results of tests with dense backfill (before yielding of material of structure)

AD67F3A500 test (relative density of 67%, Structure-A)

Fig.6.48(a) illustrates the results of calculation from AD67F3A500 test. The initial earth pressures have already exceeded the initial total overburden pressure in this test. Since AD67F3A500 test is the twelfth shaking of Model No.1, the backfill is compacted previously by shaking table tests and initial horizontal earth pressure has increased. In spite of this situation, the agreement between measured and calculated curvature seems good.

BD78F3A500 test (relative density of 78%, Structure-B)

The results of calculation from BD78F3A500 test are shown in Fig.6.48(b). Since the wall yields at 3.62 seconds in the test (see Table 6.5), profiles before this time is drawn in the figure. Since the initial earth pressure at the depth of 0.075m could not evaluated correctly by accumulation of residual earth pressure at each stage of shaking (see Table 3.21), the

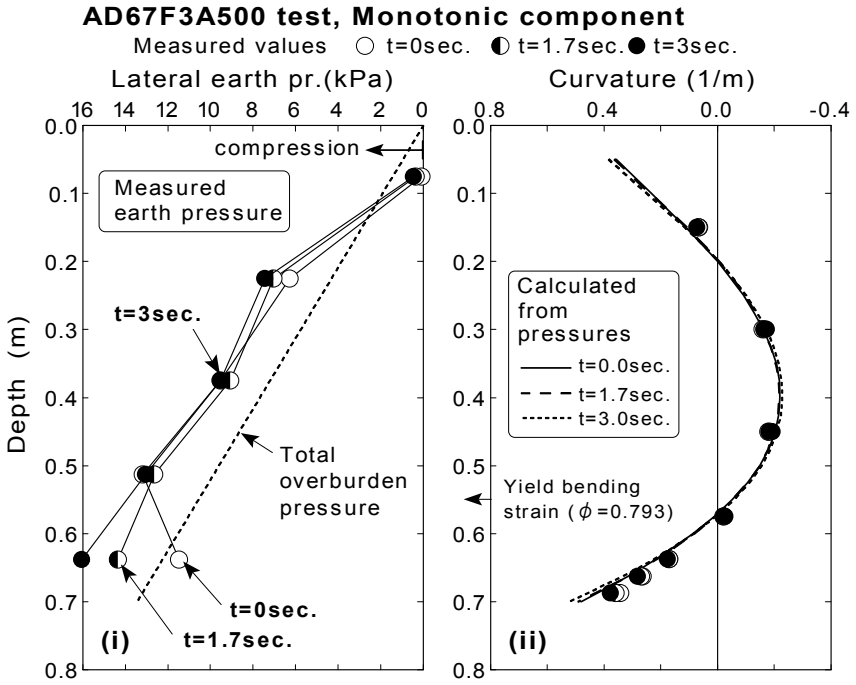

(a) AD67F3A500 test

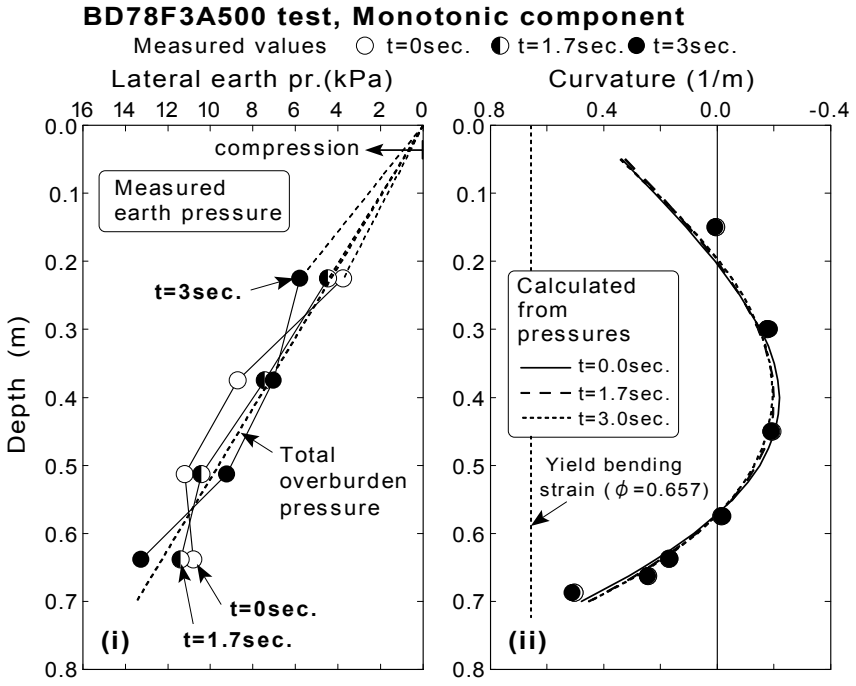

(b) BD78F3A500 test

Fig.6.48: Comparison between the monotonic components of measured and calculated curvatures (dense backfill, before yielding)

monotonic component of earth pressure became unreliable. In this respect, monotonic component of earth pressure at the depth of 0.075m was determined by linear interpolation between the surface and the depth of 0.225m (EP7) assuming the earth pressure at the surface as zero (see dotted line in Fig.6.48(b)(i)). It is seen that the calculated curvature from earth pressure agrees with measured curvature except for the curvature at 0.15m below tip.

The results of analysis suggest that the curvature of wall in box-shaped cross section of underground structure increases monotonically in accordance with monotonic component of earth pressure. It is possible that the monotonic component of curvature of wall can be evaluated quantitatively by evaluating the monotonic component of earth pressure considering build-up of excess pore water pressure as long as the structure behaves in an elastic manner.

Results from the other tests of AD39F5A50 test, AD41F3A200 test and AD61F3A200 test are presented in Fig.6.92～Fig.6.94 at the end of this chapter.

6.4.5 Analysis of fluctuating component of curvature

Fluctuating component of curvatures is calculated using Eqs.(6.35), (6.39), (6.40) and (6.41). Time histories of curvatures are derived at each measured point of bending strain at the left wall (see Fig.6.1), and profiles of curvature at selected time instance are drawn. The time when the structure undergoes resonance, and the backfill completely liquefies are selected for drawing of profiles.

Typical results (AD35F3A50 test)

Time histories of calculated curvature from AD35F3A50 test are compared with measured curvature in Fig.6.49. Measurement at 0.45m below tip at the right wall (SG10) is referred instead of measurement at the left wall (SG3) which is incorrectly measured. It is assumed that fluctuating component of curvature is identical between the left and the right wall (see Fig.6.18～Fig.6.22). It is observed that curvatures amplify during 7 seconds and 8 seconds through the depth. Based on the discussion made in Chapter 5, this amplification is due to resonance of the structure during liquefaction. (see Fig.5.10(a)).

Although it is difficult to recognize clearly because of noises of high frequency contents, phase difference can be seen before 6.5 seconds between the time history of calculated and measured curvature at 0.6875m below tip. In contrast, time histories of calculated and measured curvature are identical after 6.5 seconds. This suggests that the action of earth pressure has changed after 6.5 seconds. Further discussion on this phenomenon will be made later in this section refereeing deflection of wall.

Profiles of earth pressures and curvatures at resonance are presented in Fig.6.50(a), and during liquefaction in Fig.6.50(b). Profiles of earth pressure are shown in figure (i) in each figure. Those of measured curvature and curvature calculated from earth pressure are depicted in figure (ii). The time when the structure moved in positive (in the right) or negative (in the left) direction, and the displacement at the top of structure becomes zero between the time instances, are selected. Note that all the earth pressures and curvatures shown are fluctuating component. It is seen in Fig.6.50(a)(i) that the profile of earth pressure at 7.535 seconds when the structure displaced to the right, and profile at 7.725 seconds when the structure displaced to the left are almost symmetric. Absolute value of earth pressure amounts to about 0.8 kPa at the middle of the wall. Earth pressures at 7.630 seconds when the displacement at the top of structure is zero are seen to be small through the depth. The calculated curvature exceeds the level of 0.1 (1/m) at the stem of the wall. Calculated curvature from measured earth pressures at each time agrees with measured curvature very well through all the depth.

Fig.6.50(b) illustrates the results during complete liquefaction. Earth pressure is at the level of about 0.4 kPa, being approximately a half of earth pressure during resonance. Small earth pressures occur when displacement of structure is equal to zero (t=8.980sec). Curvatures calculated from those earth pressures are depicted in figure (ii), showing reasonable agreement with the measured curvatures. The good agreement between measured and computed curvature suggests that the fluctuating component of earth pressure on the wall and curvature as well as acceleration are internally consistent.

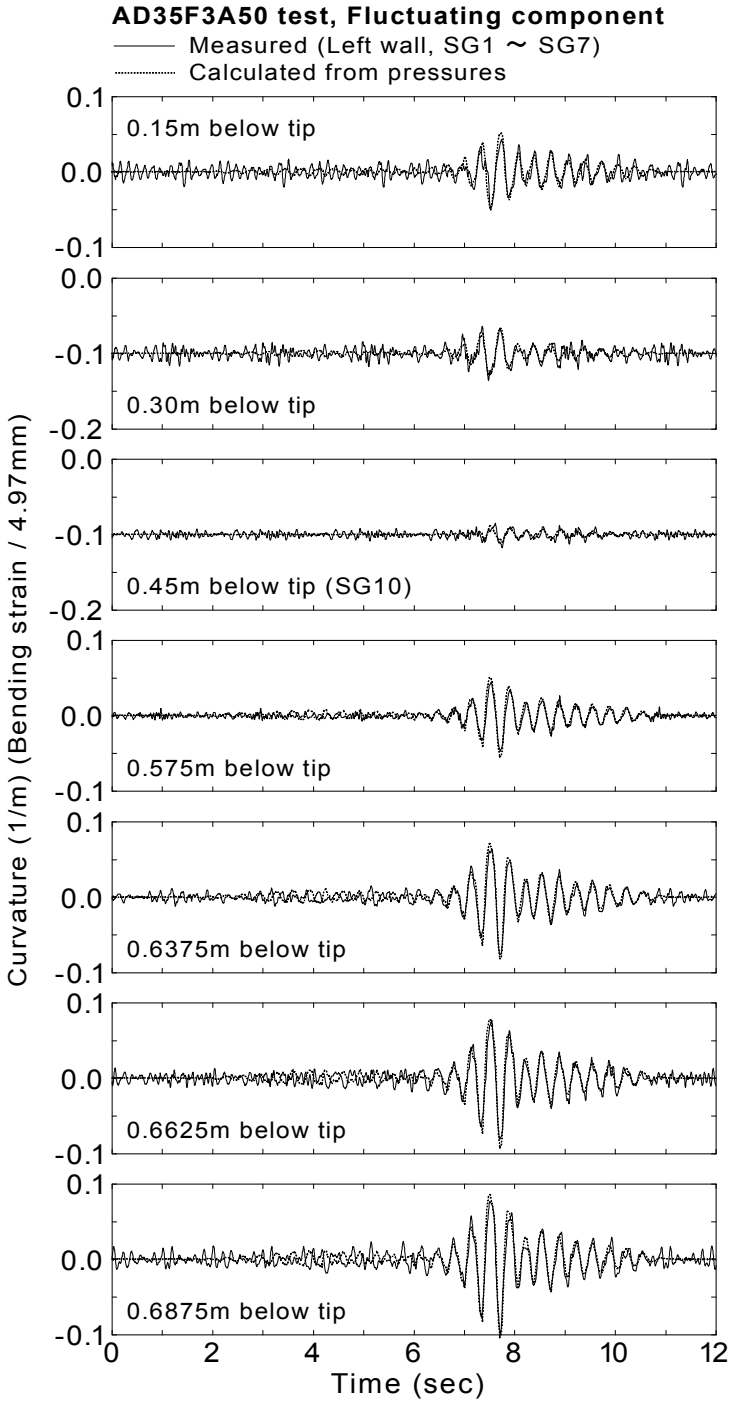

Fig.6.49: Comparison of time histories between fluctuating component of measured and calculated curvature (typical result, AD35F3A50 test)

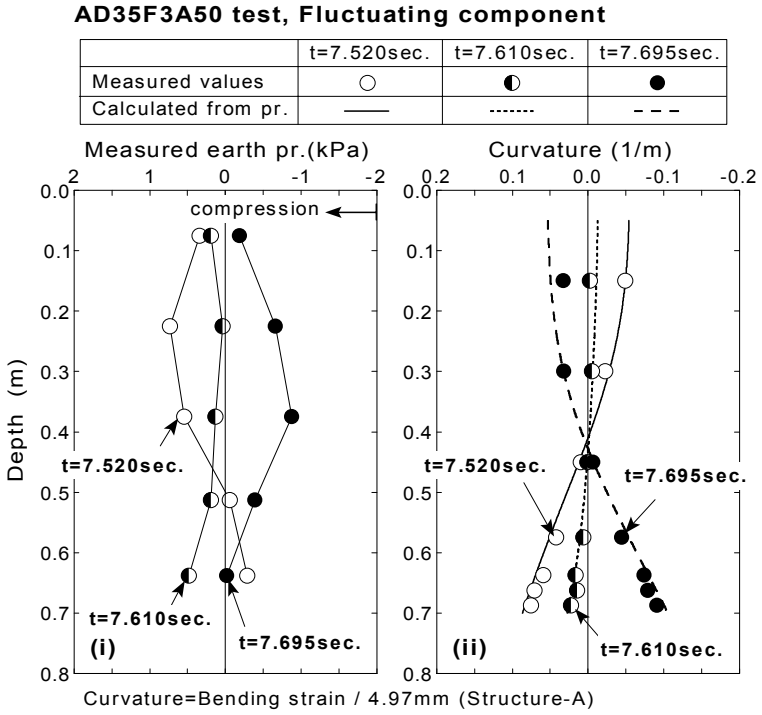

(a) Profiles at resonance of structure

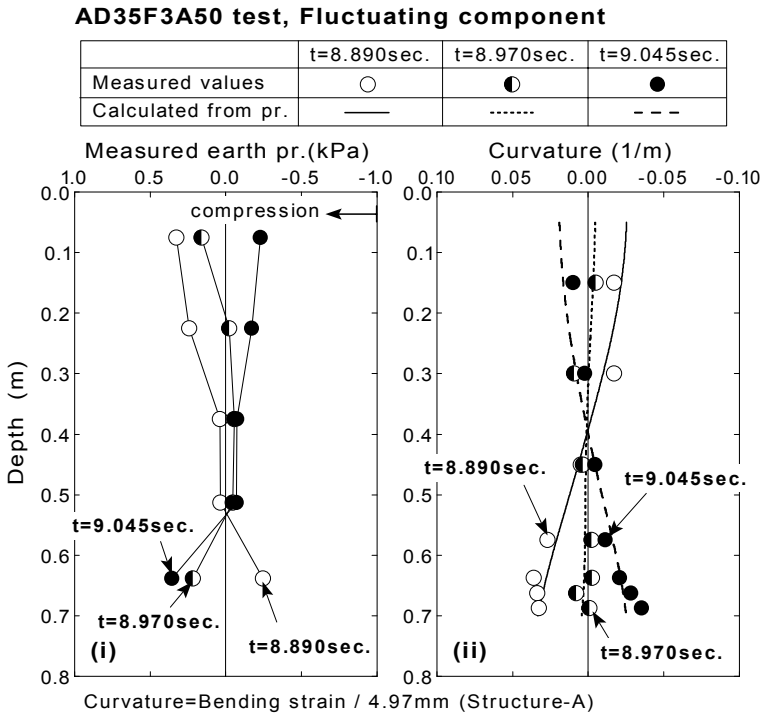

(b) Profiles during complete liquefaction

Fig.6.50: Comparison between fluctuating components of measured and calculated curvatures (typical result, AD35F3A50 test)

Results of tests with intense input motion

AD32F3A500 test (Structure-A)

Time histories of calculated curvature in AD32F3A500 test is compared with those of measured curvature in Fig.6.51. Since measurement was not obtained correctly at 0.45m below tip in the left wall (SG3) in this test, fluctuating component of curvature at the right wall (SG10) is used. The study in the previous chapter shows that the resonance occurs at about 2 seconds, and the backfill liquefies immediately after that (see, Fig.5.10(e)). No significant difference in both phase and amplitude can be observed between time histories of calculated curvature and measured curvature. The agreement between them is satisfactory. Only slight phase difference is observed after about 8 seconds, in which measured curvature delays slightly compared with the calculated curvature. This slight phase difference will be observed in results of tests which are shaken by either 2.0m/sec^2 or 5.0m/sec^2 of sinusoidal cycles. Anyhow, the reason of occurrence of slight phase difference in this test is not clear.

Profiles of earth pressure and calculated curvature as well as measured curvature from AD32F3A500 test during resonance and complete liquefaction are illustrated in Fig.6.52(a). The maximum earth pressure occurs at the top of wall when the structure deforms toward either the left or the right direction, amounting to about 2 kPa during resonance and 4 kPa during complete liquefaction. The response during complete liquefaction is larger than response at resonance in this test. In general, responses at resonance are larger than those during complete liquefaction (e.g. aforementioned result from AD35F3A50 test, see Fig.6.50). It is noted that amplitude of input motion at resonance (2.0seconds~2.3seconds) is about 2.0m/sec^2, while during complete liquefaction (7.7seconds~8.0seconds) is 5.0m/sec^2 in AD32F3A500 test (see Fig.3.19). Large input motion during liquefaction may cause the occurrence of larger earth pressure than that at resonance.

Comparison of calculated curvature and measured curvature along the depth is shown in the figures (ii) in Fig.6.52(a) and (b). Agreement is quite well both at resonance (figure (a)(ii)) and during liquefaction (figure (b)(ii)).

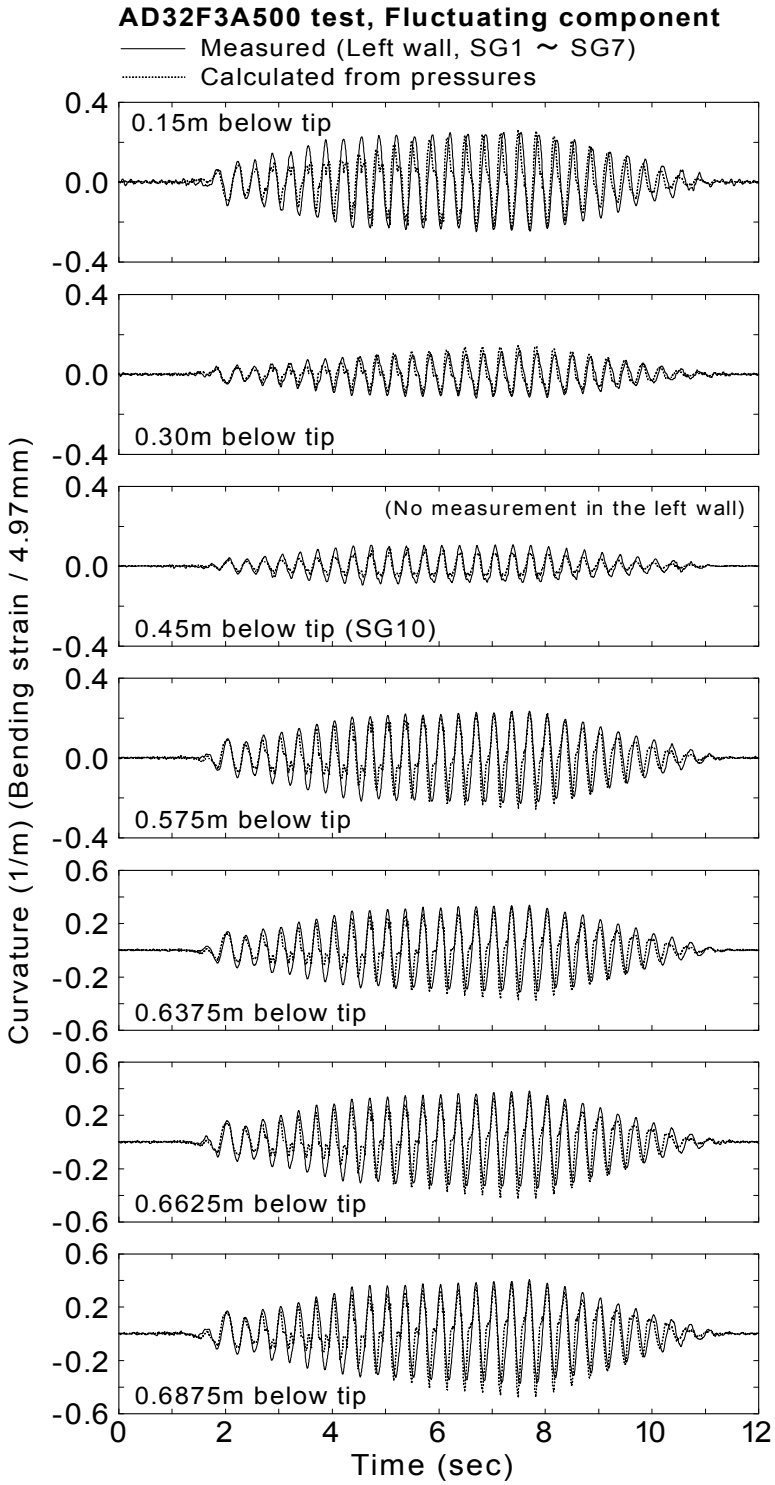

Fig.6.51: Comparison of time histories between fluctuating components of measured and calculated curvatures (intense input motion, AD32F3A500 test)

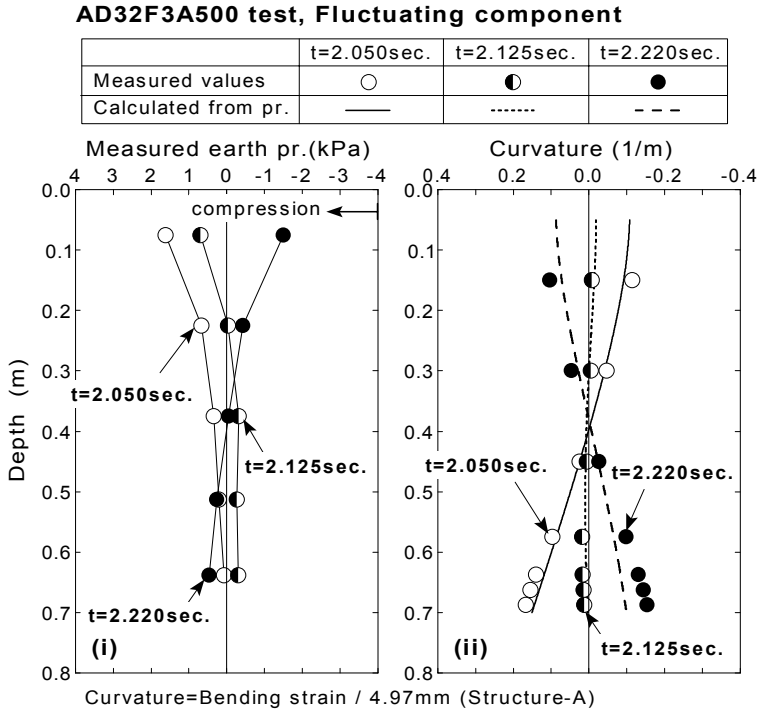

(a) Profiles at resonance of structure

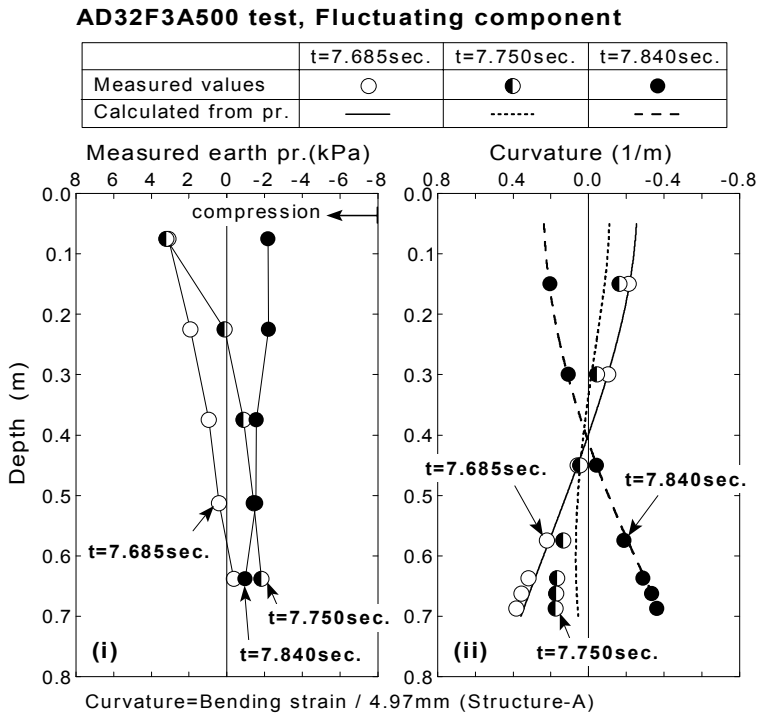

(b) Profile during complete liquefaction

Fig.6.52: Comparison between fluctuating components of measured and calculated curvatures (intense input motion, AD32F3A500 test)

BD36F3A500 test (Structure-B, before yielding of material)

Time histories of calculated curvature in BD36F3A500 test, in which the material yield during shaking, is compared with those of measured curvature in Fig.6.53. The study in the previous chapter unveiled that the resonance occurs at about 1.8 seconds, and the backfill liquefies immediately after that (see, Fig.5.10(f)). Further more, the initial yield of the wall occurred at 2.7 seconds. It is seen that time histories of calculated curvature are almost identical with measured curvature before initial yielding. It is interesting that the agreement of both time histories is still good after initial yield of wall.

Fig.6.54 illustrates profiles of earth pressures and curvatures at selected time during resonance of structure from BD36F3A500 test. Since selected time is before 2.7 seconds of initial yield (after initial liquefaction at 2.0 seconds, see Table 5.1), the behavior of structure is in an elastic region. Earth pressure at upper portion of wall is larger than at the lower portion, being similar to the aforementioned result from AD32F3A500 test (see Fig.6.52). According to a previous experimental study on dynamic pressures on a rigid wall during liquefaction (Tuchida, 1968), the maximum pressure occurs at the bottom of wall and pressure becomes smaller as the depth decreases (see Fig.1.7). It is noted that the distribution of earth pressure in this series of tests is quite different from a distribution of dynamic pressure on a rigid wall. This suggests that a flexibility of a structure affects a profile of earth pressures during earthquakes. Further discussion on the profile of dynamic earth pressure on a flexible wall will be made in Chapter 8, comparing with dynamic pressures on a rigid wall.

Agreement between calculated and measured curvature is very good. The fact of good agreement between measured and calculated curvature means that curvature of wall of underground structure can be evaluated from fluctuating component of earth pressure both during resonance in the process of liquefaction and during complete liquefaction. The theoretical method to evaluate fluctuating component of earth pressure will be presented in Chapter 8.

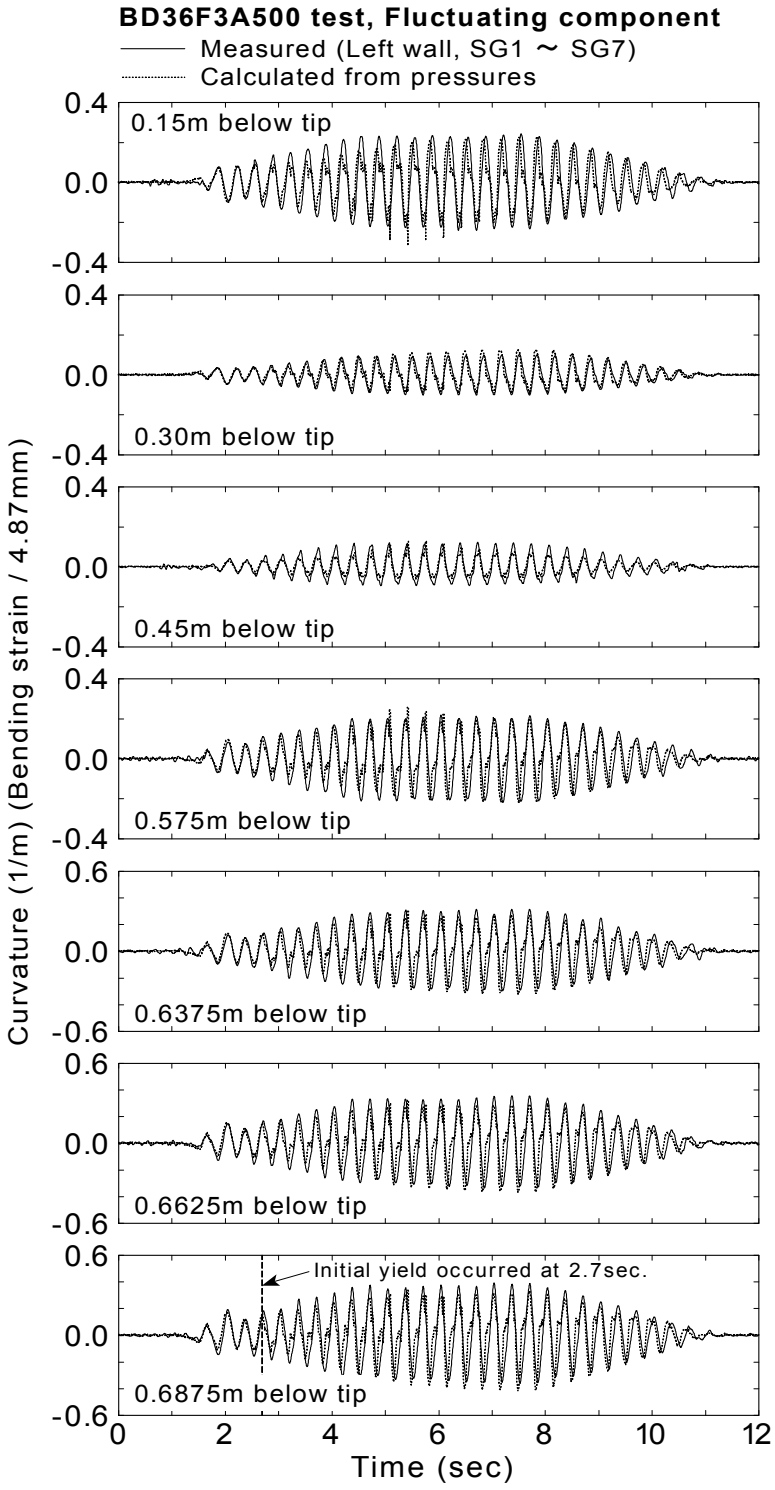

Fig.6.53: Comparison of time histories between fluctuating components of measured and calculated curvatures (intense input motion, BD36F3A500 test)

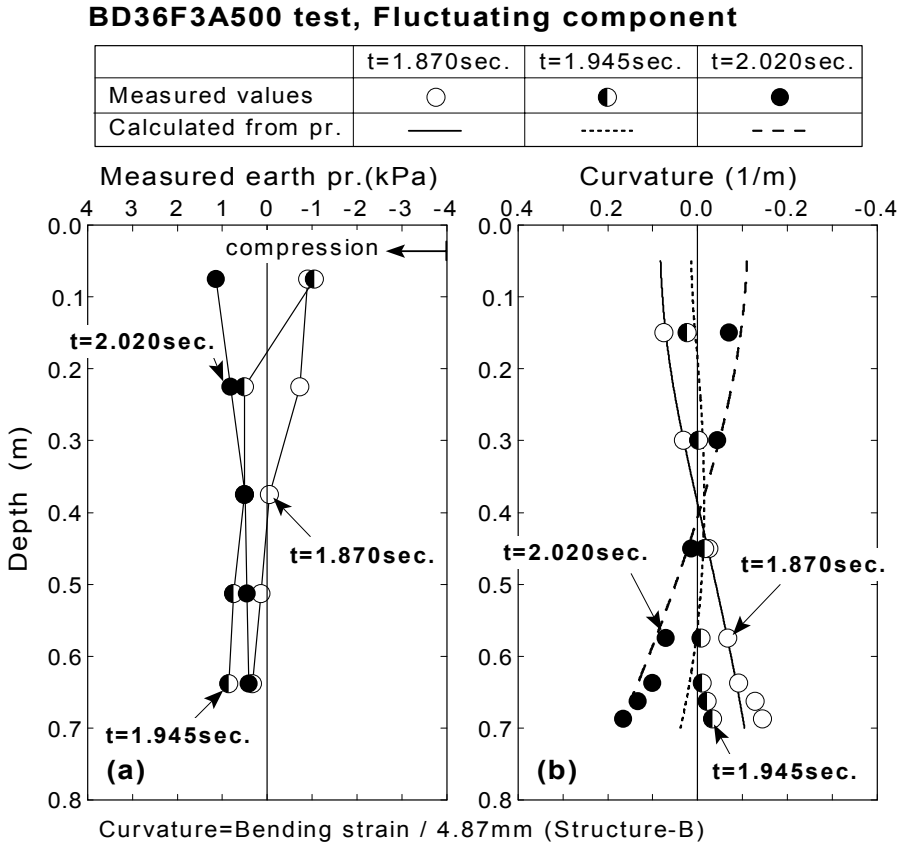

Fig.6.54: Comparison between fluctuating components of measured and calculated curvatures (intense input motion, BD36F3A500 test)

Results of tests with dense backfill (before yielding of material)

AD67F3A500 test (relative density of 67%, Structure-A)

Fig.6.55 depicts the results from AD67F3A500 test with dense backfill of relative density at 67%. Resonance occurs at about 2 seconds (Fig.5.10(g)) and the wall yields initially at 3.69 seconds (see Fig.6.7), indicating the time of initial yielding in the time history of 0.6875m below tip. Agreement between calculated and measured time histories seems well. In contrast, some disagreements are seen at the initial of shaking, being pointed by circles in the figure. The same feature of disagreements at the initial of shaking or before resonance was observed in AD61F3A200 test (see Fig.6.97). But it was not observed in AD32F3A500 test and BD36F3A500 test in which loose backfill was used (see Fig.6.51, Fig.6.53). It is inferred that this phenomenon could occur in tests with dense backfill.

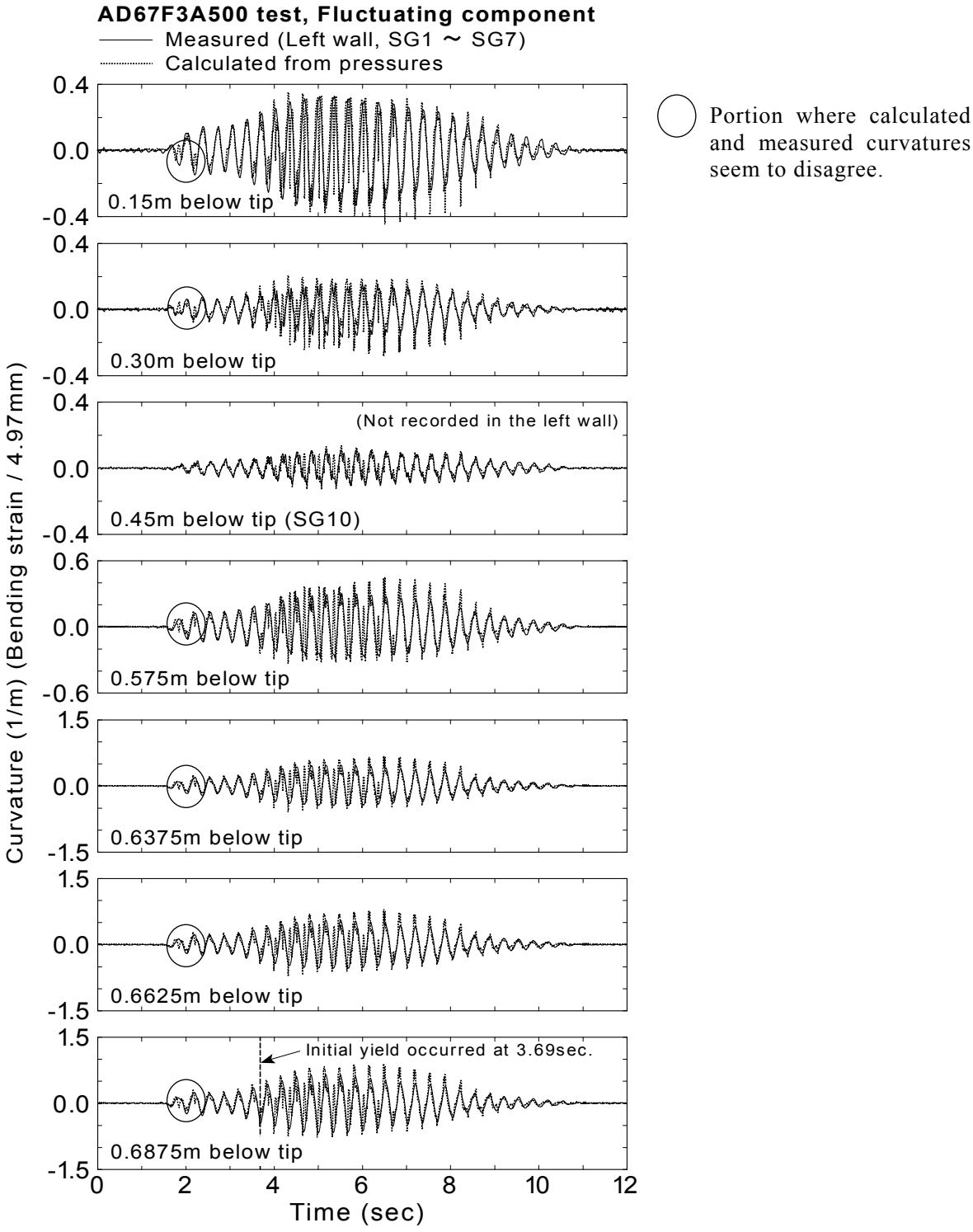

Fig.6.55: Comparison of time histories between fluctuating components of measured and calculated curvatures (dense backfill, AD67F3A500 test)

Profiles of earth pressure and calculated curvature as well as measured curvature from AD67F3A500 test during resonance and liquefaction before yielding of material are illustrated in Fig.6.56. Not like a profiles of loose backfill, the earth pressure at the deep portion of backfill is larger than that at the shallow portion. Although the reason is not clear, the similar feature appears before resonance. Comparison of calculated curvature and measured curvature along the depth is shown in the figures (ii) in Fig.6.56(a) and (b). Agreement is reasonable both at resonance and during liquefaction.

BD78F3A500 test (relative density of 78%, Structure-B)

Fig.6.57 illustrates the results from BD78F3A500 test with the densest backfill of relative density at 78% in this series of tests. Resonance due to liquefaction of backfill did not occur because of the high initial density (Fig.5.4(h)). Initial yielding of wall occurred at 3.62 seconds (see Fig.6.9). It is characterized in this calculation that curvature calculated from earth pressure does not agree with measured curvature at all during an elastic behavior of structure. This kind of disagreement has been seen partially in AD67F3A500 test, in which denser backfill is used. Since soil behaves in a dilative manner through the duration time in BD78F3A500 test (see time history of pore pressure ratio in Fig.4.116), the occurrence of disagreement between measured and calculated curvature is possibly related to a dilative behavior of dense soil. It is considered that the evaluation of curvature of wall from the earth pressure is difficult when the soil behaves in a dilative manner.

Profiles of measured and calculated values from BD78F3A500 test are depicted in Fig.6.58. It is seen that the earth pressure distribution is very complicated. In addition, the fluctuating component of calculated curvature does not agree with the measured curvature at all. It suggests that the procedure of calculation is not valid for the underground structure with dense backfill which exerts the significant dilative behavior.

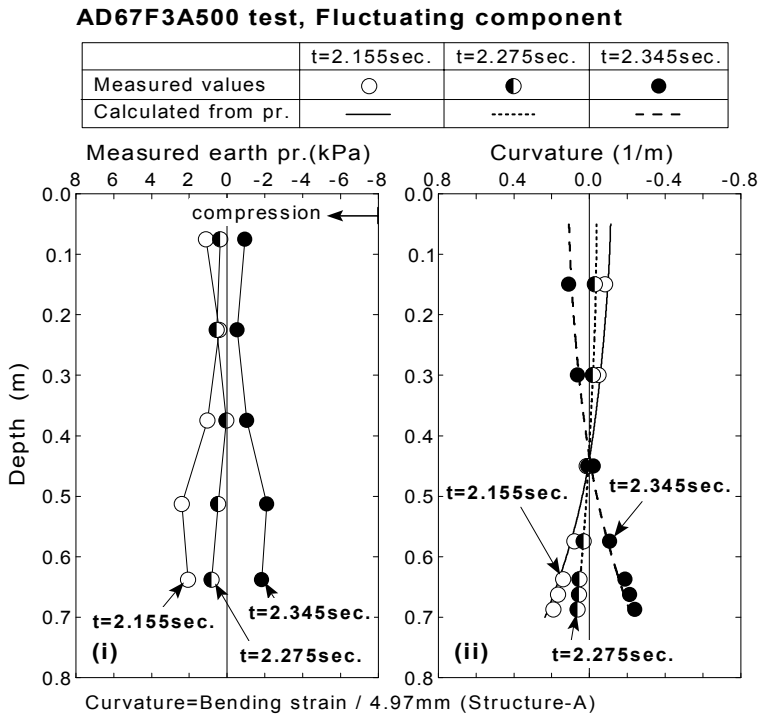

(a) Profiles at resonance of structure

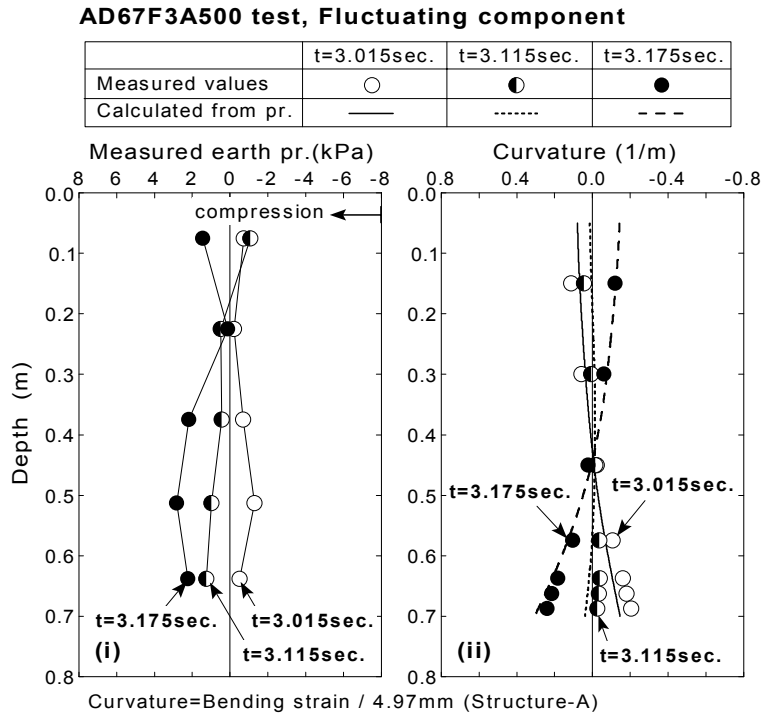

(b) Profile during complete liquefaction

Fig.6.56: Comparison between fluctuating components of measured and calculated curvatures (dense backfill, AD67F3A500 test)

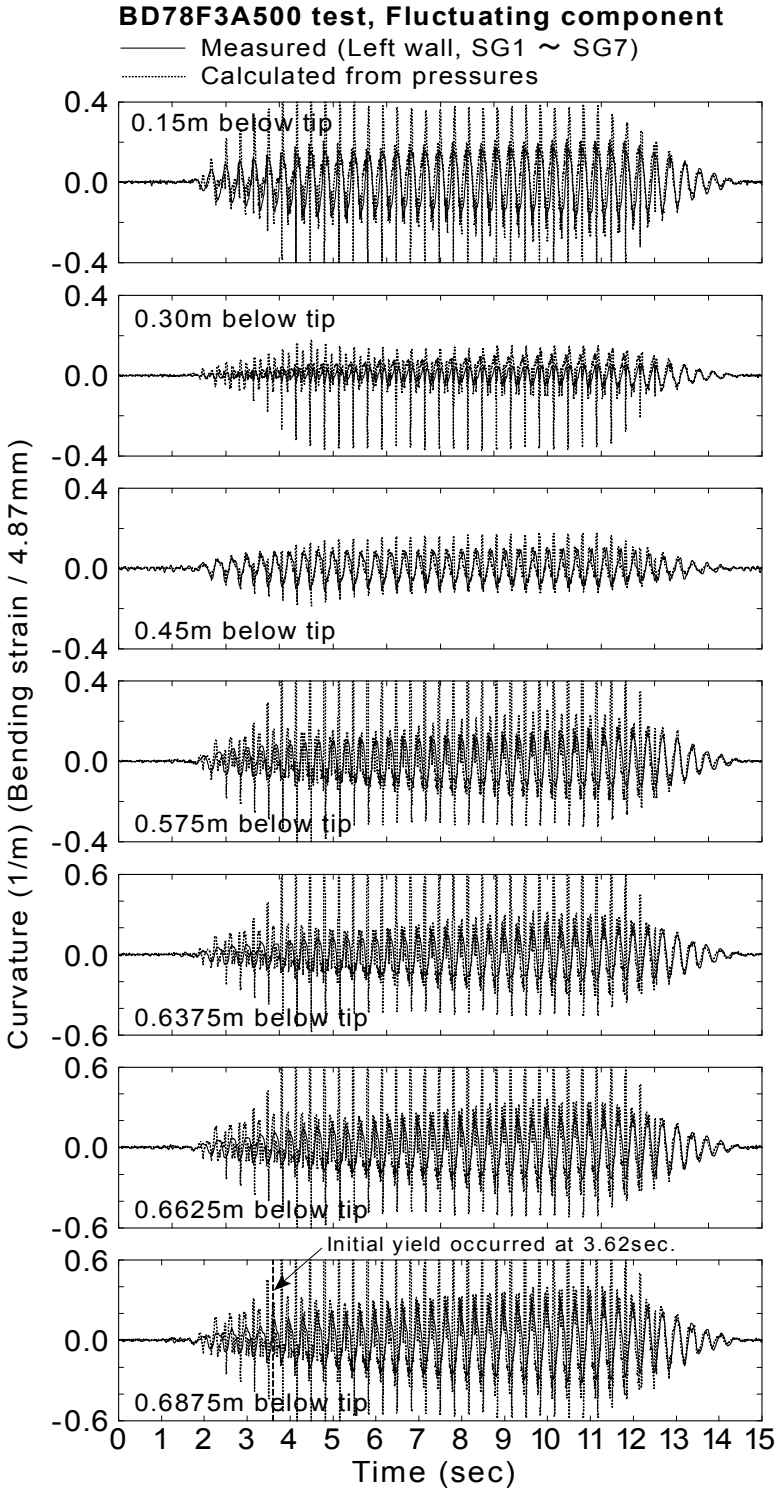

Fig.6.57: Comparison of time histories between fluctuating components of measured and calculated curvatures (dense backfill, BD78F3A500 test)

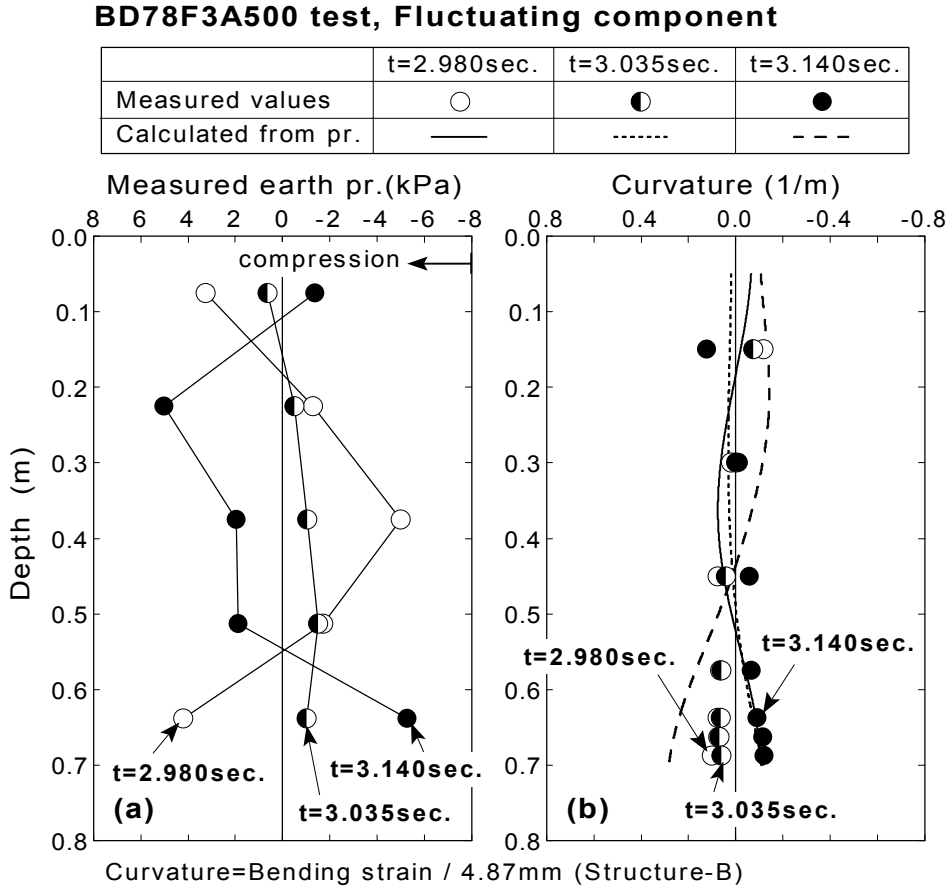

Fig.6.58: Comparison between fluctuating components of measured and calculated curvatures (dense backfill, BD78F3A500 test)

Time histories of curvatures at each portion of wall from the other tests are presented in Fig.6.95～Fig.6.97 at the end of this chapter. The profiles are shown in Fig.6.98～Fig.6.100.

6.4.6 Analysis of deflection of wall

Deflection of the wall of structure is calculated considering both monotonic and fluctuating component as

$$u(z,t) = u_{mono.}(z,t) + u_{fluc.}(z,t) \tag{6.46}$$

where $u_{mono.}(z,t)$ is the monotonic component of deflection (see Eq.(6.20)), and $u_{fluc.}(z,t)$ is the fluctuating of component of deflection (see Eq.(6.42)). Profiles of deflection are also drawn for selected time instances. Time when peak acceleration occurs at the top of the structure (AC2) was chosen to select the time for drawing profiles. The time instances are selected from each state of soil-structure model which are illustrated in Fig.6.59 as

(i) when the structure undergoes resonance
   1. Amplification is the maximum of 2.5～3.0
   2. Phase difference is approximately 90 degrees.
   3. Natural frequency of backfill is lower than about 0.4 times (or 0.67 times) that of the structure (0.4×7.5Hz＝3Hz, 0.67×7.5Hz＝5Hz).

(ii) when the backfill completely liquefies
   1. Amplification is 1.0～1.5.
   2. Phase difference is 120～150 degrees.
   3. Natural frequency of backfill is almost zero.

(iii)before the resonance
   1. Amplification is around 1.0.
   2. Phase difference is about zero.
   3. Natural frequency of backfill is higher than 0.4～0.67 times that of the structure.

Changes of phase difference between the top and the bottom were presented in Fig.5.4 in Chapter 5. Selected time in each test is summarized in Table 6.6.

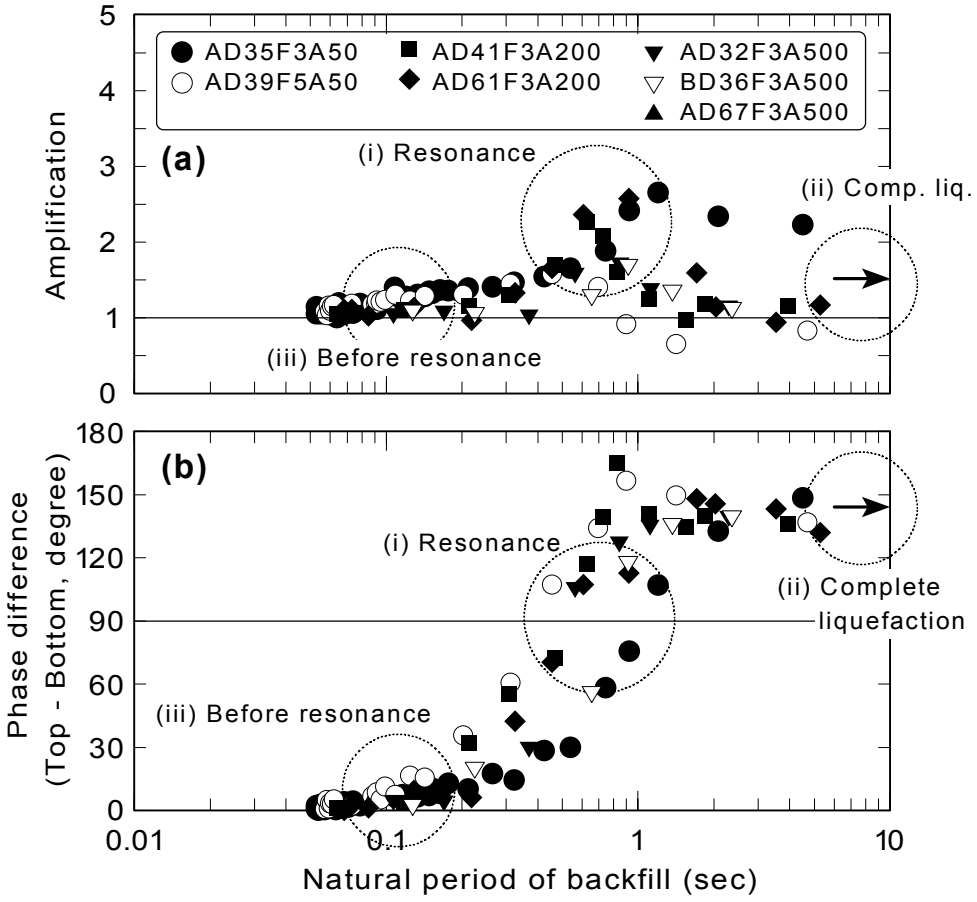

Fig.6.59: Different state of soil-structure model during shaking

Table 6.6: Selected time for drawing profiles (peak time of acc. at the top, AC2)

	Test case	Before resonance (Initial of shaking) (iii)	At resonance (Max. amplification) (i)	During complete liquefaction (ii)
Typical test	AD35F3A50	4.085 sec.	7.520 sec.	8.890 sec.
Test of intense input motion	AD32F3A500	1.465 sec.	2.050 sec.	7.685 sec.
	BD36F3F500	1.480 sec.	1.870 sec.	7.355 sec.*1
Test with dense backfill	AD67F3A500	1.470 sec.	2.155 sec.	3.015 sec.
	AD67F3A500	-	5.165 sec.*2	-
	BD78F3A500	1.800 sec.	-*3	(10.980 sec.)*4
Other tests (Test of repeated shaking)	AD39F5A50	2.870 sec.	3.320 sec.	5.125 sec.
	AD41F3A200	1.930 sec.	2.690 sec.	6.015 sec.
	AD61F3A200	2.265 sec.	3.200 sec.	6.075 sec.

*1 material yielded *2 second resonance *3 The resonance did not occur
*4 behavior in a dilative manner

Typical results (AD35F3A50 test)

Calculated time histories of deflection at the top, $u(0,t)$ from tests of initial shaking in Model No.1 (AD35F3A50 test) are compared with measured displacement at the top of structure (LV1) in Fig.6.60 Significant amplification of displacement is seen at about 7.5 seconds. It was demonstrated in Chapter 5 that this is due to resonance of structure. Phase difference between calculated and measured displacement is clearly observed during 2 seconds to 6 seconds. This time period coincides the time period when the disagreement was observed in time history of curvature in this test (see Fig.6.49). In contrast, both time histories are almost identical after 6 seconds.

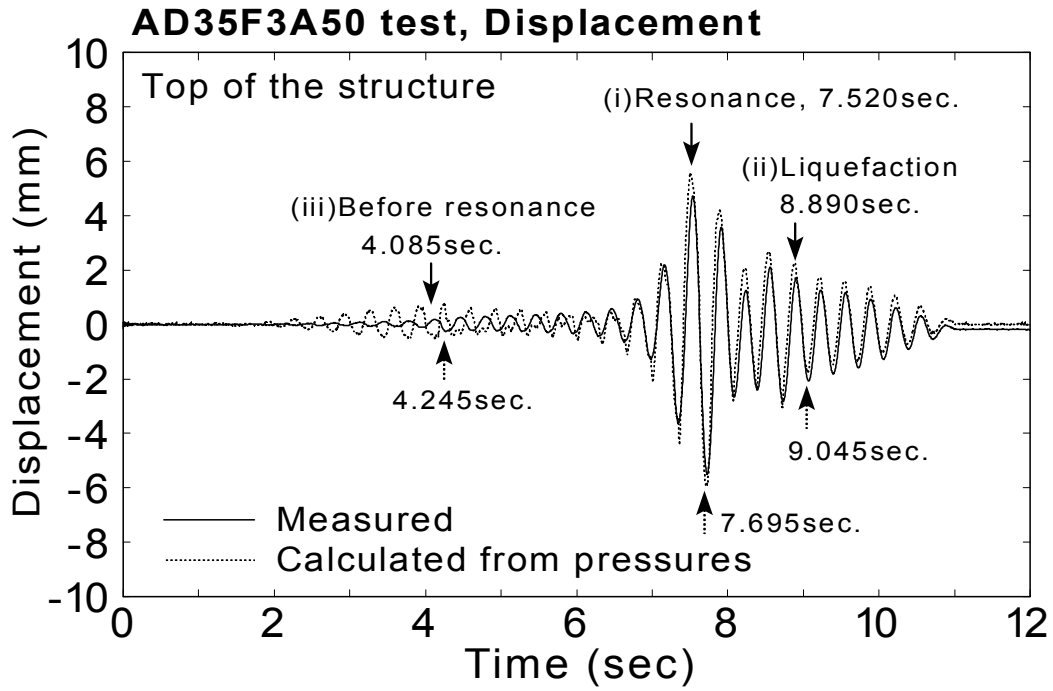

Fig.6.60: Comparison of time histories between measured and calculated displacement (Tests of initial shaking, AD35F3A50 test)

Profiles of earth pressure and deflections at the time of peak amplification (t=7.520seconds) and a half cycle after resonance (t=7.695seconds) are illustrated in Fig.6.61. The profiles of measured earth pressure and monotonic component of earth pressure are illustrated in figure (i) in Fig.6.61(a) and (b). Only the fluctuating component of earth pressure, which is derived as the difference between measured earth pressure and monotonic component, is depicted in figure (ii).

Profile of measured deflection (derived by integrating bending strains) is compared with the deflection calculated from earth pressure in figure(iii). Note that both monotonic and fluctuating component is considered for the deflection.

It is observed in Fig.6.61(a)(i) that measured earth pressure (solid line with circler symbol) is larger than the monotonic component of earth pressure (dotted line) at the portion shallower than the depth of about 0.5m. In this respect, fluctuating component of earth pressure becomes positive at the portion, meaning that the soil pushes the structure in the right direction. Consequently, the displacement of wall is calculated as positive at its top. The maximum deflection of wall is observed to occur at the depth of 0.3m. This is the effect of monotonic component of earth pressure. It is seen that the calculated deflection is consistent with that of measured deflection, which was derived by integration of measured bending strain.

It is observed in Fig.6.61(b)(i) that measured earth pressure is smaller than the monotonic component of earth pressure through the depth. Therefore, fluctuating component of earth pressure is calculated as negative. Consequently, the displacement of wall is calculated as negative at its top. It is seen that the calculated deflection is consistent with that of measured deflection. It suggests that the fluctuating component of earth pressure acts on the wall in the left direction as if the earth pressure pulls the wall to the left. Furthermore, Fig.6.61 suggests that the validity of the procedure to calculate deflections could be verified at the resonance due to liquefaction.

Calculated deflection during complete liquefaction is compared with measured deflection in Fig.6.62. It is observed in Fig.6.62(a)(i) that the fluctuating component of earth pressure is about 0.35kPa at the top and -0.2kPa at the bottom, resulting in displacement of 2mm at the top of the structure. The calculated deflection is consistent with the measured deflection through the depth. It is seen that the profile of fluctuating component of earth pressure in positive displacement at the top (Fig.6.62(a)(ii)) is approximately symmetric with that of negative displacement (Fig.6.62(b)(ii)). The measured displacement amounts to about –2mm at the top. It is observed that the calculated deflection is reasonably consistent with measured deflection. It suggests that the deflection of wall of underground structure can be calculated from both monotonic and fluctuating component of earth pressure.

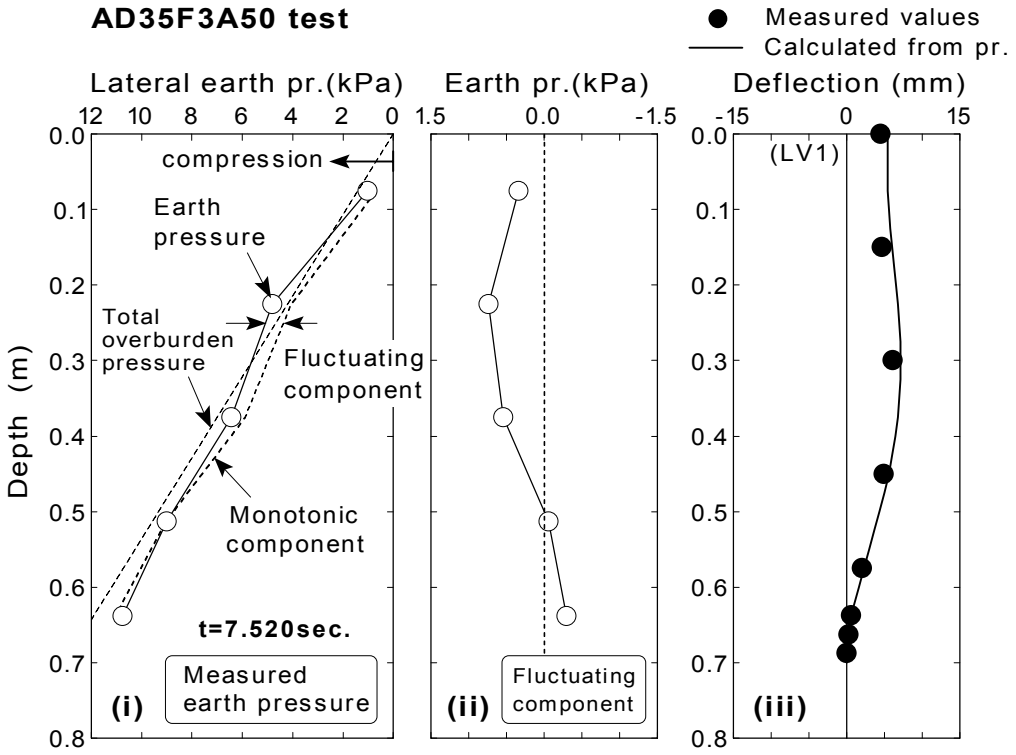

(a) At resonance (t=7.520 seconds)

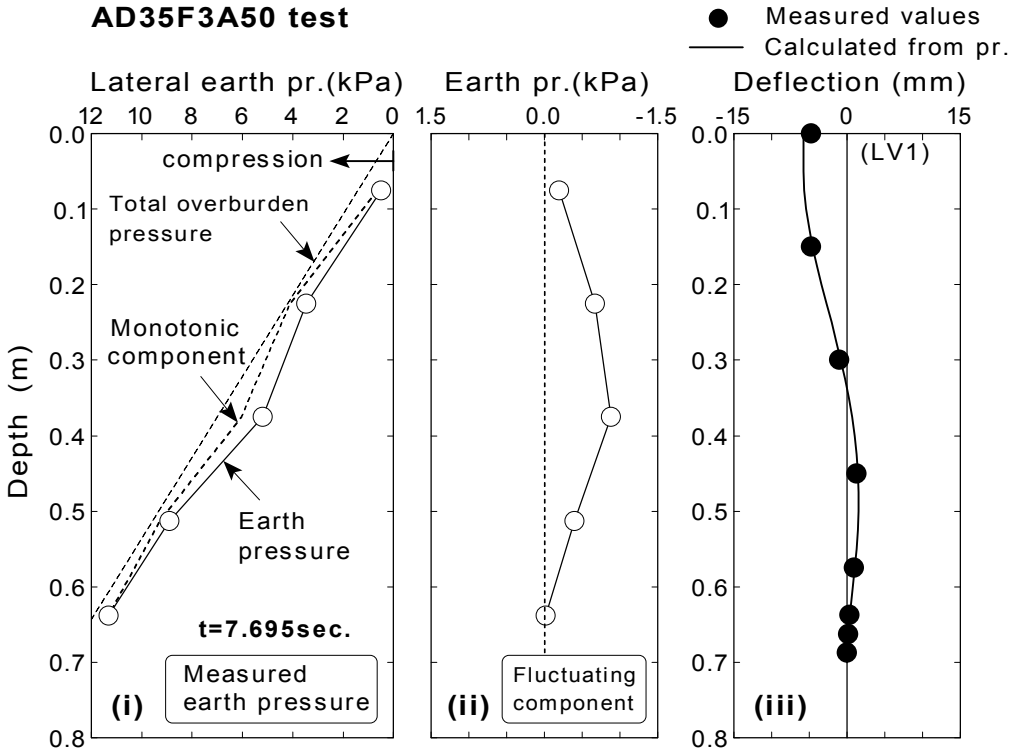

(b) A half cycle after resonance (t=7.695sec.)

Fig.6.61: Earth pressure and deflection (AD35F3A50 test, at resonance)

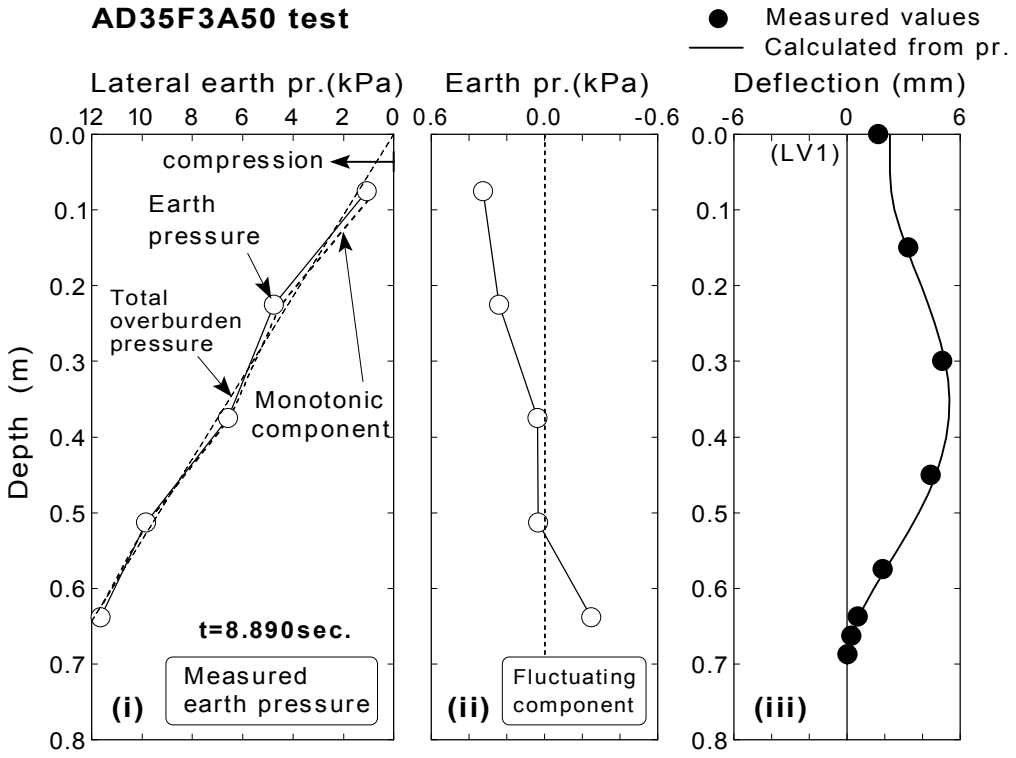

(a) t=8.890 seconds

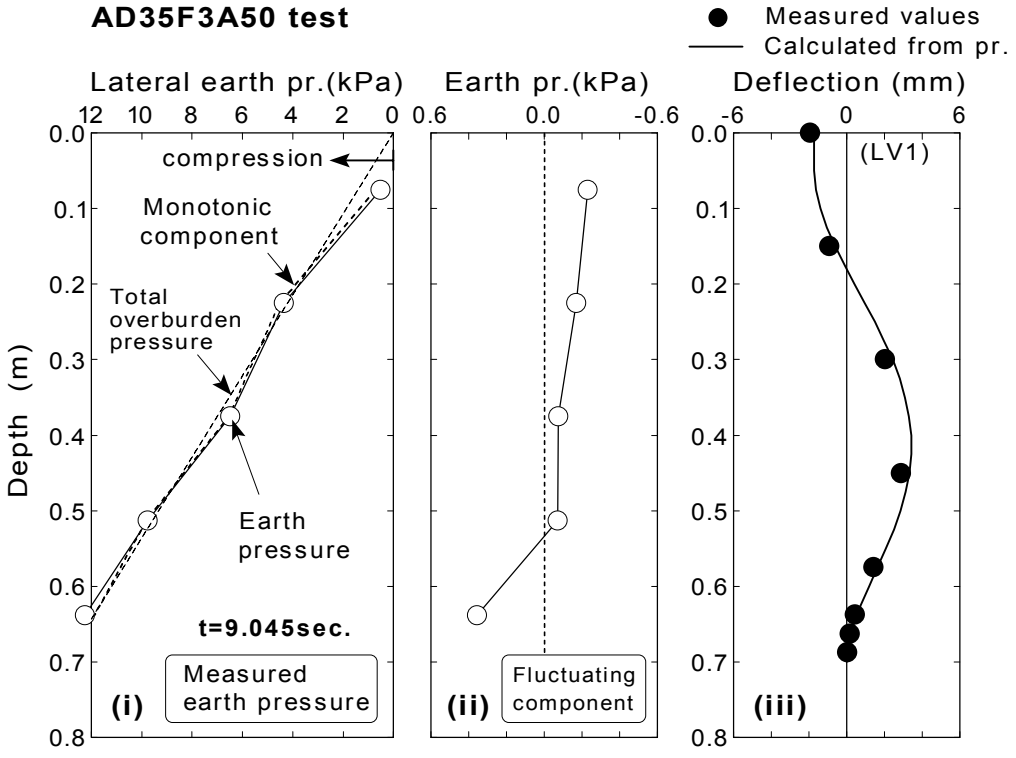

(b) t=9.045 seconds

Fig.6.62: Earth pressure and deflection (AD35F3A50 test, during liquefaction)

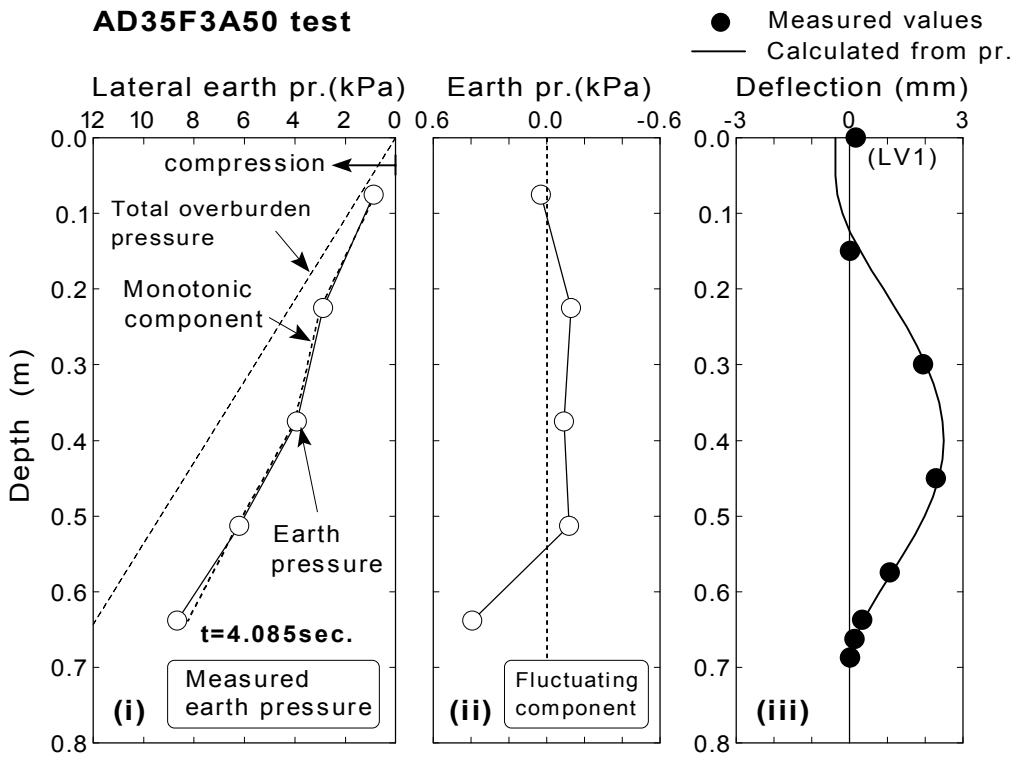

(a) t=4.085 seconds

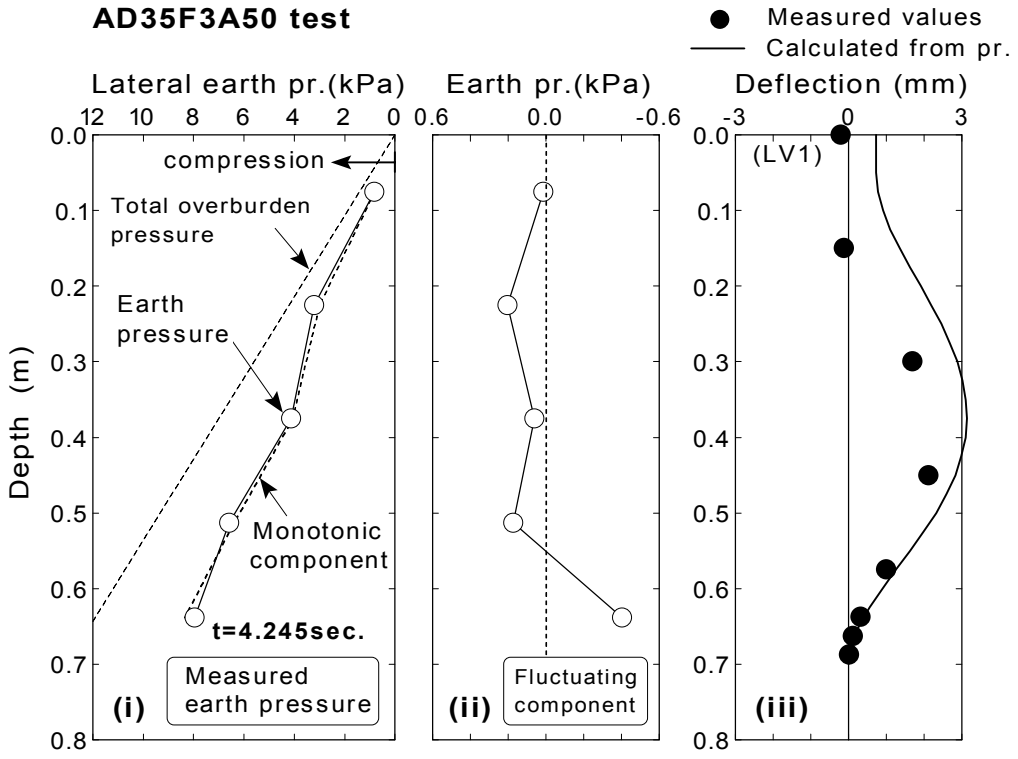

(b) t=4.245 seconds

Fig.6.63: Earth pressure and deflection (AD35F3A50 test, before resonance)

Fig.6.63 illustrates the earth pressures and comparison of deflection before resonance, when little excess pore water pressure of approximately 5.0% builds up. It is seen in Fig.6.63(a)(i) that fluctuating component of earth pressure is positive between the depth of 0.1m and 0.5m. In the calculation, the fluctuating component of earth pressure acts on the structure to move in the right direction. Therefore, positive value of fluctuating component of earth pressure results in the positive displacement at the top in calculation. Observing the measured deflection in Fig.6.63(a)(iii), however, it is seen that displacement at the top of the structure and at the depth of 0.15m occurs in the negative direction. This means that the flexible underground structure pushes the backfill which has not become soft yet. Actually, the natural frequency of backfill is higher than that of the structure in this time period of 4.115 seconds to 4.265 seconds (see Fig.5.12(a)(i)). It shows that the fluctuating component of earth pressure acts on the structure as a reaction when the backfill is harder than the structure.

In contrast, the earth pressure is assumed to push the structure always in the calculation. In this respect, calculated deflection cannot be consistent with the measured deflection. It is seen that in Fig.6.63(b), measured deflection and calculated deflection at the top of the structure is not consistent. Detailed mechanism of action of earth pressure will be discussed in the following chapter.

Results of the test with intense input motion

AD32F3A500 test (Structure-A)

Calculated time histories of deflection at the top from tests of initial shaking in Model No.2 (AD32F3A500 test, see Table 6.5) are compared in Fig.6.64 with measured displacement at the top of structure. Although calculated displacement is seen to be slightly smaller than measured displacement in the time period of 3 seconds to 5 seconds, agreement of time histories are satisfactory.

Based on the examination in Chapter 5, the resonance occurred at 2.050 seconds at the top of the structure (AC2). Profiles of earth pressures as well as measured and calculated deflection of wall at resonance are illustrated in Fig.6.65(a). It is seen that the fluctuating component of earth pressure is positive and the top of the structure moves in the right

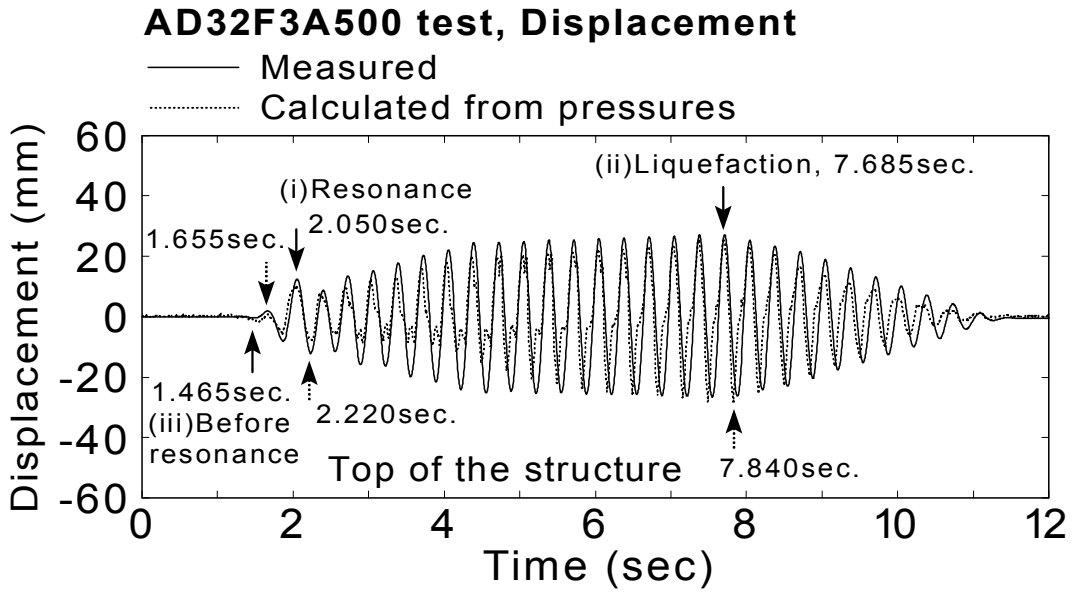

Fig.6.64: Comparison of time histories between measured and calculated displacement (intense input motion, AD32F3A500 test)

direction. It indicates that the backfill pushes the structure in the right direction. The agreement between the calculated and measured deflection is very good through the depth. It suggests that the amount of deflection can be predictable from earth pressures at resonance.

The result of a half cycle after the resonance is depicted in Fig.6.65(b). In contrast with the time of resonance, calculated deflections are rather smaller than those measured. Referencing the fluctuating component of earth pressure which is illustrated in figures (ii) in Fig.6.65, it is seen the profile of earth pressure in the negative direction (t=2.220 seconds) is slightly smaller than that of positive direction (t=2.050 seconds). This slight asymmetricity made the calculated deflection smaller than the measured deflections.

Fig.6.66 shows the results during liquefaction. Not only profiles in the positive displacement but also negative displacement are illustrated. Although the calculated deflection is slightly smaller than that of measured deflection at 7.840 seconds in the negative displacement, agreement between the calculated and measured deflection is very good at 7.685 seconds in the positive direction.

Calculated deflection before resonance is compared with measured deflection in Fig.6.67. At this moment, deflection due to monotonic component of earth pressure, which is about 3mm at the depth of 0.4m, is more dominant than that due to fluctuating component, which is

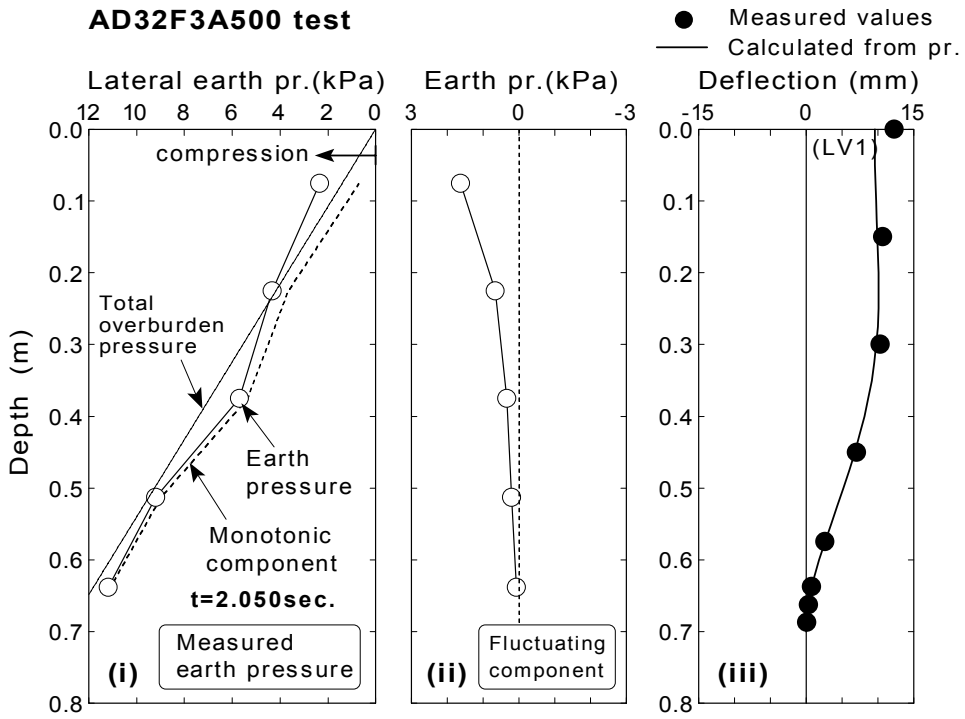

(a) At resonance, t=2.050 seconds

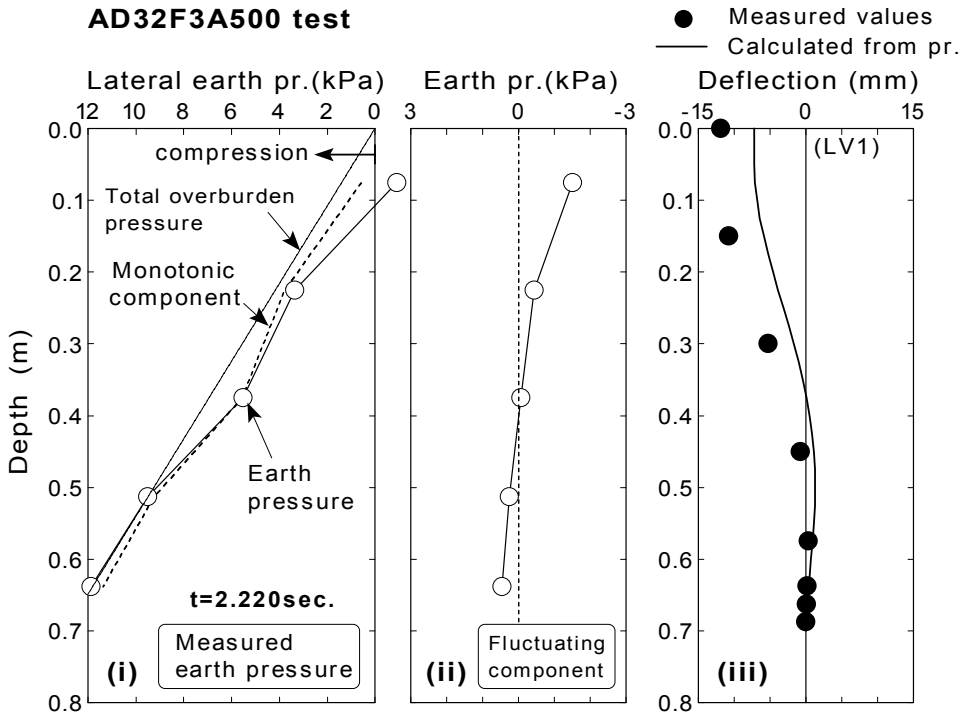

(b) A half cycle after resonance, t=2.220 seconds

Fig.6.65: Earth pressure and deflection at resonance (AD32F3A500 test)

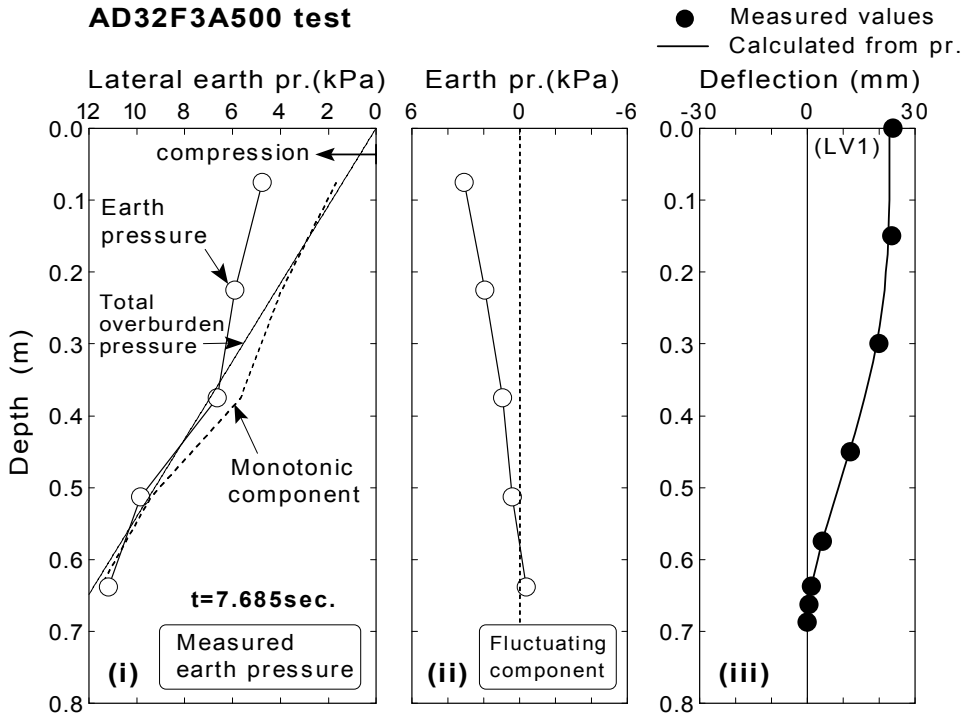

(a) t=7.685 seconds

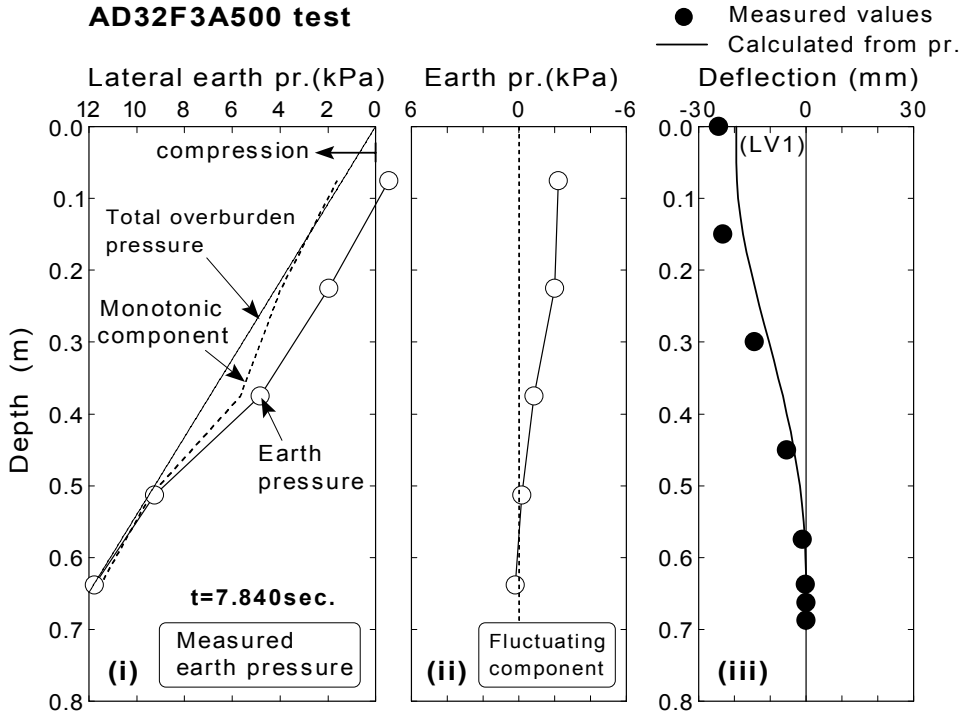

(b) t=7.840 seconds

Fig.6.66: Earth pressure and deflection during liquefaction (AD32F3A500 test)

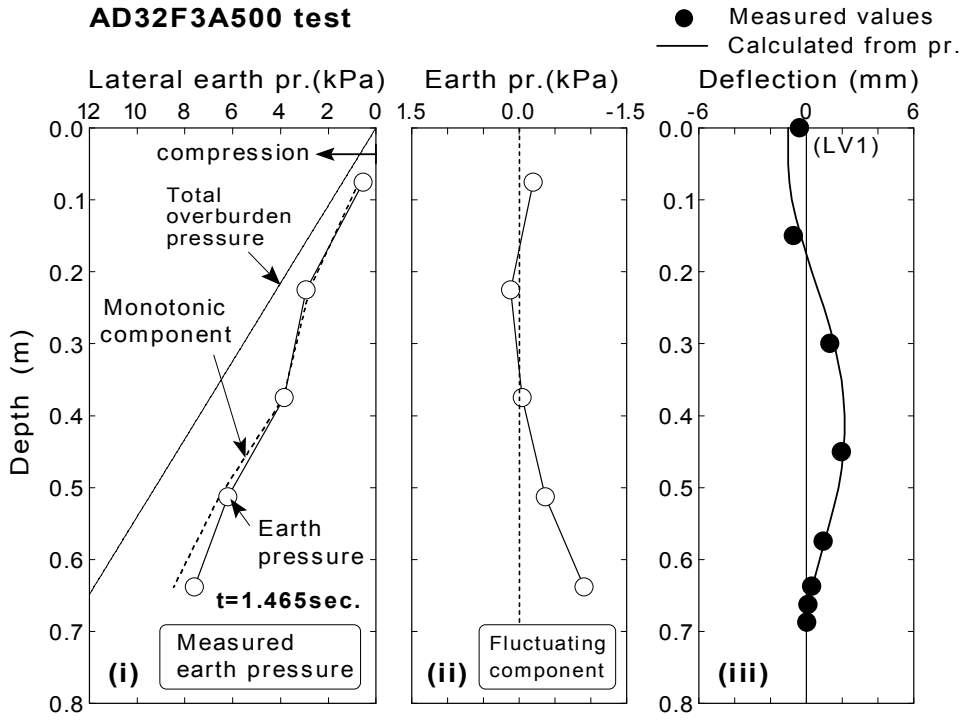

(a) t=1.465 seconds

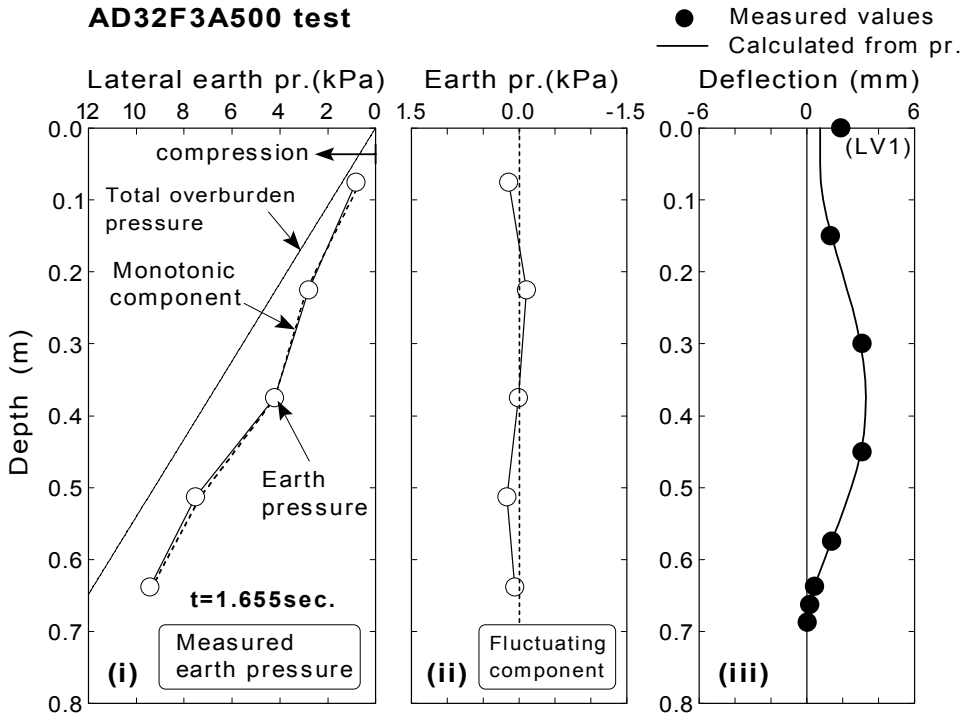

(b) t=1.655 seconds

Fig.6.67: Earth pressure and deflection before resonance (AD32F3A500 test)

less than 2mm at the top. It is seen that the fluctuating component of earth pressure at the bottom is larger than at the top, showing different feature from the resonance or during liquefaction. The agreement between the calculated and measured deflection at the top of the structure seems satisfactory.

BD36F3A500 test (Structure-B)

The time history of calculated displacement at the top of the structure from BD36F3A500 test is compared with measured time history (LV1) in Fig.6.68. The time of initial yielding of 2.70 seconds is indicated in the figure. Calculated displacement reasonably agrees with measured displacement when the structure behaves in an elastic manner. Amplitude of measured displacement seems larger than that of calculated displacement after the initial yielding, in which an elastic behavior is assumed.

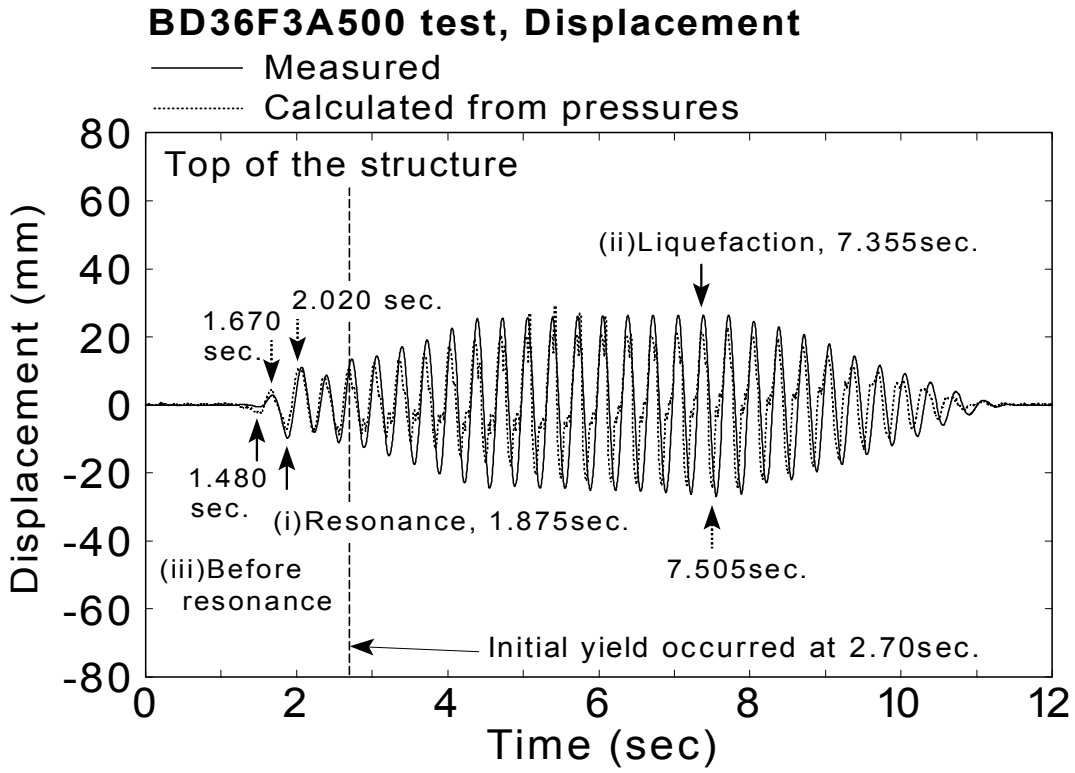

Fig.6.68: Comparison of time histories between measured and calculated displacement (intense input motion, BD36F3A500 test)

The profile of calculated deflection at resonance (t=1.870 seconds) is compared with measured deflection in Fig.6.69(a), and a half cycle after the resonance (t=2.020 seconds) in Fig.6.69(b). The comparison in the same manner during liquefaction is presented in Fig.6.70, and before the resonance is illustrated in Fig.6.71. It is noted that the wall already yielded at its bottom during liquefaction of 7.355 seconds. It is observed in Fig.6.69 at resonance that the agreement between the calculated and measured deflection is fairly good.

In contrast with this, some disagreements between the calculated and measured deflection are seen in Fig.6.70 during liquefaction of 7.355 seconds and 7.505 seconds. The measured deflection is larger than the calculated deflection at 7.355 seconds. On the other hand, the measured deflection is slightly smaller than the calculated deflection. It is considered that the yielding of wall caused the disagreement of deflection.

It is seen in Fig.6.71(a) before resonance that the fluctuating component of earth pressure is negative so that the measured displacement at the top of the structure occurs in the negative direction. The measured displacement is approximately -0.6mm, and calculated displacement is about -2.1mm at 1.480 seconds. The calculated displacement does not agree with the measured displacement at the top of the structure quantitatively. This feature was seen in Fig.6.63 before resonance of AD35F3A50 test.

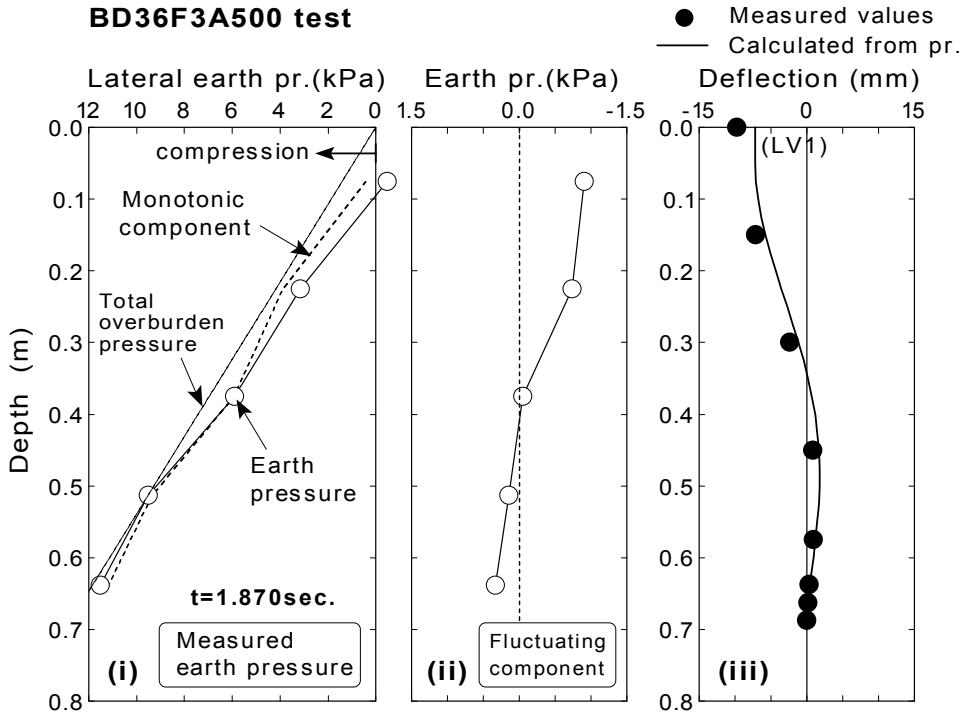

(a) At resonance, t=1.870 seconds

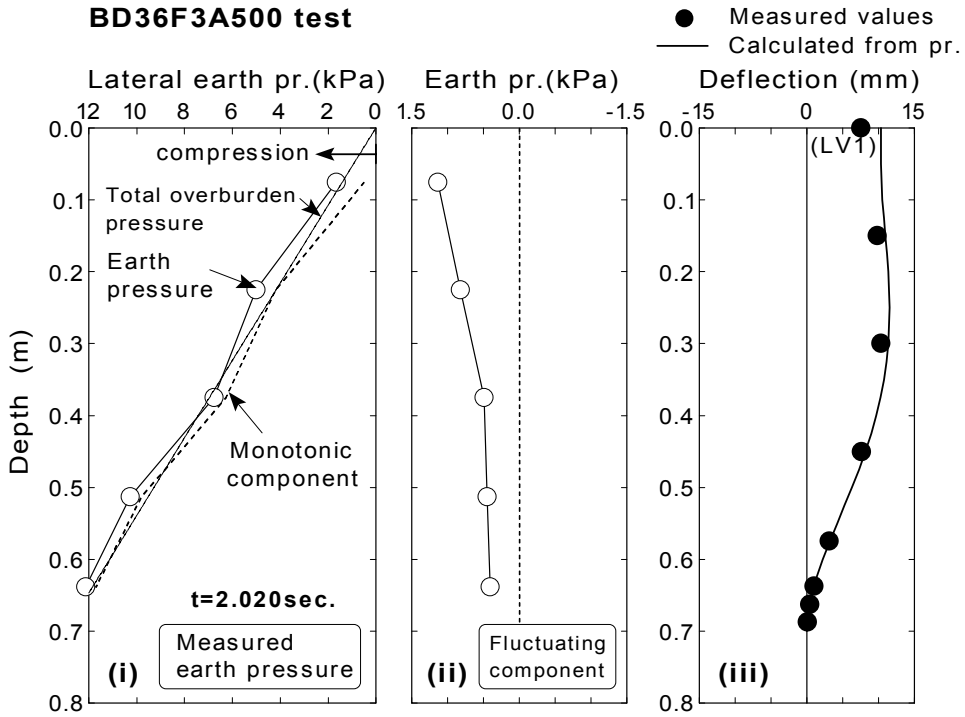

(b) A half cycle after resonance, t=2.020 seconds

Fig.6.69: Earth pressure and deflection at resonance (BD36F3A500 test)

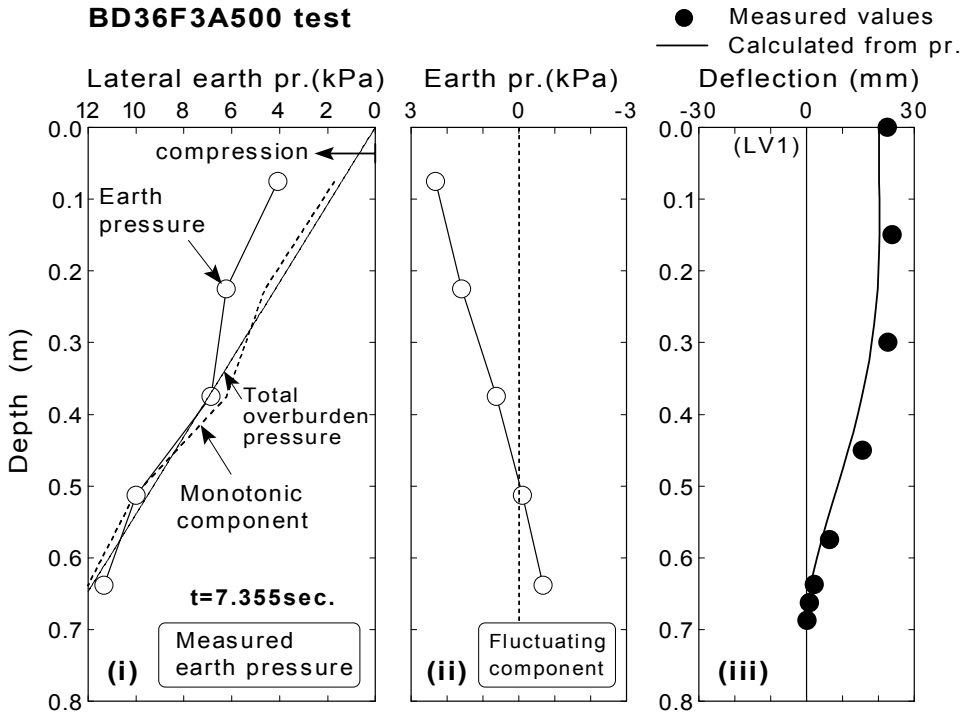

(a) t=7.355 seconds

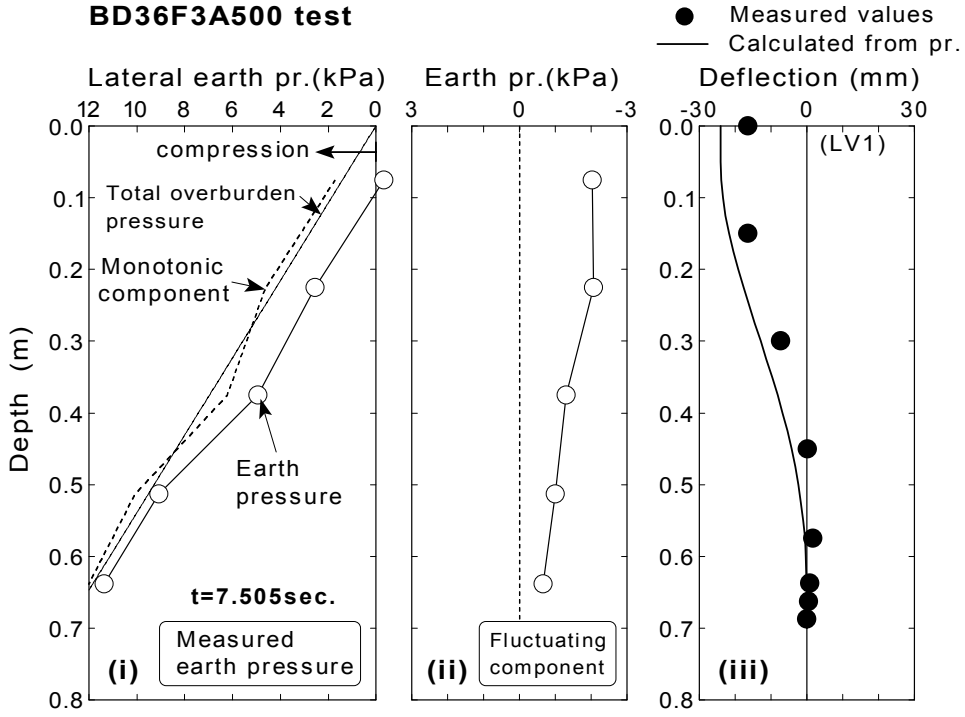

(b) t=7.505 seconds

Fig.6.70: Earth pressure and deflection during liquefaction (BD36F3A500 test, after initial yielding of wall)

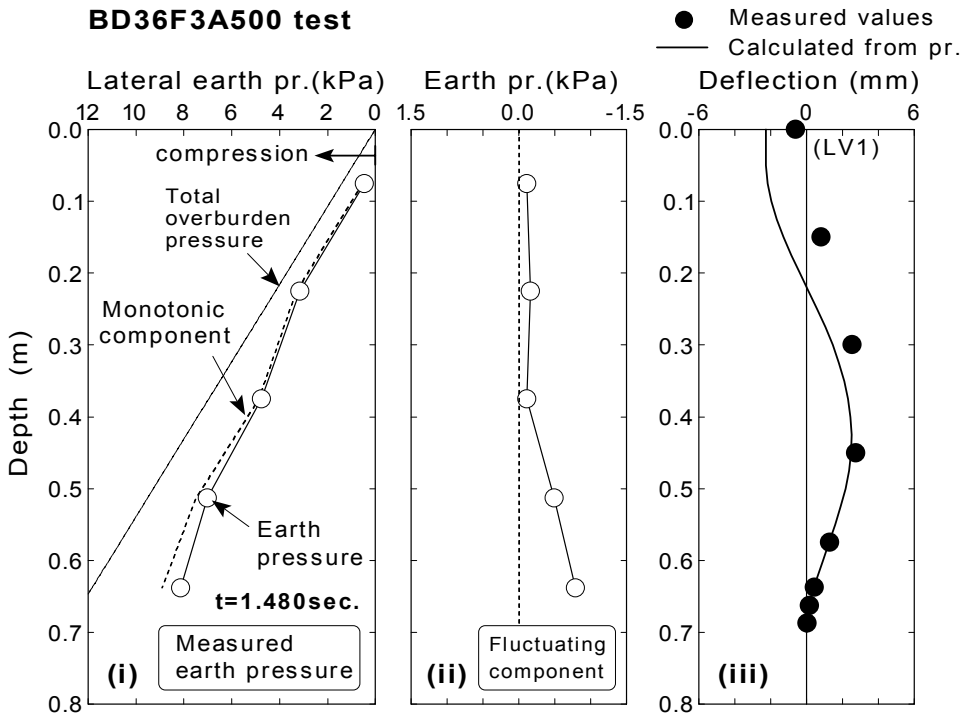

(a) t=1.480 seconds

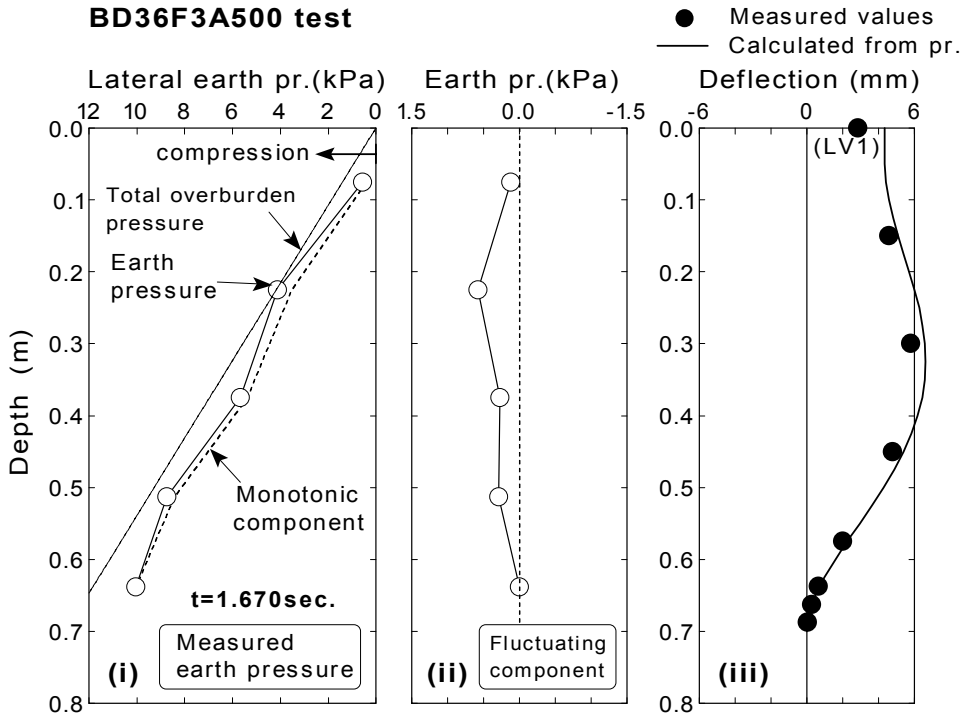

(b) t=1.670 seconds

Fig.6.71: Earth pressure and deflection before resonance (BD36F3A500 test)

Results of the test with dense backfill

AD67F3A500 test (relative density of 67%, Structure-A)

Calculated time history of displacement at the top of the structure from AD67F3A500 test is compared with the measured displacement at the top of the structure in Fig.6.72. Amplification of displacement at about 2.2 seconds indicates the occurrence of resonance. After the resonance, the amplification of displacement increased and the material of wall yielded at 3.69 seconds. Following this, the second resonance occurred at about 5.2 seconds.

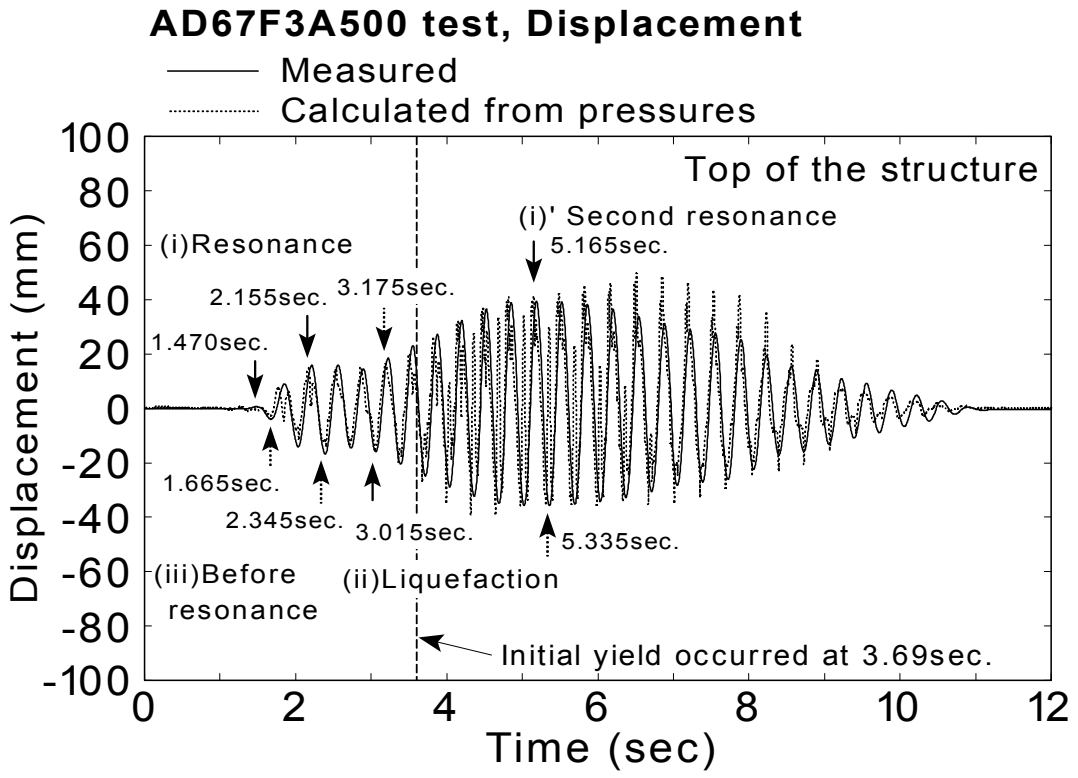

(a) 0 to 12 seconds

Fig.6.72: Comparison of time histories between measured and calculated displacement (dense backfill, AD67F3A500 test)

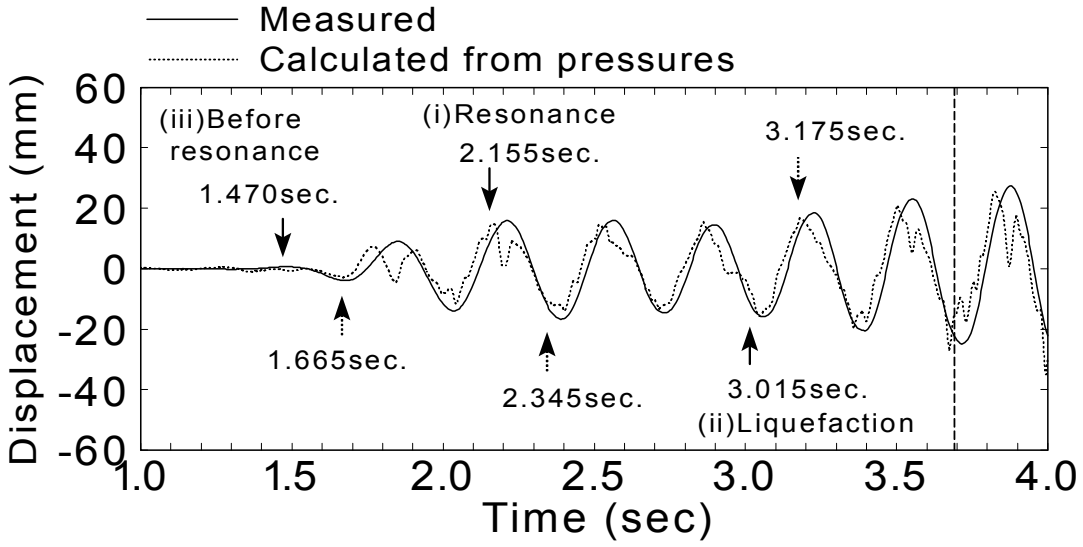

(b) 1.0 to 4.0 seconds

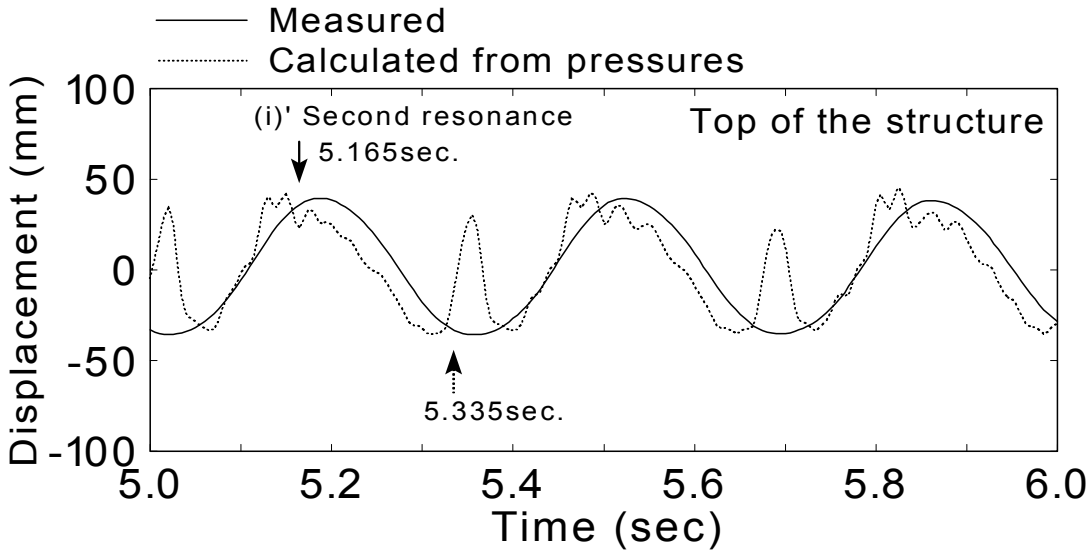

(c) 5.0 to 6.0 seconds

Fig.6.72: Continued (dense backfill, AD67F3A500 test)

It is observed that the calculated time history is reasonably consistent with the measured time history before initial yielding of the material. After that, spiky displacement is observed in the calculated time history, which is not seen in the measured one. Time history of the fluctuating component of earth pressure which is used in the calculation is presented in Fig.6.90 at the end of this chapter. The high frequency component is seen in the time history of especially EP7 and EP8. The high frequency component in the calculated displacement was produced as a result of the high frequency component in the earth pressures.

The profile of calculated deflection at resonance (t=2.155 seconds) is compared with measured deflection in Fig.6.73(a), and a result of a half cycle after the resonance (t=2.345 seconds) is depicted in Fig.6.73(b). It is interesting that the complicated profile of fluctuating component of earth pressure at resonance (Fig.6.73(a)(ii)) is symmetric with that of a half cycle later the resonance (Fig.6.73(b)(ii)). Although the calculated deflection is larger or smaller than the measured deflection, agreement between them is reasonable at resonance.

The results during liquefaction (t=3.015 seconds and 3.175 seconds) are presented in Fig.6.74. It is seen that the calculated deflection is slightly smaller than the measured deflection when the structure moves in the negative direction (left direction). In contrast with this, agreement between them is good when the structure moves in the positive direction (right direction). The results at second resonance (t=5.165 seconds and 5.335 seconds) are illustrated in Fig.6.75. Note that the material has already yielded. It is observed that the calculated deflections are inconsistent with the measured deflection. It seems difficult to calculate the deflection correctly from the earth pressure when the backfill is dense. The profiles before resonance is illustrated in Fig.6.76. It is observed that the measured displacement at the top is positive while the fluctuating component of earth pressure is negative at the middle part of the wall. This situation is the same as that observed in Fig.6.112(b) of AD61F3A200 test. The agreement between the calculated and the measured deflection seems reasonable in Fig.6.76(b).

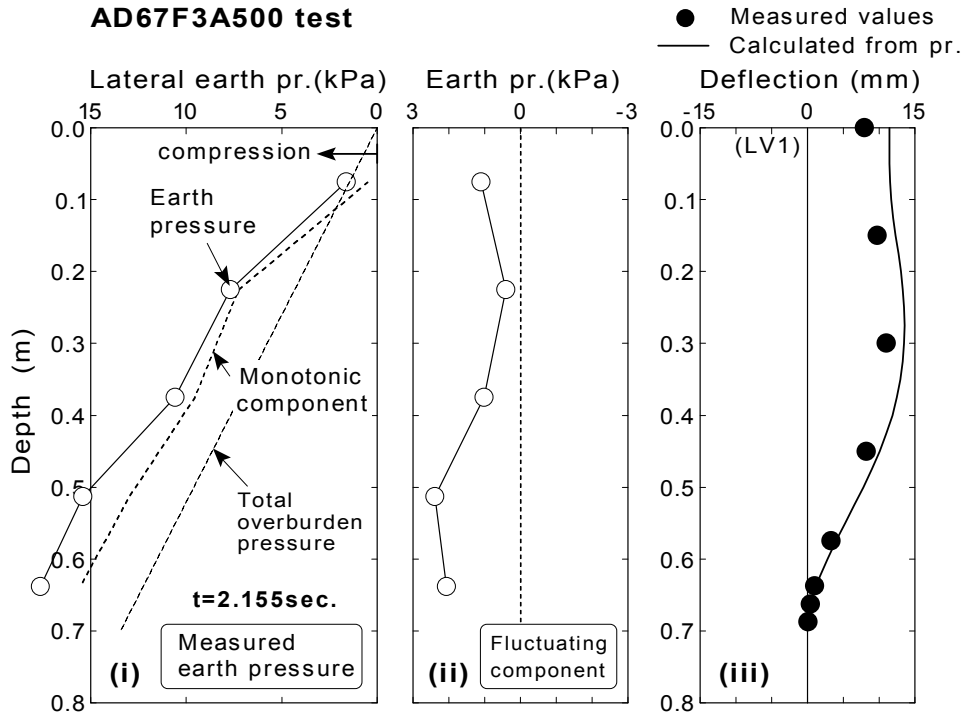

(a) At resonance, t=2.155 seconds

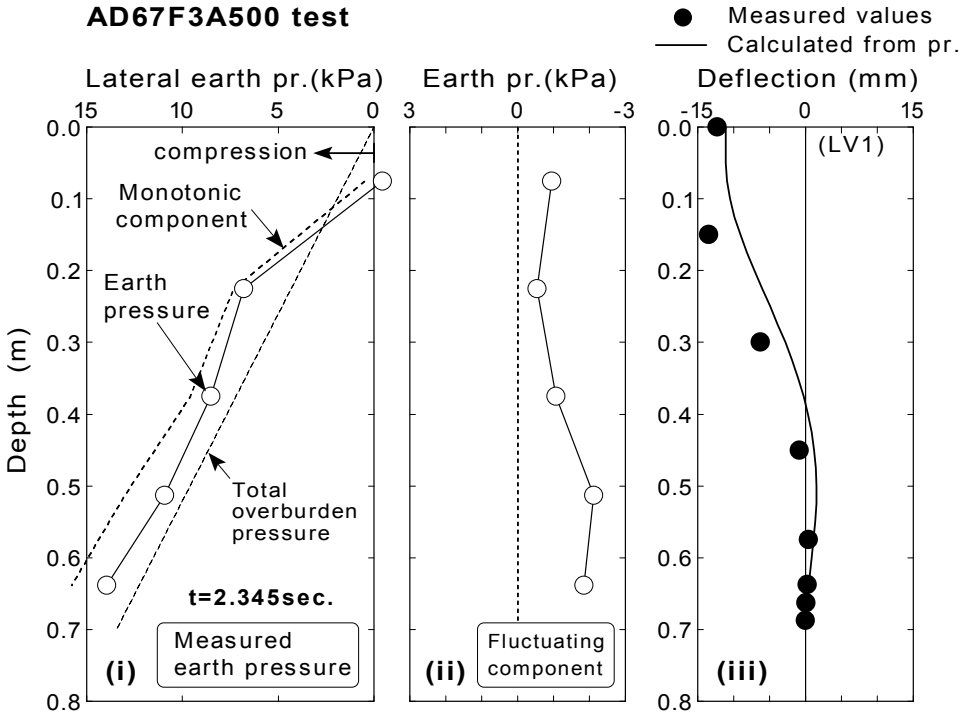

(b) A half cycle after resonance, t=2.345 seconds

Fig.6.73: Earth pressure and deflection at resonance (AD67F3A500 test)

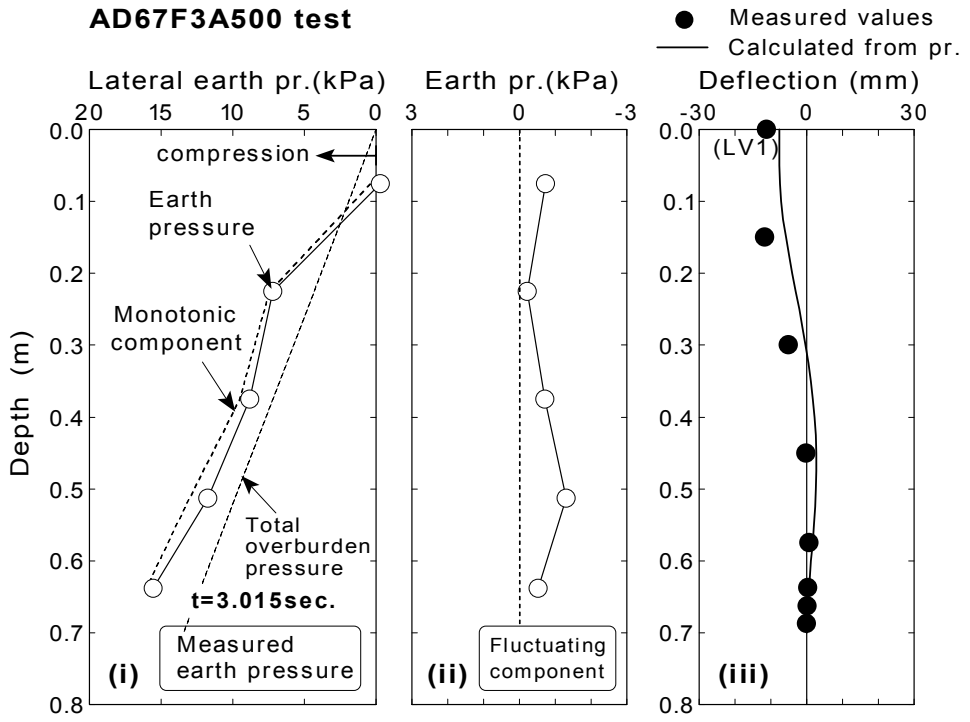

(a) t=3.015 seconds

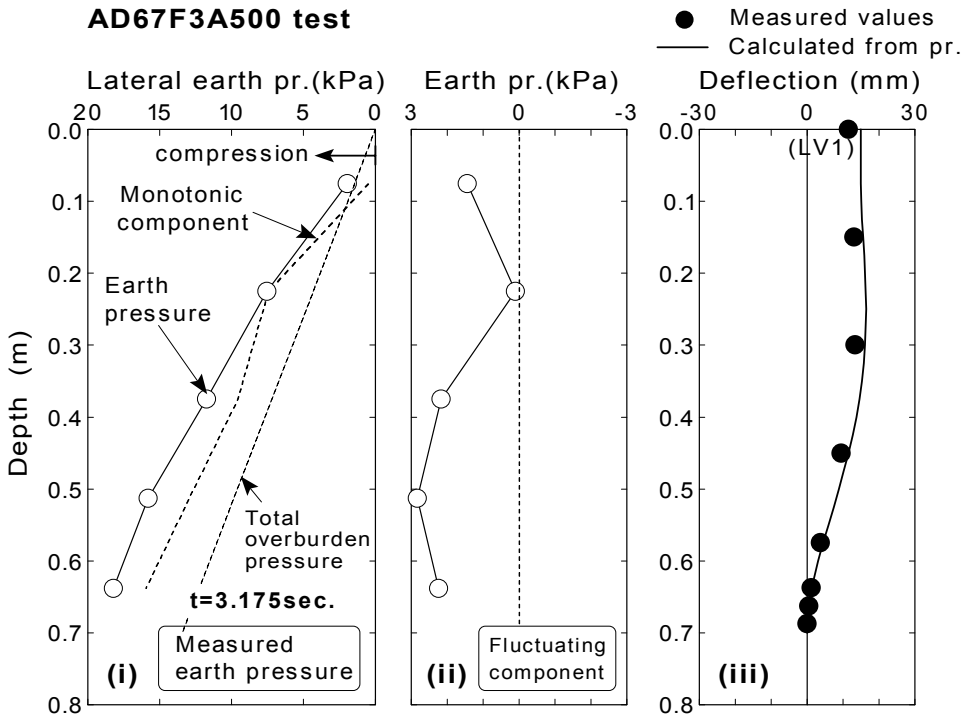

(b) t=3.175 seconds

Fig.6.74: Earth pressure and deflection during liquefaction (AD67F3A500 test)

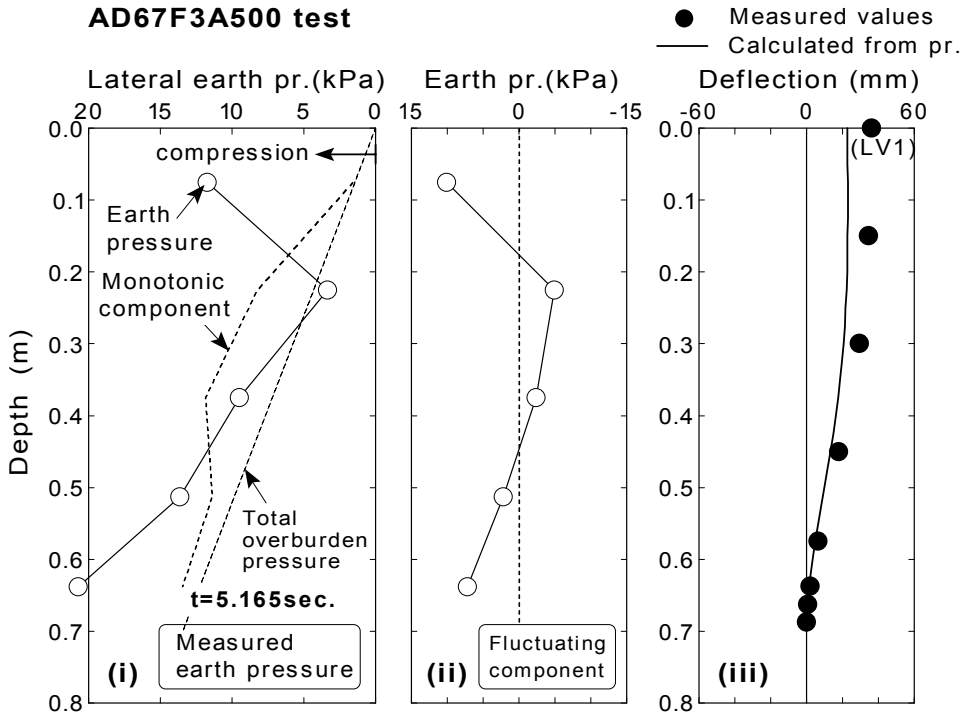

(a) t=5.165 seconds

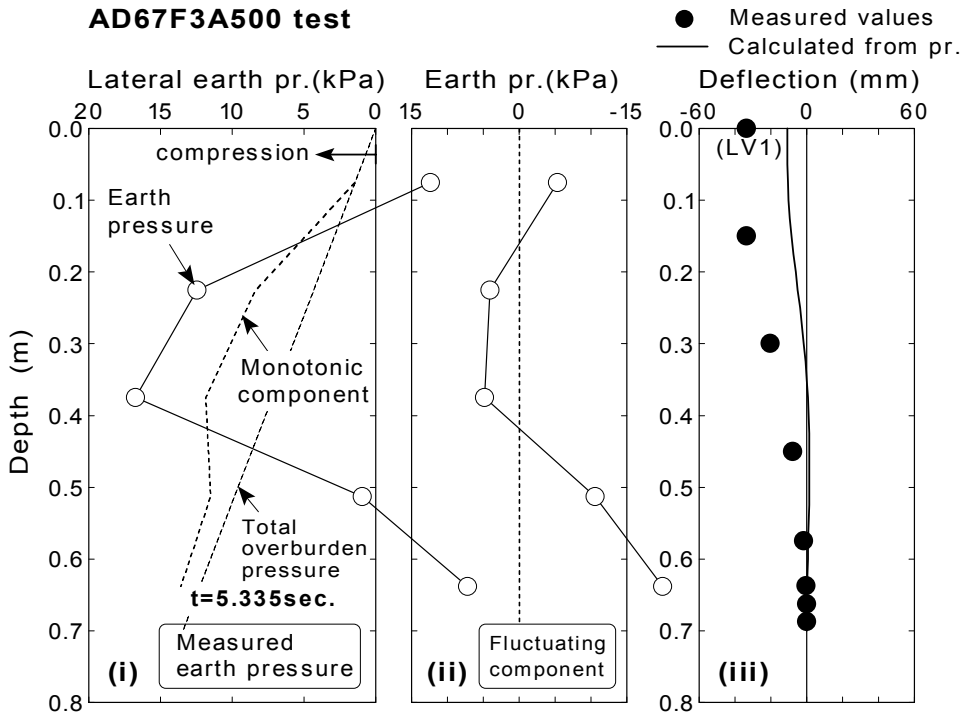

(b) t=5.335 seconds

Fig.6.75: Earth pressure and deflection second resonance (AD67F3A500 test)

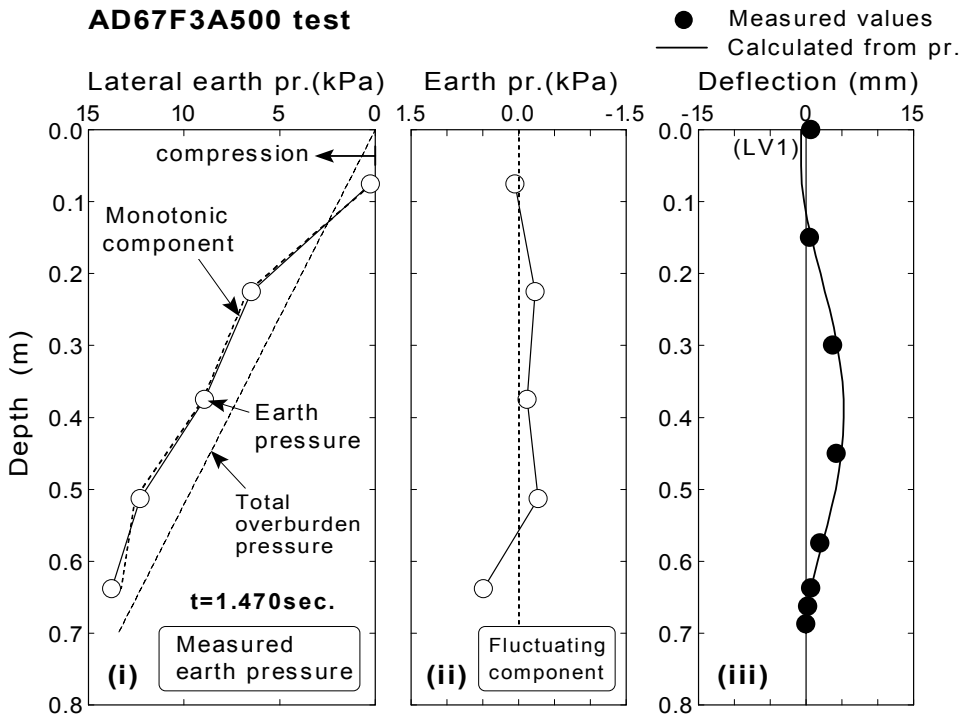

(a) t=1.470 seconds

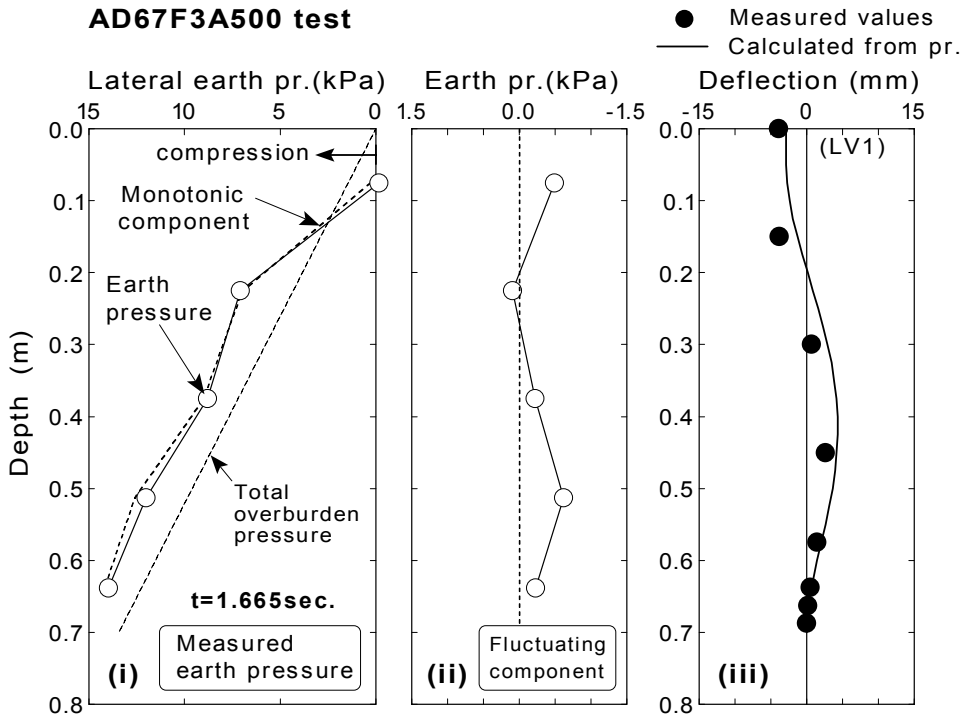

(b) t=1.665 seconds

Fig.6.76: Earth pressure and deflection before resonance (AD67F3A500 test)

BD78F3A500 test (relative density of 78%, Structure-B)

Calculated time history of displacement at the top of the structure from BD78F3A500 test is compared with the measured displacement at the top in Fig.6.77. The time of initial yielding is indicated in the figure. Time histories between 1.0 to 3.0 seconds and 10.5 to 11.5 seconds are presented in Fig.6.77(b) and (c), indicating time instances to draw profiles. Studies based on the stress strain relationship presented in the chapter 4 showed that the backfill soil behaved in a dilative manner in those tests (see Fig.4.59). According to study conducted in Chapter 5, resonance did not occur in this test. It is remarkable that calculated displacement does not agree with measured displacement at all. High frequency component are included in the calculated displacement through the duration time. Spiky change of displacement at around 11.145 seconds is also characteristic in the result. In case that the pore water pressure decreases instantaneously by a dilative behavior of soil, spiky earth pressures also appear (see Fig.6.91). Since this earth pressure fluctuates in a very short time period, it does not affect the displacement or deformation of a structure. In contrast, a sudden change of earth pressure induces directly that of the displacement in the calculation presented in this section as observed in the time history of calculated displacement at about 10.8 seconds in Fig.6.77(c).

The profile of calculated deflection at initial of shaking (t=1.800 seconds) is compared with measured deflection in Fig.6.78(a), and a result of a half cycle after that (t=1.970 seconds) is depicted in Fig.6.78(b). It is observed that the calculated deflection agrees with the measured deflection at 1.800 seconds, while it does not at all at 1.97 seconds. In this moment, it is seen that the negative value of fluctuating component of earth pressure acts on the structure and the structure deforms in the positive direction (right direction). This means that the structure moved away from the backfill so that the earth pressure decreased. It is considered that the dilative behavior of dense backfill is related to this interactive behavior, and the detail will be discussed in Chapter 7.

The profiles of calculated deflection during shaking (t=10.980 seconds and 11.145 seconds) are compared with measured deflection in Fig.6.79. It is remarkable that large fluctuating component of earth pressure more than 15 kPa occurs at the depth of 0.225m at 11.145 seconds. In the calculation, this large earth pressure acts as a load on the structure and it makes the structure deform in the positive direction (right direction). However, actually the deflection occurs in the negative direction. This large earth pressure is considered to occur when the structure clashes into

the backfill. In this time, the earth pressure is not a load but a reaction. It seems difficult to predict the deflection from earth pressure by the calculating procedure presented in this section when this phenomenon occurs.

The comparisons of time histories and profiles from other tests of AD39F5A50, AD41F3A200 and AD61F3A200 test are illustrated in Fig.6.101～Fig.6.112 at the end of this chapter.

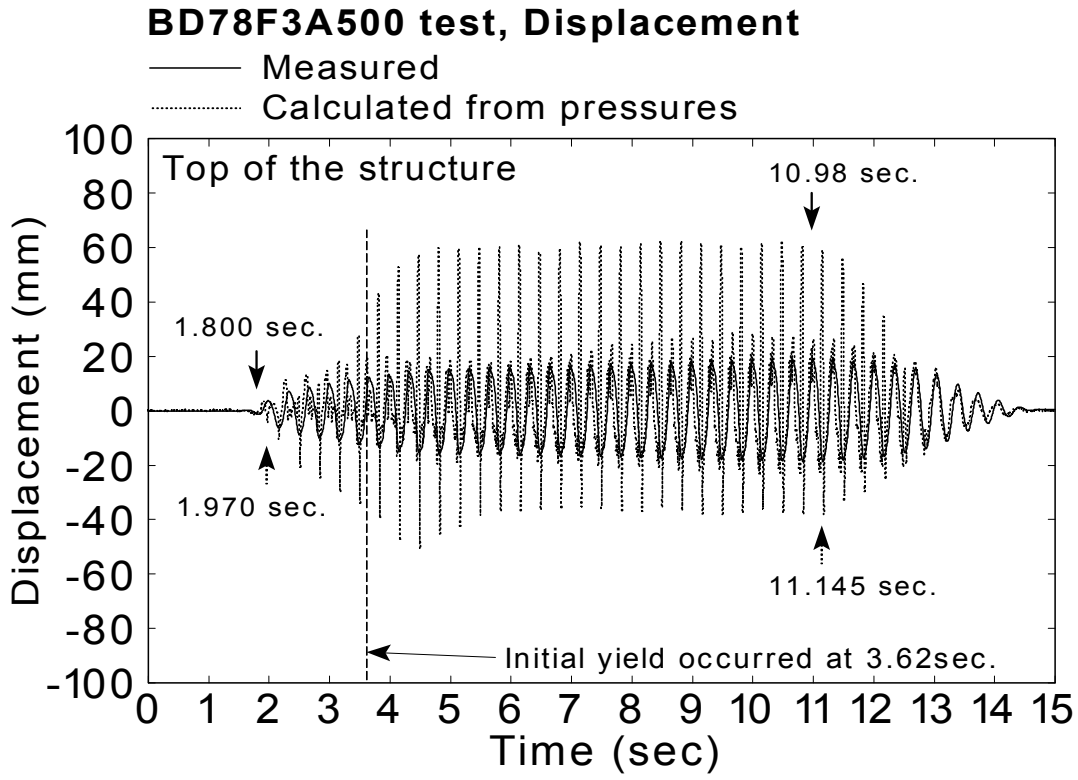

(a) 0 seconds to 15 seconds

Fig.6.77: Comparison of time histories between measured and calculated displacement (Tests of repeated shaking, BD78F3A500 test)

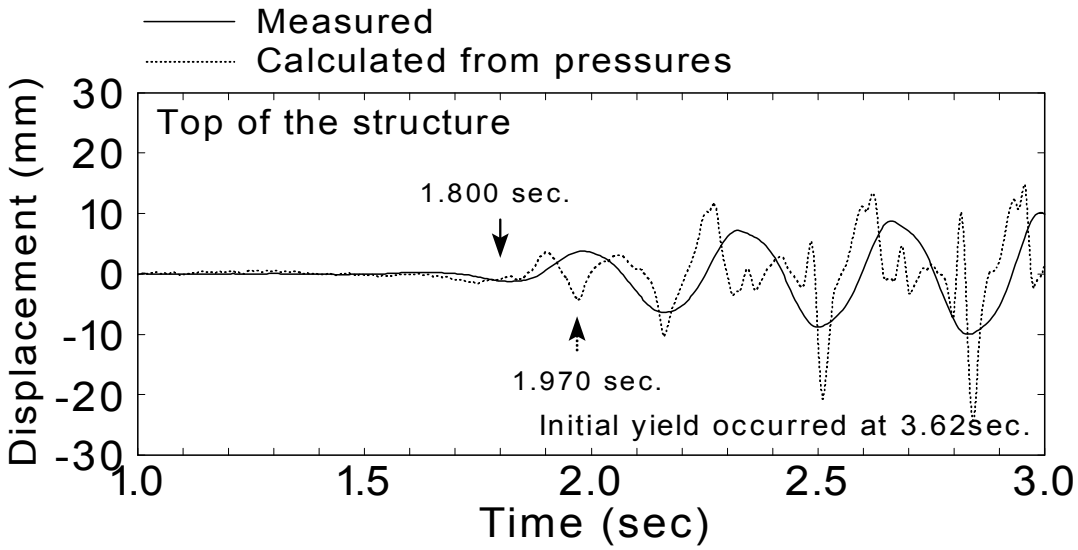

(b) 1.0 seconds to 3.0 seconds

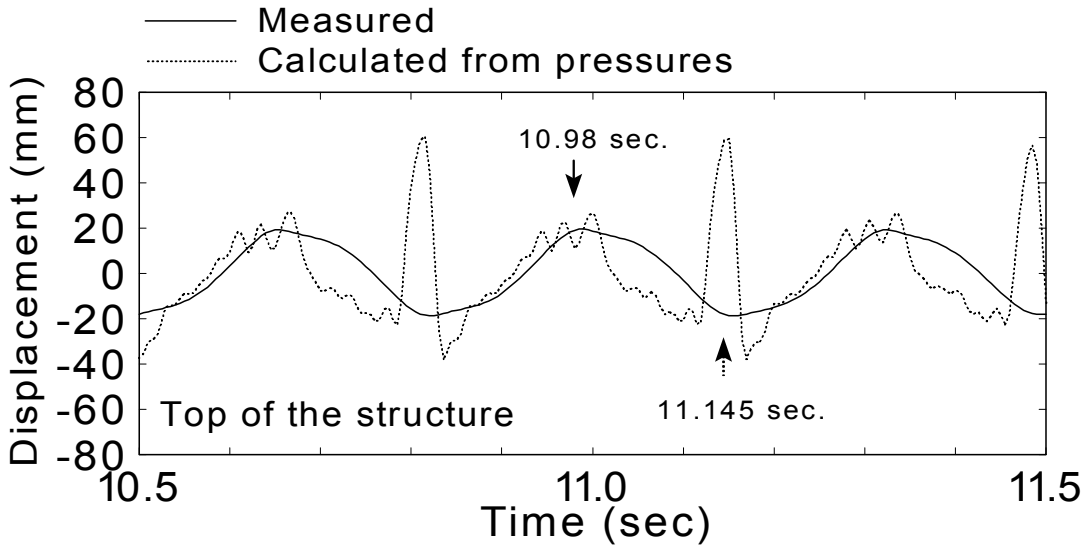

(c) 10.5 seconds to 11.5 seconds

Fig.6.77: Continued (BD78F3A500 test)

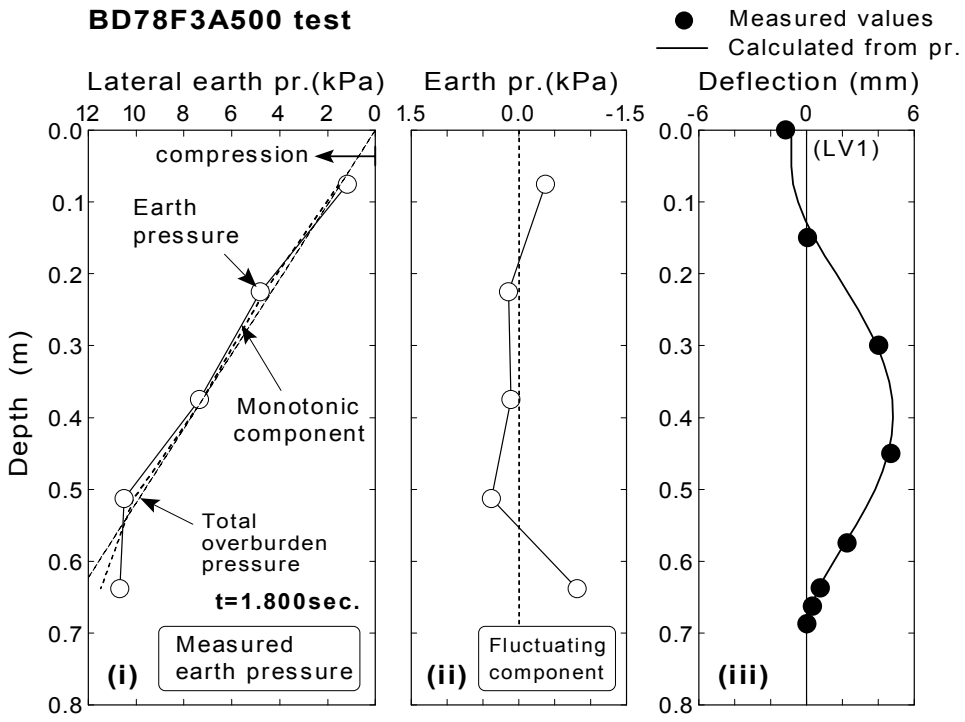

(a) t=1.800 seconds

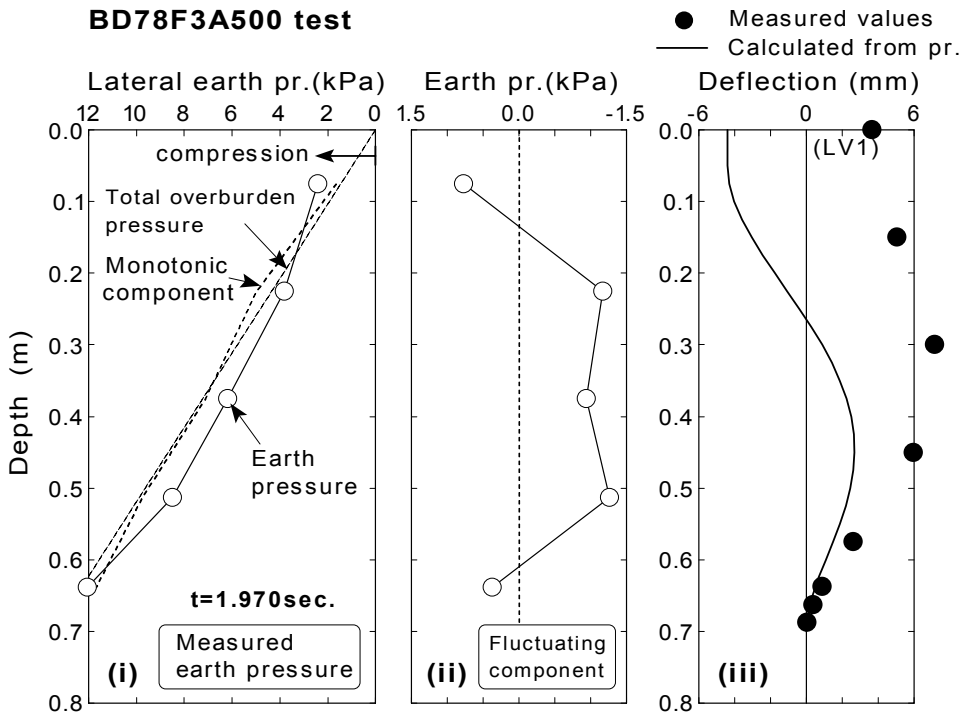

(b) t=1.970 seconds

Fig.6.78: Earth pressure and deflection before resonance (BD78F3A500 test)

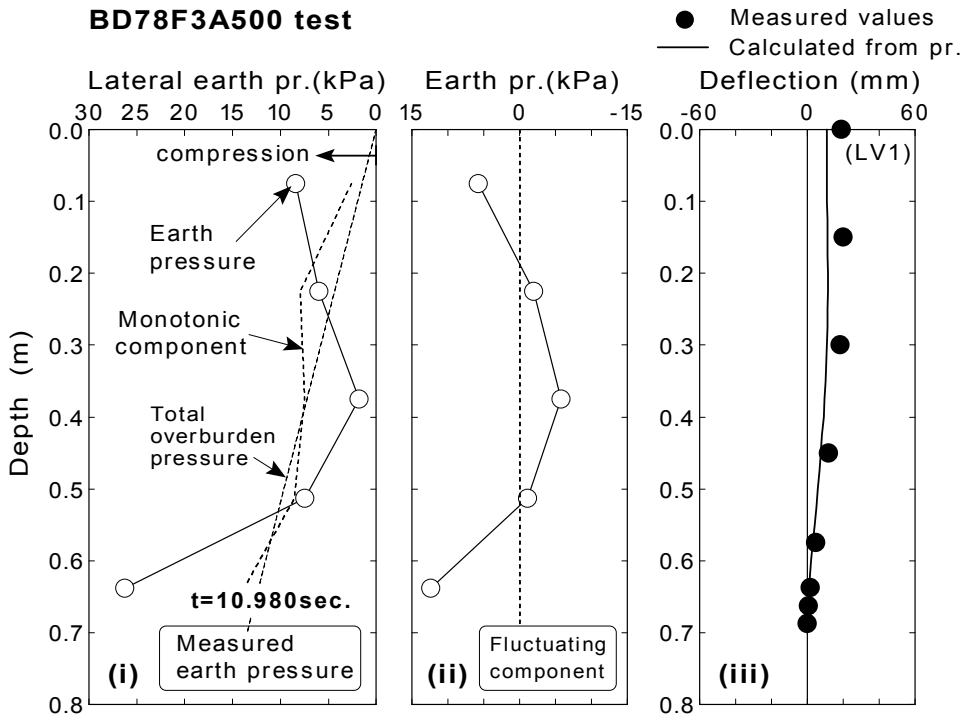

(a) t=10.980 seconds

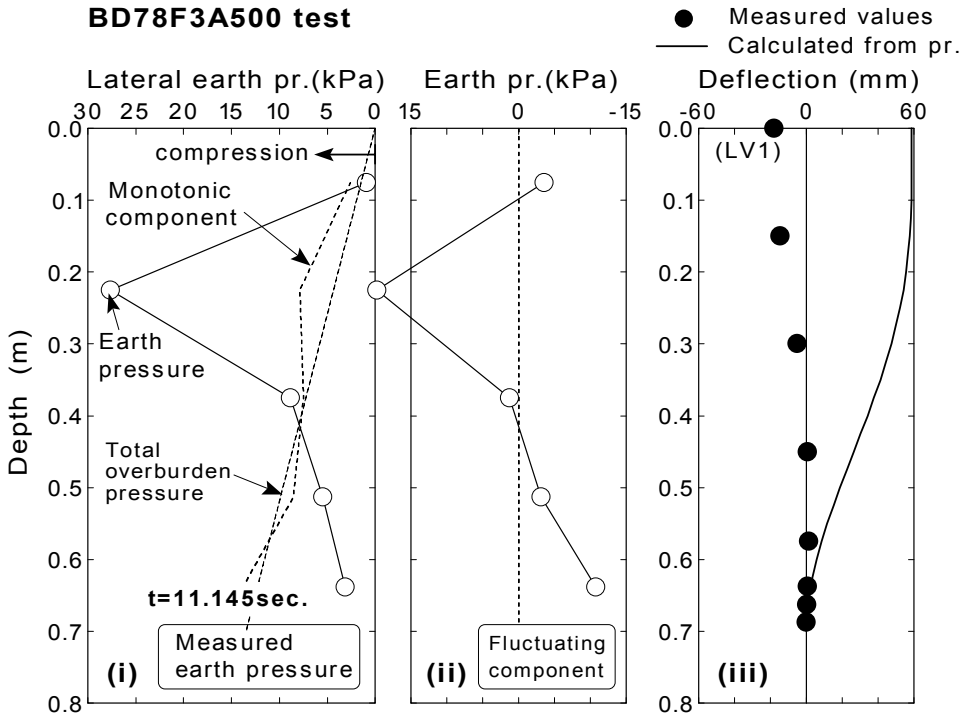

(b) t=11.145 seconds

Fig.6.79: Earth pressure and deflection during liquefaction (BD78F3A500 test)

6.4.7 Discussion

To clarify the validity of calculation procedure presented in this section, comparison of values between the calculated and the measured displacement will be made. Time history of displacement for comparison will be divided into four parts focusing on the magnitude relation of natural frequency of the backfill, $\nu_{backfill}$, and the structure, $\nu_{struc.}$, (Structure-A: 7.8Hz, Structure-B: 7.3Hz), as

1) Time period when natural frequency of backfill is higher than that of the structure.

$$\nu_{stru.} \leq \nu_{backfill} \tag{6.47}$$

2) Time period when the natural frequency of backfill is lower than that of the structure, and higher than 0.4 times of natural frequency of the structure.

$$0.4 \cdot \nu_{stru.} \leq \nu_{backfill} \leq \nu_{stru.} \tag{6.48}$$

where the coefficient of 0.4 is an approximate value derived by dividing input frequency of 3Hz by the natural frequency of the structure of 7.8Hz or 7.3Hz. It becomes 0.67 times of natural frequency of the structure for 5Hz shaking.

3) Time period when the natural frequency of backfill is lower than 0.4 times of natural frequency of the structure. Soil does not liquefy completely.

$$0 \leq \nu_{backfill} \leq 0.4 \cdot \nu_{stru.} \tag{6.49}$$

According to the study in Chapter 5, the resonance of structure occurs in this time period. As same as previous definition, the value of 0.4 for 3Hz shaking becomes 0.67 for 5Hz shaking.

4) Time period when natural frequency of backfill is almost zero. Soil liquefies completely.

$$\nu_{backfill} \approx 0 \tag{6.50}$$

Each time period is illustrated in Fig.6.80, taking AD35F3A50 and AD39F5A50 tests as examples of 3Hz shaking and 5Hz shaking, respectively. It is noted that either above mentioned 1) or 2) corresponds to the time before resonance mentioned in the previous

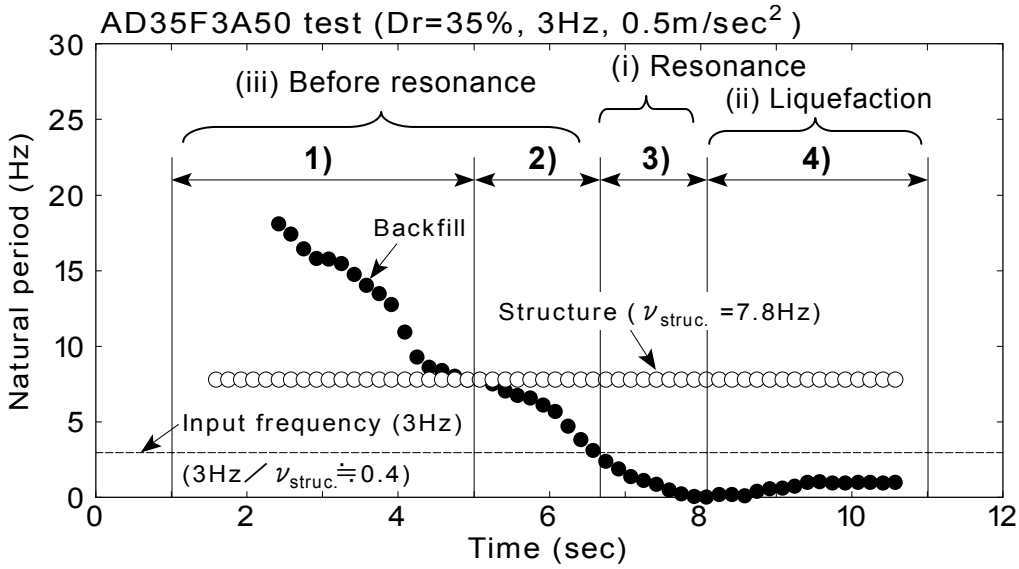

(a) Example of 3Hz shaking (AD35F3A50 test)

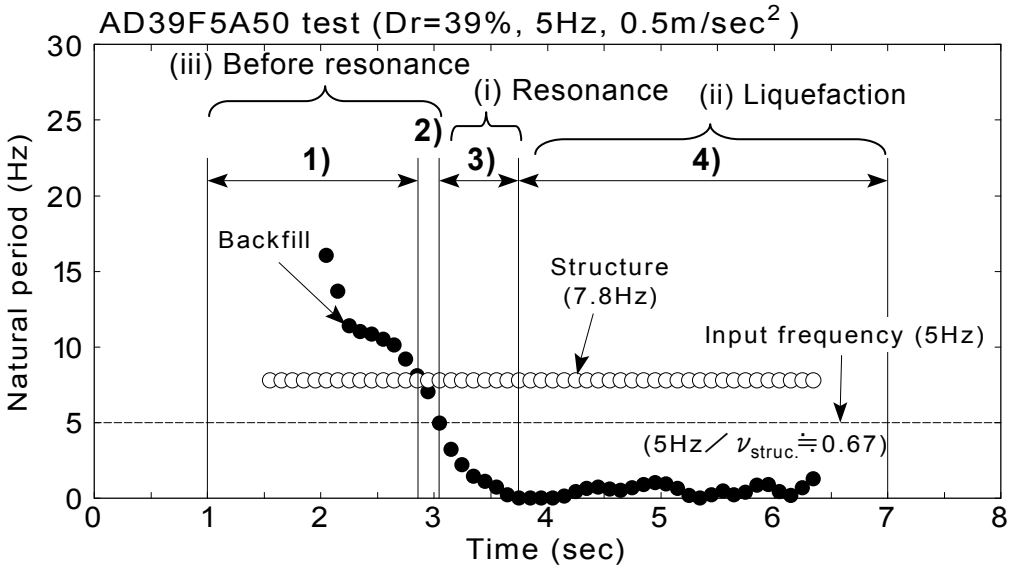

(b) Example of 5Hz shaking (AD39F5A50 test)

Fig.6.80: Change of natural frequency of backfill with time

section (Fig.6.59, (iii)), the time period 3) includes the time of resonance (Fig.6.59, (i)), and the time period 4) corresponds to the time period during liquefaction (Fig.6.59, (ii)). The coefficient of 0.4 in 3Hz shaking is replaced by the coefficient of 0.67 in 5Hz shaking as illustrated in Fig.6.80(b).

Calculated displacements in the time period of 1) when natural frequency of backfill is higher than that of the structure (see Eq.(6.47)) from all tests are compared with measured displacements at the same time instance in Fig.6.81. The line of 1:1 is drawn in each figure. It is unanimously observed that calculated displacement is inconsistent with measured displacement in every test, showing a relation of negative proportionality. A representative profile of deflection during this time period is presented in Fig.6.63(b)(t=4.245seconds) in the previous section. In this situation at 4.245 seconds, the natural frequency of structure (=7.8Hz) is closer to the input frequency (=3Hz) than the natural frequency of backfill (=approximately 12Hz, see Fig.6.80(a)). It is considered that the structure is more easily forced to shake than the backfill by input motion. Consequently, the structure pushed the backfill which was harder to move than the structure, producing earth pressure as a reaction.

The other reason also can be considered for the disagreement between the calculation and the experiment. The other possibility is that the assumption of the calculation is not suitable for the real phenomenon. For instance, the same amount and the same distribution are assumed between the left and the right walls (see, Fig.6.35). Although the amount of earth pressure on the right wall is not clear because of the absence of earth pressure transducers, there is a possibility that the amounts of earth pressures are slightly different between the both sides of wall. It is desirable for future to install earth pressure transducers on the both side when this type of experiment will be conducted. Anyhow, it is indicated that the calculating procedure presented in this section is not suitable in the state in which the natural frequency of backfill is higher than the natural frequency of the structure.

Calculated displacements in the time period of 2) (see Eq.(6.48)) from all tests are compared with measured displacements in Fig.6.82. Although some of them show positive proportionality (AD32F3A500 and BD36F3A500 test), the most of calculated displacements are inconsistent with the measured displacement. It shows still negative proportionality. It is considered that the structure still pushed the backfill which was harder to move than the structure.

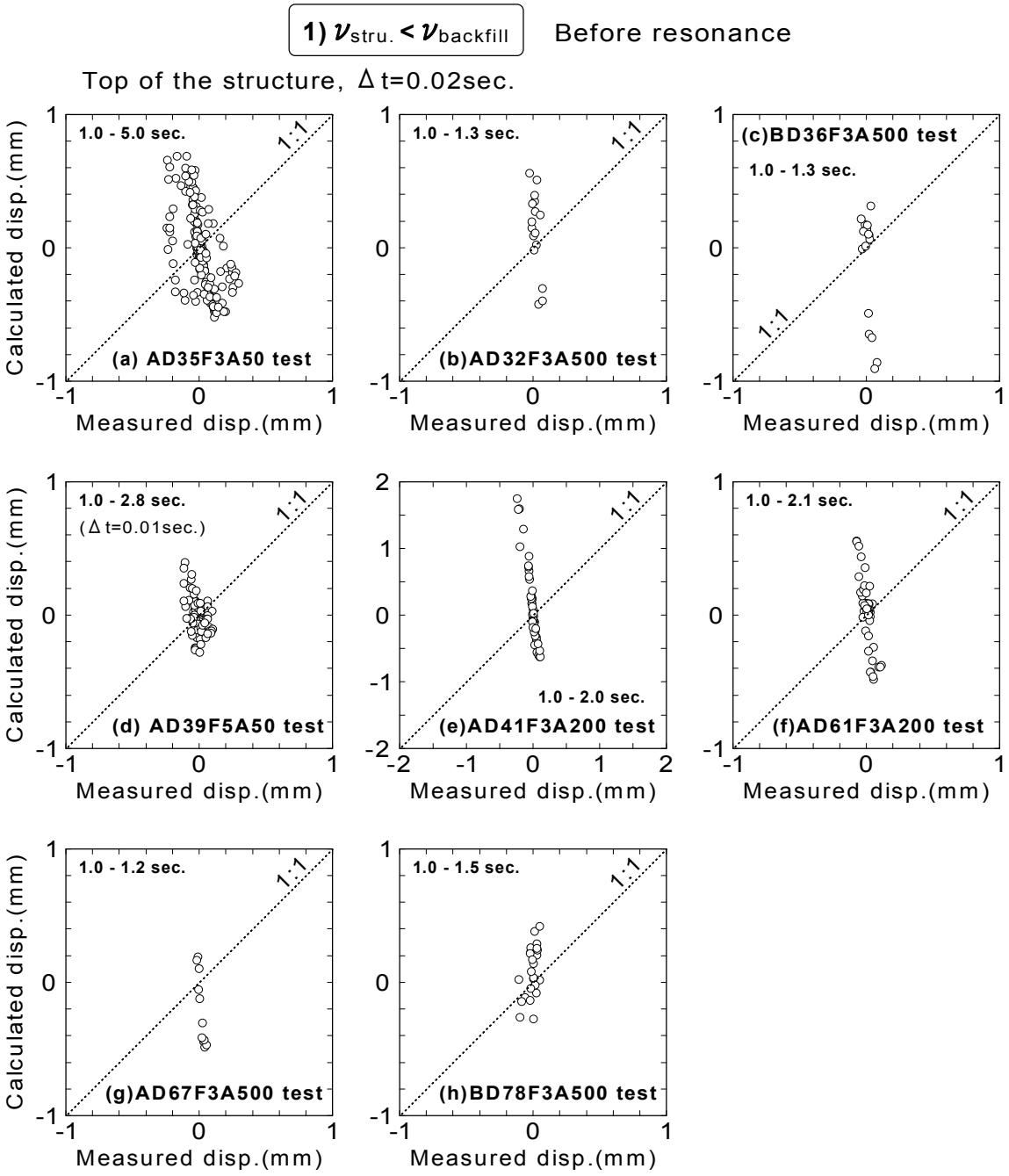

Fig.6.81: Comparison between the calculated and measured displacement at the top of the structure ($\nu_{stru.} < \nu_{backfill}$)

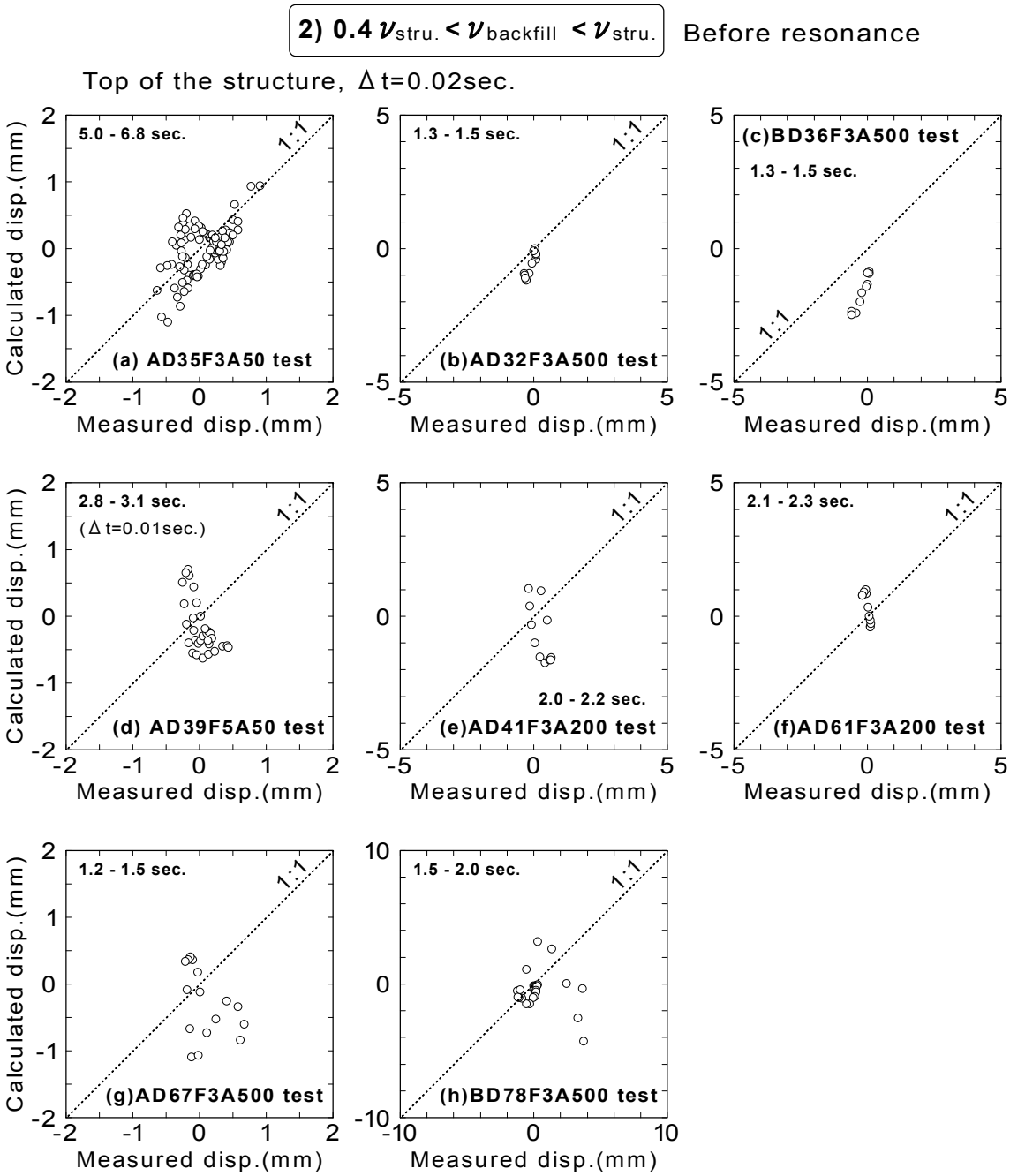

Fig.6.82: Comparison between the calculated and measured displacement at the top of the structure ($0.4\,\nu_{\text{stru.}} < \nu_{\text{backfill}} < \nu_{\text{stru.}}$)

Fig.6.83 illustrates results of comparison in the time period of 3) when the natural frequency of backfill is lower than 0.4 times that of the structure (see Eq.(6.49)). Since resonance is observed twice in one shaking in AD67F3A500 test, plots of data at the resonance and during liquefaction are presented twice (figure(g) and (h)). Before and after yield of material are distinguished in figure(h) and (i). Based on the study in Chapter 4, the significant dilative behavior of soil is observed in AD67F3A500 test and BD78F3A500 test (see Fig.4.53). Agreement between the calculated and measured displacement seems very good except for time period after yielding of AD67F3A500 test, and BD78F3A500 test.

It suggests that the calculation is valid when the natural frequency of backfill is lower or reduced by means of liquefaction to about 0.4 times that of the structure. However, it does not give good results when the soil behaves in a dilative manner. In addition, this calculation with assumption of an elastic beam theory cannot be applied after the yield of material of the structure.

The comparison in the time period 4) of complete liquefaction, in which the natural frequency of backfill becomes zero, is shown in Fig.6.84. The agreement is not so good only in the negative displacement (moves in the left direction) in AD32F3A500 and BD36F3A500 test. However, the positive proportionality of 1:1 is observed in the most of tests. This suggests that the calculation method regarding fluctuating component of earth pressure as a load is suitable during complete liquefaction.

Based on the results of series of calculation, it is assured that measured earth pressure and measured displacement of structure are internally consistent. In addition, it is possible to evaluate the displacement of structure when the natural frequency of backfill becomes lower than about 0.4 times that of the structure. It is noteworthy that calculation presented in this study is invalid when backfill behaves in a dilative manner (e.g. Fig.6.79(b)(iii)). Further discussion concerning the action of fluctuating component of earth pressure on structure will be made in the following chapter.

6.5 CONCLUDING REMARKS

The behavior of box-shaped cross section of structure during liquefaction was examined based on the measurements in a series of shaking table tests. Measured curvatures were divided

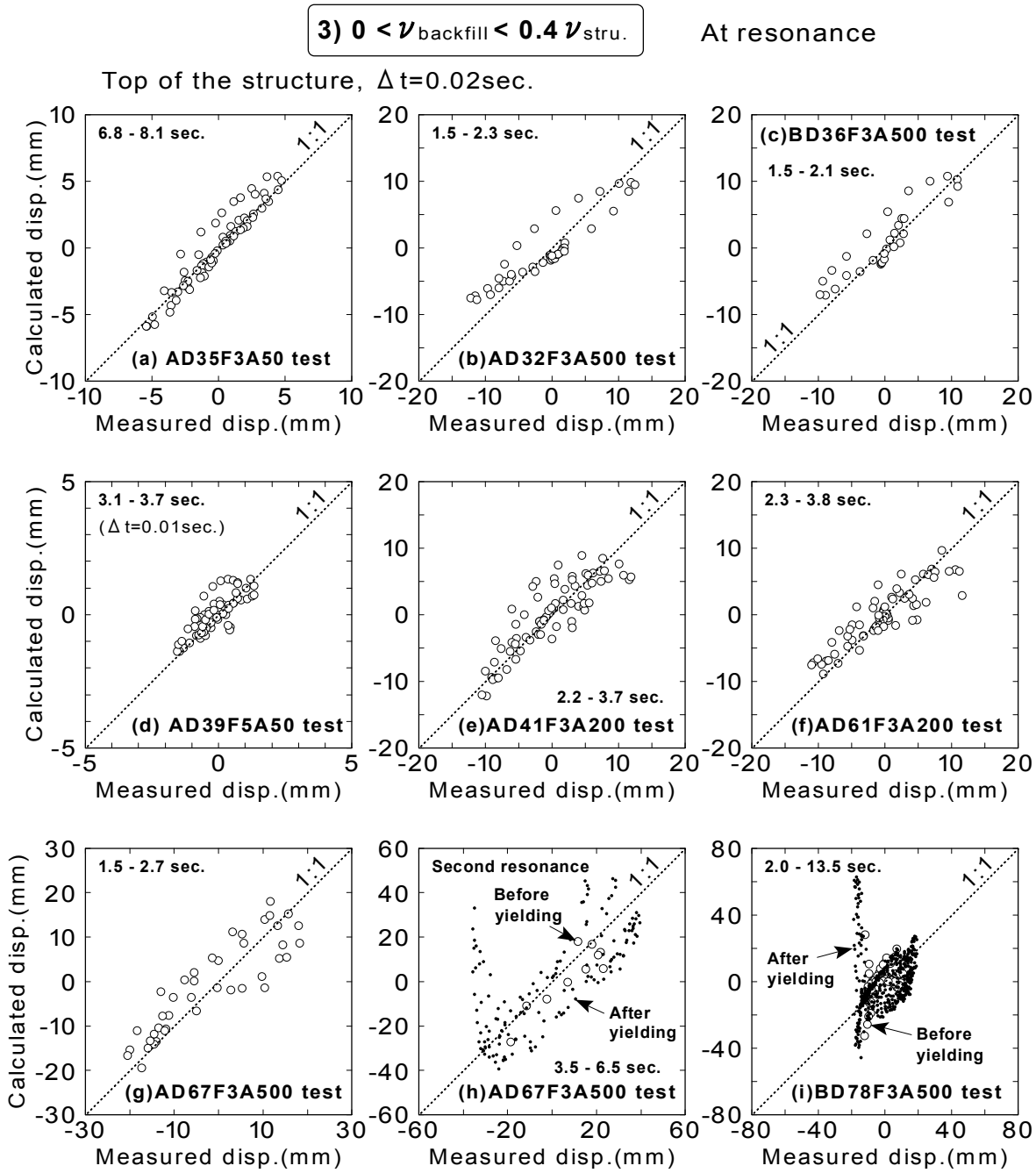

Fig.6.83: Comparison between the calculated and measured displacement at the top of the structure ($0 < \nu_{backfill} < 0.4\,\nu_{stru.}$)

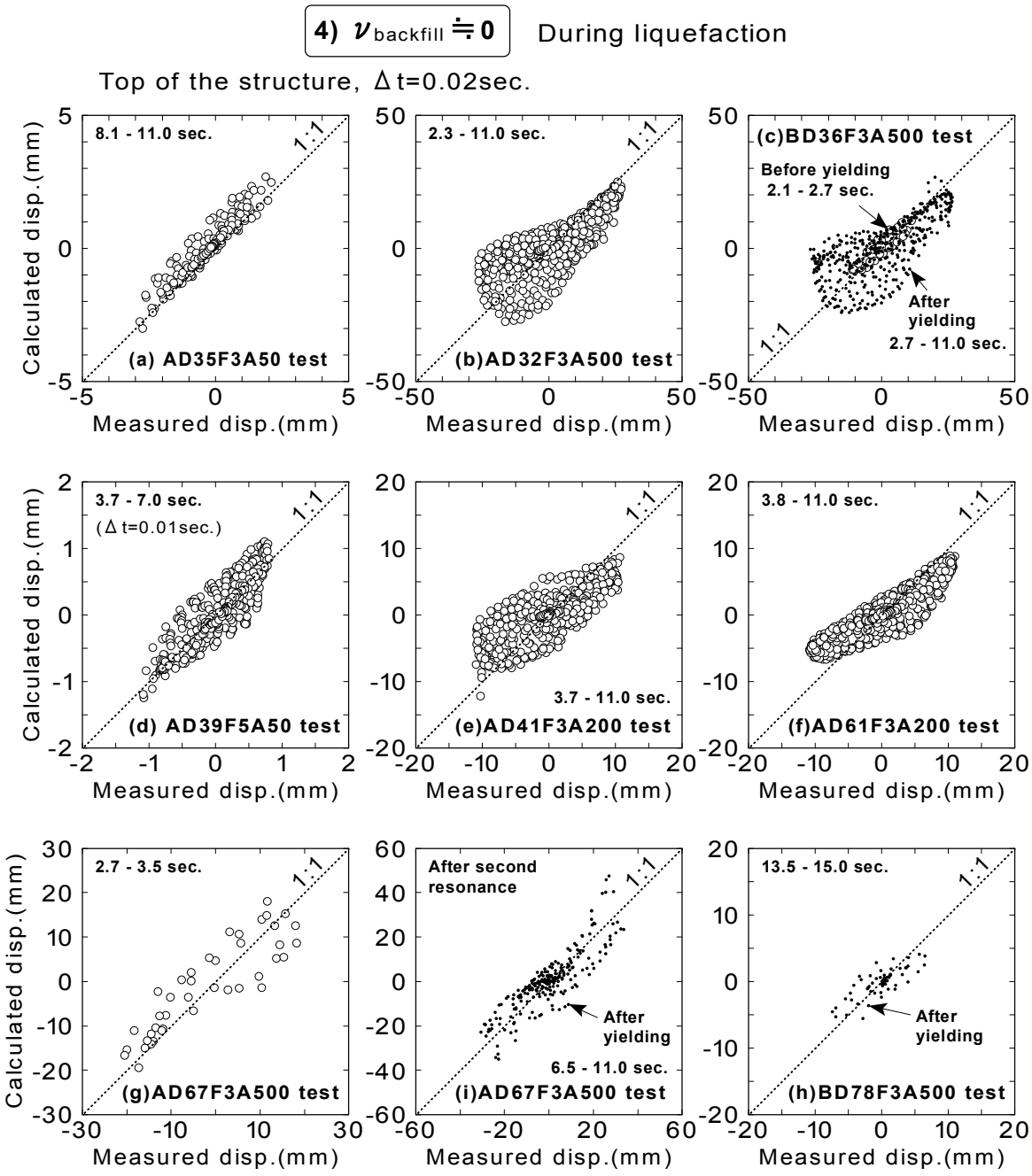

Fig.6.84: Comparison between the calculated and measured displacement at the top of the structure ($\nu_{backfill} \approx 0$)

into two components, a monotonic component and a fluctuating component, for the analysis. In addition, a study based on the calculation using an elastic beam theory was performed to assure an internal consistency among measurements. The measured earth pressure was applied on an elastic beam as a load in the calculation. The followings are conclusion from the study in this chapter:

1. From the observation of monotonic component of curvature, it was inferred that the amount of monotonic component of earth pressure is of the same magnitude between left and right, acting on both sides of structure in the opposite direction.

2. Time histories of the fluctuating component of curvature were almost identical between left and right walls except for the beginning of shaking. It was indicated that the same amount of fluctuating component of earth pressure acted on structure at both side in the same direction when the backfill became soft due to liquefaction.

3. Based on an elastic beam theory, monotonic and fluctuating components of calculated curvature of wall from earth pressure showed good agreement with the measured curvature in tests of initial shaking. Thus, it was shown the monotonic and fluctuating quantities measured on the wall (lateral earth pressures, bending strains and accelerations) were internally consistent.

4. In terms of the monotonic component, the earth pressure in the process of liquefaction was shown to act as a load on a flexible structure all the duration time.

5. Calculated displacement at the top of the structure reasonably agreed with the measured displacement when the natural frequency of backfill became lower than about 0.4～0.67 times that of the structure. It suggests that the deflection of the flexible box section could be calculated by the calculation procedure presented in this section as long as the natural frequency of backfill was lower than that of the structure itself.

6. Considerable disagreement between calculated and measured displacement was observed when the soil behaved in a dilative manner in dense backfill. It was shown that the action of fluctuating component of earth pressure becomes complicated when soil behaves in a dilative manner.

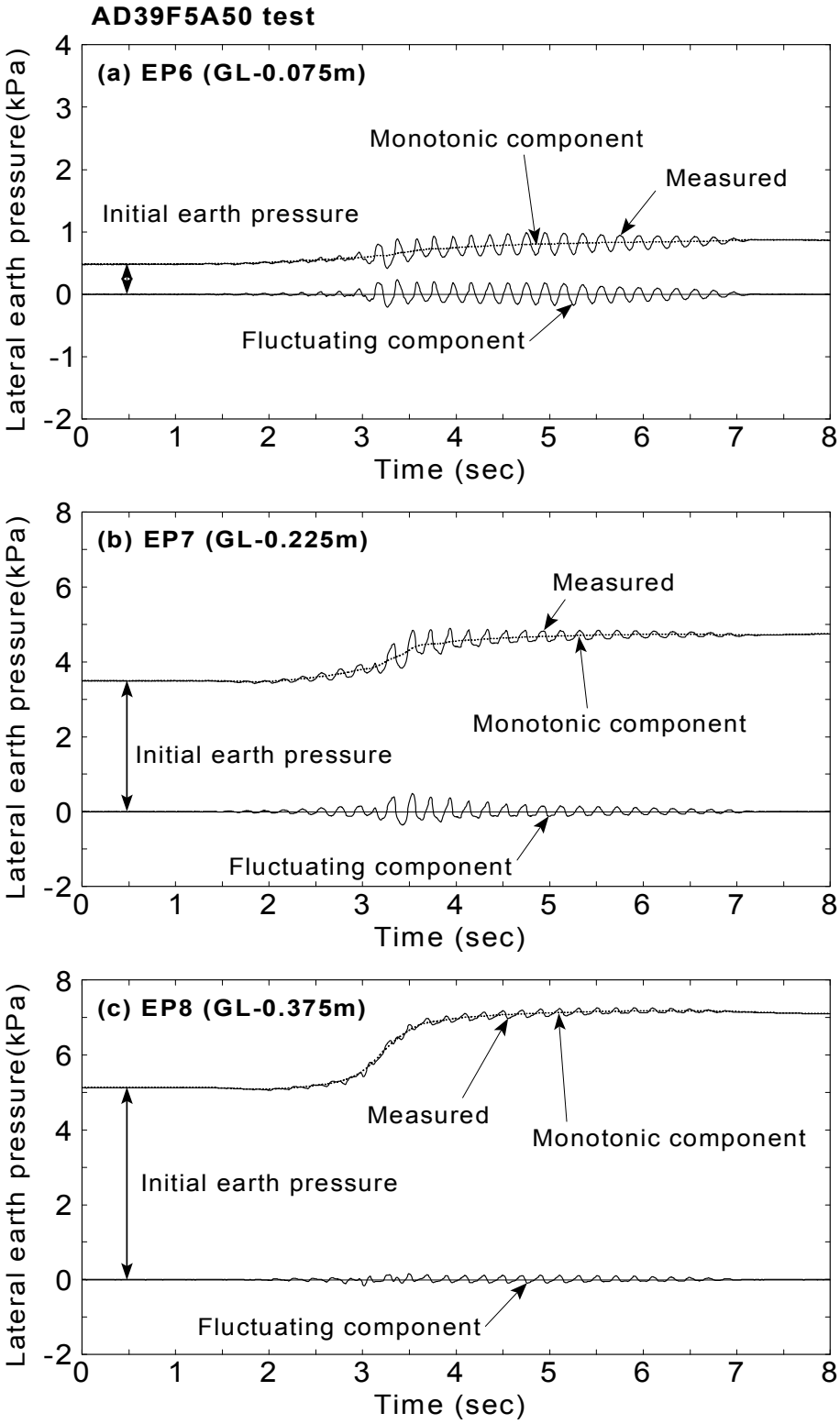

Fig.6.85: Monotonic and fluctuating component of earth pressures considered in the analysis (AD39F5A50 test)

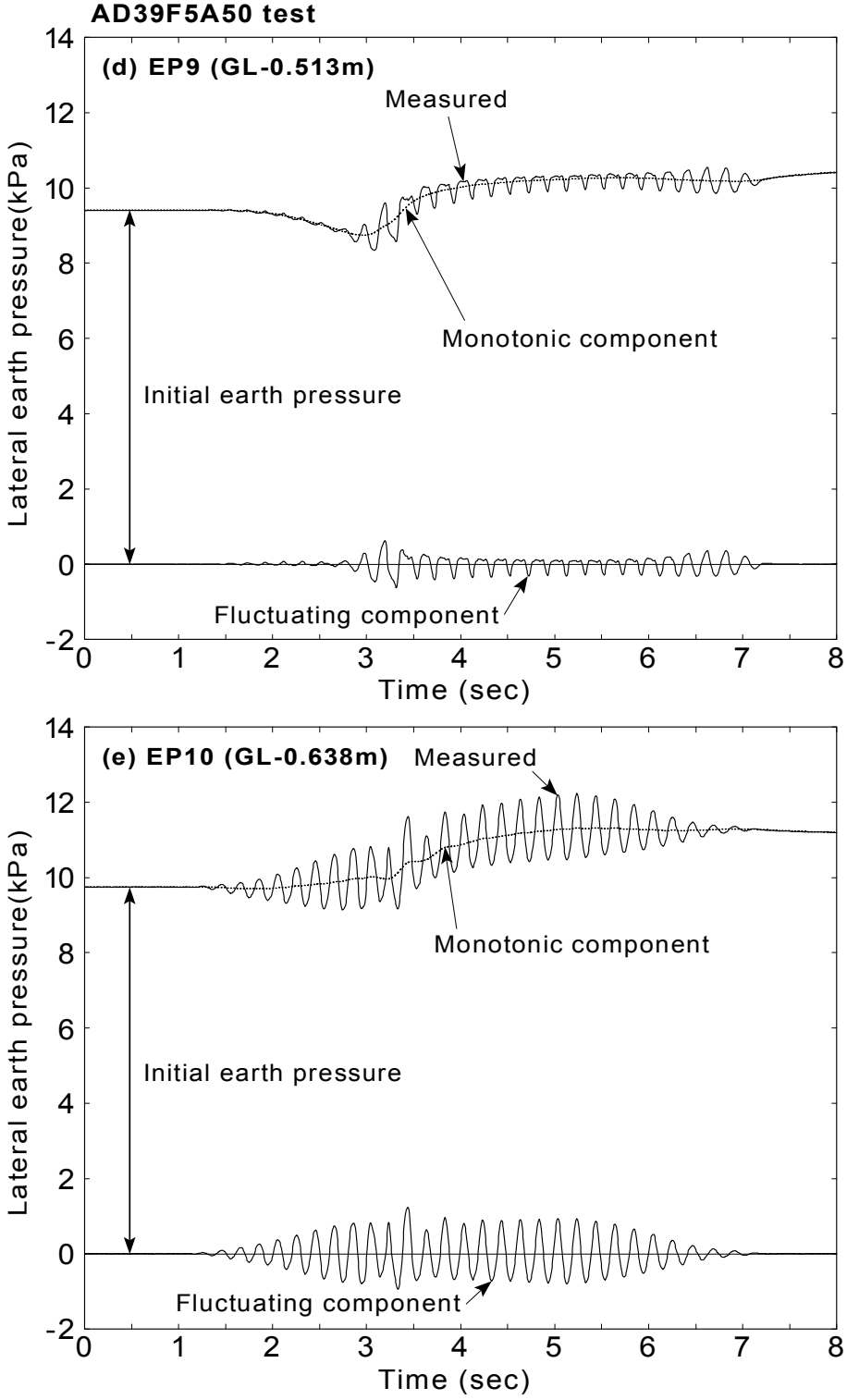

Fig.6.85: Continued

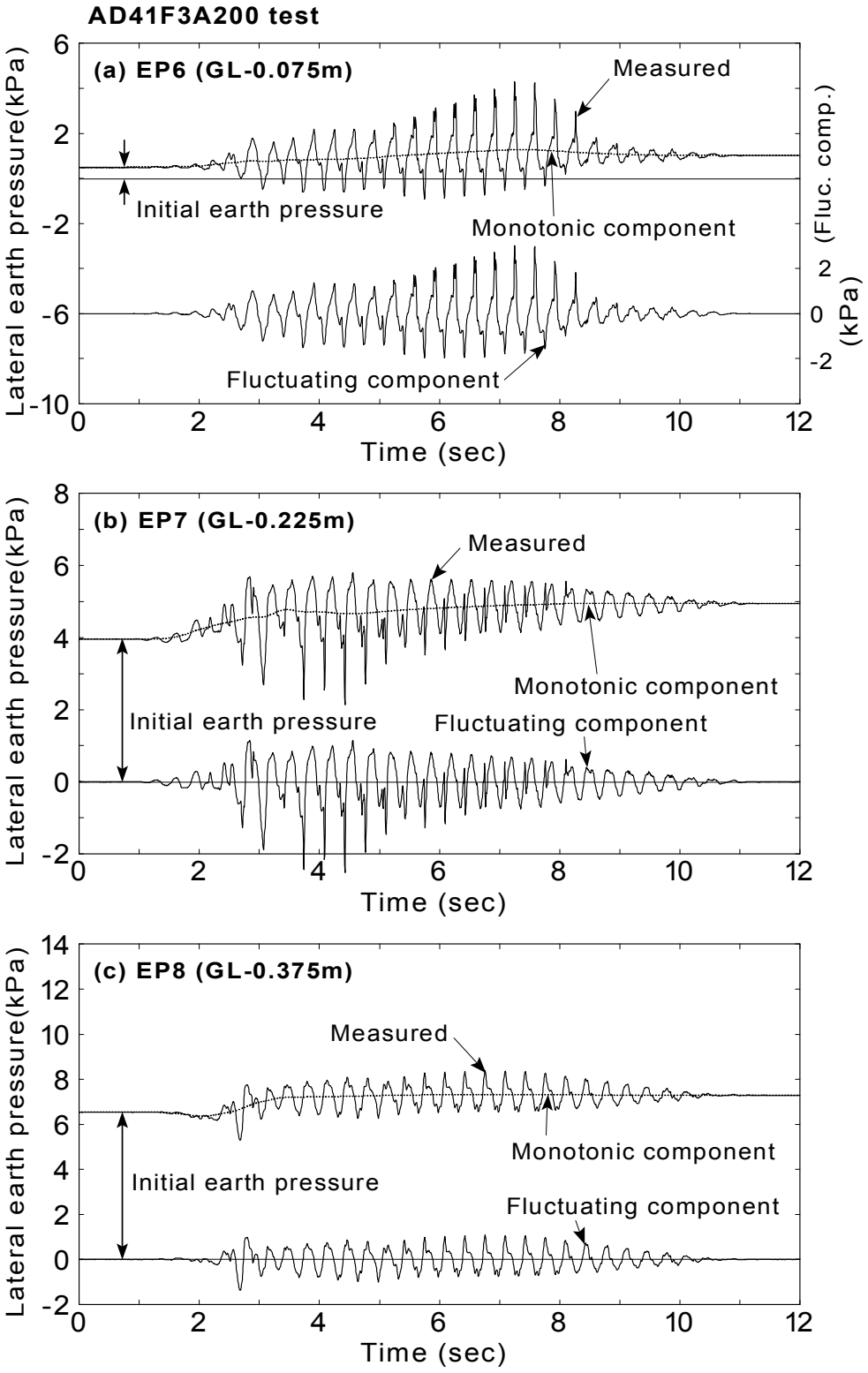

Fig.6.86: Monotonic and fluctuating component of earth pressures considered in the analysis (AD41F3A200 test)

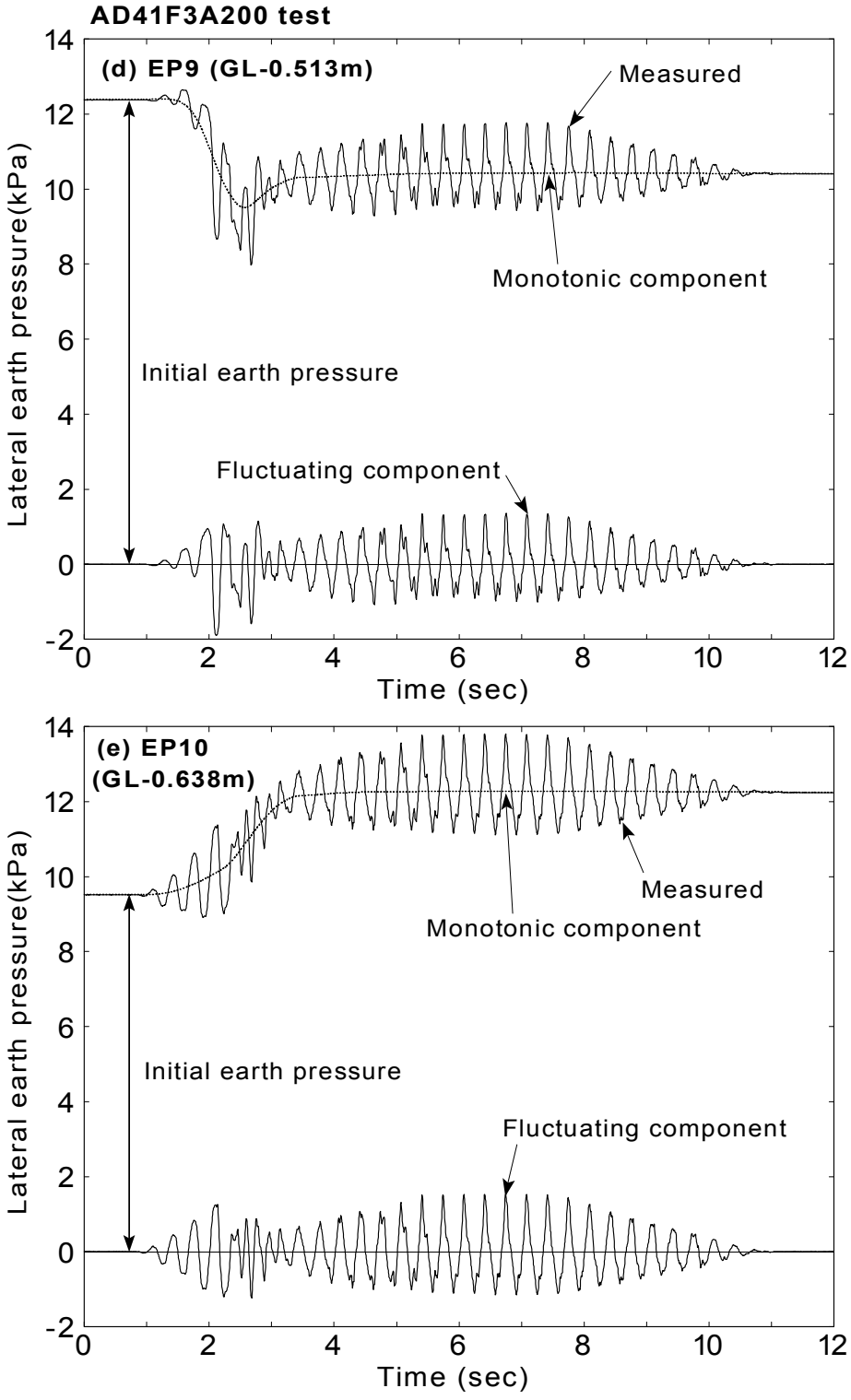

Fig.6.86: Continued

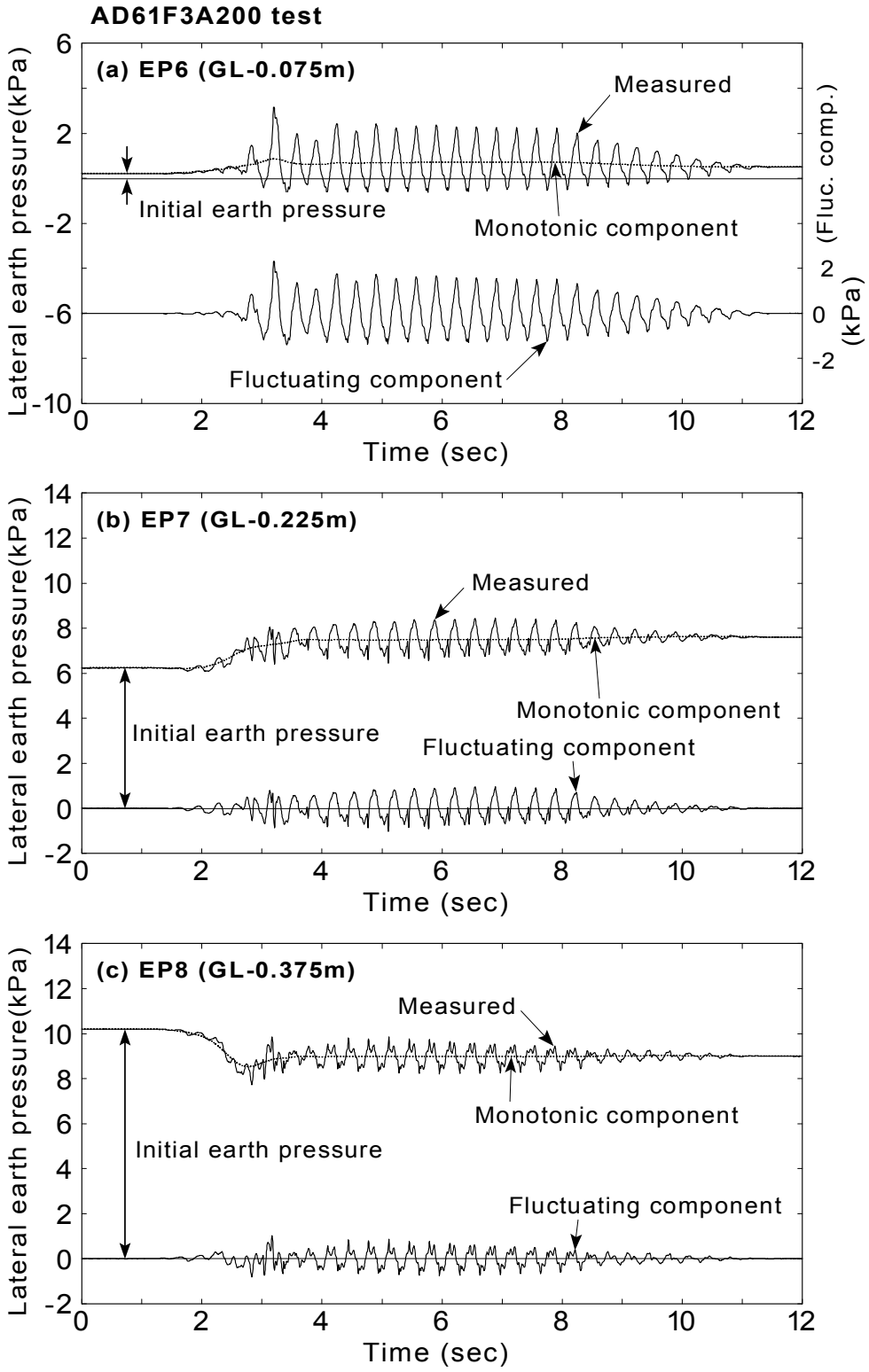

Fig.6.87: Monotonic and fluctuating component of earth pressures considered in the analysis (AD61F3A200 test)

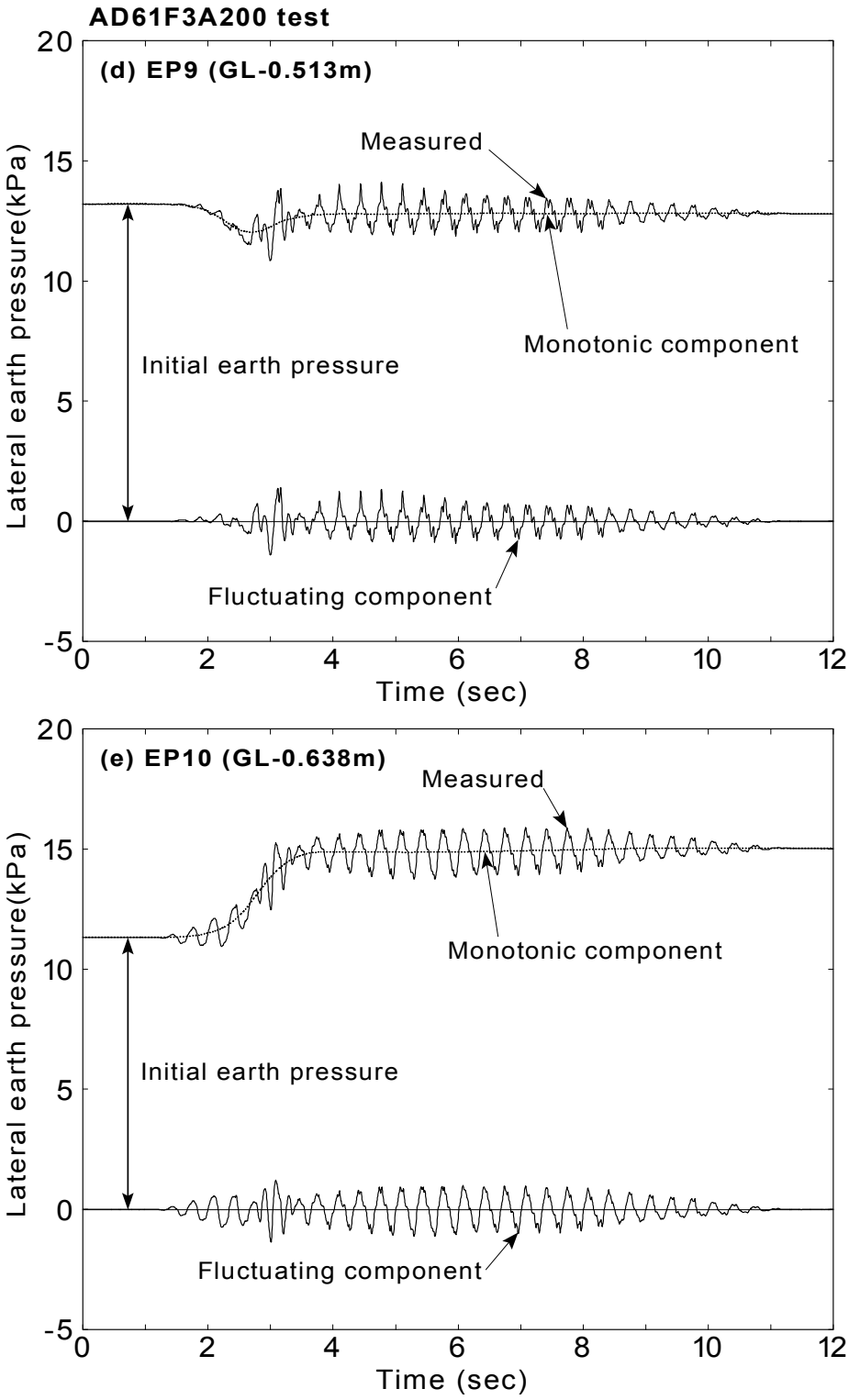

Fig.6.87: Continued

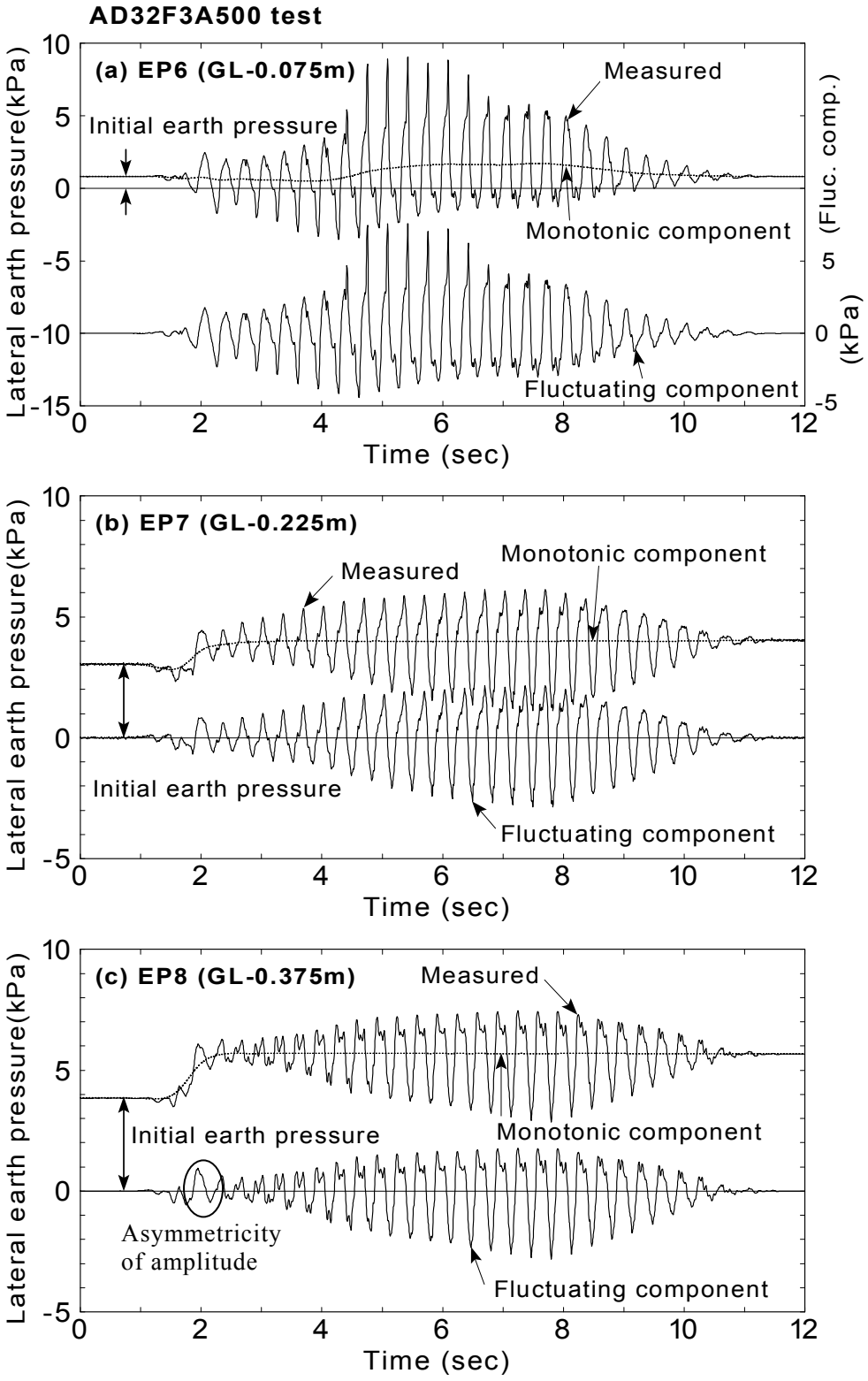

Fig.6.88: Monotonic and fluctuating component of earth pressures considered in the analysis (AD32F3A500 test)

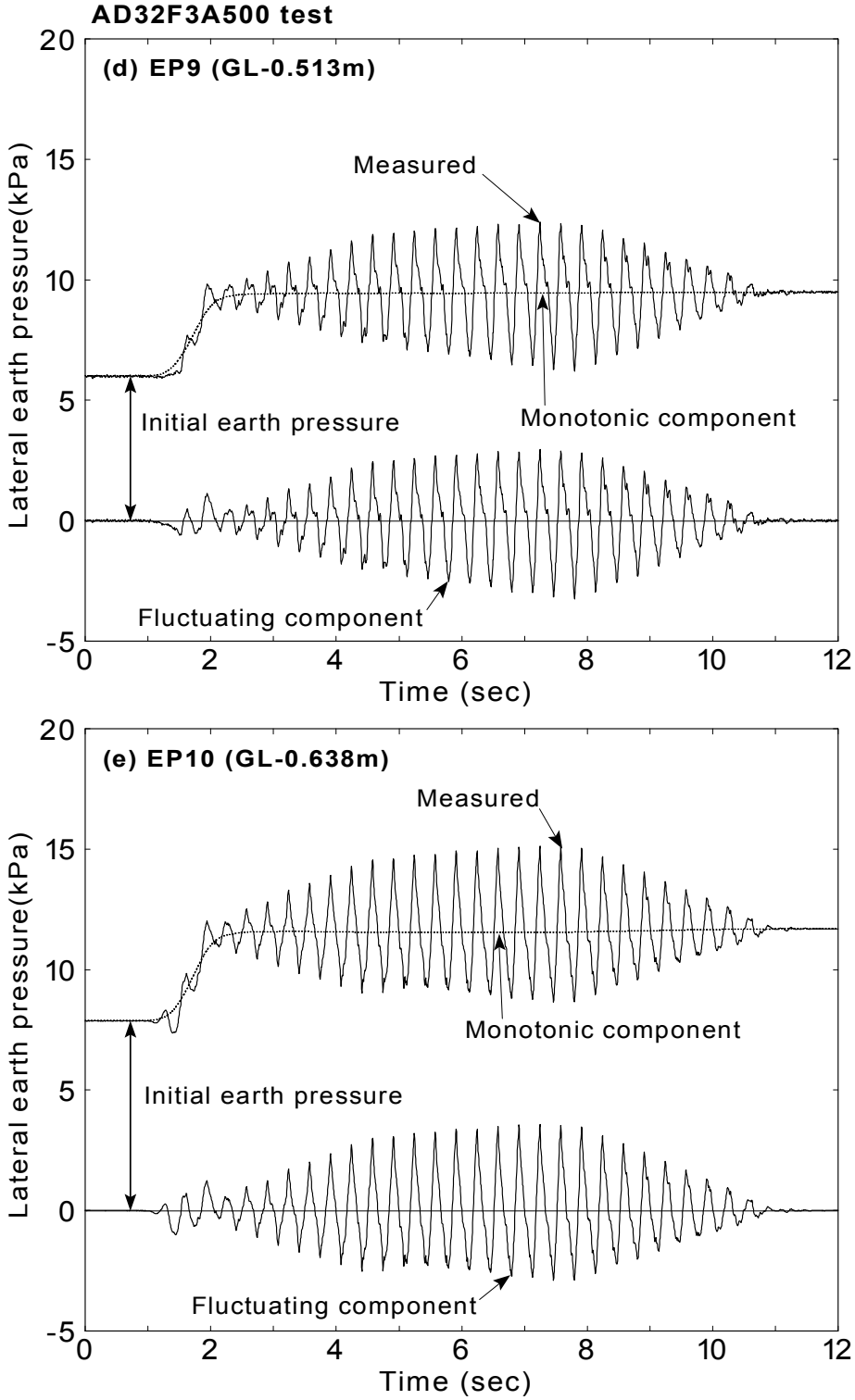

Fig.6.88: Continued

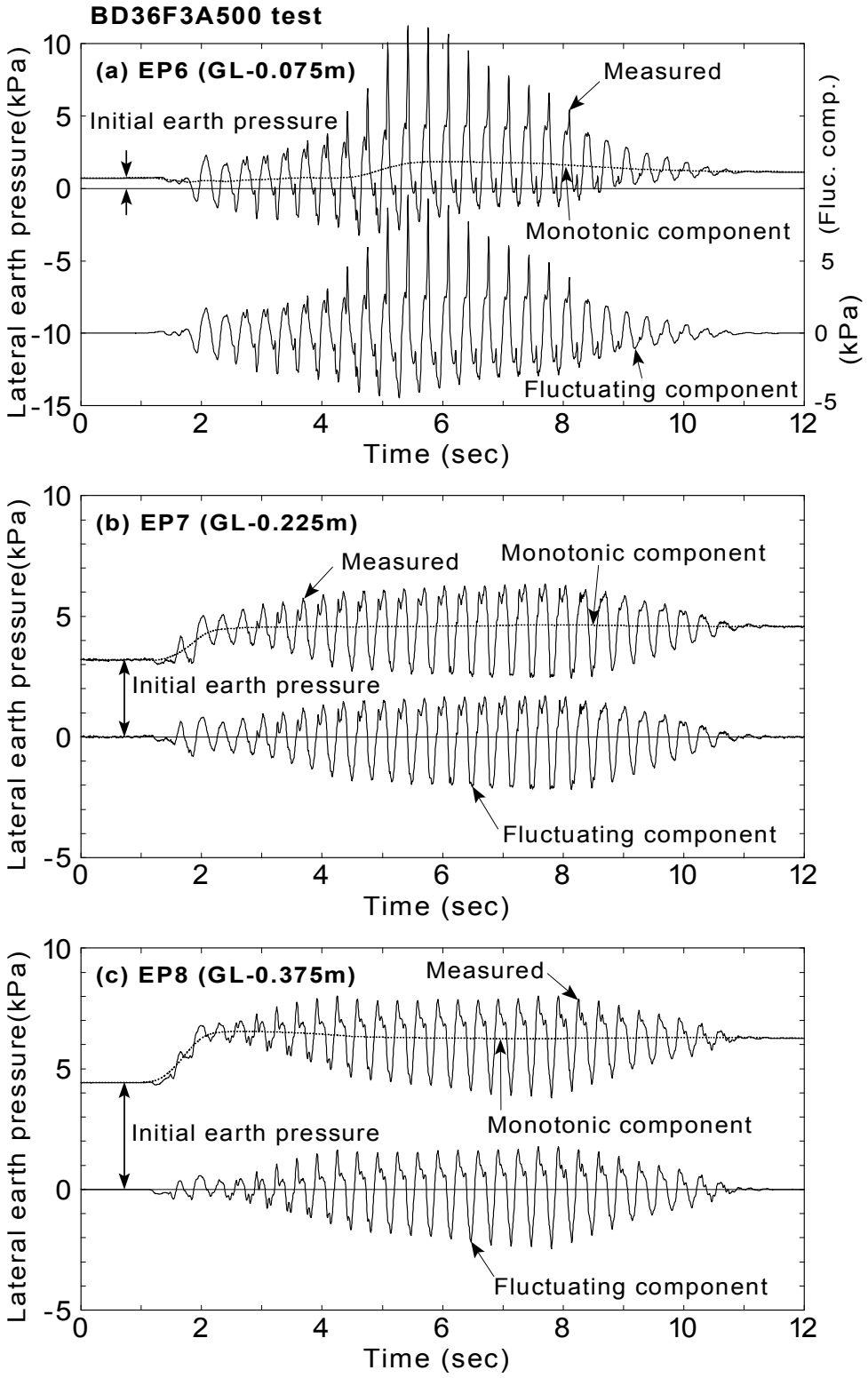

Fig.6.89: Monotonic and fluctuating component of earth pressures considered in the analysis (BD36F3A500 test)

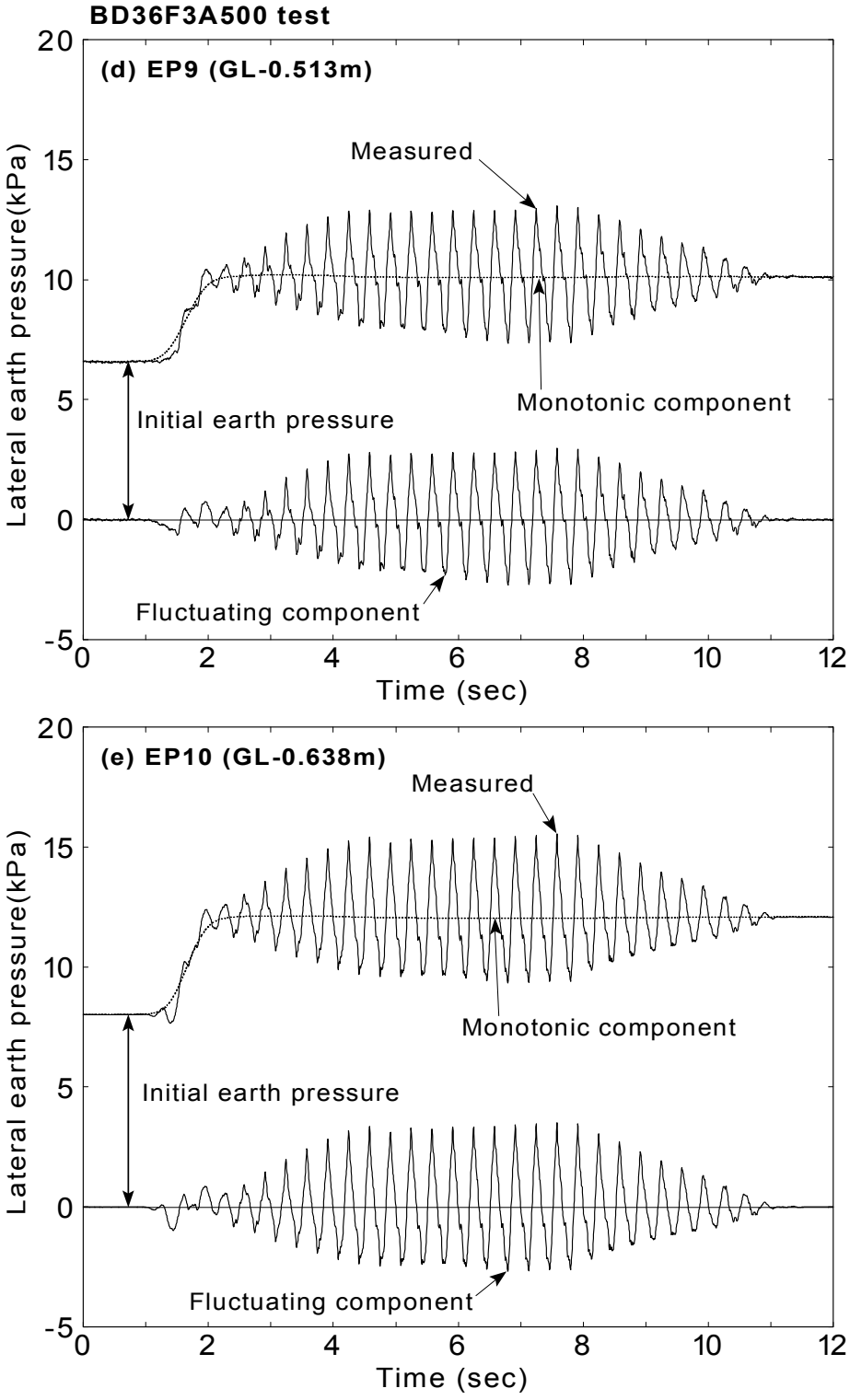

Fig.6.89: Continued

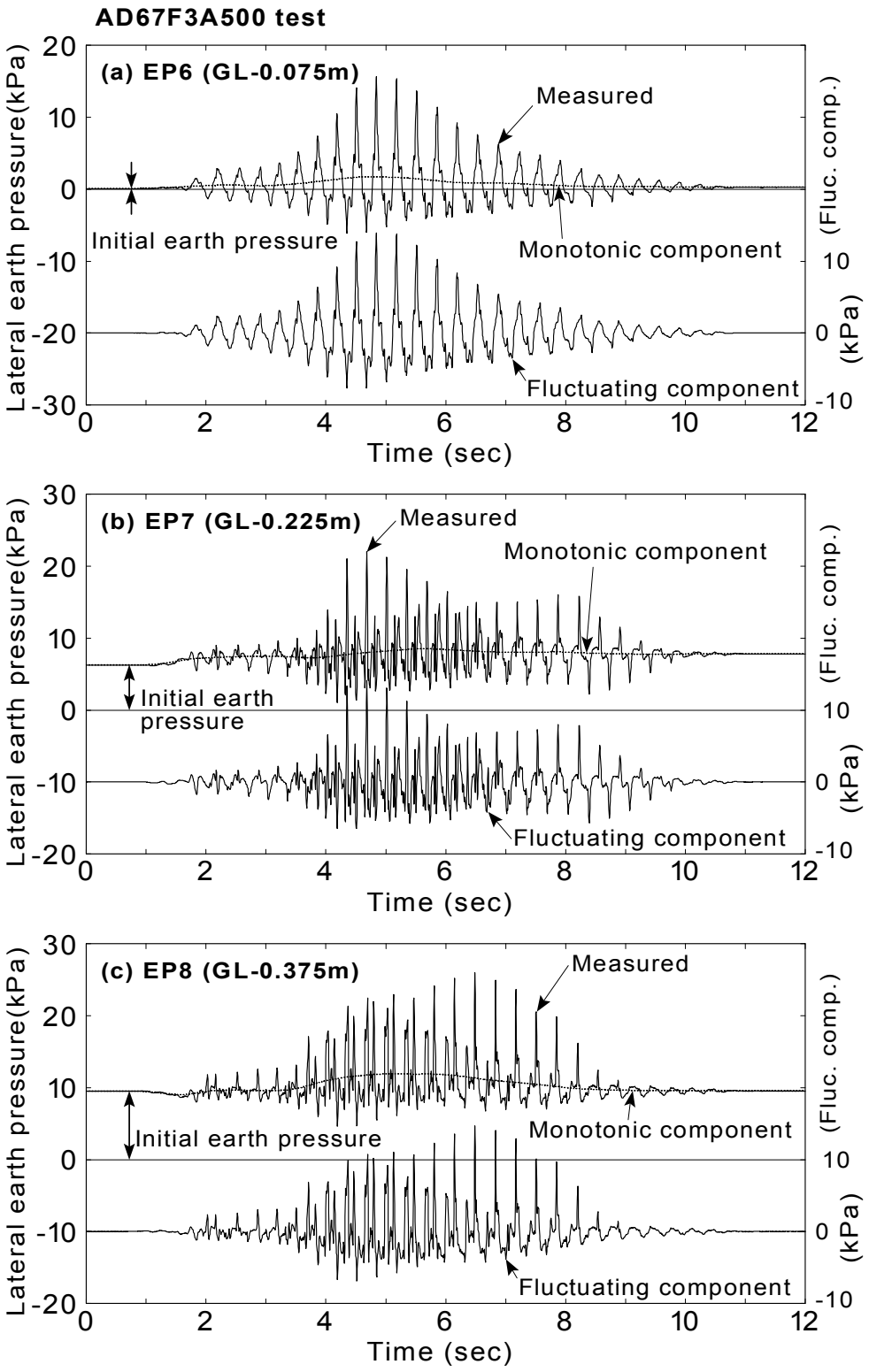

Fig.6.90: Monotonic and fluctuating component of earth pressures considered in the analysis (AD67F3A500 test)

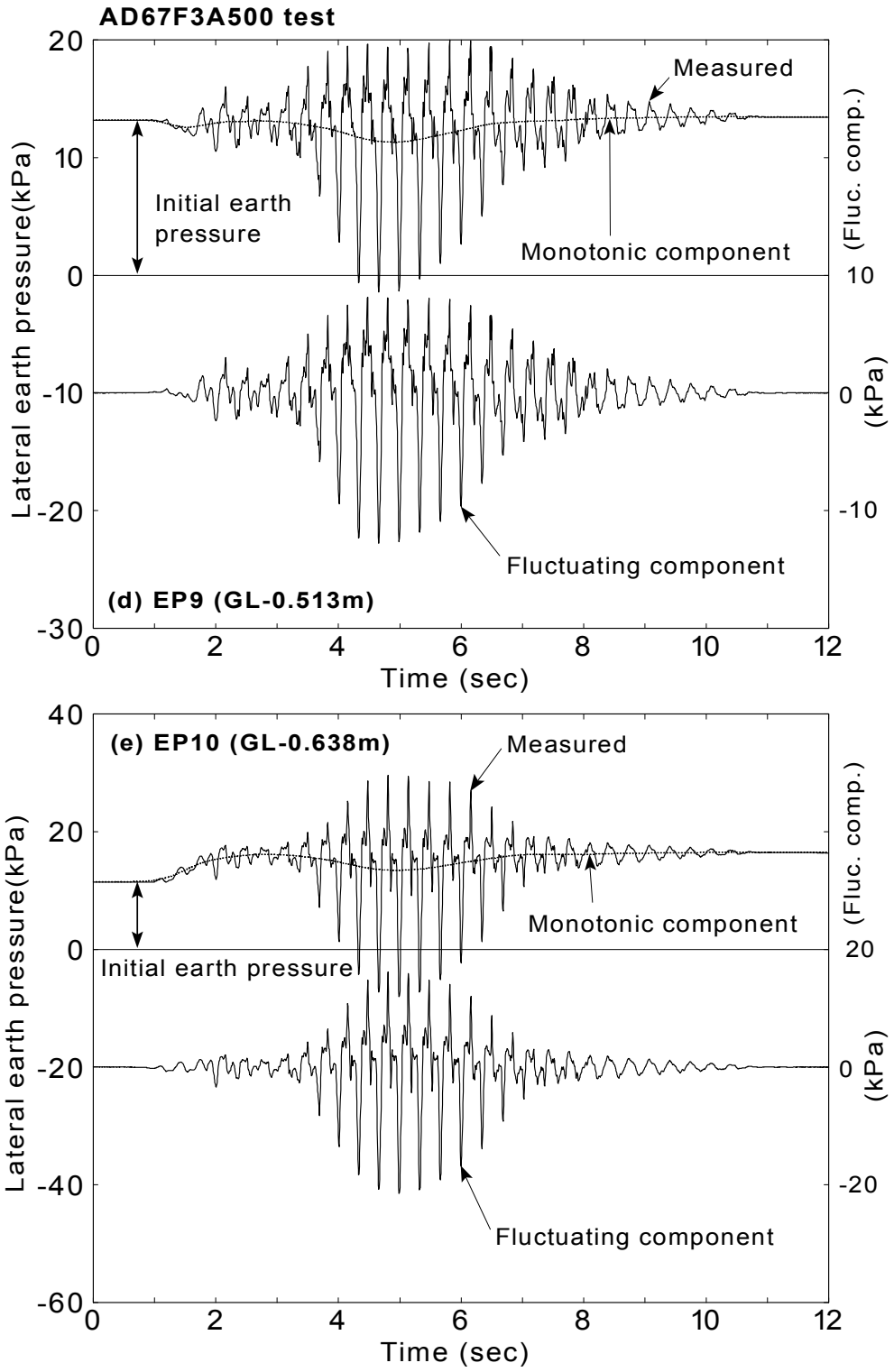

Fig.6.90: Continued

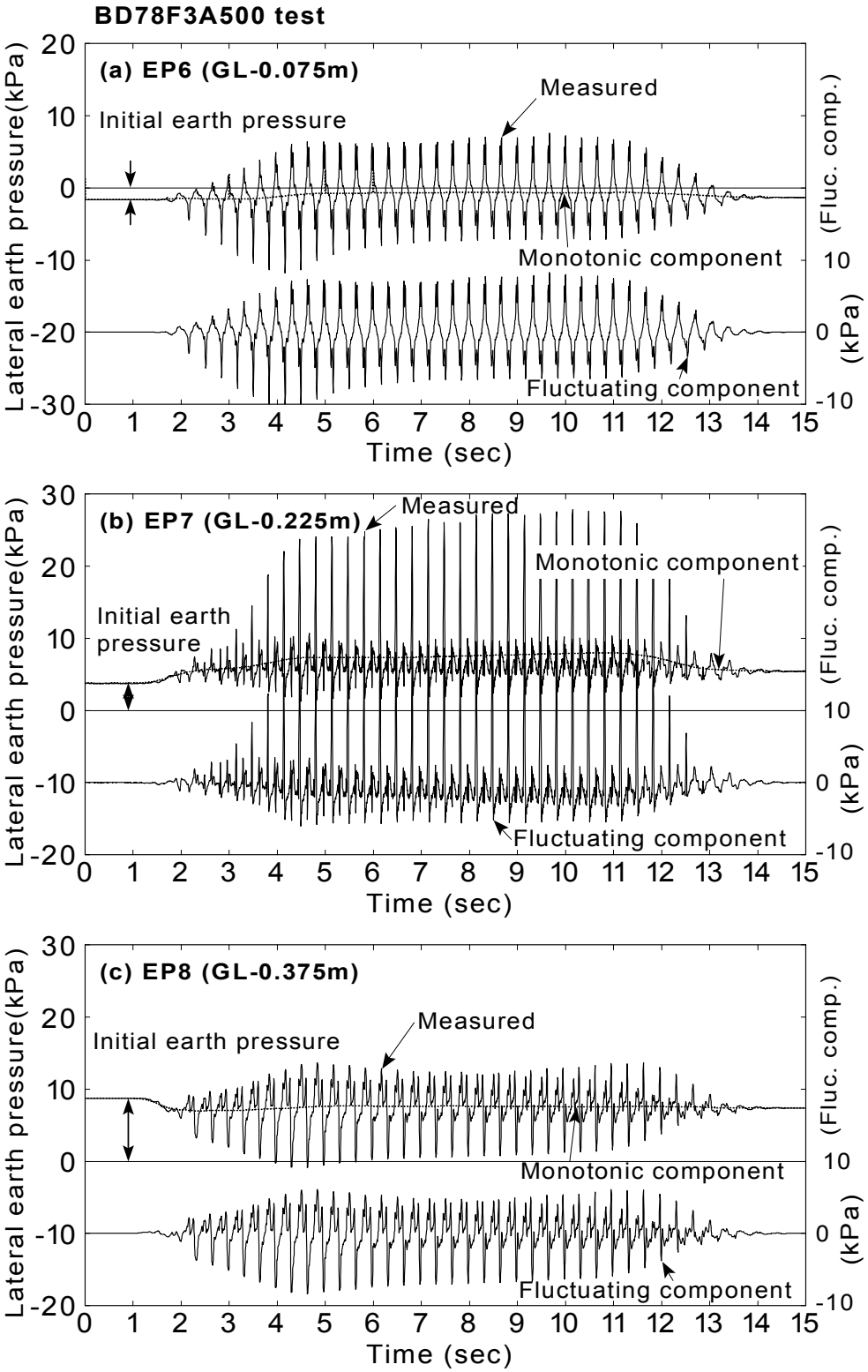

Fig.6.91: Monotonic and fluctuating component of earth pressures considered in the analysis (BD78F3A500 test)

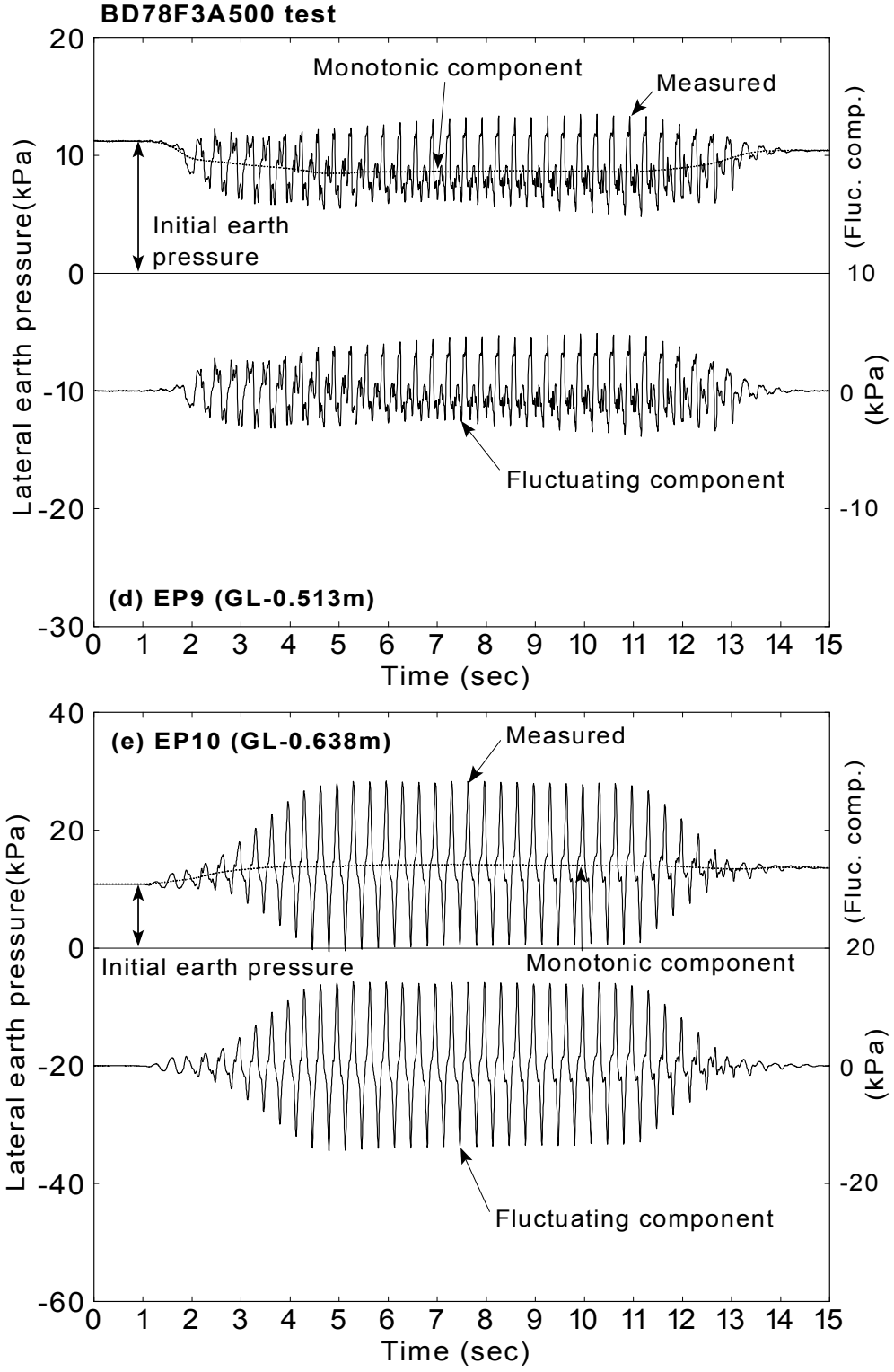

Fig.6.91: Continued

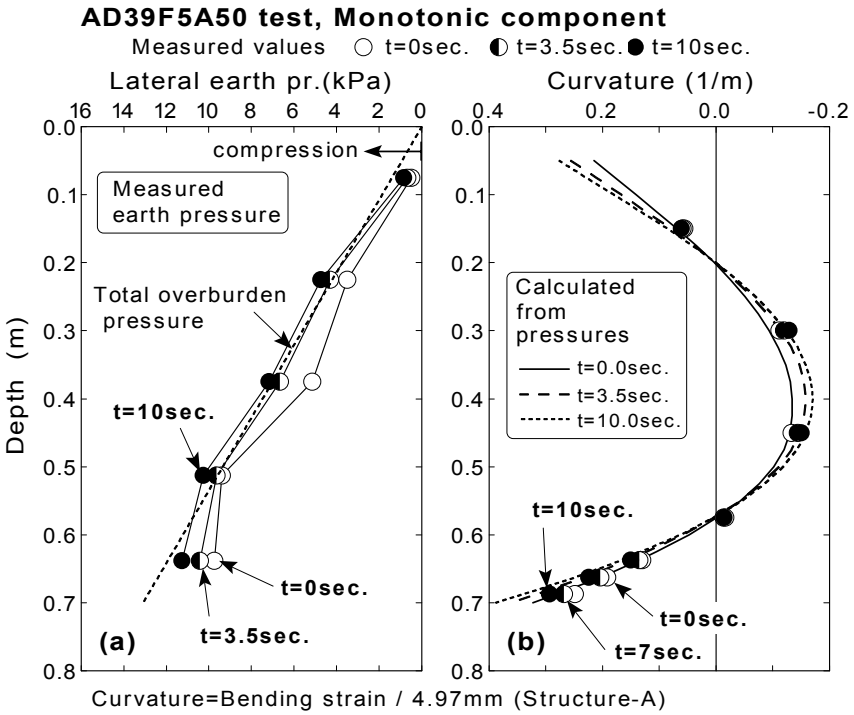

Fig.6.92: Comparison between measured and calculated curvature (Monotonic component, AD39F5A50 test)

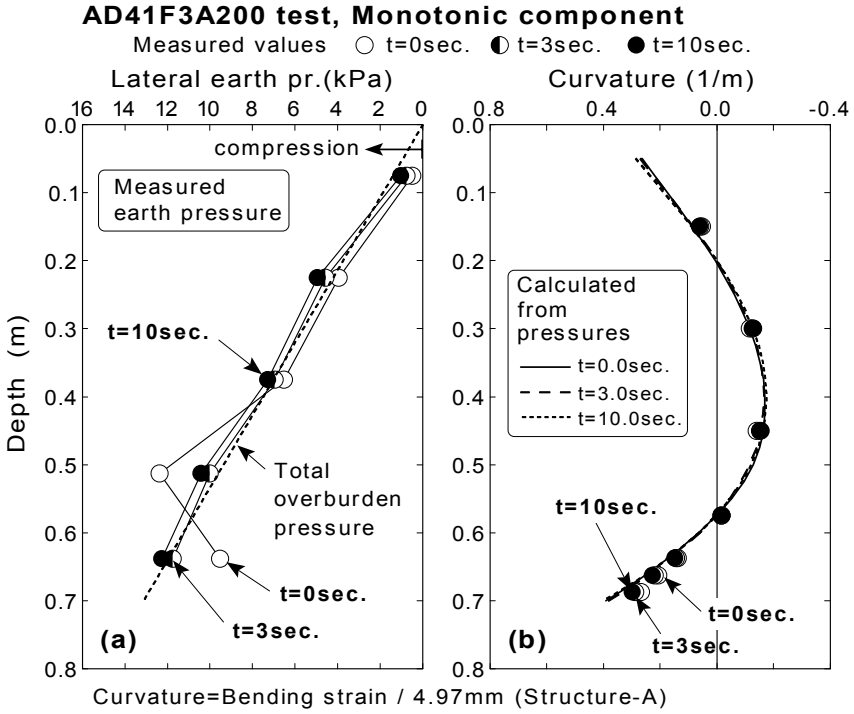

Fig.6.93: Comparison between measured and calculated curvature (Monotonic component, AD41F3A200 test)

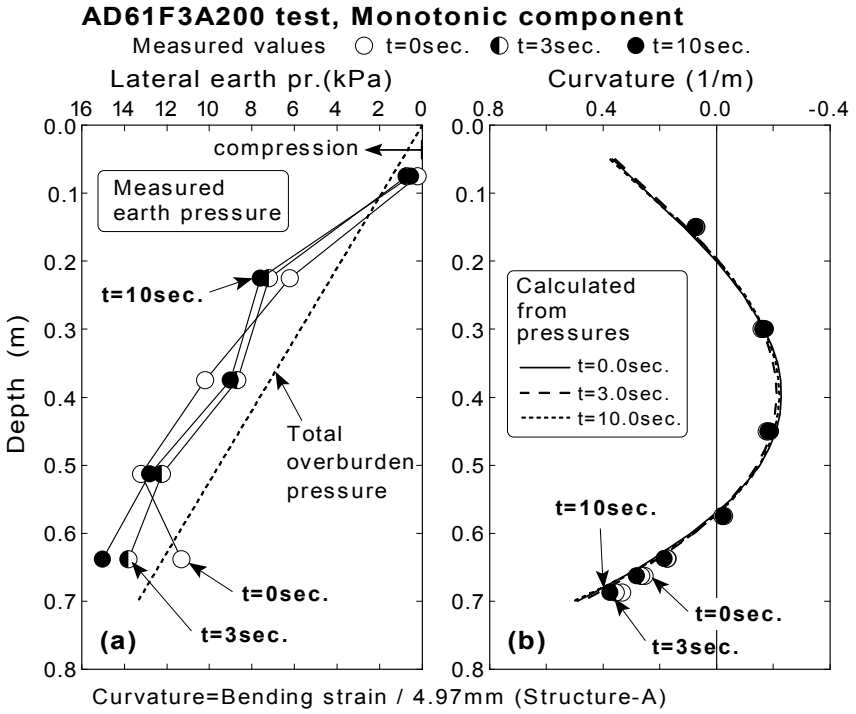

Fig.6.94: Comparison between measured and calculated curvature (Monotonic component, AD61F3A200 test)

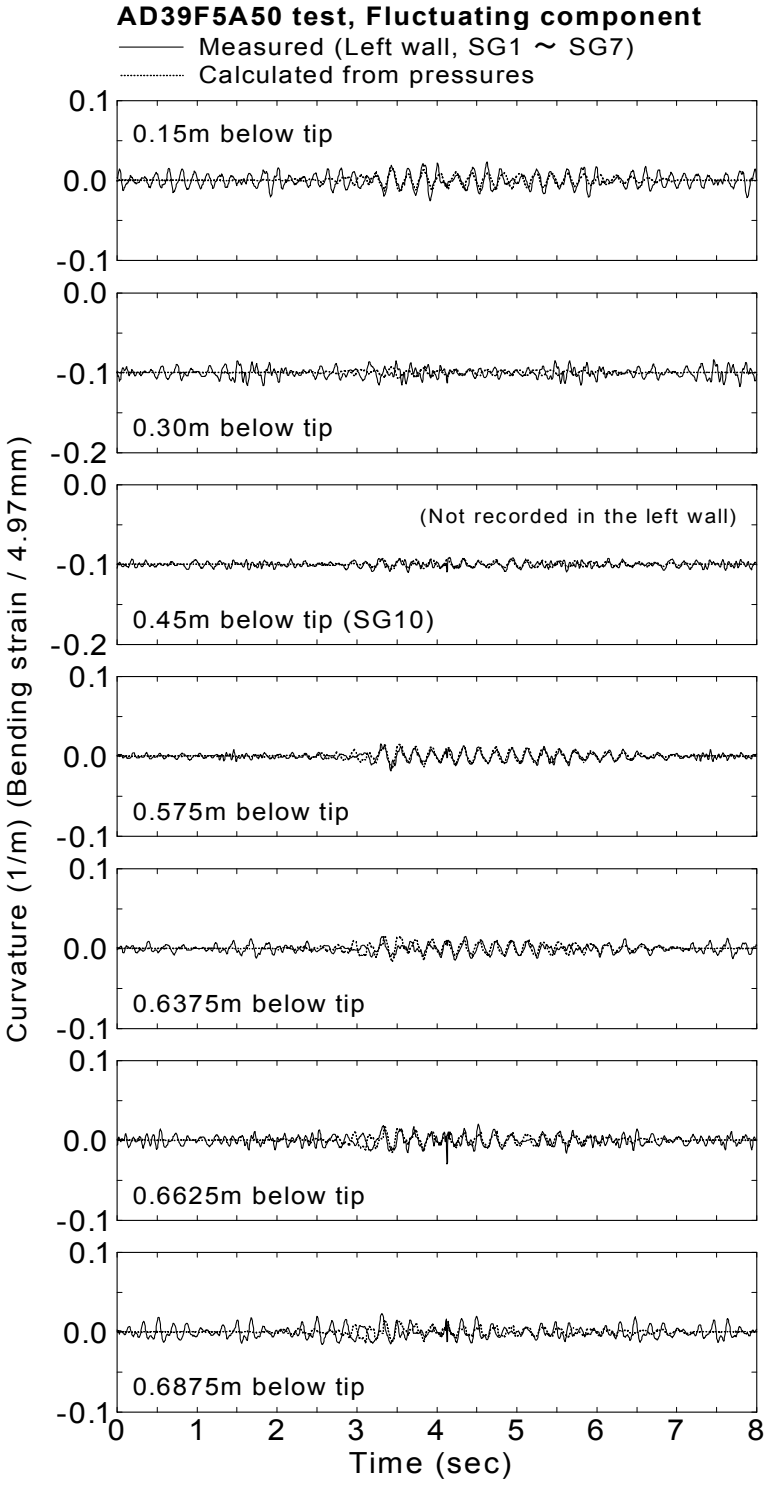

Fig.6.95: Comparison between measured and calculated curvature of fluctuating component (AD39F3A50 test)

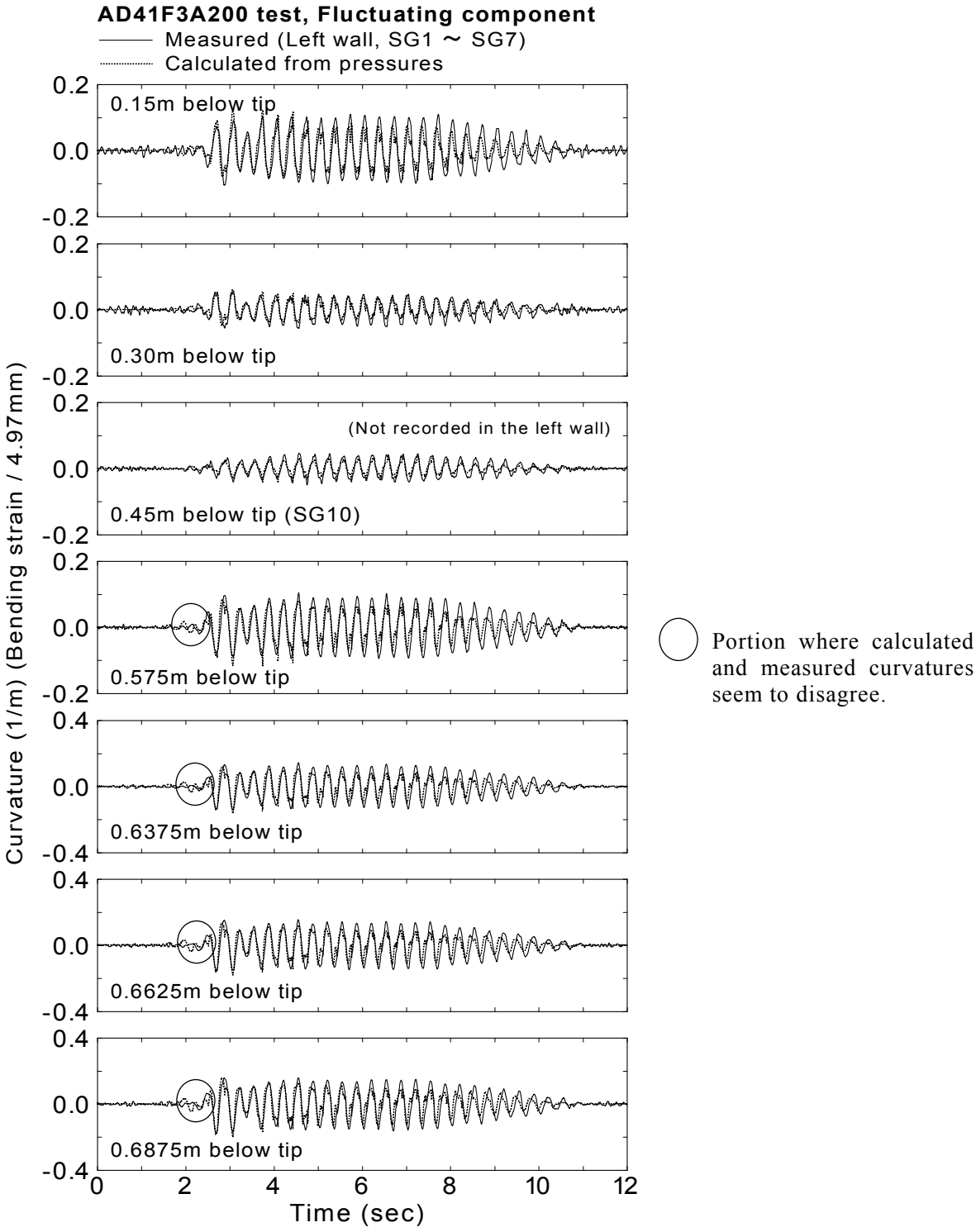

Fig.6.96: Comparison between measured and calculated curvature of fluctuating component (AD41F3A200 test)

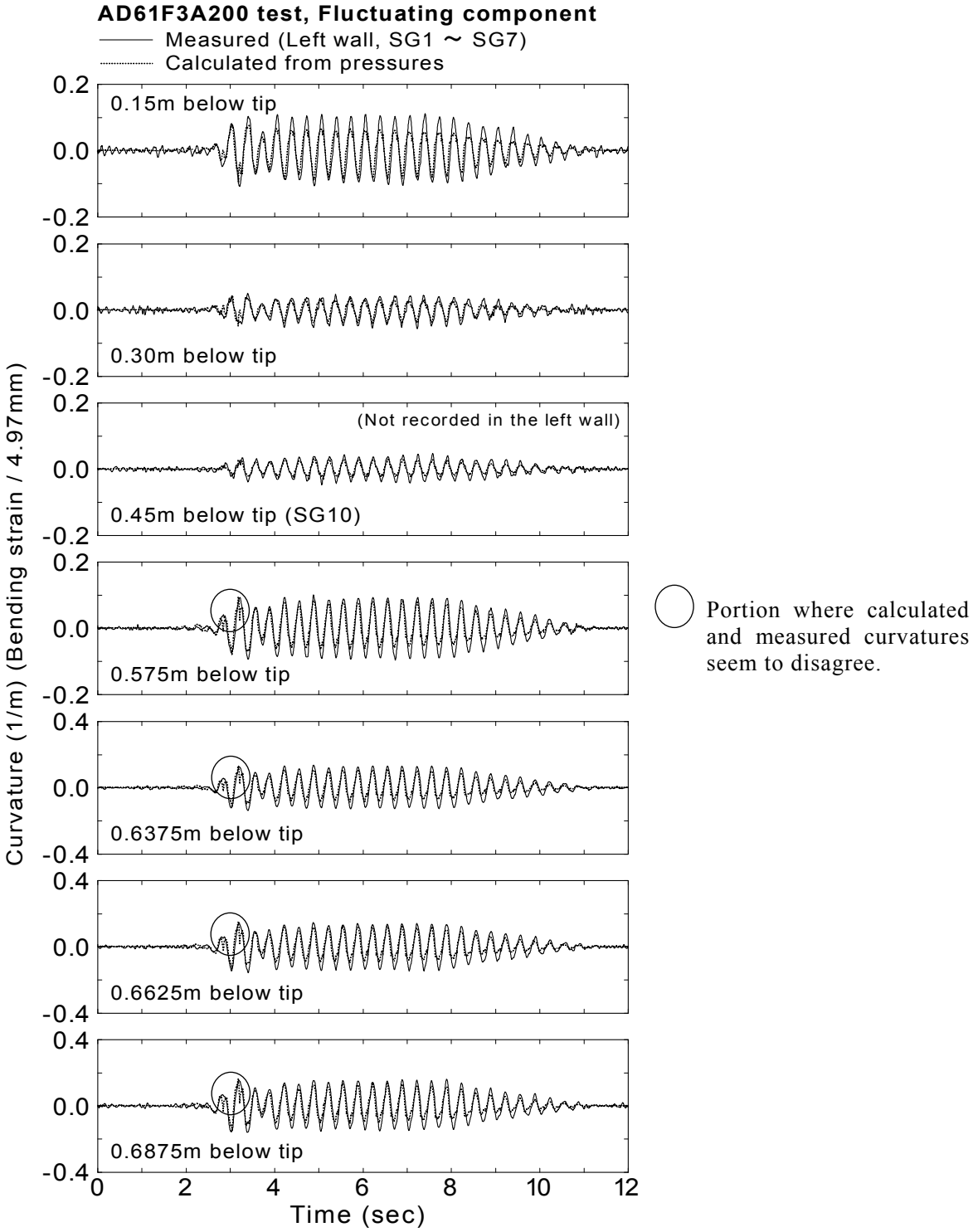

Fig.6.97: Comparison between measured and calculated curvature of fluctuating component (AD61F3A200 test)

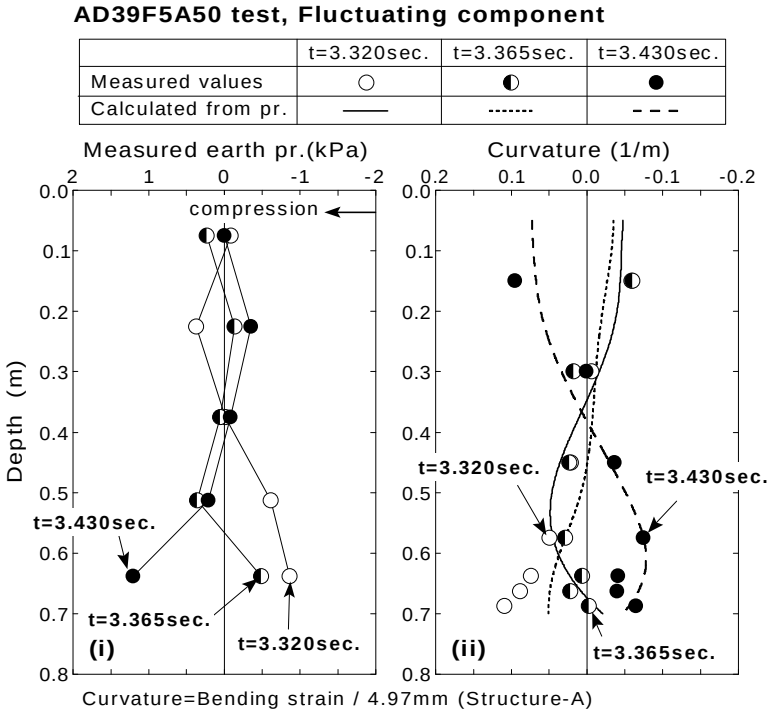

(a) Profiles at resonance of structure

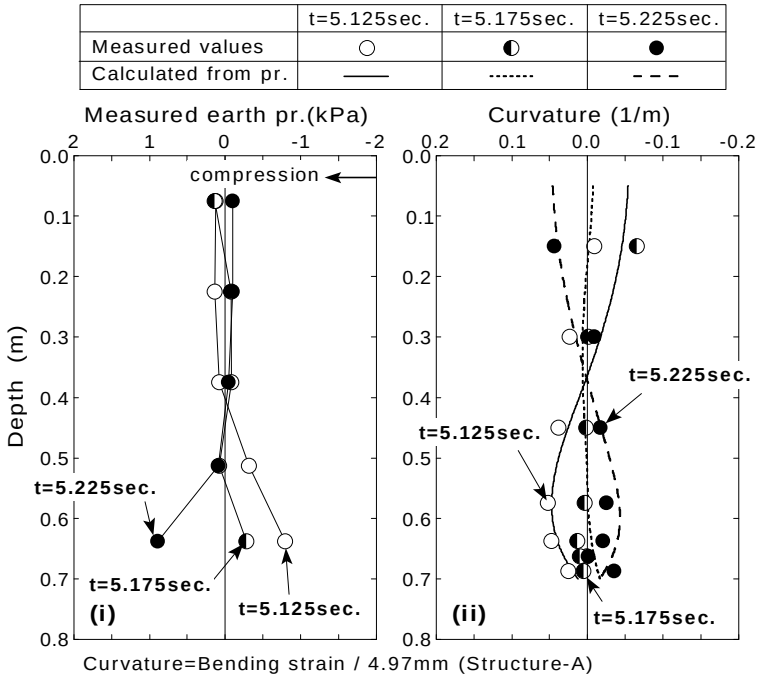

(b) Profile during complete liquefaction

Fig.6.98: Comparison between fluctuating components of measured and calculated curvatures (AD39F5A50 test)

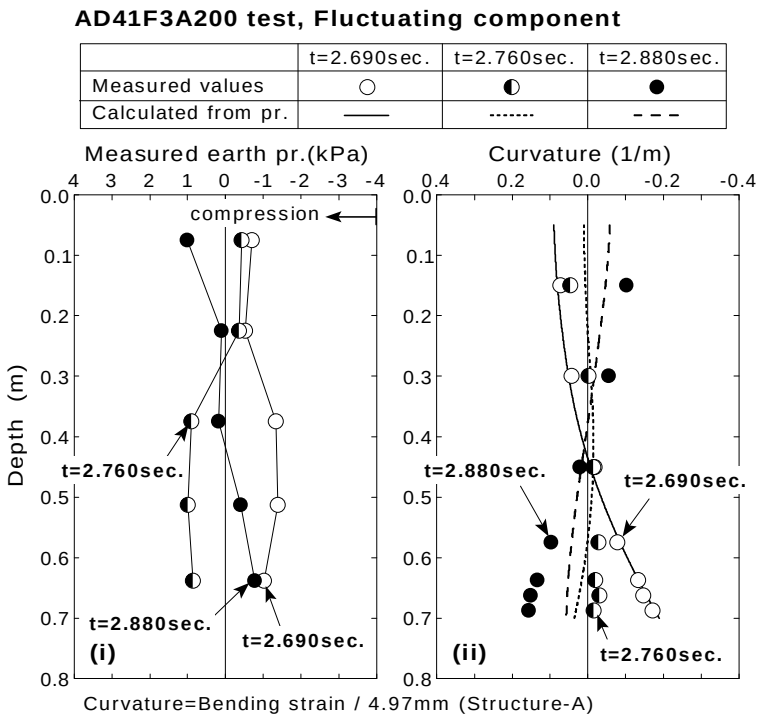

(a) Profiles at resonance of structure

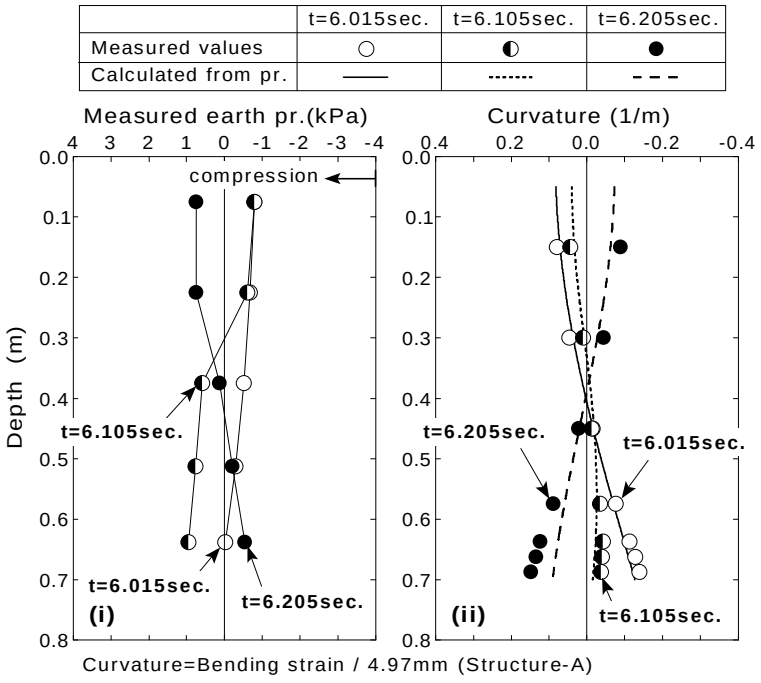

(b) Profile during complete liquefaction

Fig.6.99: Comparison between fluctuating components of measured and calculated curvatures (AD41F3A200 test)

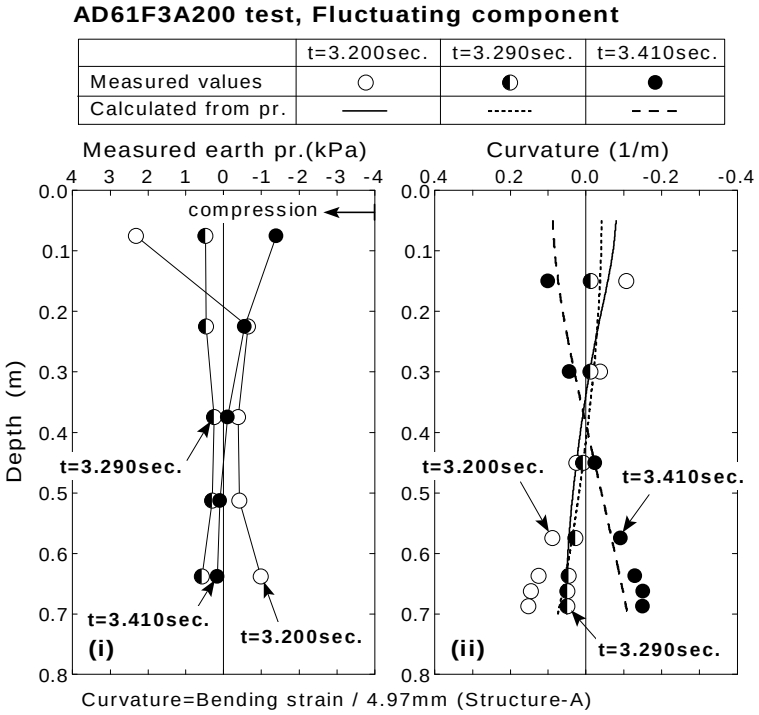

(a) Profiles at resonance of structure

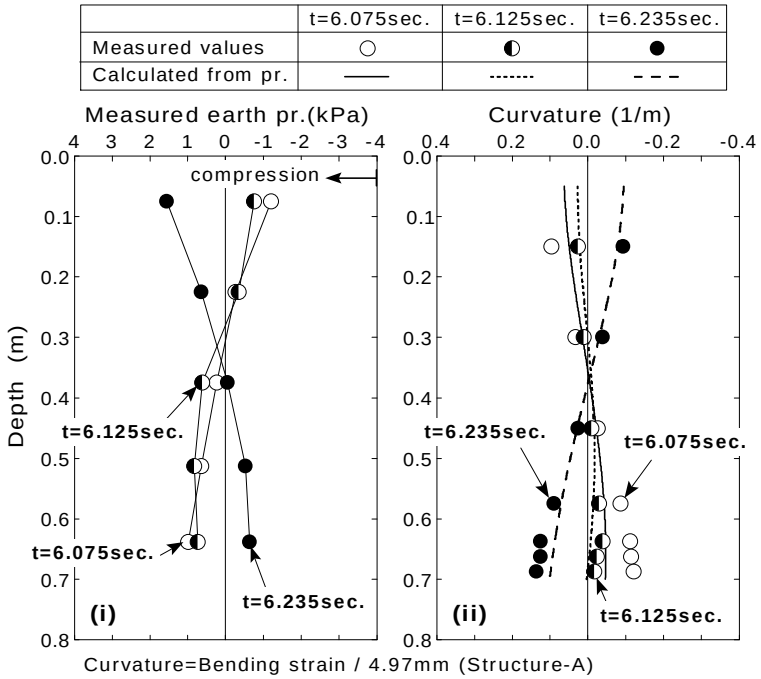

(b) Profile during complete liquefaction

Fig.6.100: Comparison between fluctuating components of measured and calculated curvatures (AD61F3A200 test)

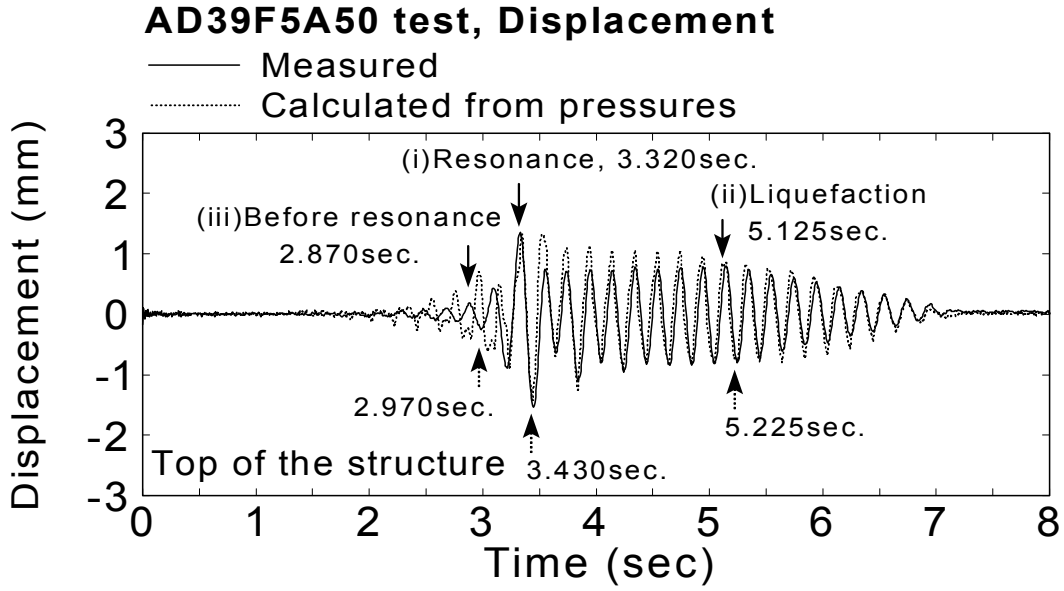

Fig.6.101: Comparison of time histories between measured and calculated displacement at the top of the structure (AD39F5A50 test)

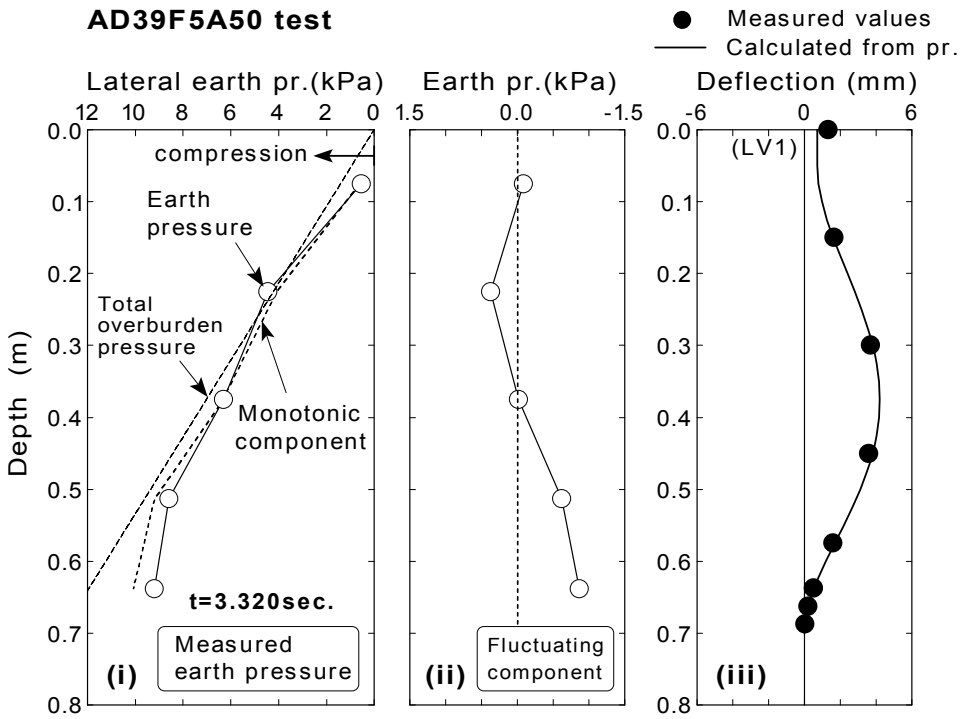

(a) At resonance, t=3.320 seconds

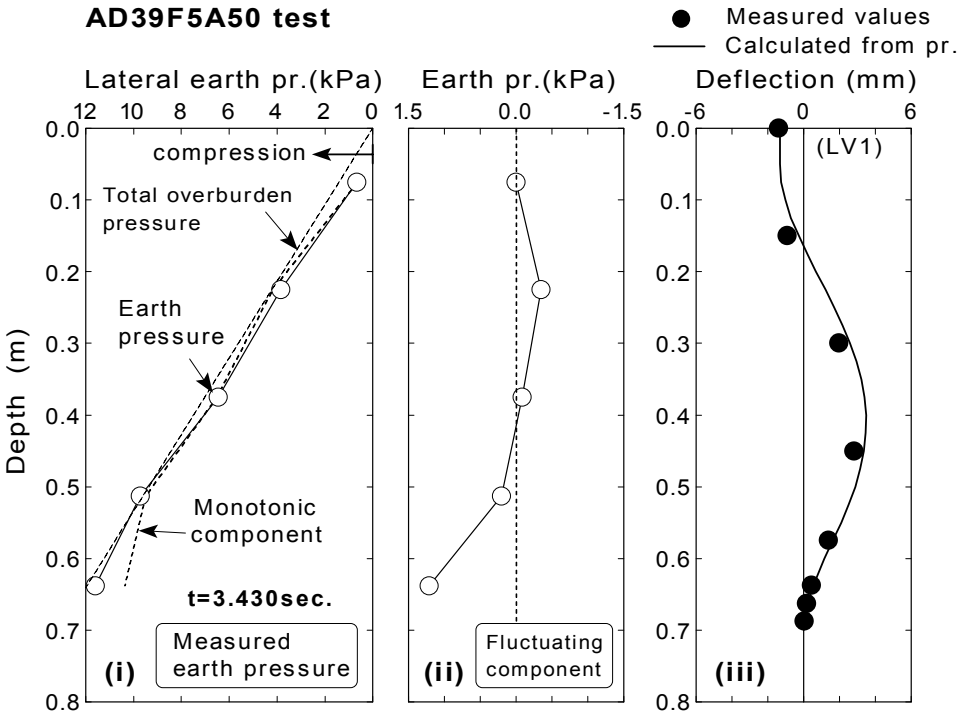

(b) A half cycle after resonance, t=3.430 seconds

Fig.6.102: Earth pressure and deflection at resonance (AD39F5A50 test)

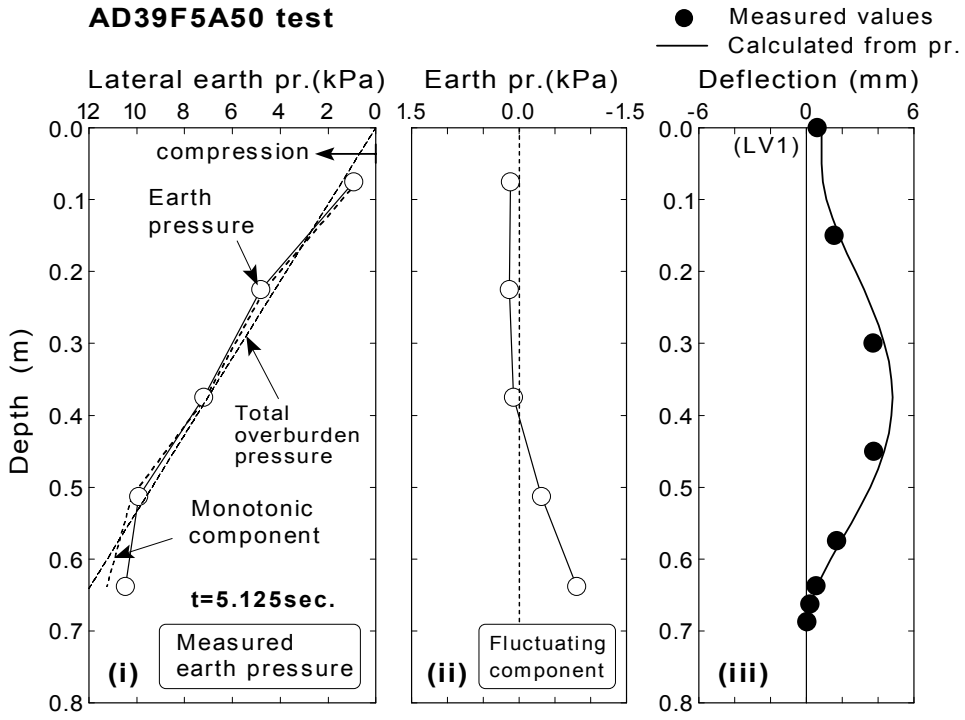

(a) t=5.125 seconds

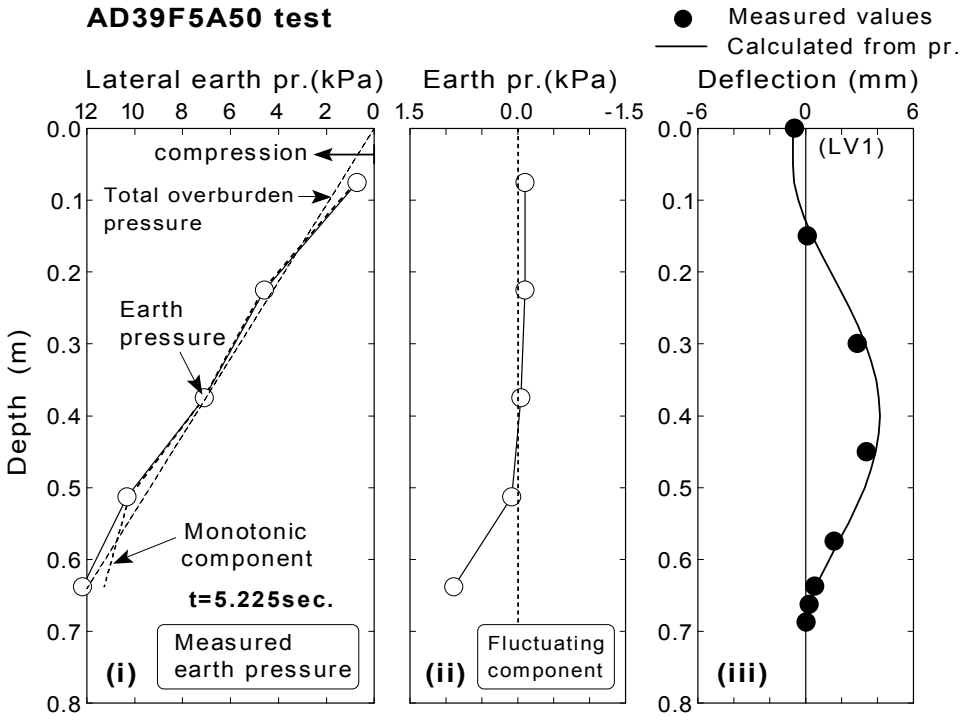

(b) t=5.225 seconds

Fig.6.103: Earth pressure and deflection during liquefaction (AD39F5A50 test)

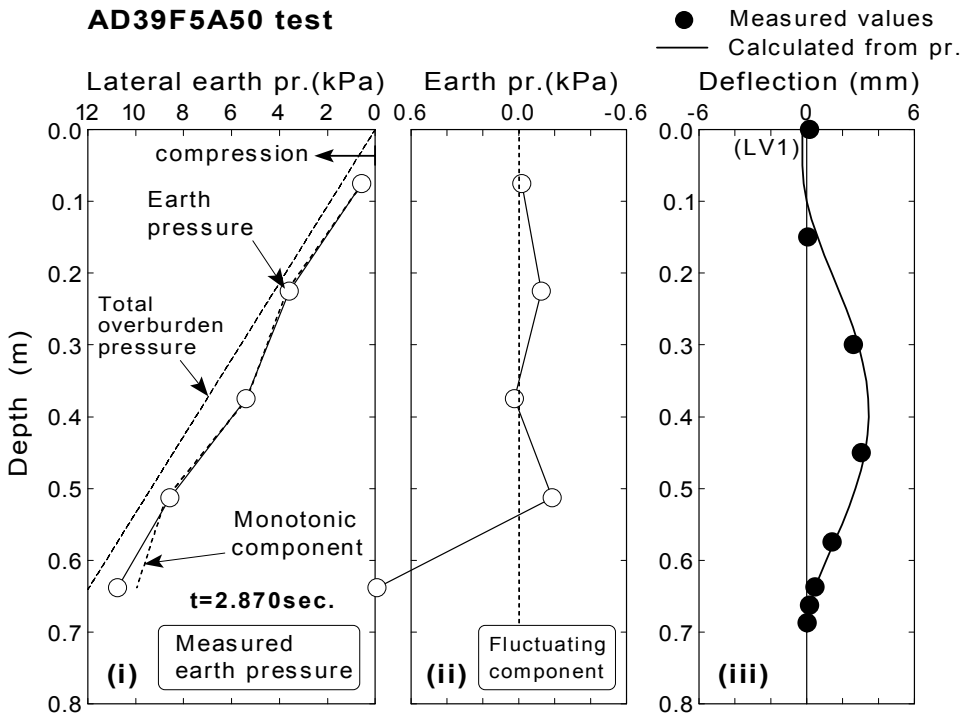

(a) t=2.870 seconds

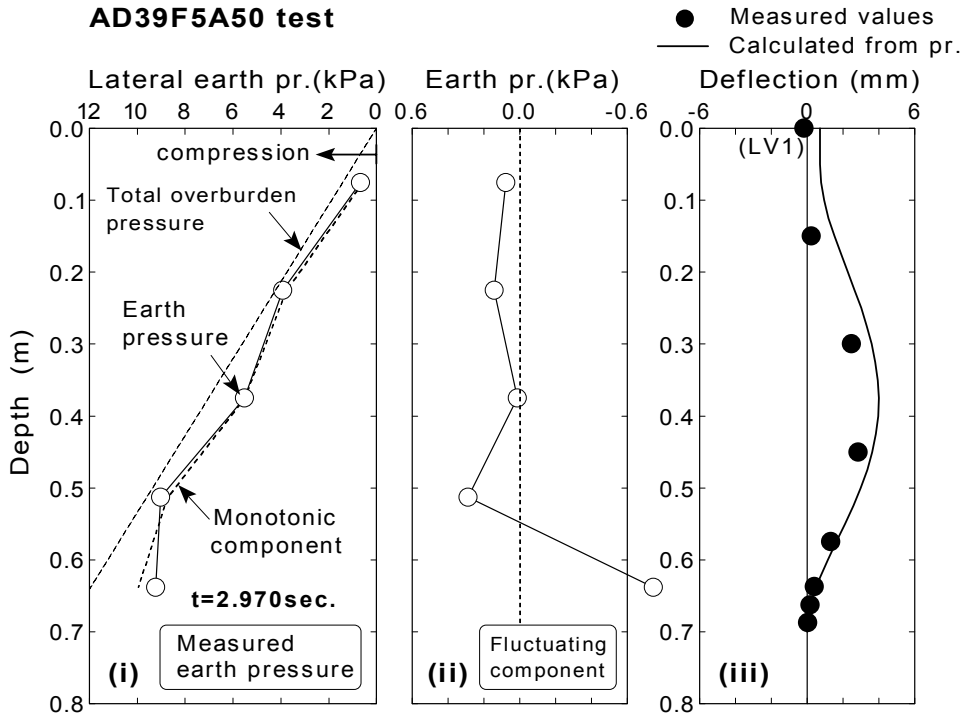

(b) t=2.970 seconds

Fig.6.104: Earth pressure and deflection before resonance (AD39F5A50 test)

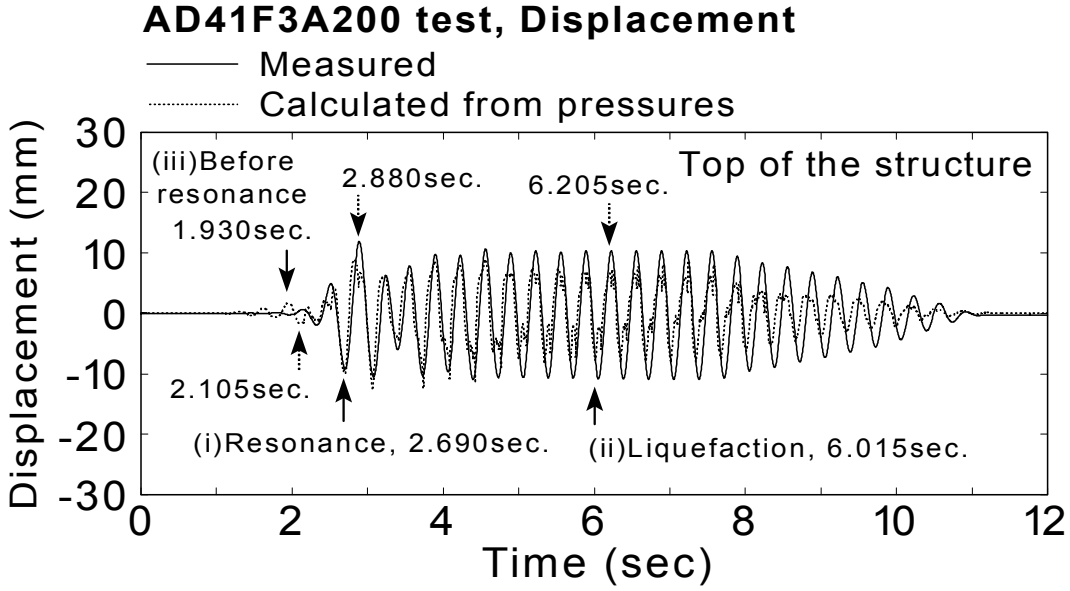

Fig.6.105: Comparison of time histories between measured and calculated displacement at the top of the structure (AD41F3A200 test)

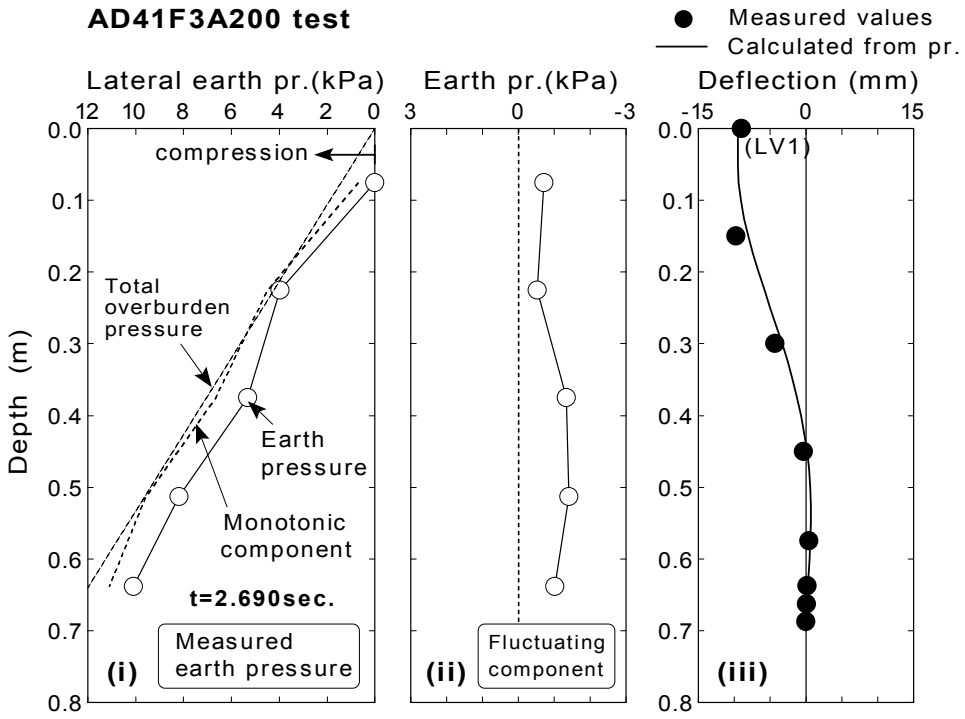

(a) At resonance, t=2.690 seconds

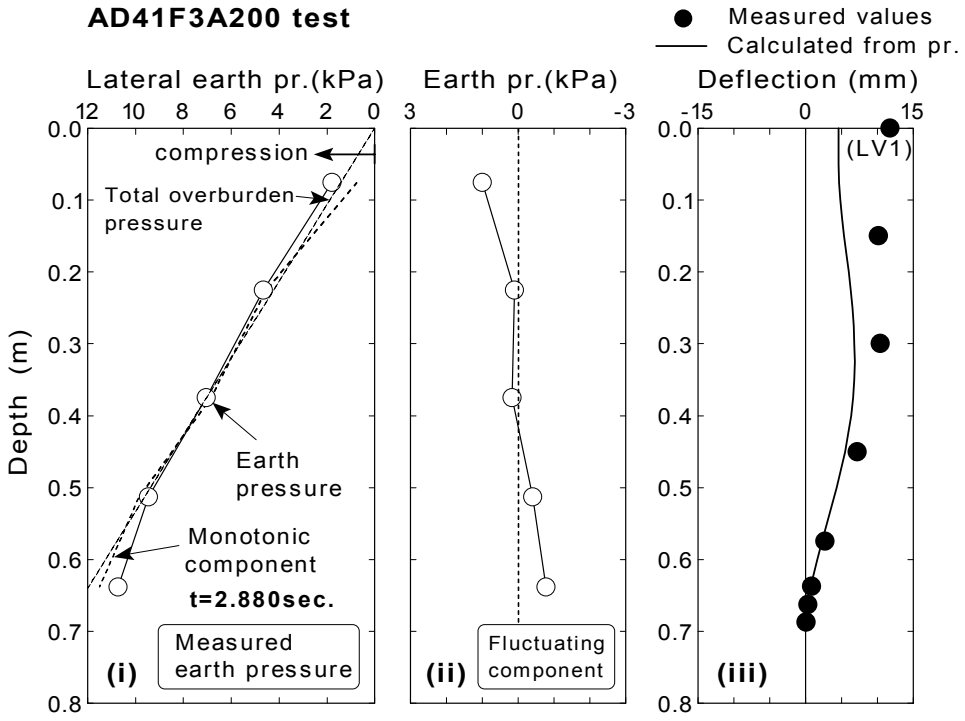

(b) A half cycle after resonance, t=2.880 seconds

Fig.6.106: Earth pressure and deflection at resonance (AD41F3A200 test)

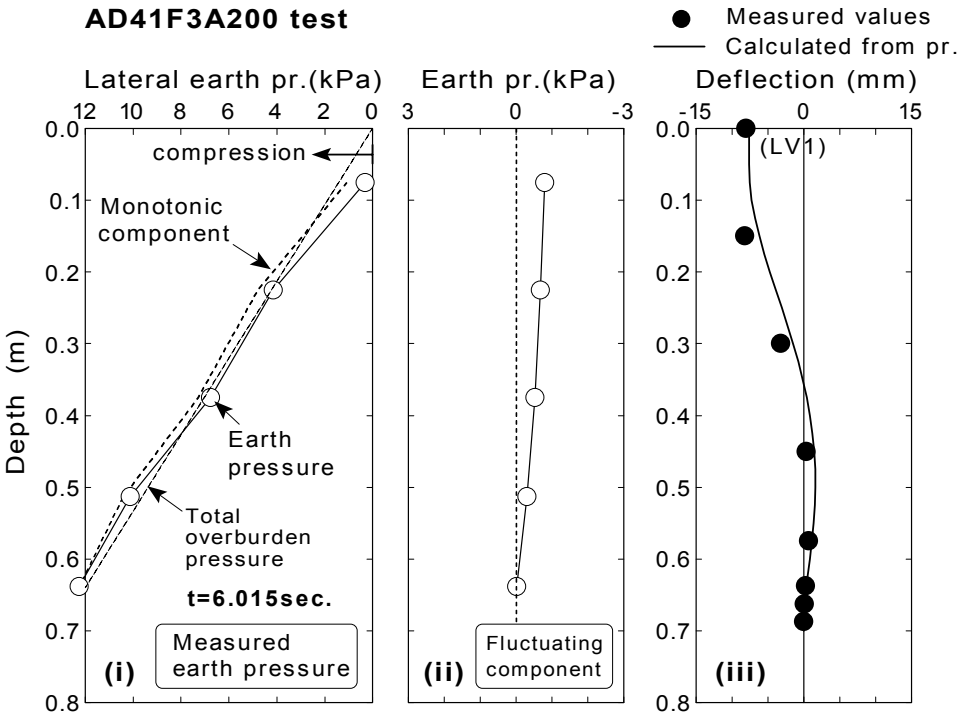

(a) t=6.015 seconds

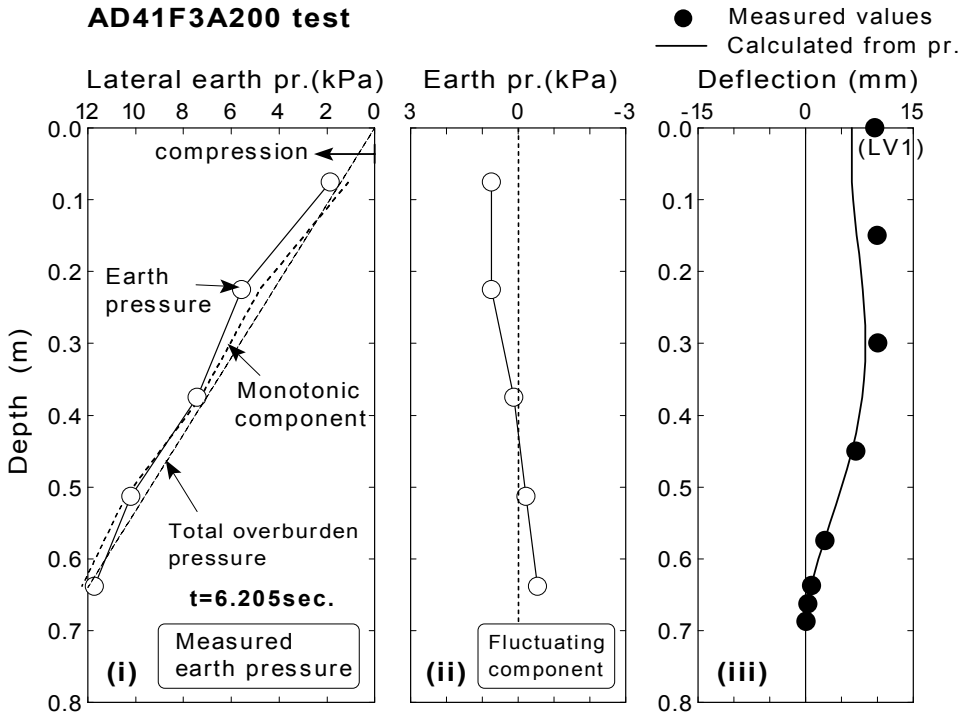

(b) t=6.205 seconds

Fig.6.107: Earth pressure and deflection during liquefaction (AD41F3A200 test)

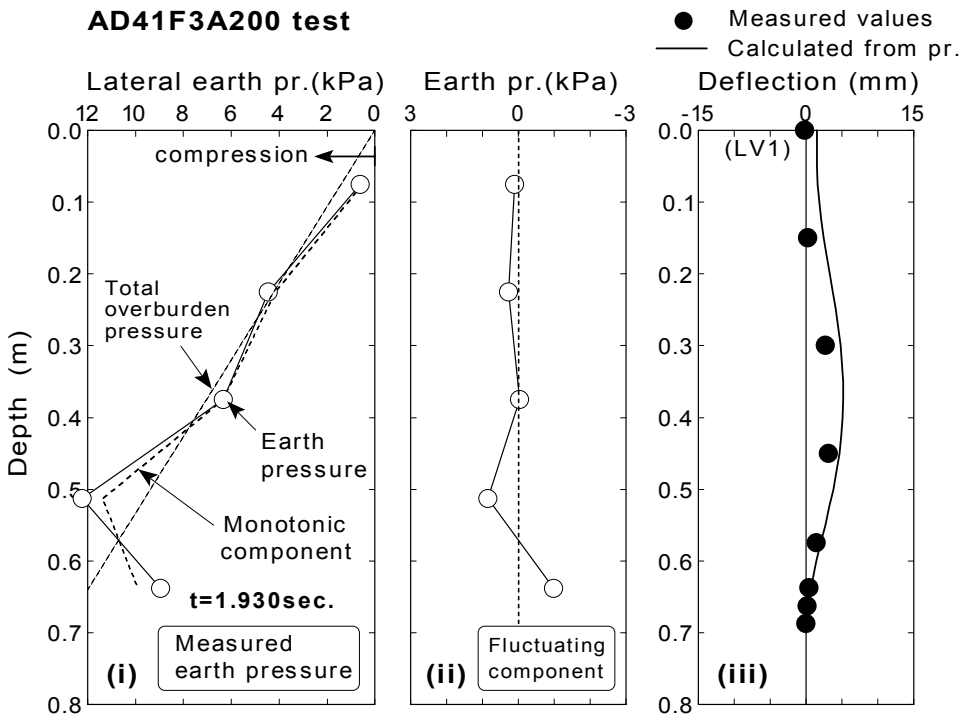

(a) t=1.930 seconds

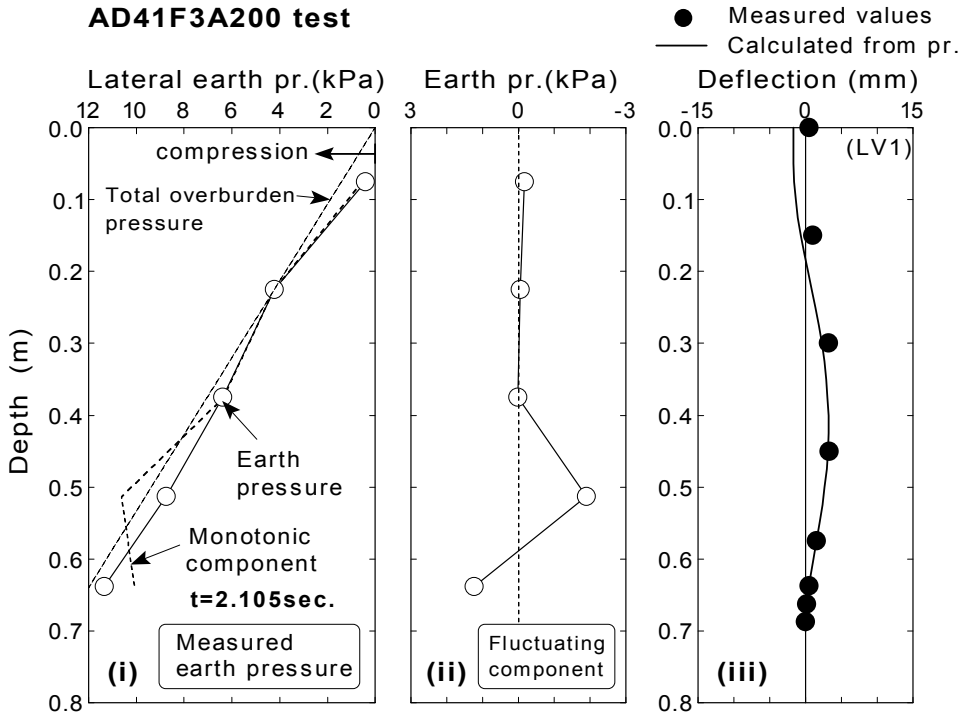

(b) t=2.105 seconds

Fig.6.108: Earth pressure and deflection before resonance (AD41F3A200 test)

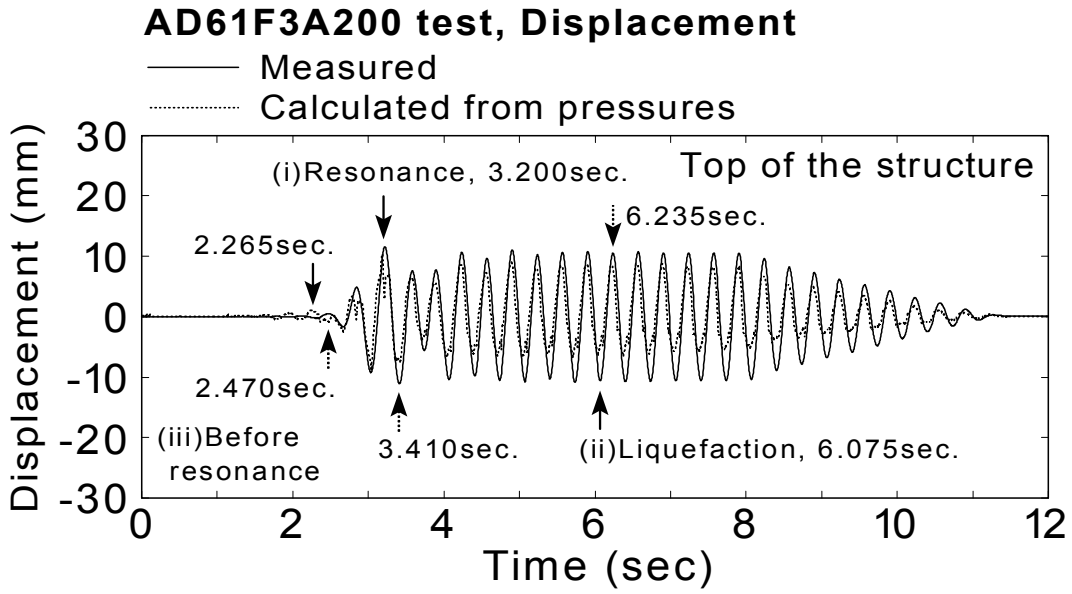

Fig.6.109: Comparison of time histories between measured and calculated displacement at the top of the structure (AD61F3A200 test)

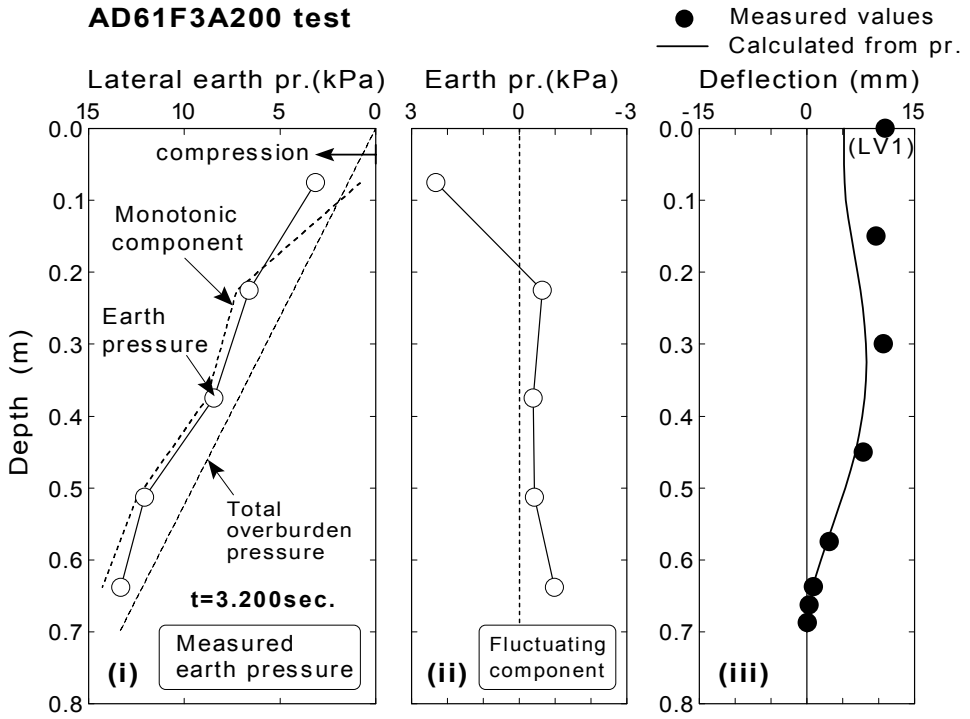

(a) At resonance, t=3.200 seconds

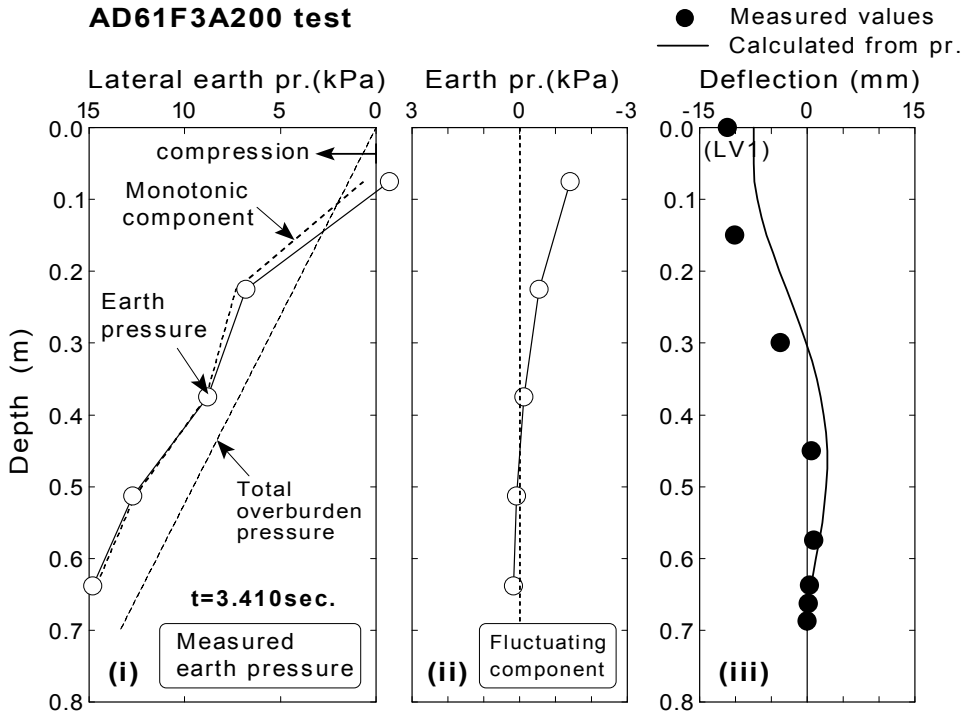

(b) A half cycle after resonance, t=3.410 seconds

Fig.6.110: Earth pressure and deflection at resonance (AD61F3A200 test)

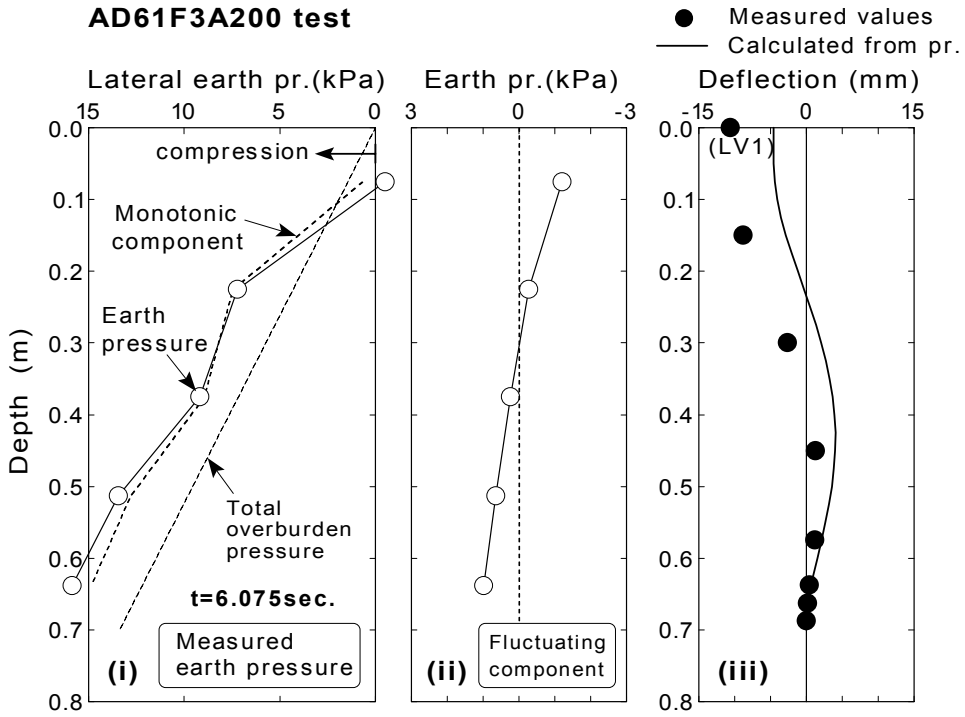

(a) t=6.075 seconds

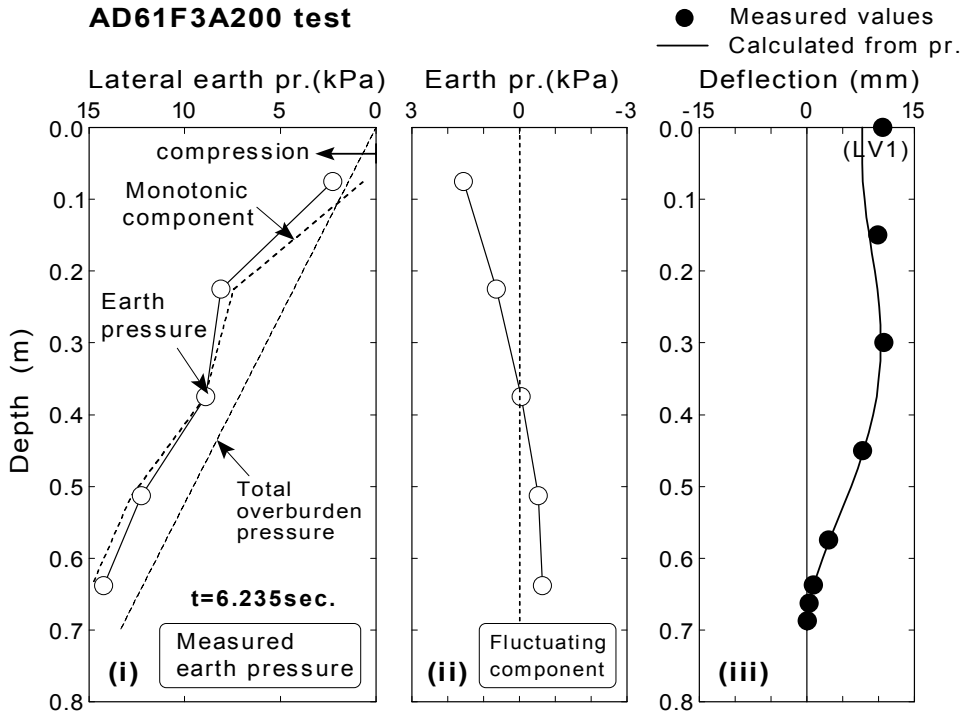

(b) t=6.235 seconds

Fig.6.111: Earth pressure and deflection during liquefaction (AD61F3A200 test)

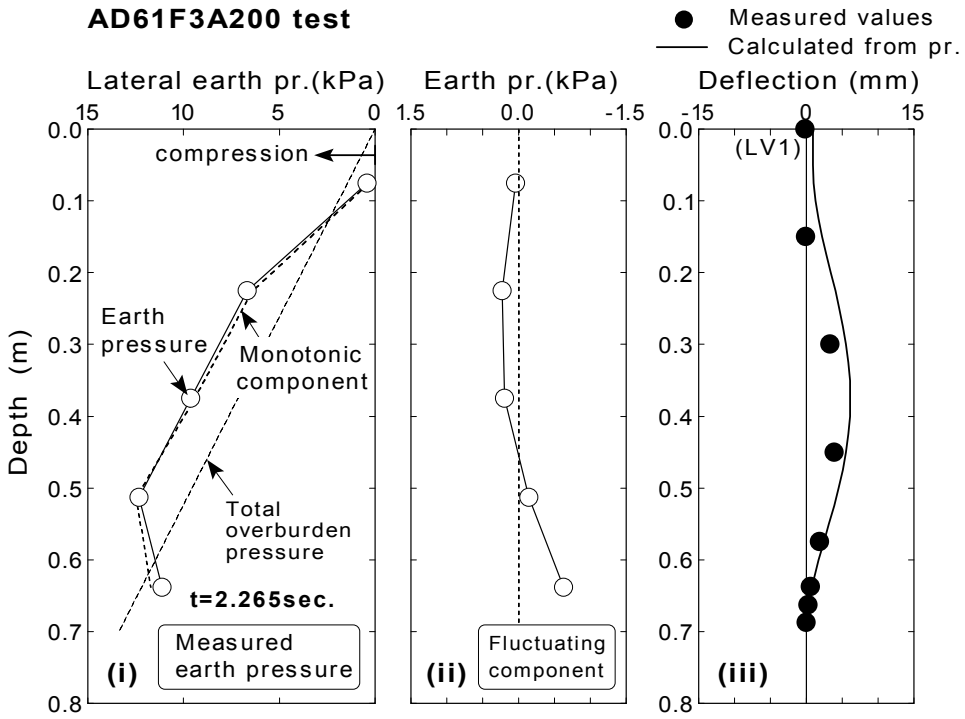

(a) t=2.265 seconds

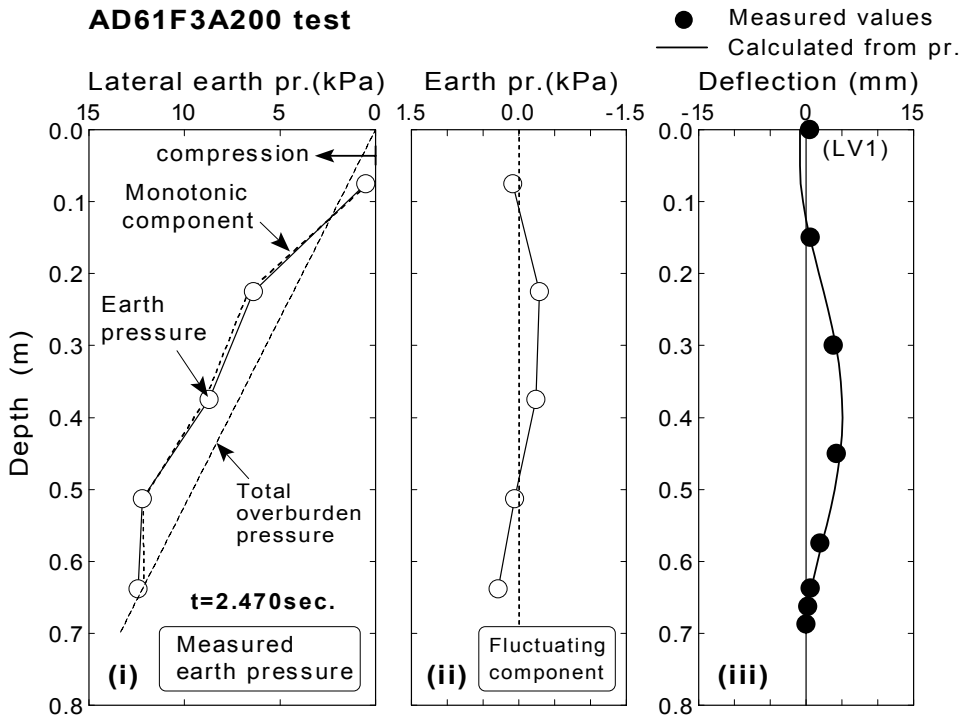

(b) t=2.470 seconds

Fig.6.112: Earth pressure and deflection before resonance (AD61F3A200 test)

Chapter 7

DYNAMIC INTERACTION BETWEEN LIQUEFIED SOIL AND STRUCTURE

7.1 GENERAL REMARKS

Dynamic effects of lateral earth pressures on structure will be examined in order to clarify the characteristics of dynamic interaction between soil and a flexible cross section before and after liquefaction. The change of shear modulus of backfill, which was analyzed in Chapter 4, will be referred to as a key parameter of soil-structure interaction. Effect of dilatancy of soil on the dynamic interaction will be discussed as well. Experimental relationship between dynamic earth pressure and normal strain of soil, as well as acceleration of wall will be used to make clear the influential parameter on dynamic pressures that act on a flexible underground structure during soil liquefaction.

7.2 EFFECTS OF NATURAL FREQUENCY OF BACKFILL ON DYNAMIC EARTH PRESSURES

Typical measurement of lateral earth pressure acting on the structure in AD35F3A50 test is presented in Fig.7.1. The frequency of input motion is 3Hz, and the peak acceleration is 0.5m/sec^2 in amplitude. As presented in the previous chapter, the earth pressures consist of i) static lateral earth pressure, ii) increase in lateral earth pressure due to accumulation of pore water pressure which is defined as monotonic component, and iii) cyclic change of lateral earth pressure which is in-phase with sinusoidal input motion, defined as fluctuating component. In this chapter, the earth pressure of fluctuating component iii) is regarded as the dynamic earth pressure. An example of time history of dynamic earth pressure (fluctuating component) is shown at the bottom part of Fig.7.1 as solid line. Time histories of dynamic earth pressure from all tests are illustrated in

Fig.6.85～Fig.6.91 in the previous chapter.

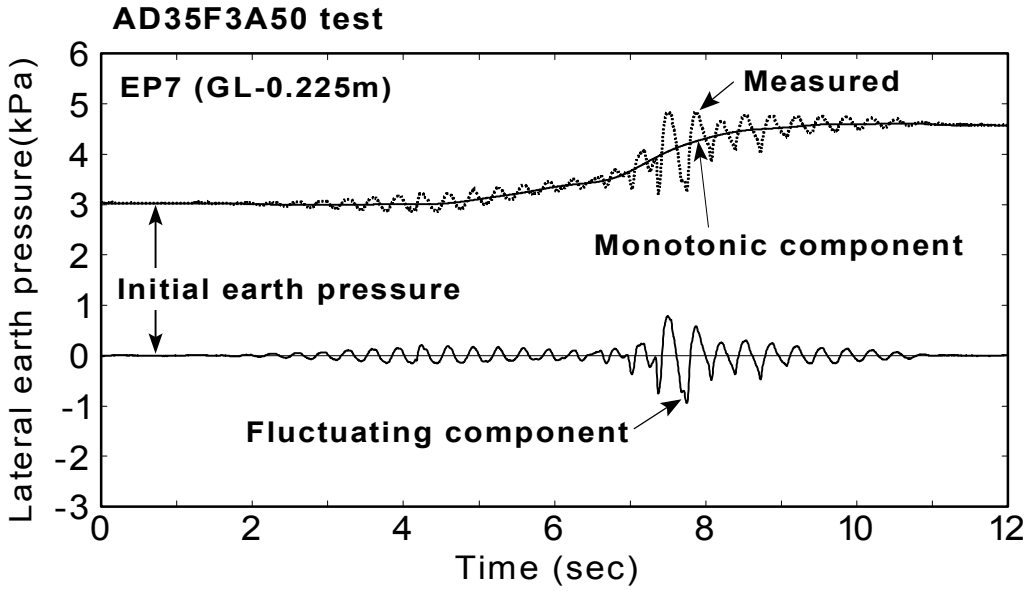

Fig.7.1: Monotonic and fluctuating components of earth pressure during shaking

7.2.1 Phase difference between earth pressures and displacements

The past experimental studies on a quay wall of gravity type have detected that the dynamic earth pressure acting on the wall and the wall displacement with inertia force became in-phase when soil liquefies (Ghalandarzadeh et al.,1998; Kohama et al.,1998). As was stated in Chapter 1, this supports the idea of seismic coefficient for dynamic pressures. Phase difference between dynamic earth pressure and displacement of the structure during liquefaction will be analyzed to make clear the interactive characteristics for a flexible underground structure.

It is possible that the dynamic earth pressures, which act on the upper part of a structure, strongly affects the displacements at the top of the structure. Therefore, the experimental relationship between the dynamic earth pressures at 0.3m from the surface (EP6, EP7) and the displacement of the structure is examined. The resultant force F_d, is introduced herein to represent the effect of dynamic pressures EP6 and EP7. The definition of the resultant force F_d, is illustrated in Fig.7.2. In this definition, the earth pressure at the ground surface is assumed as zero, and the earth pressure is interpolated by a piecewise linear function in the backfill soil. It is noted that the monotonic component of earth pressure is not included in the resultant force F_d.

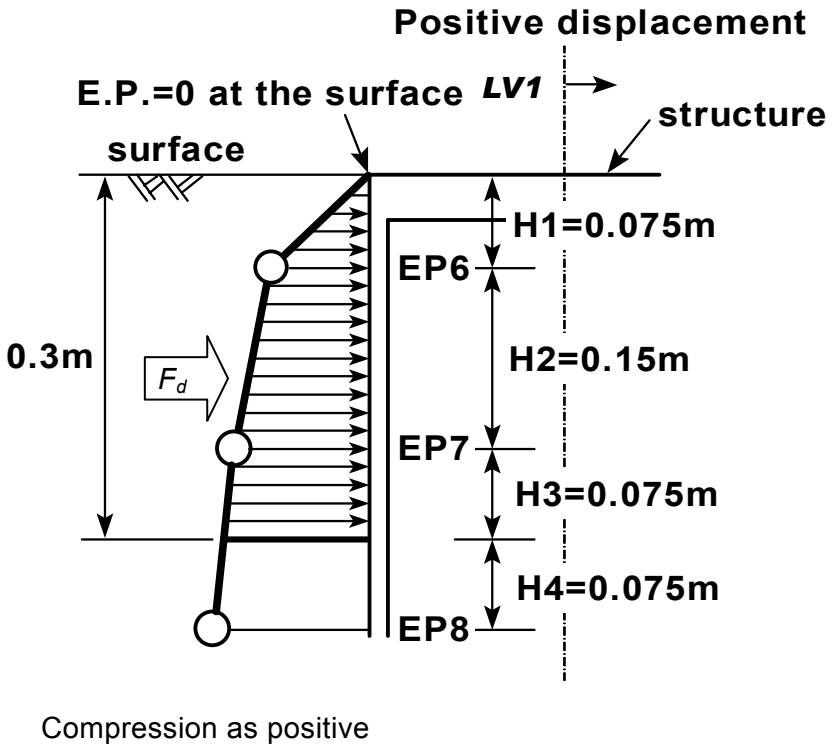

Fig.7.2: Definition of resultant force F_d due to dynamic earth pressures (Fluctuating component of earth pressure)

The typical time histories of the resultant force F_d and displacements at the top of the structure from AD35F3A50 test are presented in Fig.7.3(a). The time history of the ratio of excess pore pressure at PP2 (GL-0.375m) and the temporal change of natural frequency of backfill, which was derived in the chapter 4, are shown in Fig.7.3(b). Natural frequency of structure is also illustrated in the figure. Since the material of structure behaves in an elastic manner during shaking in this test, it does not change with time. The definition of positive displacement is illustrated in Fig.7.2. It is observed that the amplitude of the resultant force F_d, and the displacement are increased rapidly at about 7.5 seconds. At this time, the ratio of excess pore water pressure reaches about 0.8 and the natural frequency of the backfill reduces to almost zero. From the analysis made in the chapter 5, this amplification of displacement causes a resonance of the soil-structure system. It is also seen that the phase difference between two time histories in Fig.7.3(a) are recognized out-of-phase during 2.0 ～4.0 seconds when the natural frequency of backfill is larger than that of structure. In contrast, those are in-phase during 7.0 ～10.0 seconds.

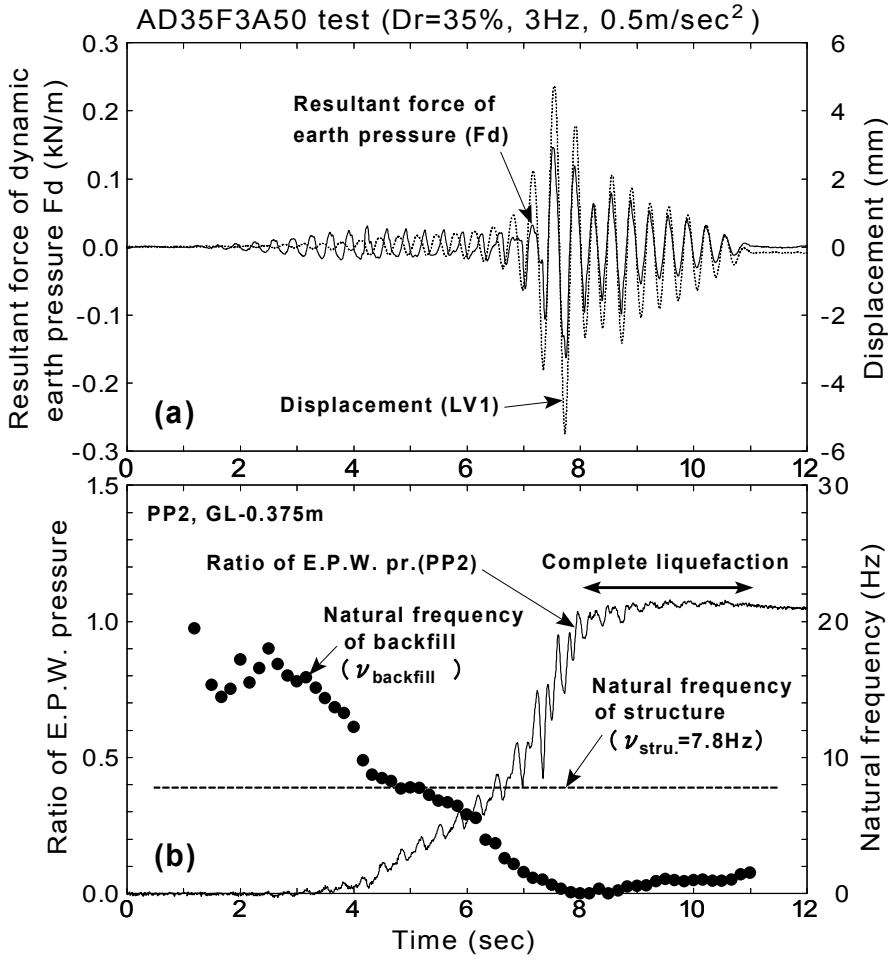

Fig.7.3: Time histories of resultant force F_d and displacements (LV1)

Fig.7.4 shows time histories of the resultant force F_d, and the displacement at the top of the structure with enlarged time axes. High frequency components are removed from the both time histories by a low pass filtering with 4Hz cut-off frequency. Filtered time histories and time differences between peaks of two time histories and phase differences are also illustrated in each figure. The phase difference is calculated from time difference as

$$\theta_i = \frac{t_{disp,peak,i} - t_{earth\ pr.,peak,i}}{T} \times 360 \quad (\text{deg.}) \tag{7.1}$$

where $t_{disp,peak,i}$ is a time instance of occurrence of peak displacement at the top of the structure at i-th half cycle, $t_{eath\ pr.,peak,i}$ of peak resultant force of dynamic earth pressure, and T is a period of the input excitation. In this definition, a phase difference of -180 degree means out-of-phase whereas zero in-phase. It should be noted that time interval of time histories Δt is 0.005 seconds in this analysis, corresponding to about 5 degree of phase difference.

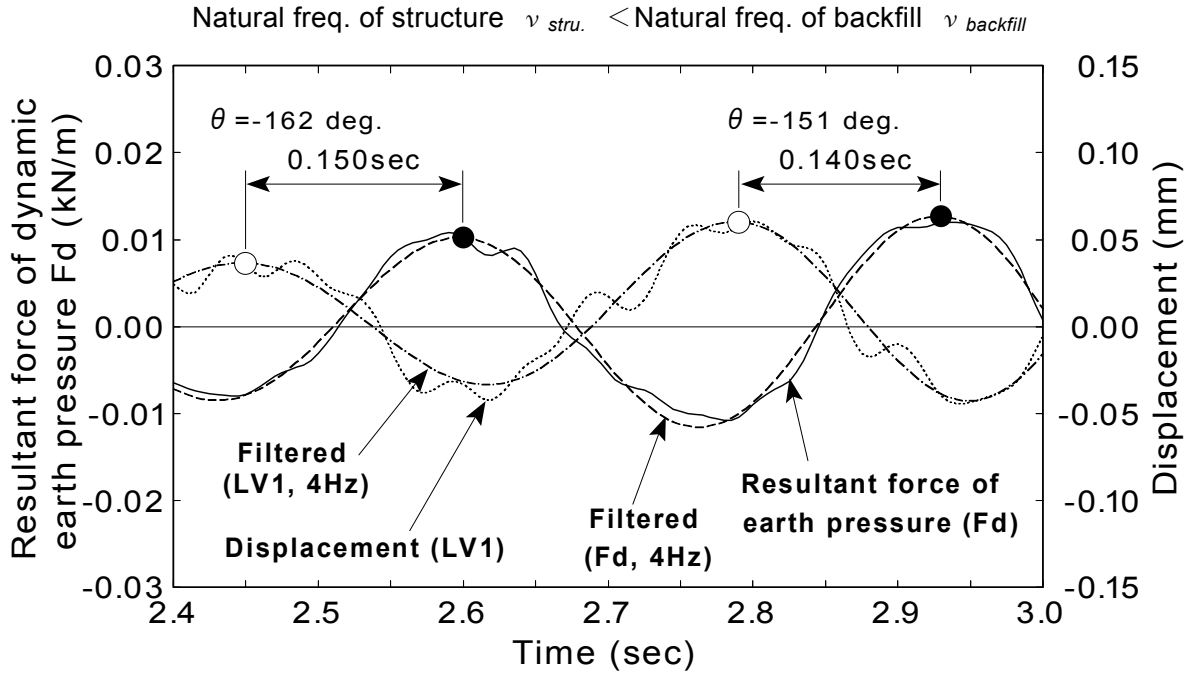

(a) 2.4sec～3.0sec (Pore pressure ratio: 0.0)

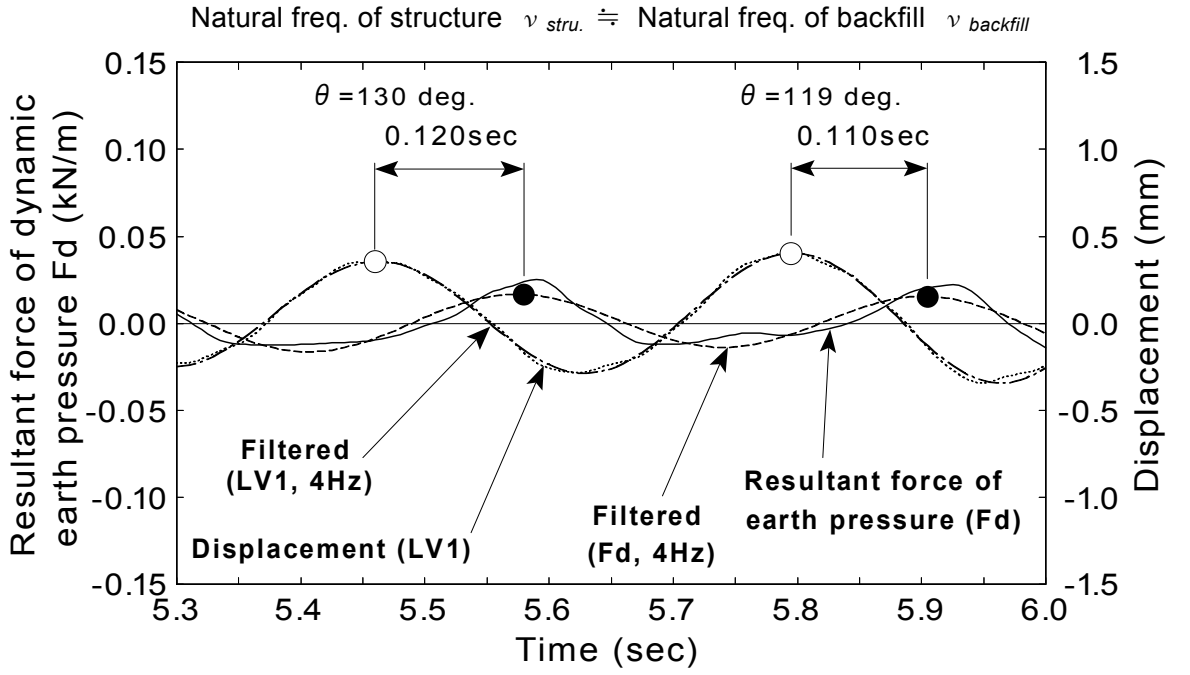

(b) 5.3sec～6.0sec (Pore pressure ratio: 0.2～0.3)

Fig.7.4: Phase difference between resultant force of earth pressure and displacement (AD35F3A50 test)

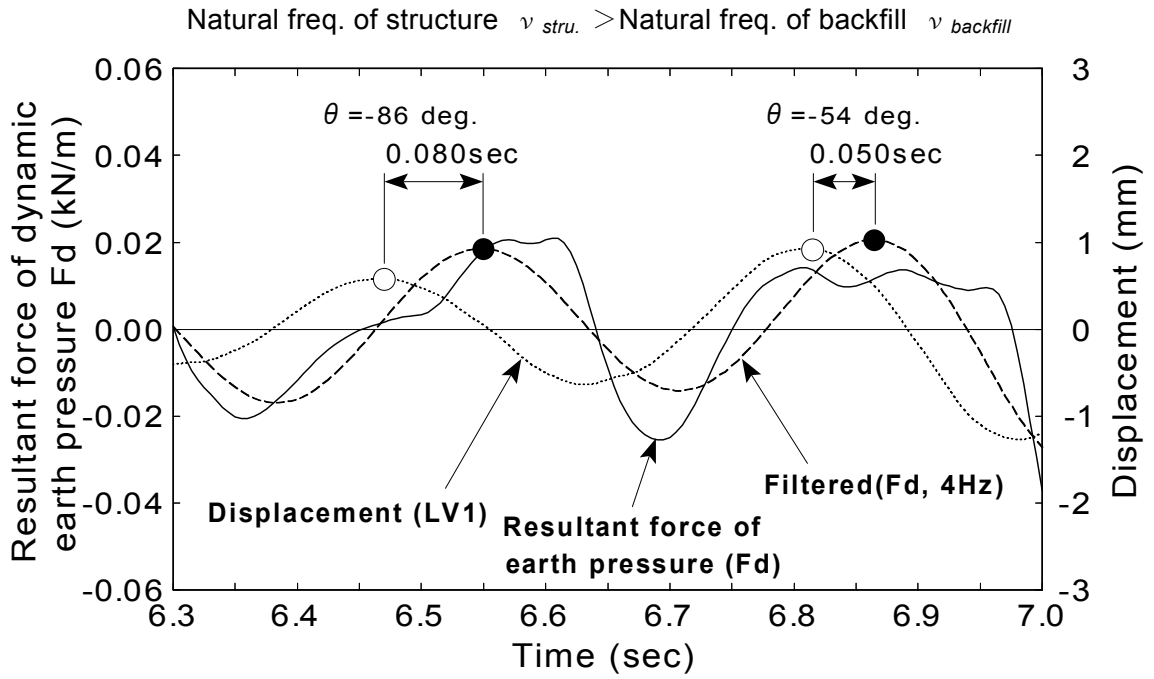

(c) 6.3sec～7.0sec (Pore pressure ratio: 0.4～0.5)

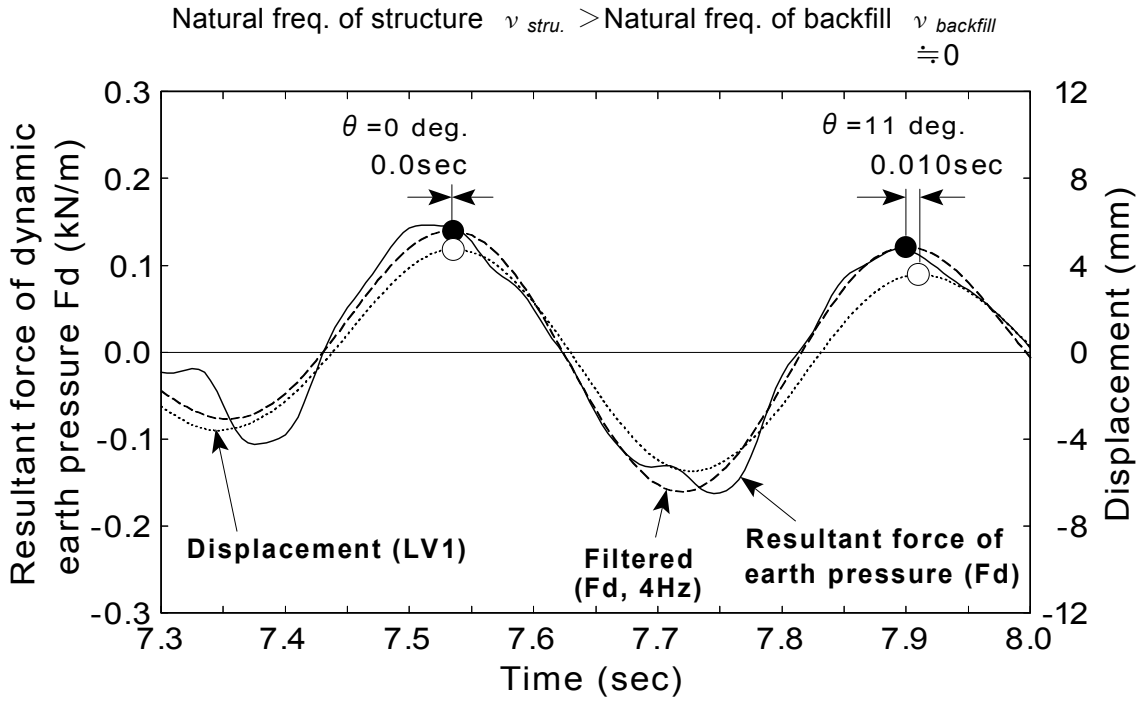

(d) 7.3sec～8.0sec (Pore pressure ratio: 0.8～1.0)

Fig.7.4: Continued (AD35F3A50 test)

Fig.7.4(a) illustrates time histories during 2.4 to 3.0 seconds. In this period, pore pressure ratio is zero, and the natural frequency of backfill, $\nu_{backfill}$, is larger than that of structure, $\nu_{struc.}$,. It is seen that the resultant force of dynamic earth pressure F_d becomes maximum in the positive direction at about 2.6 seconds when the structure moves in the negative direction. The phase difference in this time period is –162 degrees to –151 degrees, being out-of-phase.

Fig.7.4(b) and (c) depict results during 5.3 to 6.0 seconds and 6.3 to 7.0 seconds, respectively. Pore pressure ratio in the backfill is 0.2～0.5, and the natural frequency of backfill, $\nu_{backfill}$, is almost equal to or smaller than that of structure, $\nu_{struc.}$. The phase difference is seen to change from –130 degrees to –54 degrees.

Time histories during 7.3 to 8.0 seconds are shown in Fig.7.4(d). At this time period, pore pressure ratio reaches 0.8～1.0, and the natural frequency of backfill reduces nearly to zero. It is observed that two time histories are in-phase, namely the F_d becomes a peak in positive direction when the structure moves in the positive direction. It suggests that phase difference and magnitude relation of natural frequencies of backfill and structure has a close correlation.

The experimental relationships between the resultant force F_d and the displacement of the structure (LV1) at corresponding time period are illustrated in Fig.7.5. The loop indicates negative proportionality and rotates in the anticlockwise direction during 2.4 to 3.0 seconds,. This means that the dynamic earth pressure acts as a reaction to constrain the movement of the structure. In the time period of 5.3～7.0 seconds illustrated in Fig.7.5(b) and (c), the shape of the loop seems to be in transition from negative proportionality to positive proportionality. The direction of rotation is still anticlockwise. In contrast, a clear positive proportionality and clockwise rotation can be observed in the time period of 7.3～8.0 seconds. It shows that the dynamic earth pressure acts as a load to make the structure deform. These observations of time histories between the resultant force F_d and displacement of the structure are summarized in Table 7.1. This suggests that the pore water pressure build-up due to liquefaction and accompanying change of natural frequency of backfill strongly affect the action of dynamic earth pressure on the structure.

Changes of natural frequencies of backfill and phase difference with time from various tests are shown in Fig.7.6. Natural frequencies of backfill are calculated from shear modulus at each cycle of shaking by the procedure shown in the Chapter 4. Since the material of structure does not yield during shaking in these tests (see Section 3.3), its natural frequency keeps constant throughout the duration time.

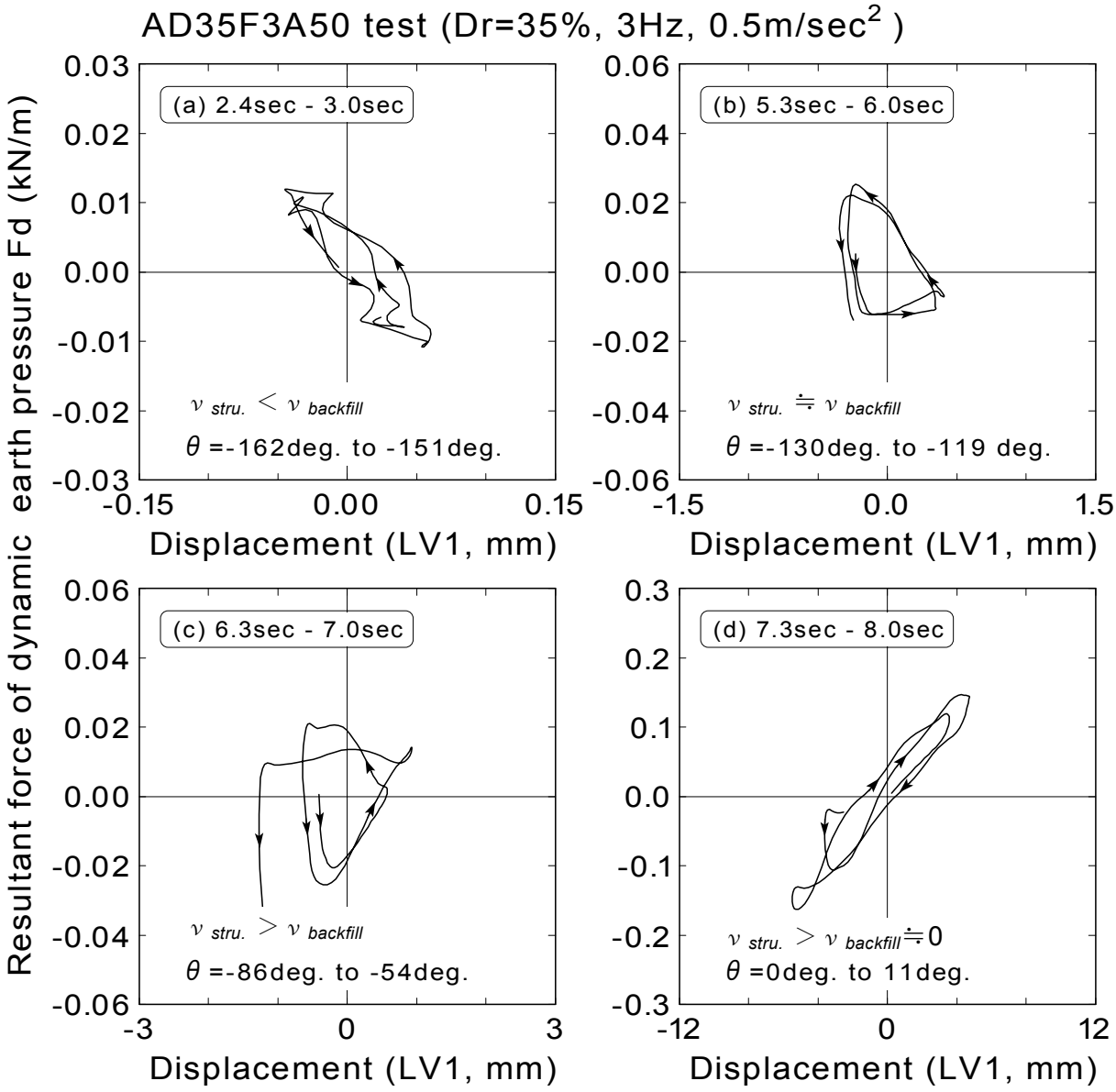

Fig.7.5: Experimental relationship between resultant force F_d and displacement of the structure (AD35F3A50 test)

Table 7.1. Summary of observations of time histories

Time (seconds)	Pore pressure ratio	Natural frequencies	Rotation of direction	Phase Difference (degree)	Action of dynamic earth pr.
2.4 to 3.0	0.0	$\nu_{stru.} < \nu_{backfill}$	Anti-clock wise	-162～-151	Reaction
5.3 to 6.0	0.2～0.3	$\nu_{stru.} \fallingdotseq \nu_{backfill}$	Anti-clock wise	-130～-119	In transition
6.3 to 7.0	0.4～0.5	$\nu_{stru.} > \nu_{backfill}$	Anti-clock wise	-86～-54	
7.3 to 8.0	0.8～1.0	$\nu_{stru.} > \nu_{backfill} \fallingdotseq 0$	Clock wise	Nearly zero	Load

The result from AD35F3A50 test is shown in Fig.7.6(a). As was expressed in previous observations, the phase difference is increasing with time from about -150 degrees towards zero when the natural frequency of backfill becomes smaller than that of structure after about 5 seconds. Natural frequencies and phase differences with time in AD39F5A50 test is illustrated in the same manner in Fig.7.6(b). Input peak acceleration is 0.5 m/sec^2, and frequency is 5Hz. It is observed that phase differences are initially less than -90 degrees (out-of-phase) when natural frequency of backfill is larger than that of structure in all test result. In contrast, phase difference is about zero, being in-phase of time histories, when the natural frequency of backfill becomes smaller than that of the structure. The results from AD41F3A200 test, AD61F3 A200 test and AD32F3A500 test are illustrated in the same manner in Fig.7.6(c)～(e). Input accelerations are 2.0 m/sec^2 and 5.0 m/sec^2. It is observed that the change of natural frequency of backfill with time becomes quicker in these test results since input acceleration is more intense. The feature of change of phase difference seems the same as that of the result from AD35F3A50 and AD39F5A50 test.

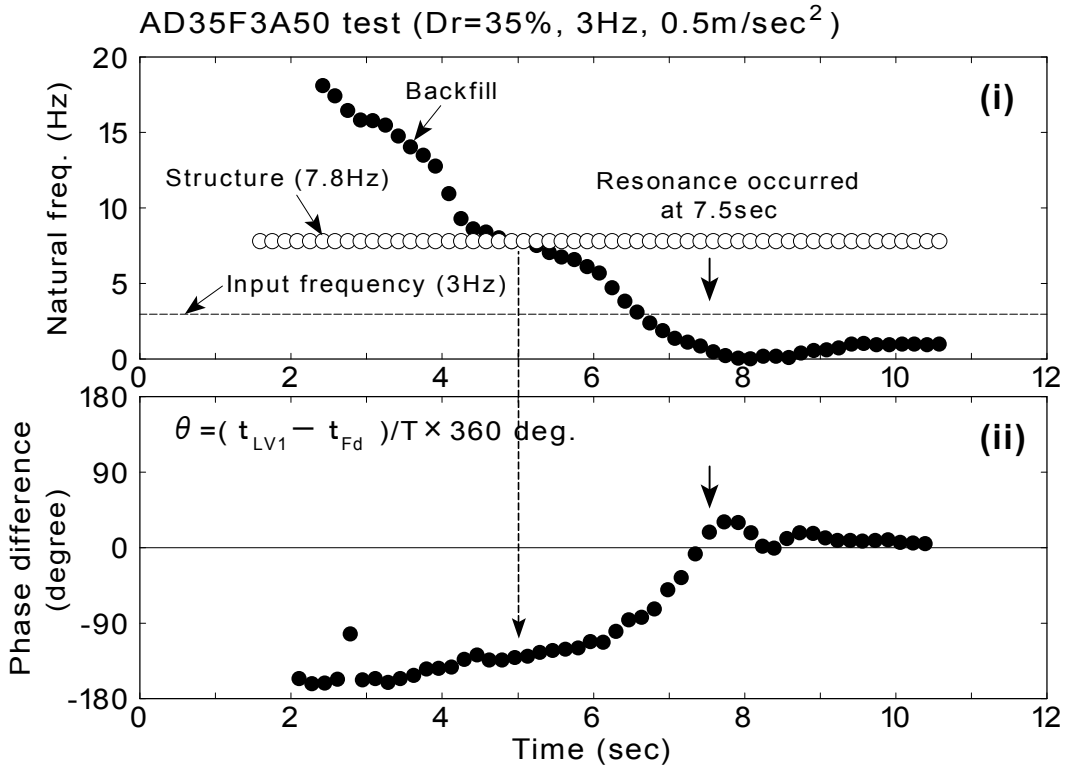

(a)AD35F3A50 test

Fig.7.6: Change of natural frequency and phase difference

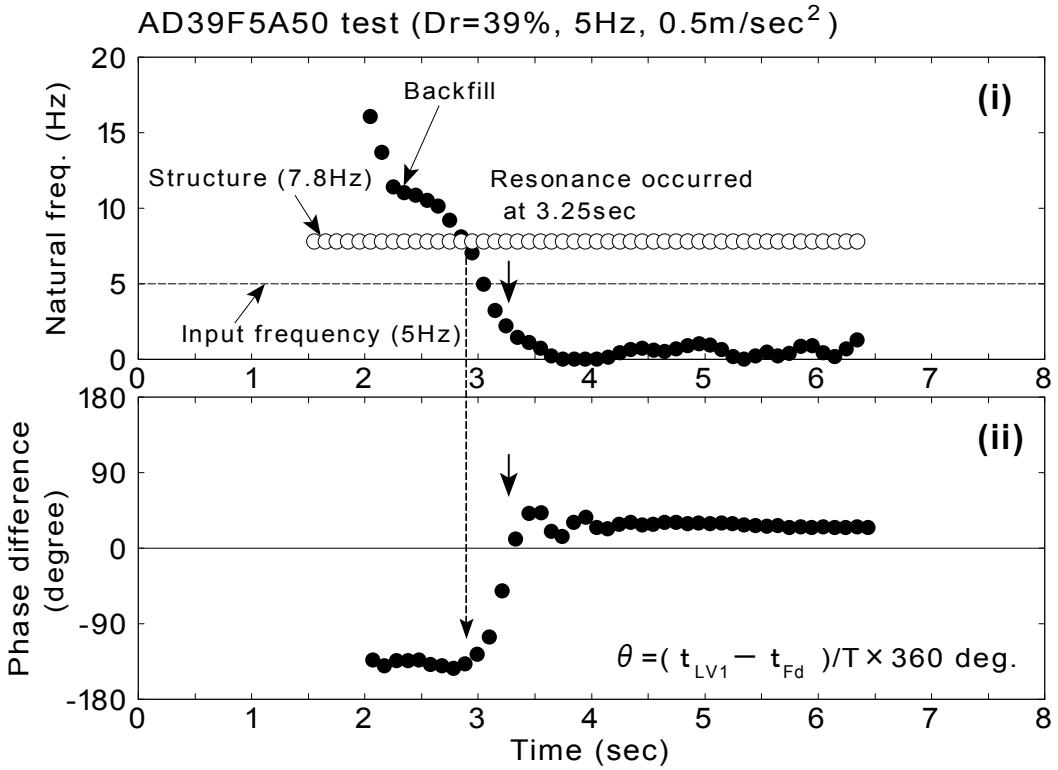

(b) AD39F5A50 test

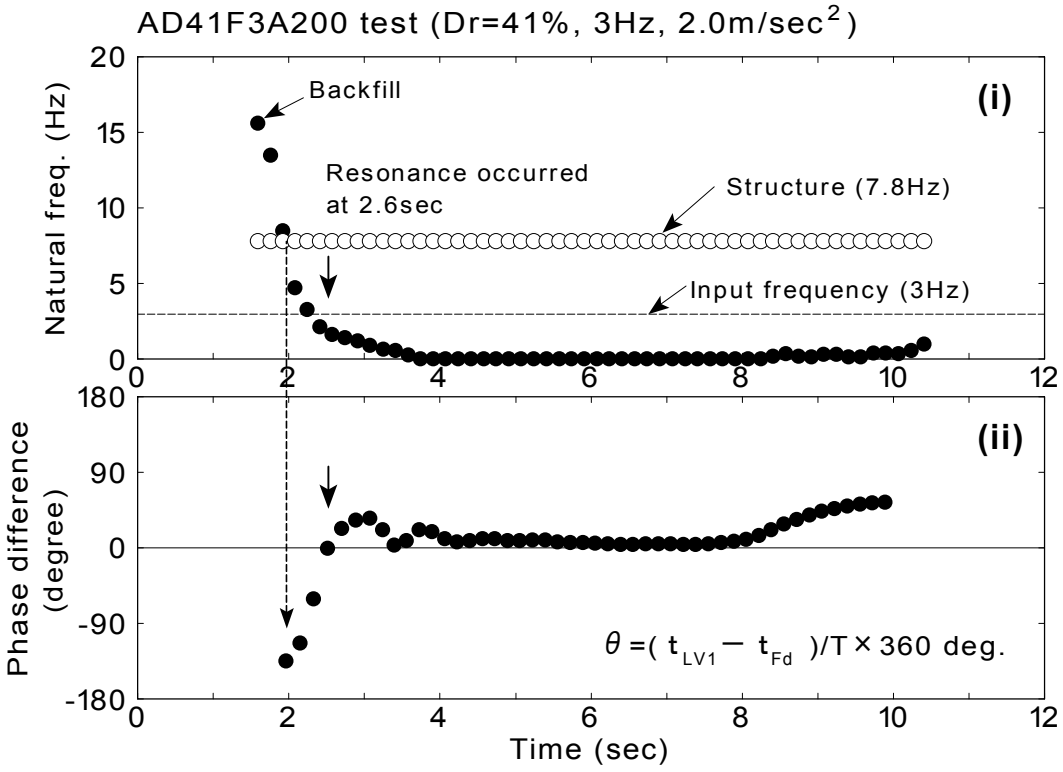

(c) AD41F3A200 test

Fig.7.6: Contined

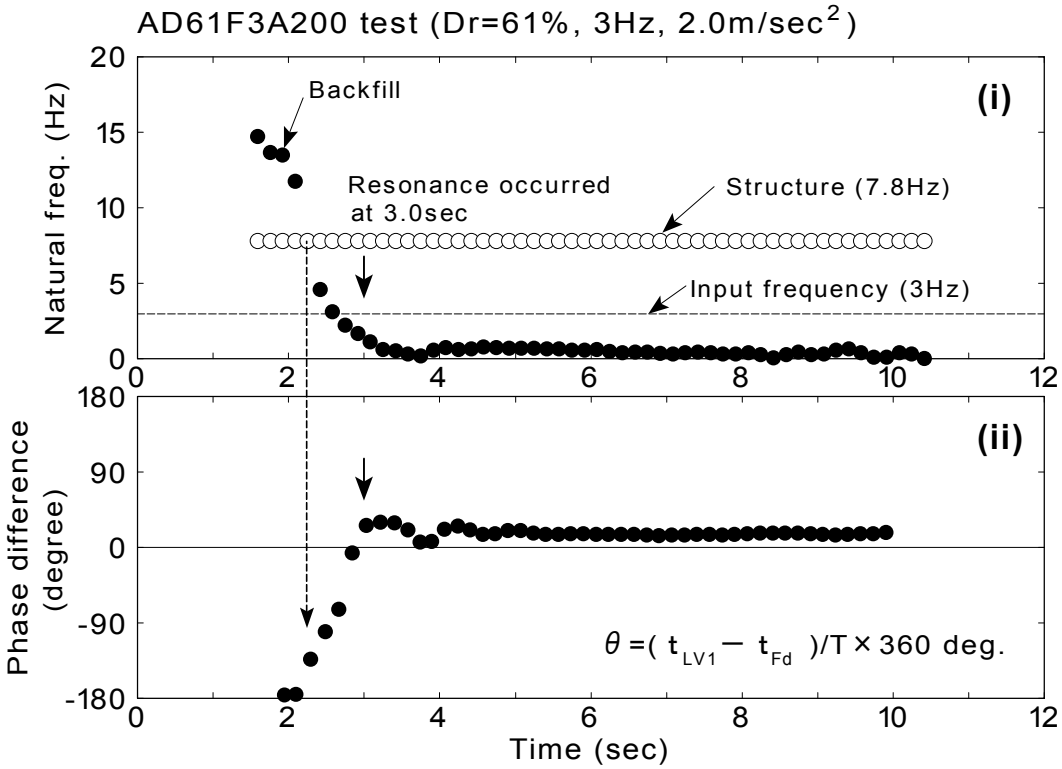

(d) AD61F3A200 test

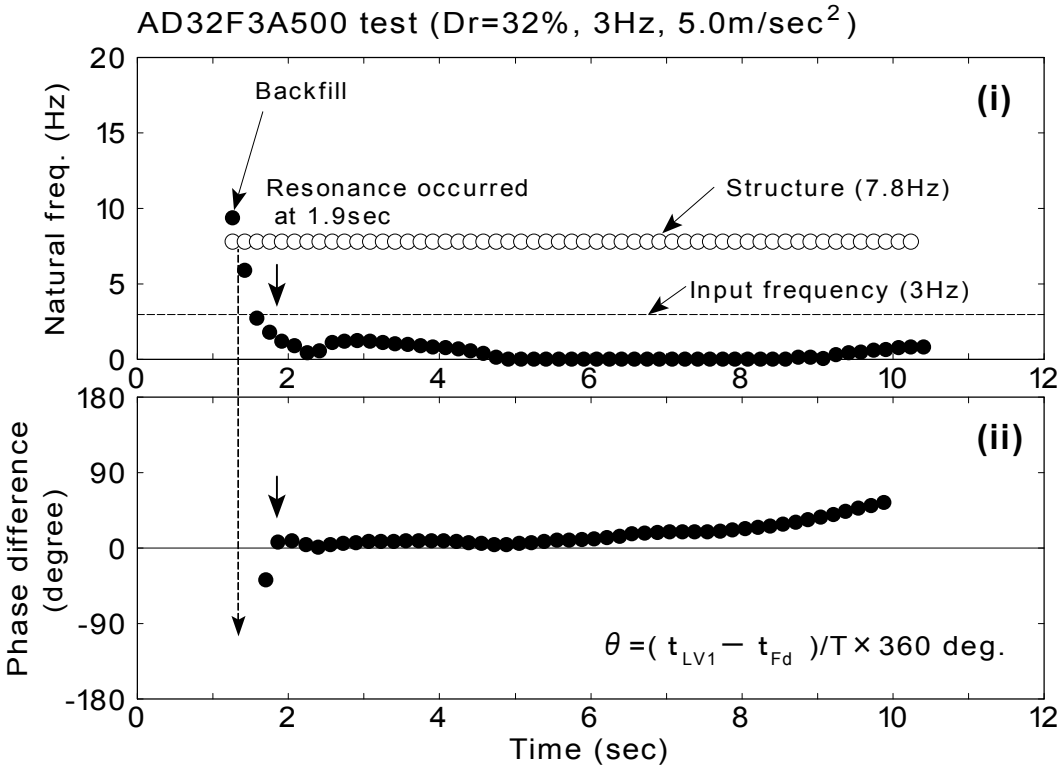

(e) AD32F3A500 test

Fig.7.6: Contined

To understand this phenomenon more clearly, change of phase difference with respect to natural period of ground are plotted in Fig.7.7. The results are illustrated with respect to intensity of input motion. It is interesting that phase difference becomes about zero at about the same natural period (0.6seconds to 1.0 second) even though the intensity of input motion is variable. It shows that phase difference is strongly affected by the natural period (or natural frequency) of backfill when it liquefies.

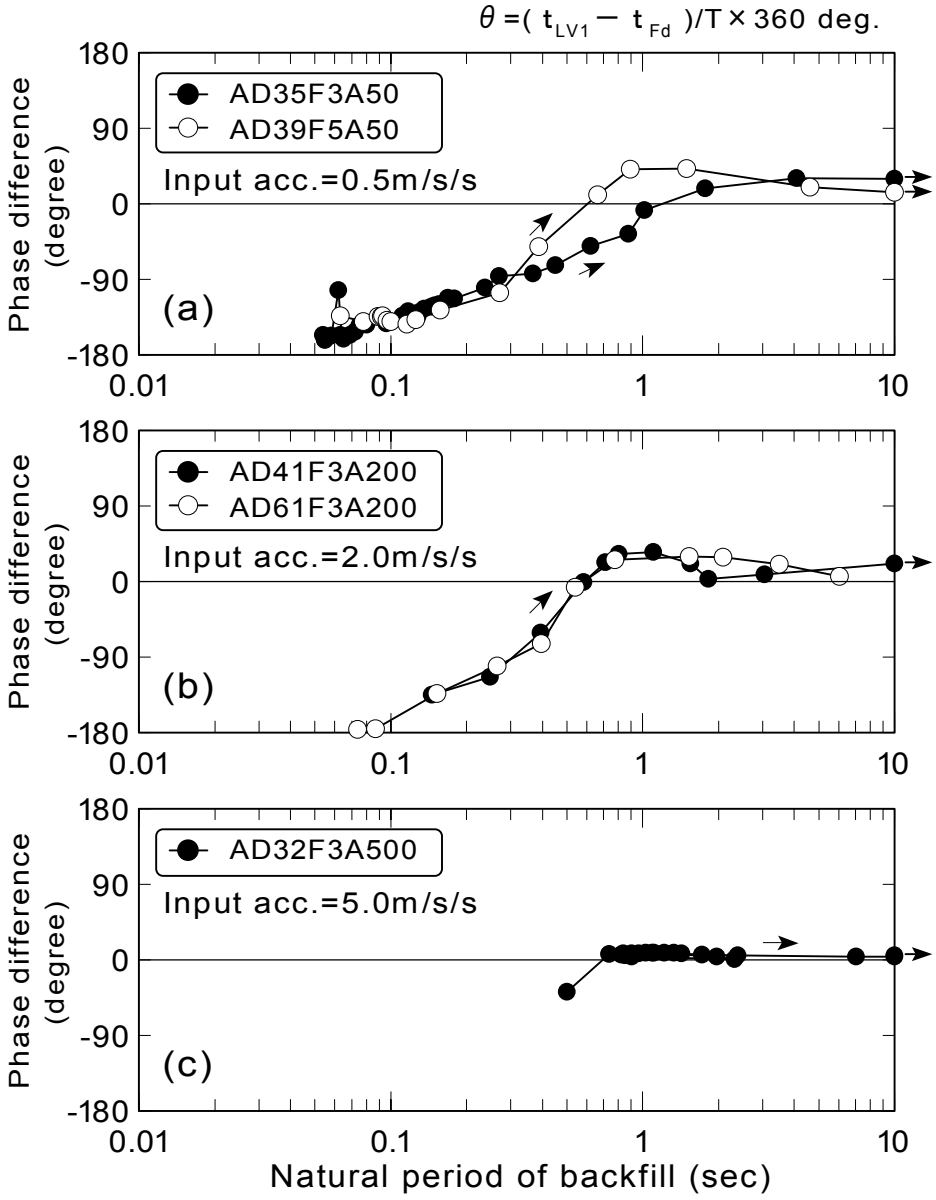

Fig.7.7: Change of the phase angle with respect to natural period

Fig.7.8 shows the experimental relationships between the phase differences and the natural period of ground. The natural period of the structure itself (0.133seconds) is indicated in the figure. It is seen that the phase difference is -180 to -120 degrees when the natural period of ground is shorter than that of the structure. In contrast, the phase difference increases to around zero as the natural period of ground becomes longer than that of the structure. The dynamic earth pressure does not act as the load on the structure until the natural period of ground near the structure becomes longer than that of the structure itself.

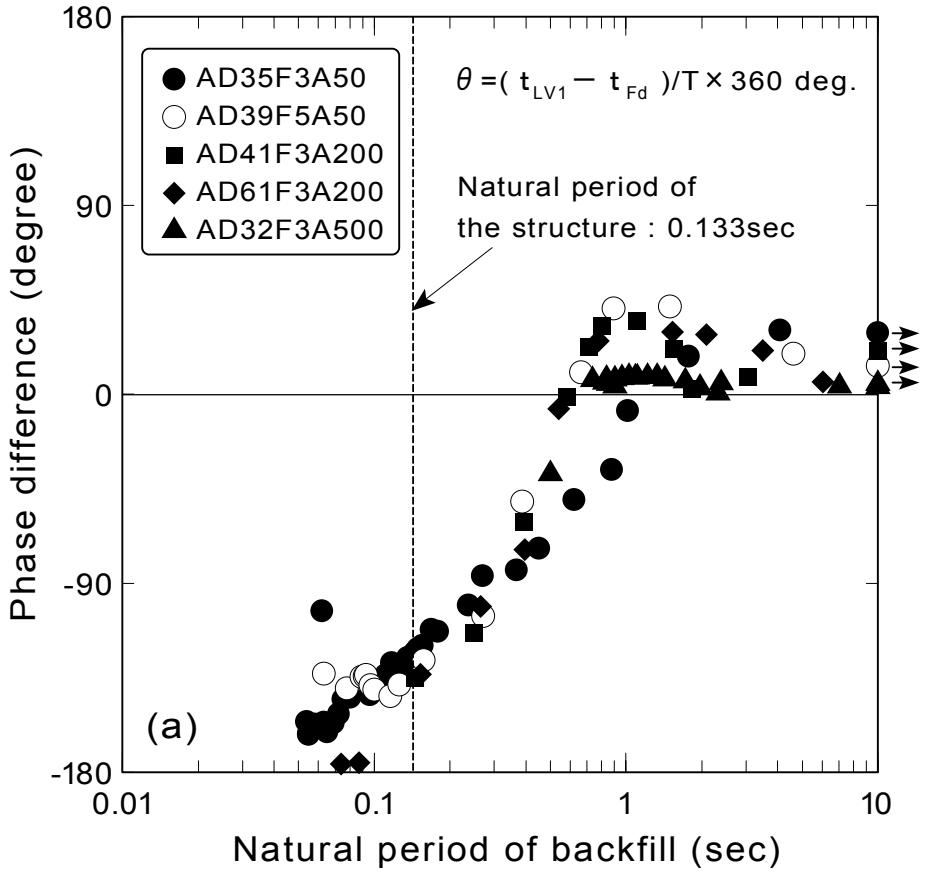

Fig.7.8: Experimental relationship between phase difference and natural period of backfill

7.2.2 Inertia force of soil mass near the structure

As shown in the equation of force equilibrium in the Chapter 4, the inertia force per unit volume of saturated soil, $-\rho\,\alpha_x$, is equal to the sum of normal stress difference, $\partial\,\sigma_x / \partial x$, and shear stress difference, $\partial\,\tau / \partial z$, in the horizontal direction. Namely,

$$-\rho\alpha_x = \frac{\partial \sigma_x}{\partial x} + \frac{\partial \tau}{\partial z} \tag{7.2}$$

When the soil mass, whose height is Δz, is located at the vicinity of the structure as shown in Fig.7.9, the force equilibrium results in

$$-\rho\alpha_x \cdot \Delta z = \frac{\partial \sigma_x}{\partial x}\Delta z + \frac{\partial \tau}{\partial z}\Delta z \tag{7.3}$$

where the height of the soil mass, Δz, is 0.3m. The quantities in Eq.(7.3) can be calculated from

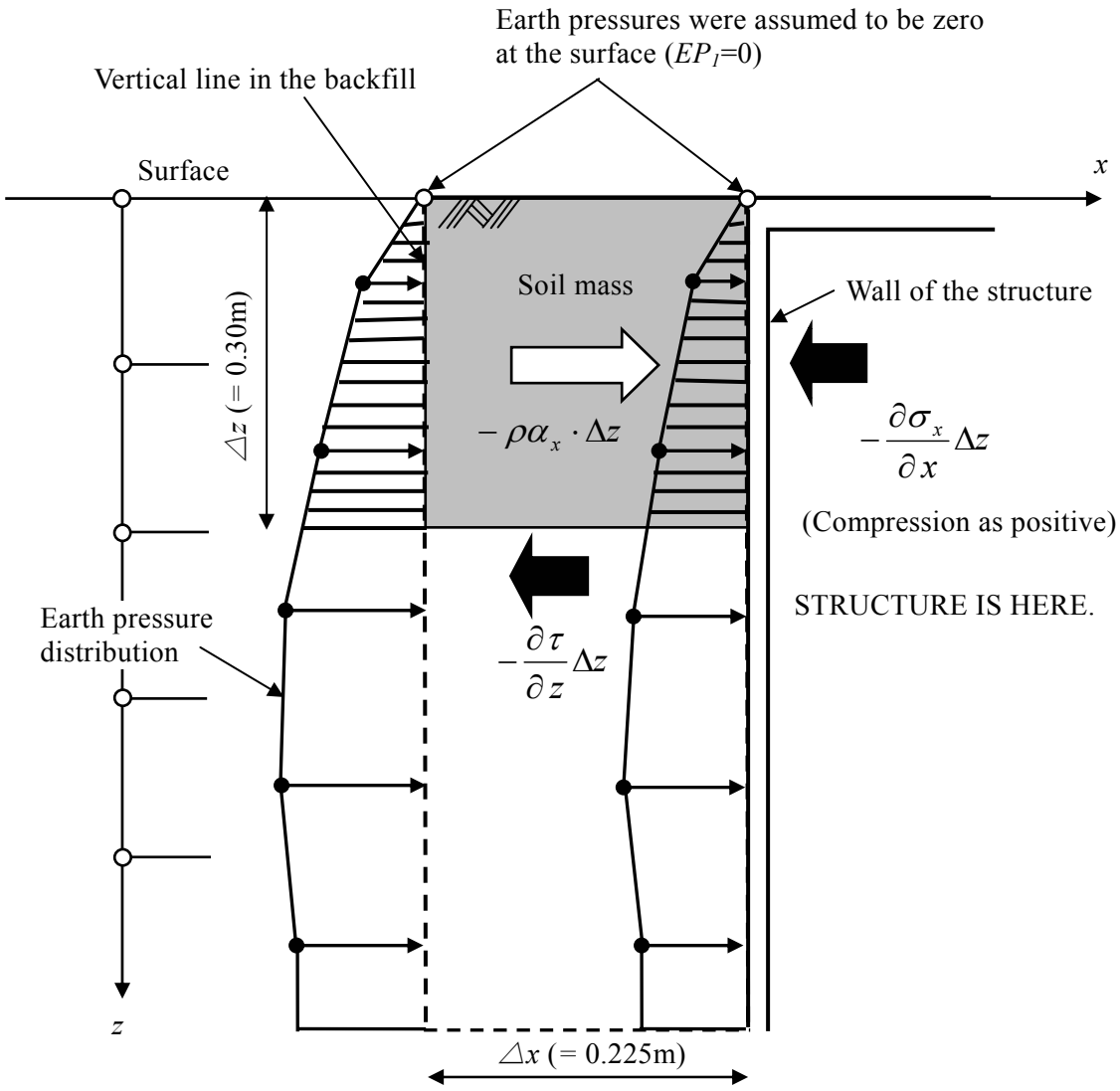

Fig.7.9: Location of soil mass and force equilibrium in the horizontal direction

the measurements of accelerations and dynamic earth pressures. The detailed procedures of calculation are presented in Section 4.2.1. In a situation presented in Fig.7.9, when a value of the inertia force, $-\rho\ \alpha_x \Delta z$, is positive, the soil mass moves toward the structure of the right direction. In the following, discussions are focused on the situation when the positive peaks of inertia force, $-\rho\ \alpha_x \Delta z$, appears.

Fig.7.10 shows the change of natural frequencies of both structure and backfill with time (figures (i)) and measured time histories of the inertia force, $-\rho\ \alpha_x \Delta z$, and the normal stress difference, $\partial\ \sigma_x / \partial x \Delta z$ (figures (ii)) from AD35F3A50 test. It is noted that the normal stress difference is calculated from the fluctuating component of dynamic earth pressure. The negative value of fluctuated component means a decrease from the monotonic component. It is not a negative pressure as illustrated in Fig.7.1.

In the time period of 4.5sec～5.0sec in Fig.7.10(a), the natural frequency of backfill is almost equal to that of the structure. At this time instance, the normal stress difference, $\partial\ \sigma_x / \partial x \Delta z$, is observed to be nearly zero (see A in the figure). It means that an inertia force, $-\rho\ \alpha_x \Delta z$, mobilized a shear stress difference , $\partial\ \tau / \partial z \Delta z$, without any effect of horizontal dynamic normal stress. A schematic diagram is illustrated in Fig.7.11(a).

During the time period of 5.0sec～7.0sec in Fig.7.11(b), the amplitude of the normal stress difference, $\partial\ \sigma_x / \partial x \Delta z$, is increasing. The amplitude of inertia force, $-\rho\ \alpha_x \Delta z$, keeps constant and it is larger than that of the normal stress difference (see B in the figure). In this time period, the natural frequency of backfill is slightly smaller than that of the structure during the time. The sum of normal stress difference and shear stress difference becomes inertia force as depicted in the conceptual diagram of Fig.7.11(b).

The amplitude of the normal stress difference is continuously increasing, and the time history of normal stress difference, $\partial\ \sigma_x / \partial x \Delta z$, coincides with that of inertia force after 7.5 seconds (see C in the figure). The natural frequency of backfill becomes zero by soil liquefaction. Considering the equilibrium of force in the soil mass, there is no shear stress difference after 7.5 second as shown in Fig.7.11(c). This phenomenon causes the reduction of shear modulus of the soil. It suggests that inertia force of soil mass becomes dominant in dynamic pressure on the structure when the backfill liquefy.

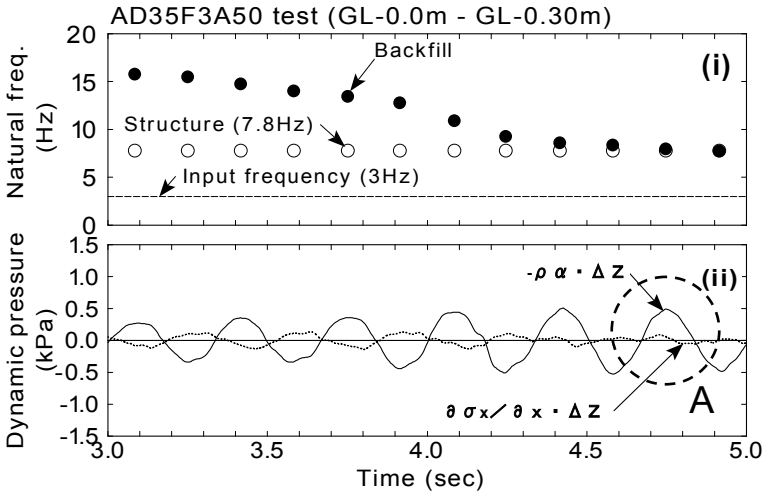

(a) 3.0sec ～ 5.0sec

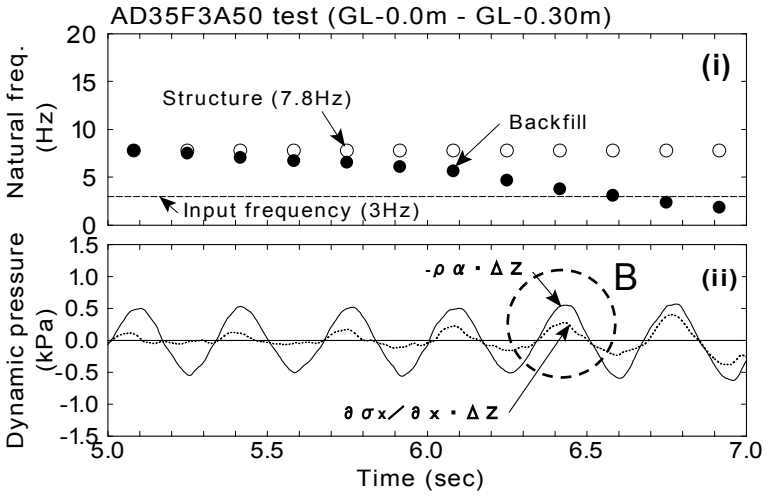

(b) 5.0sec ～ 7.0sec

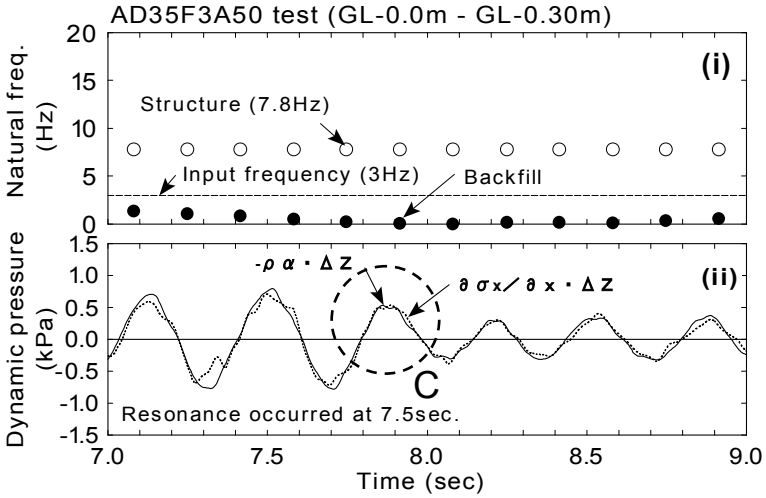

(c) 7.0sec ～ 9.0sec

Fig.7.10: Time histories of inertia force and normal stress difference (AD35F3A50 test)

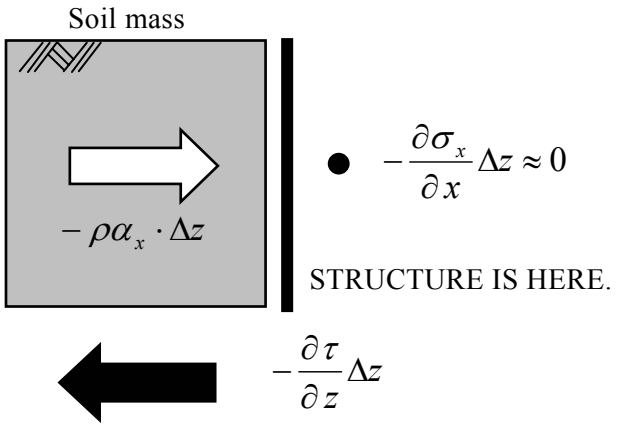

(a) Natural frequency of backfill is about equal to that of the structure (at A)

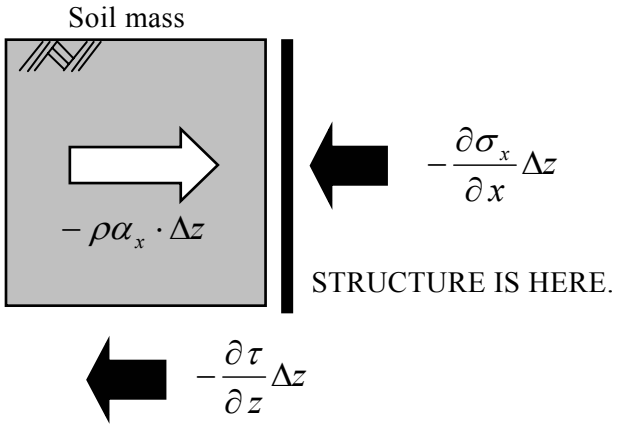

(b) Natural frequency of backfill is smaller than that of the structure (at B)

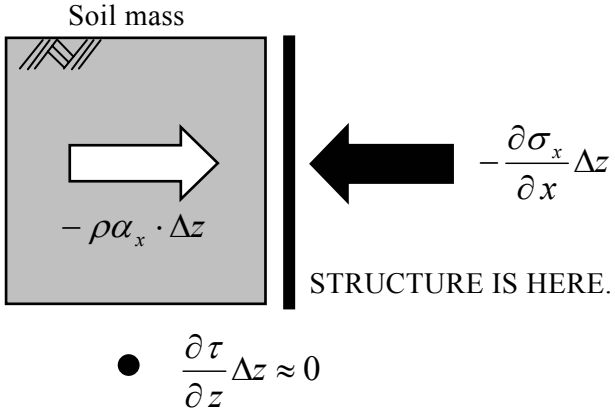

(c) Natural frequency of backfill is nearly zero by soil liquefaction (at C)

Fig.7.11: Conceptual diagram of force equilibrium at each state of soil

Fig.7.12 presents the results from AD39F5A50 test. In this test, the model with loose backfill with relative density of 39% is shaken by the sinusoidal wave with frequency of 5Hz. The input peak accelerations are 0.5m/sec^2. Since the natural frequency of backfill decreased more quickly than that of AD35F3A50 test due to high frequency of input notion, the time axes of the figures are enlarged. It is seen that the normal stress difference, $\partial \sigma_x / \partial x \Delta z$, is observed to be nearly zero at around 2.8 seconds (see A in Fig.7.12(a)). The natural frequency of backfill becomes similar to that of the structure at this time. The time history of normal stress difference is gradually changing to coincide with that of inertia force (see around B in Fig.7.12(b)). Finally, both time histories mached after the natural frequency of backfill reached zero (see C in Fig.7.12(c)).

Fig.7.13 and Fig.7.14 illustrate the results from AD41F3A200 and AD61F3A200 test, respectively. The models are shaken by an input motion of 2.0m/sec^2 in both tests. The nature illustrated in Fig.7.11 is clearly observed at A, B and C in each figure. Fig.7.15 depicts the results from AD32F3A500 test. Since the model is shaken by an intense input motion of 5.0m/sec^2, the reduction of natural frequency of backfill occurs more rapidly than other results. In spite of this, the same nature as depicted in Fig.7.11 can be seen. It seems that the contribution of an inertia force of soil mass to dynamic pressure becomes significant when the natural frequency of backfill get reduced by liquefaction.

Fig.7.16 presents the effect of natural period of ground on the normal stress difference of dynamic earth pressures during pore pressure build-up from various tests. The axis of ordinates represents the ratio of the amplitude between the normal stress difference, $\partial \sigma_x / \partial x \Delta z$, and the inertia force, $-\rho \alpha_x \Delta z$. Before amplitudes were calculated from each time history, high frequency components were removed from each time history by low pass digital filter of 6Hz for tests of 3Hz input motion, and filter of 10Hz for 5Hz input motion. The ratio is seen to be about zero when the natural period of backfill becomes equal to that of the structure, representing the state A as shown in Fig.7.11(a). The ratio increases toward unity as the natural period of ground becomes longer by liquefaction, representing the state B or C as shown in Fig.7.11(b) and (c). This suggests that the inertia force of the soil mass adjacent to the structure becomes dominant in the dynamic earth pressures when soil liquefies.

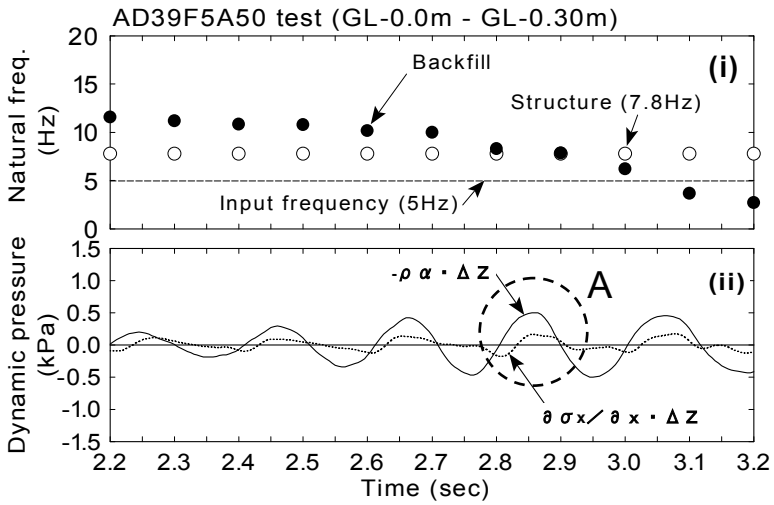

(a) 2.2sec ～ 3.2sec

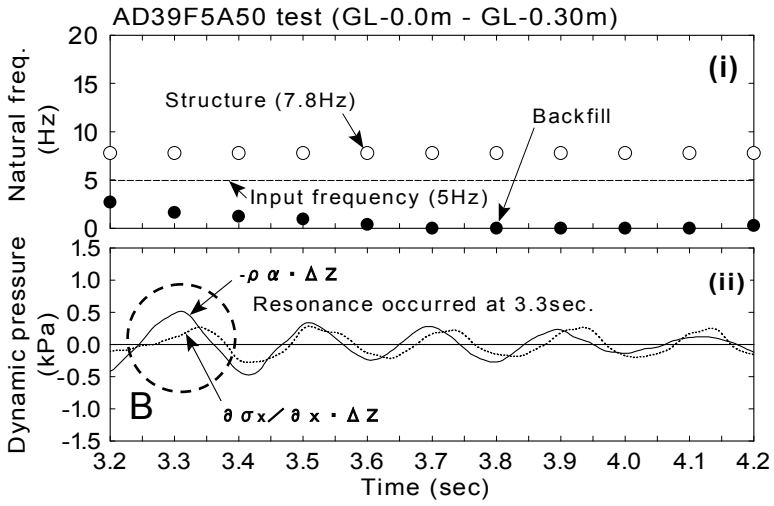

(b) 3.2sec ～ 4.2sec

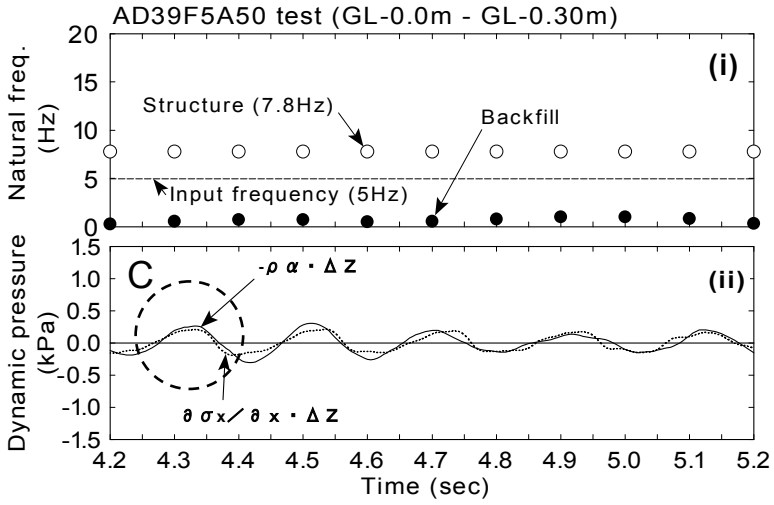

(c) 4.2sec ～ 5.2sec

Fig.7.12: Time histories of inertia force and normal stress difference (AD39F5A50 test)

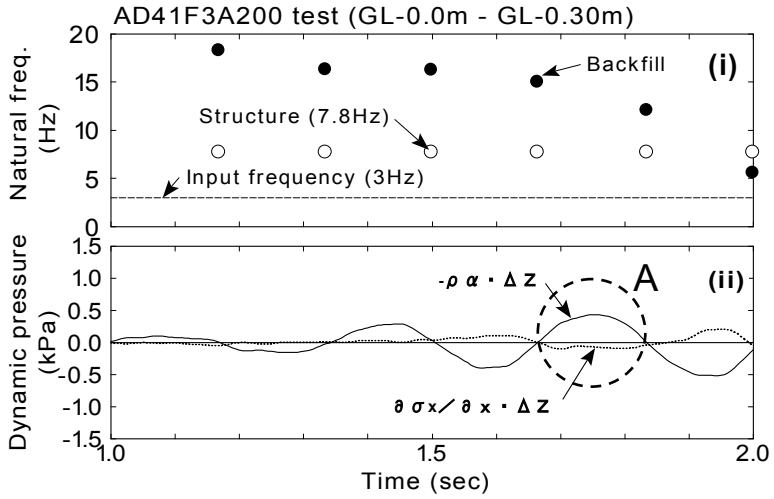

(a) 1.0sec ～ 2.0sec

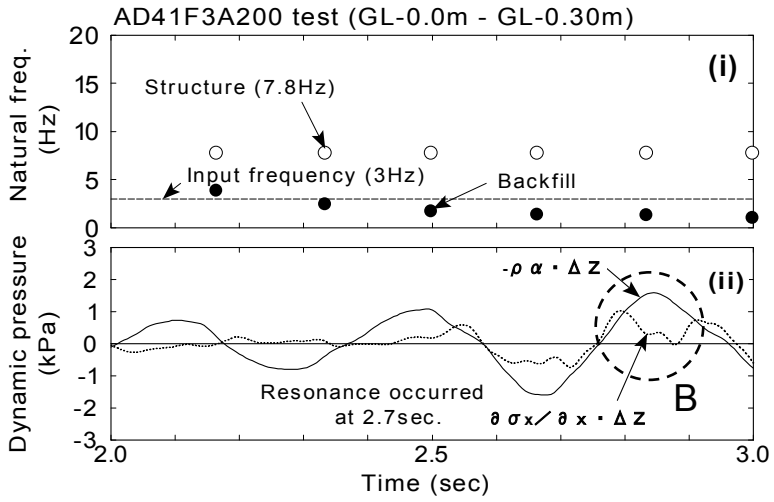

(b) 2.0sec ～ 3.0sec

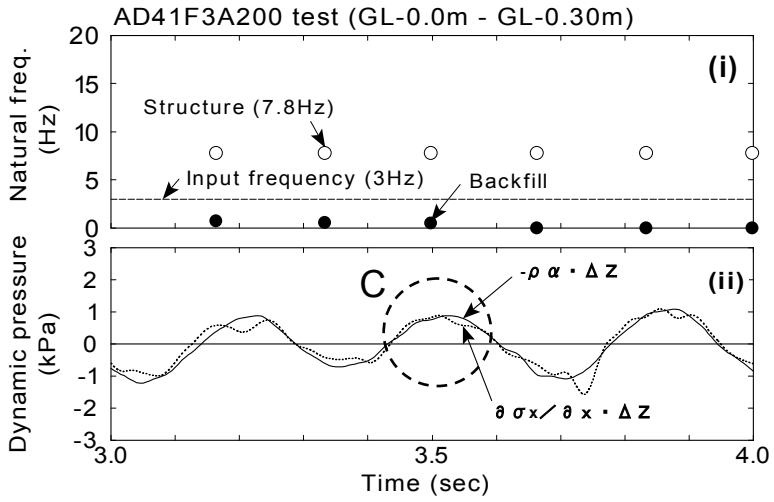

(c) 3.0sec ～ 4.0sec

Fig.7.13: Time histories of inertia force and normal stress difference (AD41F3A200 test)

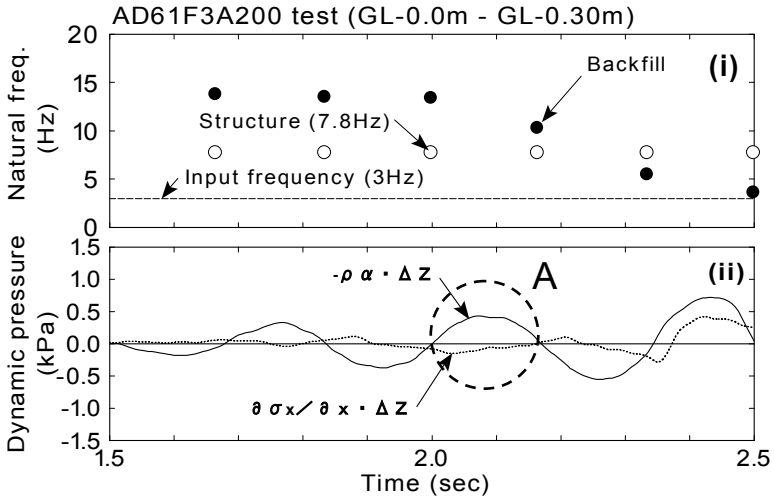

(a) 1.5sec ～ 2.5sec

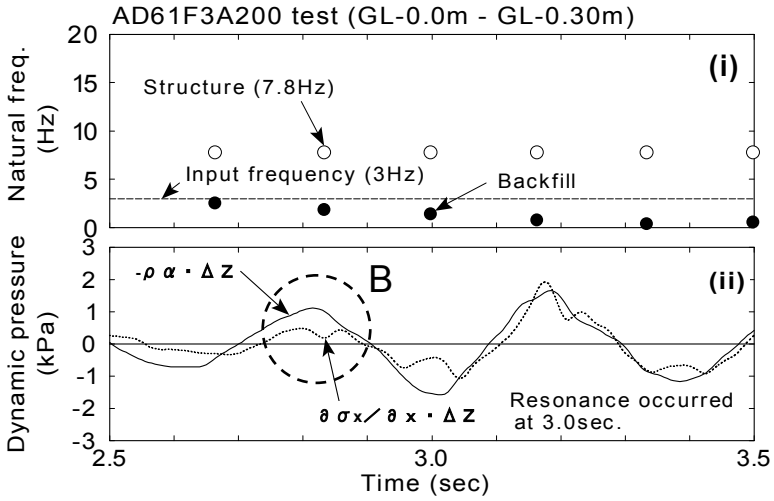

(b) 2.5sec ～ 3.5sec

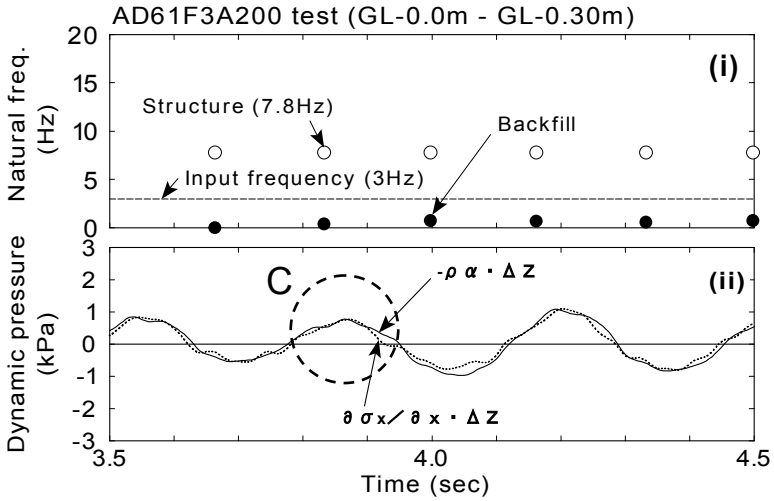

(c) 3.5sec ～ 4.5sec

Fig.7.14: Time histories of inertia force and normal stress difference (AD61F3A200 test)

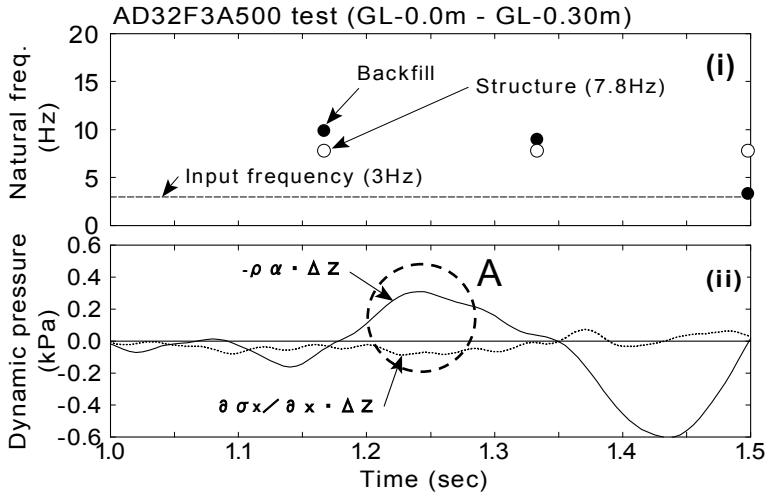

(a) 1.0sec ～ 1.5sec

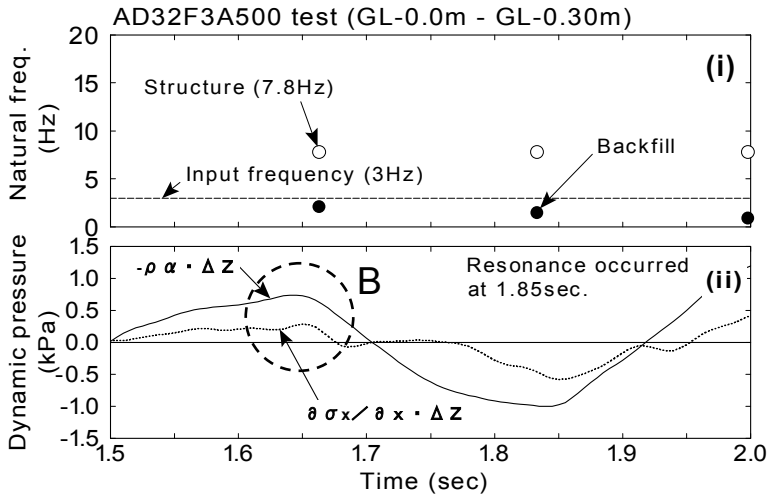

(b) 1.5sec ～ 2.0sec

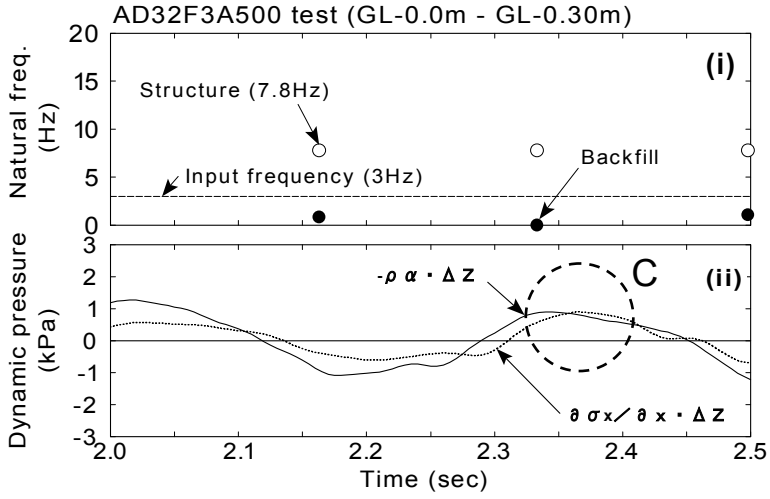

(c) 2.0sec ～ 2.5sec

Fig.7.15: Time histories of inertia force and normal stress difference (AD32F3A500 test)

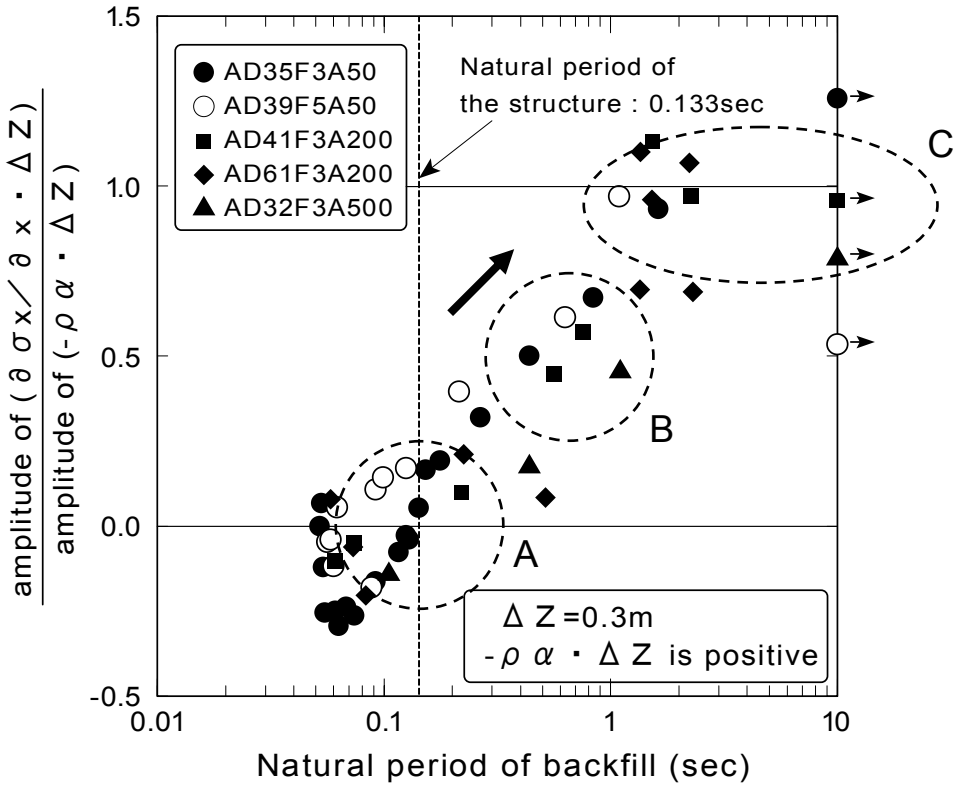

Fig.7.16: Effect of natural period of ground to the normal stress increment by dynamic earth pressure

7.3 EFFECTS OF DILATANCY OF SOIL

In the previous study based on the stress-strain relationship of soil in the Chapter 4, it was observed that dense backfill soil near the embedded structure behaves in a dilative manner during shaking. The effect of dilatancy on dynamic soil-structure interaction is examined here.

7.3.1 Dilative behavior of backfill in shaking table tests

According to the stress-strain relationship derived in Chapter 4, the dilative behavior of soil is observed in the test results from AD67F3A500 and BD78F3A500 test in which dense backfill had 67% and 78% of relative density. Fig.7.17 shows the stress strain relationship of a soil mass adjacent to the structure (GL-0.30m – GL-0.45m) in those tests. The result from AD32F3A500 test, which does not show the dilative behavior, is illustrated in Fig.7.17(a) for comparison. When the shear strain reaches a level of about 4%, the shear stress is only 2 or 3 kPa. In the case of the same

intensity of motion (5.0m/sec^2), the feature of stress-strain relationship for 78% relative density shown in Fig.7.17(b) is different from the 32% relative density. The shear stress at about 4% shear strain reaches about 20kPa at A in the figure. The same feature is seen at 67% relative density shown in Fig.7.17(c).

The acceleration responses at the top of structure (AC2) are shown in Fig.7.18. In the test for 32% relative density, the response acceleration was about 7 m/sec^2 as shown in Fig.7.18(a). The higher response acceleration for dense sand deposit was produced as shown in Fig.7.18 (b)(c) by the dilative behavior of sand that allowed the greater magnitude of shear stress.

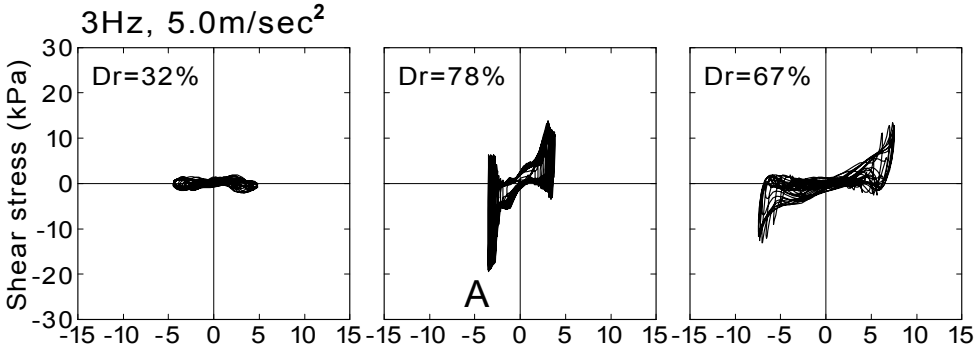

(a) AD32F3A500 test (b) BD78F3A500 test (c) AD67F3A500 test

Fig.7.17: Stress-strain relationships of soil mass

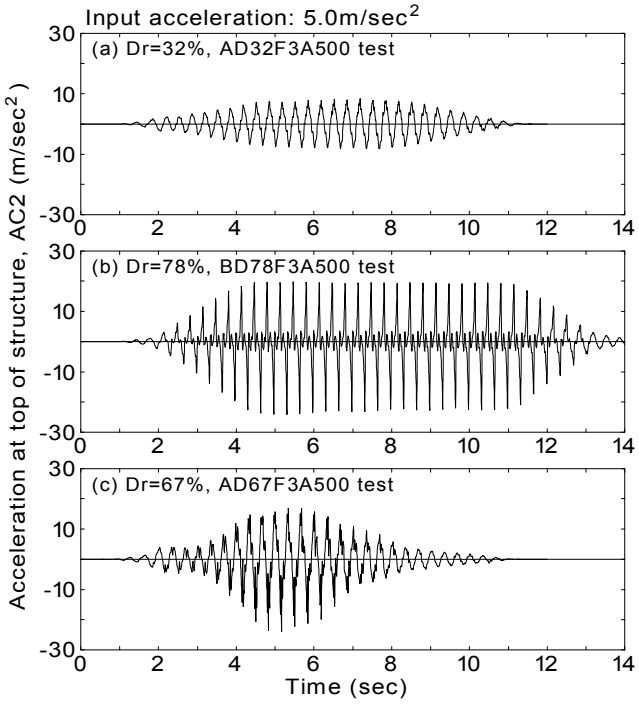

Fig.7.18: Acceleration responses at the top of the structure (AC2)

7.3.2 Dynamic earth pressures during dilative behavior of backfill

Fig.7.19 presents the experimental relationship between the resultant force F_d and the displacement of the structure (LV1) from AD32F3A500, BD78F3A500 and AD67F3A500 test. The relative densities of backfill of those tests are 32%, 78%, 67%, respectively. The models are shaken by sinusoidal wave with the peak acceleration of 5.0 m/sec^2. Different from the 0.5 m/sec^2 shaking presented in Fig.7.5, the 5.0 m/sec^2 shaking shows that liquefied sand generates load basically on the wall, being positive proportionality of the experimental relationship.

The shape of the hysteresis loop at 32% relative density is almost positive proportionality (see B to A in Fig.7.19(a)). When the wall translated away from the backfill soil (positive displacement is illustrated in Fig.7.2) the earth pressure still increased. Thus, it is interesting that the liquefied soft sand tends to move laterally more significantly than the wall, making this positive proportionality. On the other hand, the shape of the hysteresis loop at 78% and 67% relative density is very complicated. The spiky earth pressures at the negative displacement (C in Fig.7.19 (b)(c)) appears in the hysteresis loop.

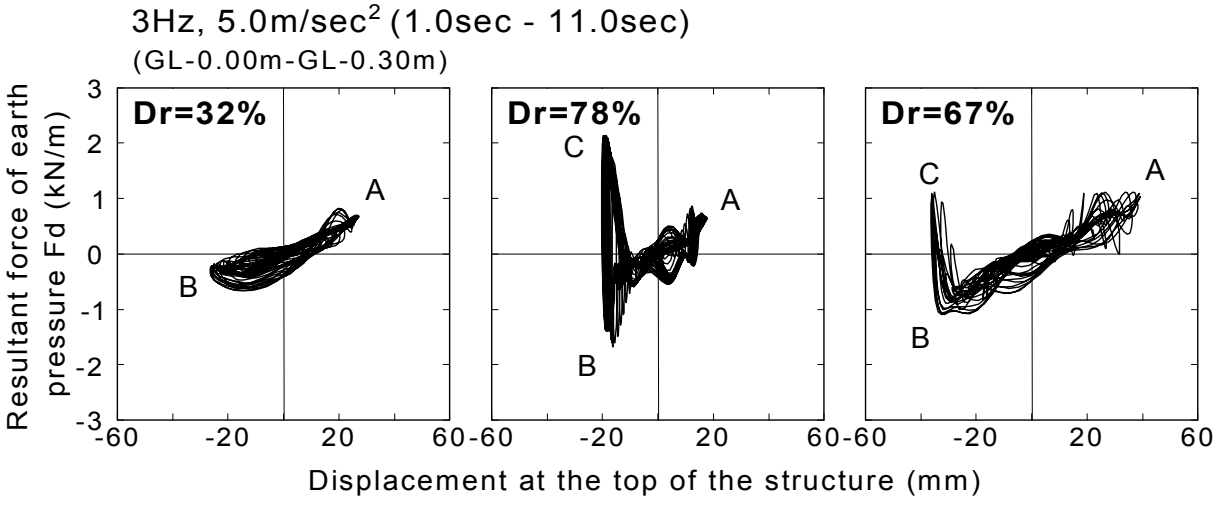

(a) AD32F3A500 test (b) BD78F3A500 test (c) AD67F3A500 test

Fig.7.19: Experimental relationship between resultant force F_d and displacement of the structure

Fig.7.20 demonstrates the hysteresis loops in the time periods of 4.0 to 4.3 seconds and 5.0 to 5.3 seconds for (i) relationship of the resultant force F_d and displacement, (ii) stress-strain relationship and (iii) effective stress path from AD32F3A500, BD78F3A500 and AD67F3A500 tests.

As shown in Fig.7.20(a)(i) of AD32F3A500 test at 32% relative density, the hysteresis loop between resultant force of earth pressure and displacement is of positive proportionality. The shape of stress-strain relationship is almost flat, indicating the loss of shear modulus of soil. In this case, the effective stress path stays at the origin as indicated in Fig.7.20(a)(iii), showing complete liquefaction of the backfill soil.

The spiky earth pressures are seen in Fig.7.20(b)(i) from BD78F3A500 test when the displacement is minimum at 4.14 and 5.14 seconds respectively. In this time, the resultant force of dynamic earth pressure, which once decreased to the level of about -1.5kN/m, increased to the level of 2 kN/m. This time moment corresponds to the time when the minimum shear stress occurred as shown in the stress-strain relationship of Fig.7.20(b)(ii). The effective vertical stress reached the level of 10 kPa as shown in Fig.7.20(b)(iii). It shows that the spiky earth pressures occurred due to the effect of dilatancy.

The same feature of resultant force of earth pressure and displacement can be seen in Fig.7.20(c)(i) at 67% relative density. The resultant force of earth pressure increased rapidly as much as 1kN/m in the negative displacement at 5.02 seconds. The effective stress path indicates that the effective stress increased at this instance, showing the soil behaved in a dilative manner. Since the soil which became rigid by a dilative behavior was hard to deform suddenly, it is considered that the structure clashed to the backfill causing the rapid increase of earth pressure.

Fig.7.21(a) depicts one cycle of hysteresis loop of stress-strain relationship in the time period of 4.0 to 4.3 seconds extracted from Fig.7.20(c)(ii). The path of the hysteresis loop is indicated in the figure by the arrows. Dilative behavior is clearly observed when the shear strain exceeds about 5% in either positive or negative direction. It is also seen that the shear stress of soil, which is about 5kPa before dilative behavior, is rapidly increased as twice as much at the portion pointed by circles in the figure.

Fig.7.21(b) shows the corresponding relationship between the resultant force F_d and the displacement of the structure. It is seen that the earth pressure increases as the displacement increases to the positive direction between B and A. It is inferred that the liquefied soft backfill tends to move laterally more significantly than the wall. The earth pressures act as a load to the

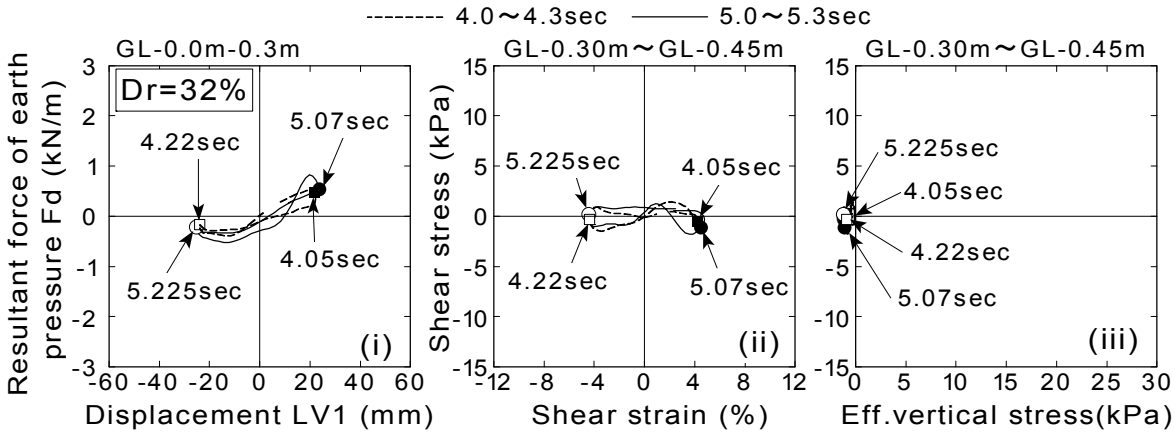

(a) Relative density Dr=32% (AD32F3A500 test)

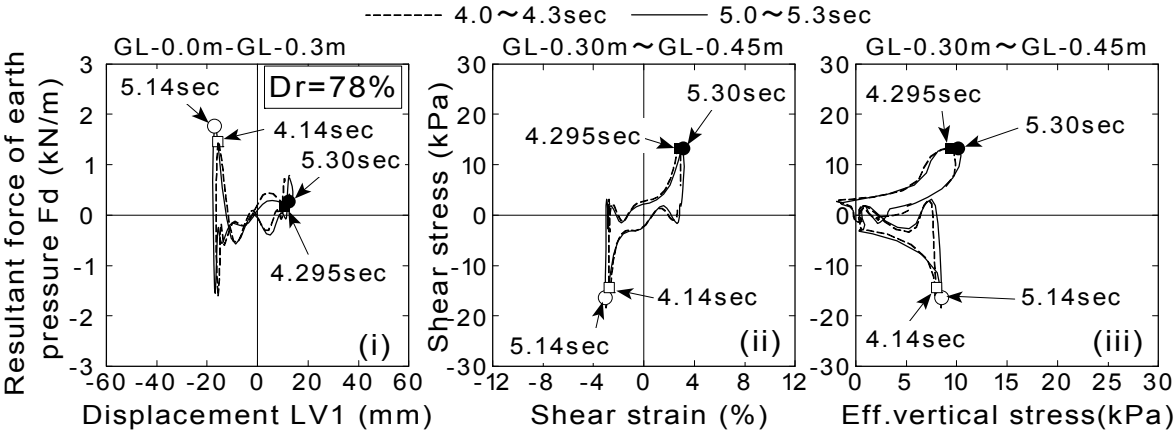

(b) Relative density Dr=78% (BD78F3A500 test)

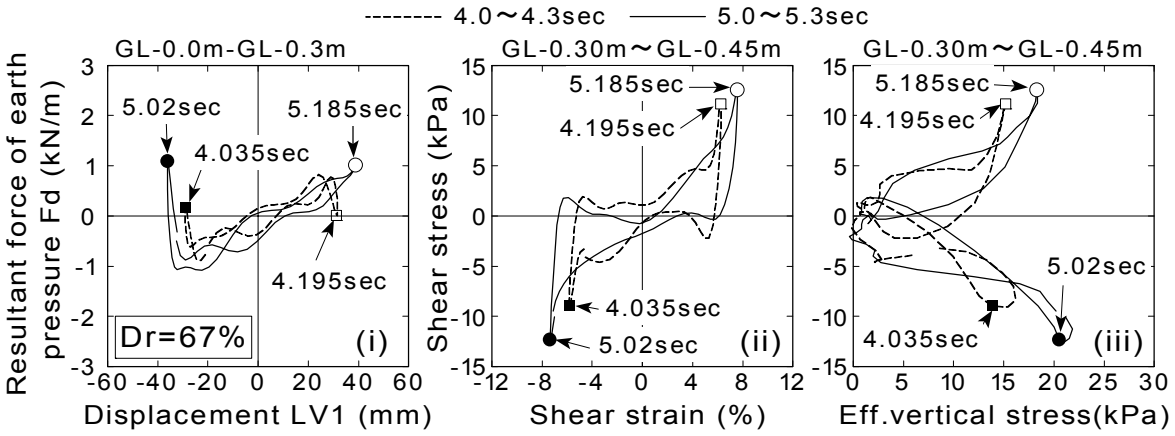

(c) Relative density Dr=67% (AD67F3A500 test, the wall started to yield at about 4 sec.)

Fig.7.20: Hysteresis loop of earth pressure and displacement of the structure (i), stress-strain relationship (ii),effective stress path (iii) shaken by the same intensity of input motion

structure in this moment. The quick decrease of earth pressure with positive displacement is observed at A to D in a positive displacement. In contrast, the earth pressure increased rapidly from B to C in a negative displacement.

Scaled-up of relationships at the portion of A to D and B to C are presented in Fig.7.21(c) and (d), respectively, with the stress-strain relationship of backfill at the same time period. Corresponding times between two relationships are also shown in each figure. It is observed in figure (c) that the soil becomes rigid by dilatancy during 4.165 seconds to 4.220 seconds (bold line), and shear stress of the soil mass increase from about 5kPa to more than 10 kPa. The resultant force of dynamic earth pressure F_d decreases quickly in this time period. It suggests that the structure moved away from backfill soil that became more rigid than the structure instantaneously by increasing of effective stress (see Fig.7.20(c)(iii)).

In contrast with this, it is seen in Fig.7.21(d)(ii) that the earth pressure increased rapidly from B to C in the negative displacement. The direction of rotation at this portion is anticlockwise, suggesting that the earth pressure acts as a reaction. Referencing the stress-strain relationship at this time period (4.000～4.060 seconds), the backfill soil becomes rigid again, and the shear stress which is about –5kPa changes more than twice as much in a negative direction. The soil, which is made rigid by dilatancy, seems to constrain the motion of the structure instantaneously.

Fig.7.22 illustrates the results from BD78F3A500 test during the time period of 4.00 seconds to 4.315 seconds. The change of resultant force of earth pressure during dilative behavior of soil is very complicated in the positive direction of displacement as seen in figure(b)(ii). However, when the structure deforms in the negative direction, the resultant force of earth pressure increases as much as 1.5 kN/m (point C in figure(d)(ii)) by dilatancy of soil. This shows that backfill constrains the movement of structure and the earth pressure occurs as a result of a reaction.

Based on the observation in this section, the behavior of dynamic earth pressures in a dilative behavior of soil can be illustrated as shown in Fig.7.23. Figure (a) represents the behavior in the positive displacement of structure, and figure (b) in the negative displacement. Increasing of rigidity and shear stress of soil mass adjacent to the structure by dilative behavior causes the quick change of dynamic earth pressure either in the positive direction or the negative direction. The dilative behavior of backfill thus influences the occurrences of dynamic earth pressures. Especially, backfill strongly constrains the structure during the dilative behavior in a negative direction, suggesting the inhibition of complete collapse of a box section of underground structure by dense backfill during earthquakes.

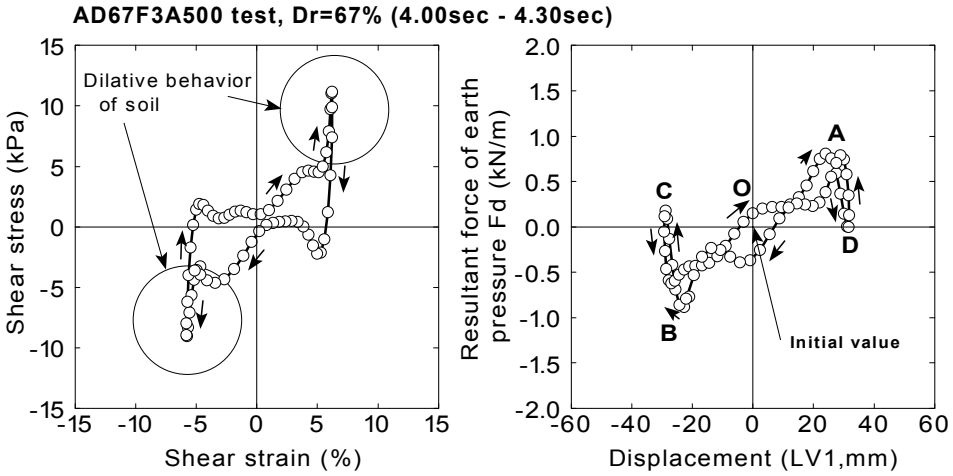

(a) Stress-strain relationship of soil mass (b) F_d and displacement of the structure

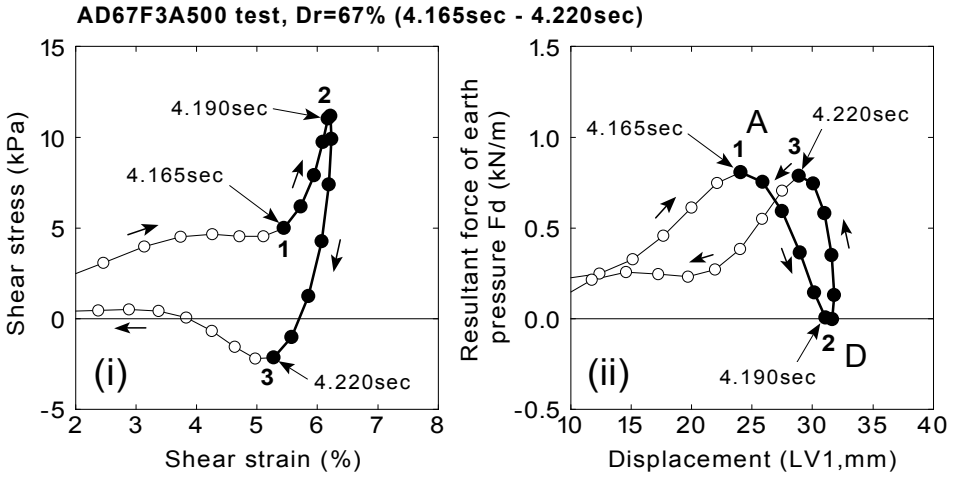

(c) Scaled-up of relationships at the portion of A to D

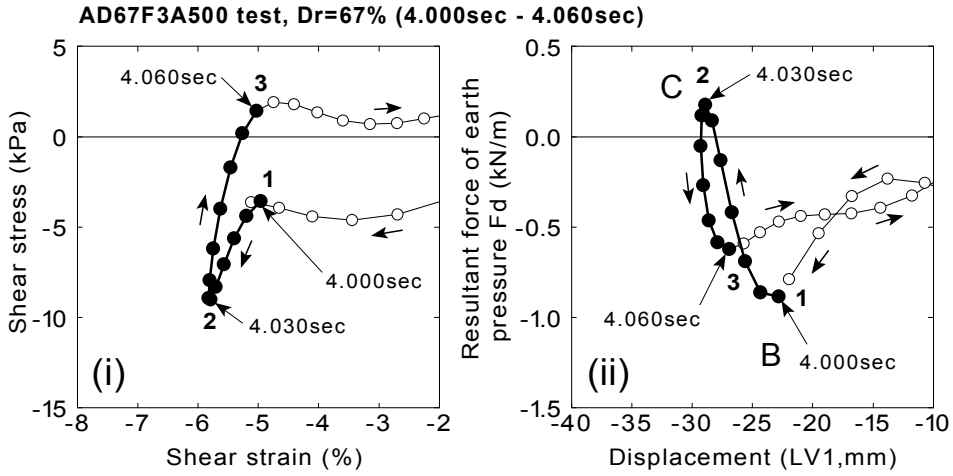

(d) Scaled-up of relationships at the portion of B to C

Fig.7.21: Behavior of soil mass and the structure in one cycle (AD67F3A500 test)

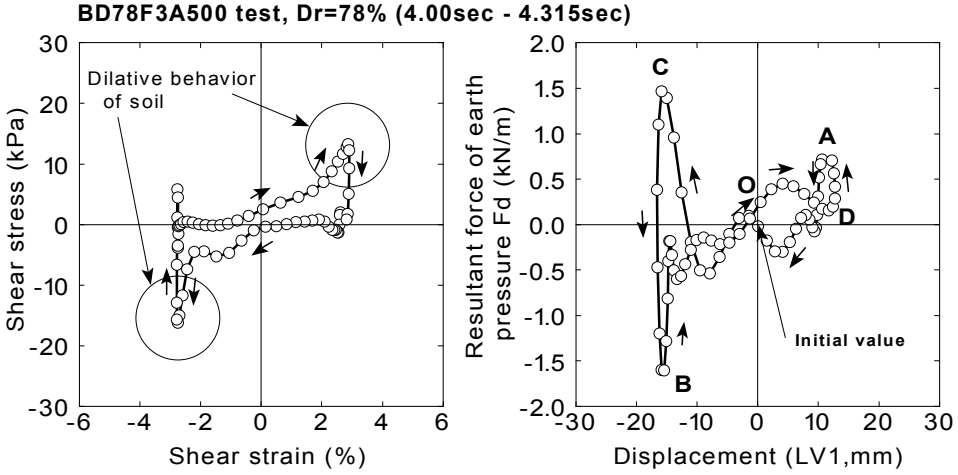

(a) Stress-strain relationship of soil mass (b) F_d and displacement of the structure

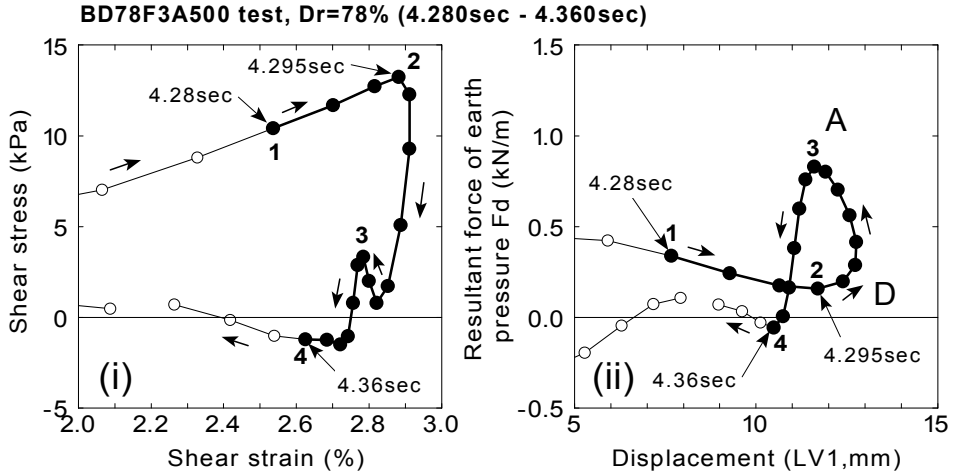

(c) Scaled-up of relationships at the portion of D to A

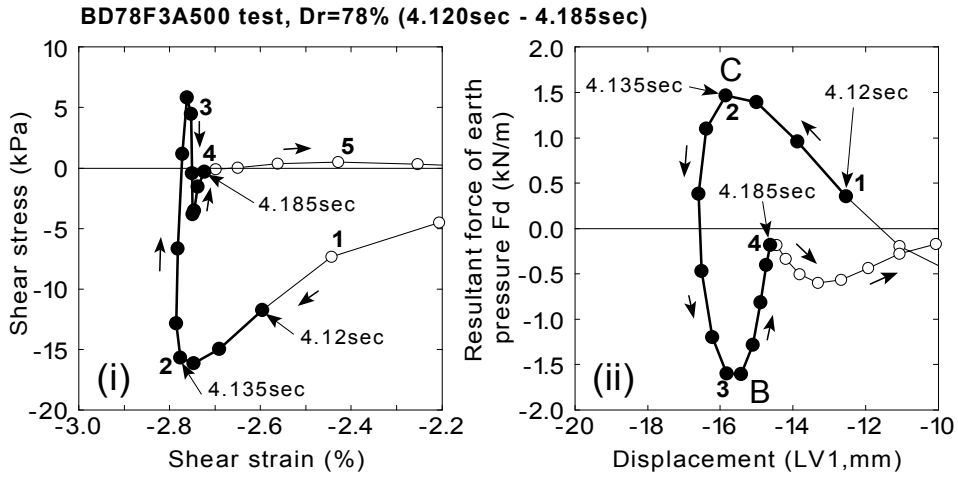

(d) Scaled-up of relationships at the portion of C to B

Fig.7.22: Behavior of soil mass and the structure in one cycle (BD78F3A500 test)

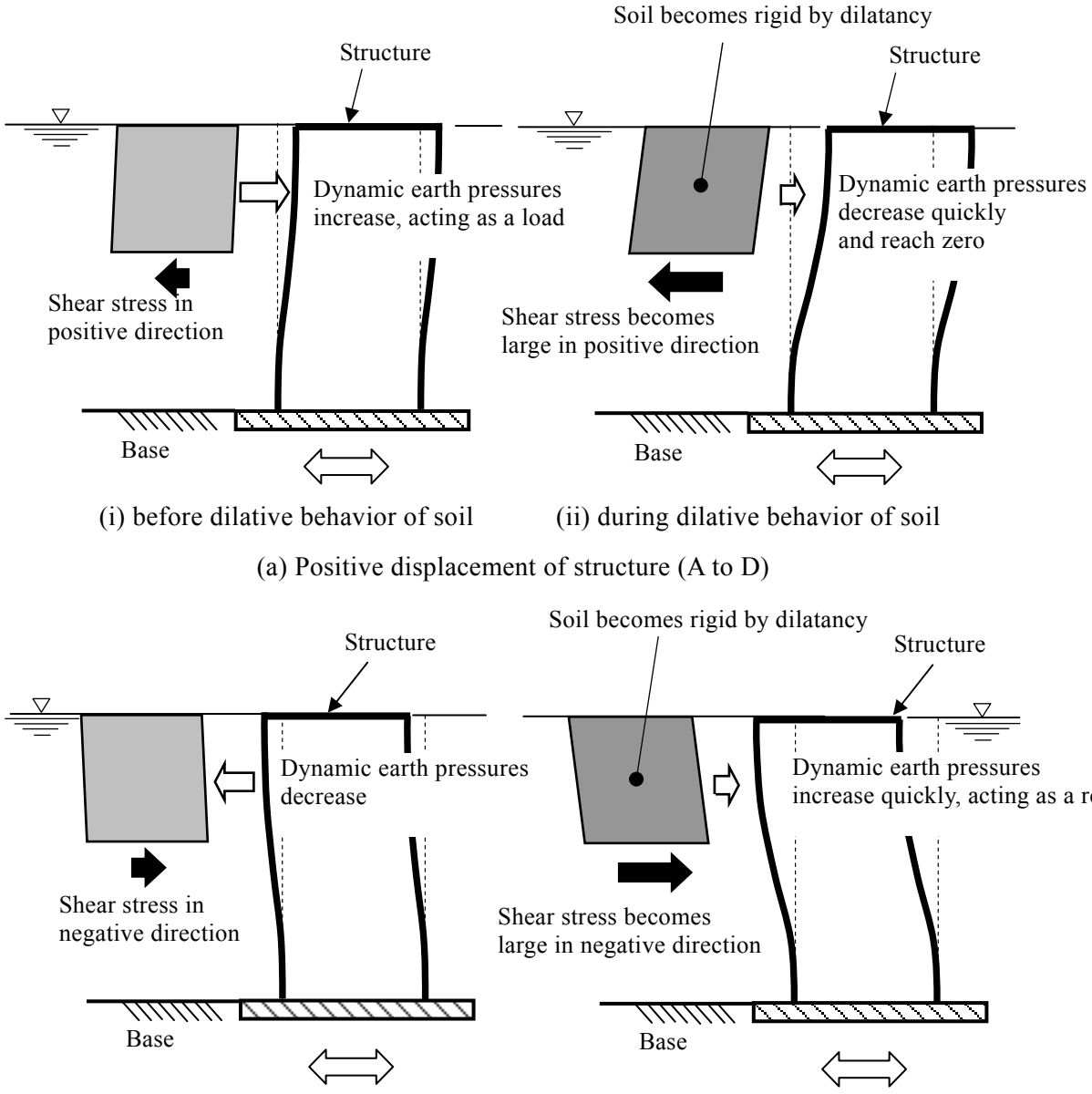

Fig.7.23: Schematic figure of dynamic earth pressures in a dilative behavior of soil

In this respect, the occurring of a dilative behavior of backfill soil during seismic excitation can be one of key phenomenon to evaluate the seismic behavior of underground structure. When the shear strain of backfill becomes as large as certain shear strain which exerts a dilative behavior of soil, the seismic load should not be considered as a dominant effect from backfill to structure. In this case, the supporting mechanism by the backfill should be considered. Further discussion on the action of backfill on structure will be made in the following section.

7.3.3 Dilative behavior of backfill after yielding of material

Fig.7.24 shows the time histories of bending strains at the bottom of the wall (SG7, SG14) and the relation between the bending strain and effective vertical stress at the point of PP2 (GL-0.375m, see at the 500gal shaking of input motion. The approximate yield bending strain of the wall ($\pm$ 3750 μ) is depicted in each figure.

Fig.7.24(a) illustrates the bending strain of Structure-A at the 32% relative density. The positive bending strain is depicted in the inset of Fig.7.24. The bending strains of wall are smaller than the yield strain through the duration of shaking. The effective vertical stress is almost zero as shown in Fig.7.24(b) so that the soil liquefies completely at time period of 4.0 to 8.0 second.

Fig.7.24(c) shows the bending strain of Structure-B at the 36% relative density. The tensile strength of the wall in Structure-B is about 3/5 of the strength of Structure-A. The bending strain at the bottom of wall at left side (SG7), gradually increased with cyclic change up to about 8 seconds, exceeded the yield bending strain at 3.4 second. The bending strain at the bottom of wall at right side (SG14) is gradually decreasing with cyclic change, and exceeded the yielding strain at 3.2 second. The effective vertical stress keeps around zero as shown in Fig.7.24(d), indicating that the loose soil behaves in the manner of negative dilatancy.

Fig.7.24(e) illustrates the bending strain of Structure-A at the 67% relative density. The bending strain of the wall exceeded the yield strain cyclically during the time of 4.0 to 8.0 second. The effective vertical stress of the backfill soil increased significantly due to dilatancy when the bending strain exceeded the yield bending strain as shown in Fig.7.24(f). It is considered that the yielding of the aluminum caused large deformation of the structure, consequently, the dense soil strain becomes large and the soil behaves in a more dilative manner.

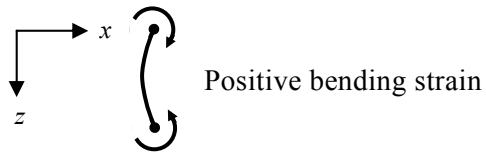

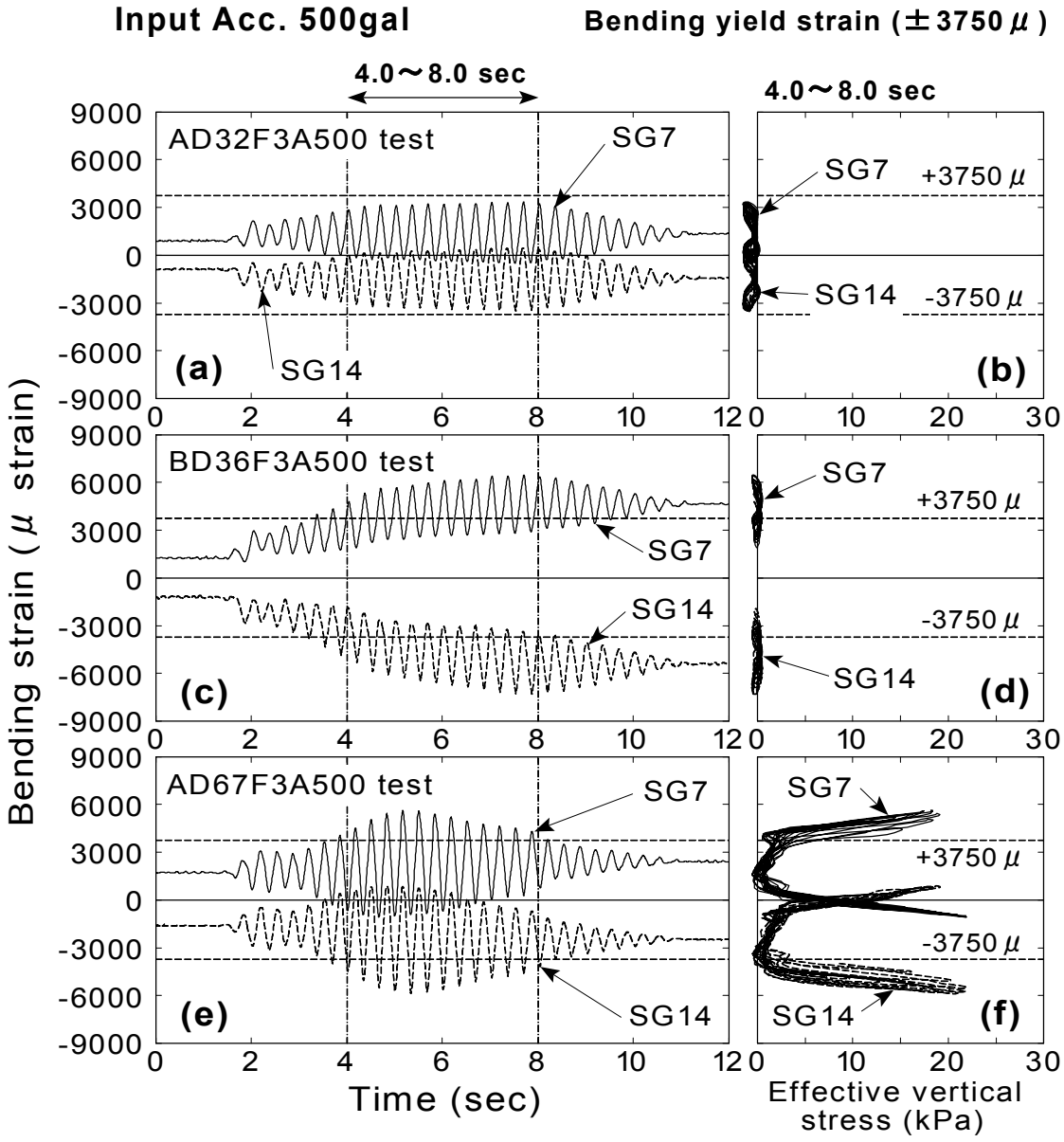

Fig.7.24: Bending strain of the wall and effective vertical stress

7.4 INFLUENTIAL PARAMETER ON DYNAMIC EARTH PRESSURES DURING SOIL LIQUEFACTION

As pointed in the Chapter 1, past studies have shown that a cross section of flexible underground structure is under the control of deformation unless the backfill does not liquefy. However, many studies associated with liquefied soil and rigid walls have shown that a rigid structure is under the control of inertia force. In this section, an influential parameter on dynamic earth pressures which act on a flexible wall of underground structure during soil liquefaction is examined. Both accelerations of wall of a flexible underground structure, and dynamic relative displacements between the ground and the structure are focused on as influential parameters.

7.4.1 Definition of horizontal normal strain of backfill and wall acceleration

Horizontal normal strain

Generally, the horizontal relative displacement δ is defined as,

$$\delta = \delta_{soil} - \delta_{struc.} \tag{7.4}$$

where δ_{soil} is the horizontal displacement at the free field, $\delta_{struc.}$ is the horizontal dynamic displacement of structure. In this section, the horizontal normal strain ε_h is defined in a simplified manner in terms of the horizontal relative displacement as,

$$\varepsilon_h = (\delta_{soil} - \delta_{struc.}) / B \tag{7.5}$$

where B is the width of the model ground in shaking table test, 0.45m. The model ground and the depth to calculated horizontal normal strain are illustrated in Fig.7.25. The measured displacement at the edge of a container (LV3, LV4) and the displacement on the wall by the measured bending strain (SG2, SG4) are the displacement δ_{soil} and $\delta_{struc.}$, respectively. The horizontal normal strain at each depth of GL-0.30m and GL-0.575m is expressed as

$$\varepsilon_{h,GL-0.3m} = (\delta_{soil,LV3} - \delta_{struc.,SG2}) / B \tag{7.6}$$

$$\varepsilon_{h,GL-0.575m} = (\delta_{soil,LV4} - \delta_{struc.,SG4}) / B \tag{7.7}$$

Since horizontal displacements at the outside of container, LV3 and LV4 are measured in AD32F3A500, BD36F3A500, and BD78F3A500 test (see Fig.3.70, Fig.3.71, Fig.3.74 in Chapter3), the horizontal normal strain defined by Eqs.(7.6) and (7.7) can be calculated only in those three tests. Although the wall displacement by the measured bending strain, $\delta_{struc.}$, contains monotonic component of displacement, the amount is relatively smaller than that of fluctuating component of displacement in above-mentioned tests which are shaken by the input motion of 5.0m/sec^2 acceleration (see, Fig.6.29～Fig.6.31 in Chapter 6).

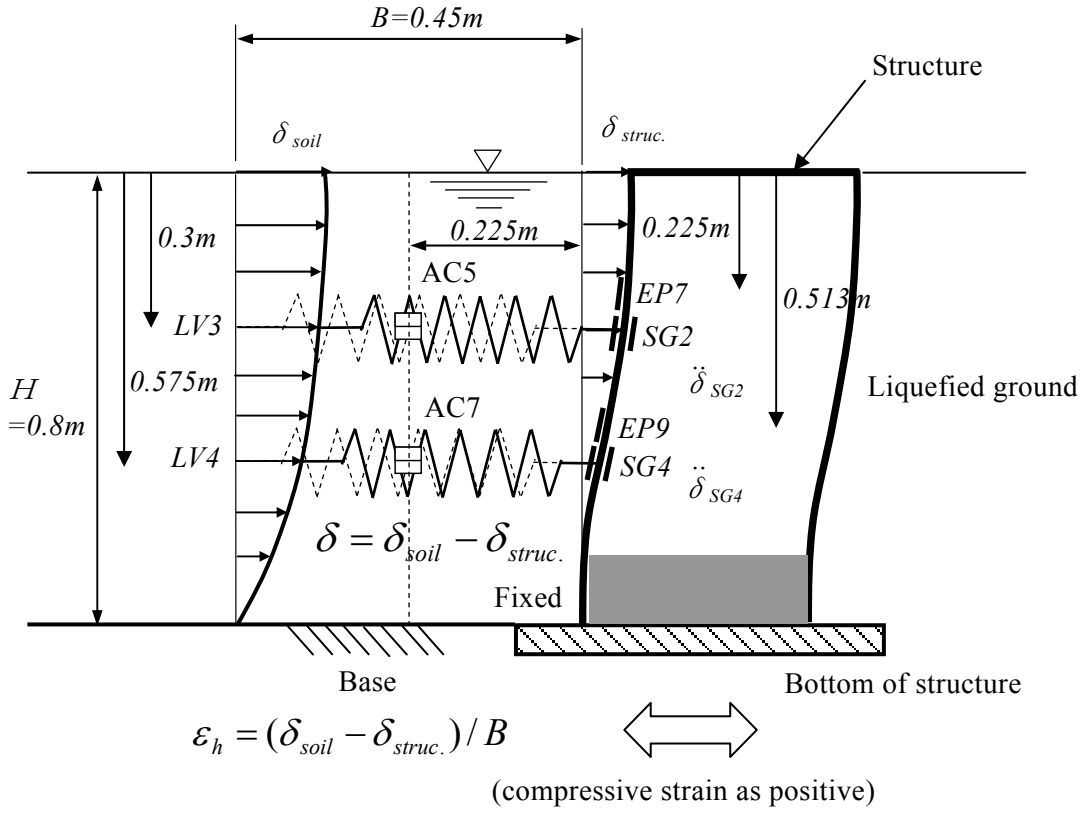

Fig.7.25: Definition of horizontal normal strain of ground.

Wall acceleration

The wall acceleration will be calculated at the depth where strain gauges SG2 and SG4 are attached. The wall accelerations are denoted as $\ddot{d}_{struc,SG2}$, and, $\ddot{d}_{struc,SG4}$ in Fig.7.25, respectively. Since the acceleration on the wall was not directly measured in the series of shaking table tests, the wall acceleration was calculated from the wall displacement, $d_{struc,SG2}$, and $d_{struc,SG4}$, by differentiating them twice with respect to time. Detailed procedure was presented in the Chapter 4.

7.4.2 Horizontal normal strain of backfill

Time histories of displacement at the edge of soil container (soil displacement) and wall displacement, as well as calculated horizontal normal strain from AD32F3A500 test are depicted in Fig.7.26. A compressive normal strain is defined as positive. The time of initial liquefaction, when the ratio of excess pore water pressure reach 100% first, is described in the figure as well.

It is seen in Fig.7.26(a) that no significant phase difference occurs between the soil displacement and wall displacement. In contrast, the amplitude of soil displacement is larger than that of wall displacement during shaking. As a result of this, the horizontal normal strain with the maximum of about 3% is produced at GL-0.300m after the initial liquefaction as shown in Fig.7.26(b). Considering that the liquefied soil is incompressible as the same level as that of water, the normal strain must occur not only in the horizontal direction but also in the vertical direction, which makes the surface heave. The level of the maximum horizontal normal strain is about 2% at GL-0.575m, being smaller than that of shallow portion. It is considered that the larger overburden pressure made constrain the deformation of soil in the vertical as well as horizontal direction.

It is observed in Fig.7.26(c) that the displacement of wall is increasing in the positive direction with fluctuation. As illustrated in the previous study made in Chapter 6, the deflection of wall increases as shaking goes on due to monotonic component of earth pressure (see Fig.6.24). It causes the accumulation of wall displacement in the positive direction.

The results from BD36F3A500 test are presented in Fig.7.27. The relative density of backfill in this test is 36%, being the same level as used in previous AD32F3A500 test. The material of wall yielded at 2.7 seconds, and the curvature of wall increased after that (see Fig.6.8). It is seen in Fig.7.27(c) that the displacement of wall is increasing in the positive direction, causing gradual decrease of horizontal normal strain. However, no phase differences are observed between them.

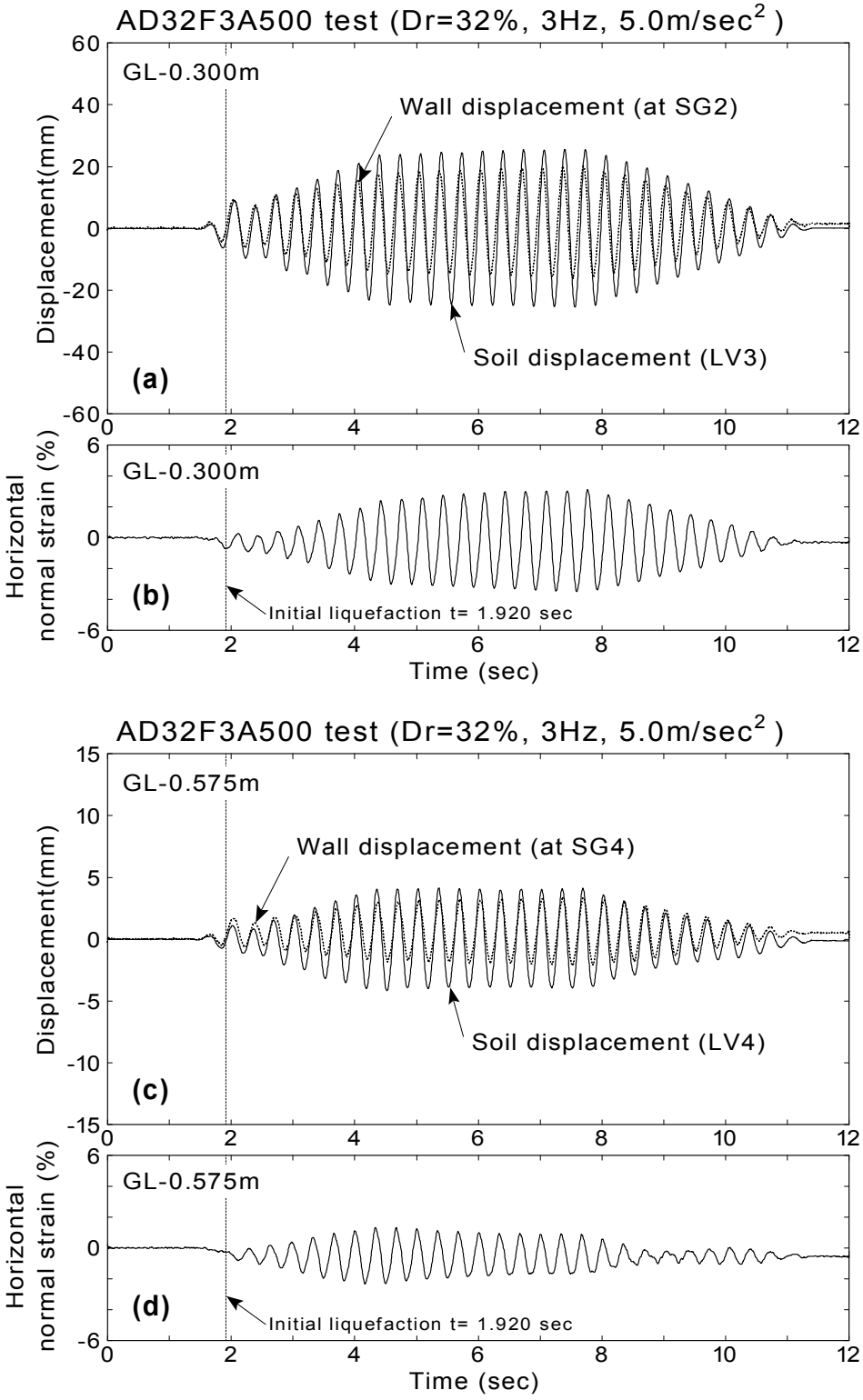

Fig.7.26: Displacement and normal strain of backfill (loose backfill, AD32F3A500 test)

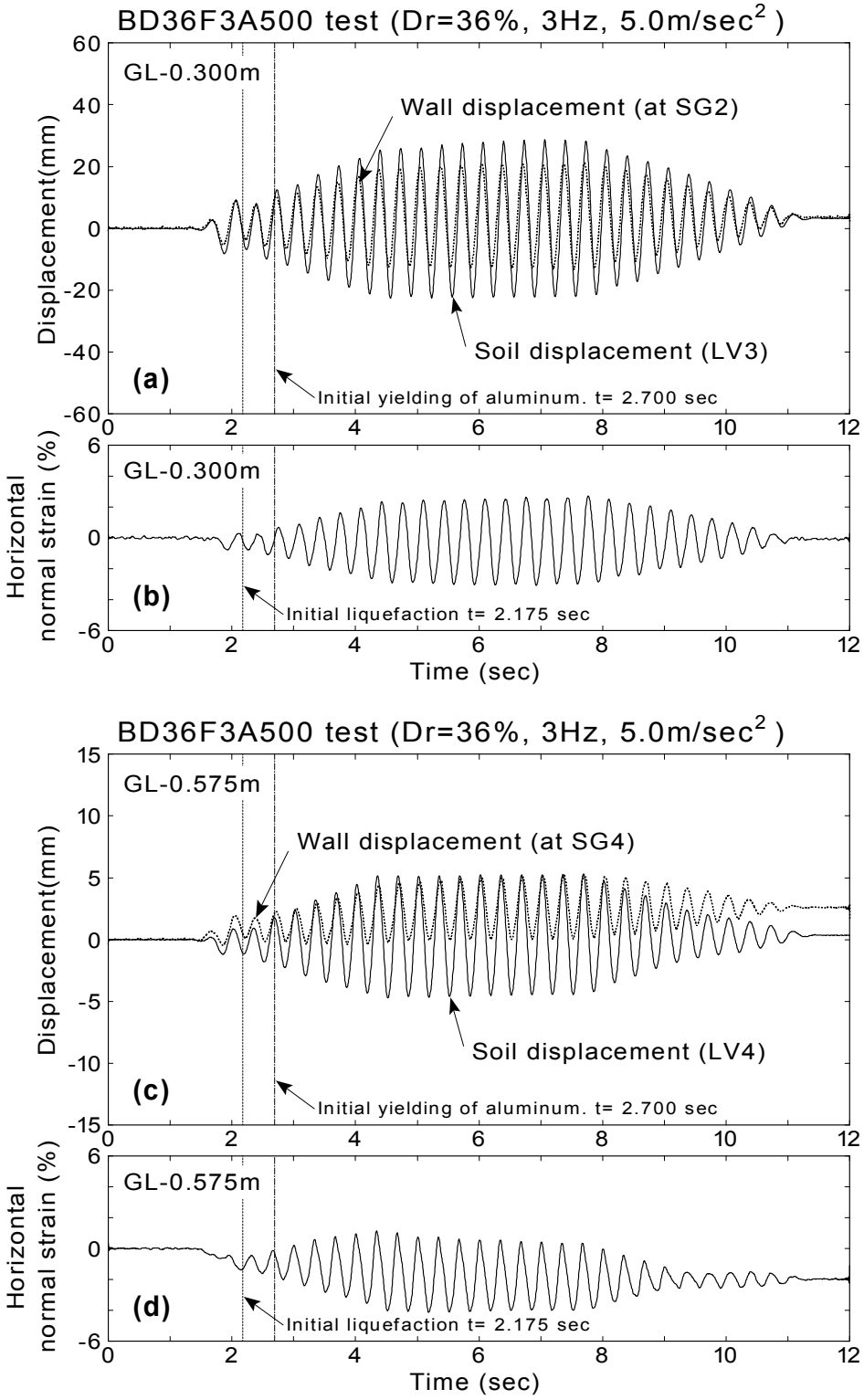

Fig.7.27: Displacement and normal strain of backfill (loose backfill, BD36F3A500 test)

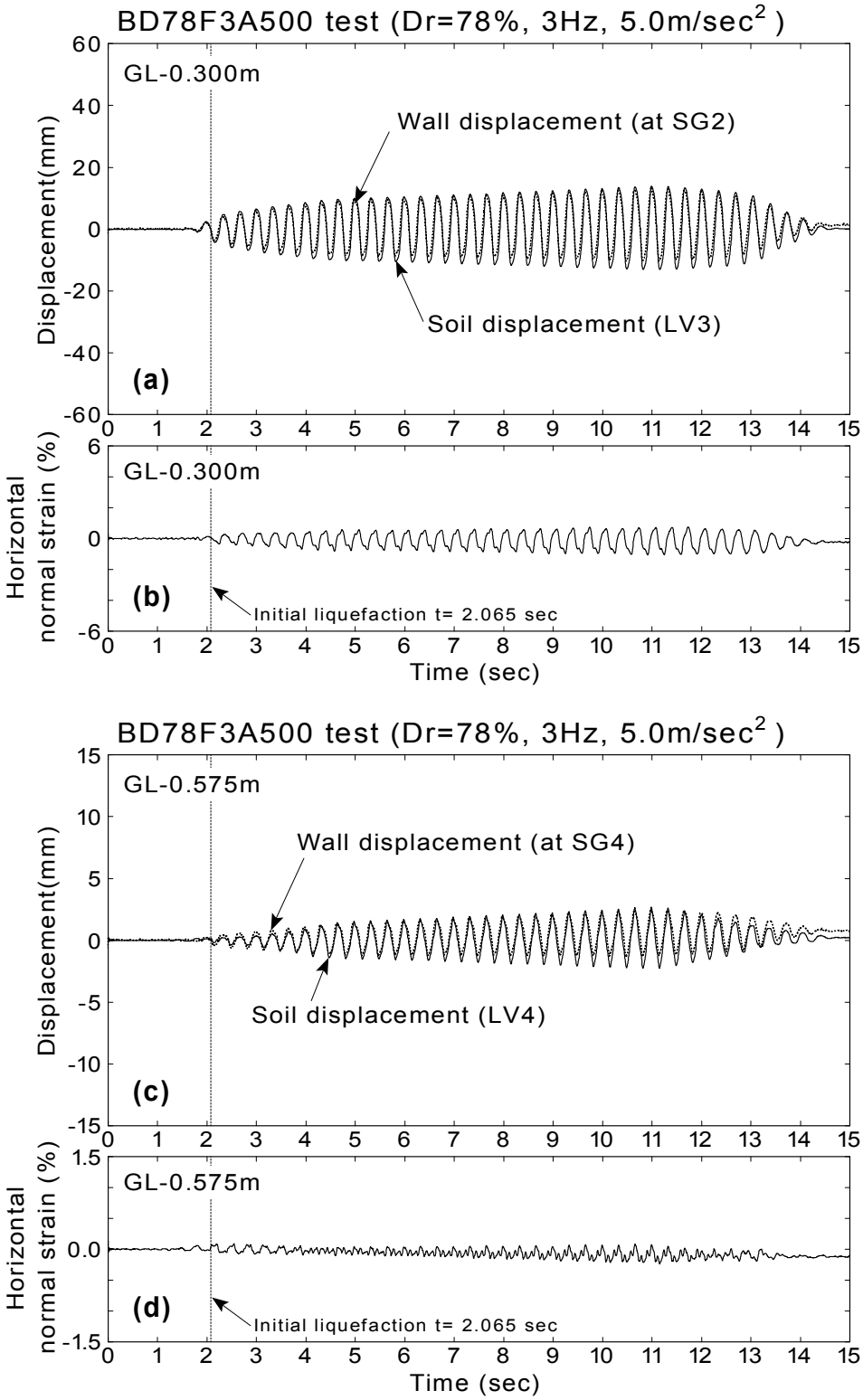

Fig.7.28: Displacement and normal strain of backfill (dense backfill, BD78F3A500 test)

The time histories of the horizontal normal strain from BD78F3A500 test, in which dense backfill is used are depicted in Fig.7.28. It is observed in Fig.7.28(a) that the soil displacement is almost identical to the wall displacement at both depths, producing small level of the horizontal normal strain of less than 1.0%. It is considered that the dense backfill prevent the deformation of soil during the intense shaking.

7.4.3 Wall acceleration

The time histories of acceleration at the wall of the structure from AD32F3A500 are presented in Fig.7.29. The time of the initial liquefaction is indicated in the figure. The acceleration time histories recorded in the backfill with distance of 0.225m from the wall at the same height are drawn by the dotted line for reference. It is seen that the amplitude of wall acceleration is about 5.0m/sec^2, which is as same as that of input motion. The wall acceleration is identical to the soil acceleration before the initial liquefaction at both depths of GL-0.30m and GL-0.575m. It suggests that little relative displacement in the horizontal direction occurs before the initial liquefaction.

Fig.7.30 shows the results from BD36F3A500 test. The amplitude of wall acceleration is seen to be about 5.0m/sec^2, which is the same level as that of input motion. The fluctuations of acceleration with high frequency contents are seen at GL-0.30m between 0.5seconds and 2 seconds. It is observed before the initiation of shaking of 1.0 second so that this fluctuation may be caused by the procedure of numerical integration and differentiation of measured curvatures.

The results from BD78F3A500 test are illustrated in Fig.7.31. The amplitude of acceleration is about 8 m/sec^2 at GL-0.30m, 5 m/sec^2 at GL-0.575m. Since the dilative behavior of soil is observed in this test (see Fig.7.20), spiky response with large amplification of acceleration is seen in the backfill. It was considered that the wall acceleration was affected by the large acceleration of dilative soil.

The time histories of acceleration at the wall of the structure from AD35F3A50, AD39F5A50 and AD41F3A200 tests are presented in Fig.7.42～Fig.7.44 at the end of this chapter.

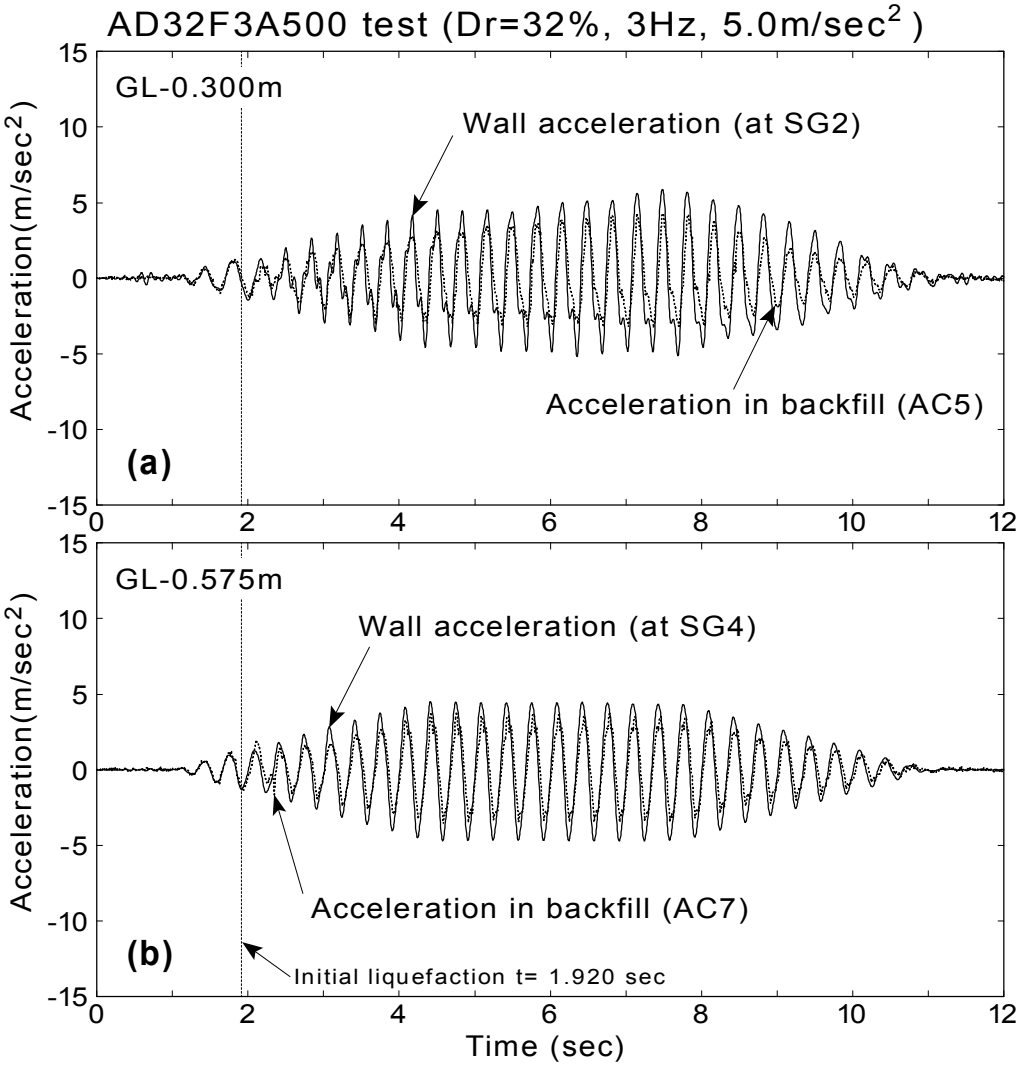

Fig.7.29: Calculated wall acceleration (loose backfill, AD32F3A500 test)

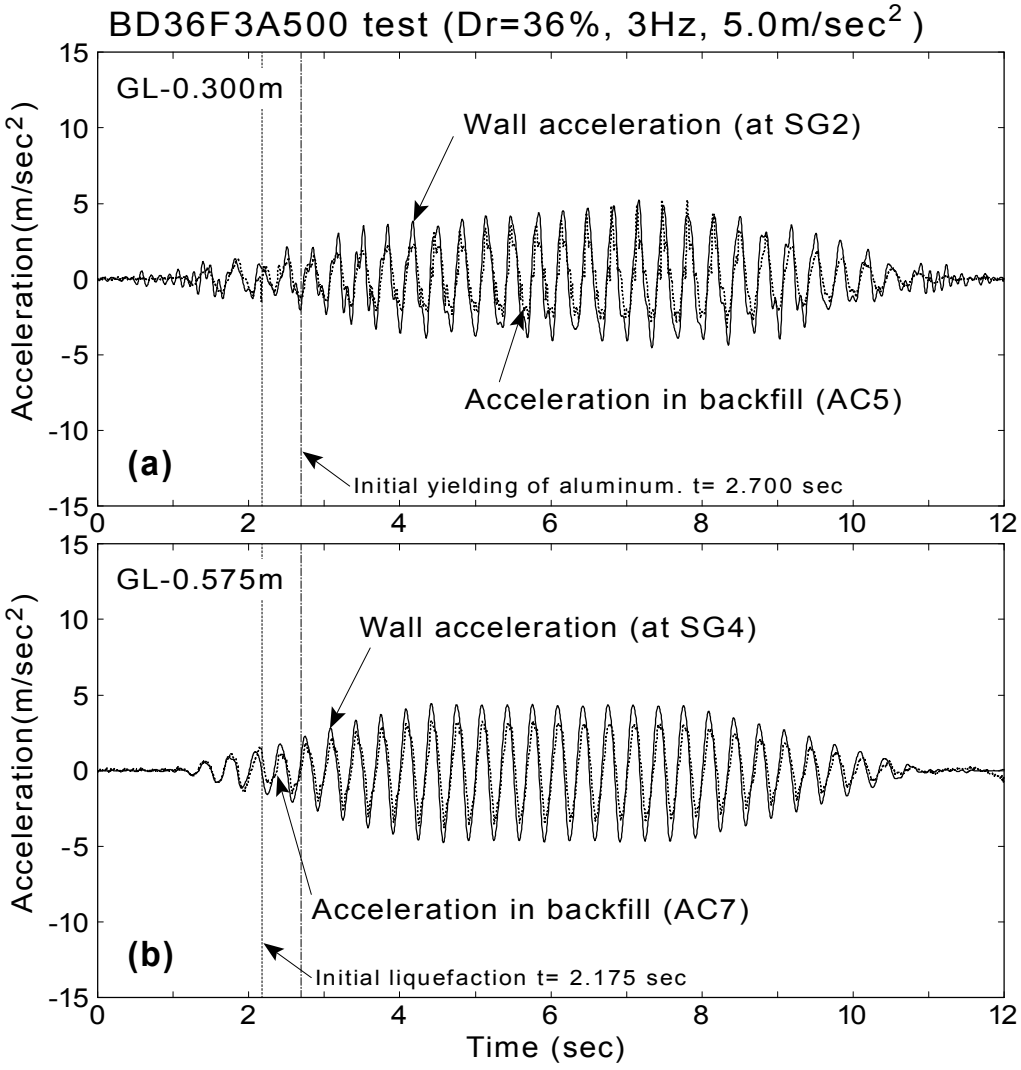

Fig.7.30: Calculated wall acceleration (loose backfill, BD36F3A500 test)

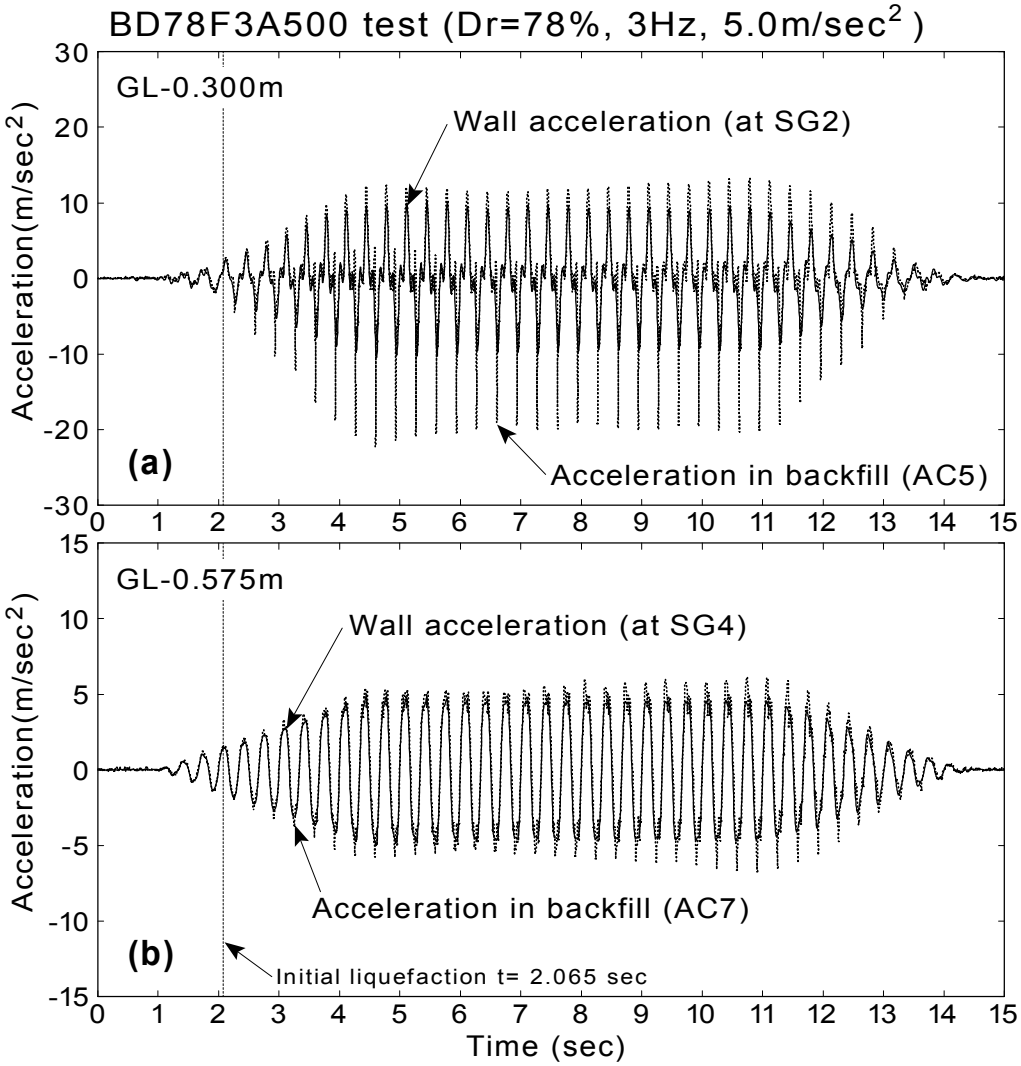

Fig.7.31: Calculated wall acceleration (dense backfill, BD78F3A500 test)

7.4.4 Dynamic earth pressure

Time histories of dynamic earth pressure at GL-0.225m (EP7) and GL-0.513m (EP9) are illustrated in Fig.7.32. These time histories are extracted from time histories of earth pressures presented in Fig.6.88, 6.89 and 6.91 in the previous section. It is seen that the dynamic earth pressures from loose backfill (AD32F3A500 and BD36F3A500 test) fluctuates in a sinusoidal manner, in contrast,

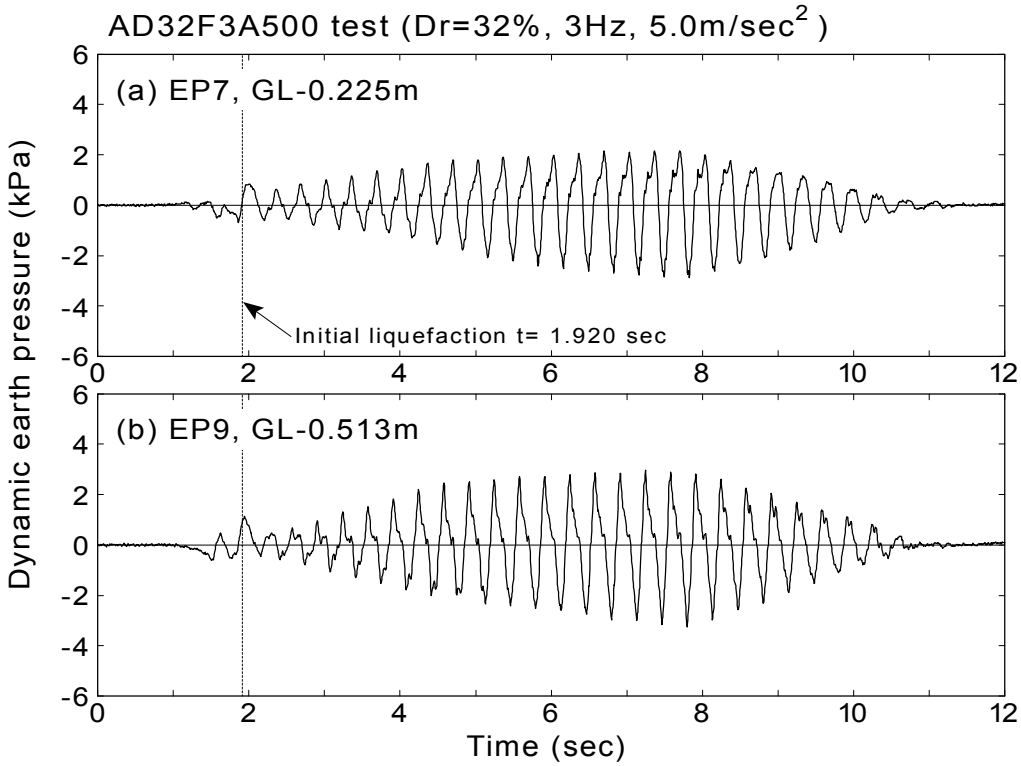

(a) AD32F3A500 test

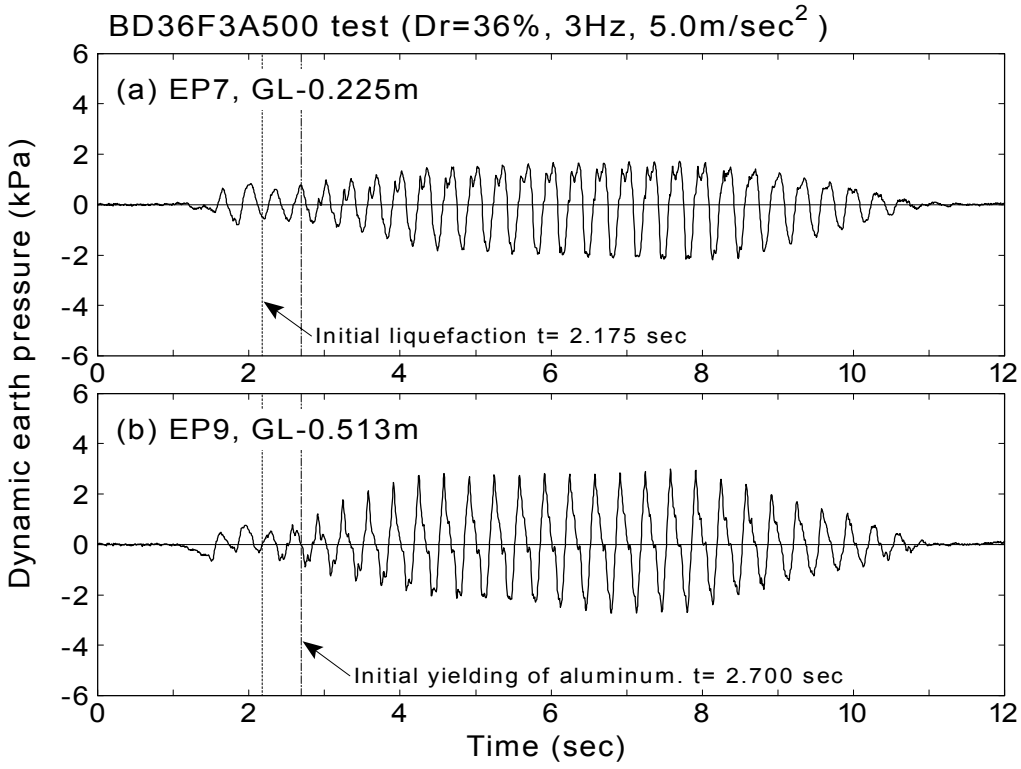

(b) BD36F3A500 test

Fig.7.32: Dynamic earth pressures at GL-0.225m and GL-0.513m

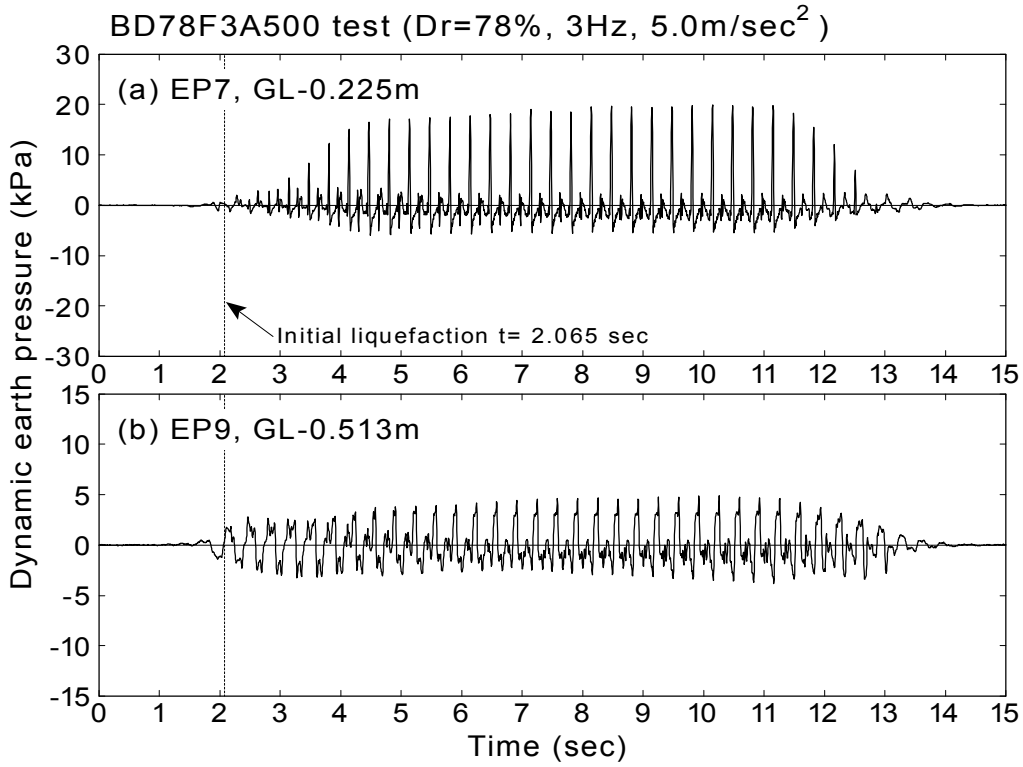

(c) BD78F3A500 test

Fig.7.32: Continued

the fluctuation of earth pressure from dense backfill is very complicated. It is due to a dilative behavior of dense soil (see Fig.7.20).

The time histories of dynamic earth pressures from AD35F3A50, AD39F5A50 and AD41F3A200 tests are illustrated in Fig.7.45(a)～(c) at the end of this chapter.

7.4.5 Experimental relationship between earth pressure and normal strain / acceleration

Time period for analysis

The analysis will be conducted selecting time periods with different state of backfill of i) before liquefaction, ii) just after initial liquefaction and, iii) during completeliquefaction The time periods selected for the analysis are summarized in Table 7.2. Only the analysis of acceleration was made on AD35F3A50, AD39F5A50 and AD41F3A200 tests because of the absence of measurement of displacement at the side of the container.

Table 7.2. Summary of time periods for analysis

Backfill	Test	Before initial liquefaction	During liquefaction or during shaking	
			Just after initial liquefaction	During complete liquefaction
Loose backfill	AD32F3A500	1.5 to 1.920 sec.	1.920 to 2.5 sec.	6.0 to 7.0 sec.
	BD36F3A500	1.5 to 2.175 sec.	2.175 to 2.5 sec	6.0 to 7.0 sec.
	AD35F3A50*	3.0 to 4.0 sec	7.535 to 8.0 sec	8.5 to 9.5 sec
	AD39F5A50*	2.0 to 2.4 sec	4.055 to 4.5 sec	4.5 to 5.0 sec
	AD41F3A200*	1.5 to 2.0 sec	2.770 to 3.5 sec	6.0 to 7.0 sec
Dense backfill	BD78F3A500	1.5 to 2.065 sec.	2.065 to 2.5 sec. (soil behaved in a dilative manner)	6.0 to 7.0 sec. (Same as in the left)

* : Analysis of acceleration only. (No measurement of displacement at the side of container)

Earth pressure and horizontal normal strain

Fig.7.33 illustrates an experimental relationship between the dynamic earth pressure and the horizontal normal strain ε_h at each depth from AD32F3A500 test. The earth pressures at the depth of GL-0.225m and GL-0.513m are corresponding to the horizontal normal strain at the depth of GL-0.3m and GL-0.575m, respectively.

It is seen in Fig.7.33(a) that a level of the normal strain is less than 0.5% before the initial liquefaction (see Fig.7.26(b)(d)), and the clear correlation between the earth pressure and the normal strain is not recognized. It is considered that the wall displacement in a small level could not be detected correctly by a numerical integration of measured curvature, consequently the small level of normal strain is not calculated with enough accuracy. A circular hysteresis loop with rotation of clockwise is observed at GL-0.225m in 1.92～2.5 seconds. It shows a phase difference of a quarter period between the earth pressure and the normal strain. In 6.0～7.0 seconds at the same depth, the normal strain and the earth pressure is much larger than that in 1.92～2.5 seconds. It is because the intensity of input motion in 6.0～7.0 seconds is about twice as much as that in 1.92～2.5 seconds. Positive proportionality is not observed clearly in either time period.

Fig.7.34 shows the results from BD36F3A500 test. Since the tensile strength of material of the structure in this test (86MPa) is smaller than that of the former test (146MPa), the large bending strain due to yielding of material is observed in this test. The hysteresis loop with clockwise is observed. Clear correlation of positive or negative proportionality is not recognized between the normal strain and the dynamic earth pressure.

Fig.7.35 illustrates the results from BD78F3A500 test in which the dense backfill is used. The fluctuation of dynamic earth pressure in a dense backfill is very complicated as illustrated in Fig.7.32(c), on the other hand, the horizontal normal strain of soil fluctuates in a sinusoidal manner as illustrated in Fig.7.28(b). Consequently, the shape of the hysteresis loop became complicated due to dilative behavior of soil.

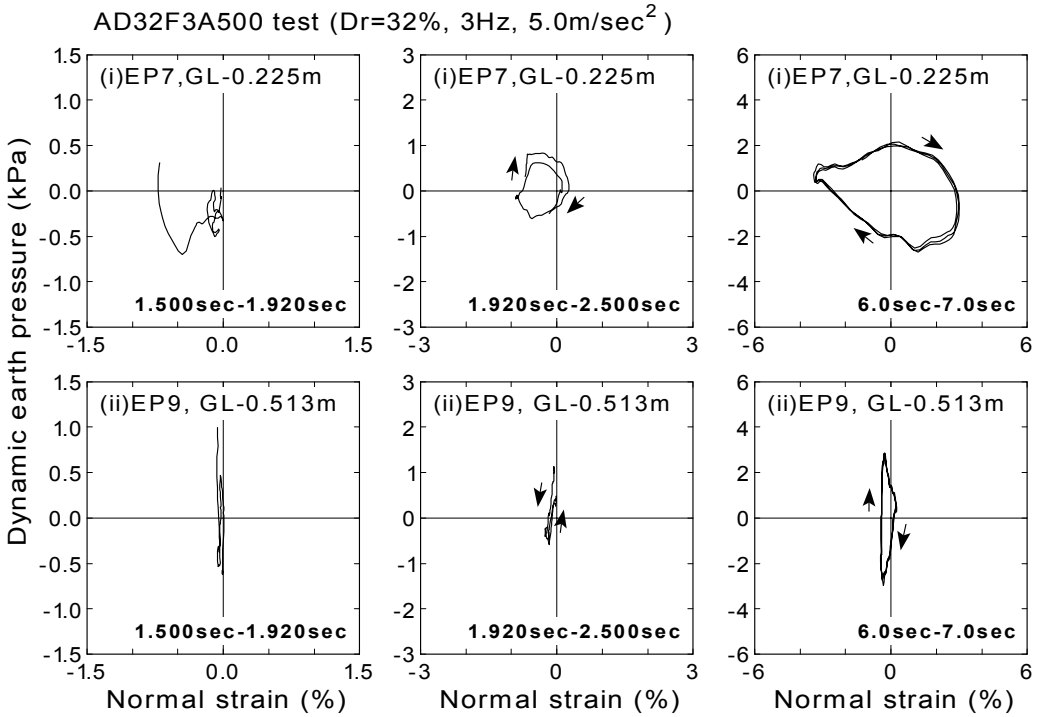

(a) Before initial liquefaction (b) Just after initial liquefaction (c) During liquefaction

Fig.7.33: Dynamic earth pressure and horizontal normal strain (AD32F3A500 test)

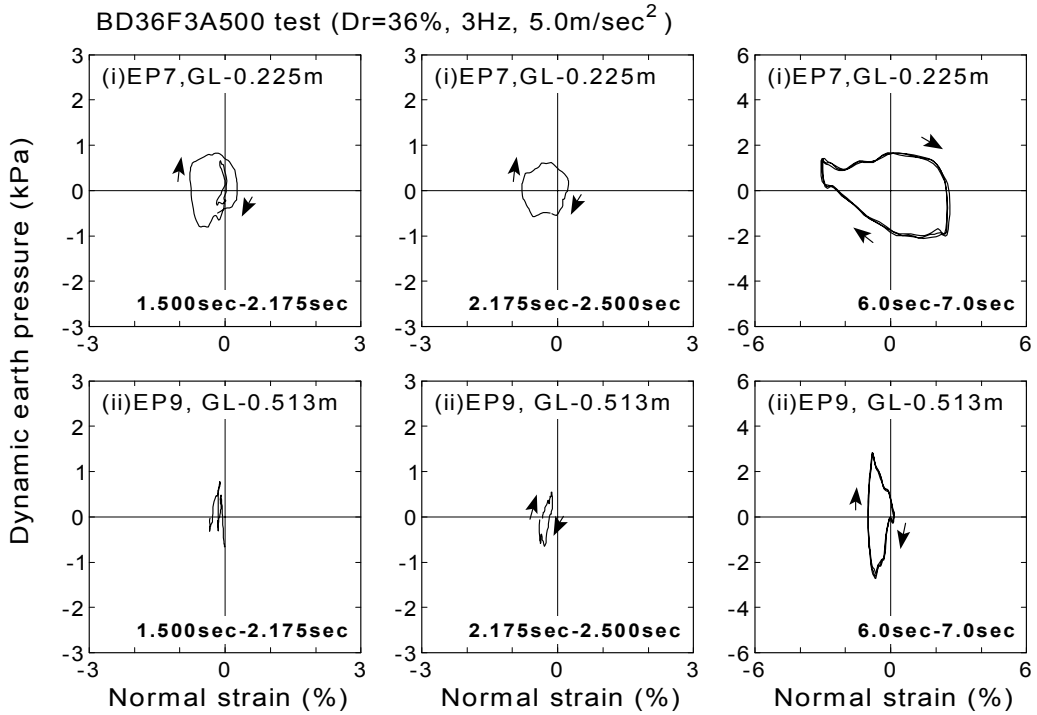

(a) Before initial liquefaction (b) Just after initial liquefaction (c) During liquefaction

Fig.7.34: Dynamic earth pressure and horizontal normal strain (BD36F3A500 test)

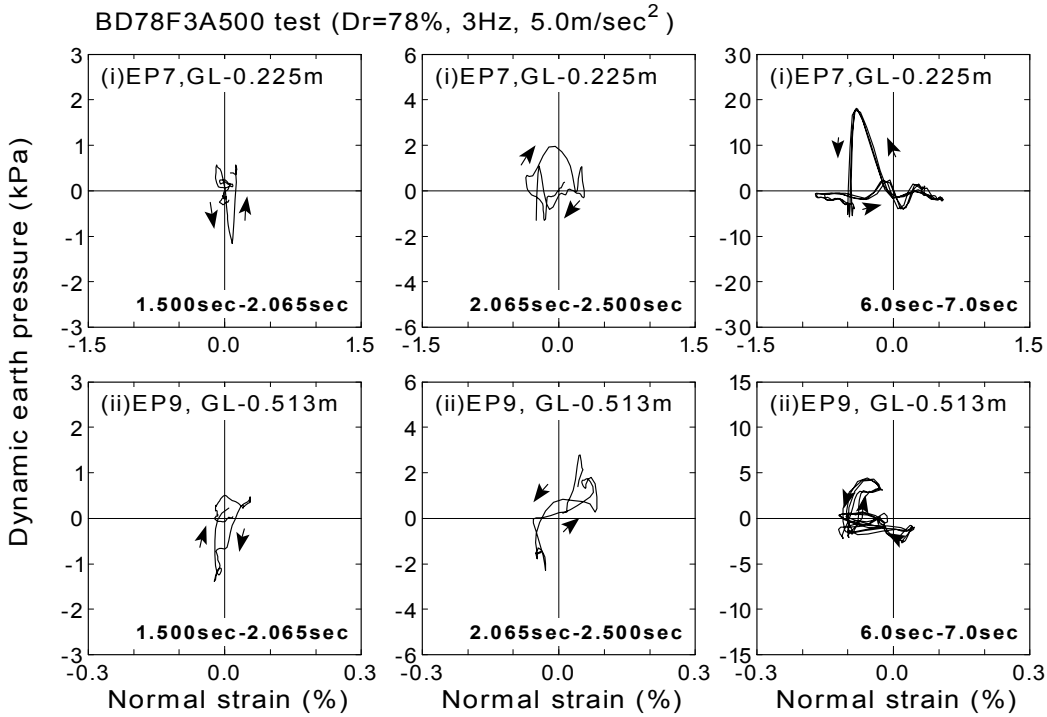

(a) Before initial liquefaction (b) Just after initial liquefaction (c) During liquefaction

Fig.7.35: Dynamic earth pressure and horizontal normal strain (BD78F3A500 test)

Earth pressure and wall acceleration

Experimental relationships between the dynamic earth pressure and the wall acceleration at the corresponding depth from AD32F3A500 test are illustrated in Fig.7.36. In contrast with horizontal normal strain, the correlation of negative proportionality is recognized clearly between the earth pressure and the wall acceleration in every selected time periods.

Since the sign of displacement is inverse with the sign of acceleration in a sinusoidal motion, the positive direction of acceleration is defined in the left direction, being opposite direction with the positive direction of displacement (see Fig.2.6). Therefore, the soil-structure system moves in the right when the acceleration at the wall is negative. The negative correlation is seen in Fig.7.36 between the earth pressure and the wall acceleration, showing that the earth pressure increase when the structure moves in the right direction. This phenomenon agrees with the relationship between the resultant force of dynamic earth pressure and the wall displacement during liquefaction which is observed in Fig.7.5(d).

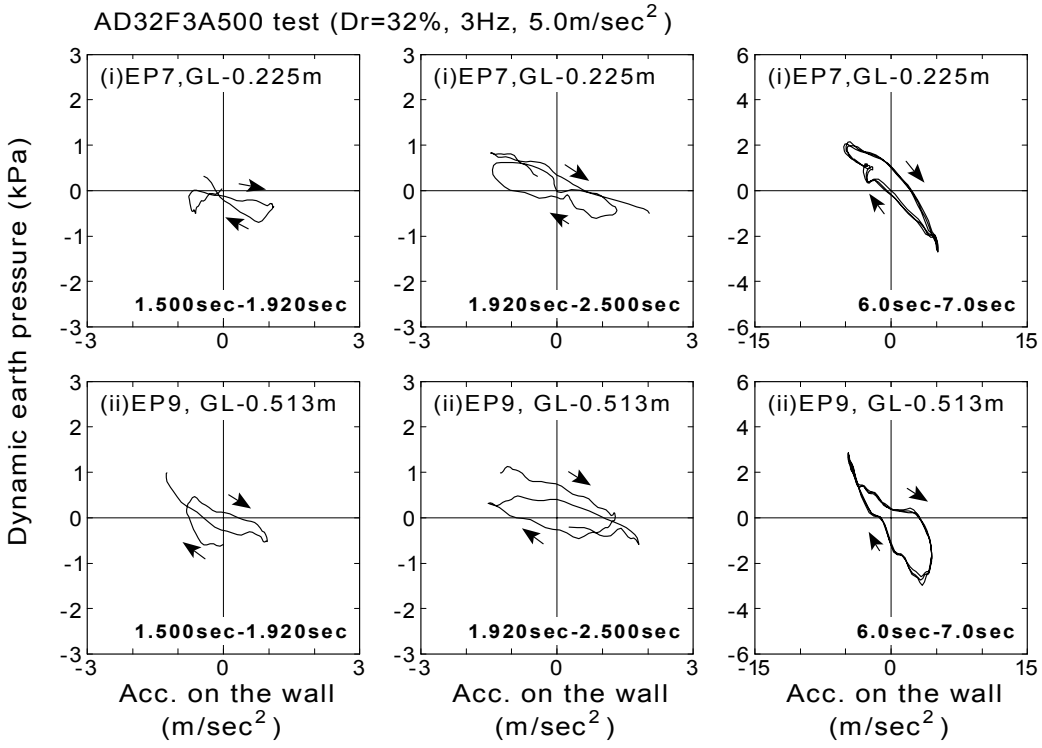

(a) Before liquefaction (b) Just after initial liquefaction (c) During liquefaction

Fig.7.36: Dynamic earth pressure and wall acceleration (AD32F3A500 test)

Fig.7.37 shows the results from BD36F3A500 test. As was observed in previous AD32F3A500 test, the negative correlation is recognized before and after initial liquefaction. Fig.7.38 illustrates the results from BD78F3A500 test. In contrast with tests with loose backfill of AD32F3A500 test and BD36F3A500 test, correlation between them is not clear. It is due to the complicated fluctuation of earth pressure in a dense backfill.

Experimental relationships between the dynamic earth pressure and the wall acceleration at the corresponding depth from AD35F3A50, AD39F5A50 and AD41F3A200 tests are depicted in Fig.7.46～Fig.7.48 at the end of this chapter.

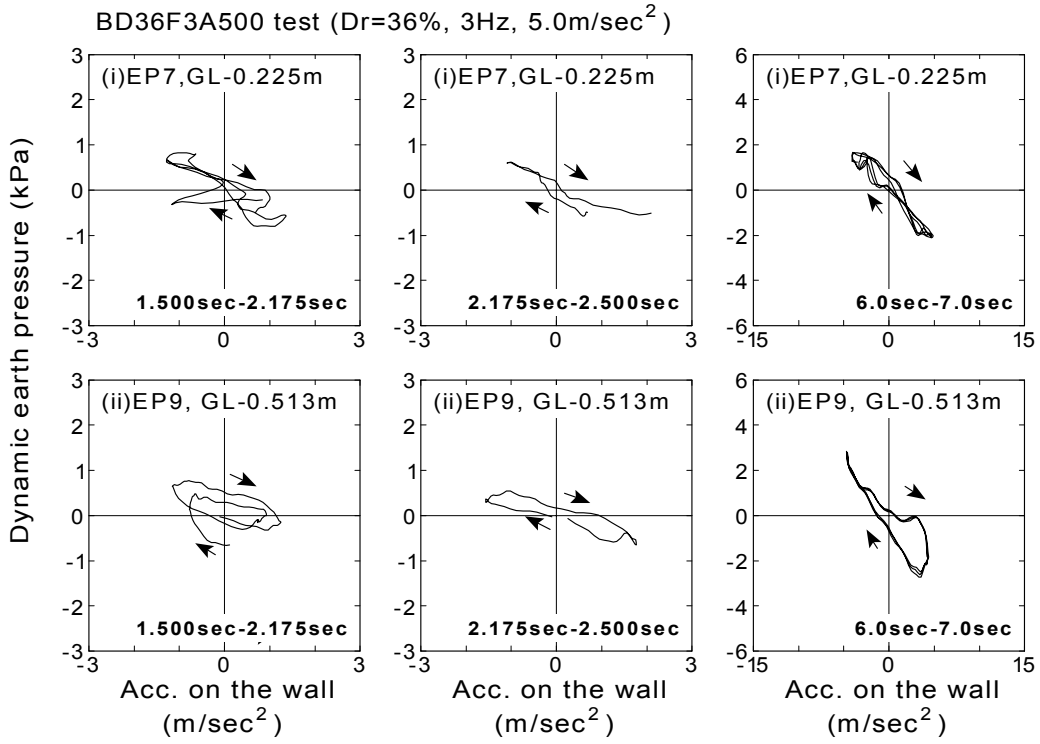

(a) Before liquefaction (b) Just after initial liquefaction (c) During liquefaction

Fig.7.37: Dynamic earth pressure and wall acceleration (BD36F3A500 test)

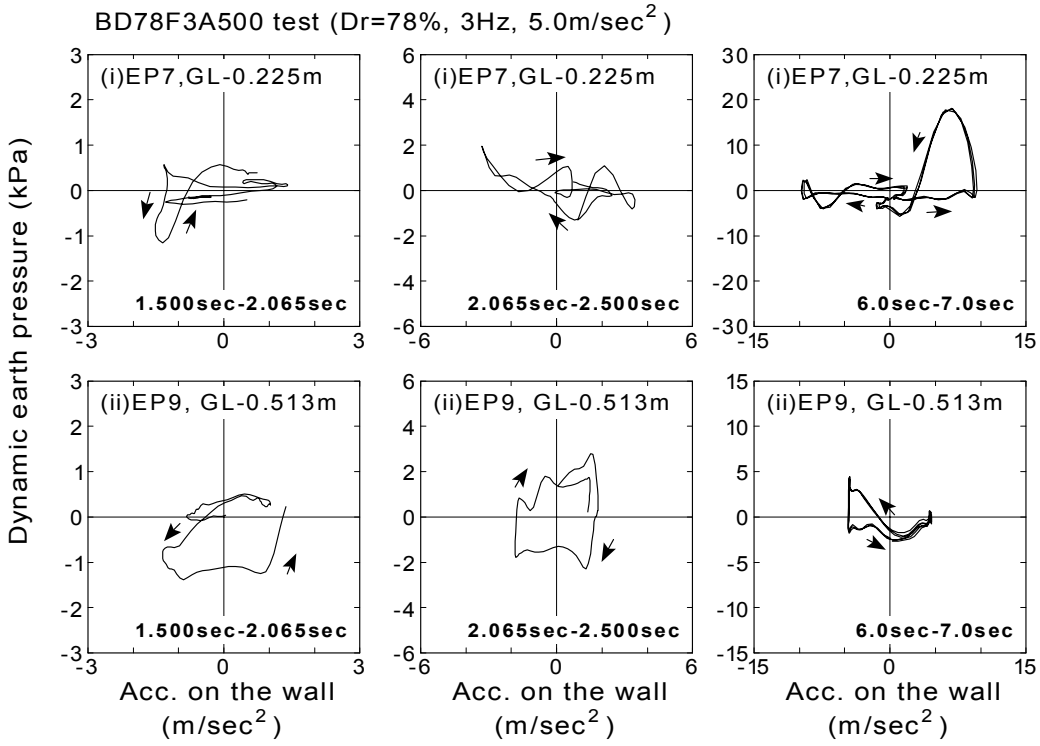

Fig.7.38: Dynamic earth pressure and wall acceleration (BD78F3A500 test)

Correlation between dynamic earth pressure and normal strain / wall acceleration

The coefficients of correlation between the time histories are calculated in each time period of before liquefaction, just after initial liquefaction and during liquefaction. In the horizontal normal strain, some amount of monotonic component is included (see, Fig.7.27(d)). As is seen, the period of monotonic component of the horizontal normal strain is much longer than that of fluctuating component. In this respect, it is considered that the coefficient of correlation is not affected by the monotonic component. The digit numbers of the coefficients are shown in Table 7.3. The shear modulus at each depth of backfill at each time instance is presented in the table referring to the shear modulus change with time derived in Section 4.5.3. Plots of the coefficients with respect to shear modulus of the backfill are presented in Fig.7.39.

Table 7.3. Coefficient of correlation between time histories

Test	Time period	Depth (m)	Shear modulus G (kPa)	Coefficient of correlation	
				Earth pressure and normal strain	Earth pressure and acc. of the wall
AD32F3A500	1.50-1.92sec	0.225 0.513	24 25	0.391 -0.042	-0.284 -0.715
	1.92-2.50sec	0.225 0.513	12 10	-0.093 0.272	-0.846 -0.641
	6.00-7.00sec	0.225 0.513	0 0	-0.398 0.199	-0.957 -0.877
BD36F3A500	1.50-2.175sec	0.225 0.513	22 4	0.007 -0.078	-0.787 -0.523
	2.175-2.50sec	0.225 0.513	3 6	0.142 0.787	-0.798 -0.796
	6.00-7.00sec	0.225 0.513	0 0	-0.464 -0.030	-0.969 -0.917
BD78F3A500	1.50-2.065sec	0.225 0.513	120 380	-0.027 0.515	0.430 0.438
	2.065-2.50sec	0.225 0.513	22 240	0.112 0.844	-0.325 0.374
	6.00-7.00sec	0.225 0.513	43 220	-0.060 -0.172	0.371 -0.387
AD35F3A50	3.00-4.00sec	0.225 0.513	2050 3860	No measurement of displacement at the side of the container	0.946 0.931
	7.535-8.00sec	0.225 0.513	0 0		-0.676 0.451
	8.50-9.50sec	0.225 0.513	20 21		-0.888 -0.072
AD39F5A50	2.00-2.40sec	0.225 0.513	1830 1580		0.936 0.355
	4.055-4.50sec	0.225 0.513	42 0		-0.531 -0.584
	4.50-5.00sec	0.225 0.513	66 0		-0.835 -0.509
AD41F3A200	1.5 to 2.0 sec	0.225 0.513	605 2110		0.912 0.716
	2.77 to 3.5 sec	0.225 0.513	0 4		-0.780 -0.505
	6.0 to 7.0 sec	0.225 0.513	0 0		-0.647 -0.914

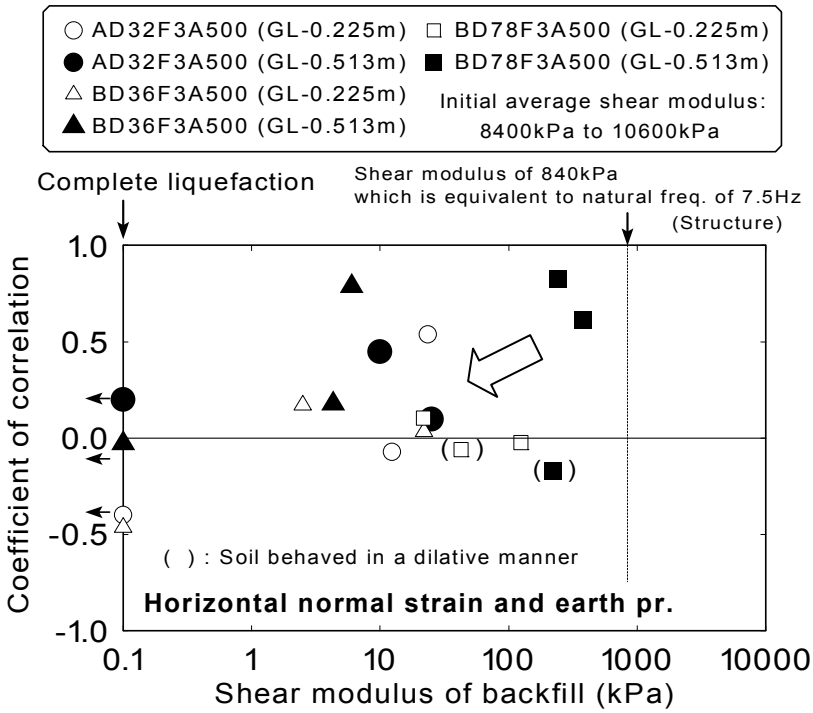

(a) Horizontal normal strain and dynamic earth pressure

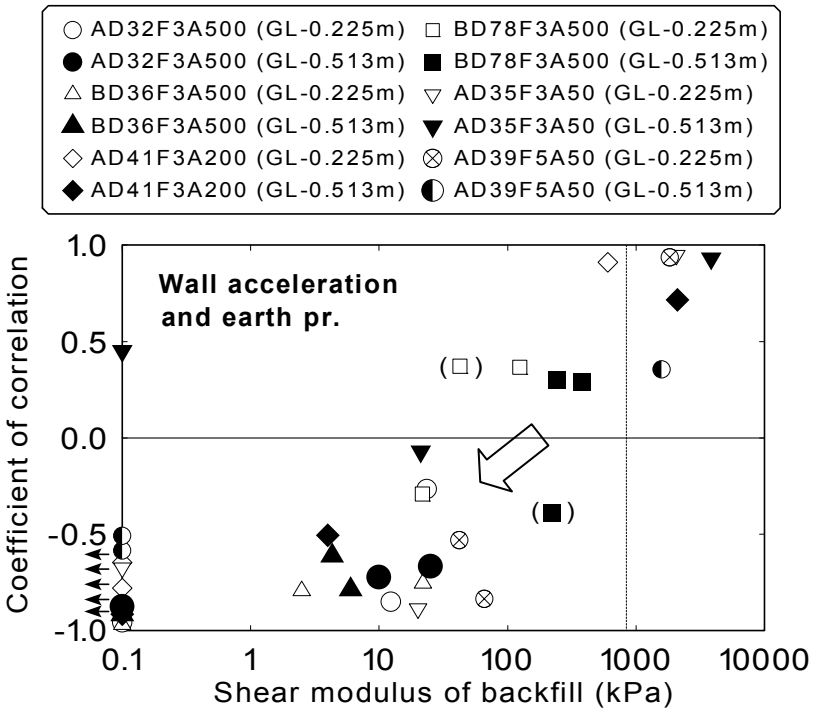

(b) Wall acceleration and dynamic earth pressure

Fig.7.39: Coefficient of correlation between dynamic earth pressure and normal strain/ wall acceleration with respect to shear modulus of backfill

It is seen in Fig.7.39(a) that the coefficient of correlation is in the range of about 0.5～0.8, showing a positive correlation between the dynamic earth pressure and normal strain, when the shear modulus of backfill is relatively large (about more than 100kPa). It suggests that the structure is under the control of deformation before soil becomes soft due to earthquakes. This fact agrees with the past knowledge of dynamic interaction of underground structure in unliquefied ground (e.g. Tateishi, 1992; Penzien et al., 1992, Kawashima, 1994).

In contrast with this, it is observed that the coefficient changes into the range of -0.5～0.5 of less correlation, when the shear modulus decreases toward zero. It means that correlation becomes weak as the soil undergoes liquefaction. It is considered that the change of the phase difference between the structure and soil causes the low correlation between the earth pressure and the normal strain of backfill during liquefaction. For instance, the measured response of acceleration during the time periods at the top of structure (AC2) and the surface of ground (AC3) are shown in Fig.7.40. The phase difference between the accelerations is not significant during 1.5 to 2.5 second around the initial liquefaction. In contrast, the phase difference about 1/5 of the period is seen between them at the period of 6.0 to 7.0 second. It indicates that the liquefied soil with little stiffness does not bring the deformation control of a structure any more.

The coefficients of correlation between the dynamic earth pressure and the wall acceleration are illustrated in Fig.7.39(b) in the same manner. In this experimental relationship, not only the results from 3Hz shaking but also 5Hz shaking are plotted. The shear modulus of backfill of 840kPa, which corresponds to natural frequency of the structure of 7.5Hz, is indicated in the figure.

Focusing on the level of shear modulus about 100kPa, it is observed that the coefficient is in the range of -0.5～0.5, being weak correlations with the acceleration. On the other hand, the coefficient of correlation becomes in the range of -0.5～-1.0 as the shear modulus decreases nearly zero. It means that the correlation between dynamic earth pressure and acceleration is strong when the soil goes into a state of liquefaction. This observation agrees with the previous fact of dynamic interaction between rigid structures and liquefied soil. (Tsuchida, 1968; Iwatate et al., 1982; Koga et al., 1996; Kohama et al., 1998; Ghalandarzadeh et al., 1998). This suggests that a flexible cross section of underground structure is initially under the deformation control, changing into the acceleration control in the process of liquefaction. From the results of this model tests, the flexible structure becomes under the acceleration control when the shear modulus decreases less than about 100kPa. This shear modulus corresponds to 1/100 of the initial value.

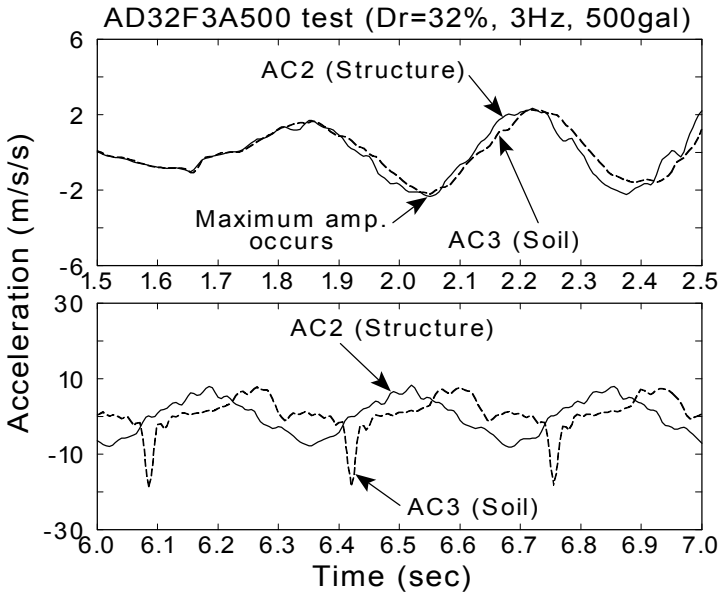

Fig.7.40: Time histories of acceleration at the top of structure (AC2) and the surface of ground (AC3) from AD32F3A500 test

Observing at the large shear modulus of backfill larger than 840kPa in Fig.7.39(b), the coefficient of correlation is near 1.0. It was observed that the action of dynamic earth pressures changes from reaction to load with the relative magnitude between the natural frequency of the backfill and the structure. It is considered that the change of coefficient of correlation from 1.0 to –1.0 causes the change of natural frequency of the backfill comparing with that of the structure.

The results from input motion of 5Hz frequency are plotted in Fig.7.39(b). It is seen that the coefficient of correlation of the test with 5Hz shaking is about –0.5 at the zero shear modulus, being slightly weaker correlation than the test with 3Hz shaking. However, overall differences are not observed between the results of 5Hz shaking and 3Hz shaking. It suggests that the frequency dependence on the correlation between the dynamic earth pressure and the acceleration is small.

It is concluded from above observations that the flexible structure is not under the deformation control when the soil liquefied. Therefore, the modeling of liquefied soil with little shear modulus by springs, which is commonly used for unliquefied soil, is not proper way to evaluate dynamic earth pressures on flexible box sections. Instead of this, the acceleration of the structure or ground near the structure is considered as a key parameter to assess the dynamic earth pressures due to liquefied soft soil.

7.5 BASIC IDEA OF SOIL-STRUCTURE ANALYSIS FOR SEISMIC DESIGN

Based on the observations and studies done previously, dynamic action of backfill on flexible underground structure during liquefaction are summarized as what follows:

1. Earth pressure of fluctuating component (dynamic earth pressure) directly acts on the structure as a dynamic load under the condition that the natural frequency of backfill becomes less than about 0.4 times as that of the structure itself. Usually, a moment at resonance of structure in the process of pore water pressure build-up as well as continuation time period of complete liquefaction correspond the condition.
2. When a deformation of the structure is small and backfill behaves without a dilative behavior, dynamic earth pressure acts from both side of structure, acting in the same direction. The dynamic earth pressure in this state of backfill has a close relation with the acceleration of wall of structure.
3. When a deformation of the structure becomes significantly large exerting large shear strain in the backfill, soil behaves in a dilative manner, especially in dense backfill. In this state, a supporting mechanism due to backfill appears at one side of structure.
4. Initial earth pressure and earth pressure of monotonic component acts on the structure as a monotonic load during seismic excitation. An increase of earth pressure of monotonic component becomes an indirect effect due to excess pore pressure generation by shaking.

According to these features of dynamic interaction, basic idea of model for soil-structure analysis can be considered as illustrates in Fig.7.41. Two patterns of simplified model are taken into consideration for such states as i) small deformation of structure without dilative behavior of backfill (Fig.7.41(a)), ii) large deformation of structure with dilative behavior of backfill (Fig.7.41(b)). First of all, the initial and monotonic earth pressures due to generation of excess pore water pressure are commonly introduced in both models. The monotonic component of earth pressure can be calculated by using Eq.(1.2) which is previously proposed by Koga et al.,(1996). The dynamic earth pressure which is related to acceleration of wall is considered in the model on both side in Fig.7.41(a). In contrast with this, a supporting mechanism is introduced at right wall instead of dynamic earth pressure as shown in Fig.7.41(b).

Since the model of structure and seismic loads are symmetric during liquefaction, it is possible to calculate the deformation of structure in a simple manner as presented in Chapter 6. Hence, it is important to evaluate magnitude of dynamic earth pressure at each depth from acceleration of structure in this model. On the other hand, the model with supporting mechanism is asymmetric with multi supports through the depth. It is difficult to verify the validity of model quantitatively using the test results in which earth pressures are measured only in one side of structure model.

Further study on dynamic earth pressure will be made focusing on the former model (Fig.7.41(a)) in the following chapter.

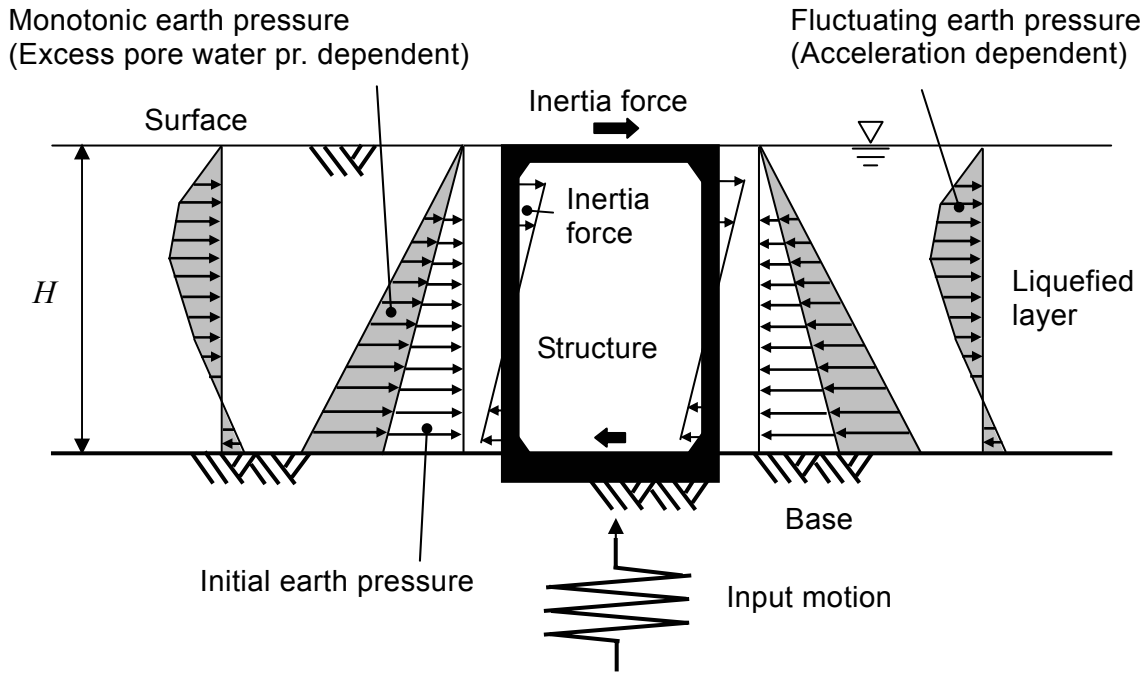

(a) Small deformation of a structure

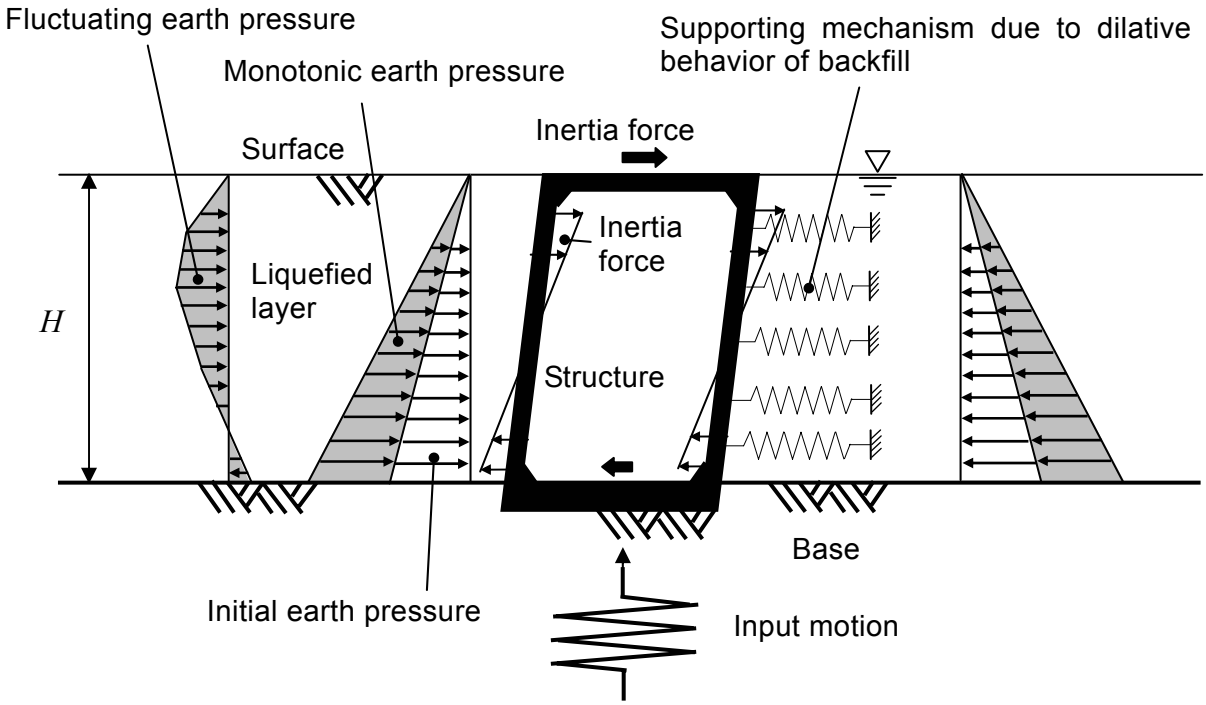

(b) Significant deformation of a structure (backfill behaves in a dilative manner)

Fig.7.41: Basic idea of soil-structure analysis for design calculation

7.6 CONCLUDING REMARKS

Dynamic effect of lateral earth pressures on flexible cross section was precisely analyzed focusing on the material change of backfill due to liquefaction. The observations were made of the effect of dilatancy of soil and influential parameter on dynamic earth pressures to find the characteristic interactive behavior of structure as well. The followings are conclusions drawn from the study in this chapter:

1. The dynamic earth pressure does not act as the load on the structure until the natural period of ground near the structure becomes longer than that of the structure itself. Since soil liquefaction results in the drastic loss of shear strength, it is possible that the dynamic earth pressure acts as a load on the underground structure during the process of pore water pressure build-up.
2. When the effective stress is increased by the dilative nature of soil under the large shear strain, the dynamic earth pressures act as not only the load but also the reaction of the structure. This situation occurs after the pore pressure ratio once reached 1.0 by seismic excitations. It suggests that a dense backfill could prevent the large shear deformation or shear type collapse of a cross section of underground structure.
3. The relation between dynamic earth pressures and accelerations on flexible wall becomes stronger than that between dynamic earth pressures and normal strain of the backfill when the shear modulus of loose backfill decreases about less than 100kPa (1/100 of the initial value). This shows that the flexible underground structure is under the control of acceleration when the backfill liquefies.

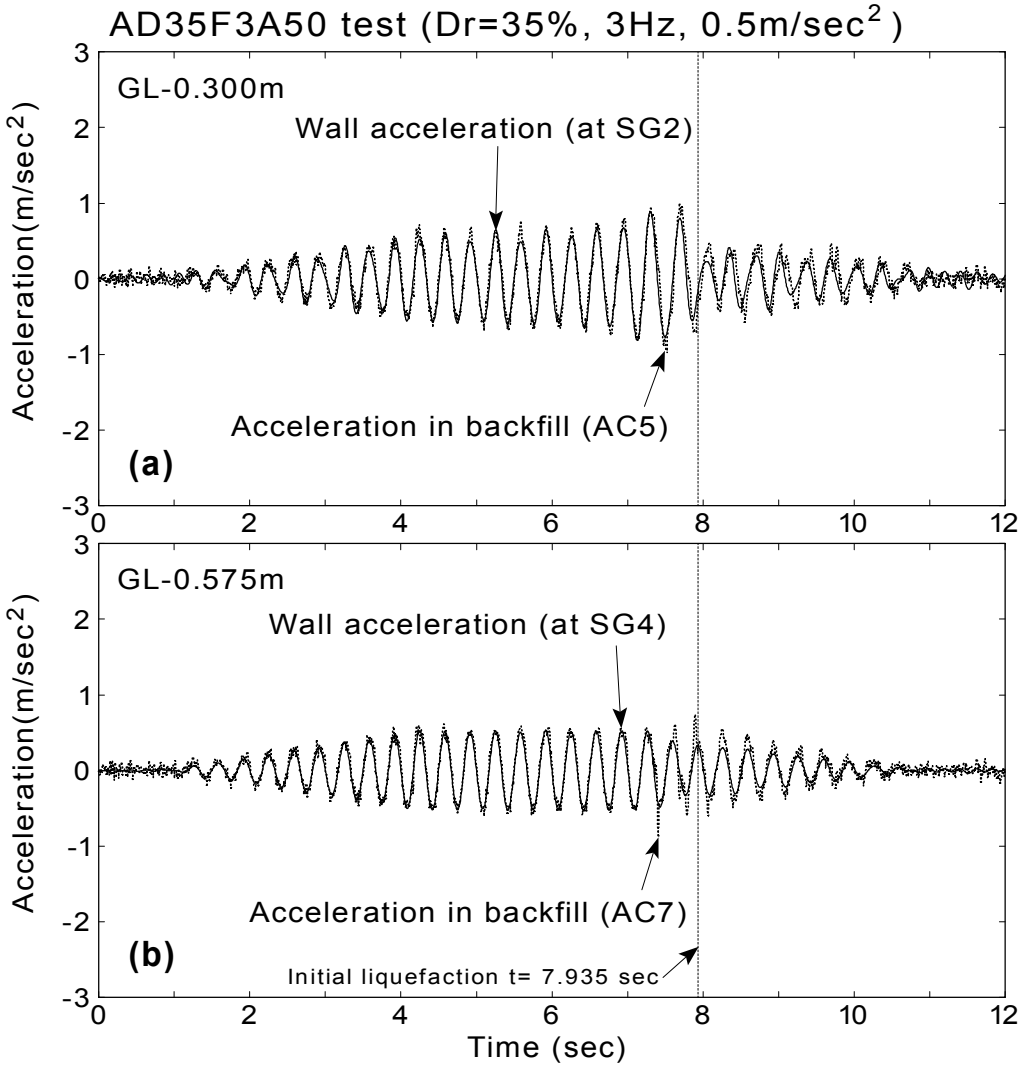

Fig.7.42: Calculated wall acceleration (loose backfill, AD35F3A50 test)

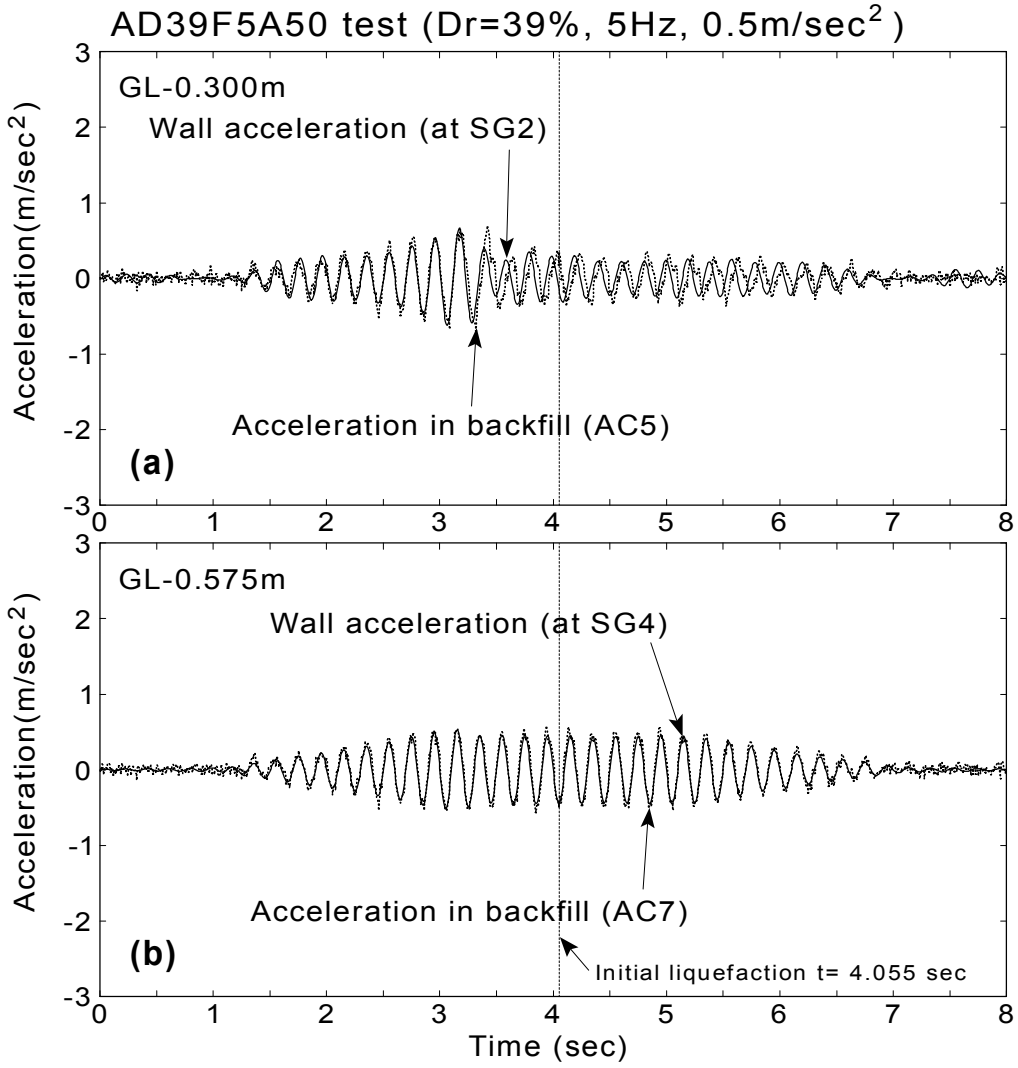

Fig.7.43: Calculated wall acceleration (loose backfill, AD39F5A50 test)

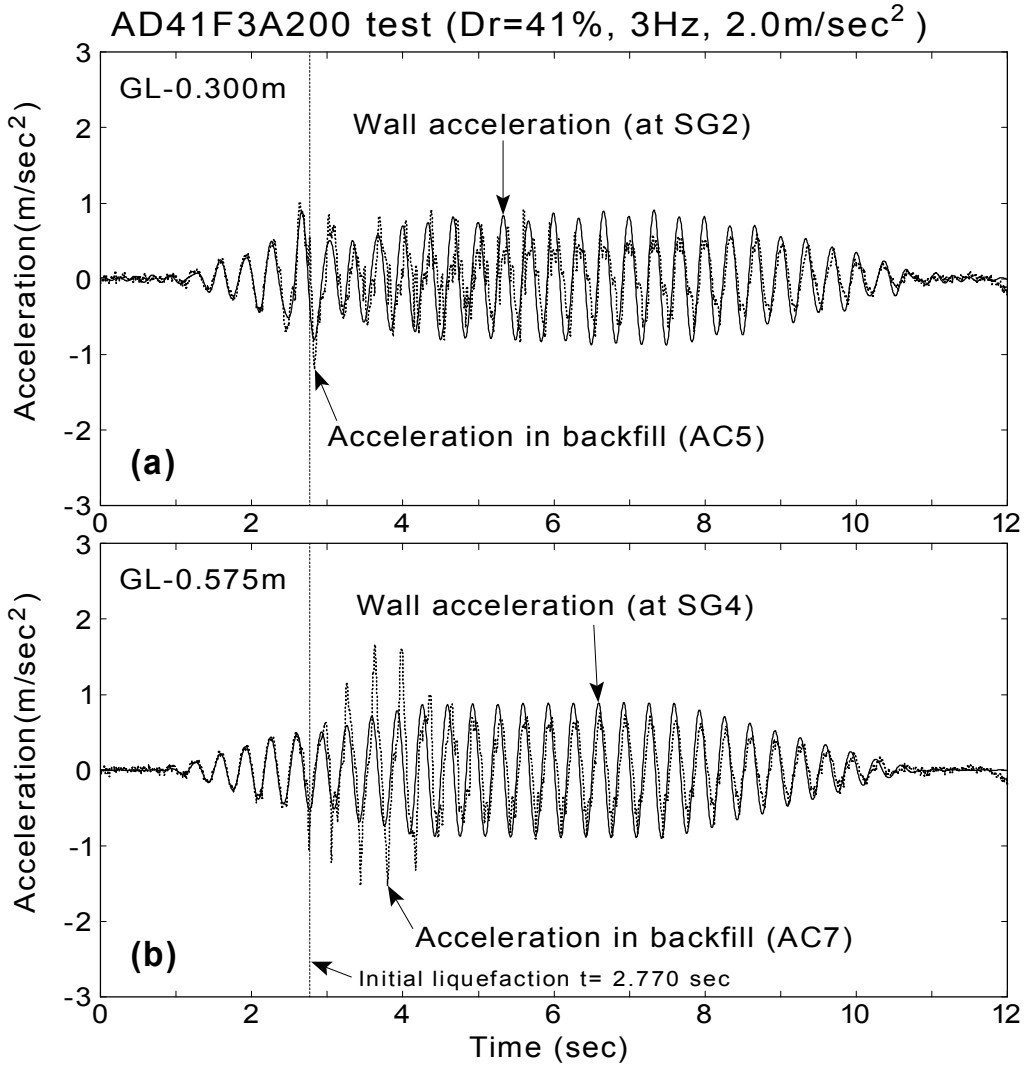

Fig.7.44: Calculated wall acceleration (loose backfill, AD41F3A200 test)

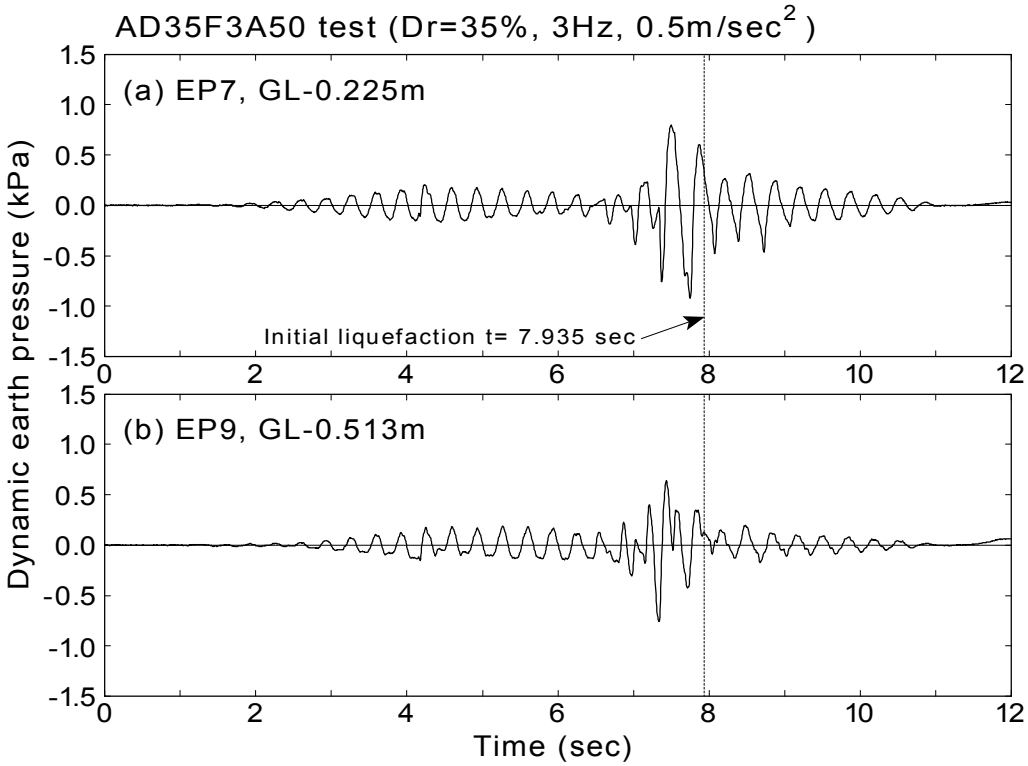

(a) AD35F3A50 test

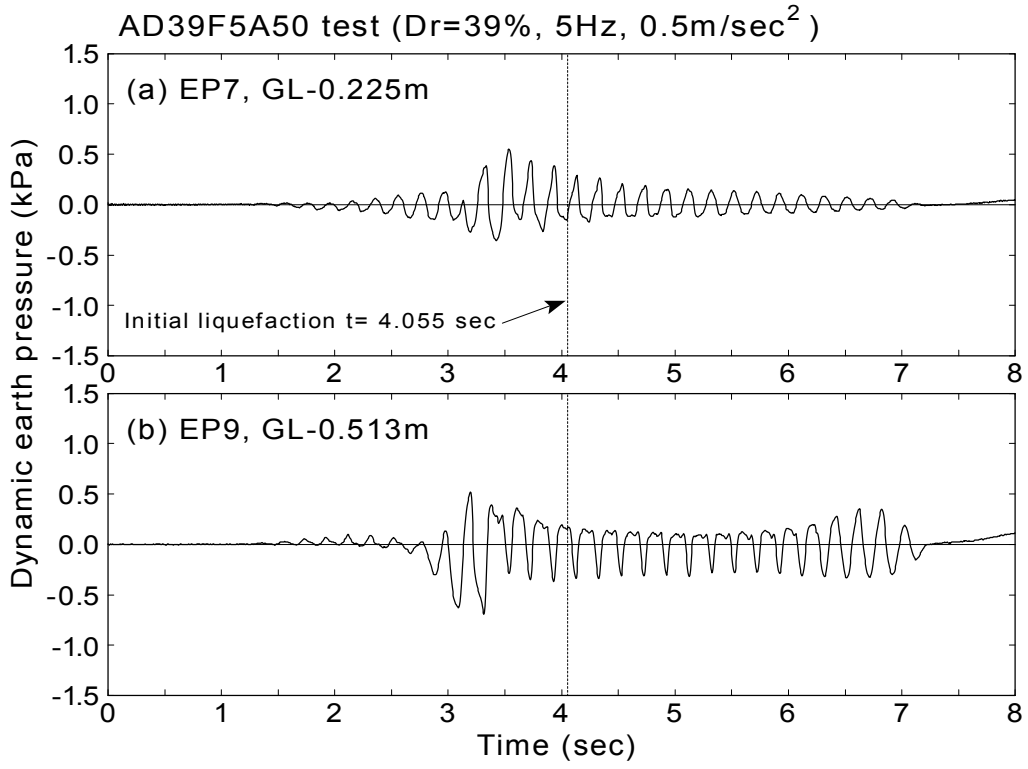

(b) AD39F5A50 test

Fig.7.45: Dynamic earth pressures at GL-0.225m and GL-0.513m

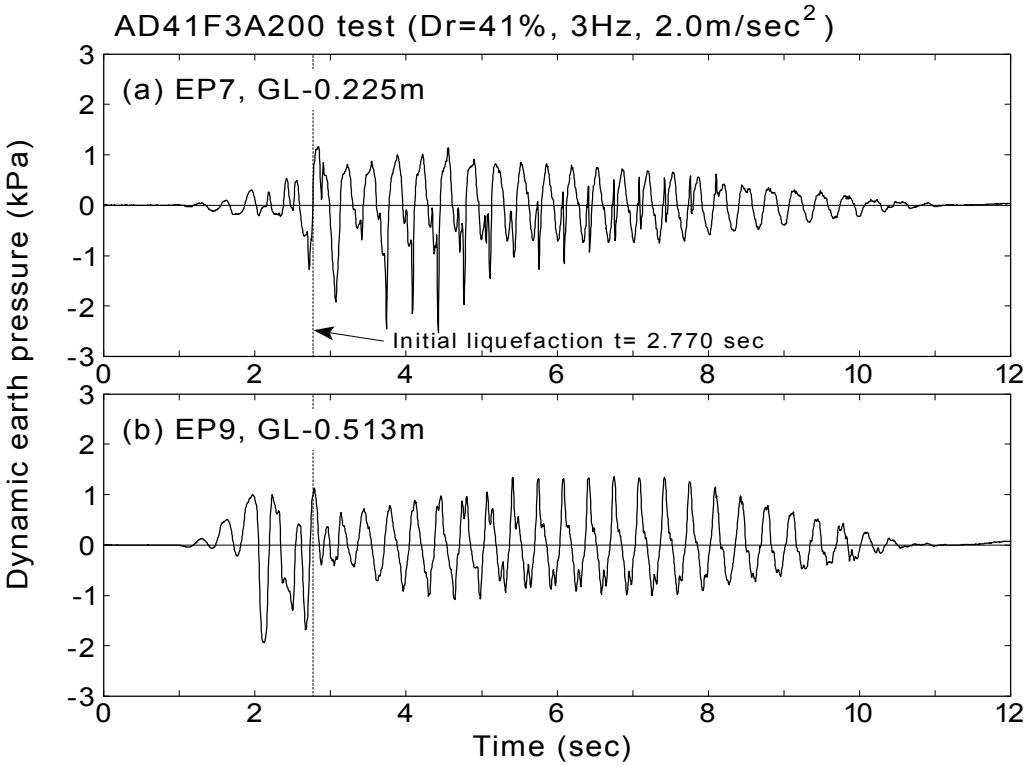

(c) AD41F3A200 test

Fig.7.45: Continued

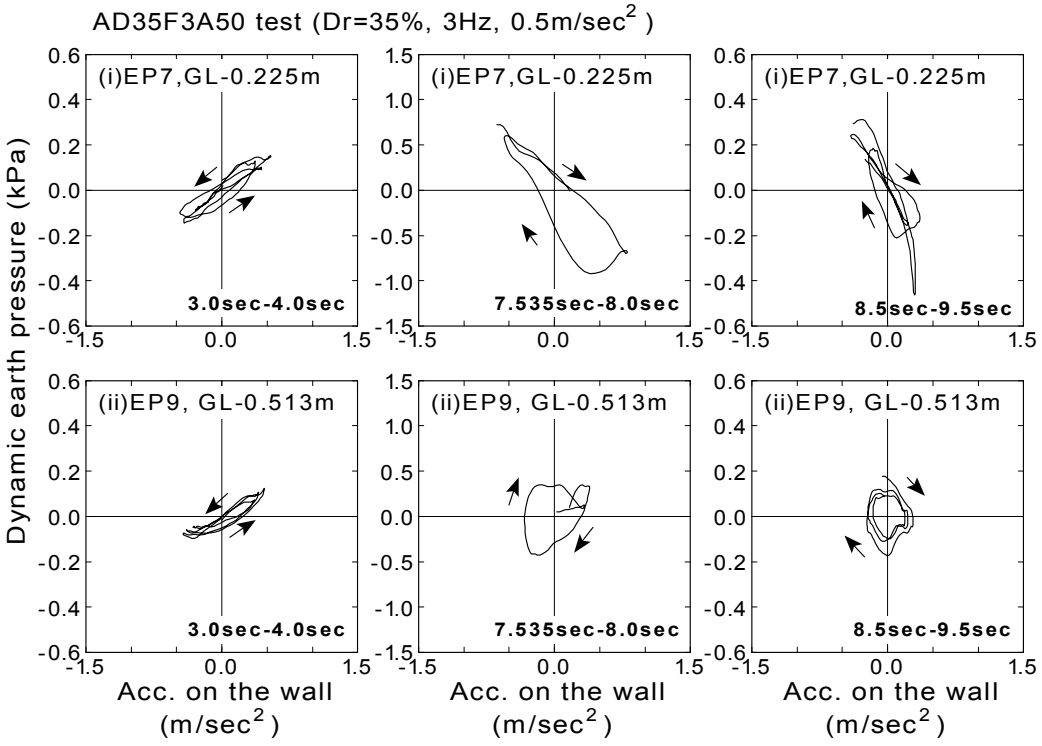

(a) Before liquefaction (b) Just after initial liquefaction (c) During liquefaction

Fig.7.46: Dynamic earth pressure and wall acceleration (AD35F3A50 test)

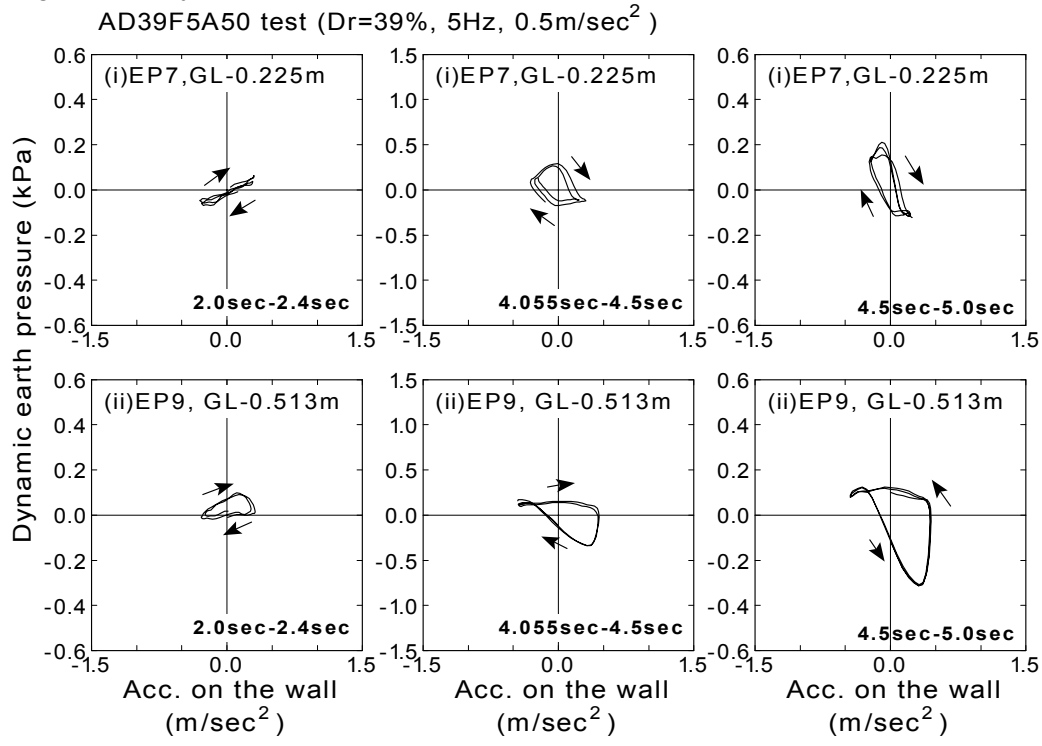

(a) Before liquefaction (b) Just after initial liquefaction (c) During liquefaction

Fig.7.47: Dynamic earth pressure and wall acceleration (AD39F5A50 test)

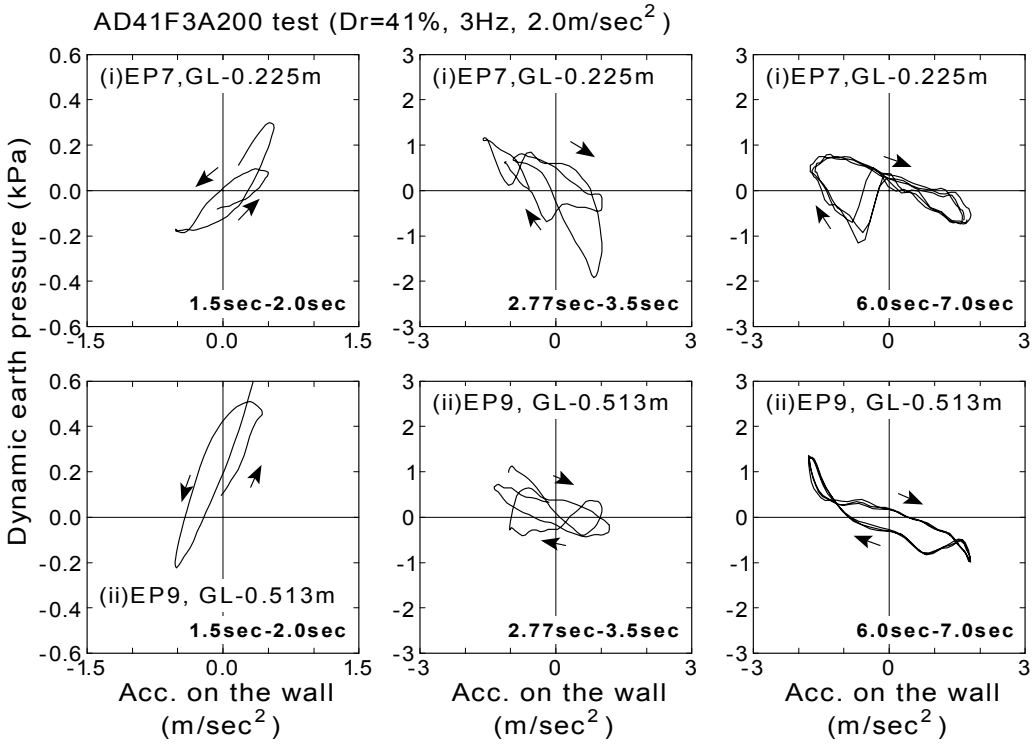

(a) Before liquefaction (b) Just after initial liquefaction (c) During liquefaction

Fig.7.48: Dynamic earth pressure and wall acceleration (AD41F3A200 test)

Chapter 8

THEORY OF DYNAMIC LATERAL PRESSURES ON FLEXIBLE WALL

8.1 GENERAL REMARKS

A theory of the dynamic lateral pressure on the flexible wall of underground structure caused by liquefied soil is going to be developed. Acceleration of the structure is selected as the major input parameter for the theory since the correlation between the dynamic earth pressure and the acceleration was found to be good in the previous study. A comparison will be made between measured and calculated dynamic pressures for several test results in order to show that the proposed theory of dynamic pressure on a flexible wall gives good results.

8.2 THEORY OF DYNAMIC EARTH PRESSURES

8.2.1 Model description

Consider a wall-soil model consisting of a semi-infinite, uniform layer of liquefiable soil of height *H*, that is free at its surface, underlain by a base unliquefied layer, and retained along one of its vertical boundaries by a flexible wall of a structure. Neither translation nor rotation was allowed at the bottom end of the flexible wall, while no rotation at its top end. The base of liquefied layer was assumed to be excited by a seismic motion. The acceleration at the base and the top of the structure at any time *t* is designated by $\ddot{x}_g(t)$ and $\ddot{x}_t(t)$, respectively. A cross section of this model along the (*x*,*y*) plane is shown in Fig.8.1. The figure also illustrates the positive directions of the horizontal and vertical displacements which are denoted by ξ and η.

In case that a harmonic excitation with angular frequency of ω is assumed for the base and the response acceleration at the top, the accelerations are expressed as,

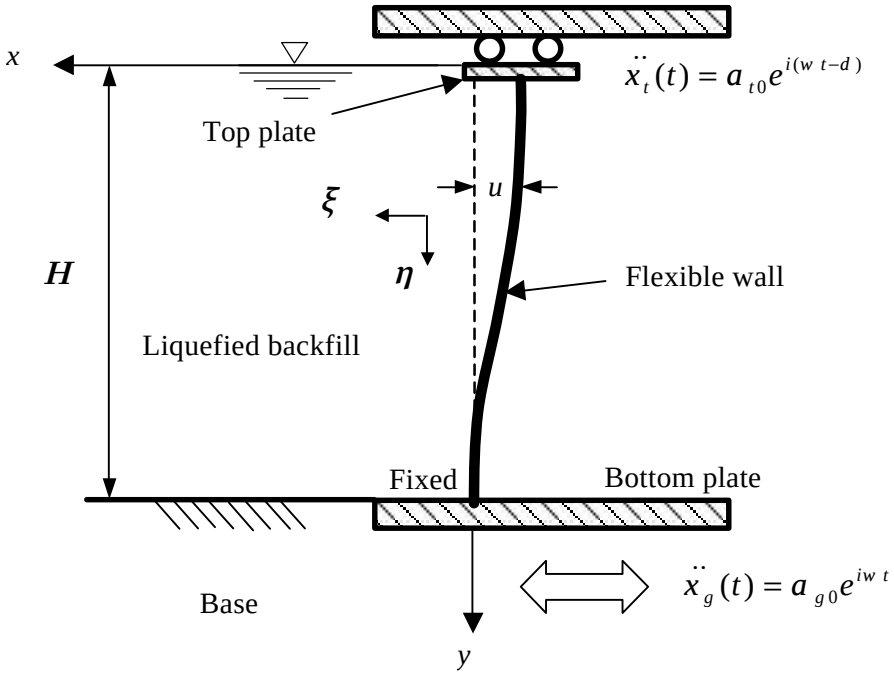

Fig.8.1 Model of structure and liquefied ground used for study

$$\ddot{x}_g(t) = a_{g0}e^{iwt} \tag{8.1}$$

$$\ddot{x}_t(t) = a_{t0}e^{i(wt-d)} \tag{8.2}$$

where, α_{g0} is the amplitude of acceleration at the bottom of structure, α_{t0} is the amplitude of acceleration at the top of structure, δ is the phase difference between the top and the bottom of structure. The value of the maximum amplification ratio, $\alpha_{t0} / \alpha_{g0}$, and the phase difference, δ, are experimentally shown from the results of shaking table tests as summarized in Table 8.1.

Table 8.1: Amplification and phase difference based on series of shaking table tests

	At the resonance	At complete liquefaction	Remarks
Maximum amplification ratio, $\alpha_{t0} / \alpha_{g0}$	2.5 to 3	1 to 1.5	See Table 5.4 and Fig.5.15.
Phase difference, δ	90 deg.	150 deg.	

The horizontal dynamic displacement of a flexible wall (x=0) is modeled by a deflection of beam with an embedded end in a vertical cross section. The deflection u is expressed as,

$$u = \left(\xi_t - \xi_g\right)\left(1-\frac{y}{H}\right)^2\left(3-2\left(1-\frac{y}{H}\right)\right) \tag{8.3}$$

where ξ_t and ξ_g are the horizontal displacements at the top and the bottom of the flexible wall, respectively. The value of ξ_t depends on the amplification of acceleration between the top and the bottom of the structure. Fig.8.2 illustrates the measured deflections of wall shaken by 5.0m/sec^2 of excitation. The deflections approximated by Eq.(8.3) are also shown in the figures. The good agreement implies that the approximation by Eq.(8.3) is satisfactory.

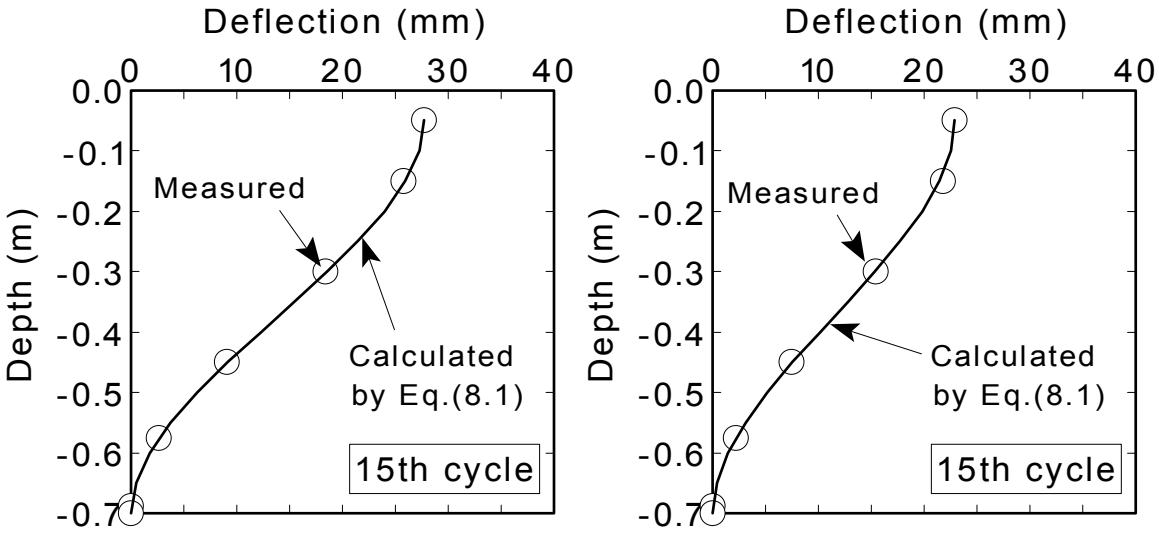

(a) AD32F3A500 test (Structure-A) (b) BD36F3A500 test (Structure-B)

Fig.8.2: Deflections of flexible wall

8.2.2 Mathematical formulation

The motion of liquefiable soil is governed by the following partial differential equations which are varid for sound propagation in liquid assuming no shear stresses in the soil (Westergaard, 1933),

$$\frac{\partial p}{\partial x} = \rho \frac{\partial^2 \xi}{\partial t^2} \tag{8.4}$$

$$\frac{\partial p}{\partial y} = \rho \frac{\partial^2 \eta}{\partial t^2} \tag{8.5}$$

$$p = K\left(\frac{\partial \xi}{\partial x} + \frac{\partial \eta}{\partial y}\right) \tag{8.6}$$

where, ρ : mass density of liquefiable soil

p : dynamic pressure (compression as negative)

K : bulk modulus of liquefied soil

The Eq.(8.4)(8.5) and (8.6) are subject to the boundary conditions:

$$p = 0 \quad at \quad y = 0 \quad (surface) \tag{8.7}$$

$$\eta = 0 \quad at \quad y = H \quad (bottom) \tag{8.8}$$

$$p = 0 \quad at \quad x = \infty \tag{8.9}$$

$$\xi_g(t) = -\frac{1}{\omega^2}\alpha_{g0}e^{i\omega t} = \xi_{g0}e^{i\omega t} \quad at\ the\ wall\ \ x = 0\ and\ \ y = H \tag{8.10}$$

$$\xi_t(t) = -\frac{1}{\omega^2}\alpha_{t0}e^{i(\omega t-\delta)} = \xi_{t0}e^{i(\omega t-\delta)} \quad at\ the\ wall\ \ x = 0\ and\ \ y = 0 \tag{8.11}$$

$$\xi(y,t) = \left(\xi_t(t) - \xi_g(t)\right)\left(1-\frac{y}{H}\right)^2\left(3-2\left(1-\frac{y}{H}\right)\right) + \xi_g(t) \quad at\ the\ wall\ x = 0 \tag{8.12}$$

where, ξ_{g0} is the amplitude of displacement at the bottom of structure, ξ_{t0} is the amplitude of displacement at the top of structure, δ is the phase difference between the top and the bottom of structure.

8.2.3 Solution

Soil displacements

The generalized solutions of Eq.(8.4) and (8.5) are expressed as;

$$\xi(x,y,t) = Ae^{-\alpha x} \cdot \sin \beta y \cdot e^{i\omega t} \tag{8.13}$$

$$\eta(x,y,t) = Be^{-\alpha x} \cdot \cos \beta y \cdot e^{i\omega t} \tag{8.14}$$

where A, B, α , β are constants. Substituting Eq.(8.13) and (8.14) in Eq.(8.6), following expression is obtained.

$$p = -K\left(A\alpha \cdot + B\beta\right)\sin \beta y \cdot e^{-\alpha x} \cdot e^{i\omega t} \tag{8.15}$$

It is obvious that Eq.(8.15) satisfies the boundary condition Eq.(8.7) and (8.9) when the constant α is positive. Substituting Eq.(8.6) in Eq.(8.4) and (8.5) respectively, the basic equation is reduced to be;

$$\rho \frac{\partial^2 \xi}{\partial t^2} = K \frac{\partial}{\partial x}\left(\frac{\partial \xi}{\partial x} + \frac{\partial \xi}{\partial y}\right) \qquad \text{and} \tag{8.16}$$

$$\rho \frac{\partial^2 \eta}{\partial t^2} = K \frac{\partial}{\partial y}\left(\frac{\partial \xi}{\partial x} + \frac{\partial \xi}{\partial y}\right) \tag{8.17}$$

Each term is expressed considering Eqs.(8.13) and (8.14) as what follows;

$$\frac{\partial^2 \xi}{\partial t^2} = -\omega^2 A \cdot e^{-\alpha x} \sin \beta y \cdot e^{i\omega t} \tag{8.18}$$

$$\frac{\partial}{\partial x}\left(\frac{\partial \xi}{\partial x}\right) = \alpha^2 A \cdot e^{-\alpha x} \sin \beta y \cdot e^{i\omega t} \tag{8.19}$$

$$\frac{\partial}{\partial x}\left(\frac{\partial \xi}{\partial y}\right) = -\alpha\beta A e^{-\alpha x} \cos \beta y \cdot e^{i\omega t} \tag{8.20}$$

$$\frac{\partial^2 \eta}{\partial t^2} = -\omega^2 B \cdot e^{-\alpha x} \cos \beta y \cdot e^{i\omega t} \tag{8.21}$$

$$\frac{\partial}{\partial y}\left(\frac{\partial \eta}{\partial y}\right) = -\beta^2 B \cdot e^{-\alpha x} \cos \beta y \cdot e^{i\omega t} \tag{8.22}$$

$$\frac{\partial}{\partial x}\left(\frac{\partial \eta}{\partial y}\right) = \alpha\beta B \cdot e^{-\alpha x} \sin \beta y \cdot e^{i\omega t} \tag{8.23}$$

Eqs.(8.18)～(8.23) are then substituted into basic Eqs.(8.16) and (8.17). The following set of equations is obtained.

$$\left\{ \begin{array}{l} \left((\frac{K}{\rho}\alpha^2 + \omega^2)A + \frac{K}{\rho}\alpha\beta B \right) \cdot e^{-\alpha x} \sin \beta y \cdot e^{i\omega t} = 0 \quad (8.24) \\ \left(\frac{K}{\rho}\alpha\beta A + (\frac{K}{\rho}\beta^2 - \omega^2)B \right) \cdot e^{-\alpha x} \cos \beta y \cdot e^{i\omega t} = 0 \quad (8.25) \end{array} \right.$$

Considering that both $e^{-\alpha x} \sin \beta y \cdot e^{i\omega t}$ and $e^{-\alpha x} \cos \beta y \cdot e^{i\omega t}$ are not always zero, the set of equations results in

$$\left\{ \begin{array}{l} \left((\frac{K}{\rho}\alpha^2 + \omega^2)A + \frac{K}{\rho}\alpha\beta B \right) = 0 \quad (8.26) \\ \left(\frac{K}{\rho}\alpha\beta A + (\frac{K}{\rho}\beta^2 - \omega^2)B \right) = 0 \quad (8.27) \end{array} \right.$$

Determination of coefficient α, β and *B*

It is required that the determinant *D* of the simultaneous linear equation, (8.26) and (8.27), must be zero to produce the effective solution. Hence,

$$\begin{vmatrix} \frac{K}{\rho}\alpha^2 + \omega^2 & \frac{K}{\rho}\alpha\beta \\ \frac{K}{\rho}\alpha\beta & \frac{K}{\rho}\beta^2 - \omega^2 \end{vmatrix} = 0 \tag{8.28}$$

$$\left(\frac{K}{\rho}\alpha^2 + \omega^2\right)\left(\frac{K}{\rho}\beta^2 - \omega^2\right) - \left(\frac{K}{\rho}\alpha\beta\right)^2 = 0 \tag{8.29}$$

$$\frac{\rho}{K}\omega^2 + \alpha^2 - \beta^2 = 0 \tag{8.30}$$

Referring to the boundary condition (8.8) at the bottom, $y = H$,

$$h(x,y,t) = Be^{-ax} \cdot \cos b\ H \cdot e^{iw\,t} = 0 \tag{8.31}$$

where $Be^{-ax} \cdot e^{iw\,t}$ is not necessarily zero. Hence,

$$\cos b\ H = 0 \tag{8.32}$$

and

$$b_n = \frac{2n-1}{2}\frac{p}{H} \qquad (n = 1,2,3,\cdots) \tag{8.33}$$

where β_n is the value of β at n=1,2,3$\cdots$. Substituting this into Eq.(8.30) considering $w = 2p/T$, we obtain

$$a_n = \frac{2n-1}{2}\frac{p}{H}\sqrt{1-\frac{16rH^2}{(2n-1)^2KT^2}} \quad (n = 1,2,3,\cdots) \tag{8.34}$$

where α_n is the value of α at n=1,2,3$\cdots$. In this equation, α_n is regarded as a positive value to satisfy the boundary condition (8.9). Eq.(8.34) is expressed as

$$a_n = \frac{2n-1}{2}\frac{p}{H}C_n \quad (n = 1,2,3,\cdots) \tag{8.35}$$

where

$$C_n = \sqrt{1-\frac{16rH^2}{(2n-1)^2KT^2}} \quad (n = 1,2,3,\cdots) \tag{8.36}$$

Substituting Eq.(8.30) into Eq.(8.26), we have

$$B = -\frac{b}{a}A \tag{8.37}$$

Considering Eqs.(8.33)(8.34), Eq.(8.37) is expressed as

$$B_n = -\frac{A_n}{\sqrt{1-\frac{16rH^2}{(2n-1)^2KT^2}}} \qquad (n = 1,2,3,\cdots) \tag{8.38}$$

or simply,

$$B_n = -\frac{A_n}{C_n} \qquad (n = 1,2,3,\cdots) \tag{8.39}$$

Substituting Eqs.(8.33)(8.35) and (8.38) into the right-hand side of Eqs.(8.13) and (8.14) respectively, displacement of soil, ξ and η, are derived,

$$x_n(x,y,t) = A_n \cdot e^{-\frac{(2n-1)p}{2H}C_n x} \cdot \sin\frac{(2n-1)p}{2H} y \cdot e^{iwt} \tag{8.40}$$

$$h_n(x,y,t) = -\frac{A_n}{C_n} \cdot e^{-\frac{(2n-1)p}{2H}C_n x} \cdot \cos\frac{(2n-1)p}{2H} y \cdot e^{iwt} \tag{8.41}$$

where $n = 1,2,3,\cdots$. Based on the principle of superposition of the linear equations, the generalized solutions Eq.(8.13) and Eq.(8.14) result in

$$x(x,y,t) = e^{iwt} \cdot \sum_{n=1}^{\infty} A_n \cdot e^{-\frac{(2n-1)p}{2H}C_n x} \cdot \sin\frac{(2n-1)p}{2H} y \tag{8.42}$$

$$h(x,y,t) = -e^{iwt} \cdot \sum_{n=1}^{\infty} \frac{A_n}{C_n} \cdot e^{-\frac{(2n-1)p}{2H}C_n x} \cdot \cos\frac{(2n-1)p}{2H} y \tag{8.43}$$

where A_n will be determined in the following section.

Determination of the coefficient A_n

The coefficient A_n in the generalized solution Eqs.(8.42) and (8.43) is still unknown. The problem is the determination of A_n to satisfy the boundary condition on the flexible wall herein. The boundary condition on the wall (x=0) is expressed as

$$x(x=0,y,t) = (x_{t0}e^{i(wt-d)} - x_{g0}e^{iwt})\left(1-\frac{y}{H}\right)^2\left(3-2\left(1-\frac{y}{H}\right)\right) + x_{g0}e^{iwt} \tag{8.44}$$

Substituting Eq.(8.44) into Eq.(8.42),

$$(x_{t0}e^{i(wt-d)} - x_{g0}e^{iwt})\left(1-\frac{y}{H}\right)^2\left(3-2\left(1-\frac{y}{H}\right)\right) + x_{g0}e^{iwt} = e^{iwt} \cdot \sum_{n=1}^{\infty} A_n \cdot \sin\frac{(2n-1)p}{2H} y \tag{8.45}$$

Considering that $e^{i\omega t}$ is not always zero, Eq.(8.45) becomes

$$(x_{t0}e^{-id}-x_{g0})\left(1-\frac{y}{H}\right)^2\left(3-2\left(1-\frac{y}{H}\right)\right)+x_{g0}=\sum_{n=1}^{\infty}A_n\cdot\sin\left(\frac{2n-1}{2}p\,\frac{y}{H}\right) \tag{8.46}$$

Multiplying Eq.(8.46) by $\sin\left(\frac{2m-1}{2}p\,\frac{y}{H}\right)$ (m is a positive integral number), and integrating it with respect to y from 0 to H, one obtains

$$\int_0^H\left[(x_{t0}e^{-id}-x_{g0})\left(1-\frac{y}{H}\right)^2\left(3-2\left(1-\frac{y}{H}\right)\right)+x_{g0}\right]\cdot\sin\left(\frac{2m-1}{2}p\,\frac{y}{H}\right)dy= \tag{8.47}$$
$$\sum_{n=1}^{\infty}A_n\cdot\int_0^H\sin\left(\frac{2m-1}{2}p\,\frac{y}{H}\right)\sin\left(\frac{2n-1}{2}p\,\frac{y}{H}\right)dy$$

The integration of the right-hand side of Eq.(8.47) is proved as

$$\int_0^H\sin\left(\frac{2m-1}{2}p\,\frac{y}{H}\right)\sin\left(\frac{2n-1}{2}p\,\frac{y}{H}\right)dy=\begin{cases}\frac{H}{2} & n=m\\ 0 & n\neq m\end{cases} \tag{8.48}$$

Considering Eq.(8.48), the coefficient A is determined as

$$A_m=\frac{2}{H}\int_0^H\left[(x_{t0}e^{-id}-x_{g0})\left(1-\frac{y}{H}\right)^2\left(3-2\left(1-\frac{y}{H}\right)\right)+x_{g0}\right]\cdot\sin\left(\frac{2m-1}{2}p\,\frac{y}{H}\right)dy \tag{8.49}$$

which implies

$$A_n=2\int_0^1\left[(x_{t0}e^{-id}-x_{g0})(1-s)^2(3-2(1-s))+x_{g0}\right]\cdot\sin\left(\frac{2n-1}{2}p\cdot s\right)ds$$
$$+2x_{g0}\int_0^1\sin\left(\frac{2n-1}{2}p\cdot s\right)ds\;=2(x_{t0}e^{-id}-x_{g0})\int_0^1(1-3s^2+2s^3)\cdot\sin\left(\frac{2n-1}{2}p\cdot s\right)ds \tag{8.50}$$

where $s=y/H$ and $dy=Hds$. Consequently,

$$A_n=\frac{4(x_{t0}e^{-id}-x_{g0})}{p(2n-1)}\left[1+6\left(\frac{2}{p(2n-1)}\right)^2\left(1-2\cdot(-1)^{n+1}\cdot\left(\frac{2}{p(2n-1)}\right)\right)\right]+\frac{4x_{g0}}{p(2n-1)}$$
$$(n=1,2,3,\cdots) \tag{8.51}$$

Solution of soil displacement

The solution of displacement of liquefied soil is derived by substituting Eq.(8.51) into Eq.(8.42) and Eq.(8.43). The solution is expressed as what follows;

$$x(x,y,t) = -\frac{1}{w^2} e^{iw\,t} \cdot \sum_{n=1}^{\infty} A_n' \cdot e^{-\frac{(2n-1)p}{2H} C_n x} \cdot \sin \frac{(2n-1)p}{2H} y \tag{8.52}$$

$$h(x,y,t) = \frac{1}{w^2} e^{iw\,t} \cdot \sum_{n=1}^{\infty} \frac{A_n'}{C_n} \cdot e^{-\frac{(2n-1)p}{2H} C_n x} \cdot \cos \frac{(2n-1)p}{2H} y \tag{8.53}$$

$$(n = 1,2,3,\cdots)$$

$$A_n' = \frac{4(a_{t0} e^{-id} - a_{g0})}{p\,(2n-1)} \left[1 + 6 \left(\frac{2}{p\,(2n-1)} \right)^2 \left(1 - 2 \cdot (-1)^{n+1} \cdot \left(\frac{2}{p\,(2n-1)} \right) \right) \right] + \frac{4 a_{g0}}{p\,(2n-1)} \tag{8.54}$$

$$= 2B_n \left[\left\{ 1 + 6B_n^{\,2} \left(1 - 2(-1)^{n+1} B_n \right) \right\} \left\{ a_{t0} e^{-id} - a_{g0} \right\} + a_{g0} \right] \tag{8.55}$$

$$B_n = \frac{2}{p\,(2n-1)} \tag{8.56}$$

$$C_n = \sqrt{1 - \frac{16\,r H^2}{(2n-1)^2 K T^2}} \tag{8.57}$$

Dynamic earth pressures on the flexible wall

The solution of the dynamic earth pressures on the flexible wall is derived by substituting Eqs.(8.52) and (8.53) into the stress-strain relationship of liquefied soil shown again as follows

$$p = K \left(\frac{\partial x}{\partial x} + \frac{\partial h}{\partial y} \right) \tag{8.58}$$

where $\partial x / \partial x$ and $\partial h / \partial y$ are

$$\frac{\partial x}{\partial x} = \frac{1}{w^2} e^{iw\,t} \sum_{n=1}^{\infty} A_n' \frac{(2n-1)p}{2H} C_n \cdot e^{-\frac{(2n-1)p}{2H} C_n \cdot x} \sin \left(\frac{2n-1}{2} p \, \frac{y}{H} \right) \tag{8.59}$$

$$\frac{\partial h}{\partial y} = -\frac{1}{w^2} e^{iw\,t} \sum_{n=1}^{\infty} \frac{A_n'}{C_n} \frac{(2n-1)p}{2H} \cdot e^{-\frac{(2n-1)p}{2H} C_n \cdot x} \sin \left(\frac{2n-1}{2} p \, \frac{y}{H} \right) \tag{8.60}$$

Consequently the dynamic pressure p is expressed as

$$p = \frac{K}{w^2} e^{iw\,t} \frac{p}{2H} \sum_{n=1}^{\infty} A_n'(2n-1)\left(C_n - \frac{1}{C_n} \right) \cdot e^{-\frac{(2n-1)p}{2H} C_n \cdot x} \sin\left(\frac{2n-1}{2} p \frac{y}{H} \right)$$

$$= -\frac{2rH}{p} e^{iw\,t} \sum_{n=1}^{\infty} \frac{A_n'}{(2n-1)C_n} \cdot e^{-\frac{(2n-1)p}{2H} C_n \cdot x} \sin\left(\frac{2n-1}{2} p \frac{y}{H} \right) \qquad (8.61)$$

$(n = 1,2,3,\cdots)$

The solution of the dynamic pressure on the flexible wall (x=0) is derived as what follows;

$$p(y,t) = -\frac{2rH}{p} e^{iw\,t} \sum_{n=1}^{\infty} \frac{A_n'}{(2n-1)C_n} \cdot \sin\left(\frac{2n-1}{2} p \frac{y}{H} \right) \qquad (8.62)$$

where, A'_n, C_n are the coefficients as expressed in Eqs.(8.55) and (8.57), T is a period of the input motion ($=2\pi/\omega$). Note that the solution is applicable to backfill which was made soft by shaking.

Example of calculation using the solution

In the formulation presented above, it can be seen that the magnitude of the dynamic earth pressure on the flexible wall depends on the amplification α_{to}/α_{go} and the phase difference δ. In order to show the distribution of dynamic earth pressures with respect to those quantities, a model structure with a normalized height was analyzed. The liquefied soil properties are given as shown in Table 8.2.

Table 8.2: Numerical values of coefficients for the model

Shear modulus of soil	G = 0 kPa (assumed)
Density of saturated soil	ρ = 1900 kg/m^3
Bulk modulus of saturated soil	$K = 2.25 \times 10^6$ kPa

Table 8.3: Assumed values for amplification and phase difference

	At the resonance	During liquefaction
Amplification α_{to}/α_{go}	2.5	1.5
Phase difference δ	90 degrees	150 degrees

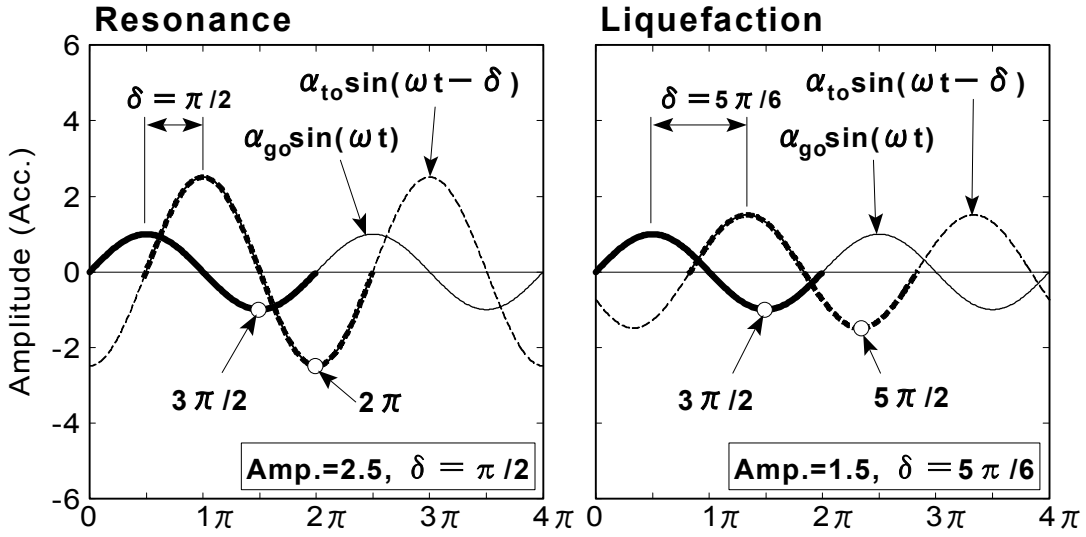

(a) At the resonance (b) During liquefaction

Fig.8.3: Time histories of harmonic accelerations for the analysis

Based on the result of shaking table tests, the amplification and phase difference between the top and the bottom of the structure are specified as shown in Table 8.3. The time histories of harmonic input motion with the amplification and the phase difference are illustrated in Fig.8.3. The solution of dynamic earth pressures expressed by Eq.(8.62) is rewritten for the calculation as

$$p(y,t) \cong -\frac{2\rho H}{\pi}\sum_{n=1}^{30}\frac{A_n''}{(2n-1)C_n}\cdot\sin\left(\frac{2n-1}{2}\pi\frac{y}{H}\right) \tag{8.63}$$

$$A_n'' = 2B_n\left[\left\{1+6B_n{}^2\left(1-2(-1)^{n+1}B_n\right)\right\}\left\{\alpha_{t0}\sin(\omega t-\delta)-\alpha_{g0}\sin\omega t\right\}+\alpha_{g0}\sin\omega t\right] \tag{8.64}$$

where B_n and C_n are constants as expressed in Eqs.(8.56) and (8.57). Fig.8.4 shows the calculated distribution of dynamic earth pressures by Eq.(8.63) with the interval of $\Delta\omega t = \pi/8$.

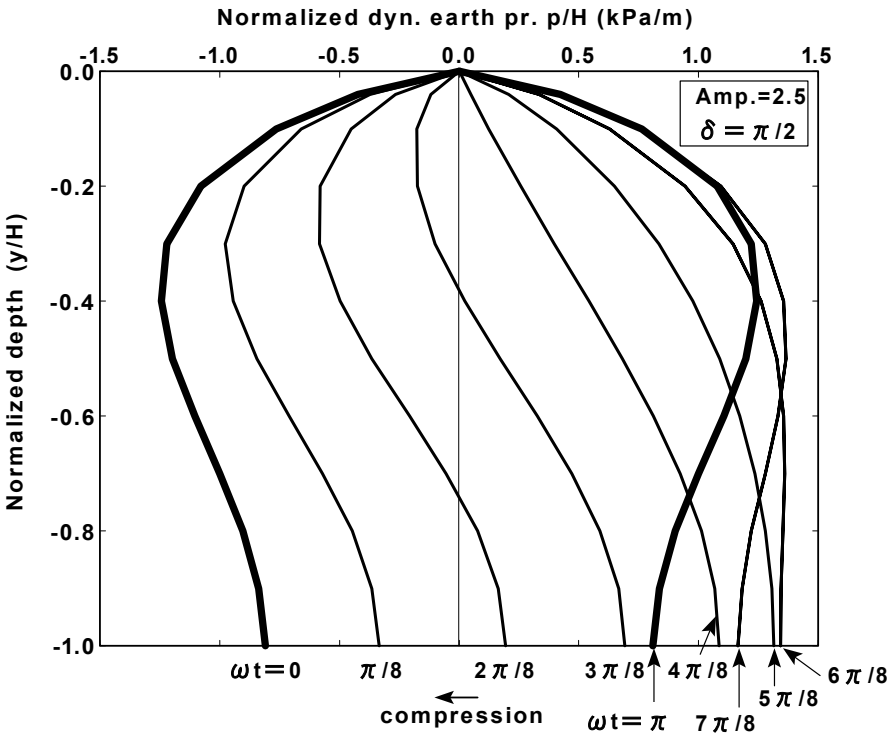

(a) At resonance (Amp.=2.5, $\delta = \pi/2$)

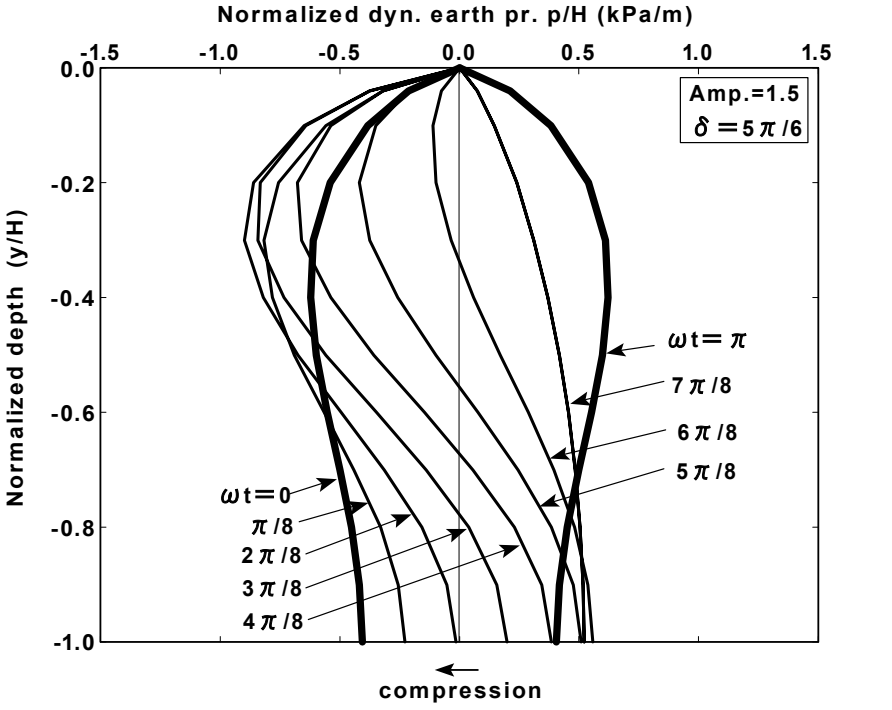

(b) Liquefaction (Amp.=1.5, $\delta = 5\pi/6$)

Fig.8.4: Normalized dynamic earth pressure on the wall

The depth and dynamic earth pressures are normalized by the height of the structure. It is observed that the dynamic earth pressures on the wall become larger as the amplification of the structure increases. The phase difference is seen at the dynamic pressures between the deep and the shallow parts of the liquefied backfill.

8.3 ANALYSIS OF TEST RESULTS

8.3.1 Time histories of dynamic pressures

To illustrate the validity of the proposed solution of Eq.(8.62), the calculations have been performed. The proposed solution is used to simulate the dynamic earth pressures observed in shaking table tests. The present study makes use of the measured acceleration at the top ($\alpha_{to}e^{i(\omega t-\delta)}$) and the bottom ($\alpha_{go}e^{i\omega t}$) of the structure as input accelerations. In addition, the bulk modulus of liquefiable soil K was specified as 2.25×10^6 kPa assuming the velocity of P wave to be 1500m/sec in water. The dynamic earth pressures were calculated by means of Eq.(8.62) considering the summation up to n =100.

The calculated and measured time histories of dynamic earth pressures for AD35F3A50 test are shown in Fig.8.5(a) and (b). The time history of the ratio of excess pore water pressure in saturated soil at GL-0.375m (PP2) is presented in Fig.8.5(c), and the change of amplification between the top and the bottom of the structure with time is illustrated in Fig.8.5(d). It is observed that the calculated dynamic earth pressures (EP7, EP9) are inconsistent with the measured dynamic earth pressures before about 7.5 seconds. On the other hand, the calculated earth pressure becomes consistent with the measured earth pressure after 7.5 seconds. It is seen that the amplification of shaking attained the maximum value at about 7.5 seconds in the process of pore water pressure build up. From the observation made in Chapter 5, the natural frequency of the backfill is about 0.8 Hz at this time instance (Fig.5.12(a)), showing that the backfill becomes substantially soft. Considering that the initial natural frequency of the backfill is 19.5Hz (see, Fig.4.75(a)), the shear modulus of the backfill becomes about 1/600 of the initial shear modulus. It suggests that the proposed solution is applicable when the shear modulus of backfill significantly decreases due to liquefaction.

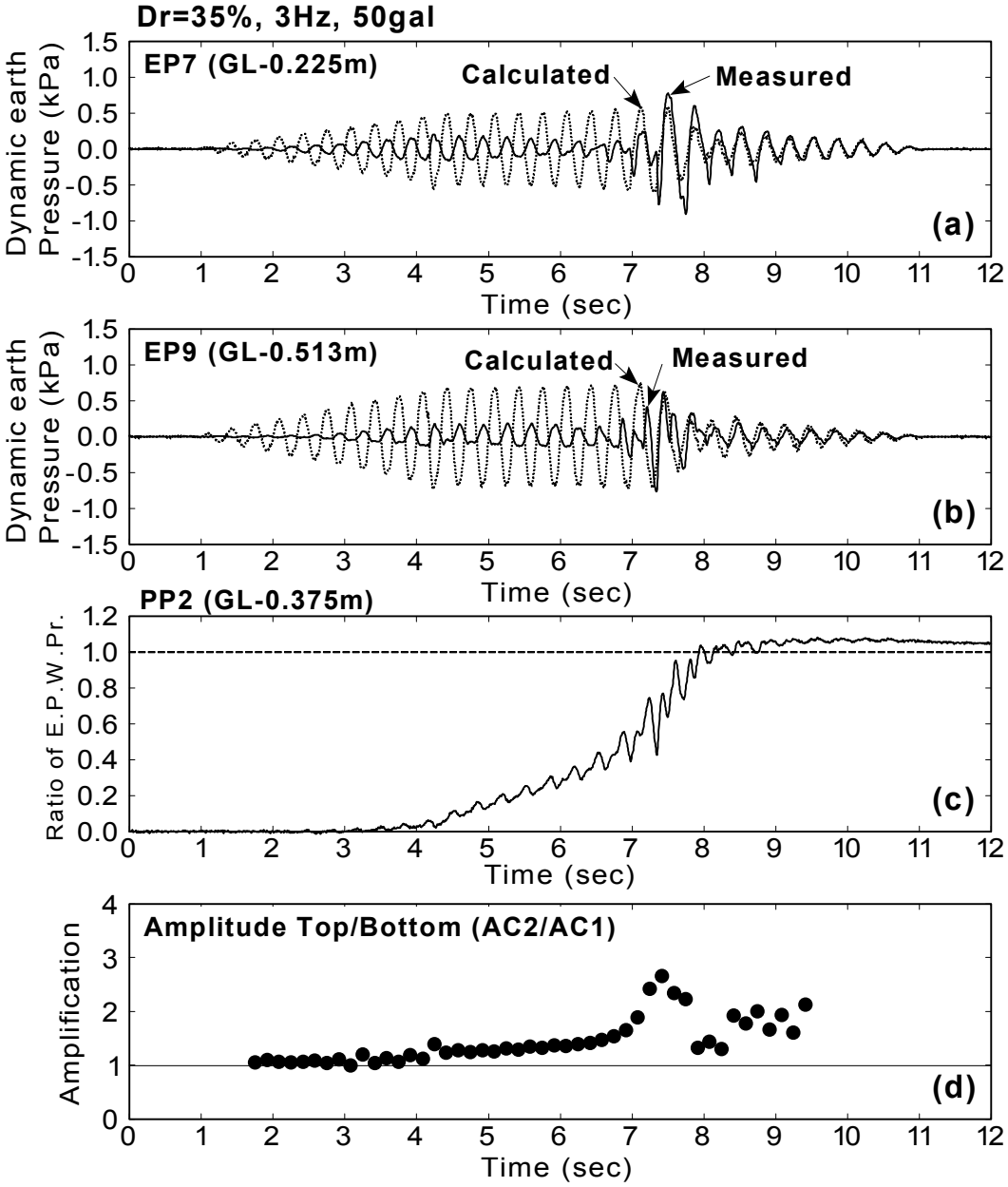

Fig.8.5: Time histories of the measured and the calculated dynamic earth pressures (AD35F3A50 test)

Fig.8.6 shows the results from AD39F5A50 in which the model is shaken by 5Hz input motion. At first, it is seen in figure (d) that the amplification reaches the maximum at about 3.2 seconds. It is observed in figure (a) that the calculated time history of dynamic earth pressure at GL-0.225m is inconsistent with the measured dynamic pressure before the maximum amplification of 3.2 seconds. In contrast, the calculated dynamic earth pressure becomes consistent with the measured dynamic earth pressure after 3.2 seconds especially in terms of phase. The same feature before and after 3.2 seconds is seen in the result at the depth of GL-0.513m. At this depth, the amplitude of calculated dynamic earth pressure only after about 6.0 seconds is apparently larger than that of the measured one, being different feature from the depth of GL-0.225m. Referring to the time history of the pore pressure ratio at GL-0.513m (see, Fig.3.68, PP3 and PP8), it can be seen that the backfill is not liquefied completely. It causes the inconsistency between the calculated and the measured values at GL-0.513m.

Fig.8.7 illustrates the results from AD41F3A200 test. The amplification becomes the maximum at about 2.5 seconds in this test. The calculated dynamic earth pressures at both GL-0.225m and GL-0.513m are inconsistent with the measured dynamic earth pressures before 2.5 seconds. As was observed previously, the calculated time histories are changed to be consistent after the maximum amplification. Assuming that the initial natural frequency of ground is 19.5Hz (see, Fig.4.123(a)), and 1.6Hz (see, Fig.5.12(c)) at 2.5 seconds, the shear modulus of the backfill is approximately 1/150 of the initial shear modulus.

The results from AD32F3A500 and BD36F3A500 tests are illustrated in Fig.8.8 and Fig.8.9, respectively. Both tests were shaken by input acceleration of 5.0m/sec^2 with 3Hz frequency. Since the tensile strength of the material used in BD36F3A500 test was lower than that in AD32F3A500 test, the material of the structure was yielded at 2.7 seconds only in BD36F3A500 test, causing the increase of curvature of the wall (see, Fig.6.8). The amplification reached the peak at about 1.8 seconds in both tests.

The calculated dynamic earth pressures in both tests are consistent with measured dynamic earth pressure in terms of phase after the peak amplification. But the amplitudes of calculated dynamic earth pressures are larger than those of the measured pressures in both tests. Referring to the results from AD35F3A50 and AD41F3A200 tests with weaker input motion, this feature seems significant in tests with intense input motion of 5.0m/sec^2 in which the level of shear strains are amounted to more than 4% (see, Figs.4.57 and 4.63). Although it may cause the effect of liquefied soil with large shear strain, the exact reason is not clear.

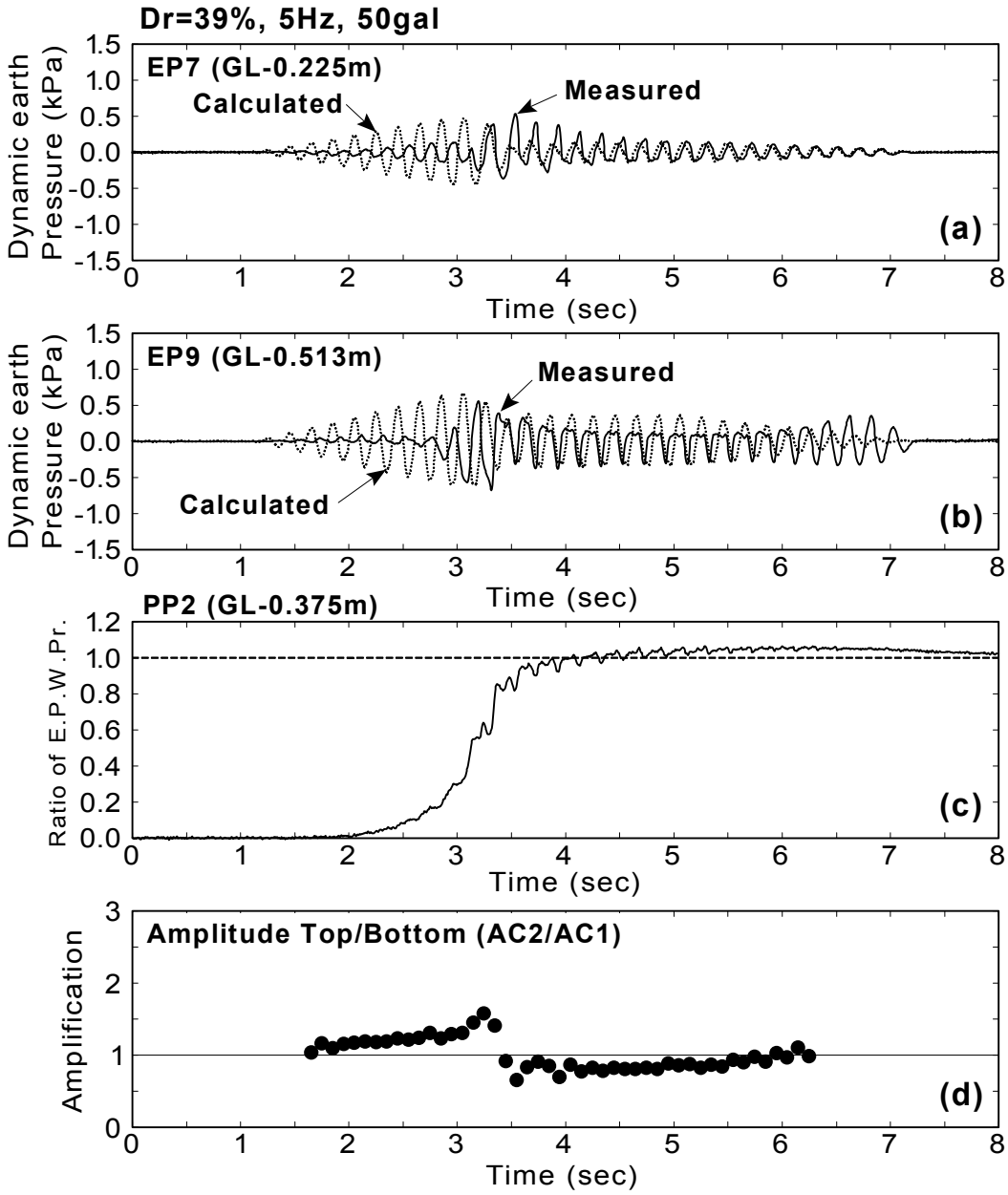

Fig.8.6: Time histories of the measured and the calculated dynamic earth pressures (AD39F5A50 test)

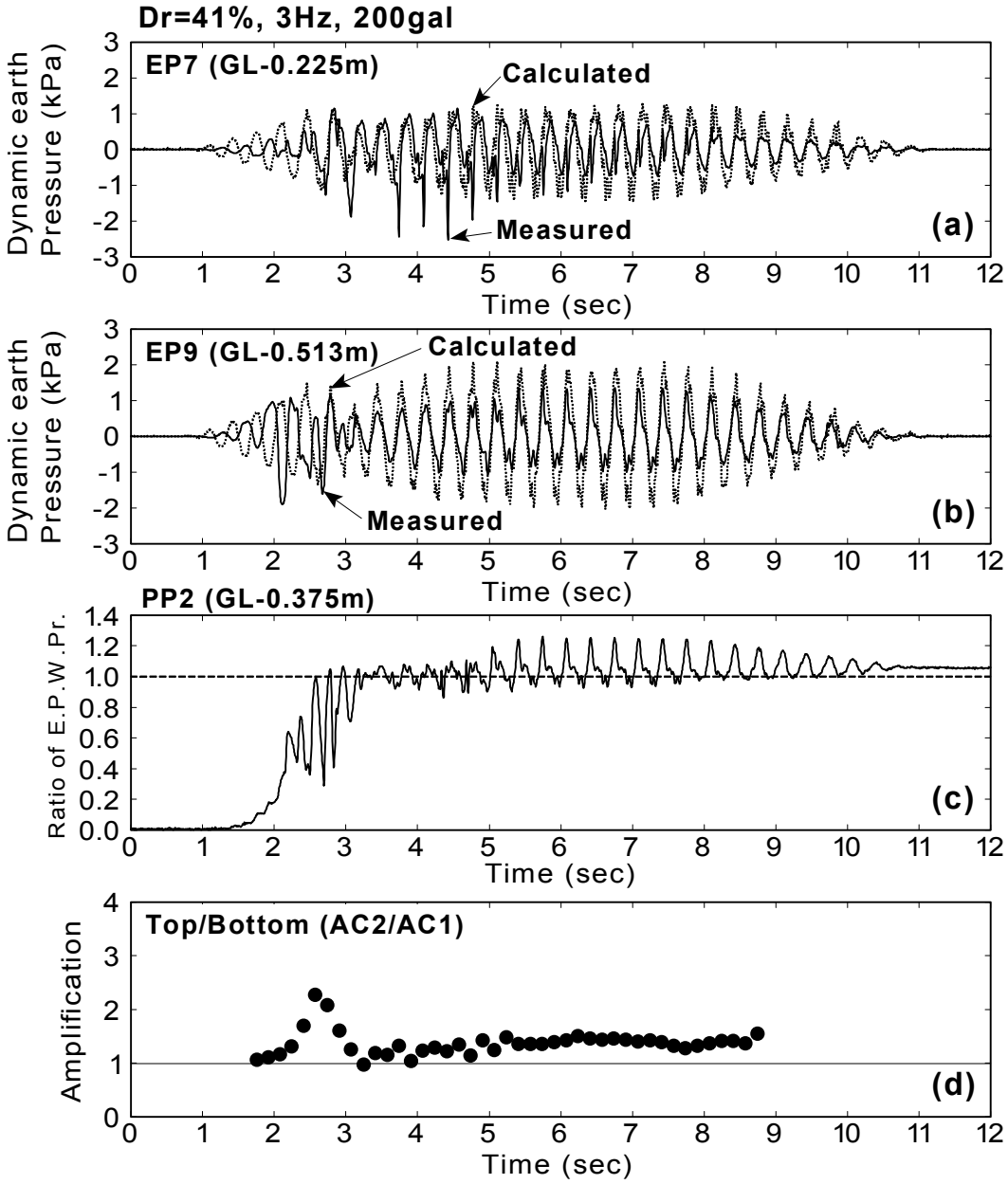

Fig.8.7: Time histories of the measured and the calculated dynamic earth pressures (AD41F3A200 test)

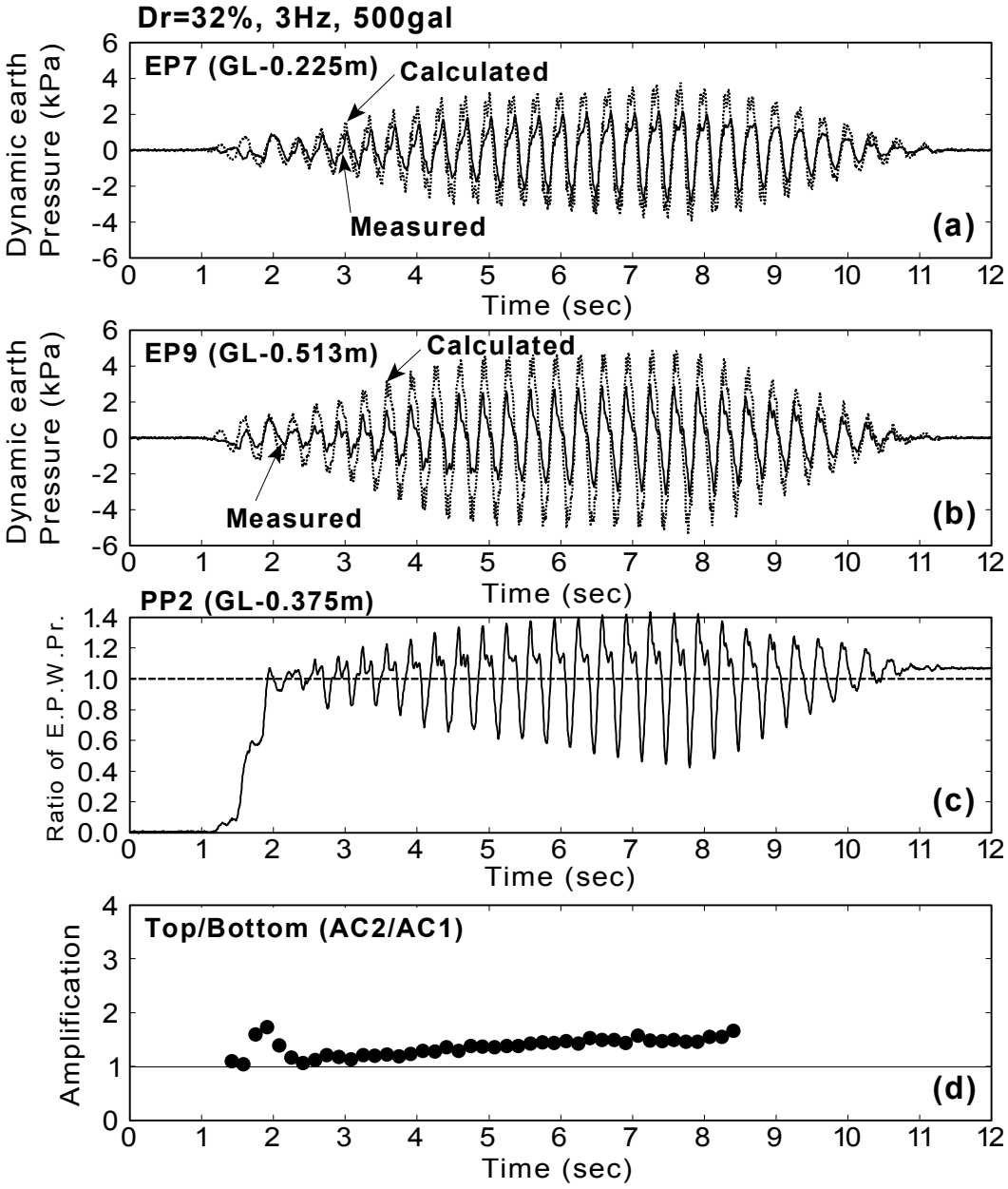

Fig.8.8: Time histories of the measured and the calculated dynamic earth pressures (AD32F3A500 test)

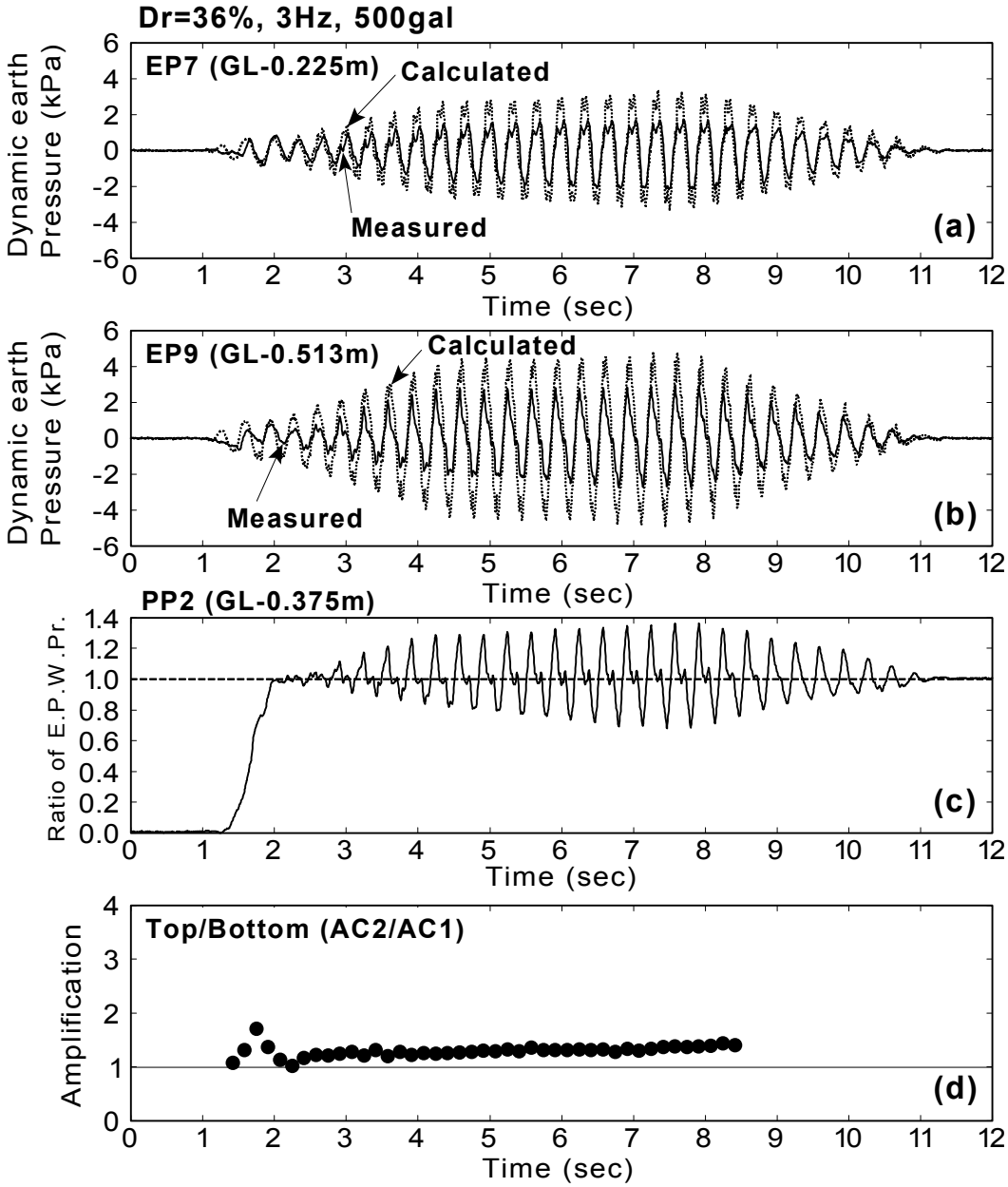

Fig.8.9: Time histories of the measured and the calculated dynamic earth pressures (BD36F3A500 test)

Comparing both results of AD32F3A500 and BD36F3A500 tests, no significant differences due to the yielding of the material after 2.7 seconds can be recognized. It is considered that the acceleration of wall, which is influential to dynamic earth pressures, is not affected by the gradual increase of curvature after yielding of material in BD36F3A500 test.

8.3.2 Distributions of dynamic pressures

The comparison between the calculated and the measured dynamic earth pressures will be made at the time instance when i) the resonance occurs and the amplification becomes the maximum, and ii) the soil liquefies completely. The dynamic pressures are calculated by two methods: the proposed solution expressed in Eq.(8.62) and the dynamic pressures due to Westergaard theory (1933), which is often used in practical calculation assuming a structure as a rigid wall. The simplified equation of dynamic pressures due to Westergaard theory is expressed using same coordinate shown in Fig.8.1 as,

$$p(y,t) = -\frac{7}{8} \cdot \alpha_{b0} e^{i\omega t} \cdot \rho\sqrt{H \cdot y} \tag{8.65}$$

where ρ is the mass density of liquefied soil.

Fig.8.10 shows the time histories and the distributions of calculated and measured dynamic pressures. Fig.8.10(a) illustrates the time histories of input acceleration for $\alpha_{to} e^{i(\omega t - \delta)}$ at the top (AC2) and $\alpha_{go} e^{i\omega t}$ at the bottom (AC1). The cycle in which the amplification becomes the maximum due to resonance (20th cycle), and the representative cycle when soil liquefy completely (24th cycle), are indicated by bold lines.

Fig.8.10(b) indicates the calculated and the measured time histories of dynamic earth pressures at the depth of 0.225m from the surface. The calculated dynamic earth pressure by Eq.(8.65), which assumes the flexible structure as a rigid wall, is illustrated in the same figure. The phase difference is seen between the calculated dynamic pressures assuming a rigid wall and the measured dynamic pressures through the period. On the other hand, the calculated dynamic pressures by the proposed solution show a good agreement with the measured dynamic pressures.

Fig.8.10(c) shows the distribution of dynamic earth pressures with respect to the depth at the same time instance. The time instances selected are illustrated in the time histories of input accelerations shown in Fig.8.10(a). The distributions by the proposed solution show a good agreement with the measured distributions than the calculated distributions assuming a rigid wall.

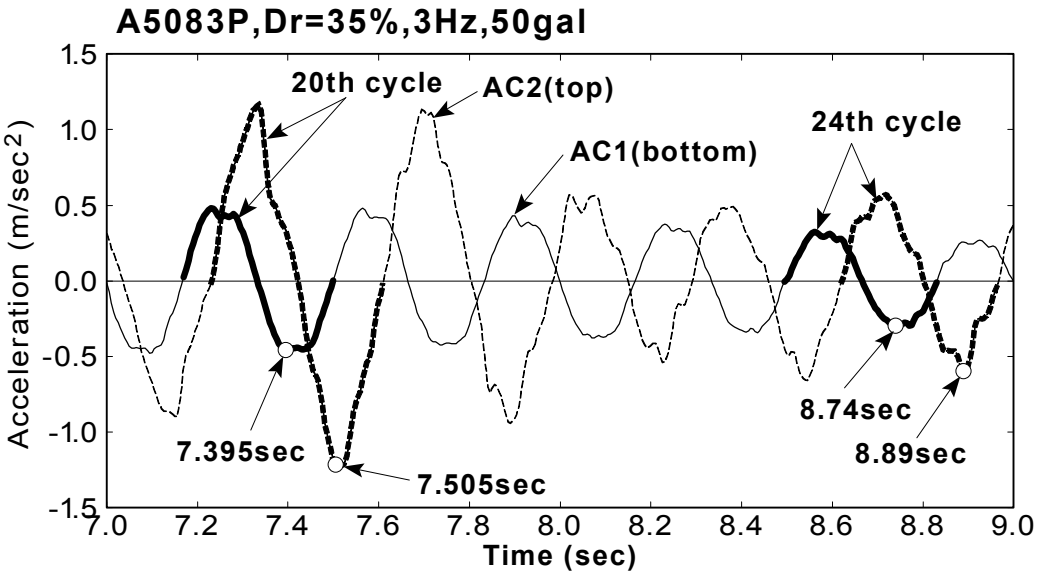

(a) Accelerations

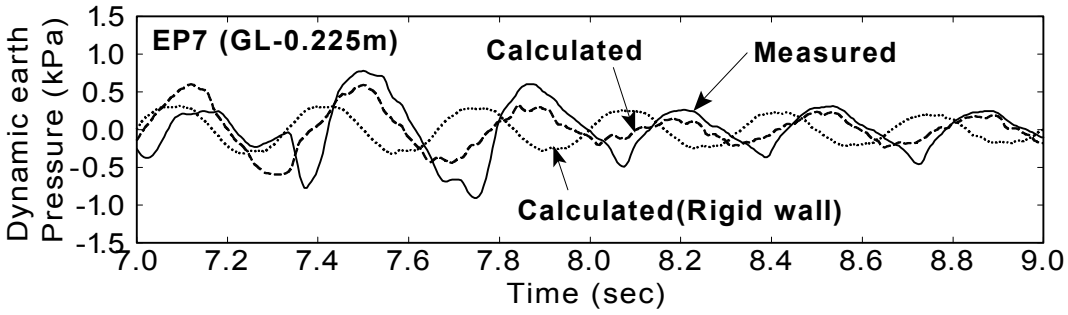

(b) Dynamic earth pressures

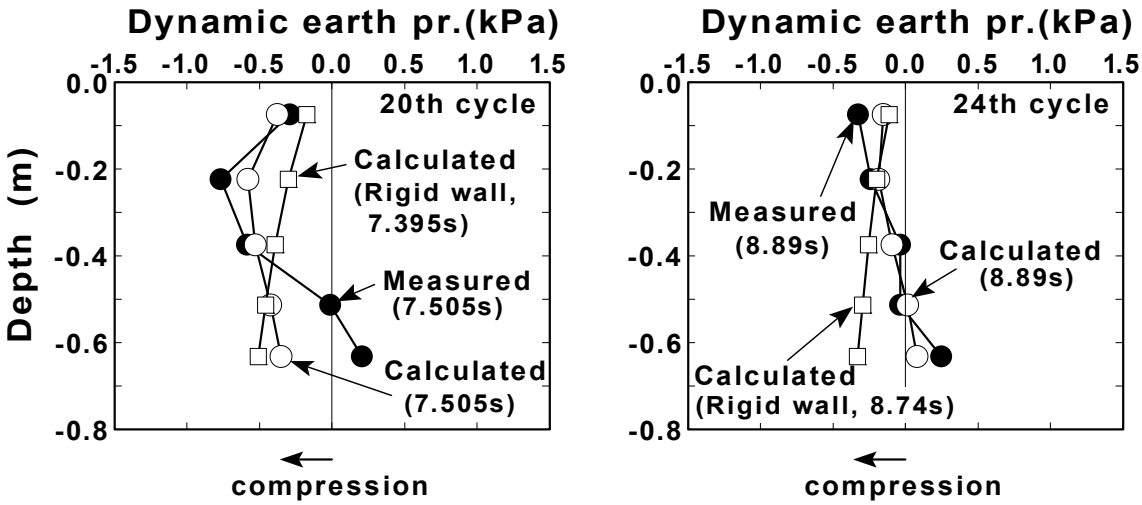

(i) At the resonance (ii) During liquefaction

(c) Distribution of dynamic pressures

Fig.8.10: Measurement and analysis (AD35F3A50 test)

This is because the amplification and the phase difference of accelerations are taken into account appropriately in the proposed solution. Only the calculated distribution by the proposed solution at the resonance is slightly different from the measured distribution. Both are almost consistent at complete liquefaction. The effect of the shear modulus at the resonance, assuming zero in calculations, can be considered for the cause of slight inconsistency at the resonance.

The time histories and the distributions of calculated and measured dynamic pressures of AD39F5A50 test are illustrated in Fig.8.11. It is seen in the distributions of the dynamic earth pressures in figure (c) that the calculated distribution by the proposed solution is almost consistent with the measured distribution during liquefaction. On the other hand, some differences are observed between them at the resonance especially below the depth of about GL-0.4m. This is due to the incomplete liquefaction at the depth of below GL-0.4m (see, Fig.3.68, PP3 and PP8). However, the proposed solution gives better distribution than the calculation by assuming a rigid wall in both time instances.

The results from AD41F3A200 test are shown in Fig.8.12(c). As was observed in previously, slight differences were seen at the resonance between the calculated by the proposed solution and the measured distribution. The calculated distribution agrees with the measured distribution during liquefaction.

Fig.8.13 and Fig.8.14 illustrate the results from AD32F3A500 and BD36F3A500 tests, respectively. In these tests, the agreements between the calculated distribution by the proposed solution and the measured distribution are very good in both time instances. It is interesting that the agreement during liquefaction after the yielding of the material in BD36F3A500 test is also very good, suggesting the less effect of monotonically increasing deflections on the dynamic earth pressures.

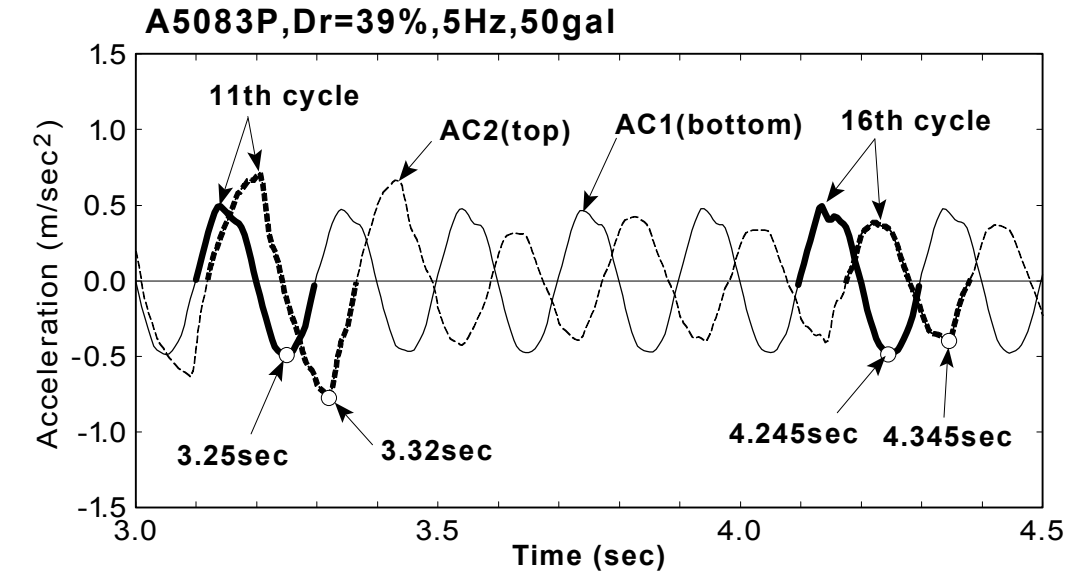

(a) Accelerations

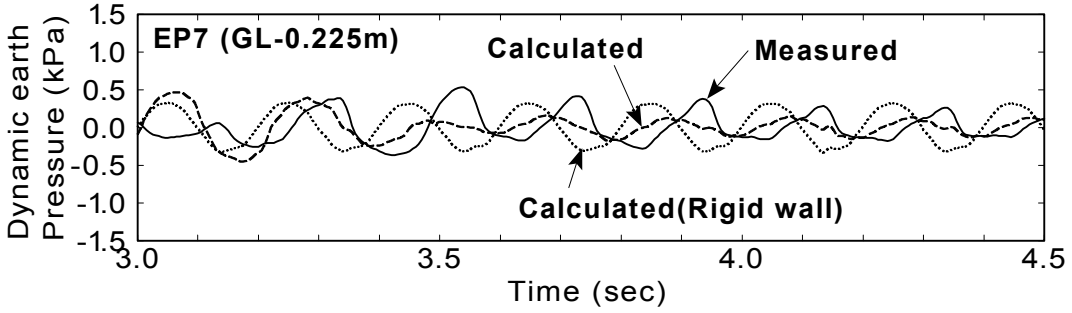

(b) Dynamic earth pressures

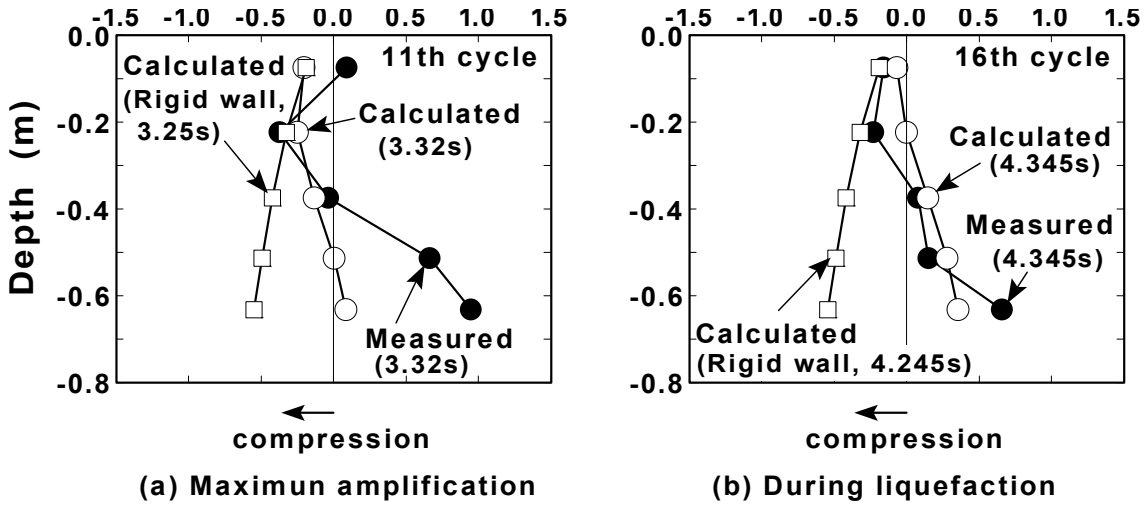

(i) At the resonance (ii) During liquefaction

(c) Distribution of dynamic pressures

Fig.8.11: Measurement and analysis (AD39F5A50 test)

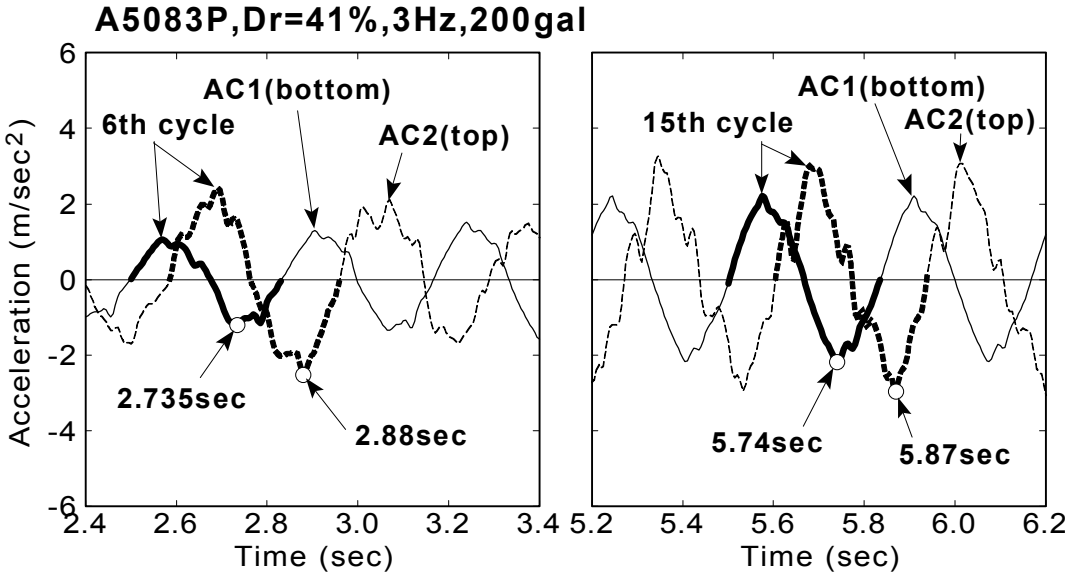

(a) Accelerations

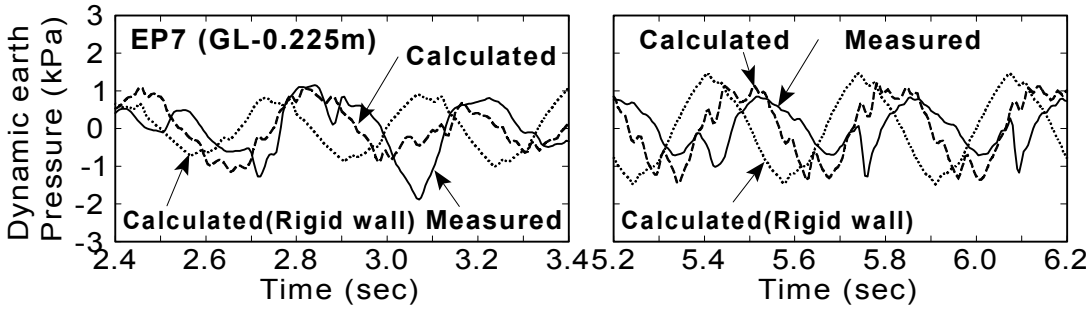

(b) Dynamic earth pressures

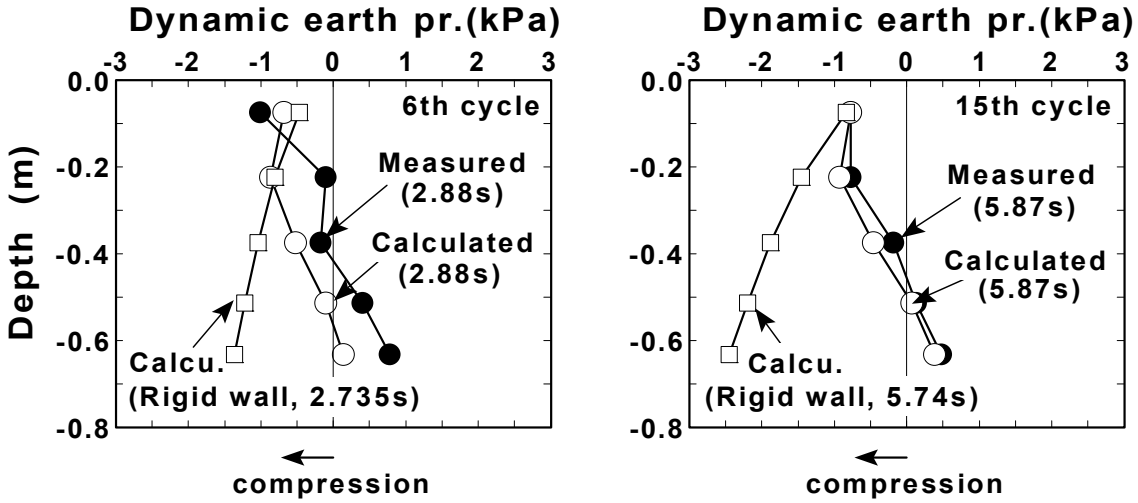

(i) At the resonance (ii) During liquefaction

(c) Distribution of dynamic pressures

Fig.8.12: Measurement and analysis (AD41F3A200 test)

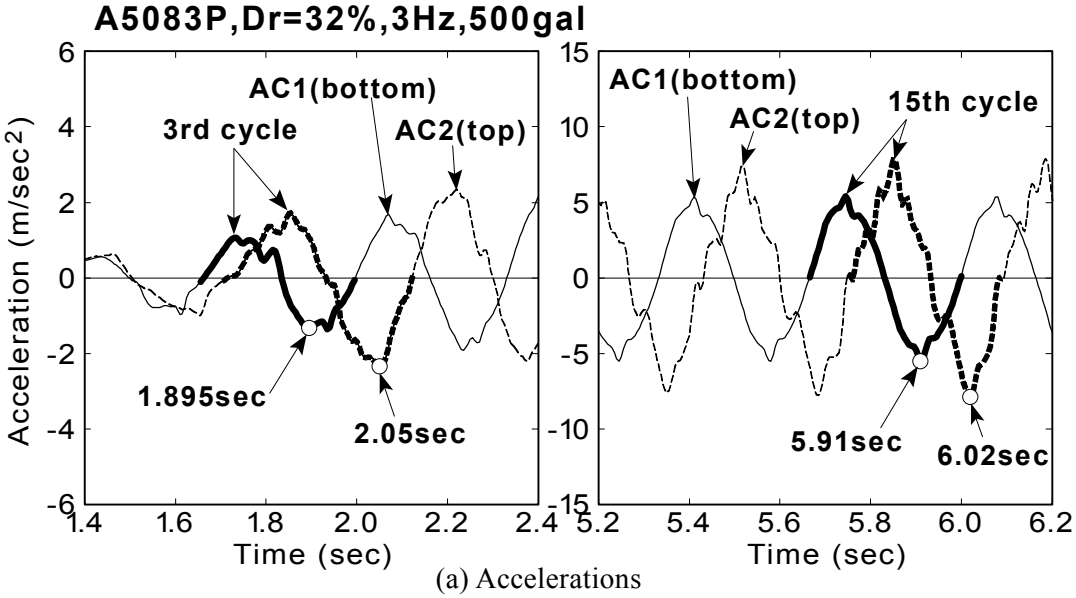

(a) Accelerations

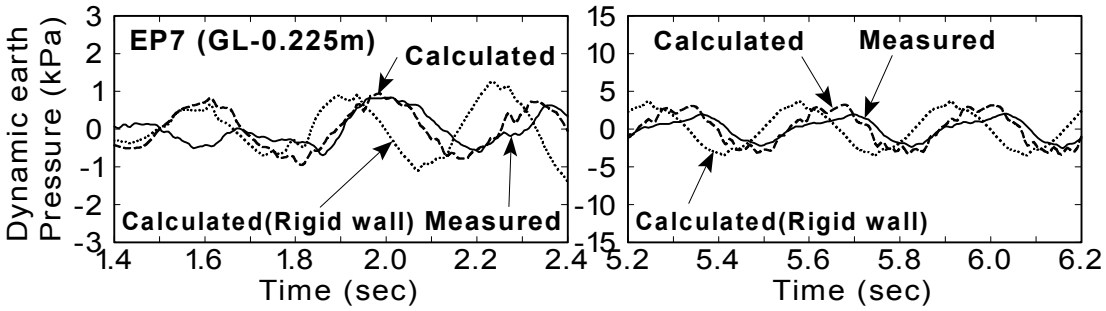

(b) Dynamic earth pressures

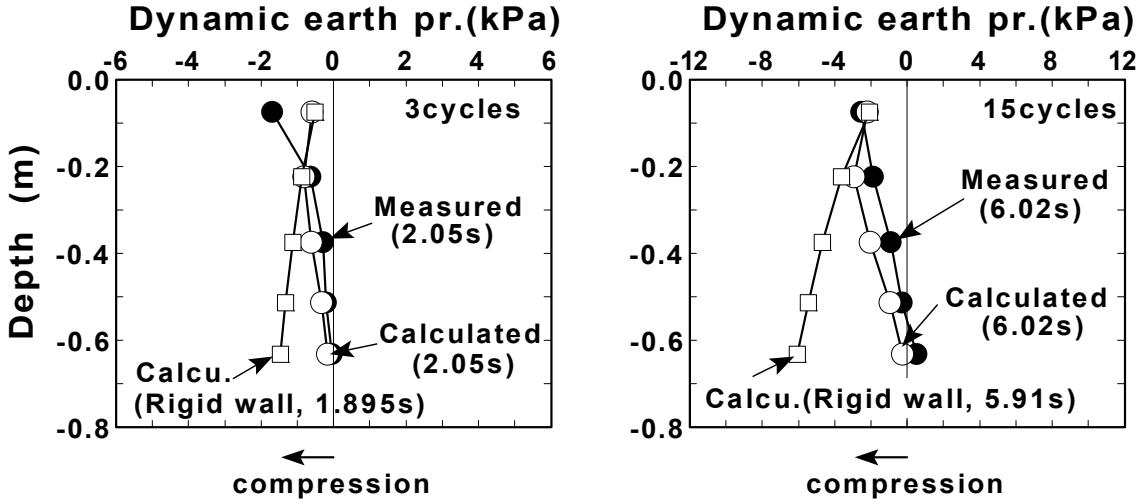

(i) At the resonance (ii) During liquefaction

(c) Distribution of dynamic pressures

Fig.8.13: Measurement and analysis (AD32F3A500 test)

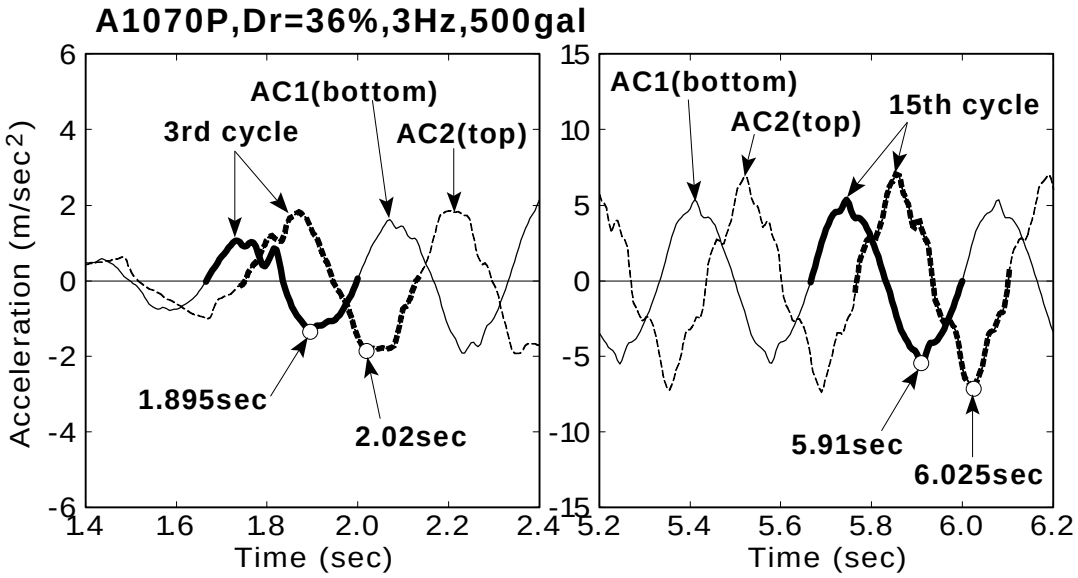

(a) Accelerations

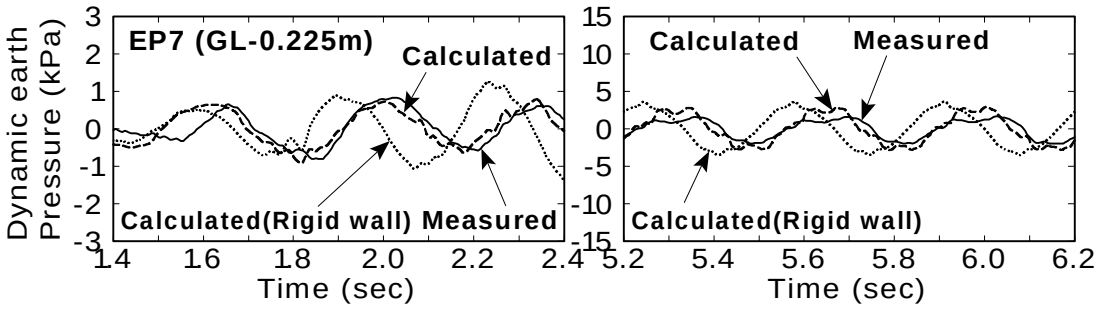

(b) Dynamic earth pressures

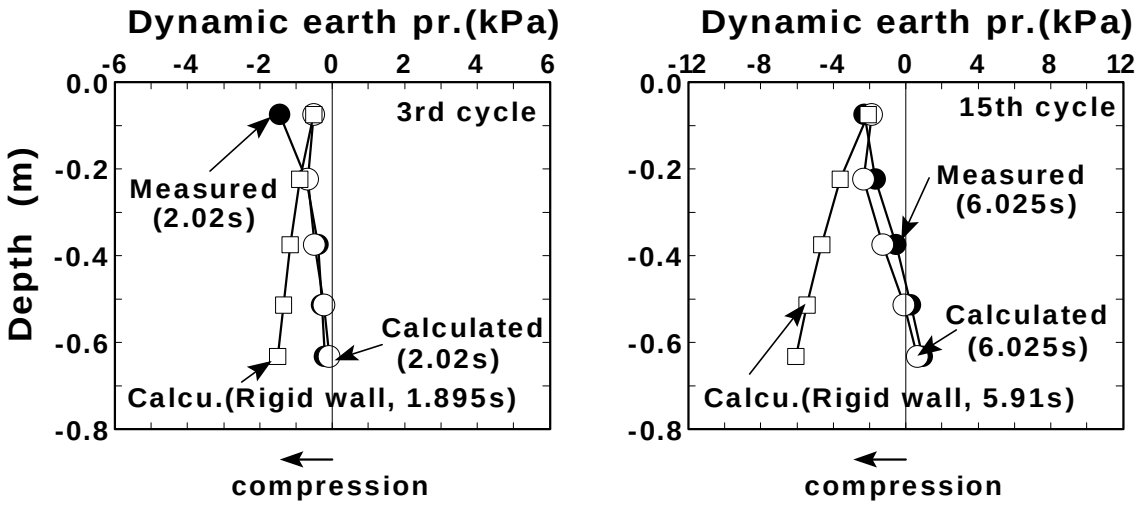

(i) At the resonance (ii) During liquefaction

(c) Distribution of dynamic pressures

Fig.8.14: Measurement and analysis (BD36F3A500 test)

8.3.3 Discussions

Discussion will be made on the proposed solution based on the comparison between the calculated and the measured dynamic earth pressures as presented in the previous section.

Scope of application of the proposed solution

It was shown qualitatively that the calculated dynamic earth pressures by the proposed solution became consistent with the measured dynamic earth pressures after the resonance. It is because that the solution of dynamic earth pressure is derived assuming that the shear modulus of soil is zero. The suitable results could be calculated after the shear modulus of soil decreases to some amount due to liquefaction.

The shear modulus ratios at the resonance are summarized in Table 8.4. The ratio of shear modulus is calculated from the ratio of natural frequencies both the initial and at the resonance. It is seen that the range of shear modulus ratio at the resonance is between 1/80 and 1/600 of the initial shear modulus, in contrast, it is between 1/2400 and zero during liquefaction. Considering that the calculated results at the resonance gives good agreements except for AD39F5A50 and AD41F3A200 tests, the proposed solution assuming zero shear modulus can be applicable to the backfill with shear modulus less than about 1/250 of the initial value.

Table 8.4: Approximate ratio of shear modulus at resonance

Case No.	Natural frequency of the backfill (Hz)			Approximate ratio of shear modulus		Remarks
	Initial	At resonance	Liquefaction	At resonance	Liquefaction	
AD35F3A50	19.5	0.8	0.4	1/600	1/2400	
AD39F5A50*	19.5	2.2	0.4	1/80	1/2400	Inconsistent at resonance
AD41F3A200*	19.5	1.6	0.0	1/150	1/∞	Inconsistent at resonance
AD32F3A500	19.5	1.2	0.0	1/250	1/∞	
BD36F3A500	19.5	1.1	0.0	1/300	1/∞	

*: tests of repeated shaking.

It was observed in Fig.8.14(c)(ii) in BD36F3A500 test that the good agreements were also seen after the bending strain of the wall exceeded the yield bending strain at its bottom (SG7) at 2.7 seconds. It can be considered that the acceleration due to the deflection, which increases monotonically, is very small comparing to the acceleration due to fluctuation. Considering the fact that the acceleration of the wall of the structure has a strong relation to dynamic earth pressure, it is clear that the small acceleration due to the monotonic deflection of wall does not affect dynamic earth pressures. It suggests that the proposed solution can be applicable to flexible structures as long as the wall keeps as a boundary condition of the proposed solution (Eq.(8.3)).

Approximate errors by the proposed solution

It was shown that the calculated distribution with respect to the depth by the proposed solution becomes close to the measured distribution qualitatively. The quantitative difference between the calculated and the measured dynamic earth pressures are calculated.

The maximum value of measured dynamic earth pressure seems to appear at around GL-0.225m. The reason why is that the amplification between the top and the bottom of the flexible structure becomes about 2～3 by resonance in the tests. In this respect, the measured dynamic earth pressure at the depth of GL-0.225m is compared with the calculated values. Only tests of the initial shaking are selected to make comparison under the same condition of backfill. The dynamic earth pressures are summarized in Table 8.5 with errors as the basis for the measured values.

Table 8.5: Comparison of dynamic pressures (Tests of initial shaking, GL-0.225m)

Case No.	Time instance	Measured (kPa)	Calculated by proposed solution (kPa)	Error (%)
AD35F3A50	At resonance	0.769	0.579	-25
	Liquefaction	0.241	0.185	-23
AD32F3A500	At resonance	0.639	0.817	28
	Liquefaction	1.884	2.930	56
BD36F3A500	At resonance	0.721	0.683	-5
	Liquefaction	1.672	2.322	39

Compression as positive

The positive error means that the calculation estimates the measured dynamic earth pressure largely, and the negative error is its inverse. It is seen that the errors are in the range of –25%～56%. The maximum underestimation by the proposed solution can be less than about 30%. It should be noted that this error is derived from only results of limited number of tests.

Effects of frequency and random wave

It is important to discuss on effects of frequency of the proposed solution. However, it is difficult to make exact discussions because of a lack of test results by a variety of frequencies. As long as observing the only result from 5Hz frequency of AD39F5A50 test (see, Fig.8.11(c)), the dynamic earth pressure seems to be predicted qualitatively as good as the test with 3Hz frequency of AD35F3A50 test.

Referring to the previous experimental studies on dynamic interaction between a rigid wall and liquefied soil (see, Chapter 1), significant frequency dependence has not been reported. Also input motions with a variety of frequencies have been used for shaking table tests to study calculation methods for dynamic earth pressures due to liquefied soil (Tuchida (1968): 3Hz; Koga et al.(1996): 1.2Hz and 5Hz; Tanaka.Y. et al.(1994): 10Hz). The proposed solution in this study introduces the same modeling of liquefied soil as in previous studies, assuming zero shear modulus (see, Eqs.(8.4)(8.5)(8.6)). In this respect, it is inferred that the frequency dependence can be small for the proposed solution.

Since real earthquake motions consist of random waves, in the meantime, an applicability of the proposed solution for random waves should be discussed. Assuming that a random wave is superposed by sinusoidal waves with variety of frequencies, the proposed solution can be applicable to problems with random waves which have predominant frequencies of around 3Hz～5Hz. However, it is not clear exactly if the superposition of sinusoidal waves correctly works out for liquefiable ground. It is desirable to assure the applicability of random waves to the proposed solution by experiments. It is one of the future issues.

8.4 CONCLUDING REMARKS

An analytical model to calculate the dynamic earth pressures on flexible wall due to liquefied soil was developed considering the amplification and the phase difference of accelerations of the structure. The followings are conclusions drawn from the study in this chapter:

1. The calculated distributions by the proposed solution of dynamic earth pressures reasonably agree with the measured distributions not only during liquefaction but also at the resonance. On the other hand, the conventional method of calculation, which assumes a flexible structure as a rigid wall, tends to give overestimated dynamic earth pressures.
2. The solution seems to be applicable to the liquefied soil of which the shear modulus decreases to the order of 1/250 of the initial value. Only a result from limited number of tests, the maximum underestimation by the proposed solution can be less than about 30%.
3. The monotonic deformation of the wall seems to give less effect on dynamic earth pressures. The proposed solution can be applicable to flexible box sections as long as the wall keeps the dynamic deflection which is defined as a boundary condition. The slight yielding of the material does not matter when it gives less effect on dynamic deflections of wall.
4. From the observation of the result from the test with input motion of 5Hz frequency, the dynamic earth pressure seems to be predicted as good as the test with input motion of 3Hz frequency. It is desirable to assure the less effects of frequencies and the applicability of random waves to the proposed solution by experiments.

Chapter 9

CONCLUSIONS AND RECOMMENDATIONS

This dissertation deals with the dynamic interaction between the liquefied soil and underground structure during earthquakes. A box-shaped culvert, which has a flexible cross section, is selected as a typical type of underground structure. Study has been conducted in order to investigate experimentally the nature and mechanism of dynamic interaction between underground structure and liquefied soil, and in order to propose a method to quantitatively evaluate the dynamic earth pressure which acts on the flexible wall of underground structure.

A series of 1G shaking table tests was carried out on an aluminum model structure of box section which was embedded in saturated cohesionless soil to achieve those objectives. A special attempt was made to experimentally reproduce a stress-strain relationship as well as an effective stress path of soil around the embedded structure by installing a variety of transducers in the backfill as well as on the structure model. The parameters such as initial relative density of backfill, intensity and frequency of base horizontal motion were varied in tests.

The change of shear modulus of liquefied soil with time, amplification of shaking, and the phase difference between displacement and earth pressures on structure's side face were produced based on the recorded quantities. Analysis of those quantities was made in various aspects of both backfill and structure.

The major results of this study are summarized below.

STRESS-STRAIN RELATIONSHIP OF BACKFILL SOIL DURING EARTH-QUAKE

The stress-strain relationship and the effective stress path were reproduced considering not only the inertia force of a soil mass but also the normal stress difference in the horizontal direction for

shear stress. The shear modulus in each cycle of shaking was calculated from the reproduced stress-strain relationship. The following observations were made:

1. The shape of a reproduced stress-strain curve in a cycle became similar to an ellipse with an inclined axis before the build-up of the excess pore water pressure. The direction of rotation was found to be clockwise. It showed the stress-strain relation ship was reasonably reproduced.
2. The amplitude of shear stress in the loose backfill decreased accompanied by the rise of the excess pore water pressure. In contrast, the amplitude of the shear stress in the dense backfill increased with spiky response as the shaking was continued due to the dilative behavior of soil.
3. It was found that the average shear modulus during liquefaction in the loose backfill at the relative density of 30～40% decreased to the level of 1/500～1/2800 of the initial shear modulus. In the dense backfill of relative density greater than about 70%, the reduction of shear modulus was up to about the level of 1/90～1/300. A dilative behavior of soil prevented the complete loss of shear modulus.
4. Based on the study on the stress-strain relationship of the backfill, the useful information of the property change for backfill near the structure, such as the shear modulus and the natural frequency of backfill, was successfully obtained.

RESPONSE CHARACTERISTICS OF FLEXIBLE UNDERGROUND STRUCTURE SUBJECTED TO SOIL LIQUEACTION

The response characteristics of underground structure subjected to soil liquefaction were investigated. The natural period or natural frequency of backfill was related to the response characteristics of underground structure such as the amplification and the phase difference between the top and the bottom of the structure. The followings are observed:

1. Significant change of amplification and phase difference of underground structure occur before the initial liquefaction. In this time, the shear modulus of backfill decreased rapidly due to pore pressure generation.
2. The backfill with decreased shear modulus elongates the natural period of soil-structure

system, and the process of shear modulus reduction causes the resonance of underground structure itself in the backfill.

3. The maximum pore pressure ratio at resonance is about 0.8 in tests with 3Hz shaking, and about 0.6 in the test with 5Hz shaking. It was considered that ratio of excess pore water pressure at resonance depends on the predominant period of base horizontal motion. When the period of base horizontal motion is long, the resonance occurs in the state of higher pore water pressure ratio. In contrast, when the period of base horizontal motion is short, the resonance occurs at lower pore water pressure ratio.
4. The maximum amplification at resonance of this type of underground structure was experimentally in the range of 2.5～3.0, corresponding to the damping ratio of 0.2～0.3 when the structure was assumed as a single mass spring model. In addition, the amplification during complete liquefaction is experimentally in the range of 1.0～1.5, and phase difference between the top and the bottom of the structure is about 150 degrees.
5. The damping ratio of underground structure at resonance has a correlation with the damping ratio of backfill during shaking. Although a theoretical reason is not clarified, the maximum amplification of underground structure at resonance may have some relation to the damping ratio of liquefied soil.
6. After the initial liquefaction, the backfill behaves either in a contractive manner or in a dilative manner depending on the initial relative density of the backfill. When the backfill behaves in a contractive manner, the acceleration does not amplify by the effect of state of seismic isolation due to liquefied soil. When the backfill behaves in a dilative manner, the complicated change of amplification could occur due to residual shear modulus of backfill.

BEHAVIOR OF BOX-SHAPED FLEXIBLE CROSS SECTION OF STRUCTURE DURING LIQUEFACTION

The behavior of box-shaped flexible cross section of structure during liquefaction was examined based on the measurements from shaking table tests. In addition, a study based on the calculation was performed to assure an internal consistency among measurements. For convenience of analysis, measured earth pressures and curvatures were divided into two components of a

monotonic component and a fluctuating component. The followings are conclusions from the study:

1. From the observation of monotonic component of curvature, it was inferred that the amount of earth pressure of monotonic component was of the same magnitude between left and right, acting on both sides of structure in the opposite direction.
2. The time histories of fluctuating component of curvature were almost identical between left and right walls except for the beginning of shaking. It was indicated that the same amount of fluctuating component of earth pressure acted on structure at both side in the same direction when the backfill became soft due to liquefaction.
3. Assuming a wall as an elastic beam, curvatures of both monotonic and fluctuating component were calculated with appropriate boundary conditions based on the principle of superposition applying earth pressure on the beam. The calculated curvature of monotonic component of wall showed good agreement with the measured curvature of monotonic component at resonance and during liquefaction in tests of initial shaking. In addition, reasonable agreement was also observed in a fluctuating component. It was confirmed that the monotonic and fluctuating quantities measured on the wall (lateral earth pressures, bending strains and accelerations) were internally consistent.
4. Integrating the calculated curvature twice with respect to depth along the beam either mathematically or numerically, the deflections of wall were calculated. Calculated deflection at the top of the structure and wall reasonably agreed with the measured displacements when the natural frequency of backfill decreased less than about 0.4～0.67 times that of the structure. It suggested that the deflection of the flexible box section could be calculated by applying the earth pressure on the structure as long as the natural frequency of backfill was less than about half of that of the structure itself.
5. Considerable disagreement between calculated and measured displacement was observed when the soil behaved in a dilative manner in dense backfill. It was shown that earth pressure of fluctuating component acted as a reaction instantaneously when soil behaves in a dilative manner.

DYNAMIC INTERACTION BETWEEN LIQUEFIED SOIL AND FLEXIBLE UNDERGEROND STRUCTURE

Dynamic effect of lateral earth pressures on flexible cross section was precisely analyzed focusing on the material change of backfill due to liquefaction. The observations were also made of the effect of dilatancy of soil. An influential effect of dynamic earth pressures on flexible structure was examined as well. The followings are derived conclusions:

1. The dynamic earth pressure does not act as the load on the structure until the natural period of ground near the structure becomes longer than that of the structure itself. Since soil liquefaction results in a drastic loss of shear strength, it is often the case the dynamic earth pressure acts as a load on the underground structure during the process of pore water pressure build-up.
2. When the effective stress is increased by the dilative nature of soil under the large shear strain, the dynamic earth pressures act as not only the load but also the reaction of the structure. It could occur after the pore pressure ratio once reached 1.0. It suggests that a dilative nature of soil could prevent the large shear deformation of a cross section of flexible underground structure.
3. The relation between dynamic earth pressures and accelerations on flexible wall becomes stronger than that between dynamic earth pressures and normal strain of the backfill when the shear modulus of loose backfill decreases about less than 100kPa (1/100 of the initial value). This shows that the flexible underground structure is under the control of acceleration when the backfill liquefies.

THEORY OF DYNAMIC LATERAL PRESSURES ON FLEXIBLE WALL SUBJECTED TO SOIL LIQUEFACTION

An analytical model to calculate the dynamic earth pressures on flexible wall due to liquefied soil was developed considering the amplification and the phase difference of accelerations of a structure. Since it was observed that the flexible underground structure was under the control of acceleration during liquefaction, the theory was formulated regarding acceleration of the wall as a key parameter. The followings were suggested in this study:

1. The calculated distributions by the proposed solution of dynamic earth pressures reasonably agree with the measured distributions not only during liquefaction but also at

the resonance. The amount of dynamic earth pressures by proposed solution became smaller than the calculated dynamic pressures by conventional method using Westergaard's theory (1933), which assumes a flexible structure as a rigid wall.

2. The solution seems to be applicable to the liquefied soil of which the shear modulus decreases to the order of 1/250 of the initial value. Only a result from limited number of tests, the maximum underestimation by the proposed solution can be less than about 30%.
3. The monotonic deformation of the wall seems to give less effect on dynamic earth pressures. The proposed solution can be applicable to flexible box sections as long as the wall keeps the dynamic deflection which is defined as a boundary condition. The slight yielding of the material does not matter when it gives less effect on dynamic deflections.
4. From the observation of the result from the test with input motion of 5Hz frequency, the dynamic earth pressure seems to be predicted as good as the test with input motion of 3Hz frequency. It is desirable to assure the effects of frequencies and the applicability of random waves to the proposed solution by experiments.

In those respects, a reasonable calculation method to assess seismic effects on flexible underground structures by liquefied soil is developed. Recommendations for design calculations of cross section subjected to soil liquefaction will be presented in the following section based on this knowledge.

RECOMMENDATIONS

Based on the findings obtained in this study, the following recommendations are proposed to evaluate seismic load on flexible cross section of structure subjected to soil liquefaction:

1. A flexible underground structure, whose natural period is longer than the initial natural period of surrounding ground, has a strong response by resonance in a process of liquefaction. The maximum bending strain of structure usually occurs at the resonance. When horizontal base motion during complete liquefaction is more intense than that during resonance, the maximum value of bending strain possibly occurs during liquefaction. Seismic design calculation should be conducted supposing two states, i) when the underground structure undergoes resonance, and ii) when the backfill

completely liquefies.

2. In either case, seismic loads resulting from the dynamic interaction between structure and liquefied soil are earth pressure and inertia force of the structure. (No effect has to be considered due to seismic deformation of ground). Basic idea of seismic load on the flexible box section is illustrated in Fig.9.1.
3. In addition, initial lateral earth pressure (both effective lateral earth pressure and static water pressure) and monotonic component of earth pressure due to liquefaction should be accounted for in the calculation.
4. Fluctuating component of earth pressure both at resonance and complete liquefaction can be calculated by the proposed method (see Eq.(8.63)). Amplifications and phase difference are summarized in Table 9.1.
5. Monotonic component of earth pressure should be calculated considering the ratio of excess pore water pressure at the backfill. Ratio of excess pore water pressure at resonance and complete liquefaction from test results are shown in Table 9.1. Note that the ratio of pore water pressure at resonance depends on such various parameters as a period of horizontal base motion, natural period of structure and shear strain of backfill during earthquake. Further study is desirable for exact specification.

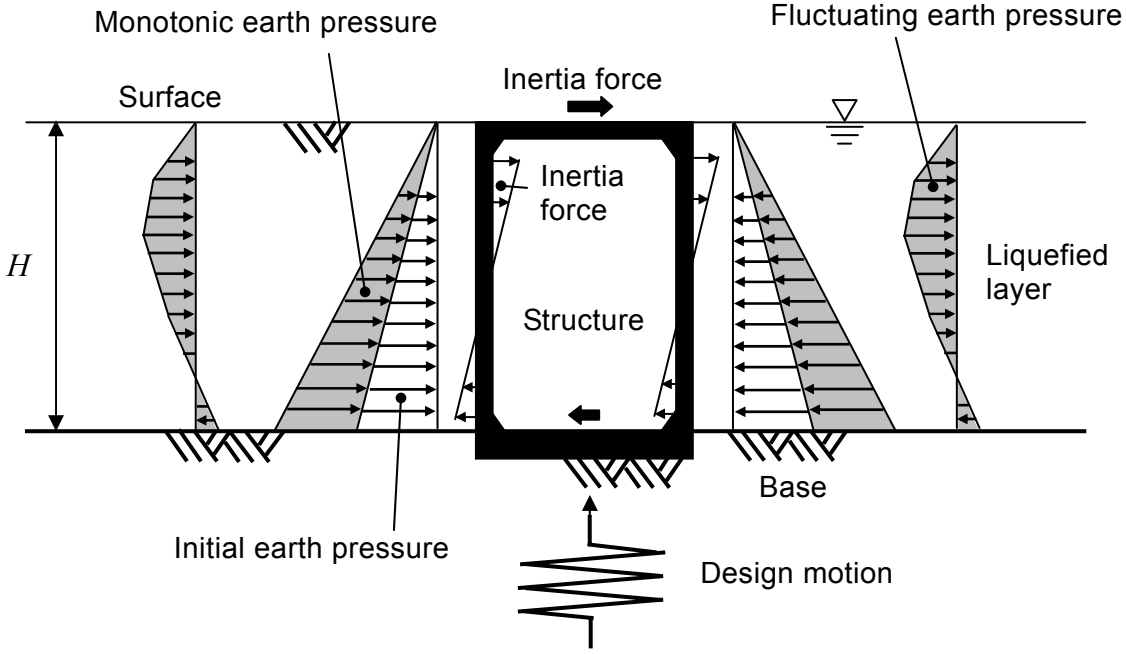

Fig.9.1: Basic idea of seismic load due to liquefied soil on cross section of underground structure

Table 9.1: Summary of key parameters from tests

	At the resonance	At complete liquefaction	Remarks
Amplification	2.5 to 3	1 to 1.5	Fluctuating earth pr. Inertia force
Phase difference	90 deg.	150 deg.	
Ratio of pore water pr.	0.6 to 0.8*	1.0	Monotonic earth pr.

*: Example value derived in a series of tests in this study.

6. When the box section of underground structure deforms significantly either to right or to left direction in the backfill by seismic excitation, a large shear strain cyclically occurs in surrounding soil and induces a dilative behavior of soil. Once the soil behaves in a dilative manner, the soil supports the structure instead of acting as a load. When an extremely strong earthquake is considered in seismic design, a supporting mechanism due to dilative soil should be taken into account in the calculation. For this reason, it is important to investigate the nature of backfill soil in advance.

ISSUES FOR FUTURE

The study presented herein clarified a part of mechanisms and method of evaluation of dynamic earth pressures related to the dynamic interaction between flexible box sections of underground structure and liquefied soil. Therefore, the method presented in this study is applicable to practical problems on underground structures. However, there still exist some issues for future.

In this study, dynamic earth pressures are assessed focusing on the state i) when the structure undergoes resonance in the process of liquefaction with the pore pressure ratio of about 0.6～0.8, and ii) when the soil completely liquefy. Therefore, dynamic earth pressures at the resonance with low pore pressure ratio (e.g. less than 0.5) have not been assessed yet. There is a scope of a future study on dynamic earth pressures at the resonance with less pore pressure ratio. According to

needs, the proposed solution in this study will have to be modified as to take some amount of shear modulus of liquefied soil into account.

Secondly, key parameters such as amplification and phase difference presented in Table 9.1 are a result of a type of small scale model tests without the effects of a rocking motion. It is desirable to confirm those values during shaking based on full scale tests considering rocking motions or records of observations of real underground structures. In addition, the validity of proposed calculation method should be verified based on case study of damaged underground structure in future earthquakes.

Thirdly, the method to evaluate the effect of dilative behavior of backfill should quantitatively be developed for seismic design calculation. It was shown that the fluctuating component of earth pressure acts not as a load but as a reaction cyclically when soil behaves in a dilative manner. It will become more reasonable for underground structure if the effect is taken into account, especially under the condition of strong earthquakes which may cause large deformation of structure.

At last, the achievement of this study is a solution for practical problems on box sections with no or less overburden soil. However, there is a possibility of significant seismic effects due to inertia forces of overburden soil on box sections when the soil-structure system undergoes resonance. In this respect, it is desirable to clarify the effect of overburden soil on box sections of underground structures during seismic liquefaction. Further experimental as well as numerical study is needed for the development.

The author believes that further investigations should be carried out to establish a reasonable seismic design method considering the effects of dynamic interaction between the liquefied soil and underground structure.

REFERENCES

Clough, R.W. and Penzien, J. (1993): “Dynamics of structures, -Second edition-,” McGraw-Hill, Inc.

Ghalandarzadeh, A., Orita, T., Towhata, I. and Yun, F. (1998): “Shaking table tests on seismic deformation of gravity quay walls,” Special Issue of Soils and Foundations, pp.115-132.

Hamada M. (1978). “Earthquake Observation and Numerical Analysis of a Large Underground Tank,” Journal of the Japan Society of Civil Engineering, No.273, 1-14 (in Japanese).

Iida, H., Hiroto, T., Yoshida, N. and Iwafuji, M. (1996): “Damage to Daikai subway station,” Special Issue of Soils and Foundations, pp.283-300.

Inagaki, H., Iai, S., Sugano, T., Yamazaki, H. and Inatomi, T. (1996): “Performance of caisson type quay walls at Kobe port,” Special Issue of Soils and Foundations, pp.119-136.

Ishihara K. (1996). Soil Behavior in Earthquake Geotechnics, OXFORD SCIENCE PUBLICATIONS, New York.

Iwatate, T., Kokusho, T., Tohma, J., Esashi, Y. and Sakurai, A. (1982): “Large Scaled Model Vibration Tests of Embedded Shaft Considering The Effect of Soil Liquefaction,” Technical reports of Central Research Institute of Electric Power Industry, No.381024 (in Japanese).

JAPAN ROAD ASSOCIATION (1992): “Specifications for design and construction of parking structures,” (in Japanese).

JSCE (1986): “Structural Engineering Formulas,” (in Japanese).

JSCE (1998): “Japanese standard for cut-and-cover tunneling,” (in Japanese).

JSCE (2000): “Earthquake Resistant Design Codes in Japan”.

Katada, T. and Hakuno, M. (1981): “Experimental Analysis on Dynamic Behavior of Underground Structures in the Liquefaction Process,” Journal of the Japan Society of Civil Engineering, No.306, pp.1-10, (in Japanese).

Kawama, I., Nishiyama, S., Muroya, K, Haya, H. and Nishimura, A. (2001): “Experimental study on the interaction between soil and structure of cut-and-cover tunnel under earthquake,” Journal of the Japan Society of Civil Engineering, No.689/I-57, pp.127-135, (in Japanese).

Kawashima, K. (1994): “Seismic design of underground structures,” Kajima Institute Publishing,

(in Japanese).

Koga, Y., Matsuo, O., Koseki, J. and Takahashi, A. (1996): ” Study on earthquake-induced earth pressure acting on semi-buried roads,” Technical memorandum of PWRI, No. 3438, (in Japanese).

Kohama E., Miura K., Yoshida N., Ohtsuka N.and Kurita S. (1998). “Instability of Gravity Quay Wall Induced by Liquefaction of Backfill During Earthquake,” Soils and Foundations, Vol.38, No.4, Japanese Geotechnical Society, 71-83.

Kokusho T. and Iwatate T. (1979), “Scaled model tests and numerical analysis on nonlinear dynamic response of soft grounds,” Journal of the Japan Society of Civil Engineering, No.285, pp.57-67, (in Japanese).

Kokusho T. (1980), “Cyclic triaxial test of dynamic soil properties for wide strain range,” Soils and Foundations, Vol.20, Japanese Geotechnical Society, 45-60.

Koseki J. and Koga Y. (1991). “Shaking Table Model Tests on Earth Pressures During Earthquakes Subjected to Soil Liquefaction,” Proceedings of the 46th National conference of civil engineering, JSCE, 224-225 (in Japanese).

Kuribayashi, E., Kawashima, K., Shibata, M. and Miyata, T. (1977): “A study on seismic design method and ultimate strength of cross sections of underground structures by means of the seismic deformation method,” Technical memorandum of PWRI, No. 1253, (in Japanese).

Matsuda, T., Ouchi, H. and Samata, S. (1997): “Seismic damage analysis on box culvert with intermadiate columns,” Journal of the Japan Society of Civil Engineering, No.563/I-39, pp.125-136, (in Japanese).

Matsuo H. and Ohara S. (1960): “Lateral earth pressure and stability of quay walls during earthquakes,” Proceedings of 2nd WCEE, Vol.1, 165-173.

Matsuzawa H., Ishibashi I. and Kawamura M. (1985). “Dynamic Soil and Water Pressures of Submerged Soils,” Journal of the Geotechnical Engineering Division, ASCE, Vol.111, No.10, 1161-1176.

M.M. Dewoolkar, H.-Y. Ko,R.Y.S. Pak. (2000): “Experimental developments for studying static and seismic behavior of retaining walls with liquefiable backfills,” Soil Dynamics and Earthquake Engineering 19, 583-593.

Nakamura, S. (2000): “Evaluation of damage mechanism of subway station based on the difference damage between two damaged subway stations due to the earthquake,” Journal of the Japan Society of Civil Engineering, No.654/I-52, 335-354 (in Japanese).

Nishimura, A. and Sawada, R. (1998): “Experimental Studies on the Seismic Behavior of Pile

Foundations in the Soft Ground," Proceedings of the 10th Japan Earthquake Engineering Symposium, pp.1581-1586 (in Japanese).

Ohtomo, K., Suehiro, T. and Kawai, S. (2002): "Development of advanced earthquake resistant performance verification on reinforced concrete underground structures, Part1 –Experimental aspects of seismically induced plastic deformation performance of underground structures–," Central Research Institute of Power Industry, CRIEPI Report, U01033, (in Japanese).

Penzien, J., Chen, C.H. and Lee, Y.J. (1992): "Seismic analysis of rectangular tunnels in soft ground," Proc. of 10th WCEE, pp.1619-1624.

Port and Harbor Research Institute (1997): "HAND BOOK ON LIQUEFACTION REMEDIATION," Ministry of Transportation, Japan, Balkema.

Railway Technical Research Institute (1999):"Seismic Design Code for Railway structures," (in Japanese).

Samata, S. (1996): "Underground subway damage during the Hyogo-ken Nanbu earthquake and reconstruction technology," Journal of the Japan Society of Civil Engineering, No.534/VI-30, 1-17 (in Japanese).

Sato H., Tanaka Y. Kanatani M., Tamari Y. and Sugisawa M. (1995): "An experimental and numerical study on the behavior of improved ground by DMM against Liquefaction," Proceedings of IS-TOKYO'95, the First International Conference on Earthquake Geotechnical Engineering, 767-772.

Sawada, R. and Nishimura, A. (1998): "Study on behavior of pile foundation during liquefaction," Proceedings of the 10th Japan Earthquake Engineering Symposium, pp.1469-1474 (in Japanese).

Tamura, C., Okamoto, S. and Hamada, M. (1975): "Dynamic behavior of a submerged tunnel during earthquakes," Report of the Institute of Industrial Science, the University of Tokyo, Vol.24, No.5.

Tanaka Y., Kanatani M., Sato H., Sugisawa M. and Tamari Y. (1994). "An Experimental and Analytical Study on the Behavior of Improved Ground by DMM against Liquefaction," Proceedings of the 9th Japan Earthquake Engineering Symposium, 913-918, (in Japanese).

Tanaka H. and Kida H. (1994). "Shaking table model tests on dynamic lateral pressures acting on a flexible wall during soil liquefaction," Proceedings of the 49th National conference of civil engineering, JSCE, 588-589 (in Japanese).

Tateishi, A. (1992): "A study on loading method of seismic deformation method," Journal of the Japan Society of Civil Engineering, No.441/I-18, pp.157-166, (in Japanese).

Tateishi, A. (1995): "A study on seismic analysis method in the cross section of underground structures by means of static finite element method," Journal of the Japan Society of Civil Engineering, No.519/I-32, pp.139-148, (in Japanese).

Tatsuoka, F., Tokida, K., Yoshida, S. and Maruyama, I. (1978): "Shake Table Tests on Dynamic Behaviors of Pile Foundation Model in Liquefying Sand Layers," Proceedings of the 5th Japan Earthquake Engineering Symposium, pp.665-672.

The Japanese Geotechnical Society (1998): "Remedial Measures against Soil Liquefaction," Balkema.

Tohda, J., Yoshimura, H. and Li, L. (1996): "Characteristic Features of Damage to the Public Sewerage Systems in the Hanshin Area," Special Issue of Soils and Foundations, pp.335-347.

Tohma, J., Kokusho, T. and Iwatate, T. (1984): "A study on seismic design for underground structures ,Part 1, -Shaking table model tests on seismic response of soil-structure system-," Central Research Institute of Power Industry, CRIEPI Report, No.383023 (in Japanese).

Tokimatsu, K. and Nomura, S. (1991): "Effects of Ground Deformation on Pile Stresses During Soil Liquefaction," Journal of Structure Construction Engineering, Architectural Institute of Japan, No.426, pp.107-113 (in Japanese).

Tsuchida H. (1968). "Dynamic Pressures on Walls due to Liquefied Sandy Ground," Tsuchi-to-kiso, Japan Geotechnical Society, No.526, 3-10 (in Japanese).

Watanabe K. and Suehiro T. (1991a). "An Experimental Study on Dynamic Earth Pressure Acting on Side Walls of Underground Conduit," Journal of the Japan Society of Civil Engineering, No.432/I-16, 155-163 (in Japanese).

Watanabe K. and Suehiro T. (1991b). "A Method to Estimate the Normal Dynamic Earth Pressure Acting Horizontally on Side Walls of Underground Conduit," Journal of the Japan Society of Civil Engineering, No.432/I-16, 165-174 (in Japanese).

Watanabe K. and Suehiro T. (1991c). "A Theory on Dynamic Earth Pressures Acting Horizontally on Underground Conduit During Earthquake," Journal of the Japan Society of Civil Engineering, No.432/I-16, 185-194 (in Japanese).

Westergaard, H.M. (1933). "Water Pressures on Dams During Earthquake," Transaction of ASCE, Vol.98, 418-472.

Yamato, T., Umehara, T., Aoki, H., Nakamura, S., Ezaki, J. and Suetomi, I. (1996): "Damage to Daikai subway station of Kobe rapid transit system and estimation of its reason during the 1995 Hyogoken-nanbu earthquake," Journal of the Japan Society of Civil Engineering, No.537/I-35, 303-320 (in Japanese).

Appendix A

PERFORMANCE OF EARTH PRESSURE TRANSDUCERS IN SATURATED SOIL

A.1 GENERAL REMARKS

One of the key measurements in this study was made of the dynamic earth pressure in saturated soil by using "earth pressure transducers". Although there were some meaningful achievements in the use of earth pressure transducers attached on the wall tightly (Dewoolkar, et al., 2000), no reliable data was obtained from earth pressure transducers embedded in saturated soil (EP1 to EP 5 shown in Fig.2.6). It was necessary to demonstrate that the earth pressure measurements in saturated soil were reliable. For this purpose, the following measure was taken. One could integrate the measured inertia forces of soil mass to calculate the dynamic earth pressures without the earth pressure transducers. When the sand deposit was shaken in the vertical direction, the dynamic earth pressure can be calculated with the boundary condition of zero at the ground surface.

In this section, the performances of the earth pressure transducers in saturated soil were investigated. A series of vertical shaking tests of model ground was conducted by using the container shown in Fig.2.2. It was assumed therein that the earth pressure transducers attached firmly on the bottom of the container provided the correct dynamic earth pressures.

A.2 MATHEMATICAL FORMULATION

A free body diagram of a simplified soil mass is shown in Fig.A.1. It is assumed that the shear stress on the wall of the container is only a friction of effective lateral pressure. Also, the coefficient of earth pressure K and the friction δ are constant with respect to the depth.

Vertical dynamic earth pressure $\sigma_z(z, t)$, vertical acceleration $\alpha_z(z, t)$, and the friction between the soil and the wall of container $\tau(z, t)$ are functions of depth z and time t. Coefficient of earth pressure $K(t)$, and coefficient of friction $\delta(t)$ are only functions of time t. The boundary

conditions are given by

1. $\sigma_z(0, t)=0$ at the ground surface (z=0)
2. $\sigma_z(H, t)$ is known (the dynamic earth pressure at the rigid bottom is measured)

Considering force equilibrium in the vertical direction, it can be shown that

$$-\rho\alpha_z = \frac{\partial\sigma_z}{\partial z} + 2\tau\frac{B+L}{BL} \tag{A.1}$$

where ρ is the mass density of saturated soil, B and L are width and length of the container (B=0.8m, L=1.2m), respectively. A frictional shear stress, τ, is expressed as;

$$\tau(\mathrm{z},\mathrm{t}) = \sigma_h' \cdot \delta = K\sigma_v' \cdot \delta = K(t)\delta(t)\cdot(\rho-\rho_w)\int_0^z [g+\alpha_z(\varsigma,t)]\,d\varsigma \tag{A.2}$$

where σ_h' and σ_v' are the effective horizontal and vertical pressures, ρ and ρ_w are mass densities of saturated soil and water, and ζ is a dummy integration valuable.

Integrating Eq.(A.1) with respect to z, the dynamic earth pressure at any depth and a particular time instance t_1 is calculated considering the boundary condition $\sigma_z(0, t)=0$ at the surface;

$$\sigma_z(z,t_1) = -\int_0^z \rho\alpha_z(\xi,t_1)d\xi - 2\frac{B+L}{BL}K(t_1)\delta(t_1)\cdot(\rho-\rho_w)\int_0^z\int_0^\xi [g+\alpha_z(\varsigma,t_1)]d\varsigma d\xi \tag{A.3}$$

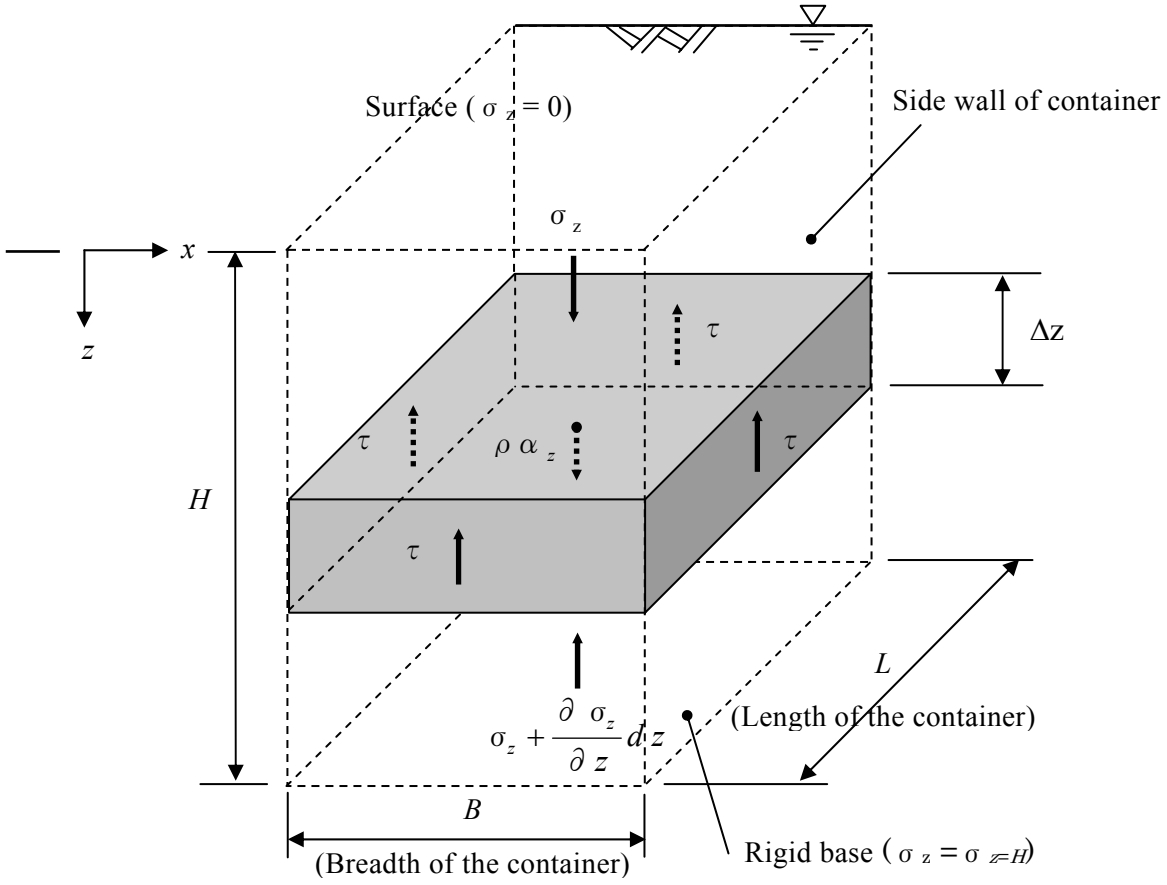

σ_z : Dynamic earth pressure in the vertical direction

α_z : Vertical acceleration in saturated soil

τ : Friction between the soil and the wall

Fig.A.1: Free-body diagram of soil mass in container in the vertical direction

where ξ is a dummy integration valuable. The dynamic earth pressure at the bottom ($z = H$) is calculated in the same manner as

$$\sigma_z(H,t_1) = -\int_0^H \rho\alpha_z(\xi,t_1)d\xi - 2\frac{B+L}{BL}K(t_1)\delta(t_1)\cdot(\rho-\rho_w)\int_0^H\int_0^\xi [g+\alpha_z(\varsigma,t_1)]d\varsigma\, d\xi \quad \text{(A.4)}$$

The product $K(t)\,\delta\,(t)$, which is unknown, is calculated from Eq.(A.4) as

$$K(t_1)\cdot\delta(t_1) = \frac{\left(\sigma_z(H,t_1) + \int_0^H \rho\alpha_z(\xi,t_1)d\xi\right)}{\left[-2\frac{B+L}{BL}(\rho-\rho_w)\int_0^H\int_0^\xi [g+\alpha_z(\varsigma,t_1)]d\varsigma\, d\xi\right]} \quad \text{(A.5)}$$

Substituting Eq.(A.5) into Eq.(A.3), the dynamic earth pressure in saturated soil is expressed as

$$\sigma_z(z,t_1) = -\int_0^z \rho\alpha_z(\xi,t_1)d\xi + \frac{\left(\sigma_z(H,t_1) + \int_0^H \rho\alpha_z(\xi,t_1)d\xi\right)\left(\int_0^z\int_0^\xi [g+\alpha_z(\varsigma,t_1)]d\varsigma\, d\xi\right)}{\left[\int_0^H\int_0^\xi [g+\alpha_z(\varsigma,t_1)]d\varsigma\, d\xi\right]} \quad \text{(A.6)}$$

When the amplification of vertical acceleration between the bottom and the surface is nearly equal to one, the denominator of Eq.(A.6) is rewritten approximately as

$$\left[\int_0^H\int_0^\xi [g+\alpha_z(\varsigma,t_1)]d\varsigma\, d\xi\right] = \left(g+\alpha_z(t_1)\right)\cdot\frac{H^2}{2} \quad \text{(A.7)}$$

Consequently, Eq.(A.6) is reduced to be

$$\sigma_z(z,t_1) = -\int_0^z \rho\alpha_z(\xi,t_1)d\xi + \left(\sigma_z(H,t_1) + \int_0^H \rho\alpha_z(\xi,t_1)d\xi\right)\cdot\frac{z^2}{H^2} \quad \text{(A.8)}$$

Thus, at each time step, by using a suitable integration scheme, the dynamic earth pressure at any depth in saturated soil is obtained. Combining calculated dynamic earth pressures at all time steps, complete time histories of dynamic earth pressures are obtained.

In a soil deposit of deal horizontal stratification, force equilibrium in the vertical direction becomes as

$$-\rho\alpha_z = \frac{\partial\sigma_z}{\partial z} \quad \text{(A.9)}$$

In this situation, the dynamic earth pressure at any depth at particular time instance t_1 is calculated by integrating Eq.(A.9) with respect to z as

$$\sigma_z(z,t_1) = -\int_0^z \rho\alpha_z(\xi,t_1)d\xi \tag{A.10}$$

In the following study, calculated dynamic earth pressures by Eqs.(A.8) and (A.10) were assumed as true dynamic earth pressures in saturated soil.

A.3 SHAKING TABLE TEST

Equipment

The experimental apparatus consisted of the shaking table, the container, and the instrumentation and data acquisition system. The same shaking table, the container, and the data acquisition system as described in the section 2.2 were used in this series of vertical shaking tests.

The dynamic earth pressures were measured by using six earth pressure transducers in saturated sand and at the bottom of the container. The vertical acceleration and excess pore water pressures in the soil were also measured by using the accelerometers and pore pressure transducers, respectively. The locations of these transducers are shown in Fig.A.2. The same transducers as shown in the section 2.3.2 were used in the test.

The earth pressure transducers were located at two places in three depths, in which two at the bottom of the container were fixed firmly by using adhesive. Each earth pressure transducer in the soil was mounted directing the sensing membrane upward. The mass density of earth pressure transducers and accelerometers were adjusted to 1.8 of the specific gravity not to sink in the soil when soil liquefied. Furthermore they were attached on thin plastic plates of which the thickness was 2mm as shown in Fig.A.3 to mitigate the rotation and translation in the vertical direction during shaking. The transducers for earth pressure and acceleration thus prepared are shown in Photo.A.1.

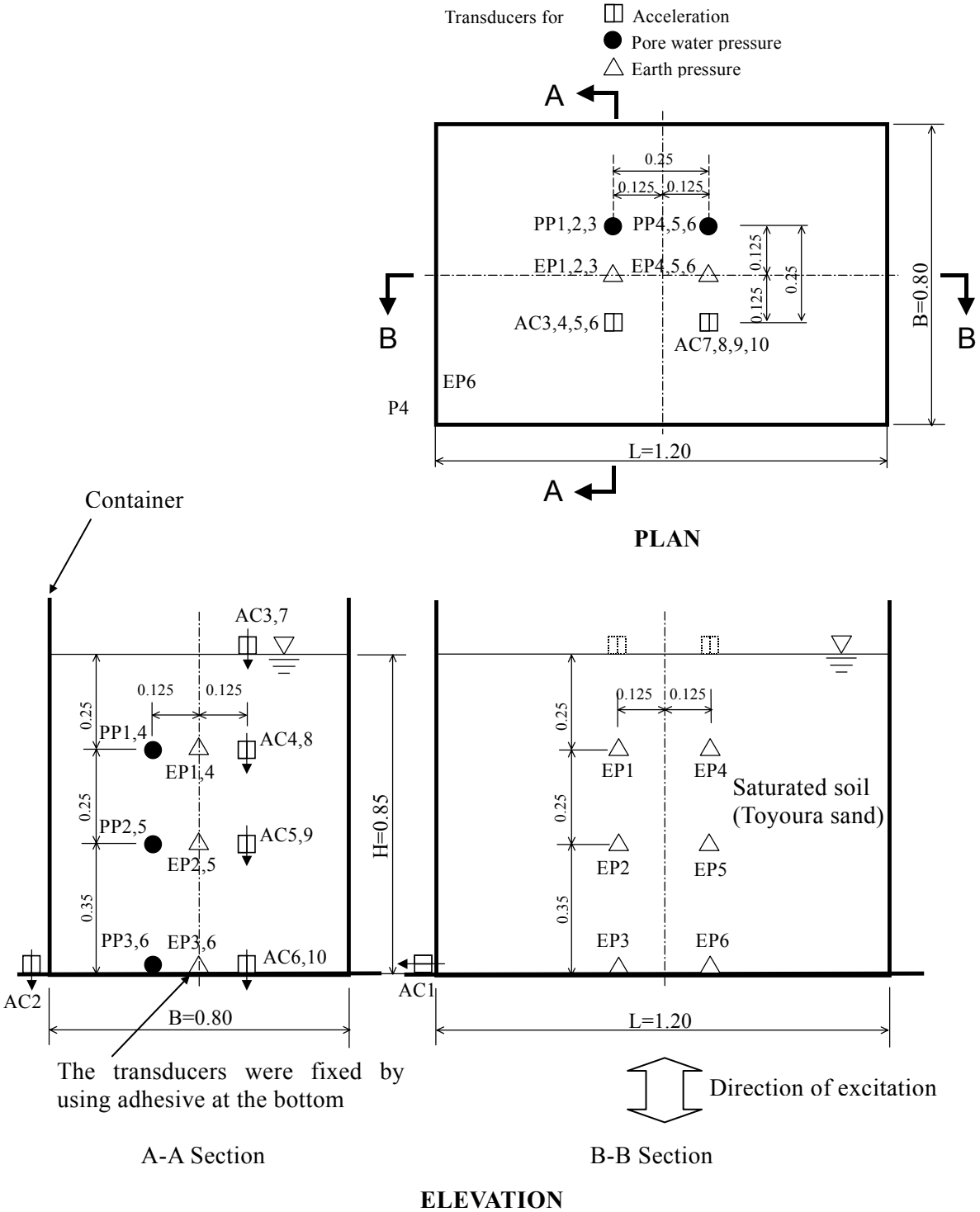

Fig.A.2: Location of transducers in the model ground

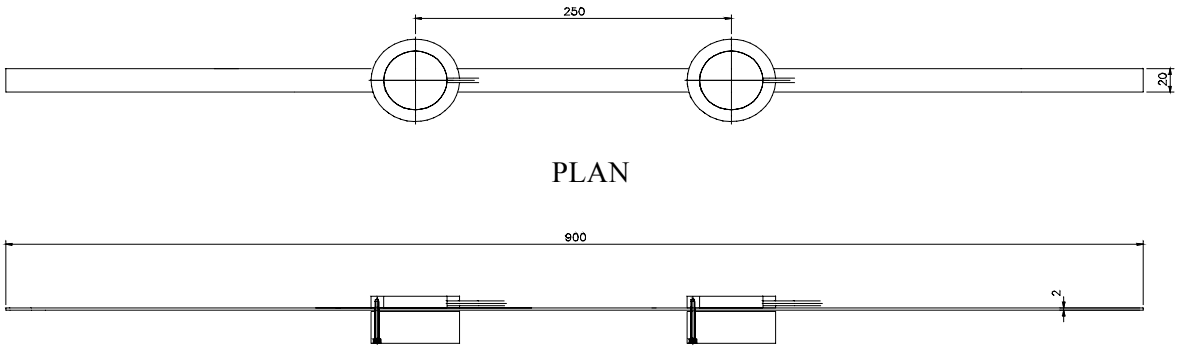

(a) Earth pressure transducers (Density adjustment, S.G.=1.8)

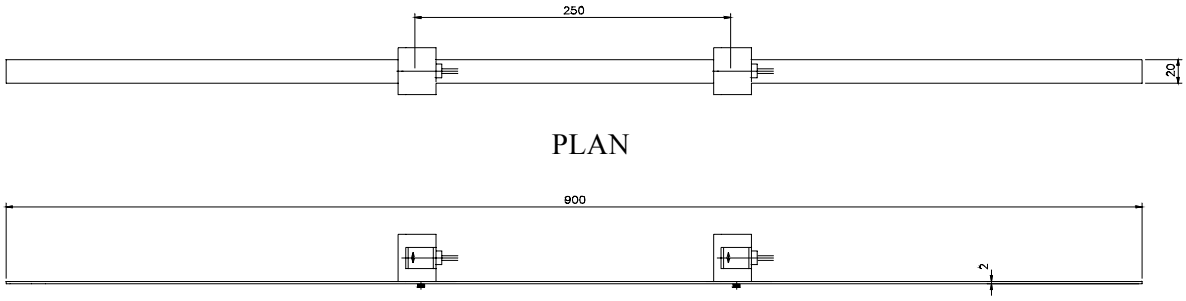

(b) Accelerometers (Density adjustment, S.G.=1.8)

Dimensions are in millimeters

Fig.A.3: Transducers placed in saturated soil

(a) Earth pressure transducer

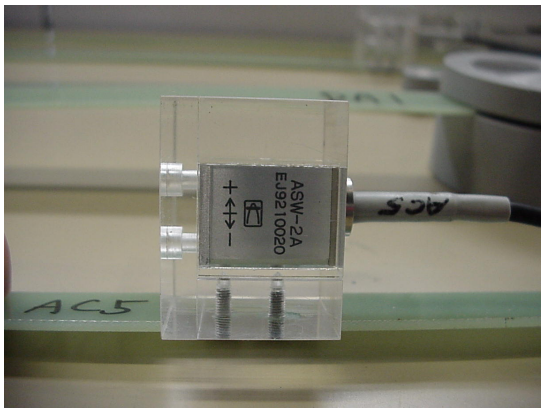

(b) Accelerometer

Photo.A.1: Transducers installed in saturated soil

Materials

All the tests herein were conducted using Toyoura sand that is the same sand as used in the shaking table tests of the underground structure. Its physical properties are shown in Table A.1.

Table A.1. Properties of Toyoura sand used in the test

Specific gravity, *Gs*	2.677
Maximum Void Ratio, e_{max}	0.972
Minimum Void Ratio, e_{min}	0.635
D50	0.2 mm

Testing Procedure

Preparation of model ground

The model ground was prepared inside the container. First, the transducers were fixed at the bottom of the container. The container was filled with deaired water and then air dried sand was rained through a sieve which was submerged slightly in the water. The transducers at the level of 0.35m and 0.60m from the bottom were placed when the surface of soil attained each determined elevations. Thus, a uniform sand deposit was prepared with a relative density of 38%. The setup of model ground is illustrated in Photo.A.2.

For tests involving denser deposits of 70% relative density, the model ground was subjected to shaking in the horizontal direction (1.0m/sec^2 or 2.0m/sec^2 acceleration at 3Hz or 5Hz frequency) until the required density was achieved. For all the tests, the level of water in the container was maintained at the surface sand and excess water on the surface of the deposit was removed by means of a tank in which the air pressure inside was lowered by vacuum pump.

Input motion

A sinusoidal vertical acceleration with a various amplitude (0.5m/sec^2, 1.0m/sec^2, 2.0m/sec^2) and frequency (3Hz, 5Hz, 10Hz) was given as the input shaking force. Initially, the input acceleration was gradually increased to the predetermined maximum value in ten cycles, and then it was maintained constant for ten cycles. Finally, the acceleration was gradually decreased to zero in ten cycles. The input motion of 5Hz is shown in Fig.A.4(a). The axis of ordinates is normalized by the maximum amplitude in the figure.

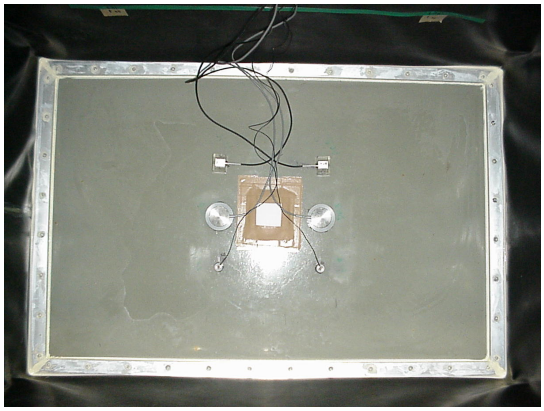

(a) Transducers fixed at the bottom of container

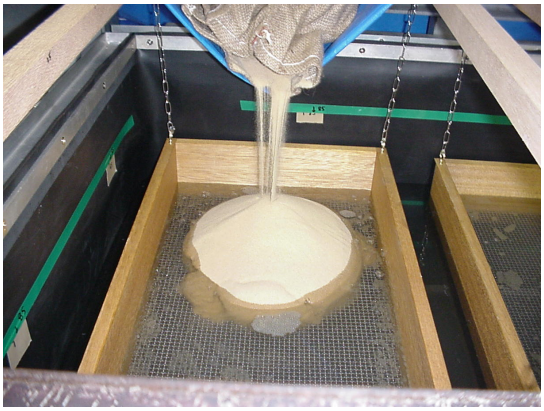

(b) Preparation of ground by water pluviation

(c) Adjustment of the installing depth

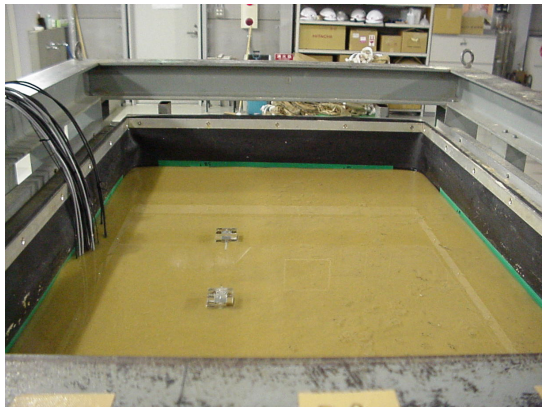

(d) Overview of the model ground

Photo.A.2: Setup of the model ground

For the tests of liquefied soil, horizontal shaking was made first in order to trigger liquefaction and then the liquefied ground was shaken in the vertical direction. The input motion in the horizontal direction is illustrated at the top of Fig.A.4(b), and the input motion in vertical direction is shown in the bottom of Fig.A.4(b).

Experimental program

A total of 22 shaking table tests were performed, in which 18 were for unliquefied soil and 4 for liquefied soil. The experimental programs are shown in Table A.2 and Table A.3 for unliquefied soil and liquefied soil, respectively. Frequency and acceleration of input motion as well as density of soil were varied in the program.

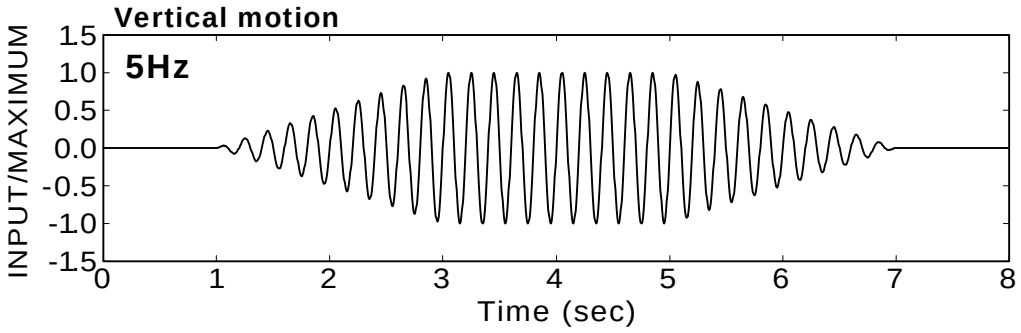

(a) Tests for unliquefied ground

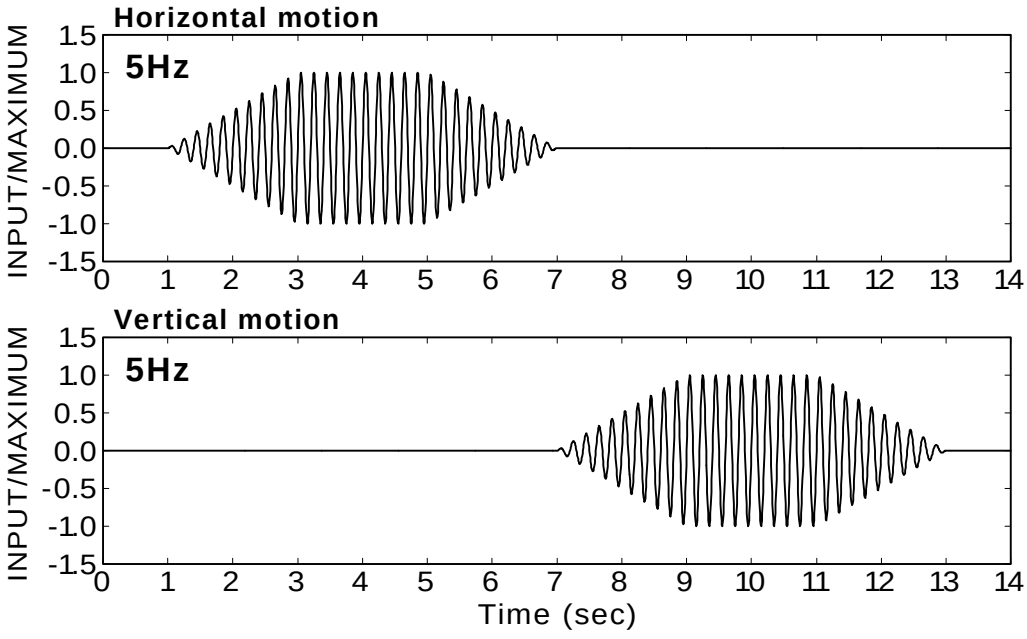

(b) Tests for liquefied ground

Fig.A.4: Example of input motion（Frequency of 5Hz）

Table A.2: Experimental program for the tests on unliquefied ground

Case No	Frequency (Hz)	Acceleration (m/sec^2)	Relative density (%)	Remarks
NLF3A50D38	3	0.5	38	
NLF3A100D40	3	1.0	40	
NLF3A200D40	3	2.0	40	
NLF3A50D70	3	0.5	70	
NLF3A100D70	3	1.0	70	
NLF3A200D70	3	2.0	70	
NLF5A50D38	5	0.5	38	
NLF5A100D40	5	1.0	40	
NLF5A200D40	5	2.0	40	
NLF5A50D70	5	0.5	70	
NLF5A100D70	5	1.0	70	
NLF5A200D70	5	2.0	70	
NLF10A50D38	10	0.5	38	
NLF10A100D39	10	1.0	39	
NLF10A200D40	10	2.0	40	
NLF10A50D70	10	0.5	70	
NLF10A100D70	10	1.0	70	
NLF10A200D70	10	2.0	70	

Table A.3: Experimental program for the tests on liquefied ground

Case No	Frequency (Hz)	Acceleration (m/sec^2)	Relative density (%)	Remarks
LIQF3A100D57	3	1.0	57	Input motion Fig.A.4(b) was applied.
LIQF3A200D60	3	2.0	60	
LIQF5A100D51	5	1.0	51	
LIQF5A200D68	5	2.0	68	

A.4 MEASUREMENT AND ANALYSIS

Measurements

Fig.A.5 shows the time histories of acceleration, earth pressure in the vertical direction, excess pore water pressures for a typical test of unliquefied soil (NLF3A100D40). It could be seen that the horizontal acceleration on the shaking table (AC1), which was not controlled as the input motion, was much weaker than the vertical acceleration. The oscillations were seen in the time histories of

earth pressure and excess pore water pressures during shaking. The post shaking residual value of excess pore water pressure was zero indicating that no liquefaction was induced by the vertical shaking.

Fig.A.6 compares the time histories for a typical test of liquefied soil (LIQF3A100D57 with those in Fig.A.5). The horizontal excitation was given first to make soil liquefy completely, and then the liquefied ground was shaken in the vertical direction. As shown in the time history of excess pore water pressure (Fig.A.6(c)), the pressure reached the initial effective vertical pressure at about 6.5 second, indicating complete liquefaction. Thus, it was considered that the friction between the wall of the container and the soil was reduced to zero, Eq.(A.10) was applicable to calculate the dynamic earth pressures in saturated soil by means of the measurement of accelerations. The oscillations of earth pressure were seen during vertical shaking from 14 seconds to 24 seconds. The residual value in AC4 recorded implies that the accelerometer tilted slightly in the liquefied soil.

The time histories of all the tests for unliquefied soil and liquefied soil are presented in Fig.A.11～Fig.A.30 at the end of the chapter. Table A.2 and Table A.3 are referred to for the specification of these tests such as frequency, acceleration, density of soil. The accelerations, amplifications and ratios of excess pore water pressure are summarized in Table A.4. The maximum vertical accelerations at the table were nearly equal to the nominal input accelerations at the frequency of 3Hz and 5Hz. In contrast, the maximum accelerations were slightly higher than the nominal accelerations at the frequency of 10Hz. In this case, the horizontal accelerations, that were intended to be zero, became 0.24m/sec^2. This suggested that the shaking table was not controlled exactly under the condition of 10Hz frequency. The amplifications of the vertical acceleration were calculated by dividing the maximum amplitude at the surface (AC3) by the bottom acceleration (AC6). It was shown that the amplifications of accelerations were approximately 1.0 in most of the tests. It suggested that Eq.(A.8), which assumes constant acceleration in the vertical direction, is safely used to calculate the dynamic earth pressures from accelerations instead of Eq.(A.6). In the tests of NLF10A100D39, NLF10A200D40, the amplifications became larger than others and the ratio of excess pore pressure rose to more than 0.9. The time histories of NLF10A100D39 test are shown in Fig.A.17. In this test, the horizontal maximum acceleration at the shaking table (AC1) was as much as 0.24m/sec^2. This horizontal acceleration that was produced by accident induced soil liquefaction. Since the reason why the horizontal acceleration was produced by 10Hz vertical shaking is not known, those tests with unexpected excess pore pressure rise are not employed in the calculation of earth pressures.

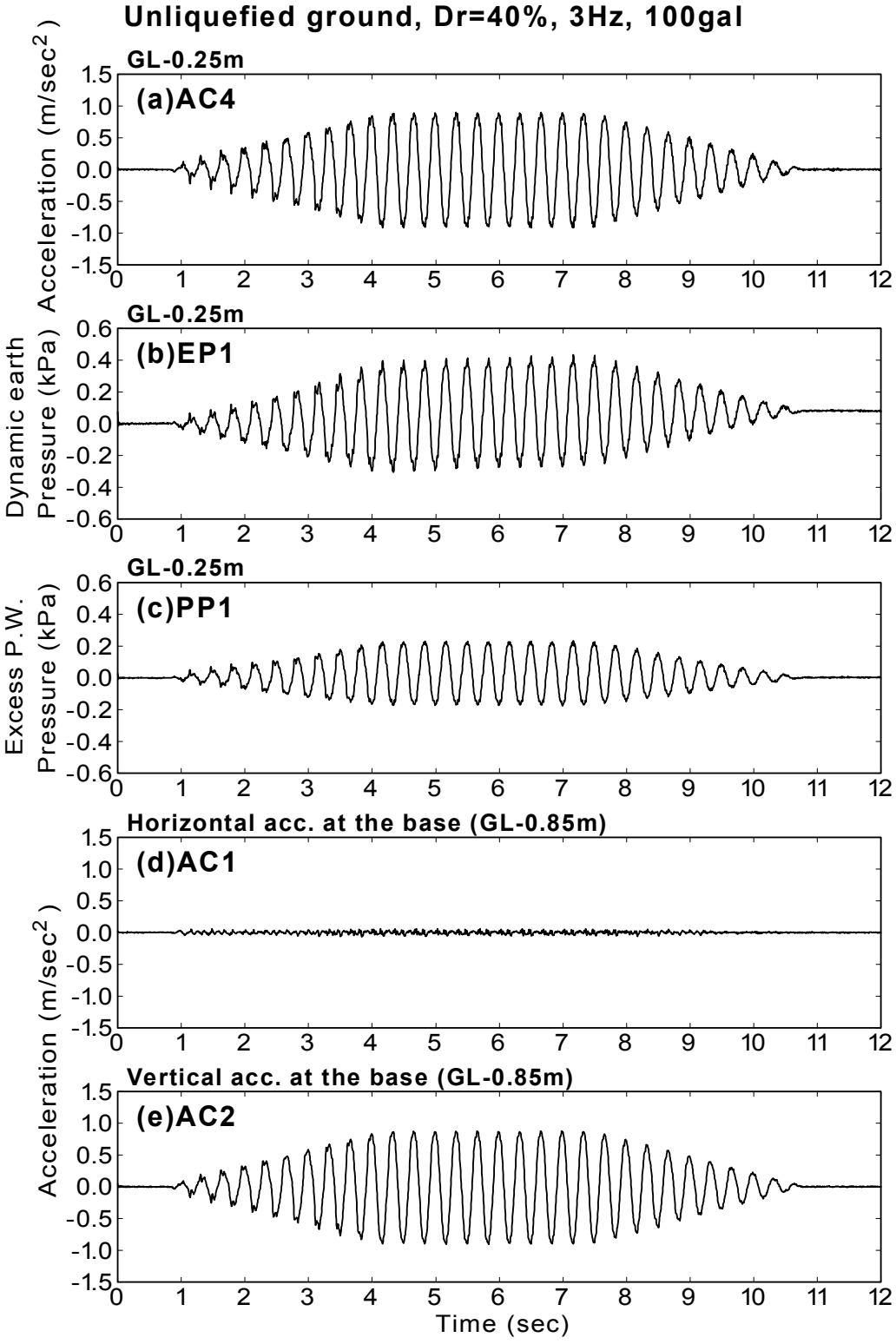

Fig.A.5: Time histories for unliquefied ground (NLF3A100D40 test)

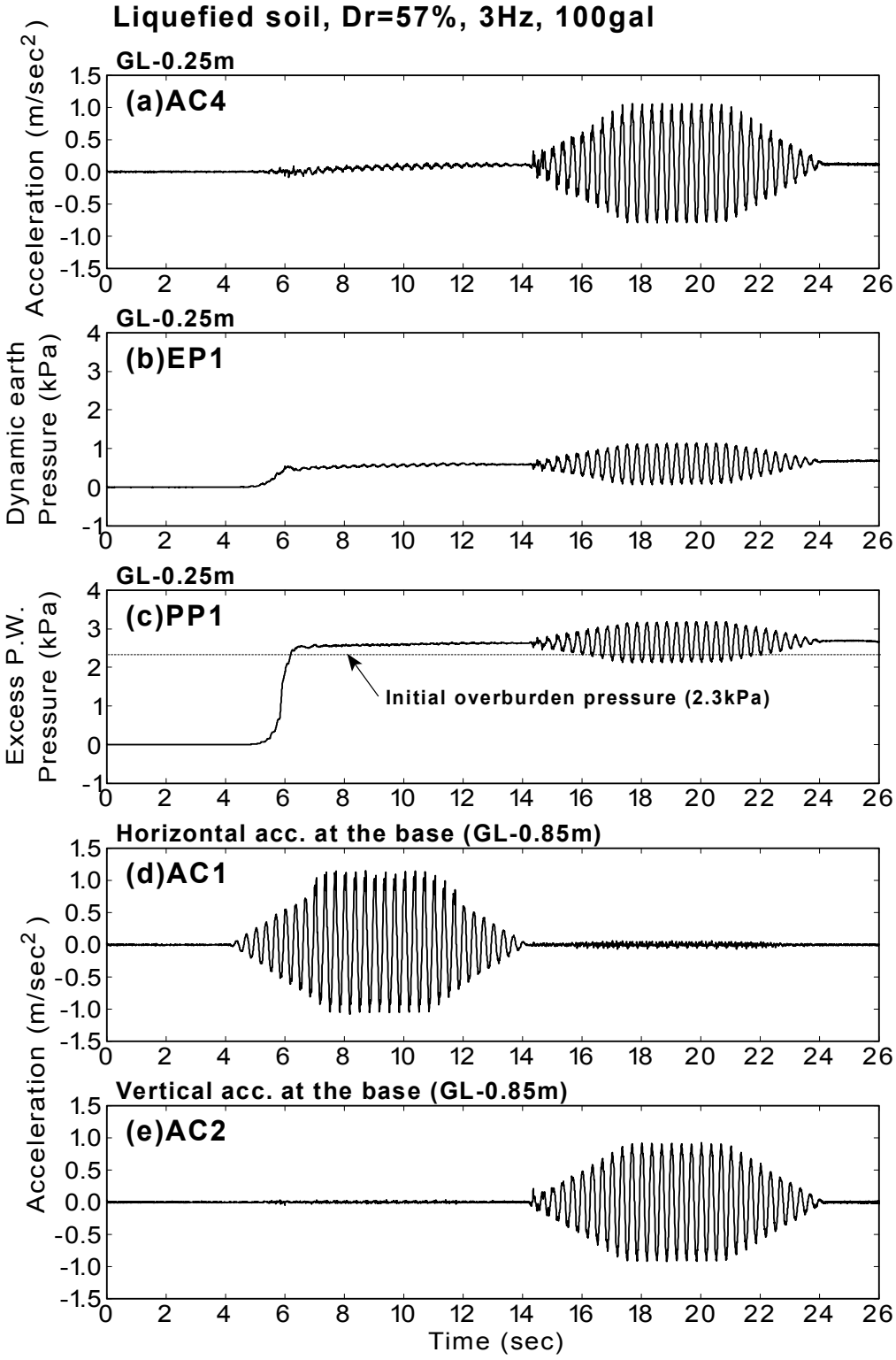

Fig.A.6: Time histories for liquefied ground (LIQF3A100D57 test)

Table A.4: Amplification and ratio of excess pore water pressures

Case No	Maximum acceleration at the table (m/sec^2)		Amplification ($AC3_{max}/AC6_{max}$)	Ratio of E.P.W. pressure
	Vertical acc. (AC2)	Horizontal acc. (AC1)		
NLF3A50D38	0.48 (0.5)	0.05 (0.0)	1.04	0.0
NLF3A100D40	0.91 (1.0)	0.07 (0.0)	1.02	0.0
NLF3A200D40	1.90 (2.0)	0.11 (0.0)	1.03	0.1
NLF3A50D70	0.48 (0.5)	0.07 (0.0)	1.04	0.0
NLF3A100D70	0.92 (1.0)	0.13 (0.0)	1.02	0.0
NLF3A200D70	1.89 (2.0)	0.12 (0.0)	1.02	0.0
NLF5A50D38	0.65 (0.5)	0.10 (0.0)	1.04	0.0
NLF5A100D40	1.16 (1.0)	0.12 (0.0)	1.08	0.05
NLF5A200D40	1.97 (2.0)	0.10 (0.0)	1.04	0.1
NLF5A50D70	0.56 (0.5)	0.07 (0.0)	1.02	0.0
NLF5A100D70	1.08 (1.0)	0.07 (0.0)	1.02	0.0
NLF5A200D70	1.93 (2.0)	0.10 (0.0)	1.02	0.0
NLF10A50D38	0.70 (0.5)	0.07 (0.0)	1.11	0.1
NLF10A100D39	1.45 (1.0)	0.24 (0.0)	1.37*	1.0
NLF10A200D40	2.67 (2.0)	0.15 (0.0)	1.23*	0.95
NLF10A50D70	0.67 (0.5)	0.12 (0.0)	1.10	0.1
NLF10A100D70	1.25 (1.0)	0.09 (0.0)	1.06	0.0
NLF10A200D70	2.62 (2.0)	0.16 (0.0)	1.11*	0.2
LIQF3A100D57	0.92 (1.0)	1.15 (1.0)	1.06	1.0
LIQF3A200D60	1.87 (2.0)	2.22 (2.0)	1.06	1.0
LIQF5A100D51	1.08 (1.0)	1.06 (1.0)	1.12	1.0
LIQF5A200D68	1.96 (2.0)	2.38 (2.0)	1.09	1.0

( ): nominal value * Excess pore water pressure built up by accident.

Analysis

Dynamic earth pressures in unliquefied models (tests of NL series) were calculated using Eq.(A.8) and those in the liquefied soil (tests of LIQ series) were calculated using Eq.(A.10). For this purpose, a piece-wise linear interpolation of acceleration profile was prepared at each time step of data acquisition. The measured dynamic earth pressures at the bottom of the container give correct quantities since the transducer is fixed at the rigid base. The time interval was 0.005sec corresponding to the sampling rate of 200Hz. The long-period components of acceleration time history were removed by a digital filtering procedure before the calculation. The frequencies of high pass filtering are shown in Table A.5.

Table A.5: Filtering frequency

Frequency of input motion	Filtering frequency (High pass filter)
3Hz	1.5Hz
5Hz	4Hz
10Hz	4Hz

The time histories of calculated dynamic earth pressures were compared with measured quantities. The calculated dynamic earth pressures are taken as true quantities in this comparison. A typical result of unliquefied soil (NLF3A100D40) is shown in Fig.A.7. Expression of "Measured" is the quantity derived by the earth pressure transducers, and "Calculated" is the dynamic earth pressures calculated from accelerations by Eq.(A.8) or Eq.(A.10).

It can be seen that the measured quantities at GL-0.25m and GL-0.50m shows very good agreements with the calculated dynamic pressures through the duration time of vertical excitation as shown in Fig.A.7(a). Both time history curves agree very well as indicated in Fig.A.7(b). Fig.A.8 illustrates time history curves of measured quantities and calculated dynamic earth pressures in a typical test of liquefied soil (LIQF3A100D57). The amplitudes of measured quantities are slightly larger than that of calculated dynamic pressures. As shown in Fig.A.8(b), no phase difference is observed between the measured and the calculated pressures.

Time histories of all the tests with unliquefied soil and all the tests with liquefied soil are presented in Fig.A.31～Fig.A.50 at the end of the chapter. Table A.2 and Table A.3 are referred to for the specification of these tests such as frequency, acceleration, density of soil.

Selected values of measured quantities are compared with the calculated dynamic earth pressures at the same time instances. The peak values of measured quantities in each cycle were selected for the comparison. Fig.A.9 shows the results for test NLF3A100D40 (Fig.A.7) and test LIQF3A100D57 (Fig.A.8) as examples. The coefficient of correlation and coefficients of linear regression are shown in each figure. Linear regression is defined as

$$\text{Measured quantities} = A \times (\text{Calculated quantities}) + B \tag{A.11}$$

The results of all the tests are summarized in Table A.6. Average value of coefficient A is 1.030 and coefficient B is -0.002, indicating that the measured quantities are equal to the calculated quantities which are based on the inertia force of soil mass.

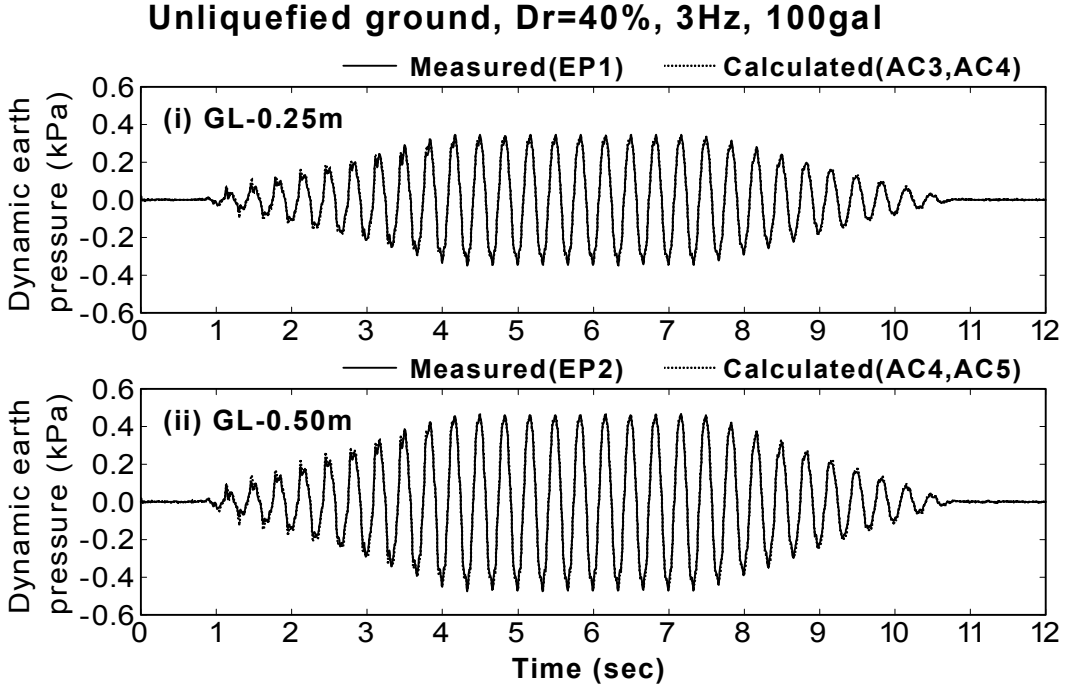

(a) During vertical excitation (0sec to 12 sec)

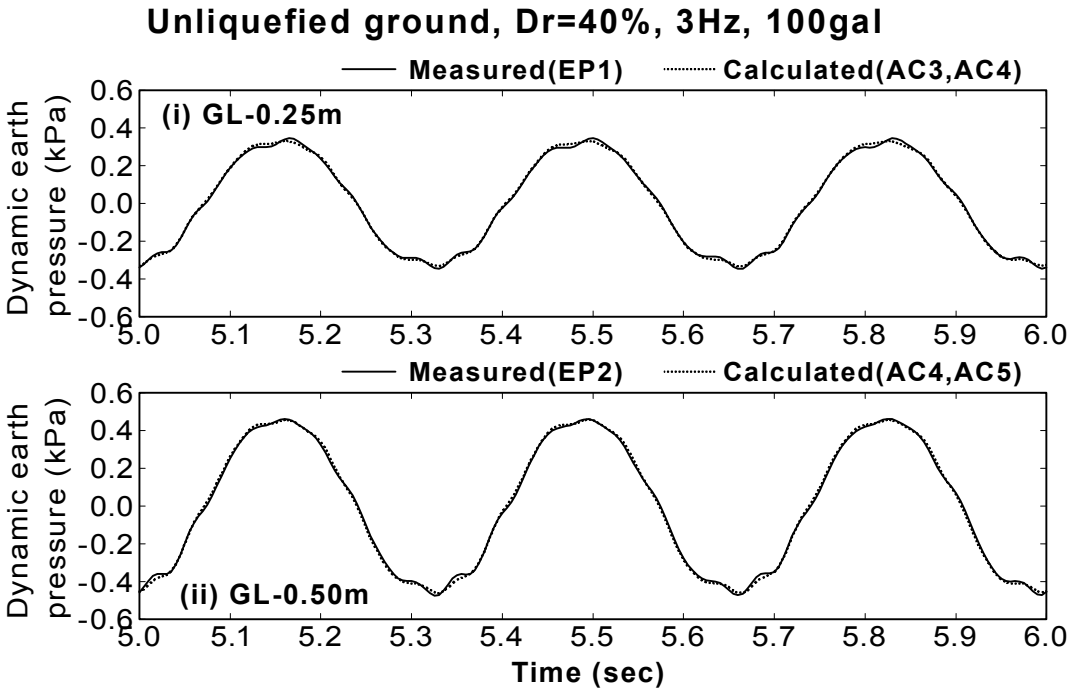

(b) Enlarged with respect to time (5.0sec to 6.0sec)

Fig.A.7: Comparison between measured and calculated dynamic earth pressures (NLF3A100D40 test)

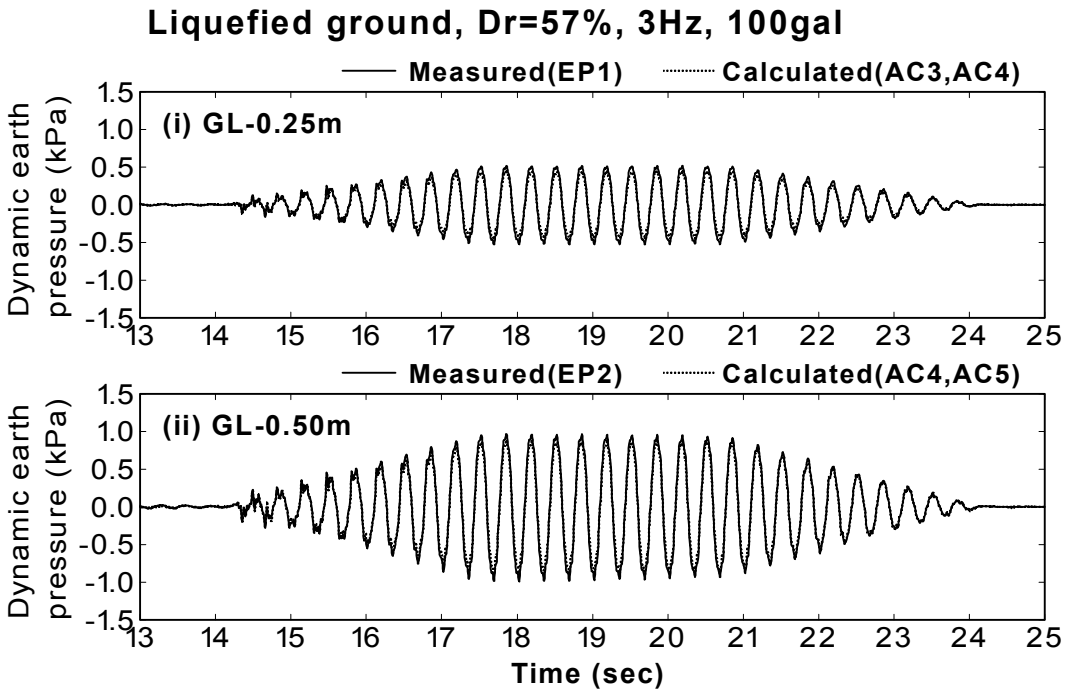

(a) During vertical excitation (13sec to 25 sec)

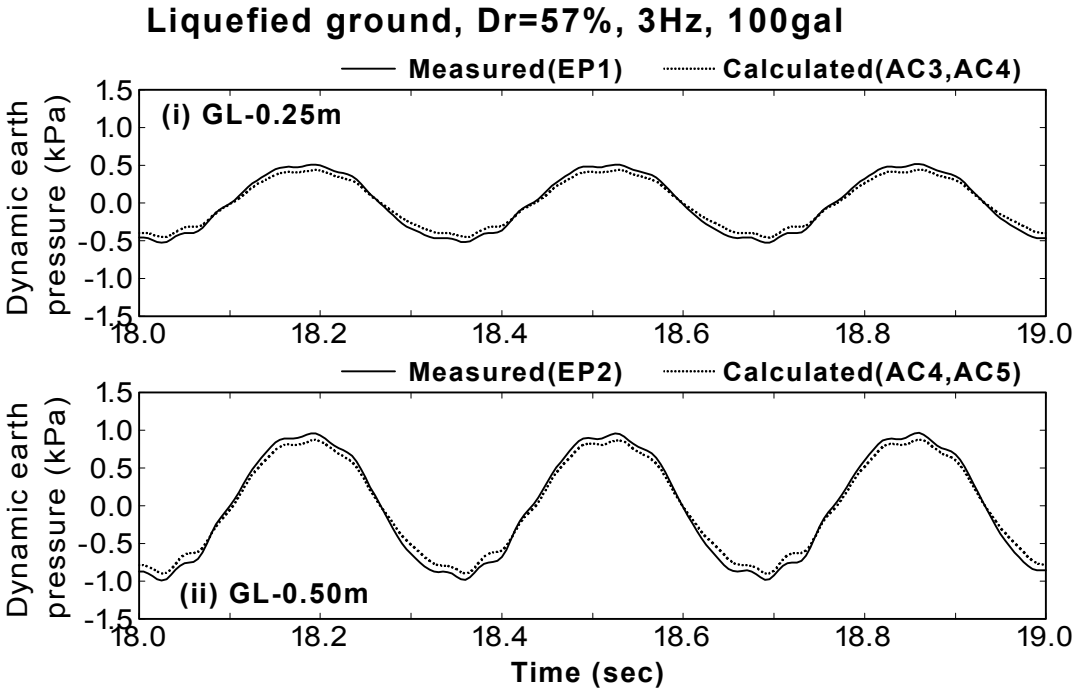

(b) Enlarged with respect to time (18.0sec to 19.0sec)

Fig.A.8: Comparison between measured and calculated dynamic earth pressures (LIQF3A100D57 test)

Table A.6: Coefficient of correlation and regression curves

Case No	GL-0.25m			GL-0.50m		
	Coeff. of correlation	A	B	Coeff. of correlation	A	B
NLF3A50D38	0.999	0.879	-0.001	0.999	0.970	0.000
NLF3A100D40	0.999	0.988	-0.003	0.998	1.034	-0.004
NLF3A200D40	0.999	1.051	-0.007	0.998	1.149	-0.007
NLF3A50D70	0.997	0.922	-0.002	1.000	0.883	0.001
NLF3A100D70	0.999	0.986	0.000	0.998	0.950	0.000
NLF3A200D70	0.998	1.058	-0.003	1.000	0.986	-0.006
NLF5A50D38	0.999	0.929	0.000	0.999	1.008	0.000
NLF5A100D40	0.999	0.994	-0.001	0.998	1.065	-0.002
NLF5A200D40	0.998	1.105	-0.011	0.997	1.174	-0.011
NLF5A50D70	0.999	0.917	0.001	1.000	0.873	-0.001
NLF5A100D70	0.998	0.981	-0.002	1.000	0.937	0.002
NLF5A200D70	0.999	1.085	-0.006	0.999	0.998	-0.009
NLF10A50D38	0.999	0.990	-0.001	0.997	1.063	-0.004
NLF10A50D70	0.998	1.019	0.002	0.987	0.980	-0.001
NLF10A100D70	1.000	1.025	0.000	0.999	0.947	-0.010
LIQF3A100D57	0.999	1.123	0.000	0.999	1.103	0.001
LIQF3A200D60	1.000	1.225	0.000	1.000	1.162	0.000
LIQF5A100D51	1.000	1.077	0.004	1.000	1.081	0.010
LIQF5A200D68	1.000	1.242	0.003	0.999	1.174	0.006

Average of coefficient A = 1.030≒1.0 Average of coefficient B = -0.002≒0.0

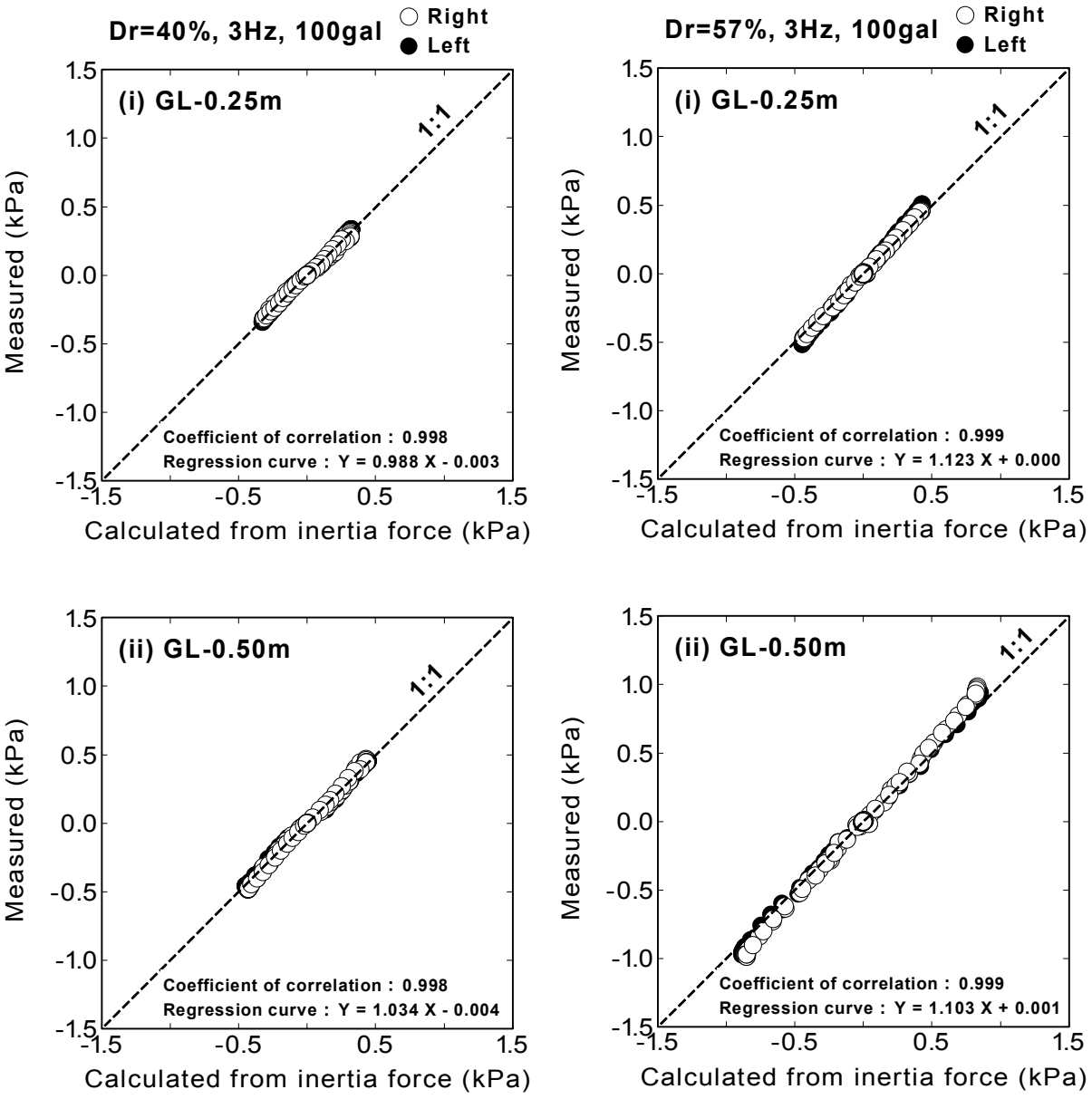

(a) NLF3A100D40 test (b) LIQF3A100D57 test

Fig.A.9: Amplitude of measured and calculated dynamic earth pressures

Fig.A.10 shows the relation between the ratio of amplitude (coefficient A) and such various conditions as those for the intensity of input motion, the frequency, the relative density of soil and the ratio of excess pore water pressure. It is seen that the values of the ratio are nearly 1.0 under the variety of conditions. It suggests that the earth pressure transducers give the appropriate dynamic earth pressures even though the transducer is placed in saturated soil.

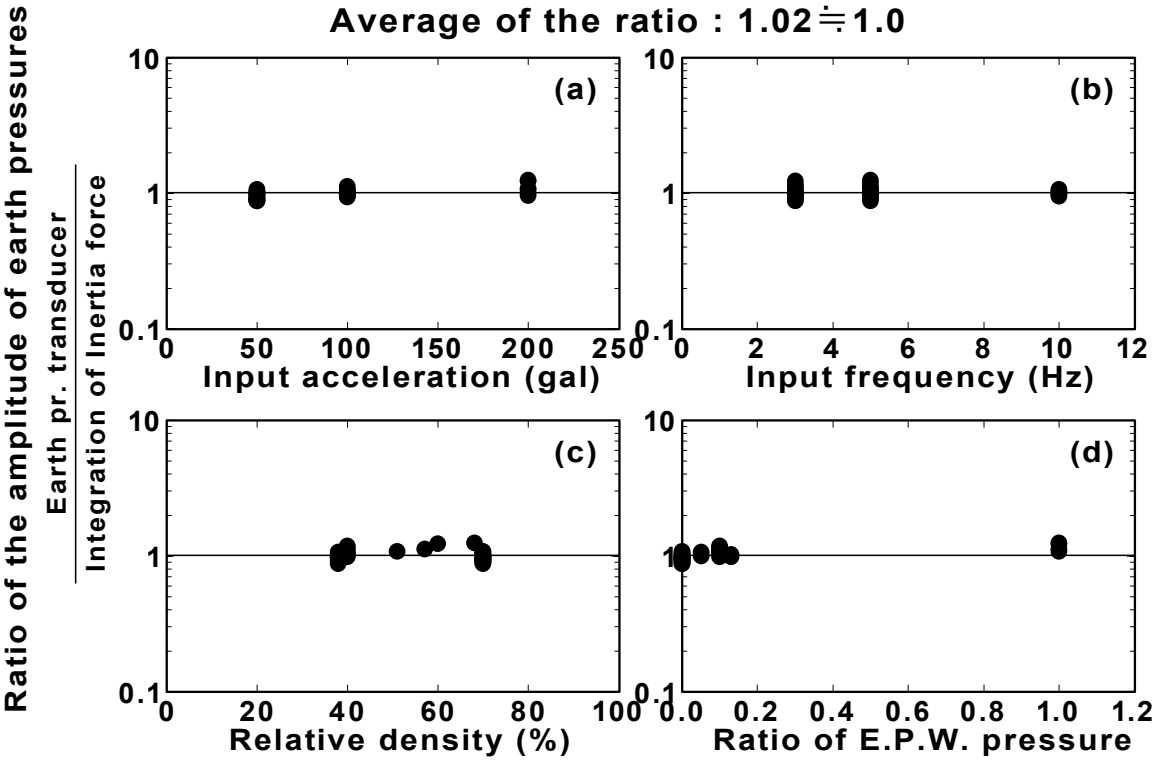

Fig.A.10: The results of calibration for the earth pressure transducers

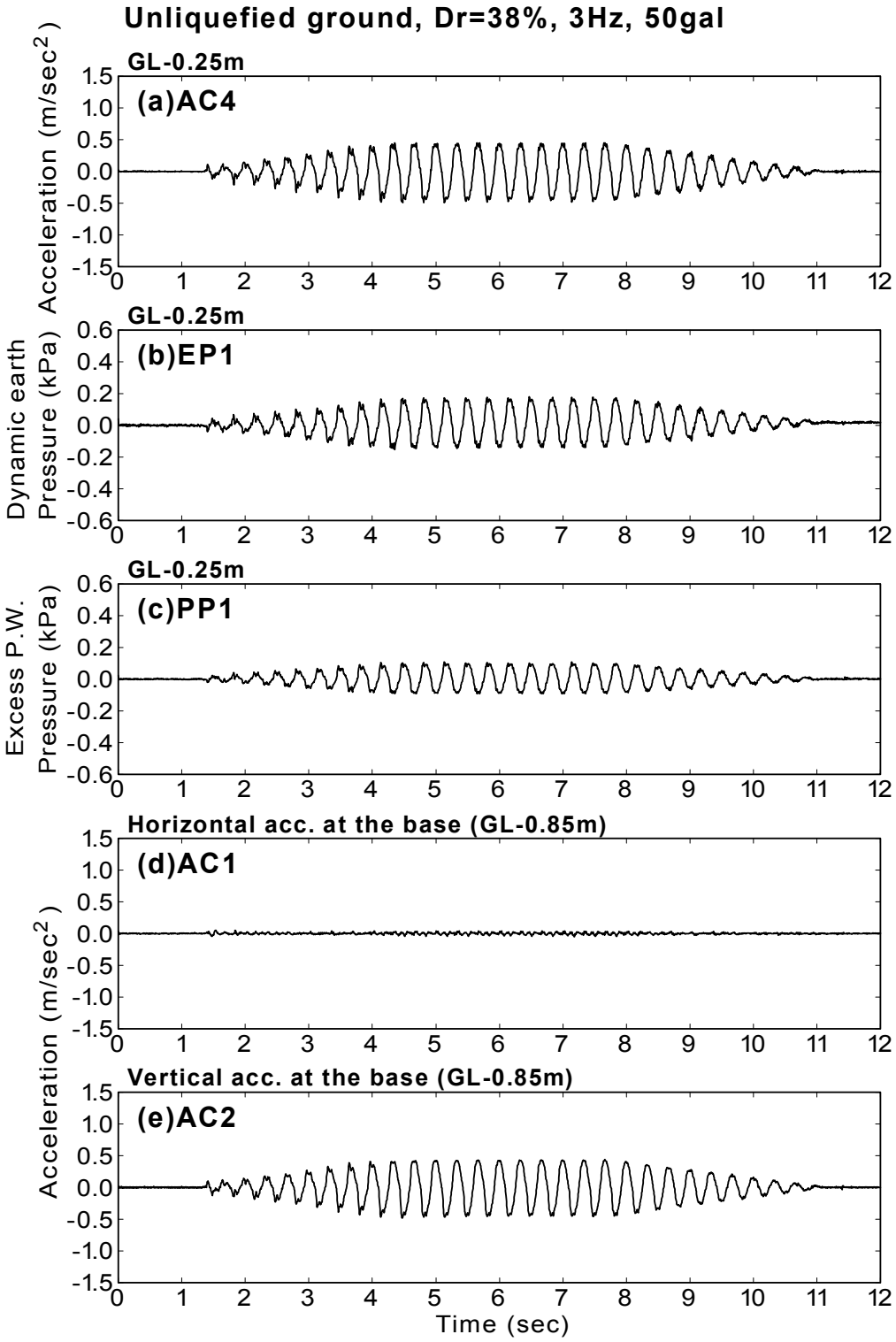

Fig.A.11: Time histories for unliquefied ground (NLF3A50D38 test)

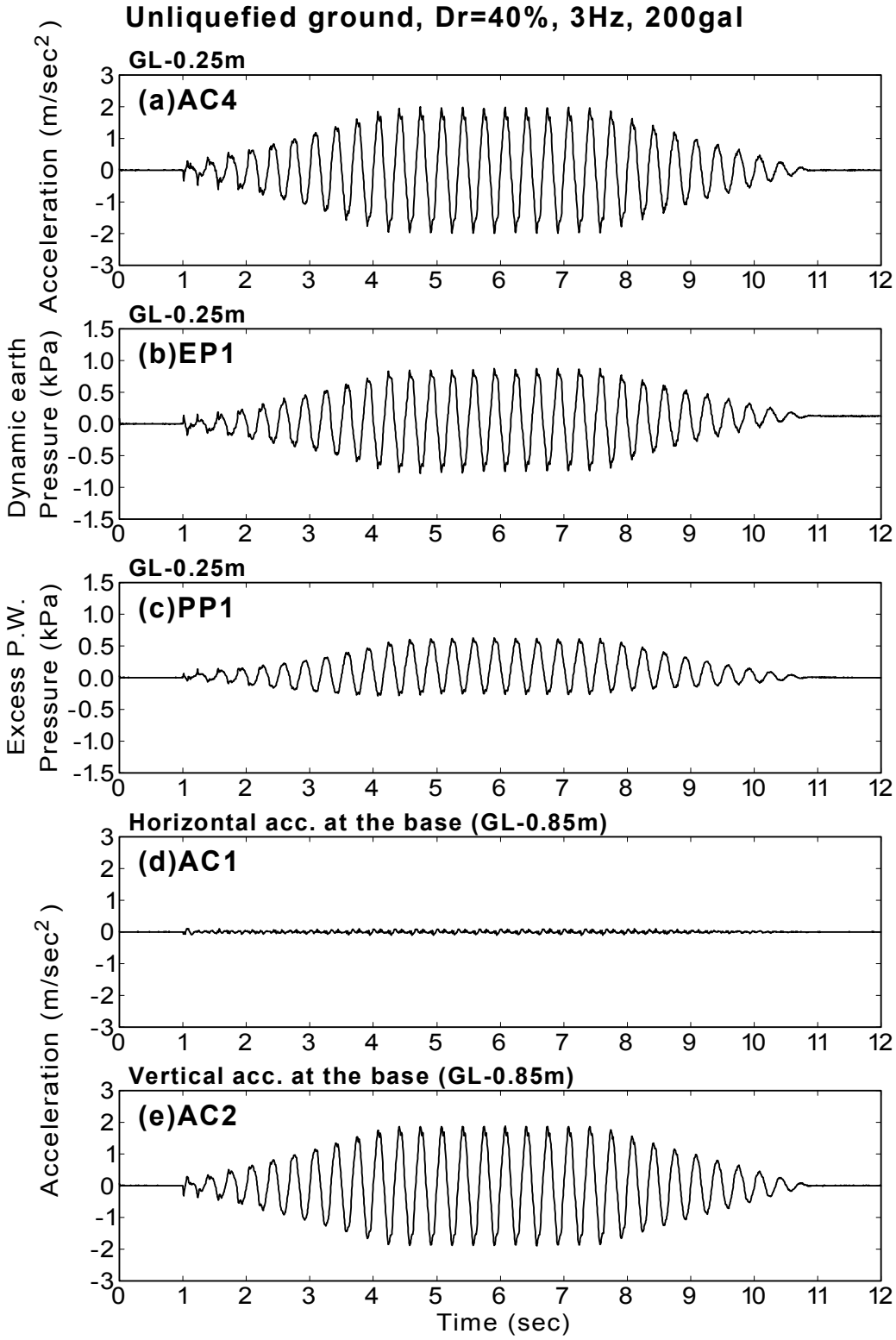

Fig.A.12: Time histories for unliquefied ground (NLF3A200D40 test)

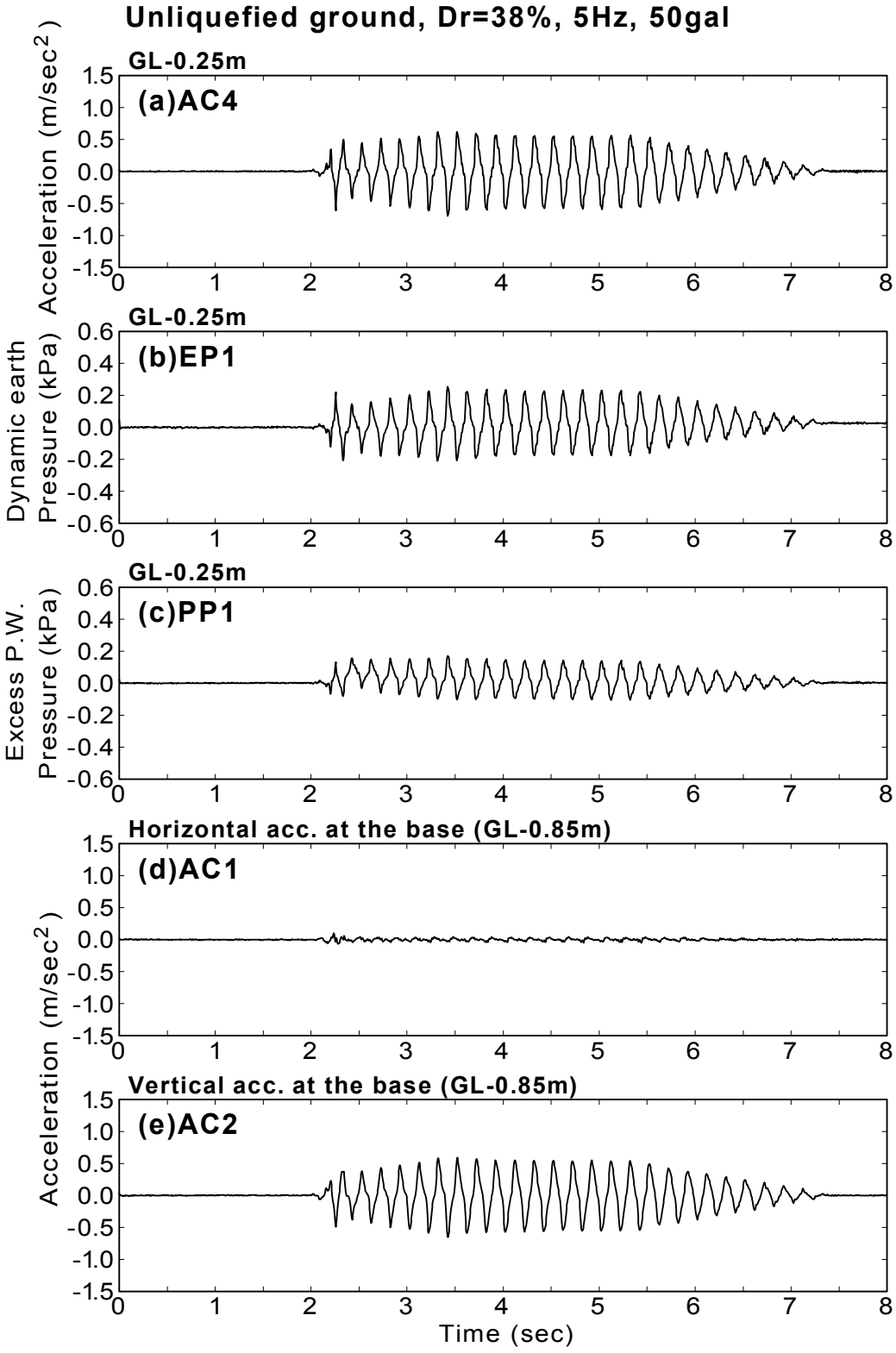

Fig.A.13: Time histories for unliquefied ground (NLF5A50D38 test)

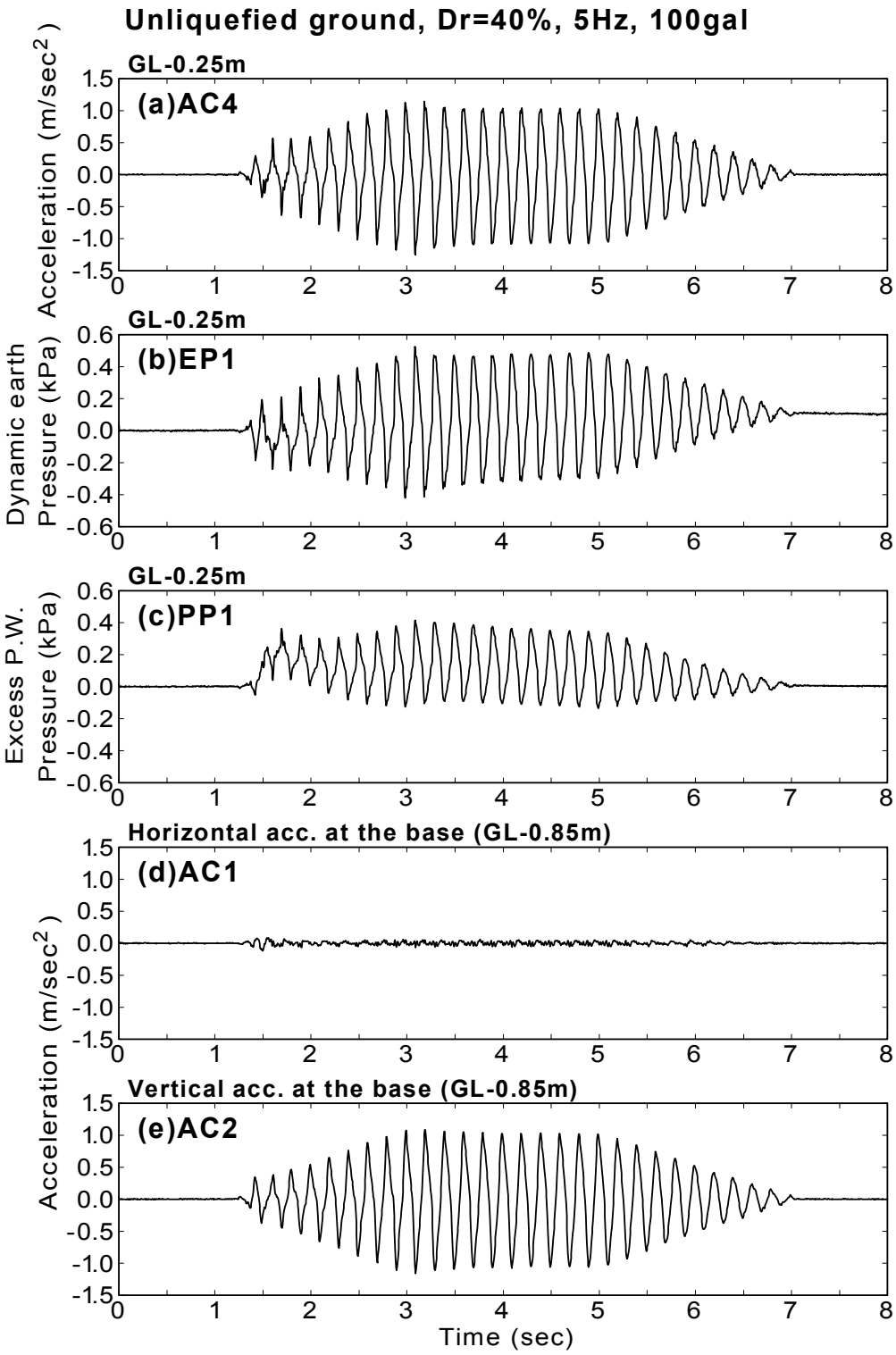

Fig.A.14: Time histories for unliquefied ground (NLF5A100D40 test)

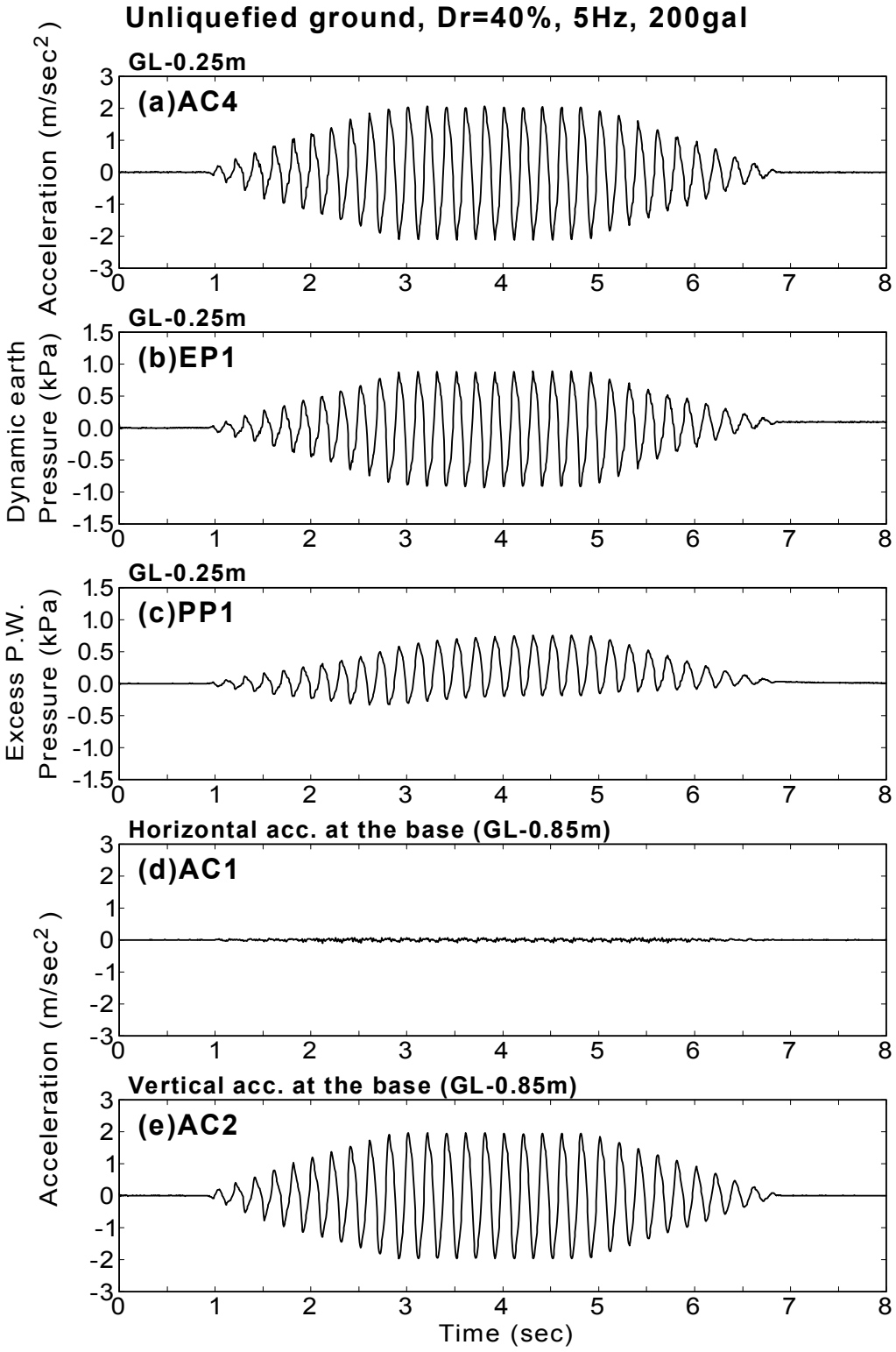

Fig.A.15: Time histories for unliquefied ground (NLF5A200D40 test)

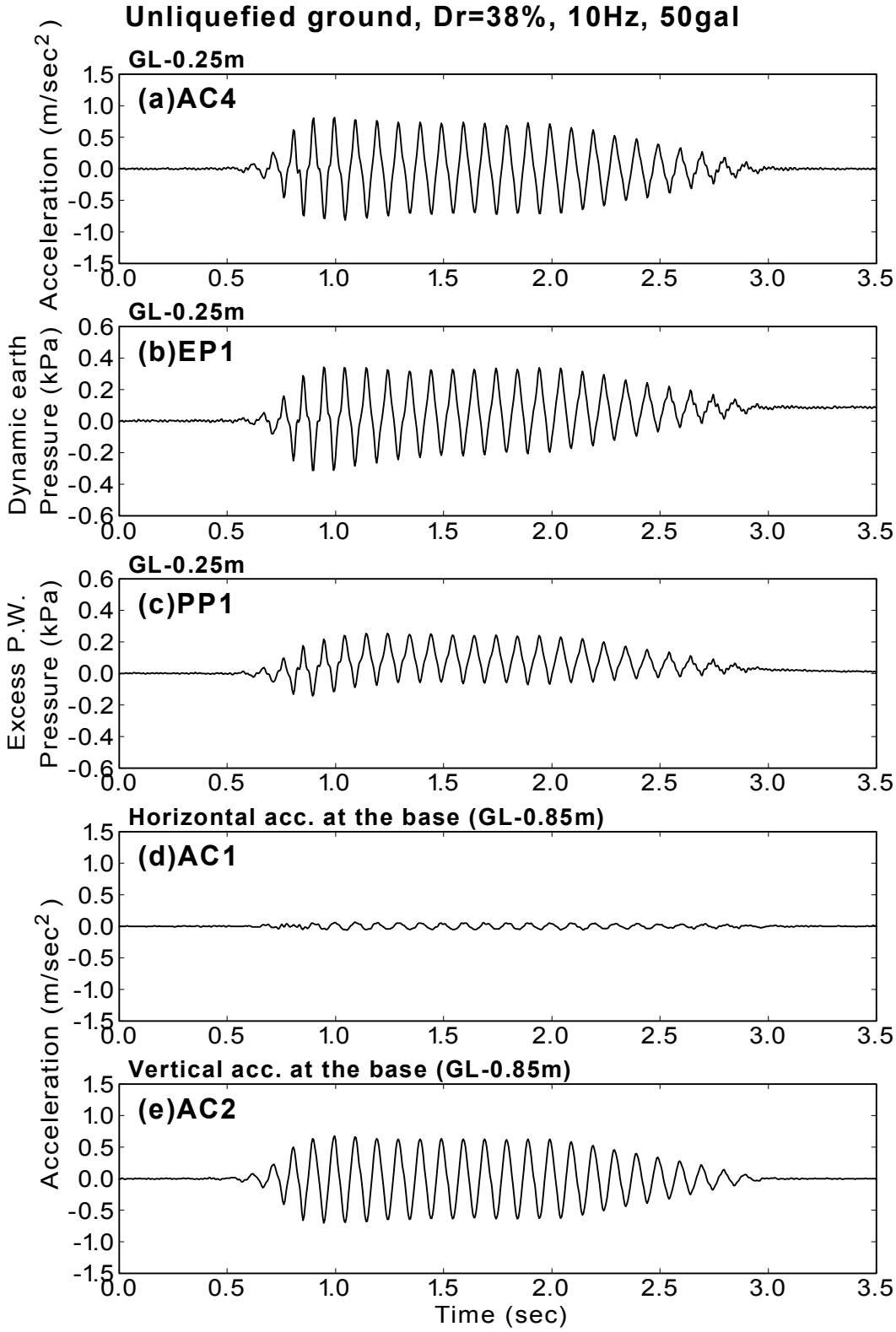

Fig.A.16: Time histories for unliquefied ground (NLF10A50D38 test)

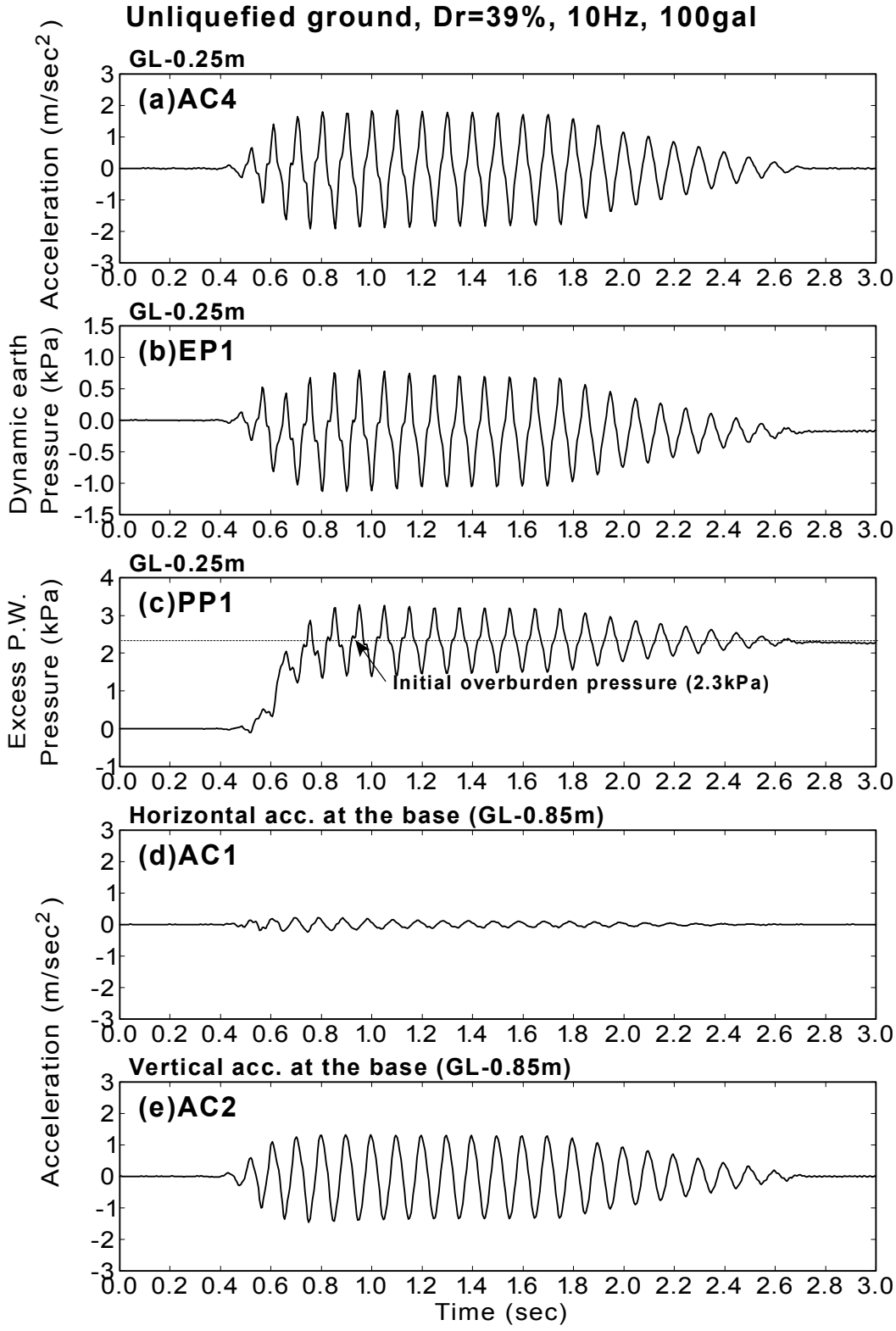

Fig.A.17: Time histories for unliquefied ground (NLF10A100D39 test)

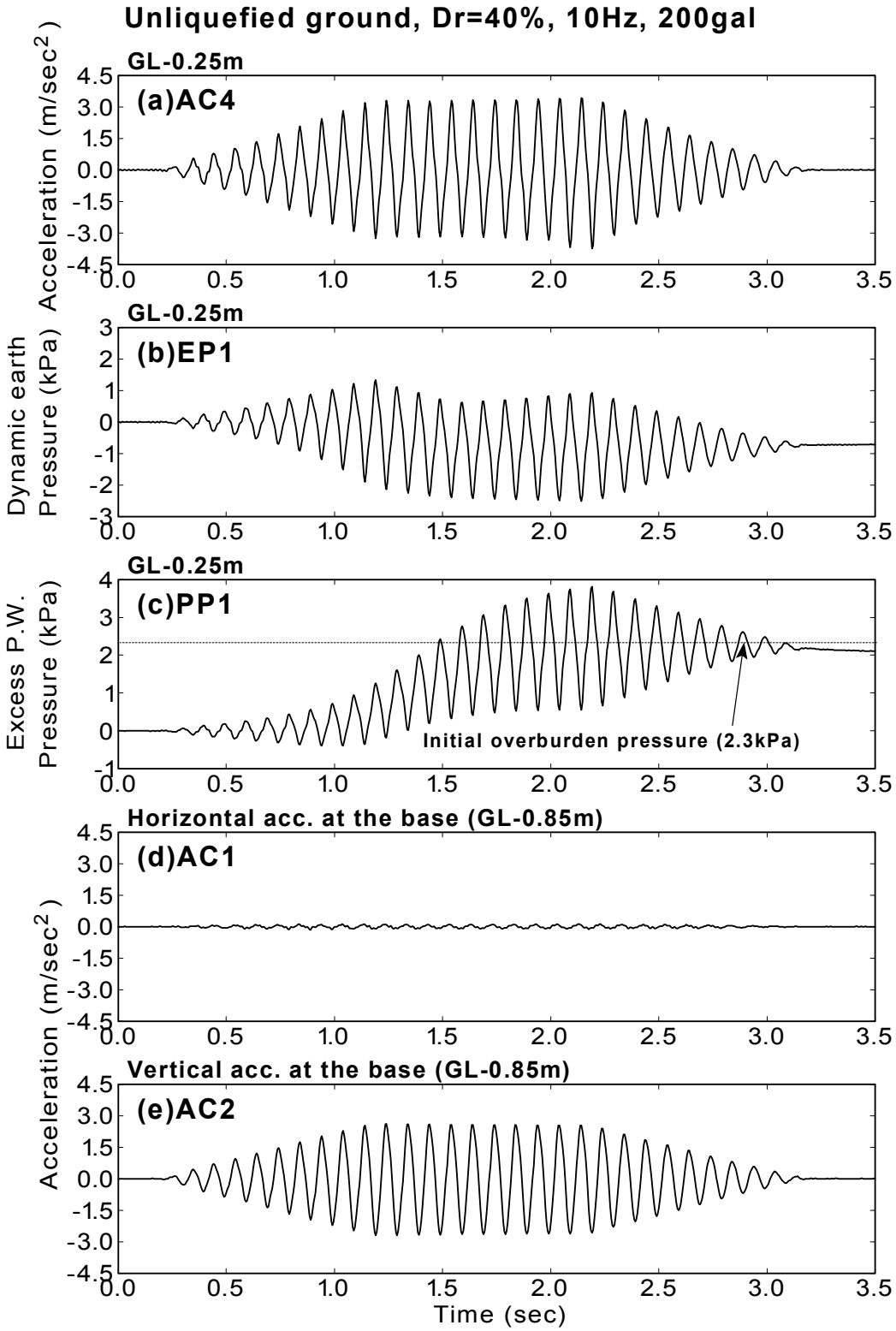

Fig.A.18: Time histories for unliquefied ground (NLF10A200D40 test)

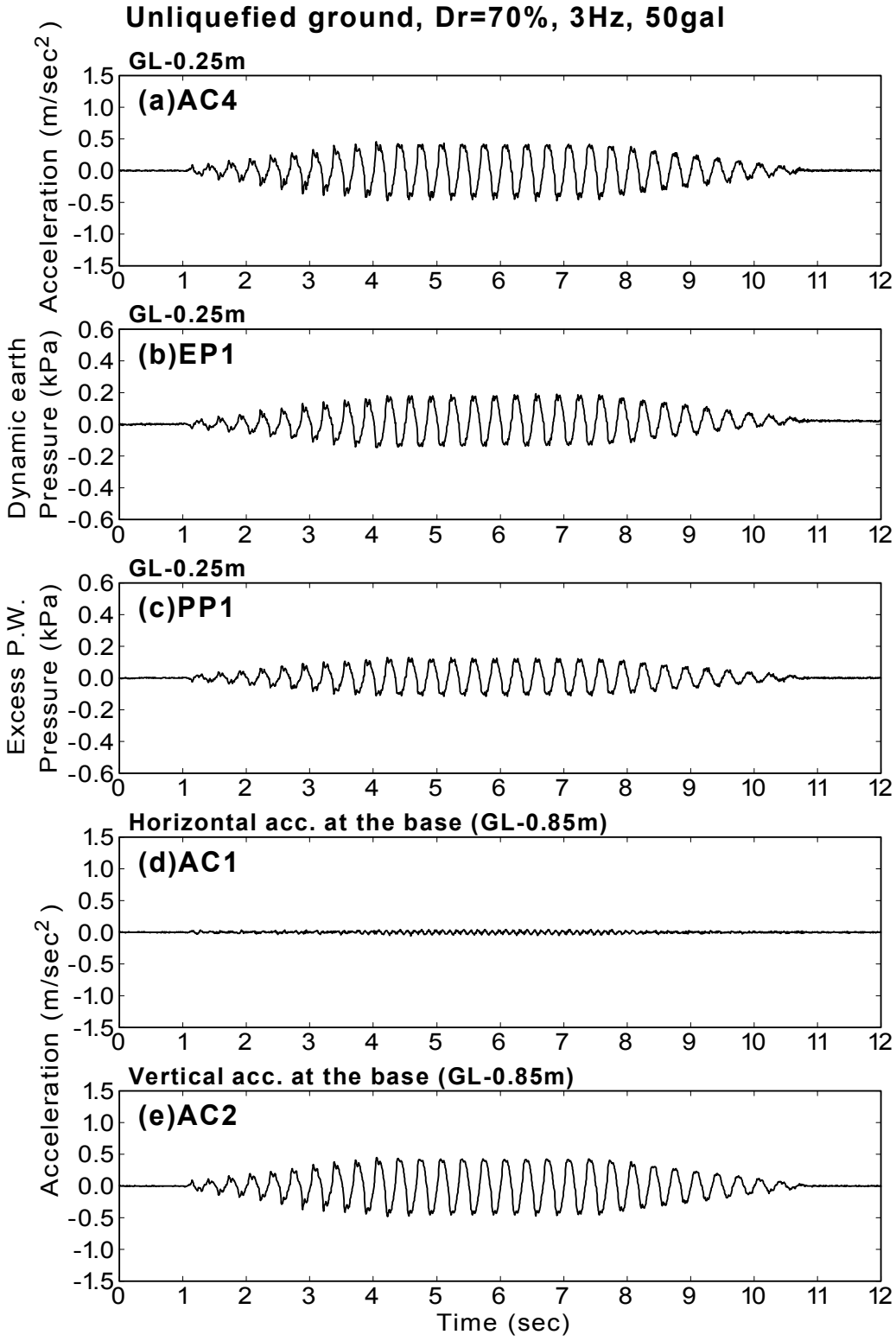

Fig.A.19: Time histories for unliquefied ground (NLF3A50D70 test)

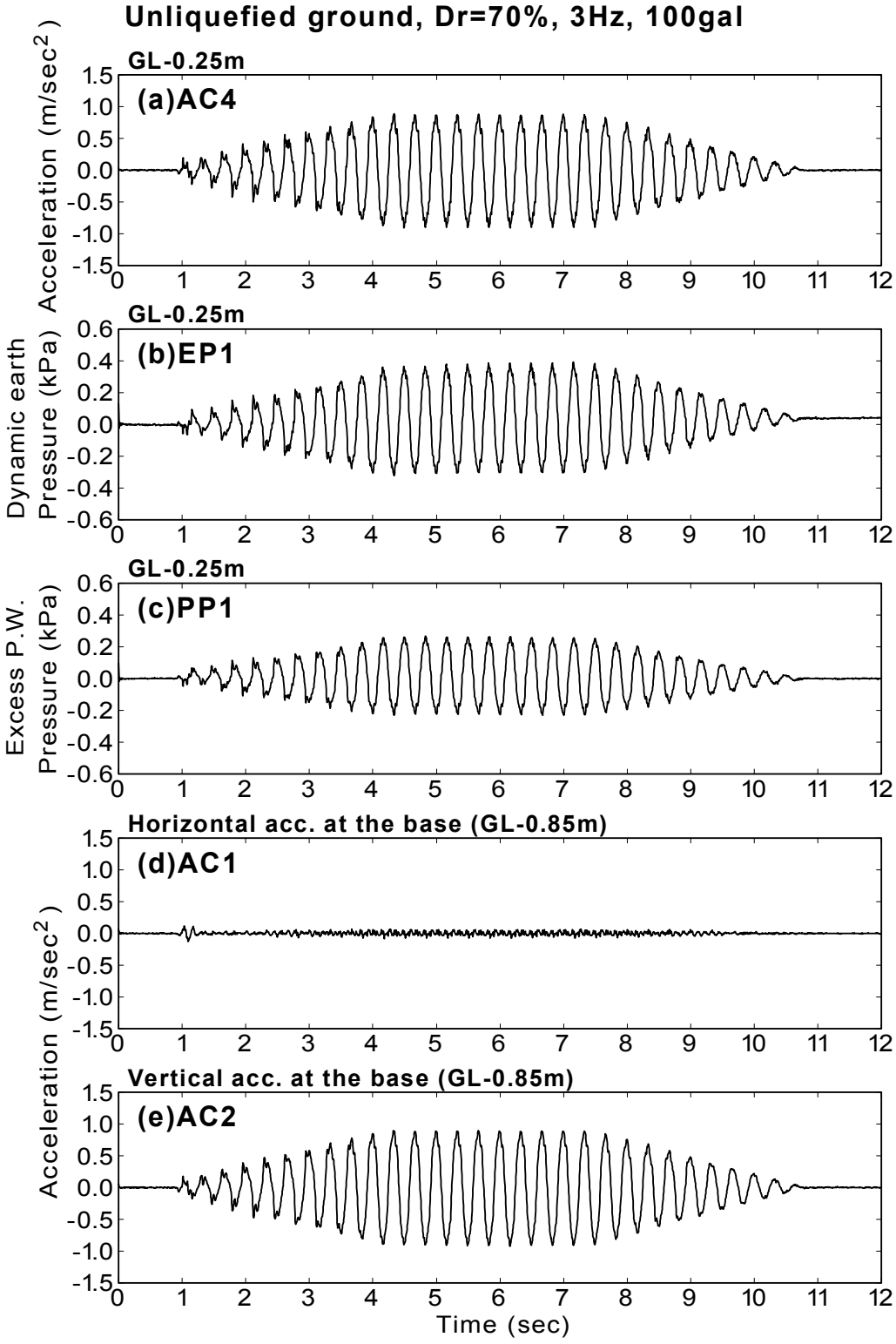

Fig.A.20: Time histories for unliquefied ground (NLF3A100D70 test)

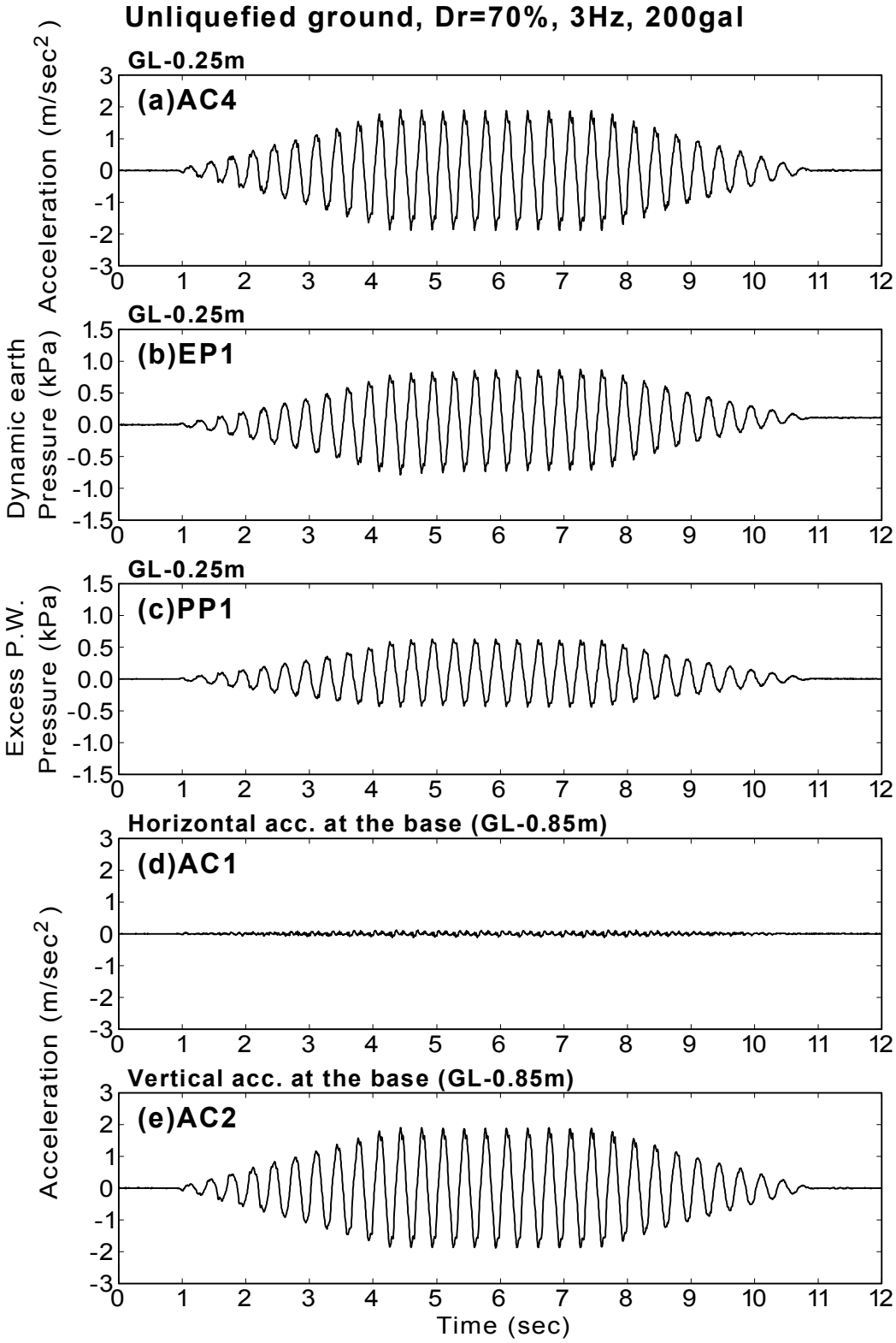

Fig.A.21: Time histories for unliquefied ground (NLF3A200D70 test)

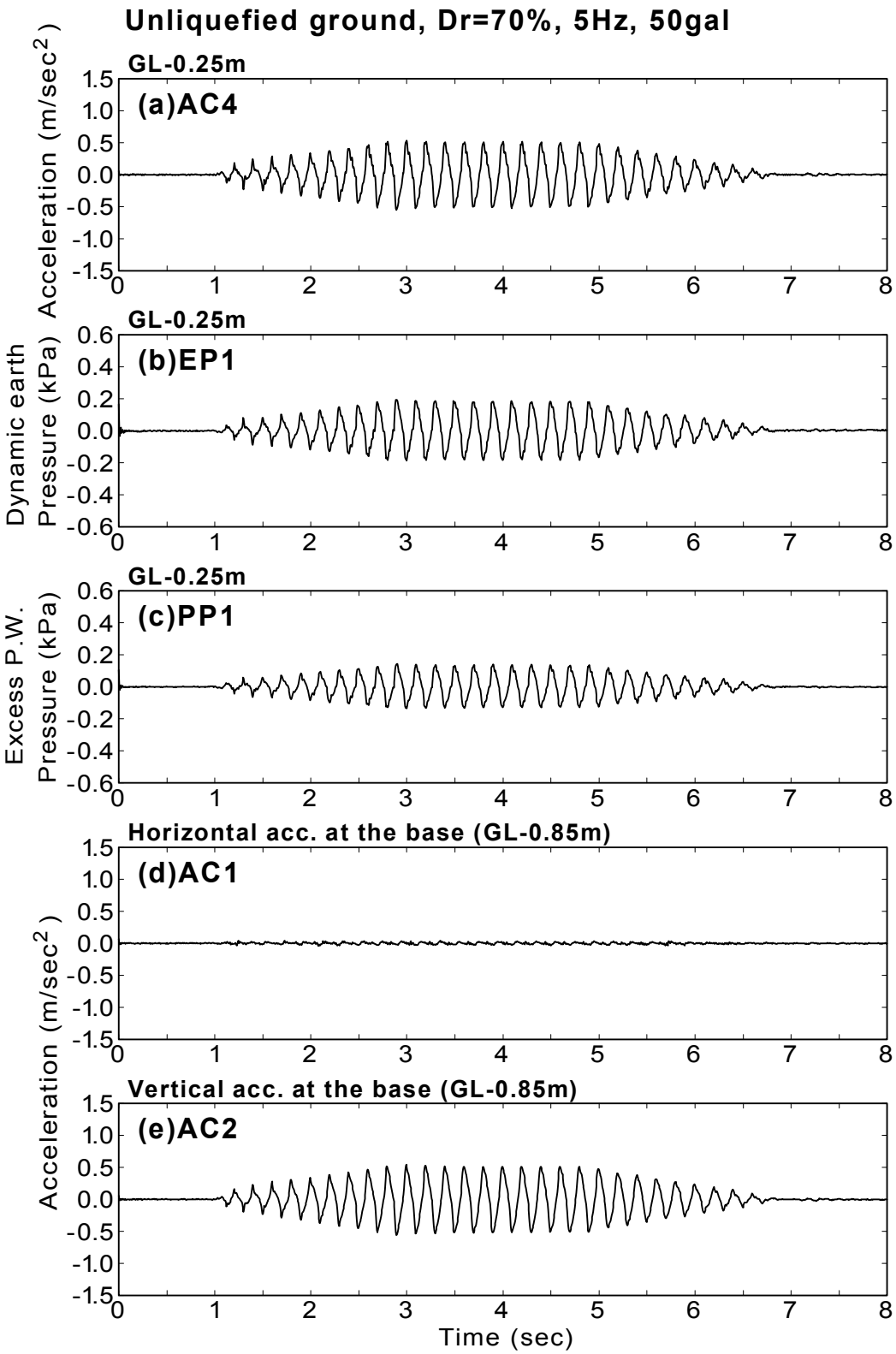

Fig.A.22: Time histories for unliquefied ground (NLF5A50D70 test)

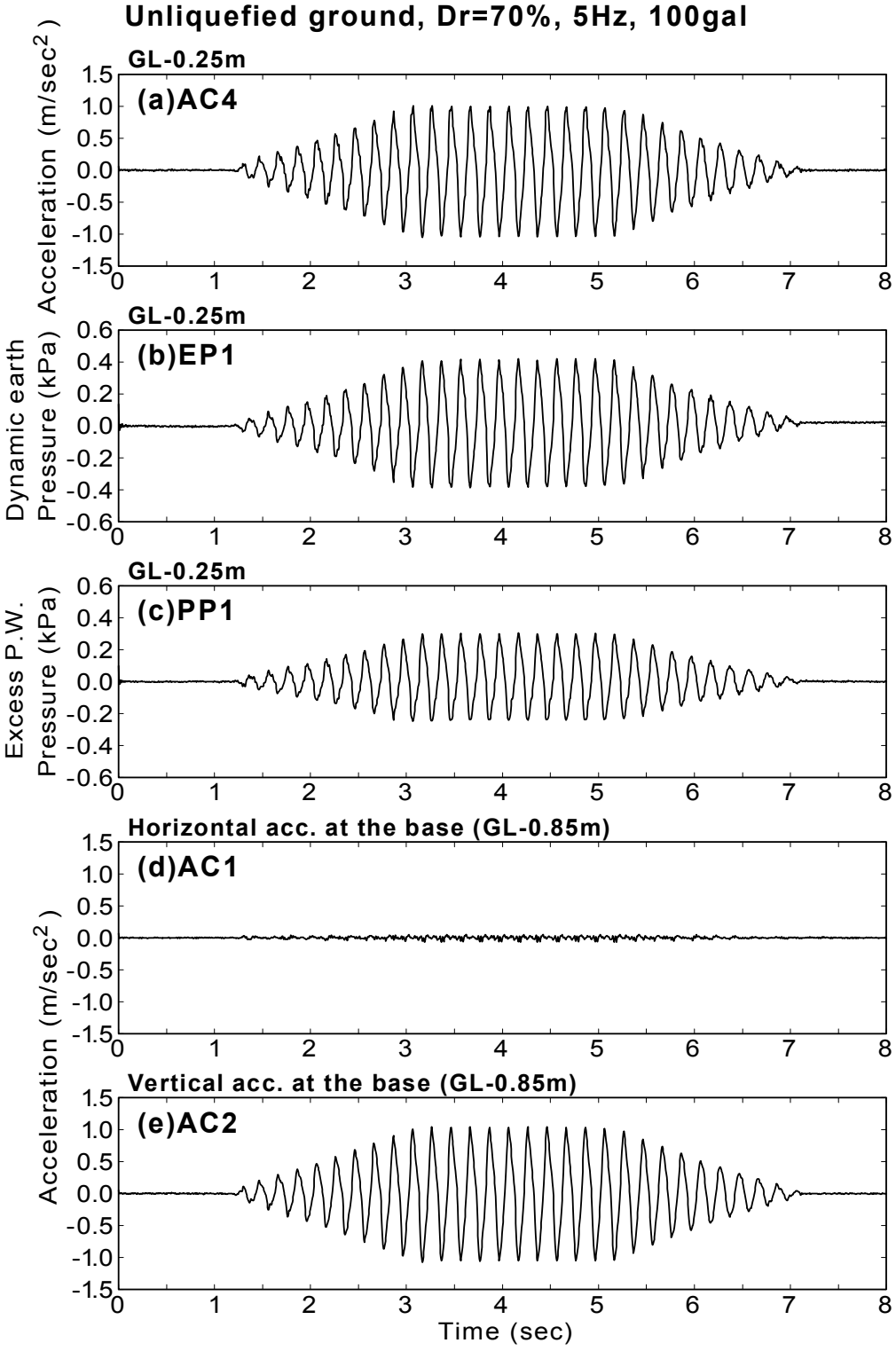

Fig.A.23: Time histories for unliquefied ground (NLF5A100D70 test)

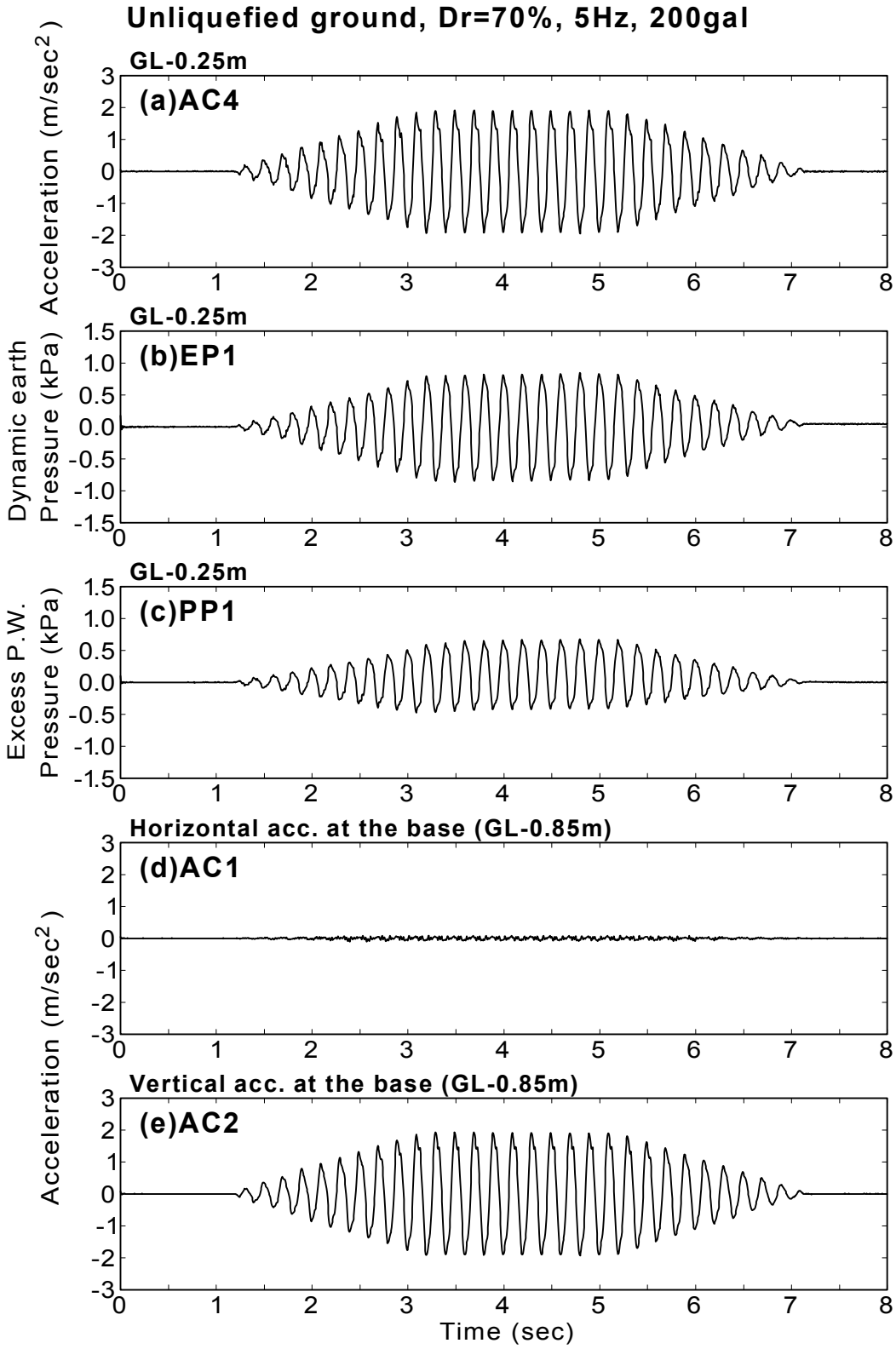

Fig.A.24: Time histories for unliquefied ground (NLF5A200D70 test)

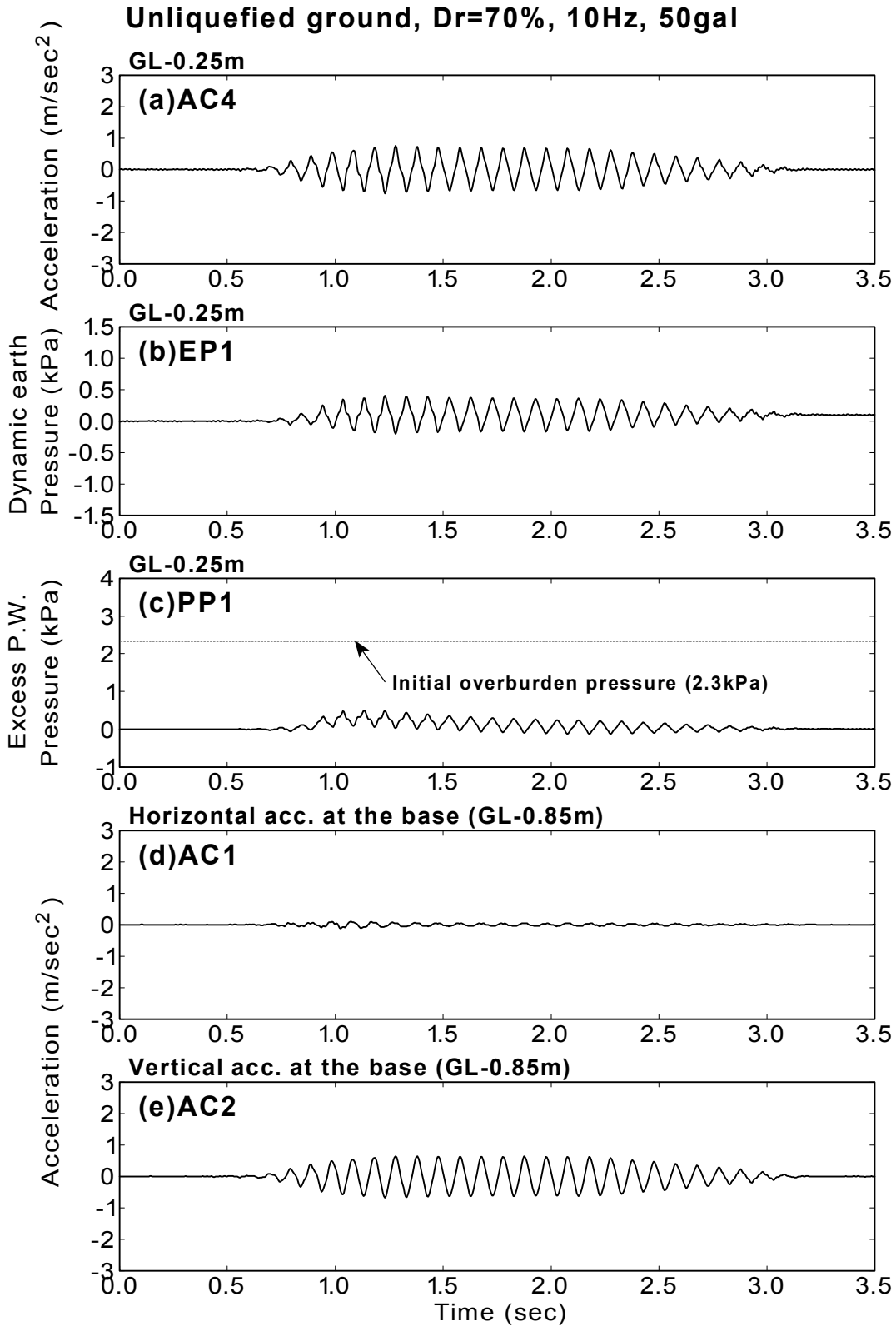

Fig.A.25: Time histories for unliquefied ground (NLF10A50D70 test)

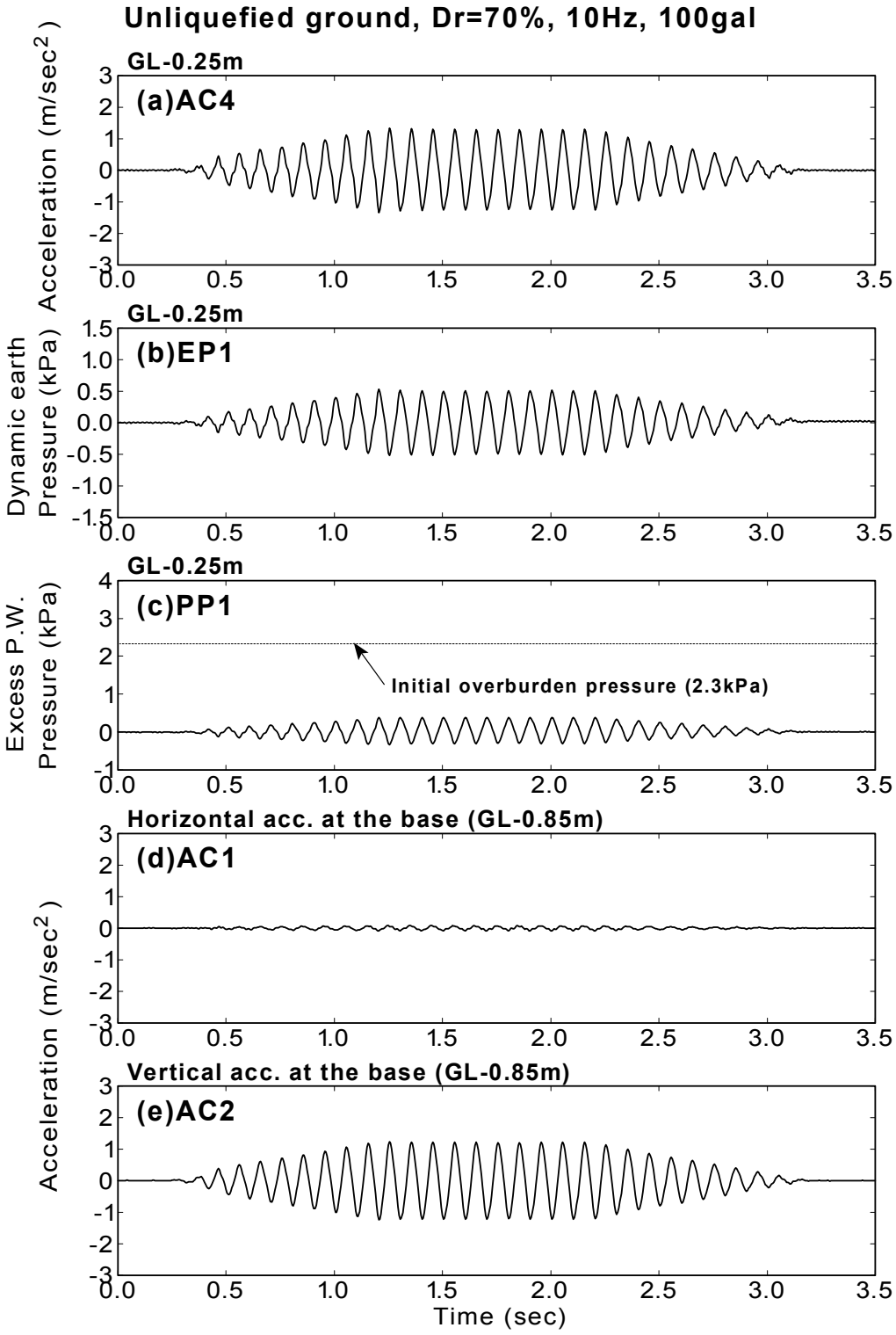

Fig.A.26: Time histories for unliquefied ground (NLF10A100D70 test)

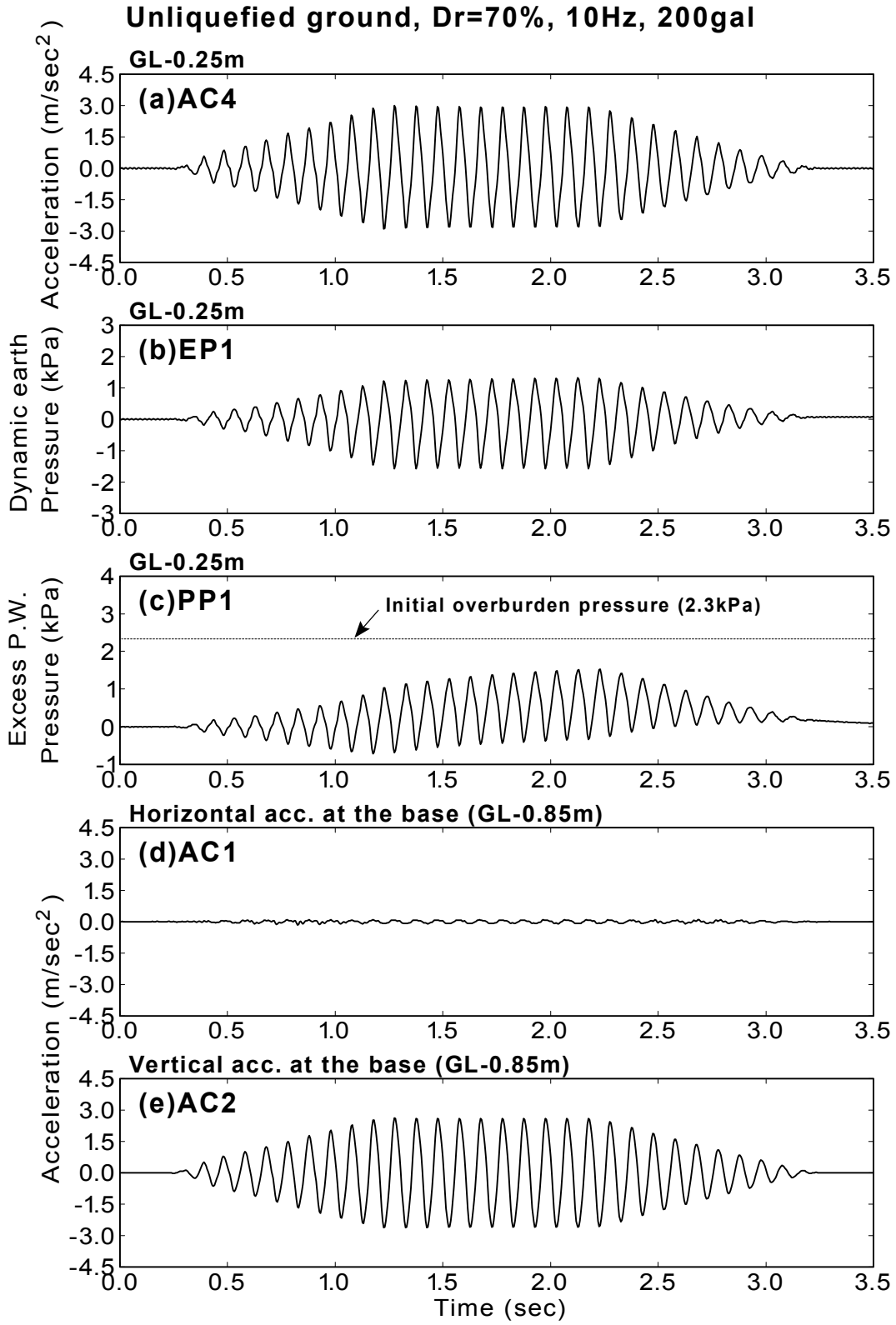

Fig.A.27: Time histories for unliquefied ground (NLF10A200D70 test)

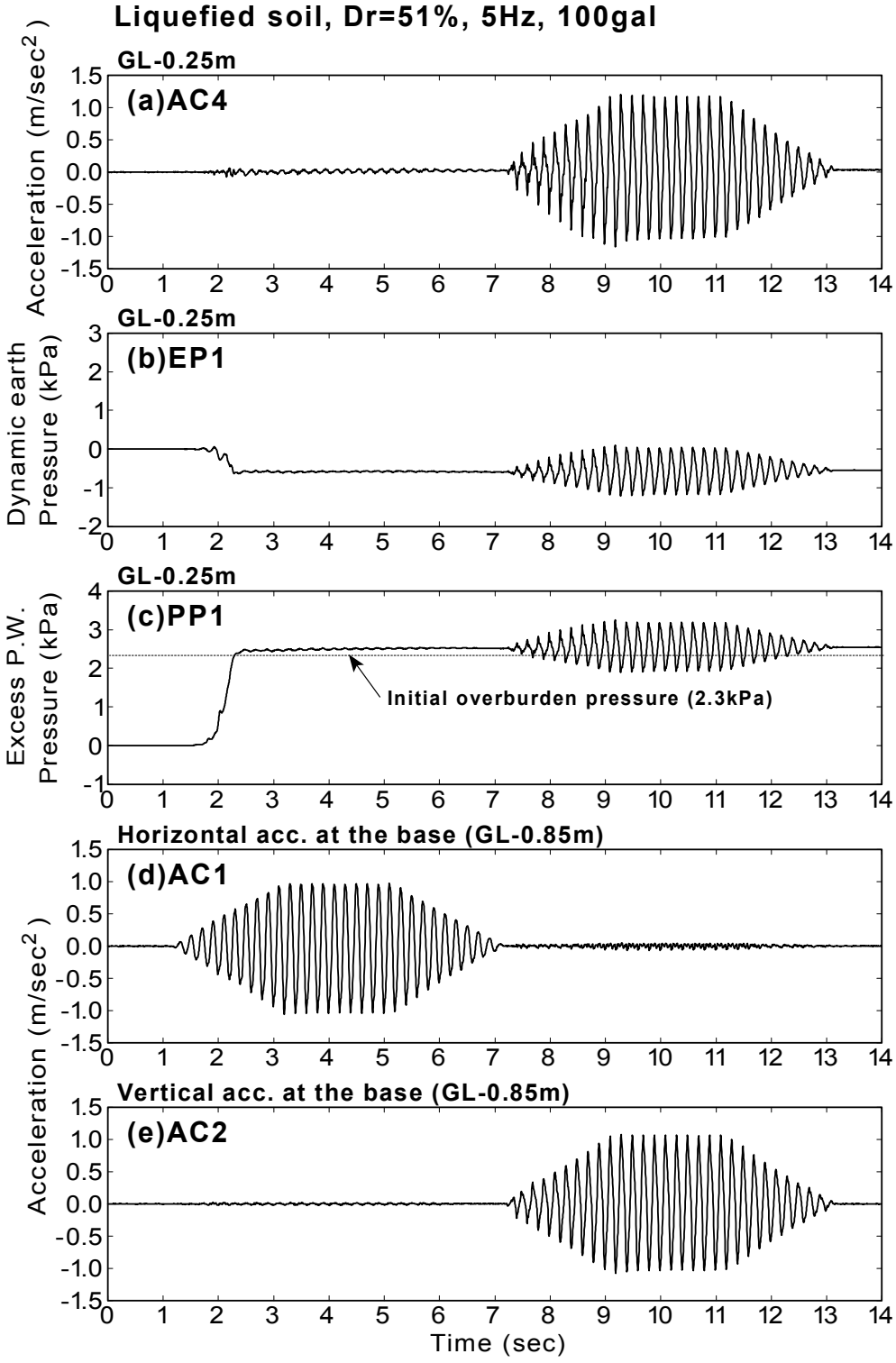

Fig.A.28: Time histories for liquefied ground (LIQF5A100D51 test)

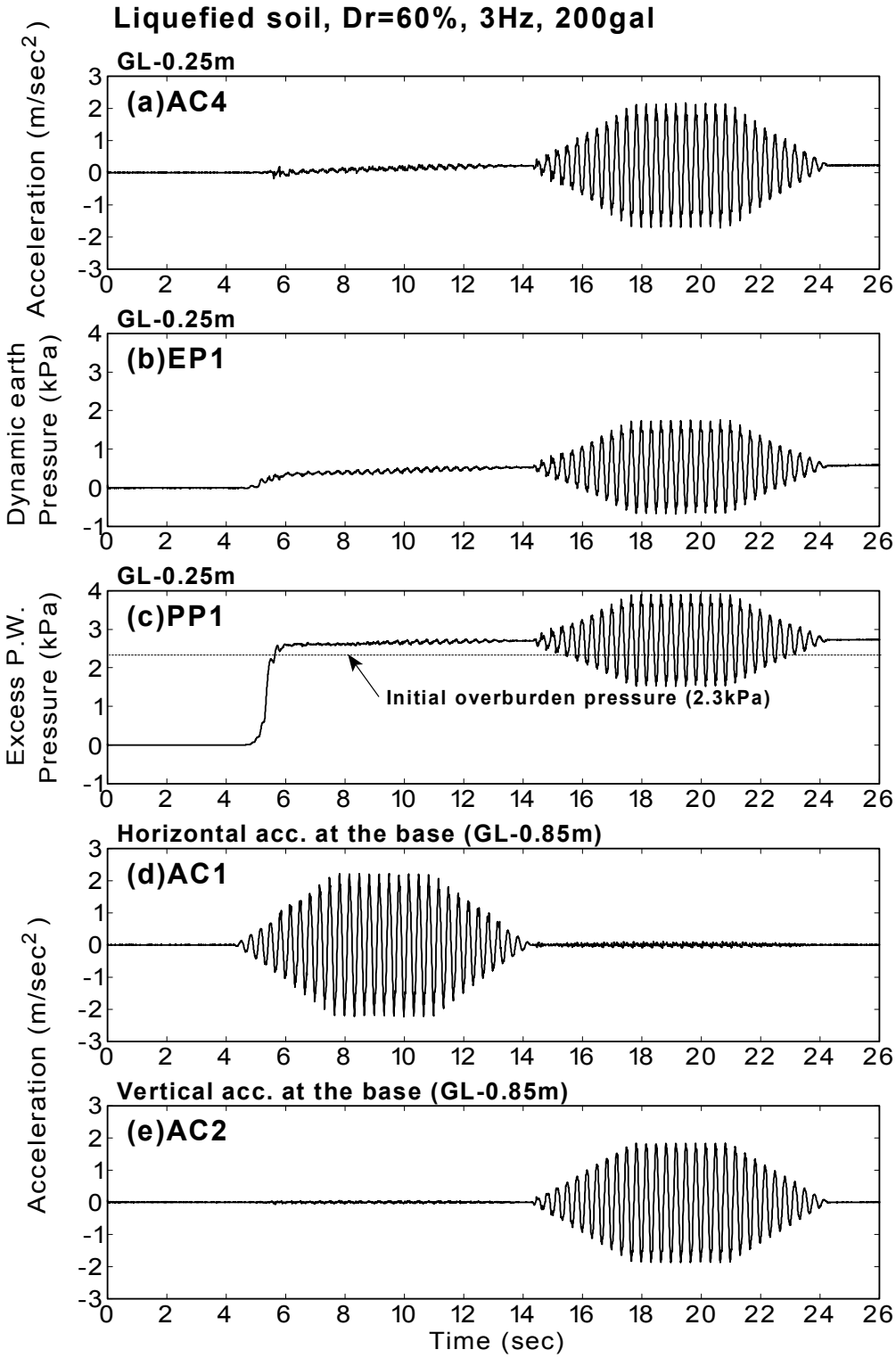

Fig.A.29: Time histories for liquefied ground (LIQF3A200D60 test)

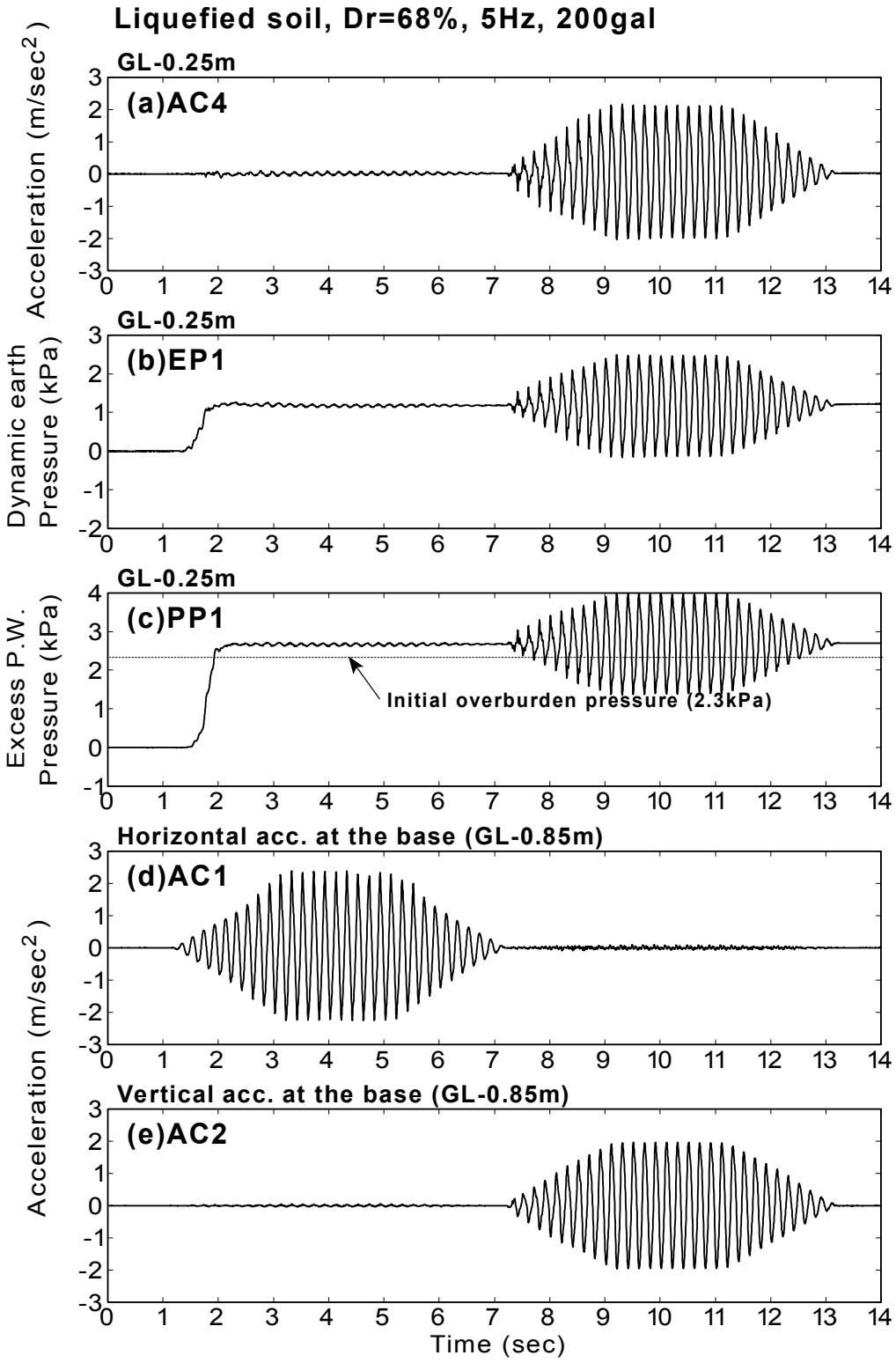

Fig.A.30: Time histories for liquefied ground (LIQF5A200D68 test)

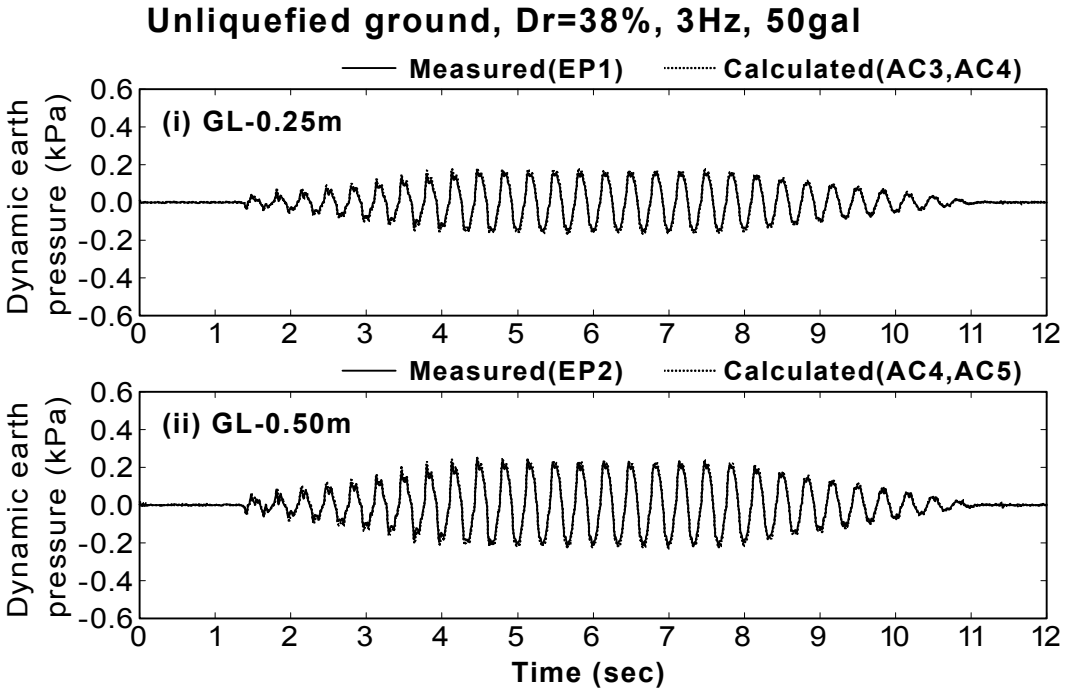

(a) During vertical excitation (0sec～12sec)

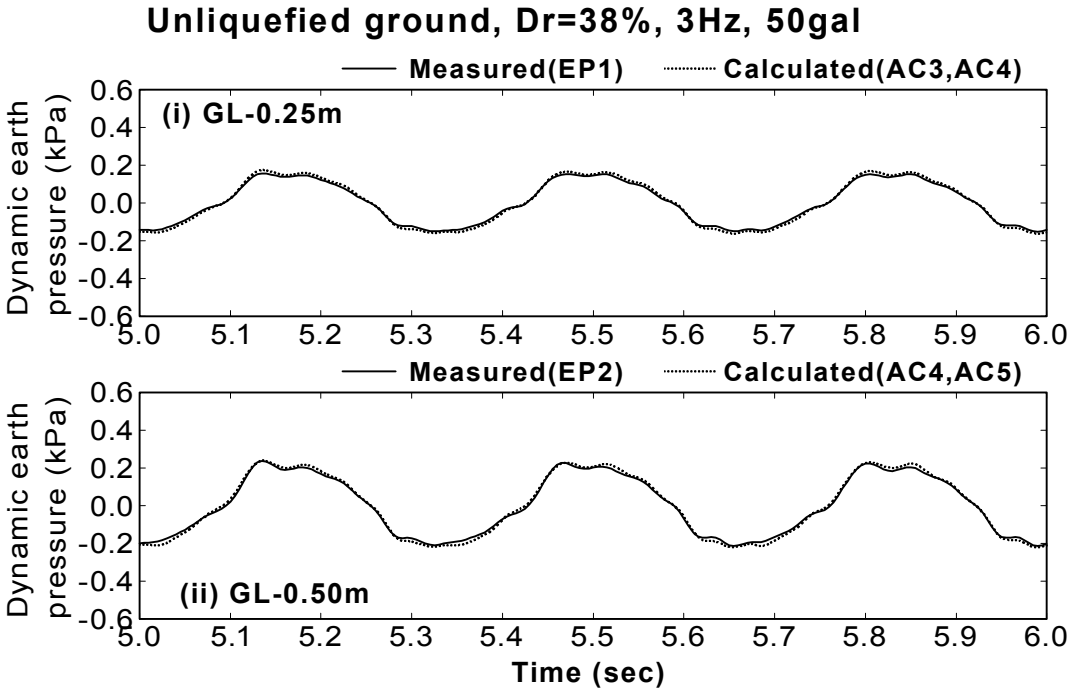

(b) Enlarged with respect to time (5.0sec to 6.0sec)

Fig.A.31: Comparison between measured and calculated dynamic earth pressures (NLF3A50D38 test)

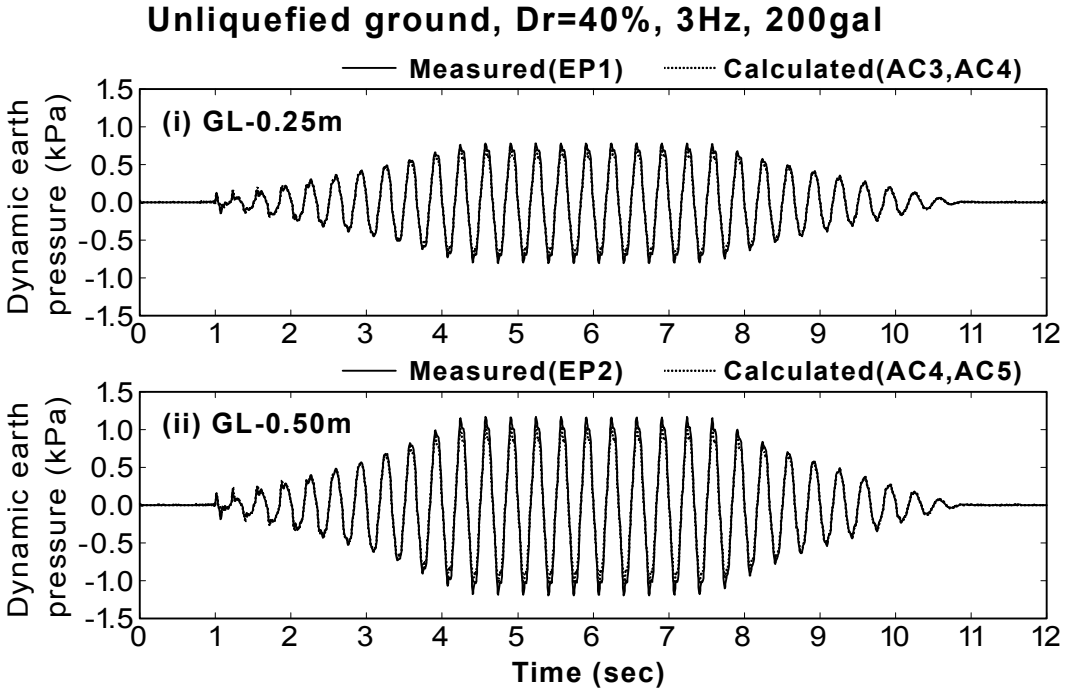

(a) During vertical excitation (0sec～12sec)

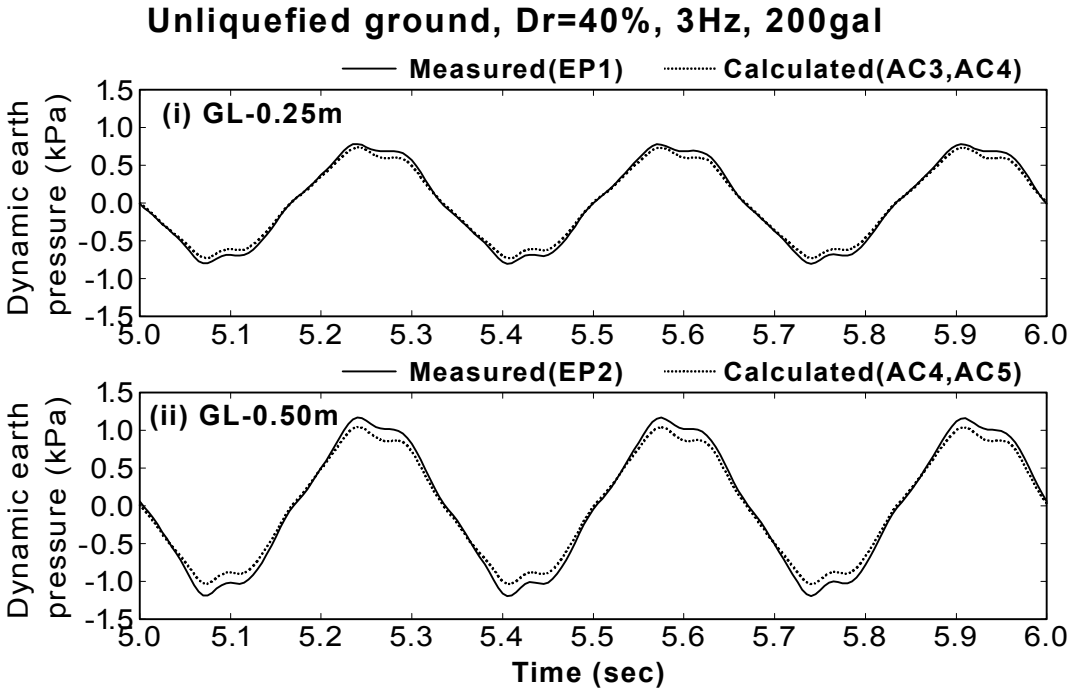

(b) Enlarged with respect to time (5.0sec to 6.0sec)

Fig.A.32: Comparison between measured and calculated dynamic earth pressures (NLF3A200D40 test)

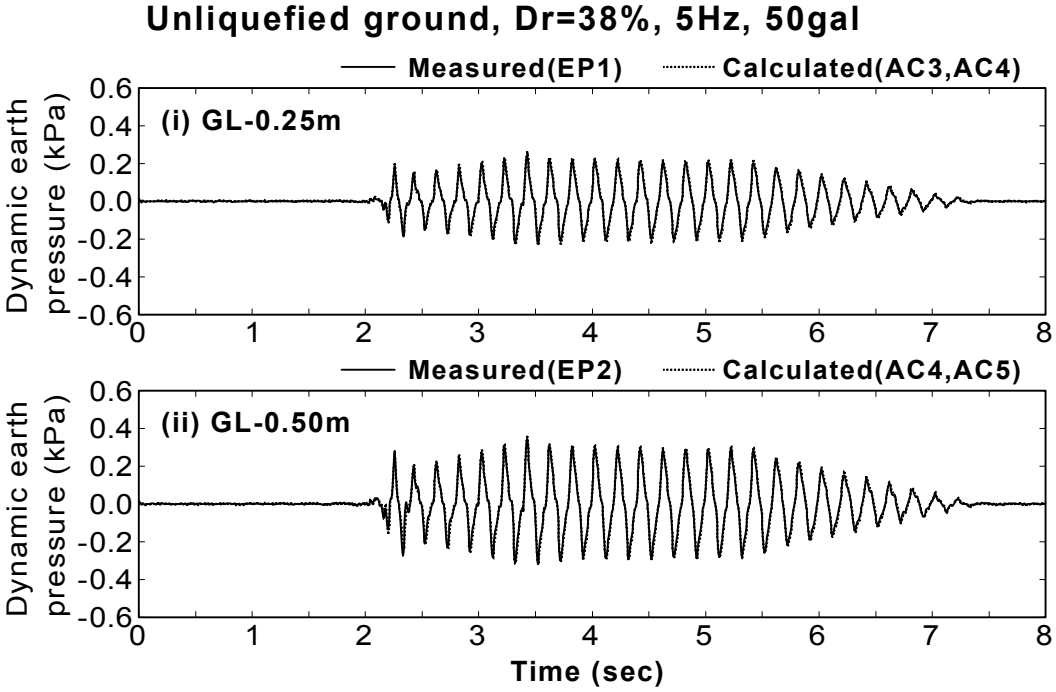

(a) During vertical excitation (0sec～8sec)

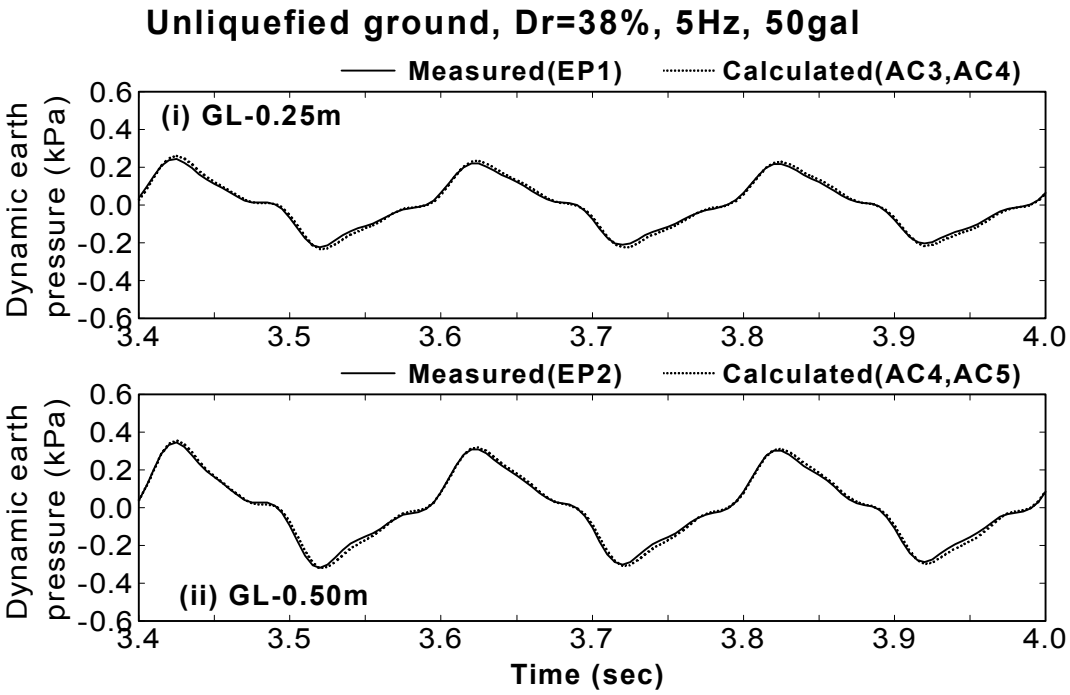

(b) Enlarged with respect to time (3.4sec to 4.0sec)

Fig.A.33: Comparison between measured and calculated dynamic earth pressures (NLF5A50D38 test)

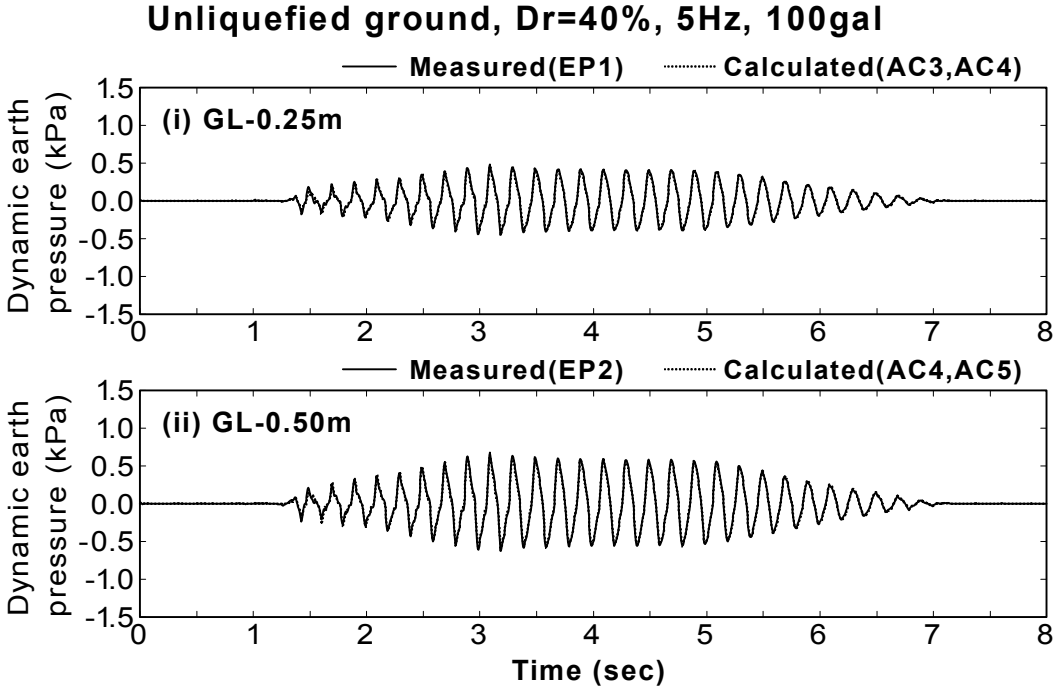

(a) During vertical excitation (0sec to 8 sec)

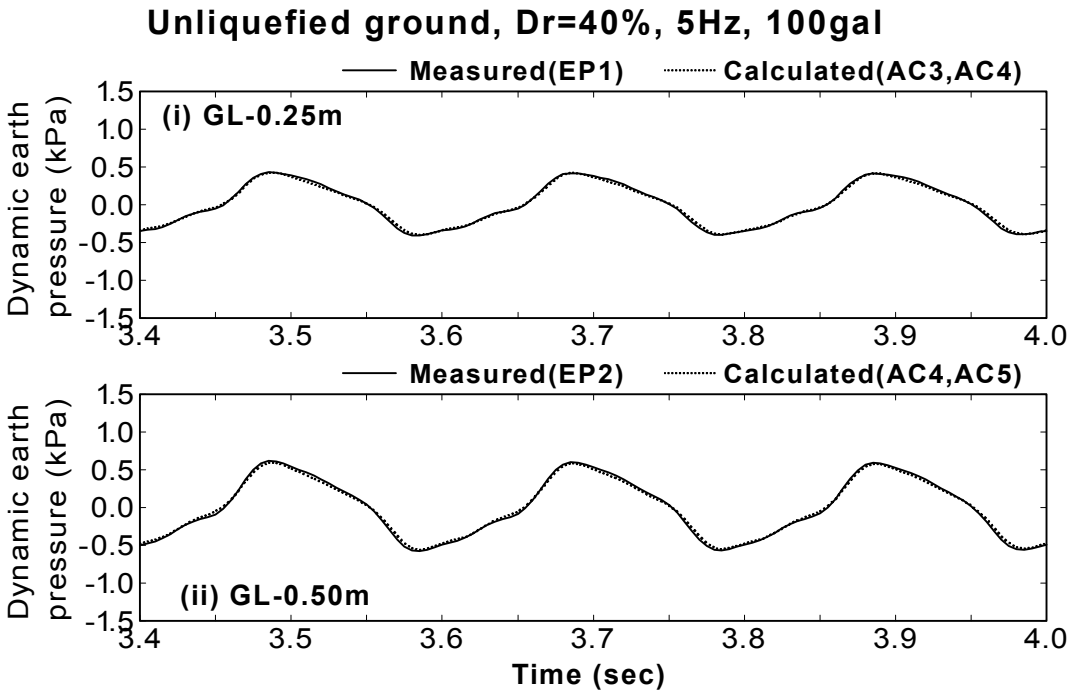

(b) Enlarged with respect to time (3.4sec to 4.0sec)

Fig.A.34: Comparison between measured and calculated dynamic earth pressures (NLF5A100D40 test)

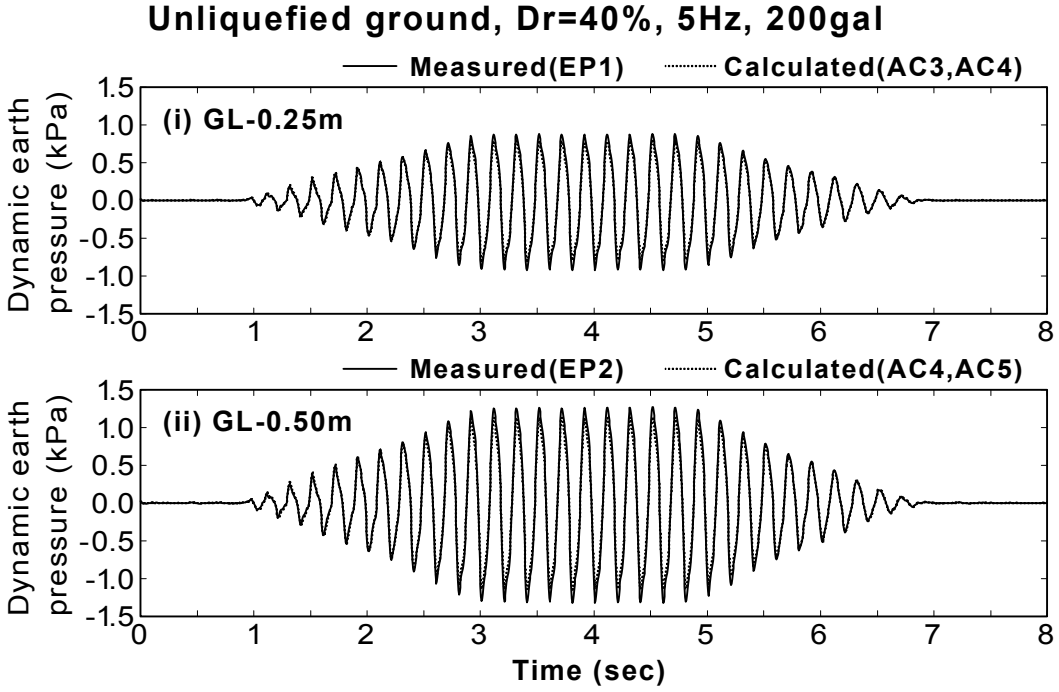

(a) During vertical excitation (0sec～8sec)

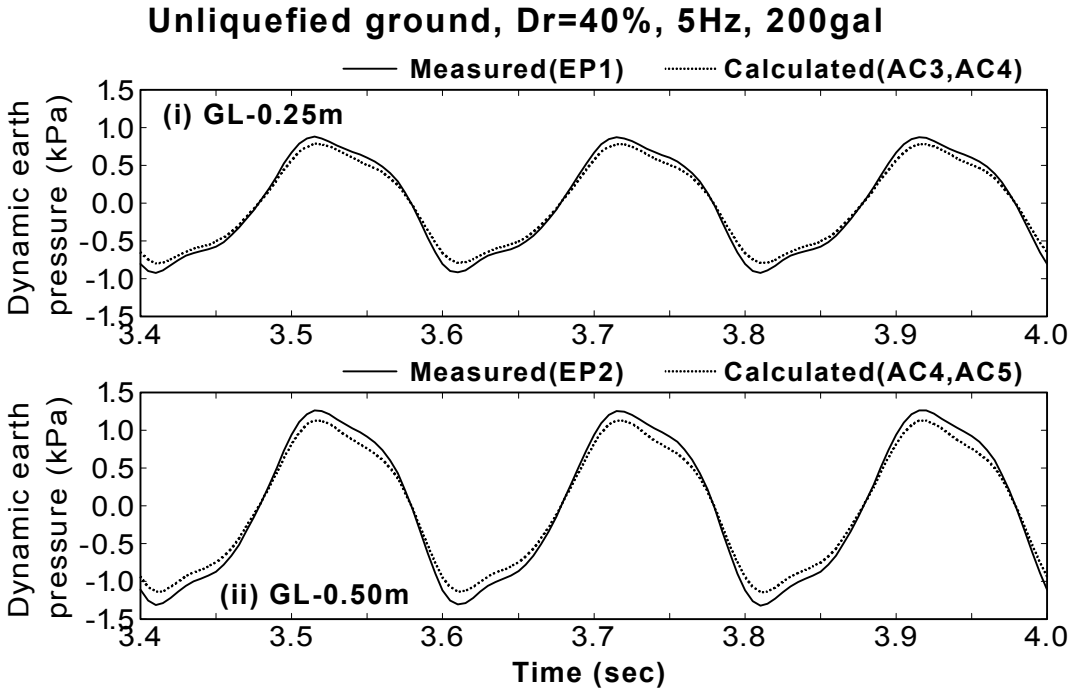

(b) Enlarged with respect to time (3.4sec to 4.0sec)

Fig.A.35: Comparison between measured and calculated dynamic earth pressures (NLF5A200D40 test)

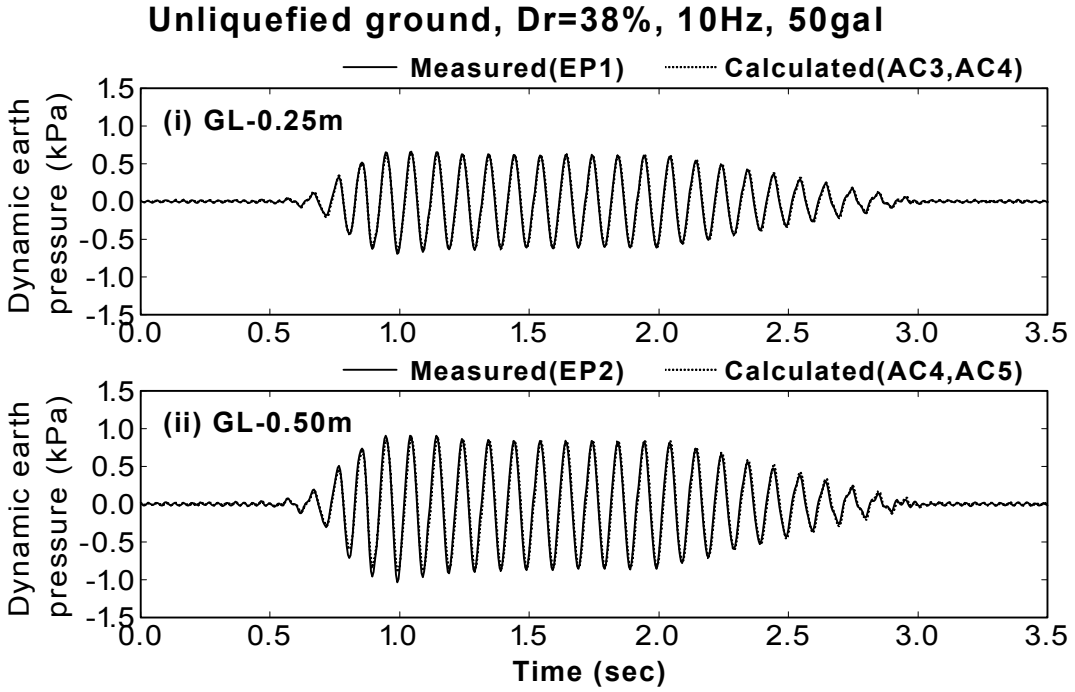

(a) During vertical excitation (0sec～3.5sec)

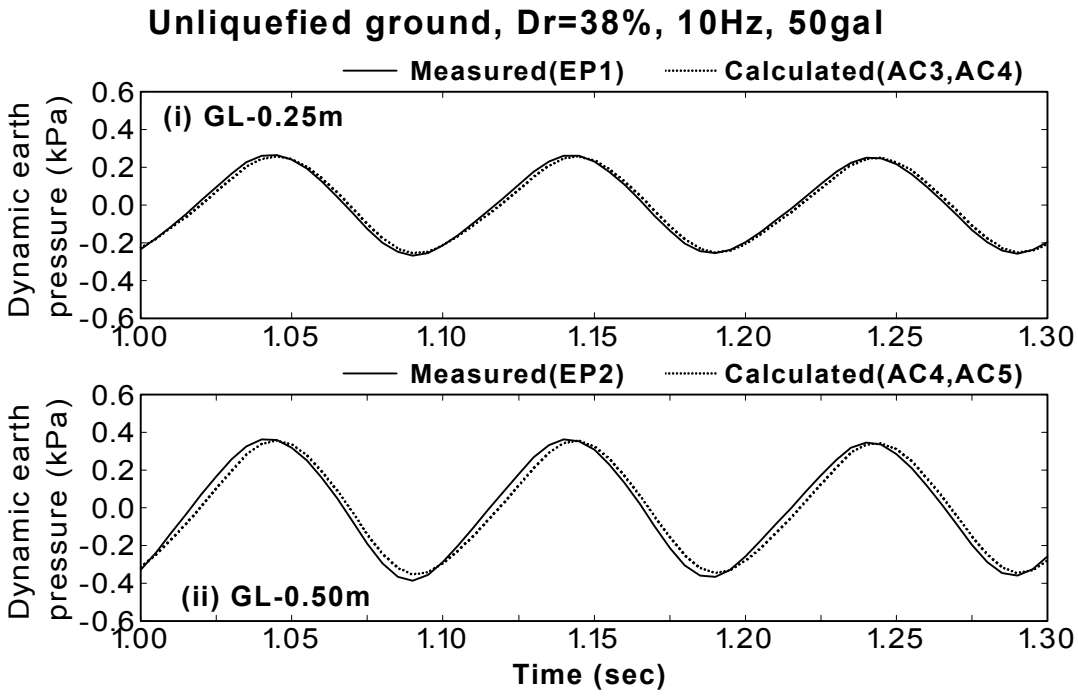

(b) Enlarged with respect to time (1.0sec to 1.3sec)

Fig.A.36: Comparison between measured and calculated dynamic earth pressures (NLF10A50D38 test)

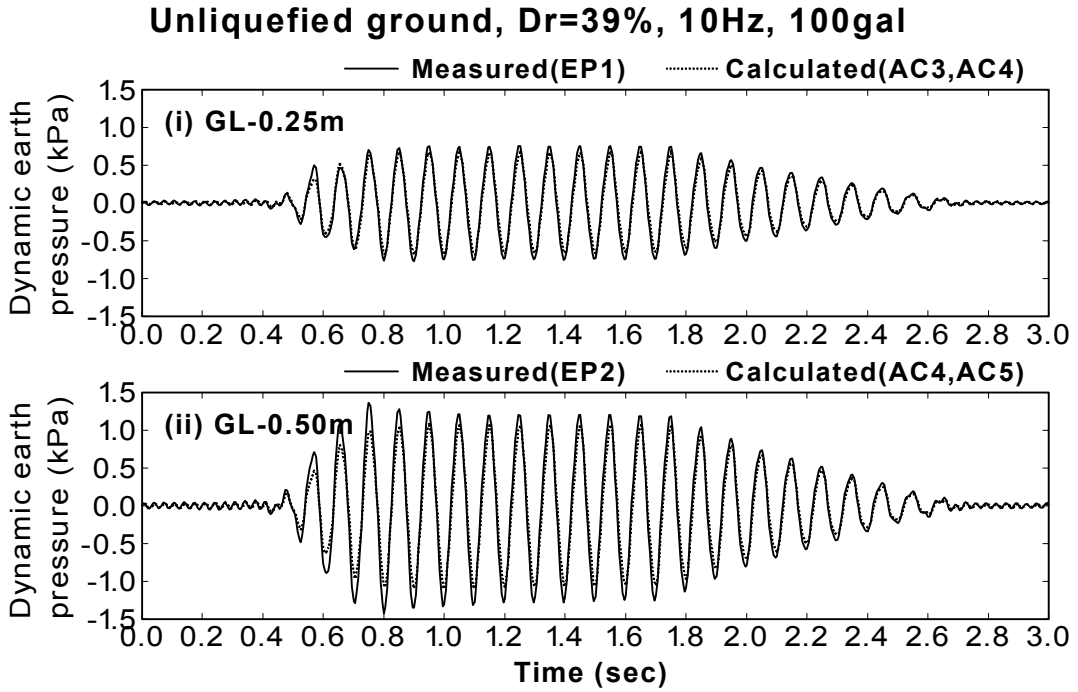

(a) During vertical excitation (0sec to 3 sec)

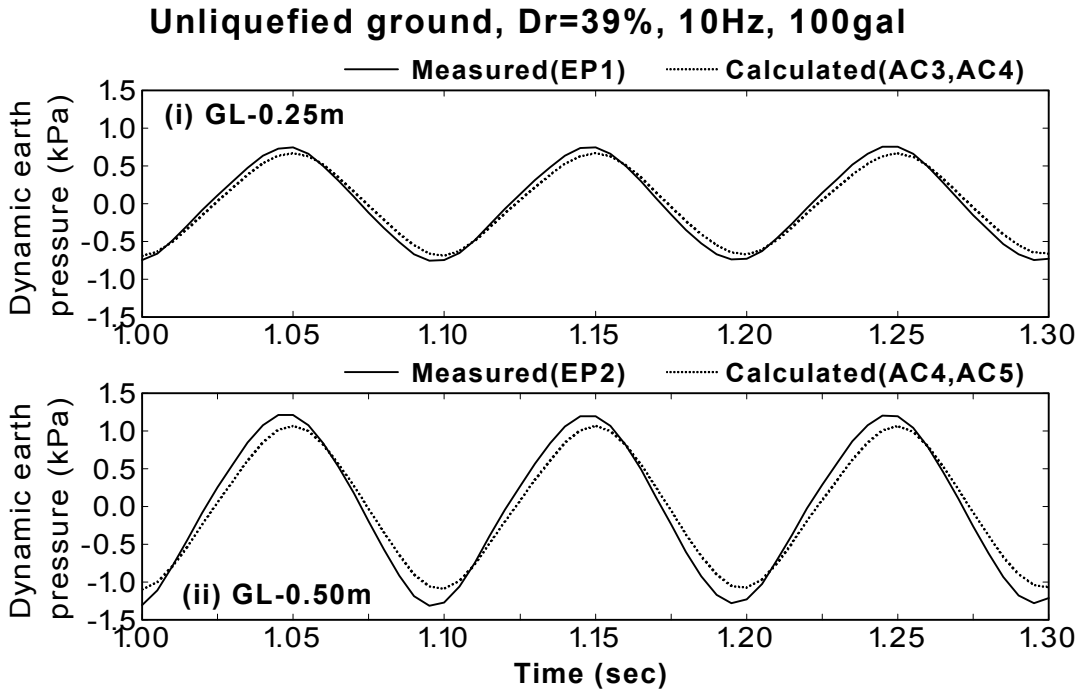

(b) Enlarged with respect to time (1.0sec to 1.3sec)

Fig.A.37: Comparison between measured and calculated dynamic earth pressures (NLF10A100D39 test)

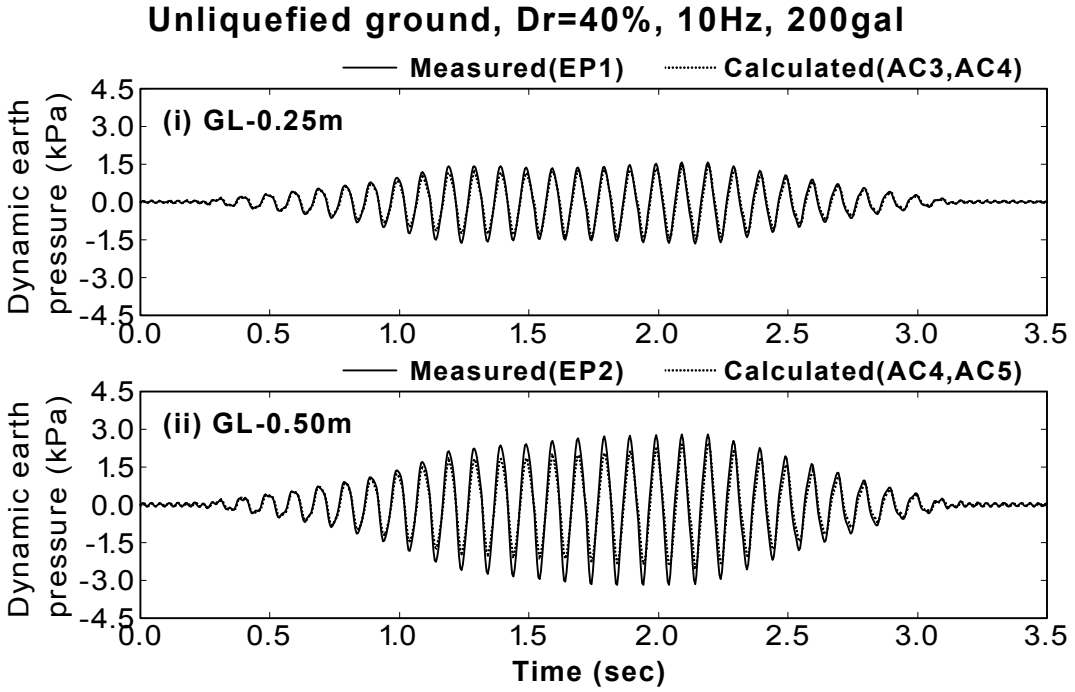

(a) During vertical excitation (0sec～3.5sec)

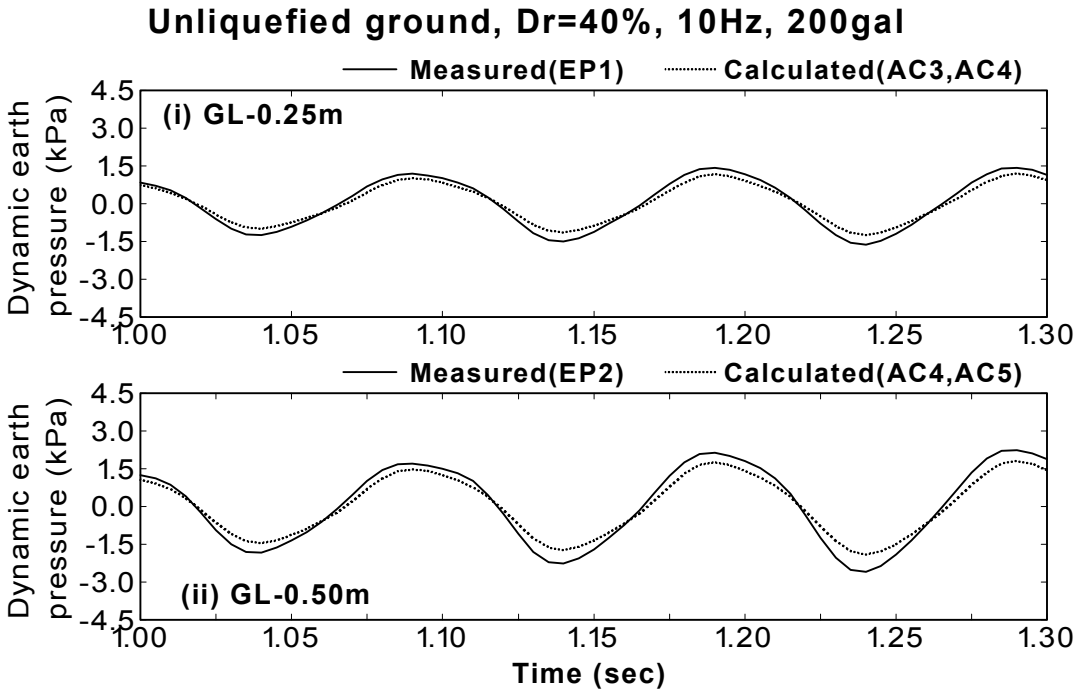

(b) Enlarged with respect to time (1.0sec to 1.3sec)

Fig.A.38: Comparison between measured and calculated dynamic earth pressures (NLF10A200D40 test)

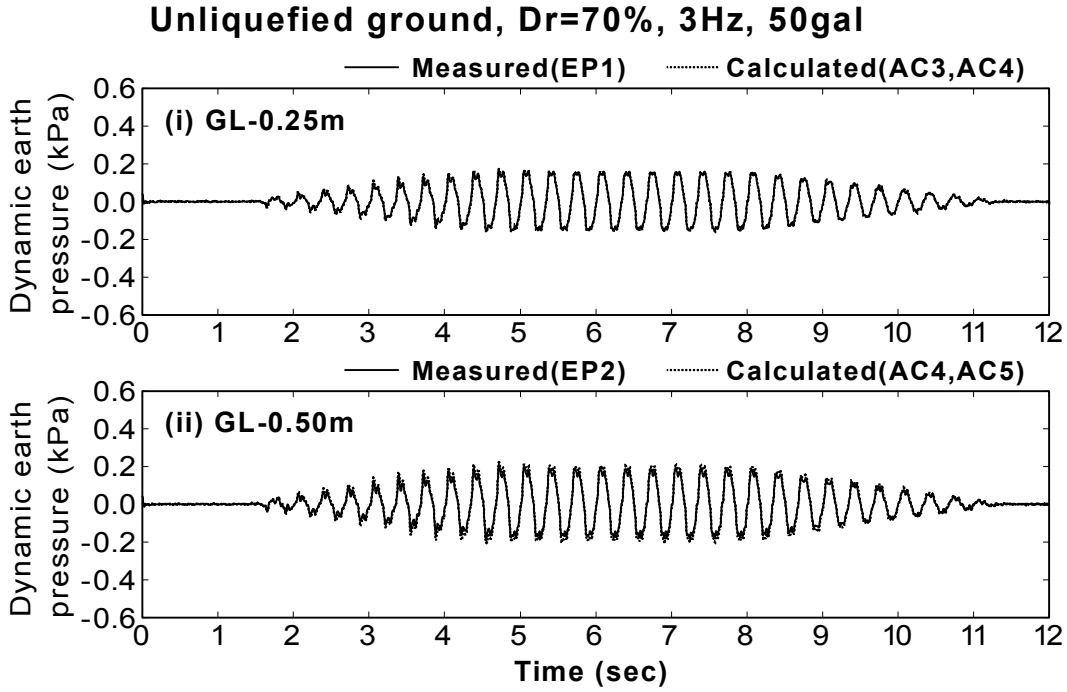

(a) During vertical excitation (0sec～12sec)

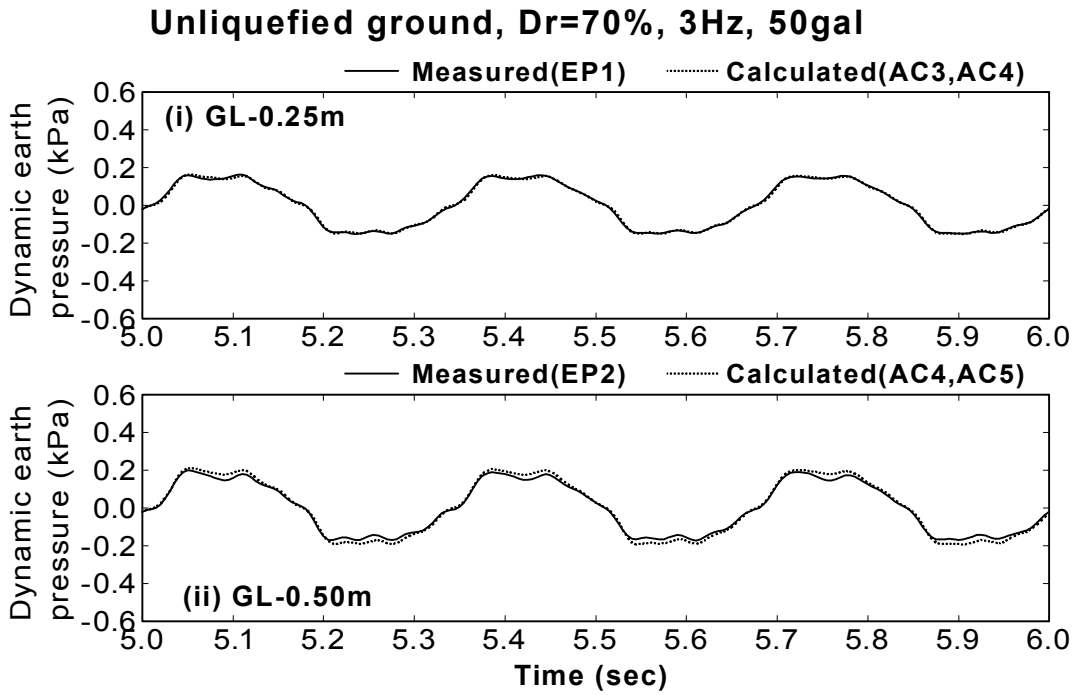

(b) Enlarged with respect to time (5.0sec to 6.0sec)

Fig.A.39: Comparison between measured and calculated dynamic earth pressures (NLF3A50D70 test)

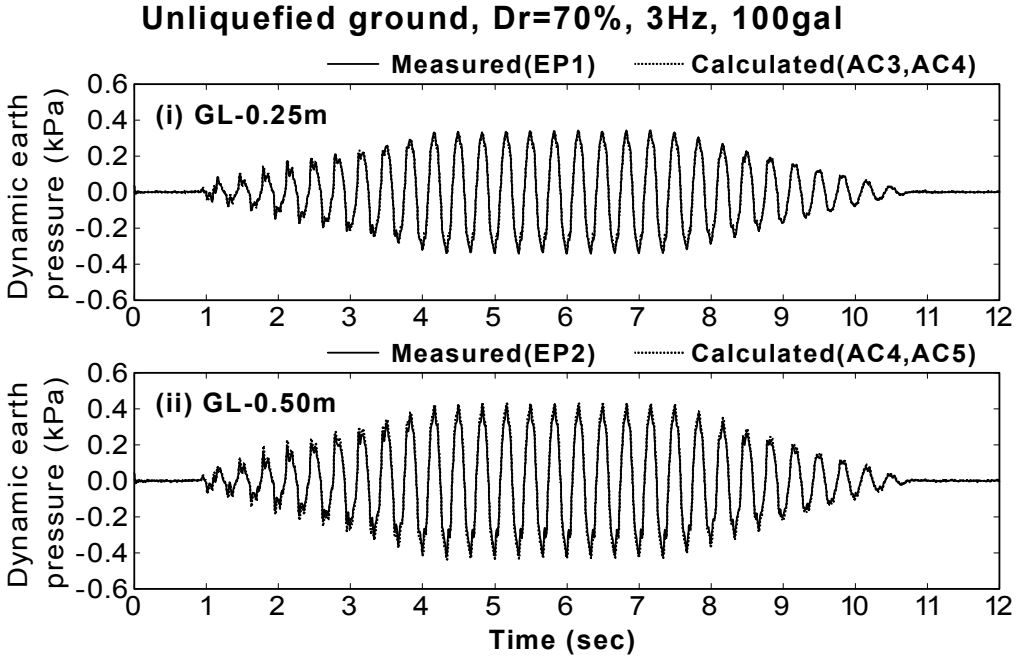

(a) During vertical excitation (0sec to 12 sec)

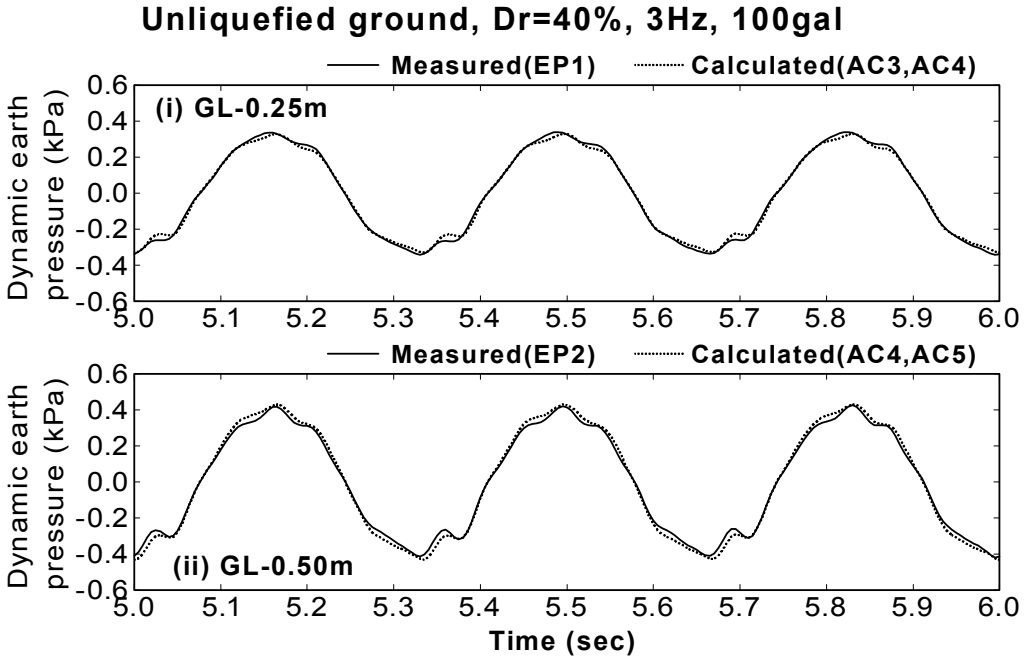

(b) Enlarged with respect to time (5.0sec to 6.0sec)

Fig.A.40: Comparison between measured and calculated dynamic earth pressures (NLF3A100D70 test)

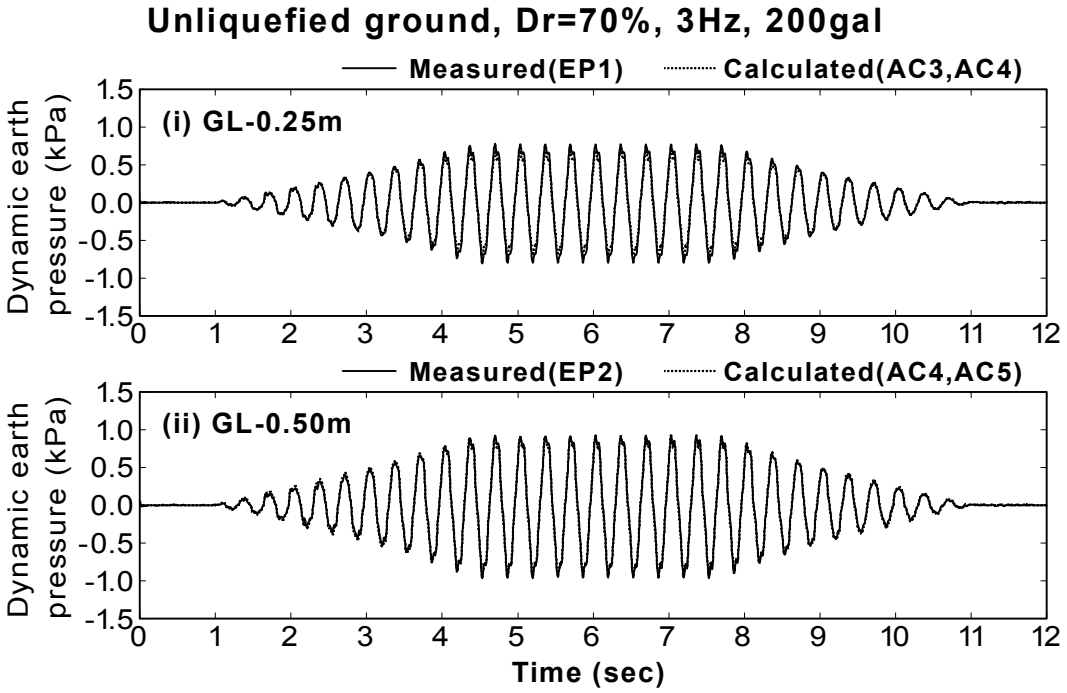

(a) During vertical excitation (0sec～12sec)

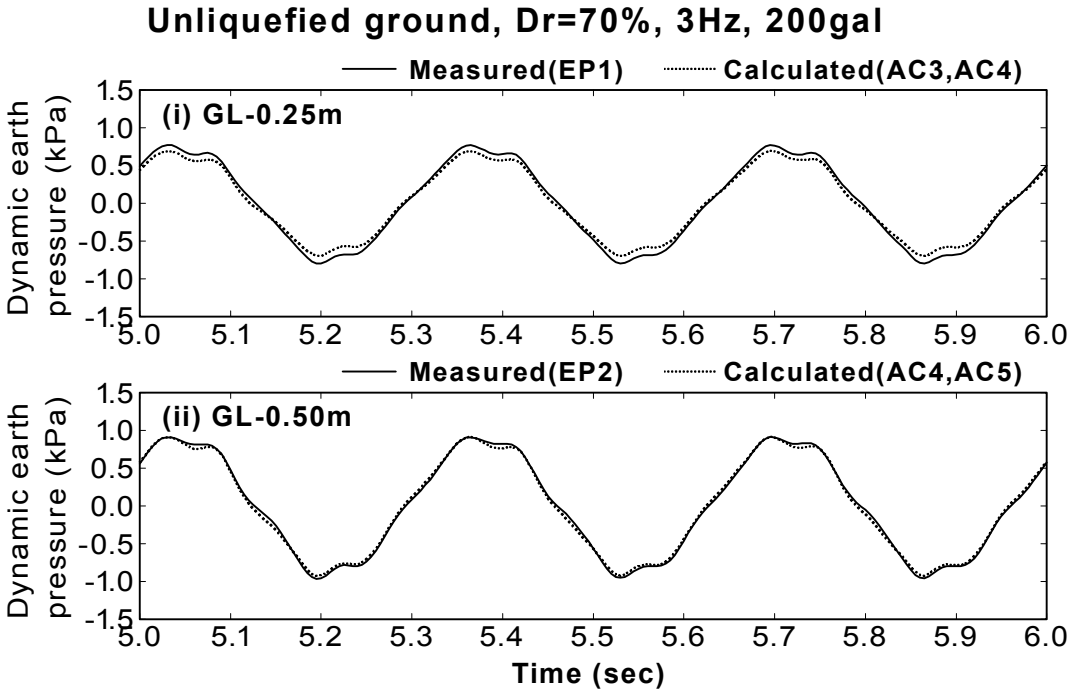

(b) Enlarged with respect to time (5.0sec to 6.0sec)

Fig.A.41: Comparison between measured and calculated dynamic earth pressures (NLF3A200D70 test)

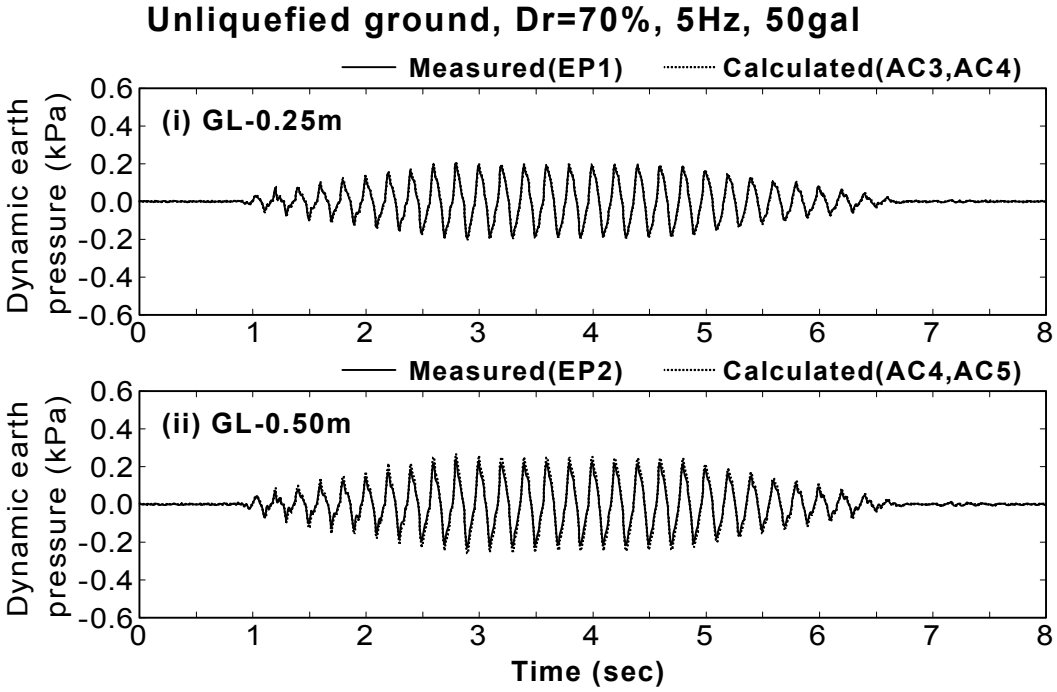

(a) During vertical excitation (0sec～8sec)

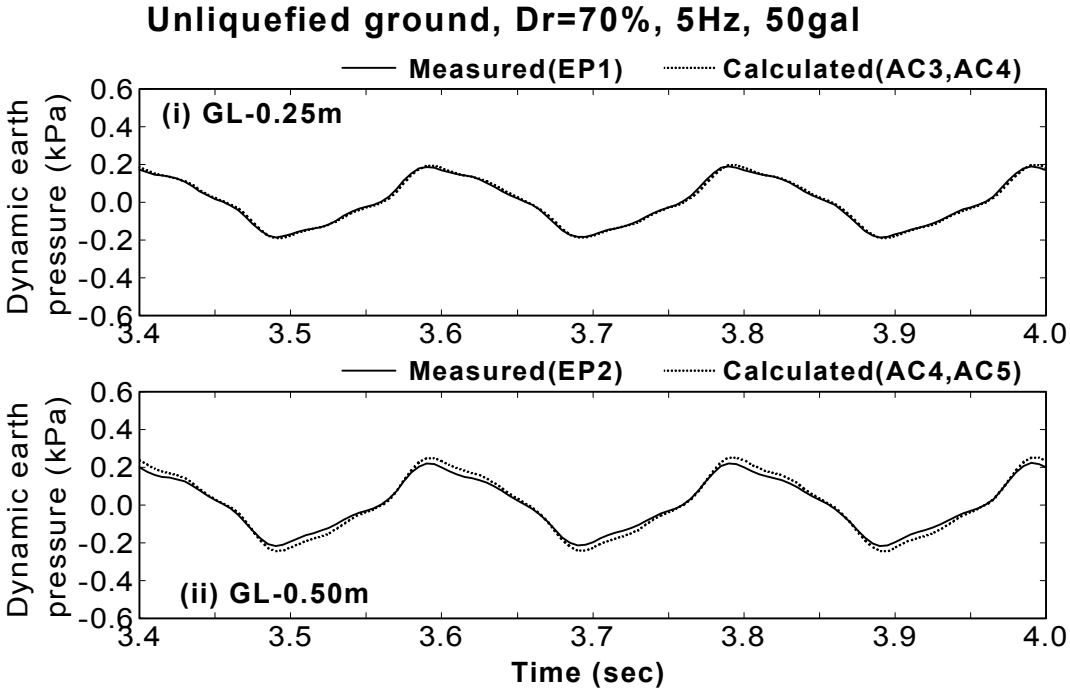

(b) Enlarged with respect to time (3.4sec to 4.0sec)

Fig.A.42: Comparison between measured and calculated dynamic earth pressures (NLF5A50D70 test)

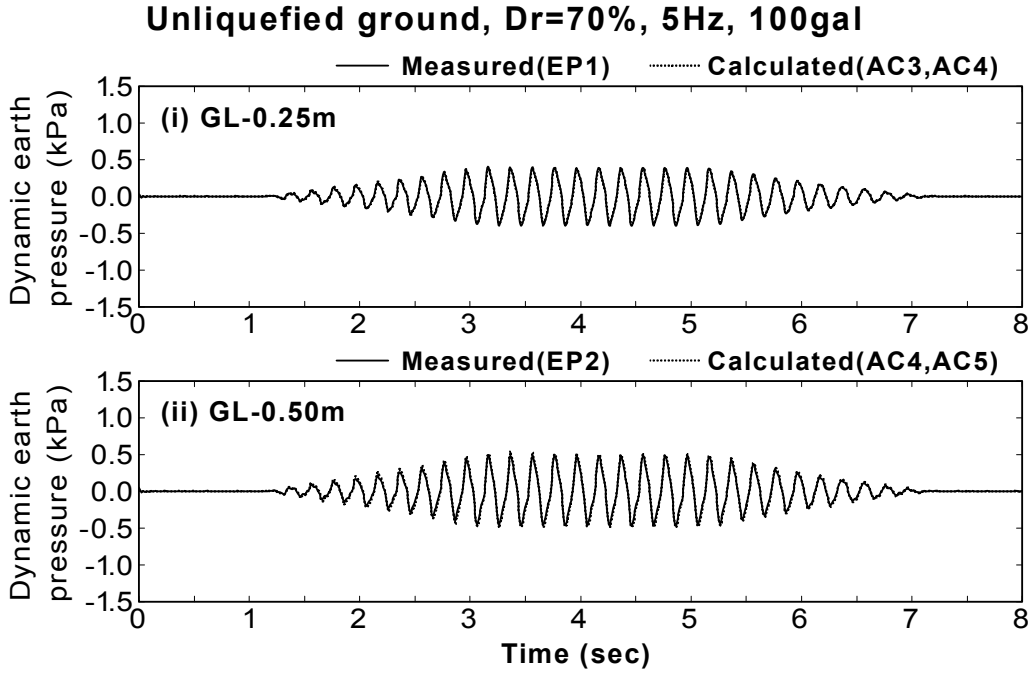

(a) During vertical excitation (0sec to 8 sec)

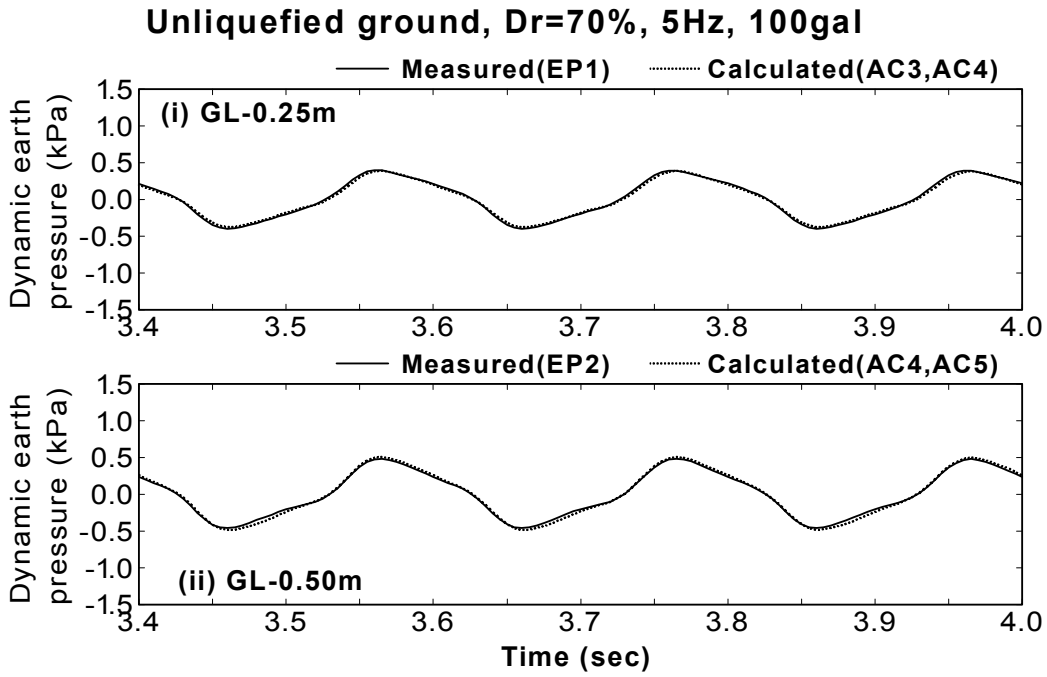

(b) Enlarged with respect to time (3.4sec to 4.0sec)

Fig.A.43: Comparison between measured and calculated dynamic earth pressures (NLF5A100D70 test)

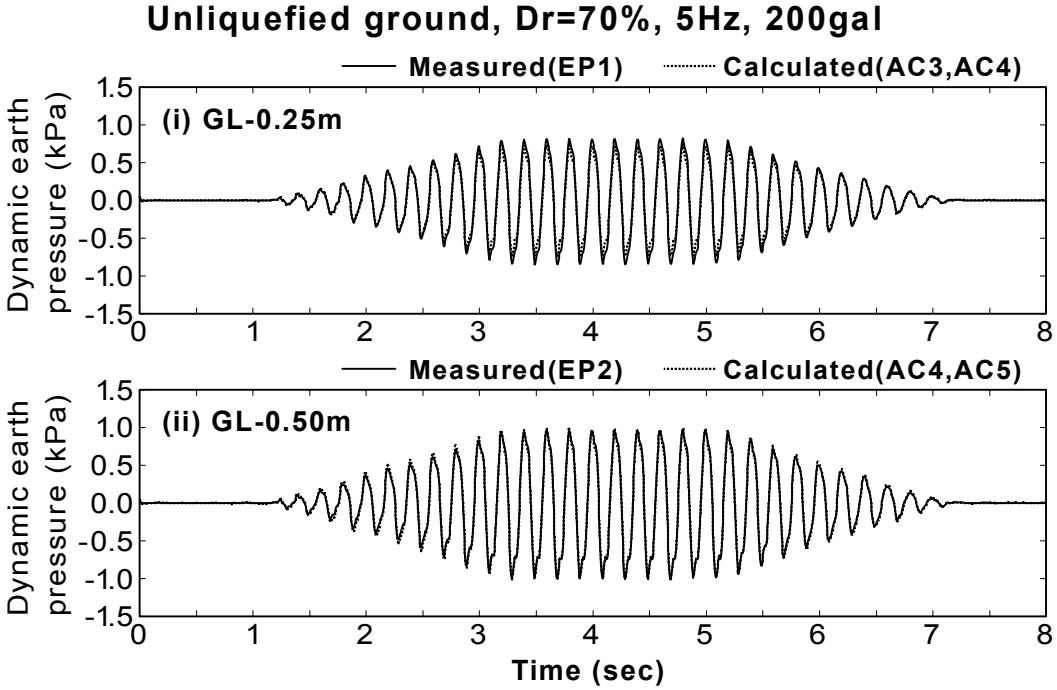

(a) During vertical excitation (0sec～8sec)

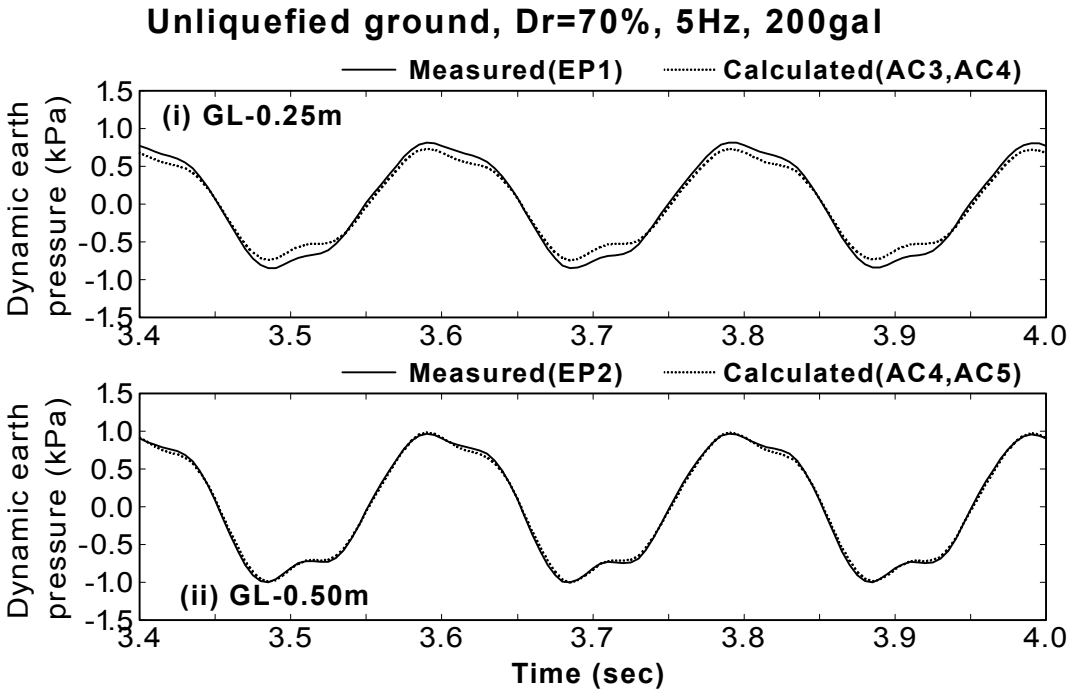

(b) Enlarged with respect to time (3.4sec to 4.0sec)

Fig.A.44: Comparison between measured and calculated dynamic earth pressures (NLF5A200D70 test)

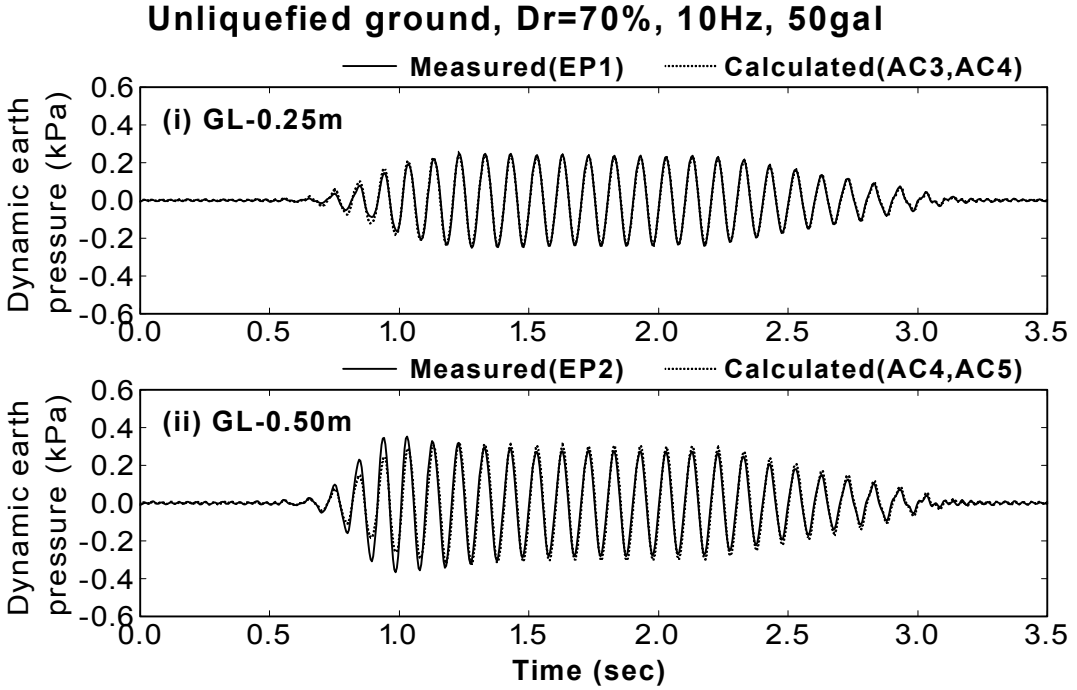

(a) During vertical excitation (0sec～3.5ec)

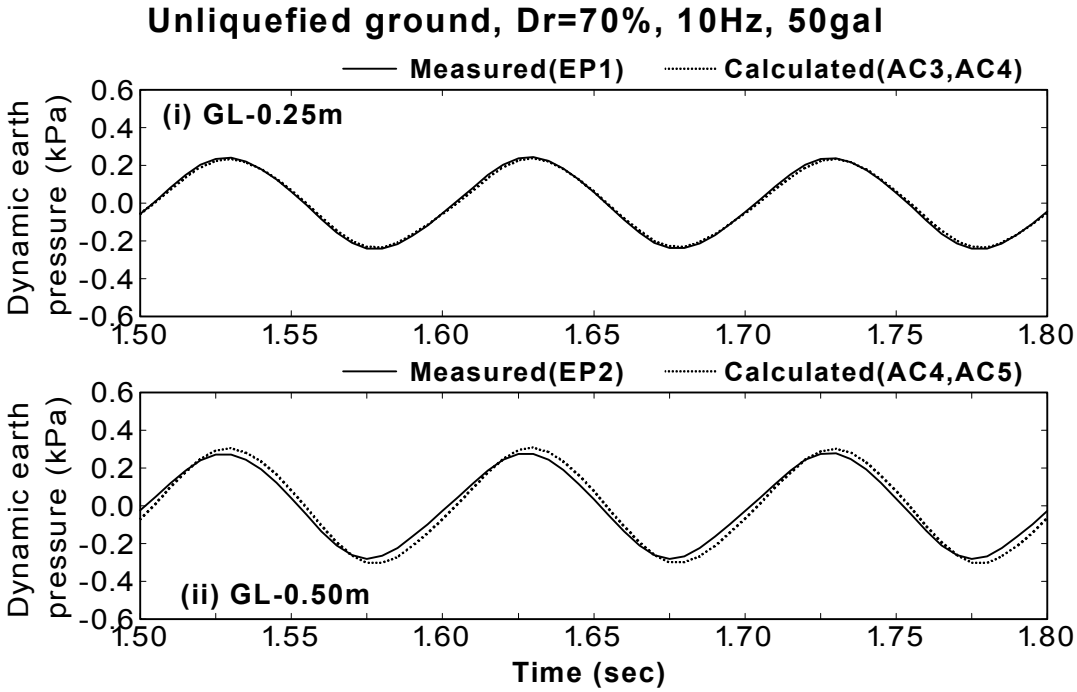

(b) Enlarged with respect to time (1.5sec to 1.8sec)

Fig.A.45: Comparison between measured and calculated dynamic earth pressures (NLF10A50D70 test)

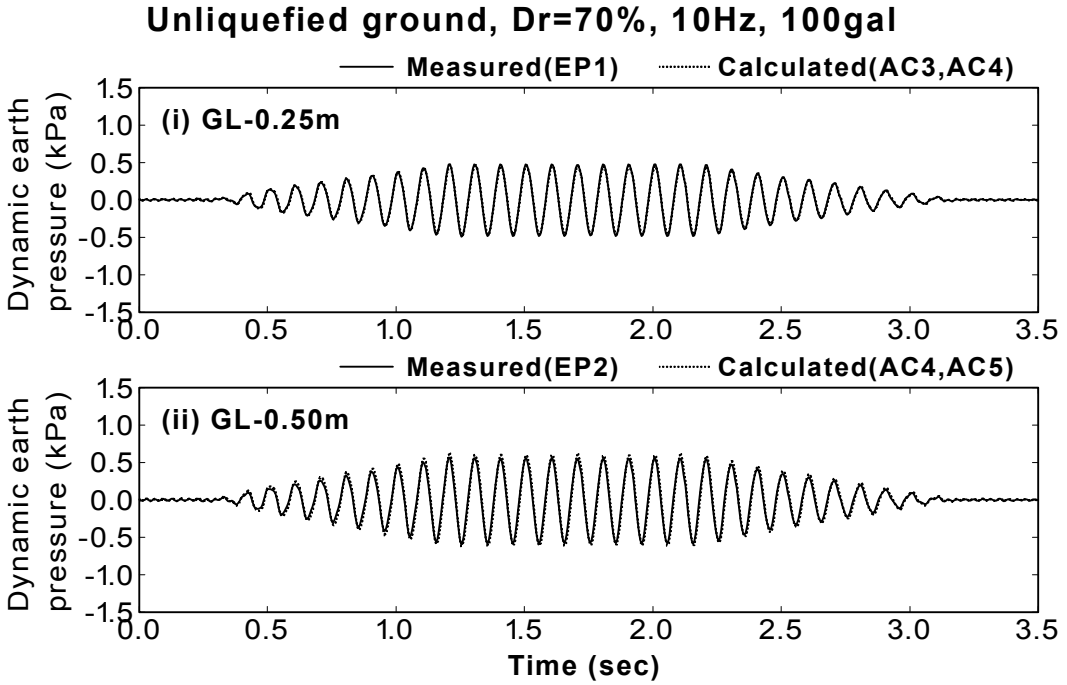

(a) During vertical excitation (0sec to 3.5sec)

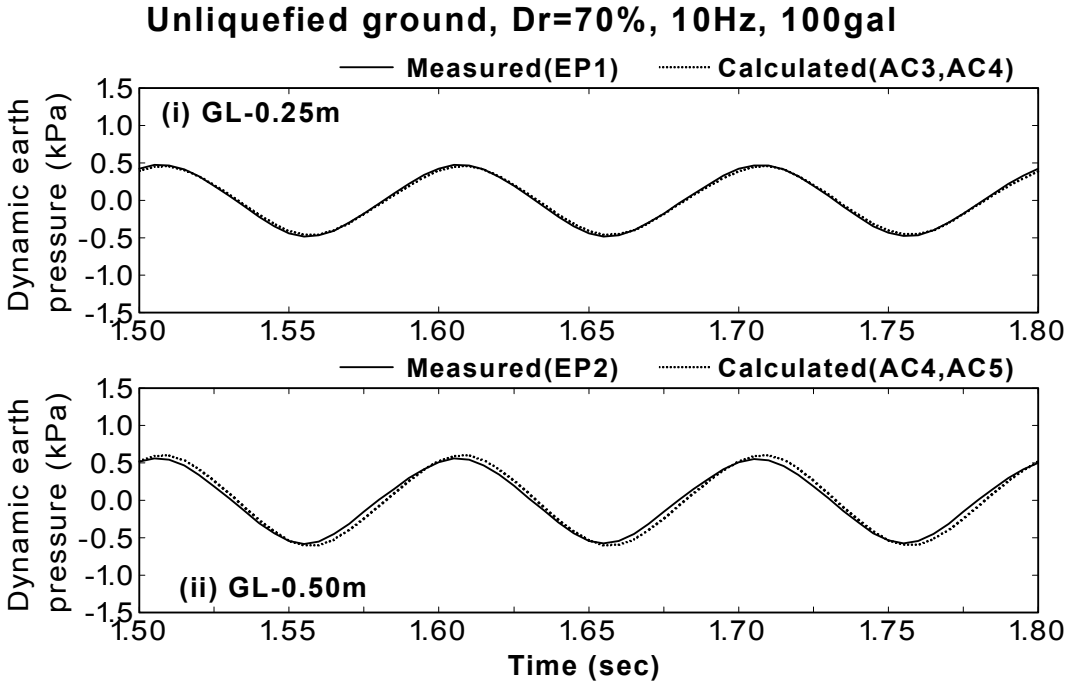

(b) Enlarged with respect to time (1.5sec to 1.8sec)

Fig.A.46: Comparison between measured and calculated dynamic earth pressures (NLF10A100D70 test)

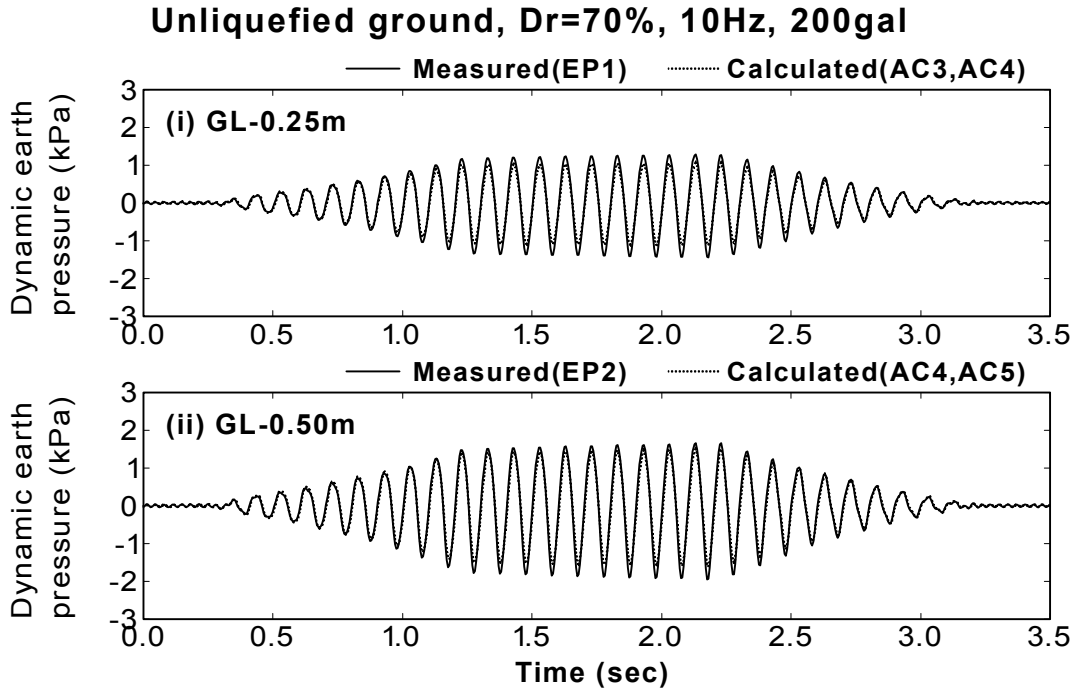

(a) During vertical excitation (0sec～3.5ec)

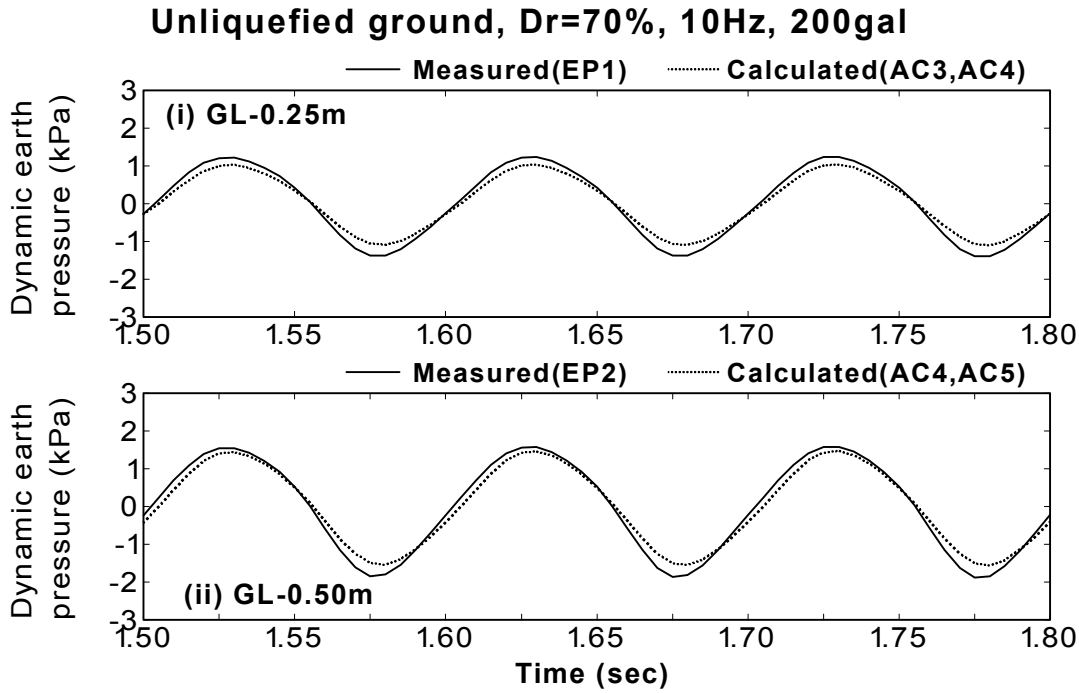

(b) Enlarged with respect to time (1.5sec to 1.8sec)

Fig.A.47: Comparison between measured and calculated dynamic earth pressures (NLF10A200D70 test)

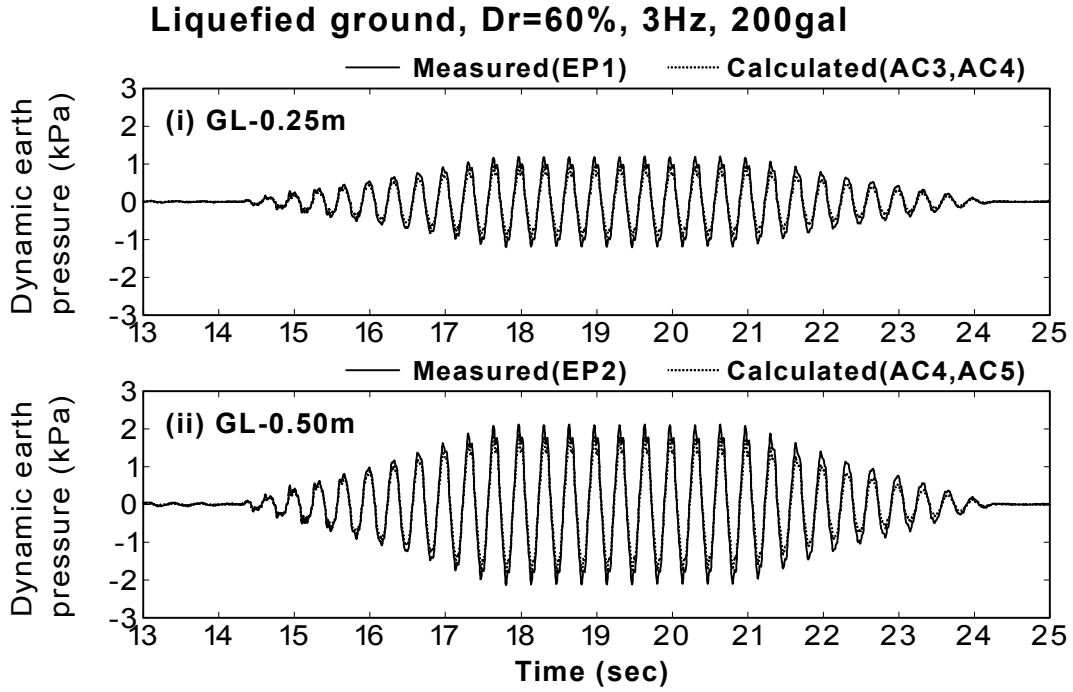

(a) During vertical excitation (13sec to 25 sec)

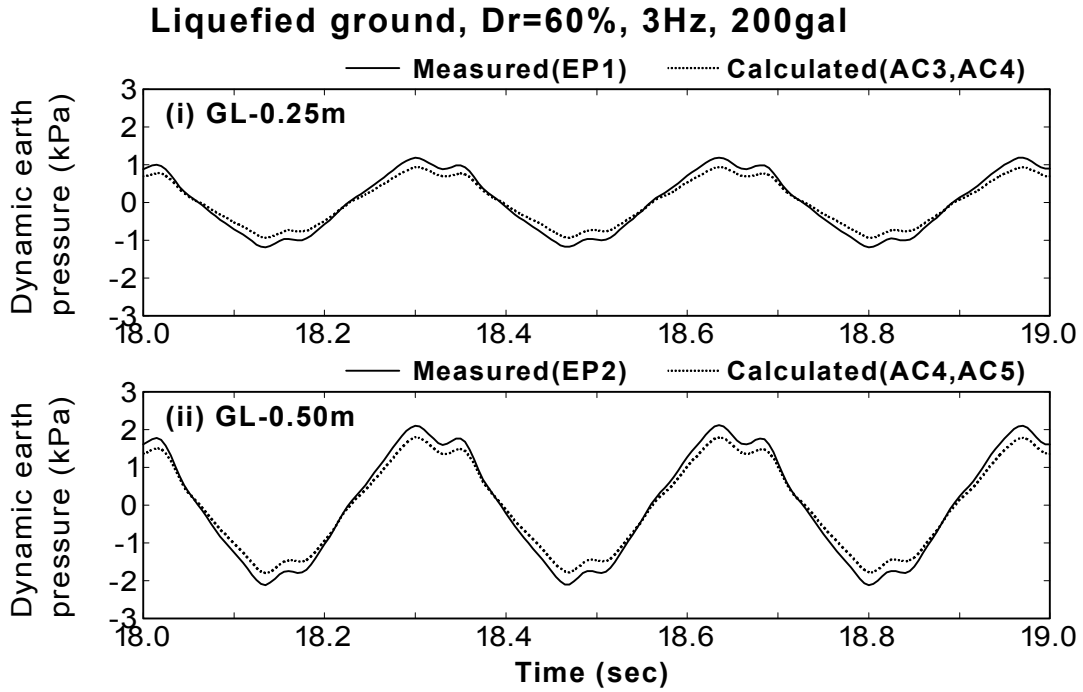

(b) Enlarged with respect to time (18.0sec to 19.0sec)

Fig.A.48: Comparison between measured and calculated dynamic earth pressures (LIQF3A200D60 test)

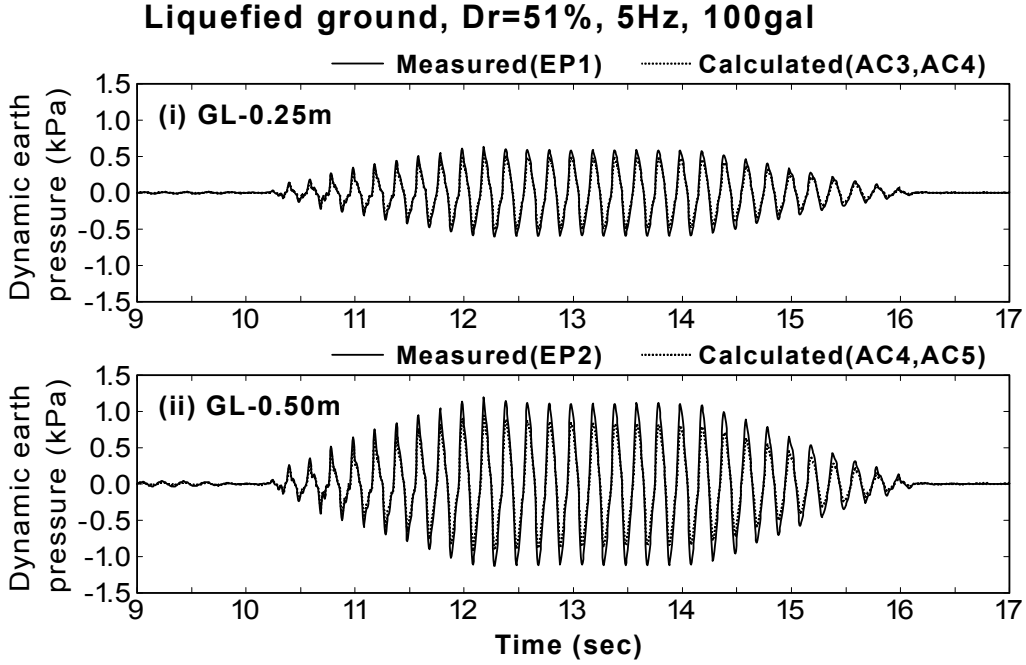

(a) During vertical excitation (9sec to 17 sec)

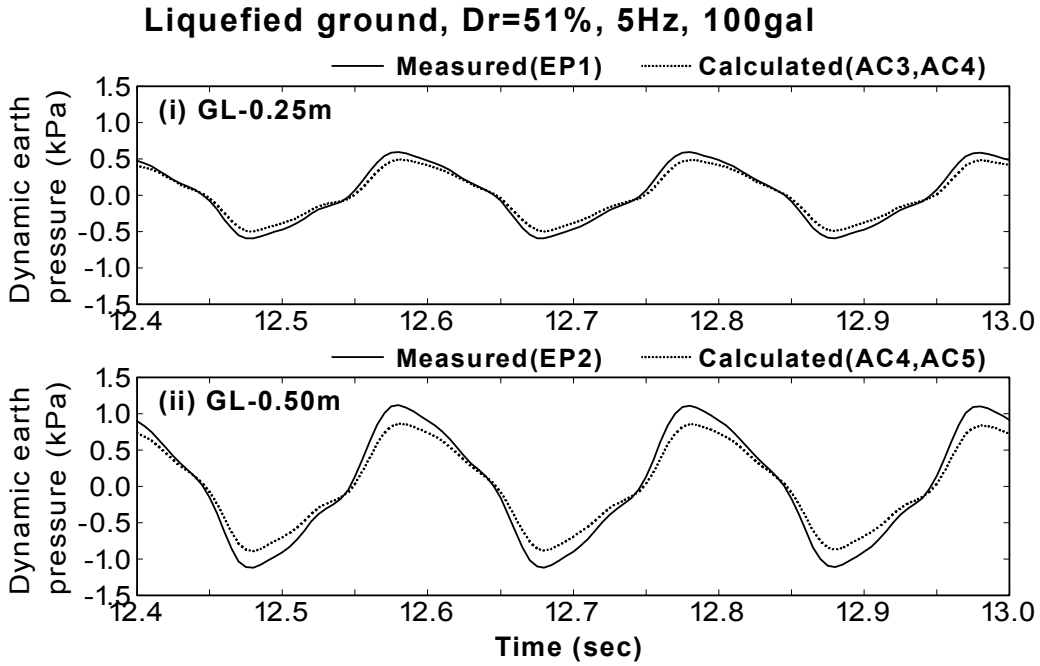

(b) Enlarged with respect to time (12.4sec to 13.0sec)

Fig.A.49: Comparison between measured and calculated dynamic earth pressures (LIQF5A100D51 test)

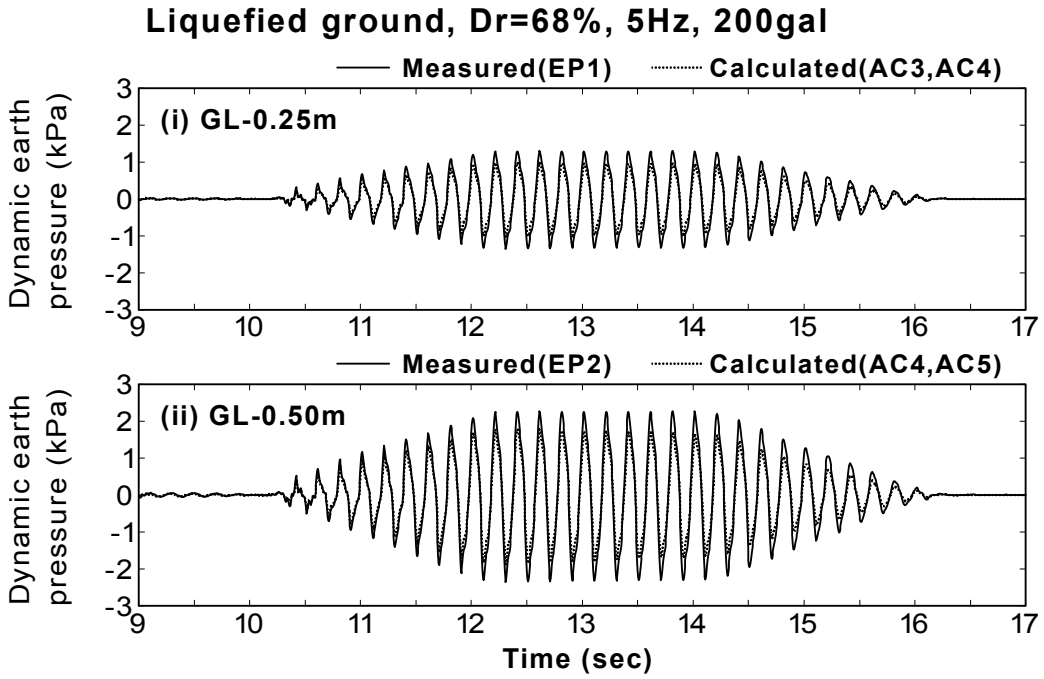

(a) During vertical excitation (9 sec to 17 sec)

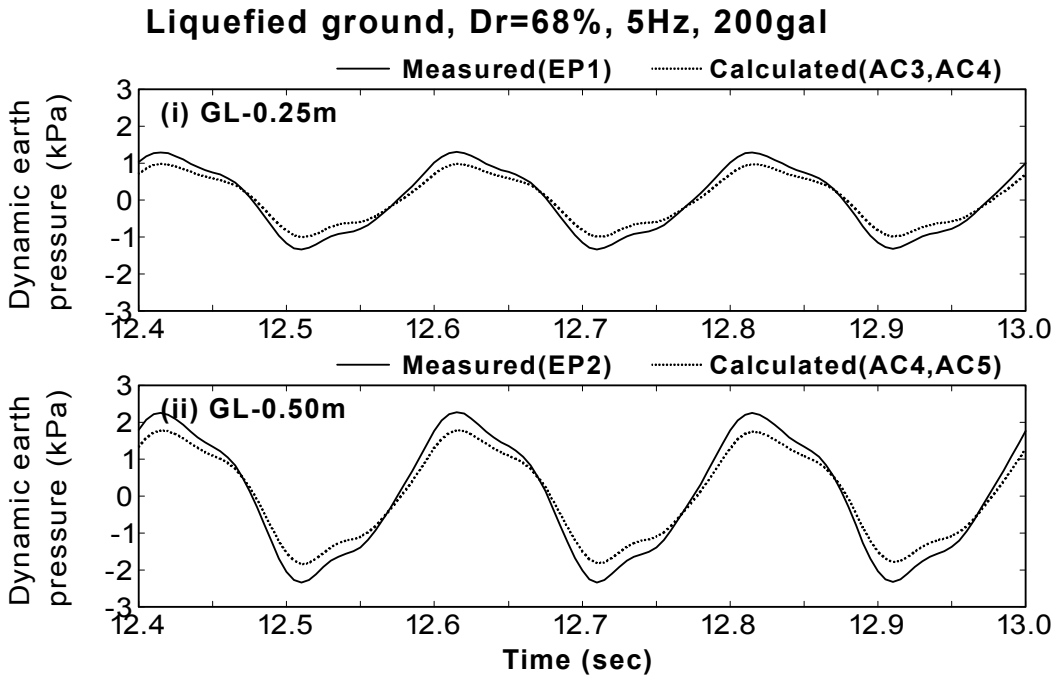

(b) Enlarged with respect to time (12.4sec to 13.0sec)

Fig.A.50: Comparison between measured and calculated dynamic earth pressures (NLF5A200D68 test)

SHAKING TABLE MODEL TESTS ON DYNAMIC INTERACTION BETWEEN CROSS SECTION OF FLEXIBLE UNDERGROUND STRUCTURES AND LIQUEFIED SOIL

液状化地盤と埋設柔構造物断面の動的相互作用に関する実験的研究

Yukio Tamari
溜　幸生

Yukio Tamari, Dr. Eng., P. E.

Tokyo Electric Power Services, 3-3-3 Higashi-Ueno, Taito-ku, Tokyo 110-0015, JAPAN
E-mail (office) : etamari@tepsco.co.jp　(home office) : tamari@tkb.att.ne.jp
Fax (office) :　+81-3-4464-5595